5th BSME International Conference on Thermal Engineering

Comparison on Evaluated Performance of Different Axis Solar Tracker

Md. Riaz Pervez[a]*, Mohd. Rafiqual Alam Beg[b], Md. Rabiul Islam Sarker[b]

[a]*Department of Mechatronics, University of Siegen, Siegen-57074, Germany*
[b]*Department of Mechanical Engineering, Rajshahi University of Engineering and Technology, Rajshahi-6204, Bangladesh*

Abstract

This paper presents the comparison of experimental study of a two axis (azimuth and elevation) and single axis automatic control solar tracking system with the fixed photovoltaic (PV) system or without tracking system. Those tracking system track solar PV panel according to the direction of beam propagation of solar radiation. The tracking unit consists of sensors, ADC, microcontroller and stepper motor. The analog input from the sensors is converted by ADC and this digital data transfer to the microcontroller. By using this data controller rotate the stepper motor in desirable direction. An experimental study is carried out to evaluate their performance under local climate. The results indicate that the average energy surplus become about 30- 38% for two axis solar tracker and 15-25% for single axis solar tracker with atmospheric influences. But there is a design difficulties exists in the two axis solar tracker which is not so considerable in the point of view of surplus energy found from two axis solar tracker compared with single axis solar tracker. Considering all above aspects two- axis sun tracking system is more beneficial than single axis sun tracking system.

Keywords: **:** Two-axis solar tracker; Single-axis tracker; surplus energy; Microcontroller, Solar energy.

1. Introduction

Dramatically decrease of fossil fuel and increase of polluted gases create a profound impact on communication, living and other consumption sectors. So human beings are largely depends on the alternatives like renewable energy. So for getting direct electricity without effort the PV system is the best choice able option. Solar panel is the fundamental energy conversion component of photovoltaic (PV) systems [1]. PV offers safe and clean energy sources [2]. With the cost of solar cells decreasing, the conversion of solar energy to electrical energy is increasingly becoming economically viable [3]. This is suitable for topical countries like Bangladesh where there is abundant solar energy available throughout the year. As solar panels are relatively expensive, much research work has been conducted to improve the utilization of solar energy. Physically, the power supplied by the panels depends on many extrinsic factors, such as insulation levels (incident of solar radiation), temperature and load condition [4].

For consuming this vast energy, an adaptive system should be developed for getting maximum power from this solar panel. But the availability of sun throughout the day is not same or maximized. This is due to the static placement of the panel which limits their area of exposure from the sun [5].In searching for the maximum power condition, many methods have been tried. The “look-up-table”, the “perturb and observe”, and the “current sweep” are some of the fundamental approach [1]. Neural Network approach [6] and Fuzzy Logic approach [7] are also reported. An automatic solar tracking system using a number of Light Detecting Registers (LDRs) is proposed [5, 8]. Researchers [9, 10] have presented the design and implementation of a computer-controlled dual-axis solar tracking system to obtain high precision positioning of the PV panel.

All the above mention research is just design and implementation of various tracking system. The aim of this work is to compare the effect of using two-axis and single axis solar tracking systems on the electrical generation of a flat photovoltaic system (FPVS) with fixed system. An experimental study is carried out to evaluate their performance under local climate.

* Corresponding author. Tel.:+ 490 176 69372865.
E-mail address: md.pervez@student.uni-siegen.de

2. Comparison of design of the tracking systems

2.1. In motor load

The Stepper Motor is an electromagnetic device that converts digital pulses into mechanical shaft rotation. Motion Control, in electronic terms, means to accurately control the movement of an object based on speed, distance, load, inertia or a combination of all these factors.

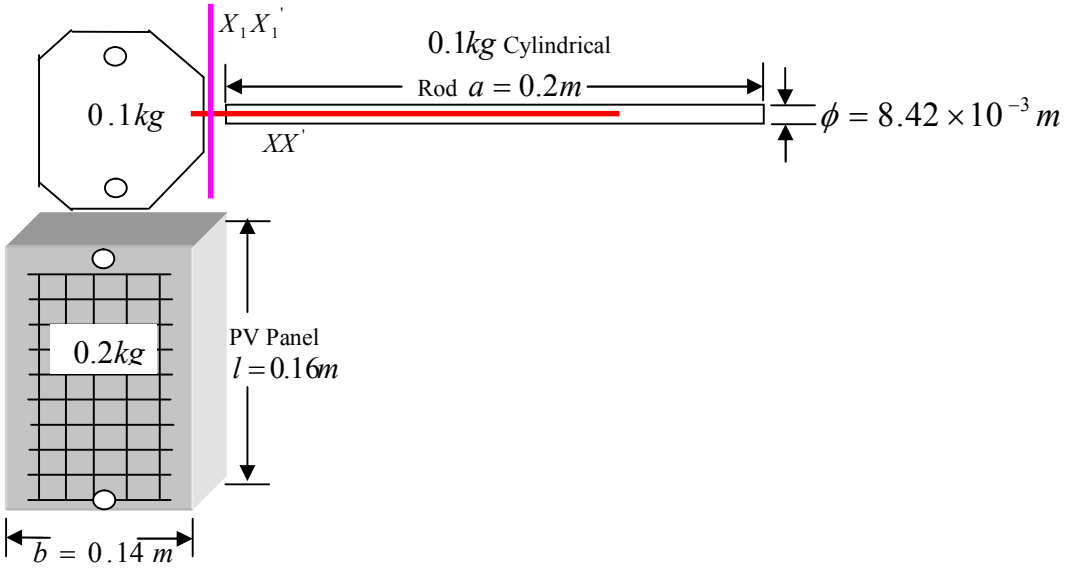

Fig. 1. Schematic diagram of the mechanical system

From above specification as shown in (Fig. 1) the power for single axis tracking is 0.092Watt and for two axes tracking the power is 1.38Watt, both are less than the single motor power (2.36Watt). The power required for Single axis tracking is much less then the two axis tracking. Though extra motor is required for two axis tracker but considering the surplus energy it is more beneficial then single one.

2.2. In Sensing Element and Signal Processing

A lot of methods have been proposed and used to track the position of the sun. The simplest of all uses an LDR– a Light Dependent Resistor to detect light intensity changes on the surface of the resistor. Other methods, such as that published by Jeff Damm in 'Home Power' [11], use two phototransistors covered with a small plate to act as a shield to sunlight.

At morning, the tracker is in state A from the previous day. The left phototransistor is turned on, causing a signal to turn the motor continuously until the shadow from the plate returns the tracker to state B. As the day slowly progresses, state C is reached shortly, turning on the right phototransistor. The motor turns until state B is reached again, and the cycle continues until the end of the day or until the minimum detectable light level is reached. Considering problems [12] three solar cells are used.

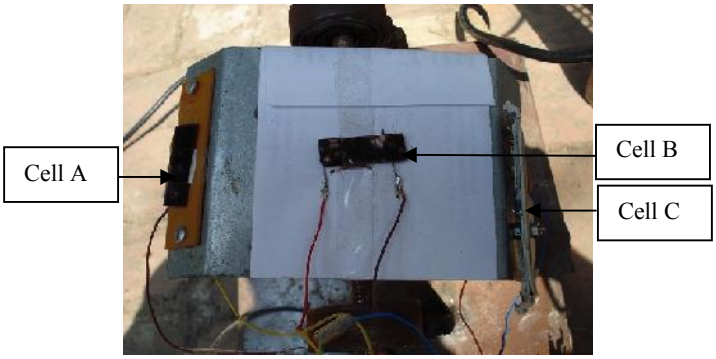

Fig. 2. Three solar cells as sensor

The cells are placed at 15^0 to each other because the sun rotates 15^0 in an hour. When maximum solar intensity falls on cell A then the motor rotates cell A direction (clockwise). On the other hand, if cell C gives the maximum then motor rotates reverse. If intensity of cell B is high than any other cell, then motor stands in that position. This is a continuous process. So the cells are always compared the intensity level and given command to the controller and the motor rotates in that direction. The rotating principle is same for the other motor.

2.3. In Software design

The designed tracking systems consists of software based online tracking method. The main components of the designed system are photocell as sun sensor, ADC0808, interfacing component with microcontroller (AT90S8515), stepper motor driver circuit (ULN2803), stepper motor and PV cell supporting metallic structure with mechanical gear mechanism.

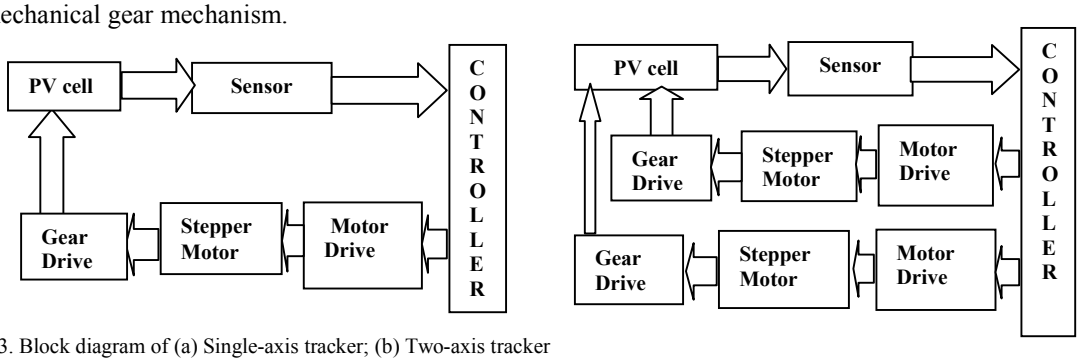

Fig. 3. Block diagram of (a) Single-axis tracker; (b) Two-axis tracker

The electromechanical system of a single-axis solar tracker consists of single drivers with single stepper motor of 0.1° per step which is used for the E-W tracking (Fig. 3 a). On the other hand, the electromechanical system of a two-axis solar tracker consists of two drivers with two steeper motor of 0.1° per step: the first for the joint rotating about the vertical axis and the second for the E-W tracking as shown in (Fig. 3 b).

Fig. 4. Experimental set-up of (a) single axis tracker; (b) Two axis tracker

The sun position sensors (Photocell) give an mV voltage proportional to the radiation beam position inside the sensor. This sensor is intended to keep the radiation beam normal with collector. Sun sensor's detector determines system misalignment (position error of solar radiation collecting unit) and then sends a signal to the controller (Microcontroller's software). The controller (Microcontroller's software) uses the sun's rate and sun sensor information as inputs to generate proper motor commands to slew the collector. The microcontroller contains database program based on sun's position for every time of a definite day. When the stepper motor gets the commands from the controller, the motor starts to rotate at a definite angle according to the controller command that slew the collector.

Control software has been developed to determine the optimum position of the panel during day light i.e. how much deviated from maximum power point. The calculated values taking from the sensor is a function of voltage which is converted to digital form is fed to the microcontroller program to control the actuator of the solar tracker. In this research the programming method of control works efficiently in all weather conditions regardless of the presence of clouds.

The software for the solar tracker is written in Bascom AVR version-11.1.8.7. Flow chart of the control software for both systems shows the basic difference in the software design which are shown in appendix A.

Software based online tracking method is used in the designed tracking system. Three PV modules of the following specifications were used to compare the energy surplus of the tracking modules where one was fixed and other two were in tracking mode. The simplest method to obtain an IV characteristic is to load the module with a variable resistor, and measure the voltage and current through digital multi-meter [13-14].

The mechanical gear mechanism used for single axis is simpler than two axis solar tracker because of the tracking complicated strategy of two axis solar tracker.

3. Experimental Results and Discussions

Measurements on the PV system with and without solar tracking at various local climatic conditions are shown in Figs 5, 6, 7 of 4th March, 2008 and 8,9,10 of 10th April, 2009. The experiment is carried out through the months February to April, 2008 & 2009.

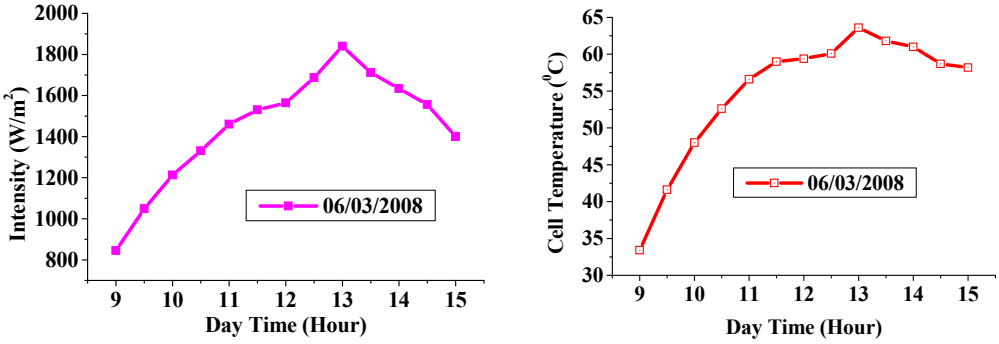

Fig. 5. (a) Intensity with day time; (b) Cell temperature with day time

3.1. Characteristics of Intensity & Temperature with respect to Day Time

From the experimental results of variation of intensity with day time characteristic it is seen that solar irradiation increases with day time up to 13.00 PM and then decreases and also there is some fluctuation of intensity due to movements of some clouds and abnormal atmosphere. Therefore during the central part of the day, the output of the solar cell will be at or near its maximum because the sunlight is arriving at more direct angle i.e. sunlight travels lesser distance to reach the earth surface. At the beginning and at the end of the day, the output fall off regardless of the orientation of the solar cell, mainly because the sunlight has to travel obliquely through the atmosphere at these times, arriving at a low angle i.e. sunlight travel more distance to reach the earth surface. This decreases the intensity of the sunlight.

In addition, since the sun travels through an angle of 15° per hour, it becomes close to perpendicular to the collector for a period of approximately two hours. Beyond this time, the intensity of the sunlight decreases due to the increase in air mass, and the angle between incident sunlight and the normal to the collector increases. These two factors cause the energy collected by the collector to decrease relatively rapidly during the hours before 11.30 A.M. and after 1.30 P.M. As a result, there is some fluctuation on PV cell characteristics.

On the other hand, temperature increases proportionally with the increase of intensity. This theory has been proved and depicts in (Fig. 5 b). Here with the increase of intensity from 9 am to 13pm the temperature is also increased and it has been shown maximum at the height intensity point. The temperature is actually the region of solar cell area. The main difference from the intensity curve the temperature moves downward not rapid like the intensity curve. Because the temperature of solar cell area largely affected by the environmental warm up.

The intensity depends on the presence of big sun. The experiment carried out in winter season. The daytime has concise to around 10 h among 24h. But the solar cell temperature largely depends on environmental temperature (as mention above). So the sensor stabilized both of these temperatures.

3.2 Characteristics of Power & surplus energy with respect to Day Time

From the curve nature in (Fig. 6 a) it is clear that with the increase of intensity with day time the power nature also increase. Because more the intensity falls on the solar cell the flow of electron also increases.

For that reason at the initial stage and the final stage the power is less only for less electron but at time around 13 pm the power shows the maximum. This not means that at 13 pm it may be any time when the intensity is high. The (Fig. 6 a) depicts power characteristics where maximum power is obtained as 5.8 watt (average) for two axis tracking mode and 4.8 watt for single axis tracking mode and 3.6 for fixed axis with 6.5 watt rated PV panel.

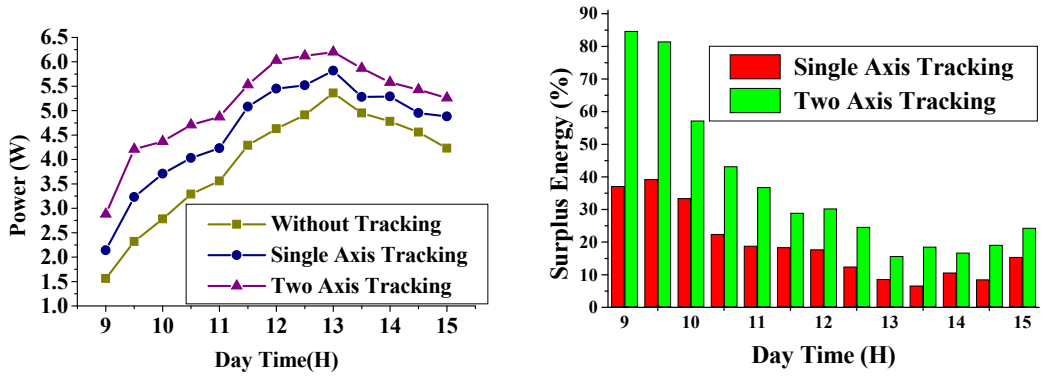

Fig. 6. (a) Power with day time; (b) Surplus energy with day time

The experimental measured variables are compared with that at fixed axis for both the single and two axis solar trackers. The results indicates that there is an overall increase of output power about 30-38% for the two-axis solar-tracking system compared to the fixed PV system and that of 15-25% for single axis solar tracking system.

The big bar chart as shown in (Fig. 6 b) shows the difference of surplus energy of tracking system to the without tracking system. When the power varies less at 13 pm then the surplus energy gives the less reading. This means that by using tracking this amount of extra energy is found which is lost by the without tracking system. On the other hand, at the initial and final stage this amount is huge. If this energy is collected by the tracking system then the fluctuation of intensity, cell temperature, and power will be less. For this reason the two axis tracking system gives the extra benefit for collecting maximum power. It has been called maximum power point tracking (MPPT). For two-axis tracking the maximum surplus energy 15% to 84% where in single axis tracking it was 6.5% to 59% throughout the day examining here. By averaging, it will be around 30-38% for two axis solar tracker and 15-25% for single axis solar tracker throughout the year.

3.3. Reproducibility:

Similar results have found after one year later. The (Fig. 7) shows that, with day time increase the intensity and cell temperature are also increased. And (Fig. 8) gives the same fashion. But the intensity range is lower than the (Fig. 5), so the cell temperature, power and the surplus energy are also lower. On the other hand, the fall of intensity is rapid than (Fig. 5) so the cell temperature, power and surplus energy also fall rapidly.

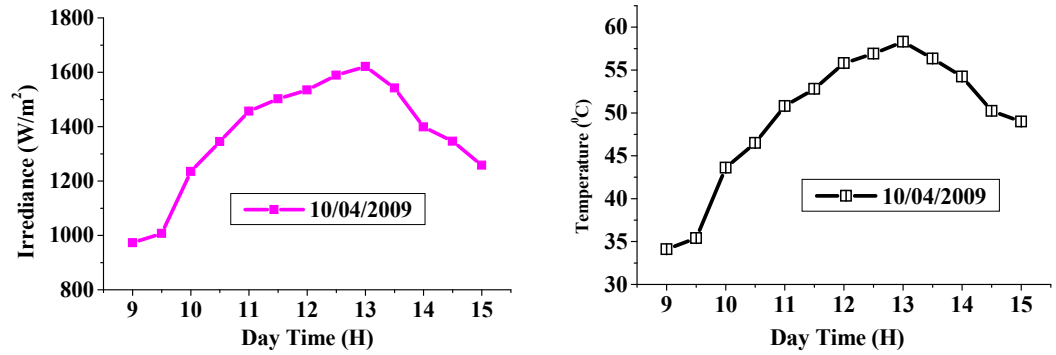

Fig 7. (a) Intensity with day time; (b) Cell temperature with day time

The main differences between the two dated curve are largely depends on the effect of both intensity and the atmospheric air mass. It has been seen that all parameter increases with the increase of intensity and decrease with respect to decrease. On the other hand, the increase of air mass causes decrease of all the parameter. Because at March 06, 2008 the season was winter in Bangladesh and April 10, 2009 the season was slightly summer. For that reason in March the sun rises about $20\text{-}32^0$ from the east position with respect to Bangladesh position but in April it was $10\text{-}20^0$.

The experimental measured variables were compared with those in case of fixed axis. The results indicate that there was an overall increase of output power about 30-45% for the two-axis solar-tracking system from the fixed PV system.

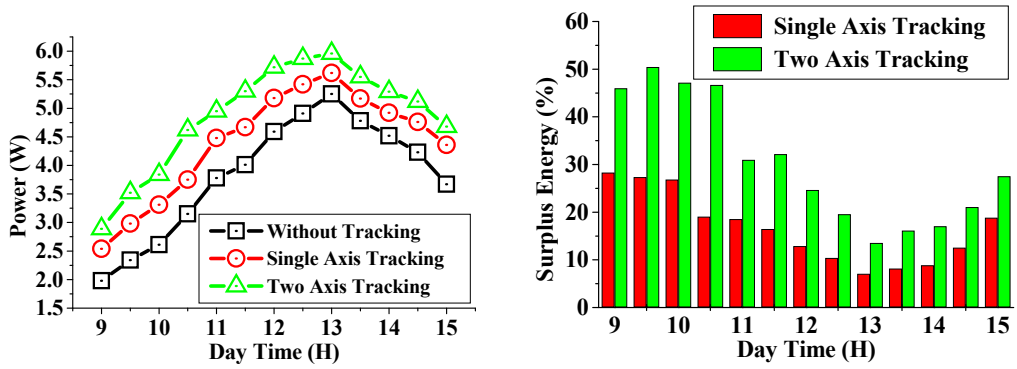

Fig. 8 (a) Power with day time; (b) Surplus energy with day time

In addition, there was an overall increase of output power about 15-23% for the single axis tracking system from the fixed tilted PV system [15]. The result obtained was approximately similar to the result found by results of George C. Bakoks (2004) designed a two axis solar tracking system for parabolic trough collector and compared the measured results with a fixed tilted trough and found that there was a surplus energy up to 46% [16].

4. Conclusion

In this research, a comparative study of experimental results are investigated on the effect of using two-axis solar tracking system and single axis solar tracking system of the PV power output.

From the result of the performance test of designed system the following conclusion can be drawn.

- The surplus output-power of the tracking solar panel with respect to fixed panel was 30-38% at average intensity 1100 W/m^2 and that of 15-25% for single axis solar tracking system i.e. about 15-18% excess energy is found from two axis solar tracking system compared with single axis solar tracking system.
- There is a design difficulties exists in the two axis solar tracker which increase the cost of fabrication.
- On the other hand the tracking electromechanical mechanism is very simple for single axis than two axis solar tracking system.
- There are no considerable difficulties in the software system for both cases.

References

[1] Chung HSH, Tse KK, Hui SYR, Mok CM, Ho MT, A novel maximum power point tracking technique for solar panels using a SEPIC or Cuk converter, IEEE Transactions on power electronics, vol. 18, no. 3, pp.717-724, 2003.
[2] HiyamaT et al. Evaluation of neural network based real time maximum power tracking controller goes PV systems, IEEE Transactions on Energy Conversion, vol. 10, no. 3, 1995.
[3] Huang F, Tien D, James O. A Microcontroller based Automatic Sun Tracker Combined with a New Solar Energy Conversion Unit, International Conference on Power Electronic Drives and Energy Systems for Industrial Growth, 1998, vol. 1, pp. 488 – 492.
[4] Mashohor S, Samsudin K, Noor AM, Rahman ARA. Evaluation of Genetic Algorithm based Solar Tracking System for Photovoltaic Panels, IEEE International Conference on Sustainable Energy Technologies, 2008, pp. 269 – 273.
[5] Koyuncu B, Balasubramanian K. A microprocessor controlled automatic sun tracker, EEE Transactions on Consumers Electronics, vol. 37, no. 4, pp. 913-917, 1991.
[6] Hayama T, Kouzuma S, Imakubo T. Identification of optimal operating of PV modules using neural network for real time maximum power tracking control. IEEE Transactions on Energy Conversion, vol.10, iss.2, pp. 360-7, June1995.
[7] Mashaly HM, Sharaf AM, Fuzzy logic controller for photovoltaic-utility interfacing scheme, In Proceedings of the 7th Mediterranean Electro technical Conference, 1994, vol. 2, pp. 715-18.
[8] Bingol O, Altinta A, Oner Y, Microcontroller based solar-tracking system and its implementation, Journal of Engineering Science, vol. 12, pp. 243-248, 2006.
[9] Yousef HA. Design and implementation of a fuzzy logic computer-controlled sun tracking system, in Proceedings of the IEEE International Symposium on Industrial Electronics, ISIE'99, vol. 3, pp. 1030-1034,1999.

[10] Yazidi A, Betin F, Notton G, Capolino GA. Low cost two-axis solar tracker with high precision positioning, in First International Symposium on Environment Identities and Mediterranean Area, ISEIMA'06, pp. 211-216, 2006.
[11] Damm J. An active solar tracking system, Home Brew Magazine, Issue #17, June/July 1990
[12] Rizk J, Chaiko Y. Solar Tracking System: More Efficient Use of Solar Panels, in proceeding of world academy of science, engineering and technology volume 31 July 2008 ISSN 2070-3740.
[13] Rai GD, Solar Energy Utilization Third Edition, Khanna Publishers Delhi-1100061987.
[14] Infield DG, Islam AKMS, Photovoltaic Technology for Bangladesh ISBN 98431-10854, pp. 87-88.
[15] Malodanado JA. Diseno y construccion de un sistema de control automatico para el posicionamiento de un pirheliometro. Memoria, Universidad Tecnica Federico Sunta Maria, Valparaiso, Chile, 1989.
[16] Maish AB, A self-aligning photovoltaic array tracking controller. In Proceedings of the 20th IEEE Photovoltaic Specialists Conference, 1988.

Appendix A. Comparison of algorithm

A.1. Software algorithm of single and two axis tracker

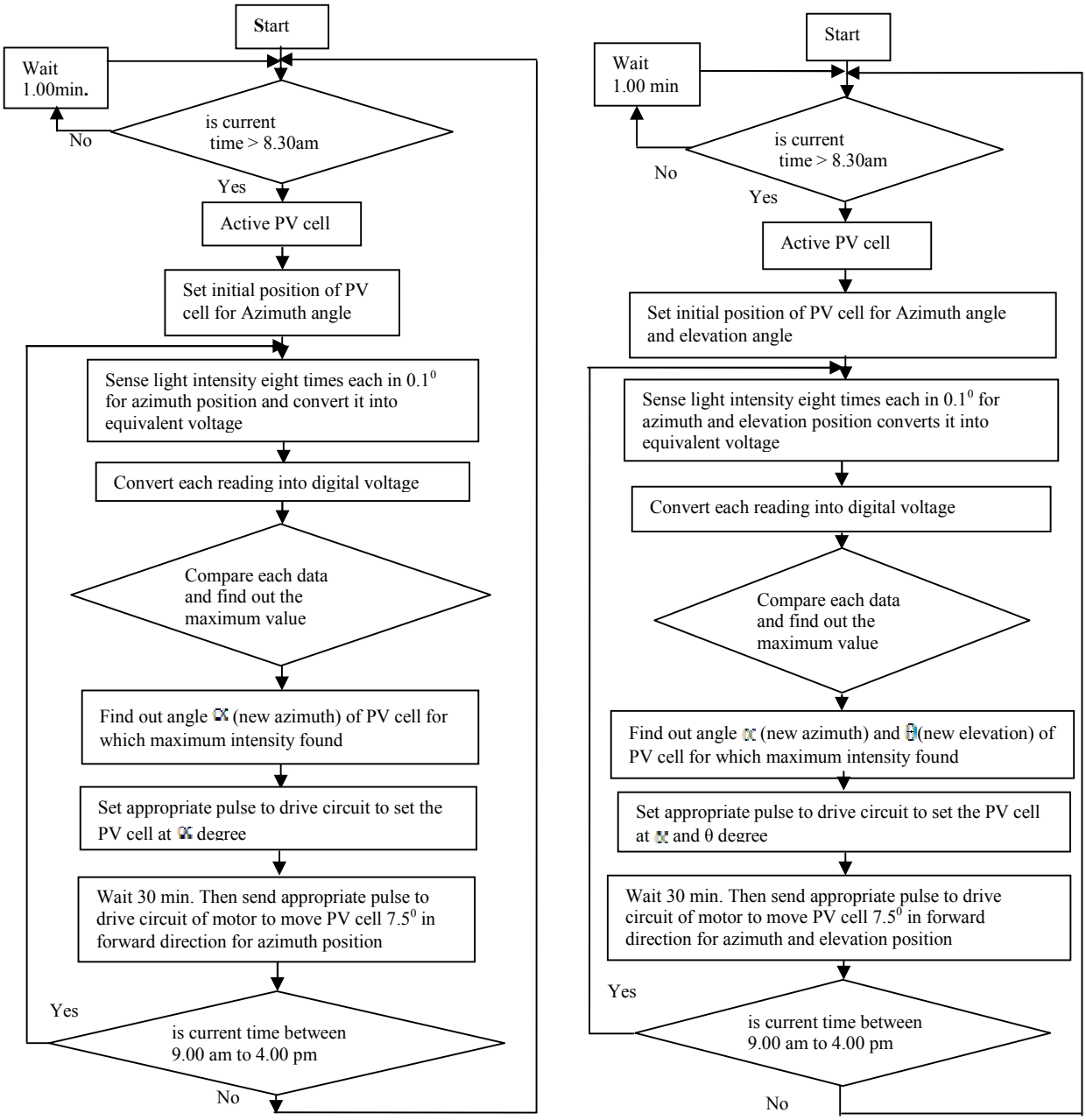

5th BSME ICTE

Modeling the performance of low concentration photovoltaic system

Muhammad N Khan[a], Abdul Arif [a], Muhammad S Khan[b]

[a] *Islamic University of Technology (IUT), MCE Department, Bangladesh*
[b] *Islamic University of Technology (IUT), EEE Department, Bangladesh*

Abstract

Concentration photovoltaic (CPV) systems are seen as a shortcut to achieve lower photovoltaic (PV) electricity costs/kWh. Within the available CPV configurations, V-trough systems are likely to succeed in the short term since they are less demanding in terms of tracking accuracy and due to their ability to make use of standard PV modules, a well-known and developed technology. The present work aims to demonstrate that the efficiency of a module can be increased by using different kinds of concentrators. In this effect we suggest to use a liquid because of its magnifying nature and difference in the refractive index between air and liquid medium, a water, water drops or controlled & proper flow of liquid can be used over a PV module in order to concentrate a diffused light up to some extent. And it also provides a great temperature reduction of a module, which leads to higher efficiency.

Keywords: Concentration photovoltaic (CPV), V-trough, liquid

1. Introduction

The energy crisis due to worldwide shortage of petroleum emphasizes the need for alternative energy sources, which expected to be both inexpensive and clean. Among possible alternative energy sources such as wind, tidal, wave, geothermal, biomass and magneto-hydro-dynamic and so forth, the most pollution free and limitless energy source is considered to be the solar energy. Solar energy can be thought of the primary source of energy as all other forms of energy sources are the derived form of the solar energy. The basic source for solar energy system is the sun. Solar energy appears to be the most promising among the nonconventional sources of energy. The sun's great energy release is the result of an elaborate chemical process in the sun's core a process of thermo-nuclear fusion like the reaction in hydrogen bomb. Sun radiates energy of about 3.5 x 10^{23} kW into space and only 2 x 10^{14} kW reaches the earth [1]. This stupendous solar energy, which is non exhaustible, could drive the civilization forever, if it could be properly and economically harnessed. The serious draw-backs associated with it, includes very low energy density per unit area. At the same time, it is available for only a part of the day; and cloudy and hazy atmospheric conditions largely reduce the energy received. Therefore, in harnessing solar energy for generation of large useful usable electrical power, a vast area is required to collect sufficient amount of energy and the means of storage will be required to use the energy when it is not available. Knowledge of the quantity and quality of the solar energy available at a specific location is of prime importance for the designing of any solar energy system. Although, the solar radiation (insolation) is relatively constant outside the earth's atmosphere, the effect of local climate can cause wide variation in available insolation on the earth's surface from site to site. In addition, the relative motion of the sun with respect to the earth will allow surfaces with different orientation to intercept different amount of solar energy [2]. From astronomical study [3], the sun converts 6 x 10^{11} kg of mass into energy each second. This is equivalent to 10^{23} kW of electric power. The diameter of the sun is 1.39 x 10^{6} km and is located 1.5 x 10^{8} km from the earth. The surface of the sun is at an effective temperature of 5762 K. This is the temperature at which the sun transmits the electromagnetic energy that is being radiated to the earth. Just outside the earth's atmosphere, the sun's energy is continuously available at the rate of 1,367 W on every square meter facing the

sun. Due to the earth's rotation, asymmetric orbit about the sun and the contents of its atmosphere, a large fraction of this energy does not reach the ground surface. Solar energy reaching the earth in tropical zones is about 1 kWh m^{-2} giving approximately 5-10 kWh/ m^2 /day. In countries within 3.200 km of the equator, the use of such energy can be economically significant. Throughout the year, the variation in the distance between the sun and the earth lead to an annual variations in the solar constant of about $\pm$3.5% (about 50 W m^{-2}) [3].

2. Use of Concentrators

The growing interest on concentration photovoltaic (CPV) technologies begins with its potential to significantly reduce the PV electricity cost/kWh. The concept behind CPV in this paper is to use a liquid such as water, water drops or a controlled flow of liquid over a PV module because of magnifying nature, that enhance the radiation falling upon the cells which allows a reduction of its area for the same output power.[6] It can be understood as a shift from the expensive PV converter material to reasonably priced optical solutions.
Within the wide variety of CPV configurations that are on the table today, Modules with a concentrator's arrangement is highlighted as a short term solution. In this case, Three main reasons should be noticed: the optical configuration (generally reflective mirrors, but in this paper it is done by a water drops and proper control of liquid flow over a module) which allows high homogeneity with moderate tracking accuracy avoiding prohibitively high costs of the final product; secondly the use of standard silicon solar cells, a technology with many years of given proofs and a well standardized industrial manufacture, benefiting from scale production.
The efficient application of standard modules in CPV systems is limited to a few suns. Ideally, as the radiation flux is enhanced through concentration, the current density increases, leading to a higher performance of the cell. However, such boost on radiation flux will lead to new challenges: higher operating cells temperature, which diminishes the open circuit voltage (Voc); high series resistance losses, due to the higher transverse flow of current from the solar emitter to the front grid (initially designed to work under a maximum irradiance of 1000 W/m^2); and possibly accelerated modules' degradation rate originated by a higher exposure to the sunlight. These issues can be somehow controlled by the presence of the liquid (water, water drops) over the module surface which reduces the temperature of the module by absorbing the module heat.[5]
Following are some concentrators:

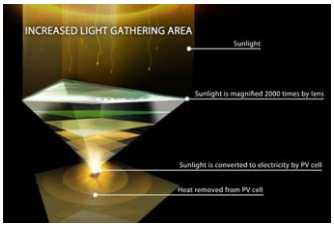

3. Experiment set up

i) Location:

This experiment was conducted in between latitude 23.6° to 23.9° North and Longitude 90.5° to 90.8° East almost centre of Bangladesh in ISLAMIC UNIVERSITY OF TECHNOLOGY (IUT).

ii) Climate:

The Experiment was conducted during the summer season. In general, maximum summer temperatures range between 38 and 41 °C (100.4 and 105.8 °F). April is the hottest month in most parts of the country.

iii) Rating of Solar Panel:

Specification:	Rated Values	Units
Power Output	60($\pm$10)	Watts(W)
Rated Voltage	17.55	Volts(V)
Rated Current	3.54	Amps(A)
Open Circuit Voltage	21.6	Volts(V)
Short Circuit Current	3.84	Amps(A)
Solar Radiation	1000	Wm^{-2}
Temperature	25	Degree(C)

4. Photovoltaic generator characteristics and models

The behavior of a PV cell can be represented by a equivalent circuit that consists of a constant current generator delivering a current I_L (so called the light current) into a network of impedances, which includes a diode, an intrinsic series resistance R_S an intrinsic shunt resistance R_{sh}, and a load resistance R_L as shown in Fig. (01). [4]

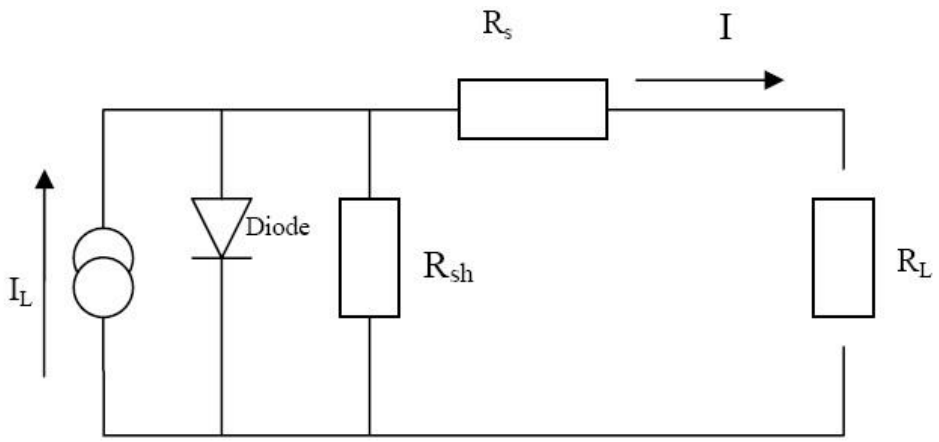

Fig: 01.
Equivalent circuit of a photovoltaic cell

The mathematical model that represents the equivalent circuit of a PV cell is then [7]:

$$I = I_L - I_O \cdot \left\{ \exp\left(\frac{e.(V + I.R_s)}{m.k.T} \right) - 1 \right\} - \frac{V + I.R_s}{R_{sh}} \qquad \text{Eq: 01}$$

Where:

***e*:** electron charge [C]
***I*:** current delivered by the cell [A]
***IL*:** light current [A]
***Io*:** saturation or dark current [A]
***k*:** Boltzmann's constant [J/K]
***m*:** curve fitting parameter
***Rs*:** series resistance [ohm]
***Rsh*:** shunt resistance [ohm]
***T*:** absolute temperature of the cell [K]
***V*:** voltage at the load [V]

The curve fitting parameter *m*, the series resistance *Rs* and the shunt resistance *Rsh* were determined based on the I-V curve given in the technical specifications of the PV modules used in the experiment.

The influence of the temperature on the PV cell characteristics can be seen in the open circuit voltage expression that follows:

$$V_{oc} = \frac{E_{go}}{k \cdot T} - \frac{k \cdot T}{e} \cdot \ln\left(\frac{K_a \cdot T^3}{I_L}\right) \qquad \text{Eq: 02}$$

Where:

***Ego*:** material band gap energy [J]
***Ka*:** constant [A/K3]
***Voc*:** open circuit voltage [V]

Values for the material band gap energy E_{go} and for the constant K_a were also determined, although indirectly, from the technical specifications of the PV modules.

In all cases the light current I_L was assumed to be proportional to the solar radiation and set equal to the short circuit current I_{sc} when the circuit was open.

5. Results and Calculations:

Two Solar Panels were used with same configuration. The Solar Panels were installed in the open field. They were exposed directly to sunlight. One was kept under normal condition without any type of concentrator. The other was subjected with concentrator. The proper flow of water had been done over a panel, and the panel was kept wet. The water drops were present over the panel surface, which acted as the concentrator and worked as the cooling agent, and kept the panels temperature low.

The panel was twice subjected to a proper flow of water over a surface, ones at 12:00pm and the other at 02:00pm.which has shown a change in an output characteristics results.

Four digital millimeters are used to measure the open circuit voltage (V_{oc}) and the short circuit current (I_{sc}) of both solar panels at a time. The readings of the digital voltmeter are recorded on regular basis. The experiment is conducted from dawn to dusk on daily basis.

The average daily, reading were obtained and plotted on voltage-time curve to illustrate the variation of voltage of solar panel with time of the day.

In this study, all necessary data related to PV panel have been collected continuously for one week

.

All collected data has been tabulated and plotted using MATLAB. Based on the observed and measured data, rests of the parameters of the panel are calculated.

Followings are the plotted Results obtained.

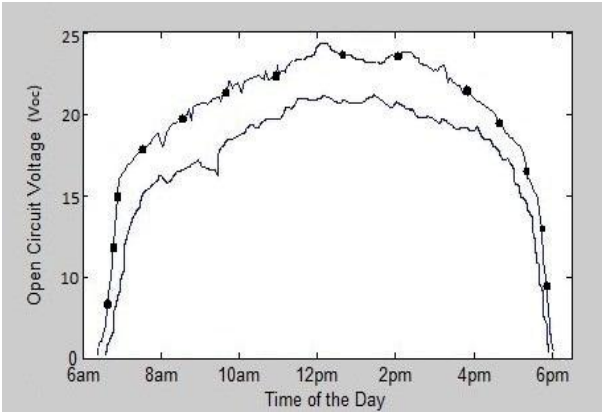

Fig: 02. Open Circuit Voltage *Vs.* Time Characteristics

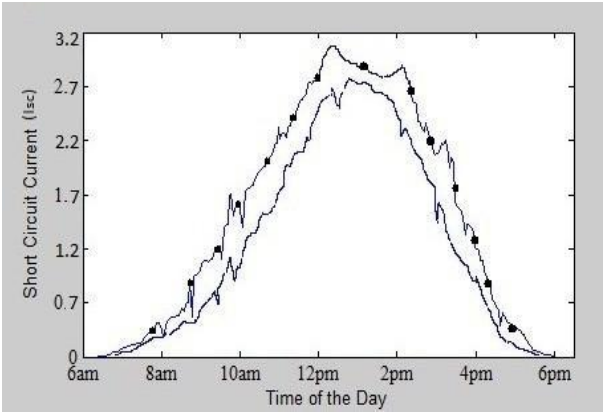

Fig: 03. Short Circuit Current *Vs.* Time Characteristics

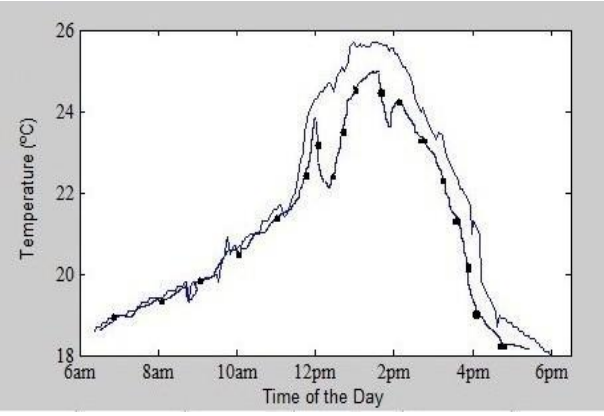

Fig: 04. Temperature *Vs.* Time Characteristics

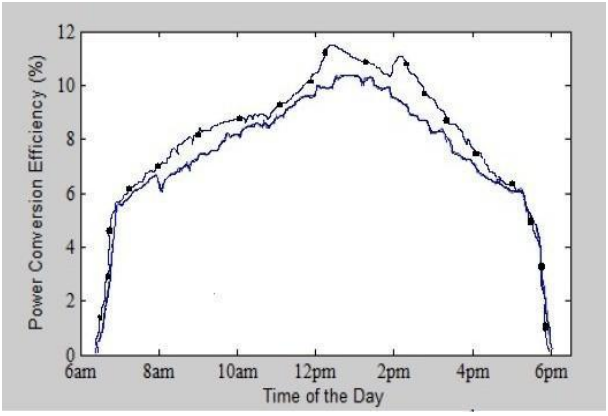

Fig: 05. Electrical Efficiency *Vs.* Time Characteristics

The above figures show the output characteristics of the two different solar panels. In the figures the panel with concentrator has much better output characteristic as compare to other panel. These better results were obtained just because of concentrator (liquid). When at 12:00pm and at 02:00pm the panel was cooled down by the flow of water over a panel surface, the increase in the output characteristic were observed & recorded.

6. Conclusion:

This paper describes model and experimental data for the performance of a PV system with a liquid concentrator, using conventional silicon modules and with active cooling. The results have shown that the radiation increase due to water drops and water flow over PV module surface which can lead to an improvement of the instantaneous output power and some increase in the daily energy yield. The effect of the concentration is less relevant in the presence of diffuse radiation, limiting the interest for this type of liquid concentration to sunny locations.

Solar panels can be used in supply power to the remote places which are not connected to the National grid. The geographical location and climatic factors in Bangladesh favored more or less the use of solar power system. Being a tropical country of south Asia, PV panels might find its way as source of alternative power. But at the same time the economic viability of the system must be considered for design and feasibility analysis purpose. The successful implementation of solar power programs in Bangladesh might show a new way of fighting against poverty and climatic changes.

7. References

[1] Patton, A.R., 1975. Solar Energy for Heating and Cooling of Building. Noyes Publications, New Jersey, USA., pp: 1-10

[2] Gupta, J.B., 2007. A Course in Power Systems. 10th Edn., Kataria S.K. and Sons, Nai Sarak, Delhi, pp: 157-161.

[3] Ekeh, J.C., 2003. Electric Power Principles. 1st Edn., Amfitop Book Lagos, Nigeria, pp: 86-99.

[4] Angrist, S. W., 1976. “Direct Energy Conversión”, Third Edition, Allyn and Bacon. Inc.

López Araujo, G., 1995. “Fundamentos de la Conversión Fotovoltaica: La Célula Solar”, Instituto de Energía Solar,Universidad Politécnica de Madrid, Ciemat.

[5] Experimental study of SOLAR RADIATION augmentation on PHOTOVOLTAIC MODULES, Gabriel Blanco, Esteban Gelso, Manuel Rodríguez

[6] Photovoltaic Concentration at the Onset of its Commercial Deployment. Luque, Antonio, Sala, Gabriel and Luque-Heredia, Ignacio. 2006, Progress in Photovoltaics, pp. 413-428.

[7] Ahmad, G.E., Hussein, H.M.S. and El-Ghetany, H.H., 2003. "Theoretical Analysis and Experimental Verification of PV Modules", Journal of Renewable Energy No.28, pp.1159-1168.

5th BSME International Conference on Thermal Engineering

Effect of tensile strength and chemical composition on corrosion properties of locally produced QT steel bars

M. A. Islam[a], Kamran Mansur[b]*

[a]*Professor, Department of Materials and Metallurgical Engineering, BUET, Dhaka-1000, Bangladesh*
[b]*Student, Department of Materials and Metallurgical Engineering, BUET, Dhaka-1000, Bangladesh*

Abstract

In structural buildings a huge amount of reinforcing steel bar is used. In advanced countries, the conventional low strength steel has been replaced by high strength steel to reduce the overall steel consumption. However, in Bangladesh, use of QT (Quenched and Tempered) grade of high strength steel in structural application is recent. The safety of any structural building depends largely on the mechanical properties of concrete and reinforcing steel bars. But, the longevity of reinforcing steel bars depend largely on their corrosion properties. Due to corrosion, mechanical properties deteriorate day by day. From this point of view, it can be said that safety of structural buildings depends on the corrosion properties of reinforcing steel bars.

The objective of this work was to compare the corrosion resistance of QT steel bars and traditional reinforcing steel bars and to identify the effect of alloying additions of Cu, Cr and Ni on corrosion properties of reinforcing steel bars. In this study, the corrosion rate of two different types of QT steel having different tensile properties, different microstructures and chemical compositions have been investigated under different environments for various time periods.

Experimental results revealed that, for any chemical composition, corrosion resistance of QT bar is lower than traditional reinforcing steel bars. Addition of alloying elements like Cu, Cr and Ni improves corrosion properties.

Keywords: Corrosion, Reinforcing steel bars, QT, traditional reinforcing steel bars;

1. Introduction

Reinforcing steel bars are used to reinforce concrete structures [1]. Their work is to hold the concrete in compression. Concrete is a porous material made of aggregates and porous cement [1].Steel reinforced concretes are used in order to increase the tensile and bending strength of the concrete. These kinds of structures are practically advantageous because they are durable against fire and require less care [2]. With the increase in number of heavy structures, strength required for the reinforcing bars is increased day by day. QT steels are now replacing traditional 60 ksi grade (Having yield strength about 60 ksi) steels because of higher mechanical properties obtained by using QT steels and they reduce consumption of steel in concrete [1, 3, and 4]. This process has made it possible to produce low carbon steels having yield strength about 75 Ksi [4].

Corrosion of reinforcement has been established as the predominant factor causing widespread premature deterioration of concrete construction [2]. Generally, due to the alkaline environment surrounding the reinforcement (PH 13.5), a passivizing layer forms on the surface of the bar and protects it from the corrosion. Carbonation and penetration of chlorides, or other mechanisms may break this layer. Then active corrosion grows. This generally leads to a loss of bond, cracking and spalling of concrete cover. Particularly severe is corrosion due to chloride contamination, [5]. After initiation of the corrosion process, the corrosion products (iron oxides and hydroxides) are usually deposited in the restricted space in the concrete around the steel [6]. These corrosion products occupy a volume of about 2– 4 times, respect to the sound bar. This in turn results in progressive deterioration of the concrete [7]. Differences within the grain structure of the metal or different residual stress levels can also lead to galvanic corrosion. When chlorides are uniformly distributed around the steel, local action micro-cells are formed and generally lead to a type of localized corrosion known as pitting corrosion. As corrosion proceeds, the condition inside the pit becomes progressively more acidic and further loss occurs from the bottom of the pit rather from the sides [8]. As a result, the repair costs nowadays constitute

* Corresponding author. Tel.: +8801932691259;
E-mail address: chapol4200@yahoo.com

a major part of the current spending [6]. Properly monitoring the structures for corrosion performance and taking suitable measures at the appropriate time could result enormous saving [6, 7, 9, 10 and 11].

All of the corrosion processes described above, in the absence of oxygen, the corrosion rate is appreciably reduced even with chloride concentrations above the threshold level (The level below which Cl is not harmful), except in acid solutions. In most of the service conditions complete removal of oxygen is not possible. But corrosion resistance of reinforcing steels must be increased to lengthen the durability of the concrete structure. To improve the corrosion resistance of reinforcing steel, effect of corrosion resisting alloying elements like Cu, Ni, Cr etc. and the extent of effect must be known.

The main objective of this work was to identify and compare corrosion rates in various environments between traditional reinforcing steels and steels produced by Thermo Mechanical Treatment. The second objective is to identify the effect of alloying elements in both of them on corrosion properties.

1.1. Experimental

1.1.1. Methods and Materials

In this work, two different QT steel samples having different compositions were taken. Ridges were cut out in both of them to make the area uniform.

Table 1: Composition of the samples taken

Sample name	Fe %	C%	Si%	Mn %	P %	S%	Cu%	Ni%	Cr%
Low Alloy Steel (LAS)	97.96	0.19	0.23	0.85	0.03	0.03	0.37	0.13	0.07
Plain Carbon Steel (PCS)	98.3	0.22	0.15	0.9	0.03	0.01	0.03	0.02	0.05

Comparing the compositions of PCS and LAS, LAS has higher amount of Ni, Cr and Cu. Difference of corrosion rate between these two revealed the effect of alloying addition.

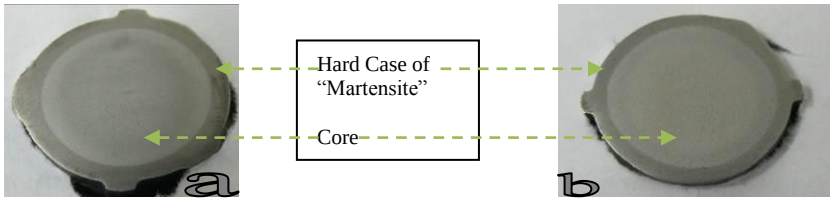

Figure 1: Macrostructures of the samples taken; a) PCS, b) LAS

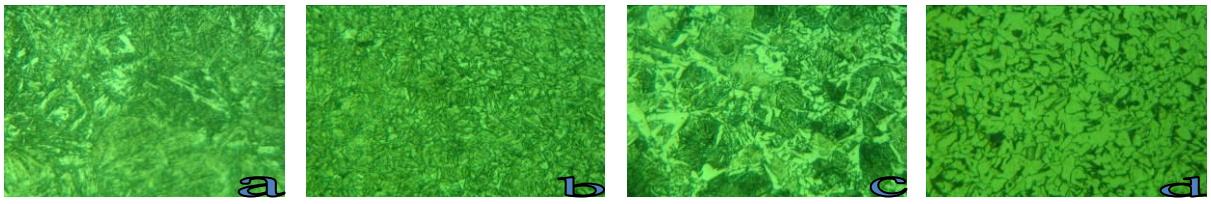

Figure 2: Microstructures of the samples taken; a) Case of PCS, b) Case of LAS, c) Core of PCS, d) core of LAS

Then from the data obtained by microstructure study, 2 types of samples were made from both of them. One type of samples kept with only ridges removed which represent QT steel. In other type of samples, the hard case of martensite was removed by machining and this type represents traditional steel sample. Thickness of martensite layer was found from macrostructure study. From this point of view, there were 4 types of samples. They are represented in figure 3.

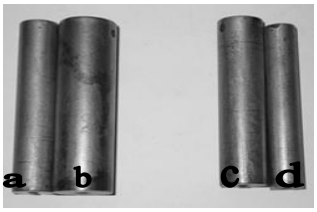

Figure 3: Prepared samples; a) PCS core, b) PCS with case, c) LAS with case, d) LAS core

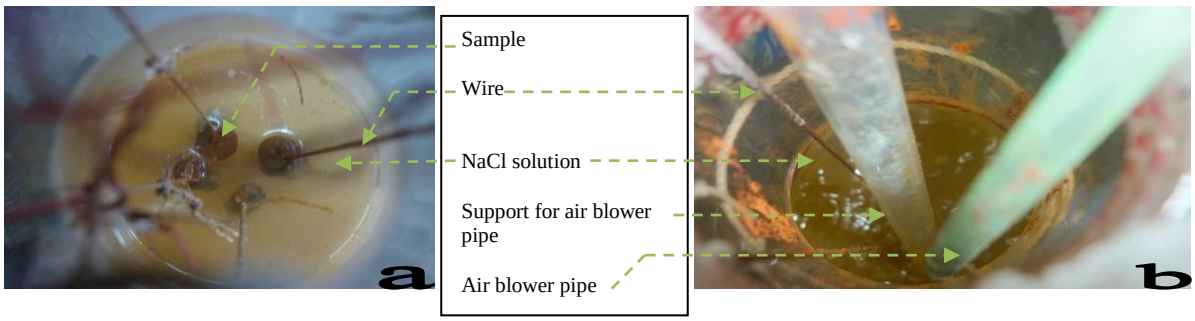

Figure 4: Experimental setups a) Without air experiment 1, b) with air experiment 1

All of these 4 types of samples were weighed and then subjected to two experiments. In experiment 1 without air, steady solution of 10% NaCl was used as the corrosive solution. In the other, effect of stirring and flow of oxygen was introduced by passing air through a pipe into 10 % NaCl solution. In both experiments, samples were hanged by rope into the solution.

In every week all samples were removed from the solution, washed into detergent, dried and weighed to measure weight in corresponding week. Reduction of area was also measured.

1.1.2. Measurement of Corrosion Rate

Corrosion rate is measured as the ratio between weight loss 'W' in desired time period and cross sectional area, 'A'. So, corrosion rate,

$$C = W/A \quad (1)$$

Here, for cores, area immersed in solution consists only of desired area, but in the case of samples with case, area of the core is very small compared to the total area exposed. So, areas of cores in these samples were ignored when calculating corrosion rate.
So, measurement of area for samples with case,

$$A = 2x3.1416*r*x(r+h) - 3.1416*r_2^2 \quad (2)$$

Where, r = outer radius
r_2= core radius
h= height of the sample

For core samples, measurement of area,

$$A = 2x3.1416x(r+h) \quad (3)$$

1.2. Results and Discussions

Chlorine attack mechanism was used to corrode the samples in solution, rapid corrosion was observed in all 4 types of samples

1.2.1. Test Data

From the data found in both experiments and by calculating corrosion rate from them, 2 different data tables are constructed. From these data Time vs. Corrosion rate curves are also constructed. These tables and curves are given below

Table 2: Corrosion rate data for without air experiment 1

Description	Corrosion after 1 wk, (gm/mm^2) *10^{-5}	2 wk (gm/mm^2) *10^{-5}	3wk (gm/mm^2) *10^{-5}	4wk (gm/mm^2) *10^{-5}	6 wk (gm/mm^2) *10^{-5}	7 wk (gm/mm^2) *10^{-5}	8 wk (gm/mm^2) *10^{-5}
PCS Case	2.1557	3.59286	7.31636	8.62286	10.9	13.2	15.18
PCS core	1.2578	2.3488	5.4505	6.70831	8.8	10.1	11.32
Las Case	2.4345	4.0575	6.8978	8.92668	10.5	11.4	13.39
LAS core	1.5874	3.1748	6.3496	7.40795	9	10.2	11.11

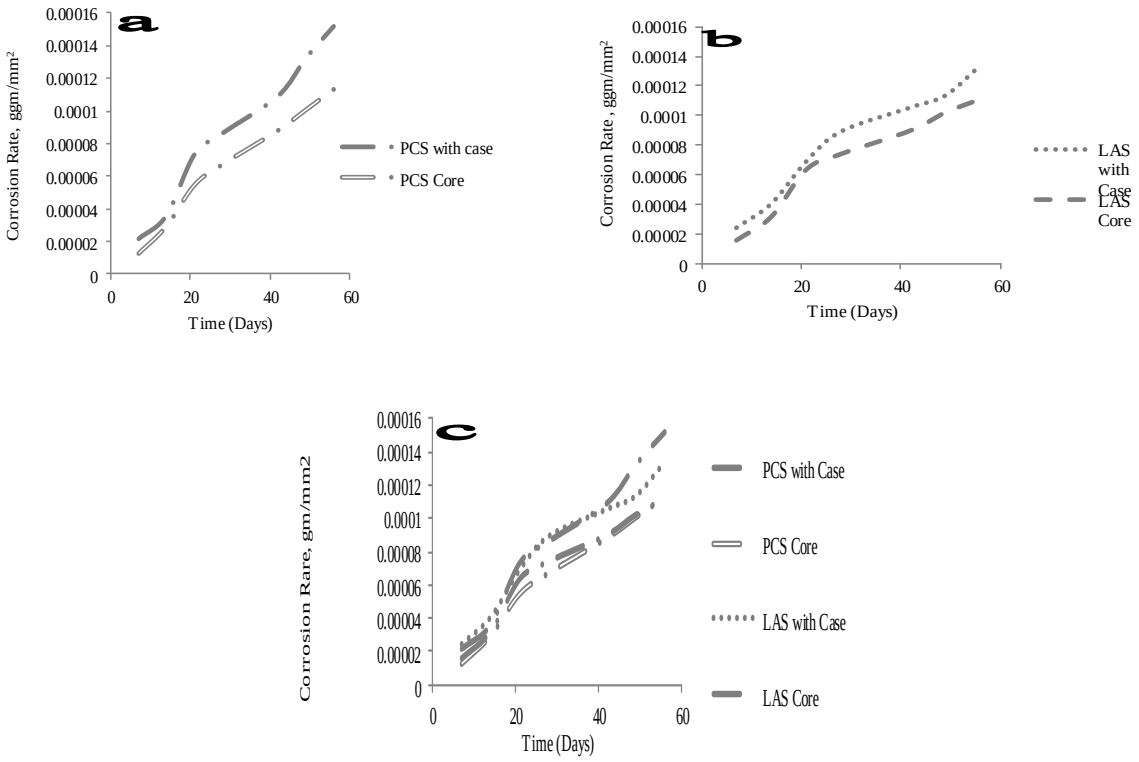

Figure 5: Time vs. Corrosion rate curves for without air experiment 1; a) PCS, b) LAS, c) all 4 curves are superimposed

From first 2 curves (a and b), it has been found that corrosion rate of samples with case (both PCS and LAS) of martensite is higher than core samples. This may be due to the presence of residual stresses in QT steel which comes during its production and heat treatment. When all 4 curves are superimposed in the third curve (c),

corrosion rate of PCS (With case and without case) has been found to be higher than LAS (Both with case and without case). Presence of corrosion resisting elements in LAS is the probable cause of lower corrosion rate of LAS. Elements like Ni, Cr and Cu accelerates the formation of protective oxide film on the surfaces of samples.

Table 3: Corrosion rate data for with air experiment one

Description	Corrosion after 1 wk, (gm/mm^2) $*10^{-4}$	2 wk (gm/mm^2) $*10^{-4}$	3wk (gm/mm^2) $*10^{-4}$	4wk (gm/mm^2) $*10^{-4}$	6wk (gm/mm^2) $*10^{-4}$	7wk (gm/mm^2) $*10^{-4}$	8wk (gm/mm^2) $*10^{-4}$
PCS Case	1.41	1.95	2.1	2.56	2.87	3.36	3.82
PCS core	1.15	1.75	1.98	2.4	2.63	3.09	3.55
Las Case	2.01	2.65	2.93	3.37	3.74	4.02	4.34
LAS core	1.28	2.05	2.25	2.51	2.71	3.17	3.63

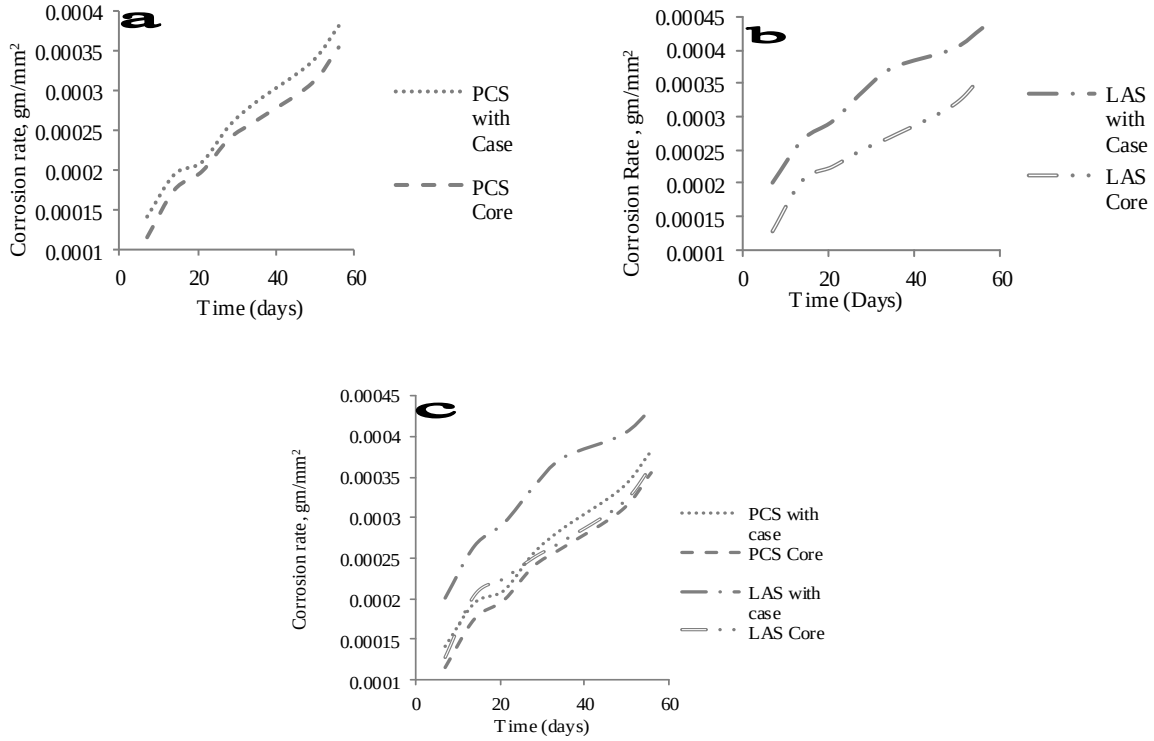

Figure 6: Time vs. Corrosion rate curves for with air experiment 1; a) PCS, b) LAS, c) All 4 super imposed

From the first 2 curves (a and b), similar results have been found i.e. samples with case of martensite corrodes faster for both PCS and LAS. But when all 4 curves are superimposed in c, corrosion rate of LAS samples has been found to be higher than corresponding PCS Samples. In LAS samples, protective oxide film is formed faster. By the stream of air in experiment 1 with air, this film is broken and reformed successively. By this way corrosion is accelerated. This is the cause of higher corrosion rate of LAS samples in with air experiment 1.

1.3. Conclusions

- In all of the selected conditions (corrosive solutions) of this work, samples with case of martensite corrode faster than core samples. For both LAS and PCS it is evident from the curves that corrosion rate of QT steel bar is higher than traditional reinforcing steel bar. Since identical compositions were compared, higher corrosion rate of samples with case might be due to the presence of residual stresses in QT steels which they get during production and heat treatment.

- In experiment 1 without air, corrosion rate of PCS is higher than LAS. This is due to the presence of corrosion resisting elements like Cr, Ni and Cu. These elements accelerate the formation of protective oxide film on the surface of steel samples. This layer protects LAS sample in corrosive media.

- In experiment 1 with air, corrosion rate of LAS samples is higher than PCS samples which is contradictory to the result of Experiment 1 without air. This unusual result may be due to the flow of air. The stream of air breaks the protective oxide film and supplies oxygen into the solution. In the samples containing Cr, Ni and Cu, this film is reformed faster. By this way, corrosion is accelerated in LAS samples in this experiment.

References

[1] Manoharan R.., Jayabalan P., Palanisamy K. “Experimental study on corrosion resistance of TMT bar in concrete”. ICCBT 2008; page2
[2] Oğuzhan Kelestemur, Servet Yildiz. “Effect of various NaCl concentration on corrosion of steel in concrete produced by addition of styrofoam”. Fırat University, Technical Education Faculty, Construction Education Department, TURKEY, 2006; page1
[3] Panigrahi B.K., Srikanth S., Sahoo G. “Effect of alloying elements on tensile properties, microstructure and corrosion resistance of reinforcing bar steel”. Journal of Materials Engineering and Performance”, Volume 18, 2009
[4] Arthur Nilson, David Darwin, Charles W. D., “Design of concrete structures”, 13th ed., 2007, page 2
[5] Imperatore S., Rinaldi Z., “Mechanical behavior of corroded rebars and influence on the structural response of R/C elements”. ISBN 978-0-415-46850-3, 2009
[6] Ha-Won Song, Velu Saraswathy, “Corrosion monitoring of reinforced concrete structures – A review”, Int. J. Electrochem. Sci., 2, 2007; page1
[7] Bentur A., Diamond S., Berke N.S., “Steel corrosion in concrete: fundamentals and civil engineering practice”. E & FN Spon, London 1997
[8] Steven F. D. “Understanding corrosion and cathodic Protection of reinforced concrete structures”. Corrpro companies, Incorporated, Ohio 1
[9] Elsener B., Buchler M., Stalder F., Bohni H., J. Corros. 55; 1999: 1155
[10] Montemor M.F., Simoes A.M.P., Ferreira M.G.S., Cem. Concr. Compos. 25; 2003: 491
[11] Saremi M., Mahallati E., Cem. Concr. Res. 32; 2002

5th BSME International Conference on Thermal Engineering

Effect of Current Supply on the Wear Properties of TIG Modified Gray Cast Iron

Sanjoy Mallick[a,*], M. A. Islam[b]

[a]*Student, Department of Materials and Metallurgical Engineering, BUET, Dhaka-1000, Bangladesh*
[b]*Professor, Department of Materials and Metallurgical Engineering, BUET, Dhaka-1000, Bangladesh*

Abstract

Gray cast iron has extensive applications in the making many machine components like gear, link, cylinder block, cylinder head, clutch plate, and piston ring due to its high cast-ability, fair mechanical properties, machinability and wear resistance. Wear is always a major industrial problem of all transmission parts. In gray cast irons, graphite flakes are embedded in the matrix of ferrite/pearlite or both. But the matrix hardness (which is very important to provide higher wear resistance) is relatively low. As a result, as cast gray iron cannot provide satisfactory wear resistance in many practical applications. In this research work, an initiative has been taken to improve the surface hardness as well as the wear resistance of as-received gray cast iron. The sliding wear behavior of gray cast iron surface remelted by tungsten inert gas (TIG) welding was studied and compared with the as-received one. To evaluate the wear behavior a pin-on-disk type wear test machine was used at room temperature in ambient air. Welding current of magnitude 5, 15, 30 amperes and potential magnitude of 15 volts have been used to melt the surface of gray cast iron. Microstructural characterization, hardness measurement, and dry sliding wear tests have been performed on these modified surfaces. Hardness has been found to increase with increase in current supply. Wear rate of the gray cast iron decreased with increase in the welding current reaching minimum value for 30 amperes and where it was about 4 times lower than that of the as-received specimens. After wear tests, worn surfaces of test specimens were observed in optical microscope and they were photographed. Wear morphologies of TIG modified and as-received gray cast iron surfaces were found to be different.

Keywords: Gray cast iron; Wear; Worn surface; TIG melting; Surface hardening ;

1. Introduction

Gray cast iron is a type of cast iron that has a graphitic microstructure. It is named after the gray color of the fracture it forms, which is due to the presence of graphite [1].Gray cast iron has graphite flakes which are embedded in the matrix of ferrite/pearlite or both. Graphite flakes are interacted together and disposed in the form of plates, constituting an easy path for fast heat dissipation, good ability for vibration damping and excellent machinability [2]. It is the most common cast iron and the most widely used cast material. They are generally used in mechanical (pumps, valves etc.), chemical, food, armament and oil industries [3, 4]0. In industries, gray cast irons find wider applications than white cast irons. There is an ever increasing demand for increased wear resistance of gray cast irons for high performance and durability of cylinder liners for machineries.

Hence, to benefit from this inexpensive cast iron in the wear applications, their surface can be modified by using surface engineering techniques. There are various kinds of surface treatment techniques for structural materials. Induction hardening, flame hardening, chemical hardening, electron beam hardening, laser hardening, Tungsten Inert Gas (TIG) welding, chill castings are some of the techniques of surface hardening. Recent research efforts have been concentrated on the development of surface layers with improved properties. Surface melting is a process in which the surface of the work-piece is melted and re-solidified. The surface melted layer has usually a finer and more homogeneous structure than its original base material [5]. Surface remelting of cast irons by high energy-intensity heating sources, specially laser and electron beam, has been investigated by researchers [6-9].Meanwhile tungsten inert gas (TIG) process as an economical and easily available method is

* Sanjoy Mallick. Tel.:+8801922529440.
E-mail address: sanjoy.mme@gmail.com

considered as an alternative for laser and electron beam [10, 11]. So it seems to be appreciable to concentrate more on this process in surface modification and effect of its variations on wear behavior of the pearlitic gray cast iron in detail. In this study improvement of wear resistance of the gray cast iron by surface remelting and the effects of the parameters of TIG process are evaluated.

2. Experimental

In this present work, commercially available gray cast iron was used. The composition of this cast iron has been presented in Table 1. The geometry of wear test specimens has been given in Fig. 1. The samples were made from gray cast iron stock and then they were TIG modified at 5A, 15A, 30A DCSP current settings and voltage was fixed (15V).These surface modified samples are now designated as GC2, GC3 and GC4 respectively and as-received gray cast iron samples are designated as GC1. After TIG modification, the modified surfaces were ground carefully to get the final wear test specimens. The surfaces of TIG modified and as-received specimens were observed under optical microscope after necessary metallographic preparations and they were photographed.

Table 1. Chemical composition of gray cast iron (weight percent)

C	Si	Mn	S	P
3.2	2.5	0.5	0.03	0.05

Surface hardness values of as-received, TIG modified samples and also the counter body was measured. Rockwell hardness tester was used for hardness measurement. Dry sliding wear tests of all samples of both as-received and TIG modified samples were carried out at room temperature in the laboratory air. Here, it is mentioned that for all samples dead load and rotational speed of counter body were kept fixed, respectively at 1 kg and 1000 rpm and the test periods were 3 hours. In Fig. 2, schematic diagram of pin-on-disk type wear test set-up has shown. Many investigators used this type of set-up for dry sliding wear test [12].After wear tests, weight losses for different test periods were measured and worn samples as well as counter bodies were also observed under microscope to know the wear behavior and again they were photographed.

Fig. 1. Wear samples before and after welding.

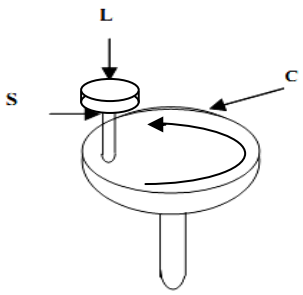

C: counter disk, L: load,
S: pin specimen

Fig. 2. A pin-on-disk type sliding wear test set-up.

3. Results and Discussions

The microstructures of as-received gray cast iron were pearlitic, embedded with typical graphite flakes as shown in Fig. 3. However, TIG melting caused graphitic flakes to be distributed and diffused inside the matrix. Due to higher rate of cooling, diffused carbon could not come back. As a result, pearlitic surface of the as-received gray cast iron become interdendritic cementite networks and dendrites of pearlite. The microstructures are given in Fig. 4.

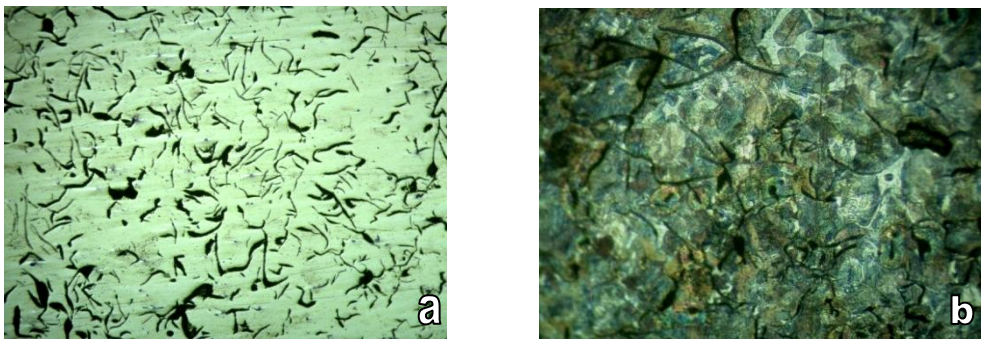

Fig. 3. Microstructures of as-received gray cast iron, (a) unetched (100x); (b) etched (200x).

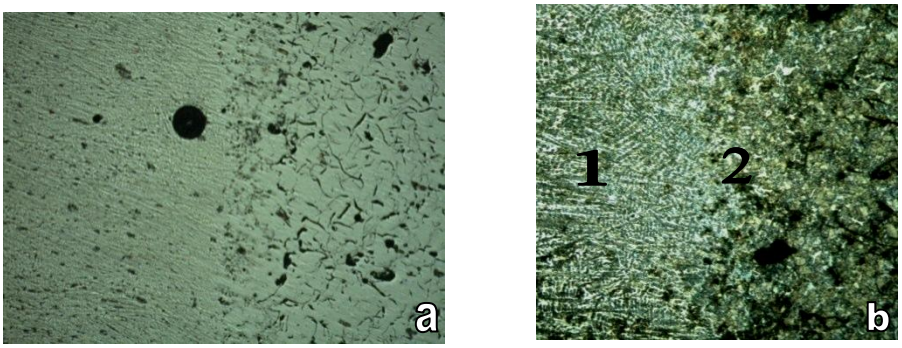

Fig. 4. Microstructures of 15A TIG modified gray cast iron, (a) unetched (50x); (b) etched (100x).

The interdendritic cementite networks and dendrites of pearlite microstructure form at the surface of TIG modified cast iron is very clear in the close-up view of marked region (1) of micrograph 4b, which is presented in Fig. 5a. With increase in depth from the TIG melted surface towards the core the microstructures become pearlitic dominating structure with surrounded by interdendritic cementite networks. After TIG melting of gray and nodular cast irons some other investigators also mentioned similar micro-structural changes from surface towards the core [13, 14].

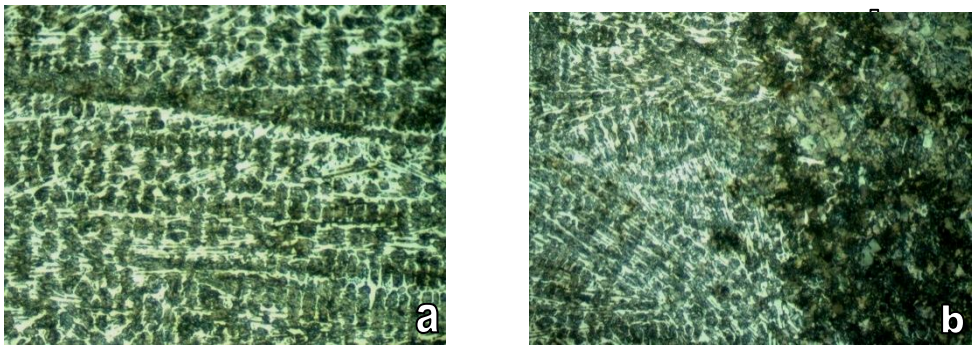

Fig. 5. Close-up view on optical micrograph presented in Fig. 4b, (a) marked area 1 (200x); (b) marked area 2 (200x).

After TIG melting and air cooling, the surface hardness of the as-received gray cast iron increased significantly. The hardness values of as-received, TIG modified samples and the counter body is presented in Table 2.The reason of this increased surface hardness is due to the increase of interdendritic cementite networks and dendrites of pearlite content in the microstructure, which is very clear from Fig. 4. and Fig. 5.

Table 2: Hardness values of as-received cast iron, TIG modified cast irons and Cast Iron counter body.

Sample Identification	Hardness Values (HRC)
Heat Treated Cast Iron counter body	35.0
As-received Gray Cast Iron	9.80
TIG modified Gray Cast Iron , 5A	41.4
TIG modified Gray Cast Iron , 15A	46.7
TIG modified Gray Cast Iron , 30A	49.6

The variation of hardness values with TIG welding current is plotted in Fig. 6.

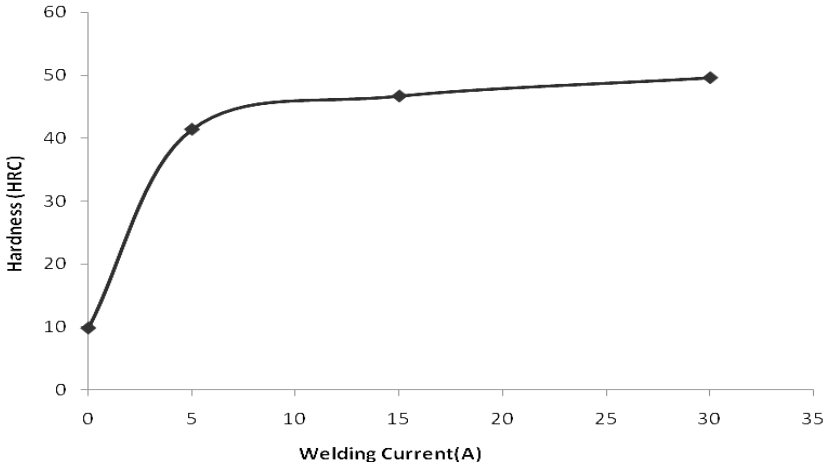

Fig. 6: Variation in Hardness of gray cast iron with TIG welding current.

After wear tests, weight losses for different test periods were measured and they are presented in the Table 3 and weight loss versus wear test time periods curves are potted, Fig. 7.

Table 3: Wear test data of as-received, 5A, 15A and 30A TIG modified gray cast iron.

Time Interval (hours)	Cumulative wt. loss of as received GCI (g)	Cumulative wt. loss of 5A TIG Modified GCI (g)	Cumulative wt. loss of 15A TIG Modified GCI (g)	Cumulative wt. loss of 30A TIG Modified GCI (g)
3	0.0438	0.015	0.0116	0.01
3	0.068	0.0274	0.0207	0.0174
3	0.0872	0.0369	0.0276	0.0215
3	0.1055	0.0441	0.0334	0.026

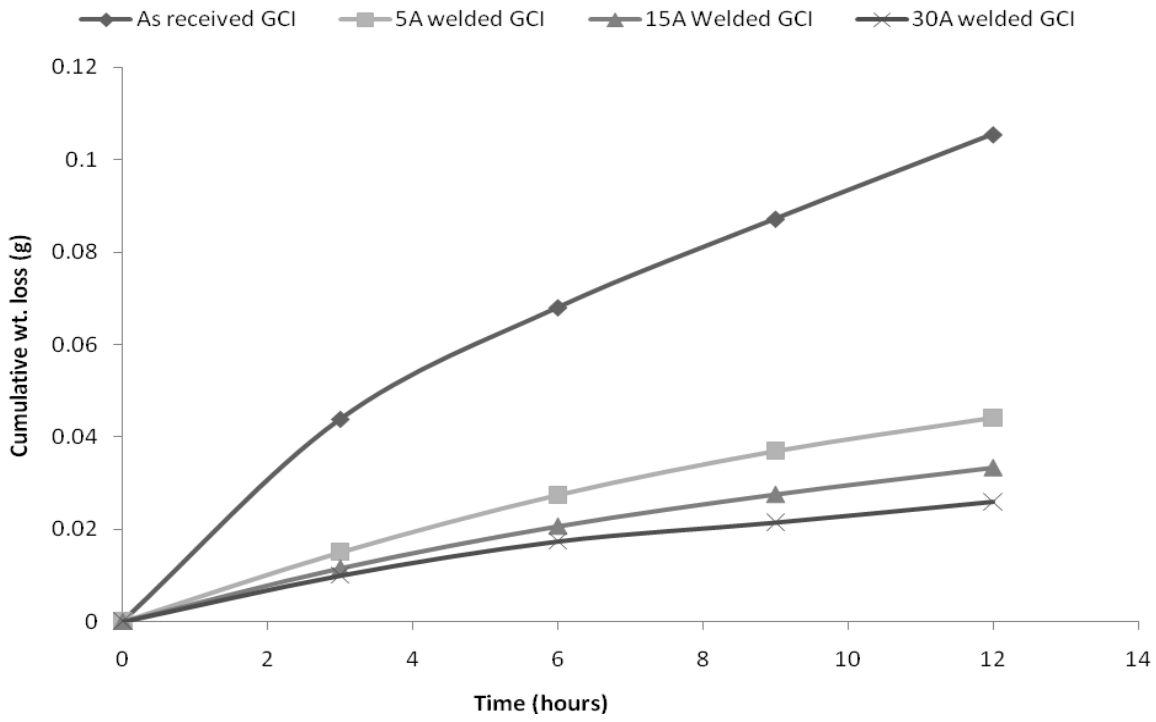

Fig. 7. Cumulative weight loss versus time period curves for as-received and TIG modified gray cast iron.

Detail investigation on worn cast iron counter body revealed that the wear patterns of counter body were almost similar (micro-cutting type abrasive wears), Fig. 8. However, wear patterns of worn samples were somewhat different. For as-received condition adhesive type wear morphology dominant Fig. 9a. On the other hand, TIG modified all samples showed micro-cutting dominating abrasive type wear mechanism Fig. 9b. In most cases of dry sliding wear test, wear patterns of samples and counter bodies are controlled by the surface hardness of the respective component. The average hardness of the counter body, as-received and TIG modified samples are given in Table 2. The worn particles from counter body or TIG modified specimens of sufficiently high hardness could not be plastically deformed or adhered on their respective surfaces. So, counter body and TIG modified specimen showed abrasive type wear patterns and as-received gray cast iron with low hardness showed adhesive type wear mechanisms.

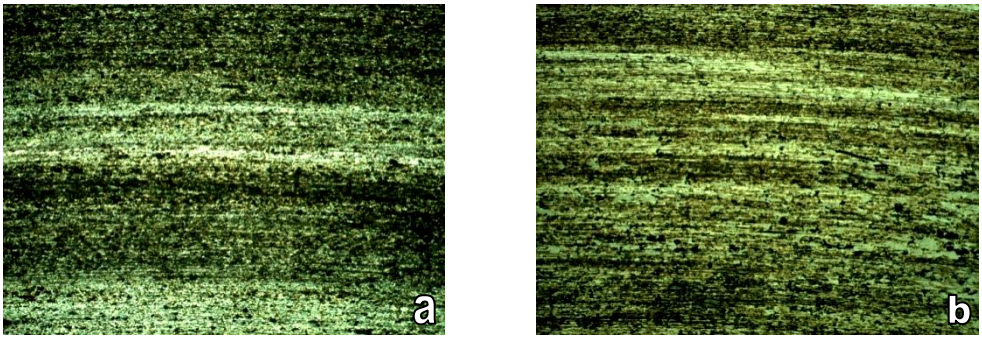

Fig. 8. Wear patterns on counter body (a) as-received; (b) TIG modified (30A) gray cast iron.

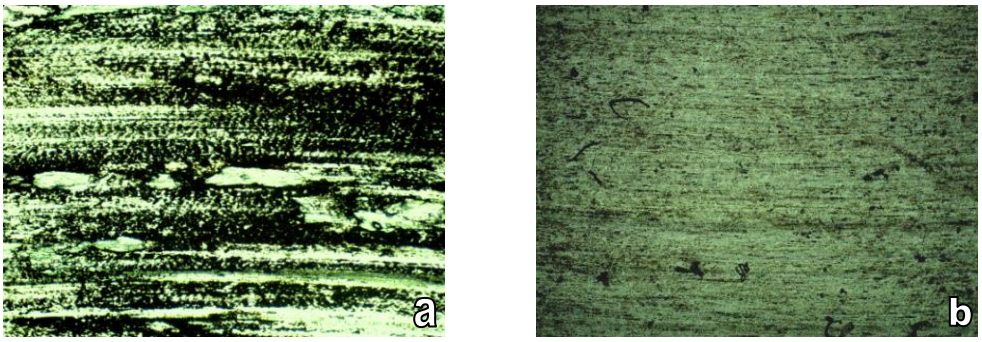

Fig. 9. Wear patterns on pin sample (a) as-received; (b) TIG modified (30A) gray cast iron.

4. Conclusions

In this present work, effect of current supply on the wear behavior of TIG modified gray cast iron has been investigated. After experimental work, following conclusions have been drawn.

- Experimental results showed that surface modification by TIG melting increased the wear resistance of the as-received gray cast iron to an unbelievable level. Wear rate of the gray cast iron decreased with increase in the welding current reaching minimum value for 30 amperes and where it was about 4 times lower than that of the as-received specimens.
- TIG melting increased the surface hardness and changed the wear pattern of as-received gray cast iron from adhesion dominating one to abrasive dominating wear. Hardness of the gray cast iron increased with increase in the welding current reaching maximum value for 30 amperes and where it was about 5 times larger than that of the as-received specimens.
- For both TIG modified and as-received sample conditions, wear pattern of cast iron counter body was found to be abrasive type.

References

[1] Avner S. H., “Introduction to physical metallurgy”, Tata McGraw Hill, Edition 1997.
[2] Cueva G., Sinatora A., Guesser W.L. and Tschiptschin A.P., Wear, 2003, 255, 1256.
[3] Properties and Selection: Irons and Steels, ASM Metals Handbook, vol. 1, 9th ed., ASM International, Metals Park, Ohio, 1990, 12-40.
[4] Kowandy C., Richard C., Chen Y.M. and Tessie J.J.: Wear, 2007, 262, 996.
[5] Sohi M.H.: Ph.D. Thesis, University of Birmingham, 1991.
[6] Mordike B.: in Proc. of the Sec. Inter. Sem. on Surface Engineering with High Energy Beams, Lisbon, Portugal, 1989, 13-26.
[7] Chen Z., D.R.F. West and Steen W.M.: in Proc.of the Fifth Inter. Cong. on Appications of Lasers and Electro-optics, ICALEO086, Arlington, VA, USA,1986, 27-35.
[8] Tsujikawa M., Yoshida N., Kswamoto M., Hino M. and Hiramatsu M.: Proc. of the Fifth World Sem. on Heat Treat. and Surf. Eng., IFHT095, Isfahan, Iran,1995, 535.
[9] HeydarzadehSohi M., Karshenas G. and Boutorabi S.M.A.: J. Mater. Proc. Tech., 2004, 153-154,199.
[10] Lansdown A.R. and Price A.L.: Materials to Resistance Wear, 1st ed., Pergamon Press, 1986.
[11] OrÃlowicz A.W. and Trytek A.: Wear, 2003, 254, 154.
[12] Islam, M.A., Haseeb, A.S.M.A. and Kurny, A.S.W., 1995, “Study of Wear of As-Cast and Heat-Treated Spheroidal Graphite Cast Iron Under Dry Sliding Condition”, J. of wear, Elsevier Sci. Ltd., 188 (61-65).
[13]Benyounis, K.Y., O.M.A. Fakron, O.M.A., Abboud, J.H., Olabi, A.G. and Hashmi, M.J.S. 2005, Surface melting of nodular cast iron by Nd-YAG laser and TIG, J. of Mat. Proc.Tech., 170(1-2), 127-132.
[14] Alabeedi, K.F., Abboud, J.H. and Benyounis, K.Y., 2009, “Microstructure and Erosion Resistance Enhancement of Nodular Cast Iron by Laser Melting”,J.of wear, 266(9-10), 225-933.

5th BSME ICTE

Study of LPG Heating Value

Niaz Bahar Chowdhury, Kazi Ekram Kamal and Iqbal Hossain*
Department of Chemical Engineering, Bangladesh University of Engineering and Technology, Dhaka-1000.

Abstract

The heating value of liquefied petroleum gas (LPG) is an important characteristic implying LPG fuel-quality. Nevertheless, the quantitative and detail study on the heating value of LPG is still in high scarcity. Hence, the heating value of LPG is analyzed extensively in the present study. A combustion reactor simulated employing Aspen-Hysys simulator is used to determine the heating value. The separate effects of the presences of additives or foreign components (e.g., ethane, hydrogen sulfide, moisture, and mercaptan), the proportion of primary LPG components (e.g., propane and butane), and the combustion temperature and pressure on the heating value of LPG are studied. Explanations of the observed effects are also provided. The present study would help the researchers, manufacturers, bottlers, and distributors of LPG immensely.

Keyword: Heating value; LPG; Aspen-Hysys process simulator; Fuel.

1. Introduction

On the basis of reserve and uses, natural gas is the main energy resource in Bangladesh. Since it is being used in the sectors of power, industrial, commercial, domestic, automobile, etc largely, the reserve of natural gas is depleting rapidly. As exploration of new gas fields in Bangladesh is not going as expected, it will not be possible for natural gas to fulfil the demand solely after a decade **[1]**. From this scenario the necessity of energy-diversification is felt. Liquefied petroleum gas, LPG is a mixture primarily of propane and butane. It has already been proved as an efficient alternative domestic fuel in Bangladesh. It can also used as a fuel in heating appliances and vehicles. To popularize and enhance the uses of LPG also require fundamentals research at various aspects. Heating value is a very important character of any combustion-fuel indicating the fuel quality or value. It is expected that the heating value of LPG is affected by the parameters like presences of additives or foreign components, proportion of primary LPG components, and combustion pressure and temperature, etc. Unfortunately, no quantitative and detail study on the effect of the important parameters stated above on the heating value of LPG is available in the literature. Therefore, the objective of the present study is to the study of the separate effects of the presences of additives or foreign components (e.g., ethane, hydrogen sulfide, moisture, and mercaptan) in LPG, the proportion of primary LPG components (e.g., propane and butane), and the LPG combustion temperature and pressure. The Aspen-HYSYS process simulator is used in this study to determine the heating value at various conditions.

Nomenclature

LPG	Liquefied petroleum gas
SI	System of international
P	Propane
B	Butane
HS	Hydrogen sulphide
W	Moisture
M	Mercaptan

*To whom correspondence should be maintained: iqbalhossain@che.buet.ac.bd

2. Methodology

Heating value is normally defined as the amount of heat obtained from the complete combustion of one unit of fuel (e.g., LPG). The pure experimental setup to determine this heating value especially for LPG is rarely available. Hence the simulation method is adopted to determine the heating value. A combustion reactor is created in Aspen-HYSYS 7.1 process simulator as shown in Fig.1. The simulation and heating value determination are briefly stated below:

A new file in aspen-hysys is opened and a package unit (e.g., SI unit) is chosen from preference tab. The various components (e. g. ethane, propane, butane, mercaptan, hydrogen sulfide, water, methanol, ethanol, oxygen, and nitrogen, etc.) are selected from the component tab. Subsequently, an appropriate fluid package (i.e., Peng Robinson) is selected from the fluid package tab. The specific reactions are also defined in the reaction tab and the selected fluid package is assigned to each reaction. After entering into the simulation environment the reactor (i.e., conversion type) is taken from object pellet. A 100 % conversion of each LPG component is added to the reactor as a parameter. Then the LPG and air streams at a given condition are finally added to the reactor [2]. An energy stream (E, in Fig. 1) is also added to the reactor to represent the heat generated by the combustion reactions. With the run of the simulation, the reactions are completed and the heating value is obtained from the energy stream, E.

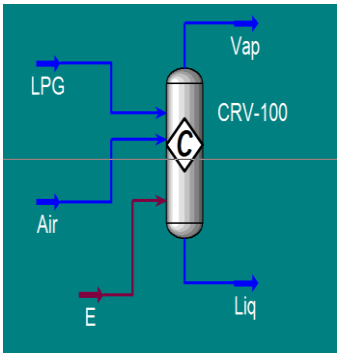

Fig. 1. Combustion reactor and associated streams in Aspen HYSYS simulator.

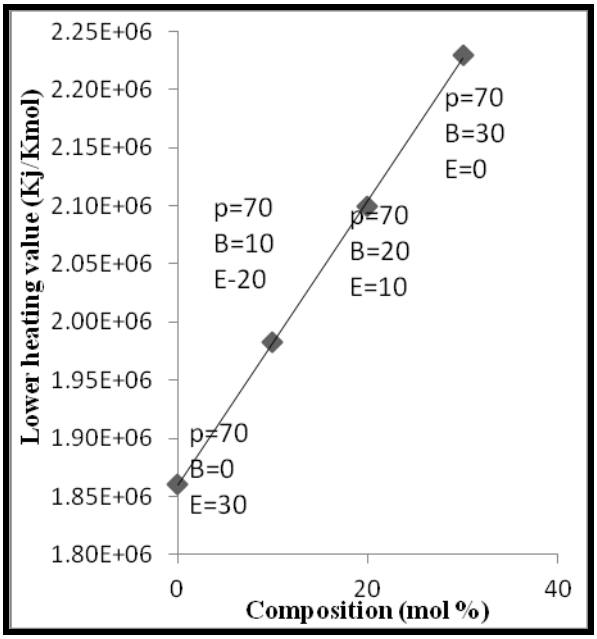

Fig. 2. Effect of ethane on the heating value of LPG.

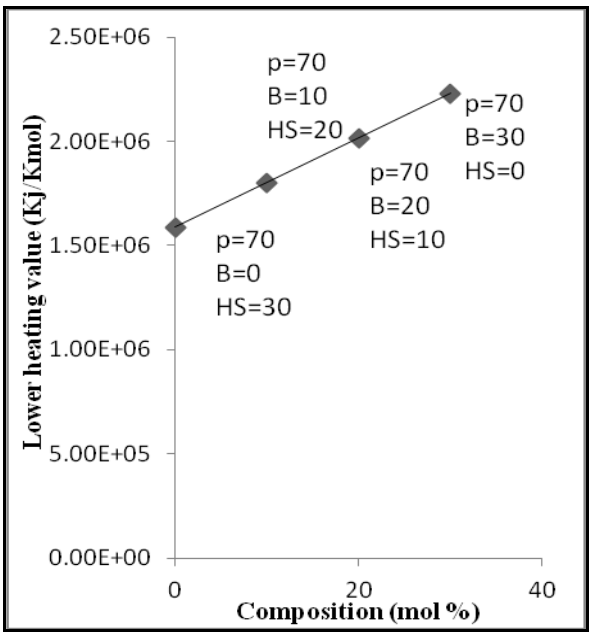

Fig. 3. Effect of hydrogen sulphide on the heating value of LPG.

3. Results and Discussions

The effects of various parameters on the heating value of LPG are presented and discussed in the following sub-sections.

3.1. Effect of additives or foreign components

During the manufacture of LPG, ethane can come into it. Similarly, H_2S and moisture can also be present in LPG. In addition, mercaptan is deliberately added to commercial grade LPG to identify the leakage of LPG from cylinder or bottle. Therefore, it is required to know the effect of these additives or foreign components on the heating value of LPG. Fig. 2 clearly shows that the heating value decreases monotonically if the proportion of ethane increases. This is because the heating value of ethane is lower than that of LPG primary components (i.e., propane and butane). Fig. 3 also indicates that the heating value decreases monotonically with the increases in the proportion of H_2S in LPG. This also happen due to the fact that the heating value of H_2S is much lower than that of propane and butane. Finally, Figs. 4 and 5 also show the same effect that is the heating value of LPG decreases with the increases in the proportions of moisture and mercaptan [3]. In addition, here the decreasing effect is severe than that of ethane and H_2S. This is because both the moisture and mercaptan are non-combustible. Therefore, it is desirable to suppress the proportions of additives or foreign components in LPG as much as possible.

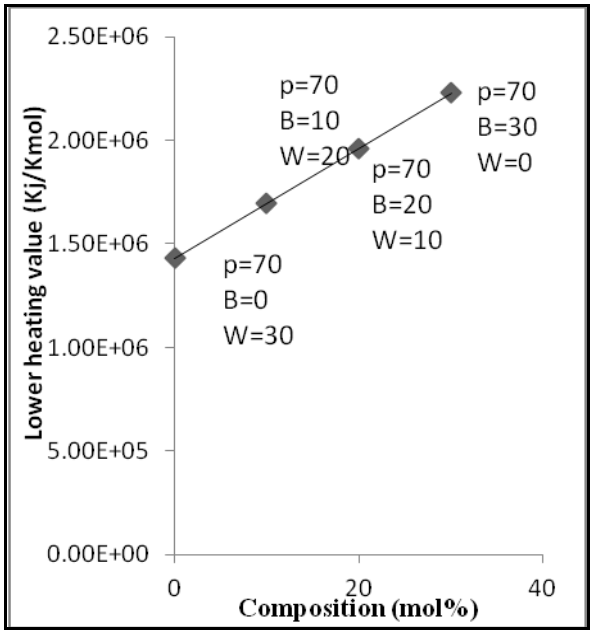

Fig. 4. Effect of moisture (W) on the heating value of LPG.

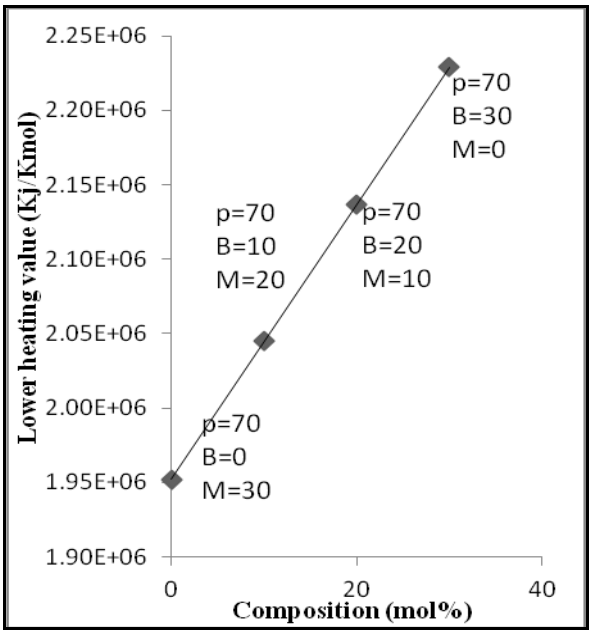

Fig. 5. Effect of mercaptan (M) on the heating value of LPG.

3.2. Effect of primary components proportion

The propane and butane are the primary components of LPG. Fig. 6 shows that with the increase in the proportion of propane, the heating value per unit volume of LPG also decreases substantially. This is because the heating value of pure propane is lower than that of pure butane in volume basis units. The actual reason behind the lower heating value of propane is that, in a unit volume, propane has the lower number of carbon atom (C) than butane, which are converted into C-O bond upon combustion generating lower amount of heat than butane [4]. Same qualitative trend is observed if the heating value is considered per unit mole and mass of LPG. Hence, it is desirable to have more butane in LPG to yield higher heating value of the mixture.

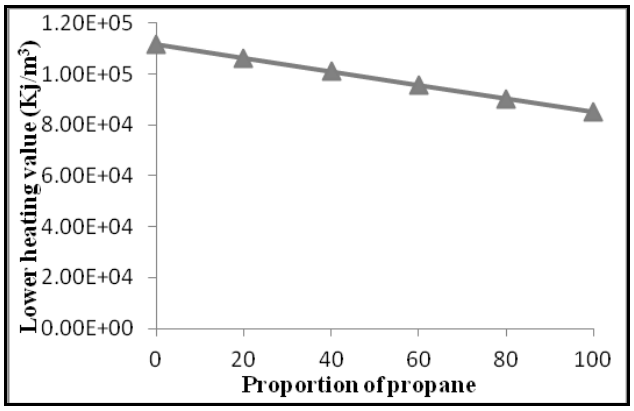

Fig. 6. Effect of primary component composition.

3.3. Effect of combustion temperature and pressure

Having the same pressure different geographical regions utilizing LPG as cooking and heating fuel can be at different temperatures. Similarly, having the same temperature the geographical regions can hypothetically be under different pressures too. In addition, numerous industrial and mechanical units employing LPG as a combustion fuel can be under different temperatures and pressures. Therefore, LPG with a particular quality can give different heating values upon combustion at different temperatures and pressures. As a result, it is also very important to know the effect of combustion temperature and pressure on the heating value of LPG [5].

The effect of combustion temperature on heating value is studied over a temperature range of -50 to 200°C under three separate pressures of 1, 5, and 10 atm. Fig. 7 clearly indicates that the heating value increases monotonically with the increase in combustion temperature at all pressures. However, three distinct regions along temperature can be observed, which have different rate of the increase of heating value with temperature. The first and last regions have nearly the same rate of increase of the heating value with temperature while the middle region has abruptly faster rate [6]. Fig.7 also shows that the first region becomes shorter with the increase of pressure. The increase on heating value with the increase in temperature would be due to the change of energy level of reacting molecules with the increase in combustion temperature.

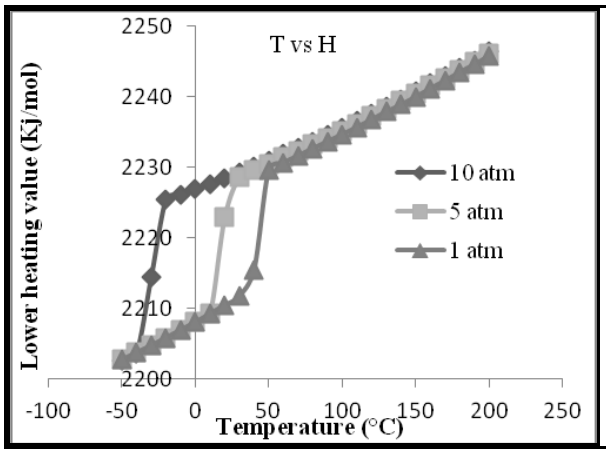

Fig. 7. Effect of combustion temperature on the heating value of LPG.

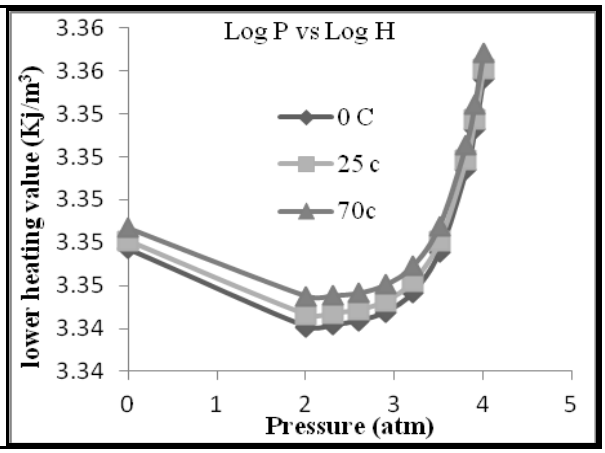

Fig. 8. Effect of combustion pressure on the heating value of LPG.

The effect of combustion pressure on heating value of LPG is studied over a pressure range of 0 to 4 atm under three separate temperatures of 0, 25, and 70°C. Fig. 8 shows that, regardless of combustion temperature considered, the heating value initially decreases to a minimum level and then increases abruptly with the increase in pressure. This complex behavior of heating value with combustion pressure is expected to involve multiple contributing factors, which are still under research.

4. Conclusion

The separate effects of additives or foreign components present in LPG, proportion of primary LPG components, and combustion temperature and pressure on the heating value of LPG are studied in this study. It is found that the presences of additives or foreign components (e.g., ethane, hydrogen sulfide, moisture, and mercaptan) always decrease the heating value. Hence, it is required to minimize the amount of the additives if the high heating value is desired. It is also found that the heating value of LPG decreases if the proportion of propane is increased through the decrease in the proportion of butane. Hence, it is required to have more proportion of butane in the LPG to ensure a higher heating value. Analysis shows that the heating value always increases with the increase in combustion temperature. Three distinct regions with different rates of increase can clearly be observed in the curve of heating value vs. combustion temperature. However, regardless of combustion temperature, the effect of combustion pressure on the heating value is complex. The heating value decreases with the increase in pressure initially up to a critical pressure level; once the pressure level is exceeded, the heating value increases with increasing pressure. Those who are involved with the research, manufacturer, bottling, and distribution of LPG are expected to be benefited immensely by the results of this study.

Acknowledgement

The supports from the Department of Chemical Engineering, Bangladesh University of Engineering and Technology are gratefully acknowledged.

References

[1] www.lpgbangladesh.com

[2] Aspen user guide (www.aspentech.com)

[3] Smith, J.M., H.C. Van Ness and M.M. Abbott, Introduction to Chemical Engineering Thermodynamics, 6th edition, Singapore: McGraw-Hill, (2001)

[4] Cengel, Y. A., M. A. Boles, Thermodynamics an Engineering Approach, 5th edition, , Singapore : McGraw-Hill (2007)

[5] Borgnakke, C., Richard E. Sonntag, Fundamentals of Thermodynamics, 1st edition, India: Apprentice Hall, (2008)

[6] Moran, J. M., Howard N. Sapiro, Fundamentals of Engineering Thermodynamics, 6th edition, New York: John Wiley & Sons (2010)

5th BSME International Conference on Thermal Engineering

Comparison on Evaluated Performance of Different Axis Solar Tracker

Md. Riaz Pervez[a]*, Mohd. Rafiqual Alam Beg[b], Md. Rabiul Islam Sarker[b]

[a]*Department of Mechatronics, University of Siegen, Siegen-57074, Germany*
[b]*Department of Mechanical Engineering, Rajshahi University of Engineering and Technology, Rajshahi-6204, Bangladesh*

Abstract

This paper presents the comparison of experimental study of a two axis (azimuth and elevation) and single axis automatic control solar tracking system with the fixed photovoltaic (PV) system or without tracking system. Those tracking system track solar PV panel according to the direction of beam propagation of solar radiation. The tracking unit consists of sensors, ADC, microcontroller and stepper motor. The analog input from the sensors is converted by ADC and this digital data transfer to the microcontroller. By using this data controller rotate the stepper motor in desirable direction. An experimental study is carried out to evaluate their performance under local climate. The results indicate that the average energy surplus become about 30- 38% for two axis solar tracker and 15-25% for single axis solar tracker with atmospheric influences. But there is a design difficulties exists in the two axis solar tracker which is not so considerable in the point of view of surplus energy found from two axis solar tracker compared with single axis solar tracker. Considering all above aspects two- axis sun tracking system is more beneficial than single axis sun tracking system.

Keywords: **:** Two-axis solar tracker; Single-axis tracker; surplus energy; Microcontroller, Solar energy.

1. Introduction

Dramatically decrease of fossil fuel and increase of polluted gases create a profound impact on communication, living and other consumption sectors. So human beings are largely depends on the alternatives like renewable energy. So for getting direct electricity without effort the PV system is the best choice able option. Solar panel is the fundamental energy conversion component of photovoltaic (PV) systems [1]. PV offers safe and clean energy sources [2]. With the cost of solar cells decreasing, the conversion of solar energy to electrical energy is increasingly becoming economically viable [3]. This is suitable for topical countries like Bangladesh where there is abundant solar energy available throughout the year. As solar panels are relatively expensive, much research work has been conducted to improve the utilization of solar energy. Physically, the power supplied by the panels depends on many extrinsic factors, such as insulation levels (incident of solar radiation), temperature and load condition [4].

For consuming this vast energy, an adaptive system should be developed for getting maximum power from this solar panel. But the availability of sun throughout the day is not same or maximized. This is due to the static placement of the panel which limits their area of exposure from the sun [5].In searching for the maximum power condition, many methods have been tried. The “look-up-table”, the “perturb and observe”, and the “current sweep” are some of the fundamental approach [1]. Neural Network approach [6] and Fuzzy Logic approach [7] are also reported. An automatic solar tracking system using a number of Light Detecting Registers (LDRs) is proposed [5, 8]. Researchers [9, 10] have presented the design and implementation of a computer-controlled dual-axis solar tracking system to obtain high precision positioning of the PV panel.

All the above mention research is just design and implementation of various tracking system. The aim of this work is to compare the effect of using two-axis and single axis solar tracking systems on the electrical generation of a flat photovoltaic system (FPVS) with fixed system. An experimental study is carried out to evaluate their performance under local climate.

* Corresponding author. Tel.:+ 490 176 69372865.
E-mail address: md.pervez@student.uni-siegen.de

2. Comparison of design of the tracking systems

2.1. In motor load

The Stepper Motor is an electromagnetic device that converts digital pulses into mechanical shaft rotation. Motion Control, in electronic terms, means to accurately control the movement of an object based on speed, distance, load, inertia or a combination of all these factors.

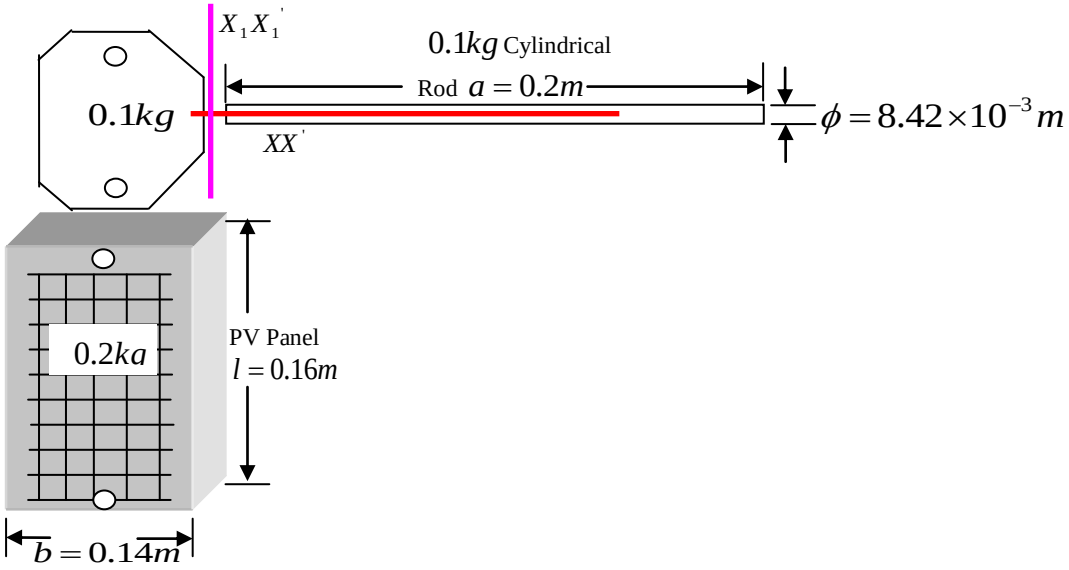

Fig. 1. Schematic diagram of the mechanical system

From above specification as shown in (Fig. 1) the power for single axis tracking is 0.092Watt and for two axes tracking the power is 1.38Watt, both are less than the single motor power (2.36Watt). The power required for Single axis tracking is much less then the two axis tracking. Though extra motor is required for two axis tracker but considering the surplus energy it is more beneficial then single one.

2.2. In Sensing Element and Signal Processing

A lot of methods have been proposed and used to track the position of the sun. The simplest of all uses an LDR– a Light Dependent Resistor to detect light intensity changes on the surface of the resistor. Other methods, such as that published by Jeff Damm in 'Home Power' [11], use two phototransistors covered with a small plate to act as a shield to sunlight.

At morning, the tracker is in state A from the previous day. The left phototransistor is turned on, causing a signal to turn the motor continuously until the shadow from the plate returns the tracker to state B. As the day slowly progresses, state C is reached shortly, turning on the right phototransistor. The motor turns until state B is reached again, and the cycle continues until the end of the day or until the minimum detectable light level is reached. Considering problems [12] three solar cells are used.

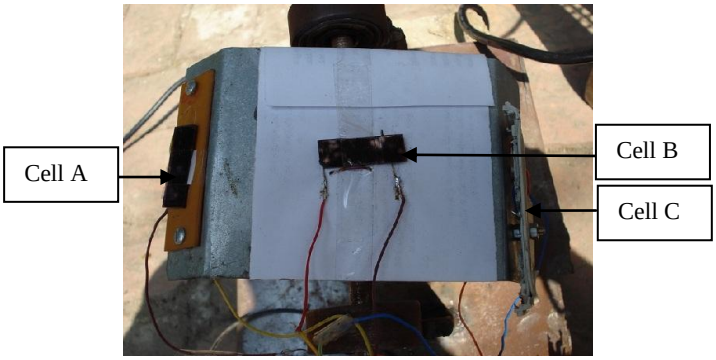

Fig. 2. Three solar cells as sensor

The cells are placed at 15^0 to each other because the sun rotates 15^0 in an hour. When maximum solar intensity falls on cell A then the motor rotates cell A direction (clockwise). On the other hand, if cell C gives the maximum then motor rotates reverse. If intensity of cell B is high than any other cell, then motor stands in that position. This is a continuous process. So the cells are always compared the intensity level and given command to the controller and the motor rotates in that direction. The rotating principle is same for the other motor.

2.3. In Software design

The designed tracking systems consists of software based online tracking method. The main components of the designed system are photocell as sun sensor, ADC0808, interfacing component with microcontroller (AT90S8515), stepper motor driver circuit (ULN2803), stepper motor and PV cell supporting metallic structure with mechanical gear mechanism.

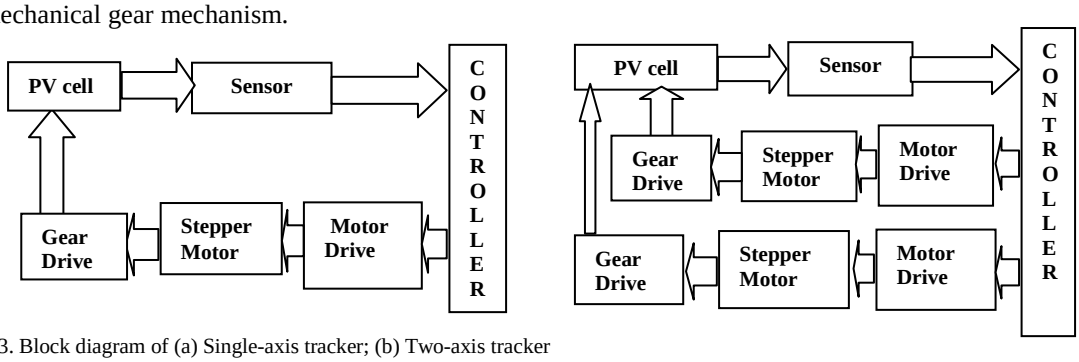

Fig. 3. Block diagram of (a) Single-axis tracker; (b) Two-axis tracker

The electromechanical system of a single-axis solar tracker consists of single drivers with single stepper motor of 0.1° per step which is used for the E-W tracking (Fig. 3 a). On the other hand, the electromechanical system of a two-axis solar tracker consists of two drivers with two steeper motor of 0.1° per step: the first for the joint rotating about the vertical axis and the second for the E-W tracking as shown in (Fig. 3 b).

Fig. 4. Experimental set-up of (a) single axis tracker; (b) Two axis tracker

The sun position sensors (Photocell) give an mV voltage proportional to the radiation beam position inside the sensor. This sensor is intended to keep the radiation beam normal with collector. Sun sensor's detector determines system misalignment (position error of solar radiation collecting unit) and then sends a signal to the controller (Microcontroller's software). The controller (Microcontroller's software) uses the sun's rate and sun sensor information as inputs to generate proper motor commands to slew the collector. The microcontroller contains database program based on sun's position for every time of a definite day. When the stepper motor gets the commands from the controller, the motor starts to rotate at a definite angle according to the controller command that slew the collector.

Control software has been developed to determine the optimum position of the panel during day light i.e. how much deviated from maximum power point. The calculated values taking from the sensor is a function of voltage which is converted to digital form is fed to the microcontroller program to control the actuator of the solar tracker. In this research the programming method of control works efficiently in all weather conditions regardless of the presence of clouds.

The software for the solar tracker is written in Bascom AVR version-11.1.8.7. Flow chart of the control software for both systems shows the basic difference in the software design which are shown in appendix A.

Software based online tracking method is used in the designed tracking system. Three PV modules of the following specifications were used to compare the energy surplus of the tracking modules where one was fixed and other two were in tracking mode. The simplest method to obtain an IV characteristic is to load the module with a variable resistor, and measure the voltage and current through digital multi-meter [13-14].

The mechanical gear mechanism used for single axis is simpler than two axis solar tracker because of the tracking complicated strategy of two axis solar tracker.

3. Experimental Results and Discussions

Measurements on the PV system with and without solar tracking at various local climatic conditions are shown in Figs 5, 6, 7 of 4th March, 2008 and 8,9,10 of 10th April, 2009. The experiment is carried out through the months February to April, 2008 & 2009.

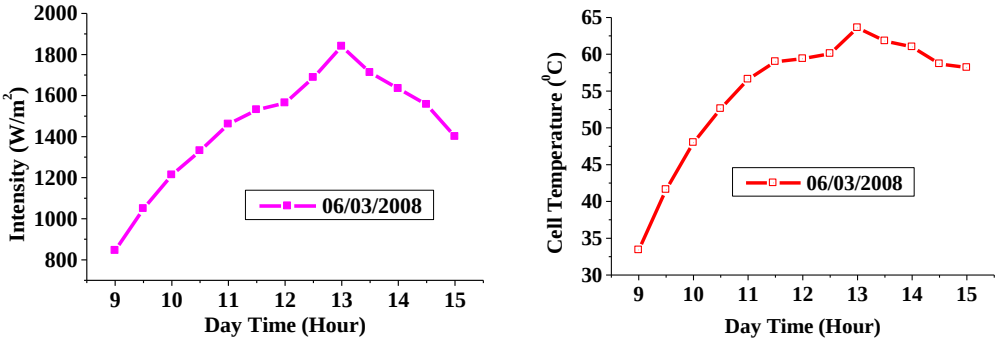

Fig. 5. (a) Intensity with day time; (b) Cell temperature with day time

3.1. Characteristics of Intensity & Temperature with respect to Day Time

From the experimental results of variation of intensity with day time characteristic it is seen that solar irradiation increases with day time up to 13.00 PM and then decreases and also there is some fluctuation of intensity due to movements of some clouds and abnormal atmosphere. Therefore during the central part of the day, the output of the solar cell will be at or near its maximum because the sunlight is arriving at more direct angle i.e. sunlight travels lesser distance to reach the earth surface. At the beginning and at the end of the day, the output fall off regardless of the orientation of the solar cell, mainly because the sunlight has to travel obliquely through the atmosphere at these times, arriving at a low angle i.e. sunlight travel more distance to reach the earth surface. This decreases the intensity of the sunlight.

In addition, since the sun travels through an angle of 15° per hour, it becomes close to perpendicular to the collector for a period of approximately two hours. Beyond this time, the intensity of the sunlight decreases due to the increase in air mass, and the angle between incident sunlight and the normal to the collector increases. These two factors cause the energy collected by the collector to decrease relatively rapidly during the hours before 11.30 A.M. and after 1.30 P.M. As a result, there is some fluctuation on PV cell characteristics.

On the other hand, temperature increases proportionally with the increase of intensity. This theory has been proved and depicts in (Fig. 5 b). Here with the increase of intensity from 9 am to 13pm the temperature is also increased and it has been shown maximum at the height intensity point. The temperature is actually the region of solar cell area. The main difference from the intensity curve the temperature moves downward not rapid like the intensity curve. Because the temperature of solar cell area largely affected by the environmental warm up.

The intensity depends on the presence of big sun. The experiment carried out in winter season. The daytime has concise to around 10 h among 24h. But the solar cell temperature largely depends on environmental temperature (as mention above). So the sensor stabilized both of these temperatures.

3.2 Characteristics of Power & surplus energy with respect to Day Time

From the curve nature in (Fig. 6 a) it is clear that with the increase of intensity with day time the power nature also increase. Because more the intensity falls on the solar cell the flow of electron also increases.

For that reason at the initial stage and the final stage the power is less only for less electron but at time around 13 pm the power shows the maximum. This not means that at 13 pm it may be any time when the intensity is high. The (Fig. 6 a) depicts power characteristics where maximum power is obtained as 5.8 watt (average) for two axis tracking mode and 4.8 watt for single axis tracking mode and 3.6 for fixed axis with 6.5 watt rated PV panel.

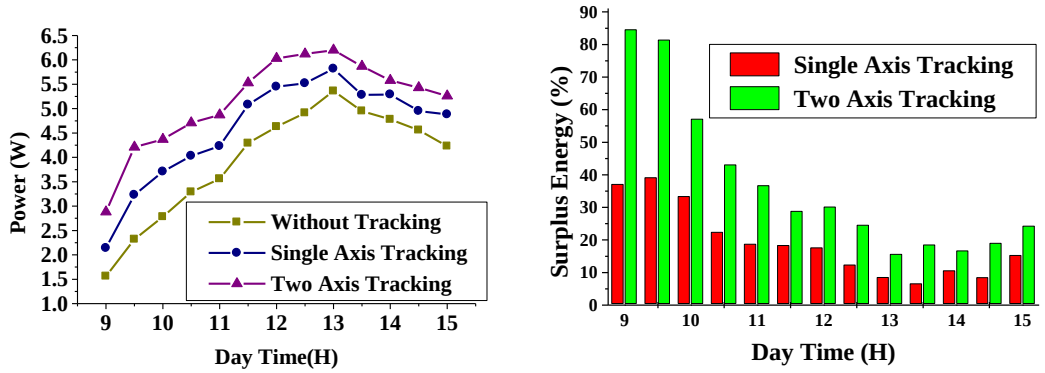

Fig. 6. (a) Power with day time; (b) Surplus energy with day time

The experimental measured variables are compared with that at fixed axis for both the single and two axis solar trackers. The results indicates that there is an overall increase of output power about 30-38% for the two-axis solar-tracking system compared to the fixed PV system and that of 15-25% for single axis solar tracking system.

The big bar chart as shown in (Fig. 6 b) shows the difference of surplus energy of tracking system to the without tracking system. When the power varies less at 13 pm then the surplus energy gives the less reading. This means that by using tracking this amount of extra energy is found which is lost by the without tracking system. On the other hand, at the initial and final stage this amount is huge. If this energy is collected by the tracking system then the fluctuation of intensity, cell temperature, and power will be less. For this reason the two axis tracking system gives the extra benefit for collecting maximum power. It has been called maximum power point tracking (MPPT). For two-axis tracking the maximum surplus energy 15% to 84% where in single axis tracking it was 6.5% to 59% throughout the day examining here. By averaging, it will be around 30-38% for two axis solar tracker and 15-25% for single axis solar tracker throughout the year.

3.3. Reproducibility:

Similar results have found after one year later. The (Fig. 7) shows that, with day time increase the intensity and cell temperature are also increased. And (Fig. 8) gives the same fashion. But the intensity range is lower than the (Fig. 5), so the cell temperature, power and the surplus energy are also lower. On the other hand, the fall of intensity is rapid than (Fig. 5) so the cell temperature, power and surplus energy also fall rapidly.

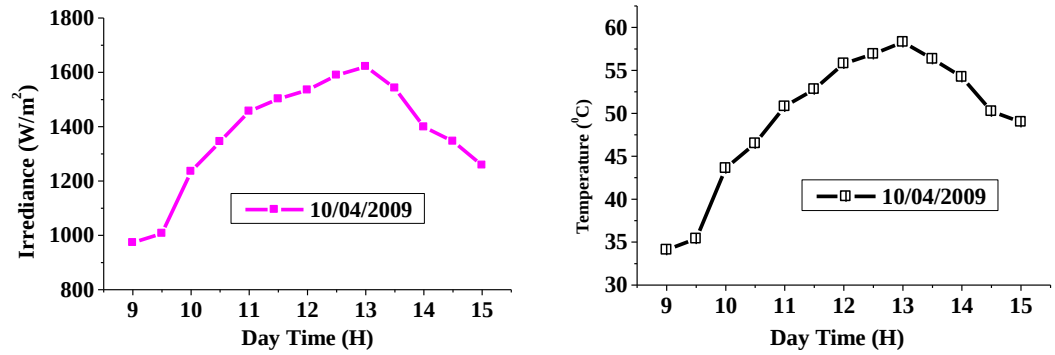

Fig 7. (a) Intensity with day time; (b) Cell temperature with day time

The main differences between the two dated curve are largely depends on the effect of both intensity and the atmospheric air mass. It has been seen that all parameter increases with the increase of intensity and decrease with respect to decrease. On the other hand, the increase of air mass causes decrease of all the parameter. Because at March 06, 2008 the season was winter in Bangladesh and April 10, 2009 the season was slightly summer. For that reason in March the sun rises about 20-32^0 from the east position with respect to Bangladesh position but in April it was 10-20^0.

The experimental measured variables were compared with those in case of fixed axis. The results indicate that there was an overall increase of output power about 30-45% for the two-axis solar-tracking system from the fixed PV system.

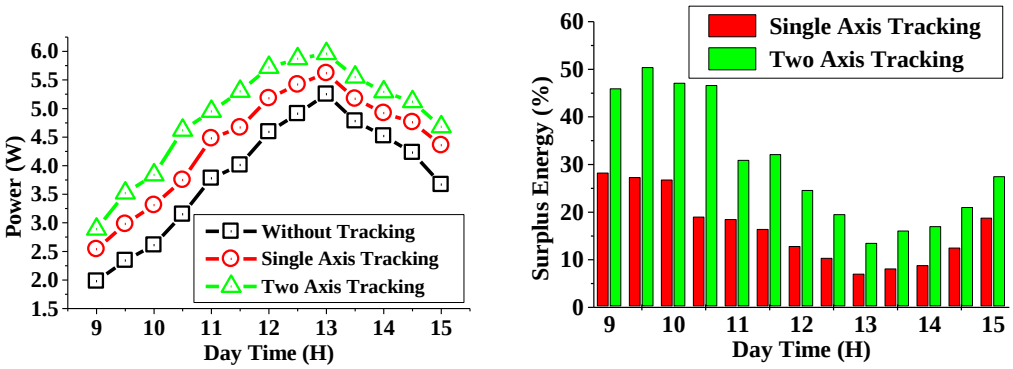

Fig. 8 (a) Power with day time; (b) Surplus energy with day time

In addition, there was an overall increase of output power about 15-23% for the single axis tracking system from the fixed tilted PV system [15]. The result obtained was approximately similar to the result found by results of George C. Bakoks (2004) designed a two axis solar tracking system for parabolic trough collector and compared the measured results with a fixed tilted trough and found that there was a surplus energy up to 46% [16].

4. Conclusion

In this research, a comparative study of experimental results are investigated on the effect of using two-axis solar tracking system and single axis solar tracking system of the PV power output.

From the result of the performance test of designed system the following conclusion can be drawn.

- The surplus output-power of the tracking solar panel with respect to fixed panel was 30-38% at average intensity 1100 W/m^2 and that of 15-25% for single axis solar tracking system i.e. about 15-18% excess energy is found from two axis solar tracking system compared with single axis solar tracking system.
- There is a design difficulties exists in the two axis solar tracker which increase the cost of fabrication.
- On the other hand the tracking electromechanical mechanism is very simple for single axis than two axis solar tracking system.
- There are no considerable difficulties in the software system for both cases.

References

[1] Chung HSH, Tse KK, Hui SYR, Mok CM, Ho MT, A novel maximum power point tracking technique for solar panels using a SEPIC or Cuk converter, IEEE Transactions on power electronics, vol. 18, no. 3, pp.717-724, 2003.

[2] HiyamaT et al. Evaluation of neural network based real time maximum power tracking controller goes PV systems, IEEE Transactions on Energy Conversion, vol. 10, no. 3, 1995.

[3] Huang F, Tien D, James O. A Microcontroller based Automatic Sun Tracker Combined with a New Solar Energy Conversion Unit, International Conference on Power Electronic Drives and Energy Systems for Industrial Growth, 1998, vol. 1, pp. 488 – 492.

[4] Mashohor S, Samsudin K, Noor AM, Rahman ARA. Evaluation of Genetic Algorithm based Solar Tracking System for Photovoltaic Panels, IEEE International Conference on Sustainable Energy Technologies, 2008, pp. 269 – 273.

[5] Koyuncu B, Balasubramanian K. A microprocessor controlled automatic sun tracker, EEE Transactions on Consumers Electronics, vol. 37, no. 4, pp. 913-917, 1991.

[6] Hayama T, Kouzuma S, Imakubo T. Identification of optimal operating of PV modules using neural network for real time maximum power tracking control. IEEE Transactions on Energy Conversion, vol.10, iss.2, pp. 360-7, June1995.

[7] Mashaly HM, Sharaf AM, Fuzzy logic controller for photovoltaic-utility interfacing scheme, In Proceedings of the 7th Mediterranean Electro technical Conference, 1994, vol. 2, pp. 715-18.

[8] Bingol O, Altinta A, Oner Y, Microcontroller based solar-tracking system and its implementation, Journal of Engineering Science, vol. 12, pp. 243-248, 2006.

[9] Yousef HA. Design and implementation of a fuzzy logic computer-controlled sun tracking system, in Proceedings of the IEEE International Symposium on Industrial Electronics, ISIE'99, vol. 3, pp. 1030-1034,1999.

[10] Yazidi A, Betin F, Notton G, Capolino GA. Low cost two-axis solar tracker with high precision positioning, in First International Symposium on Environment Identities and Mediterranean Area, ISEIMA'06, pp. 211-216, 2006.
[11] Damm J. An active solar tracking system, Home Brew Magazine, Issue #17, June/July 1990
[12] Rizk J, Chaiko Y. Solar Tracking System: More Efficient Use of Solar Panels, in proceeding of world academy of science, engineering and technology volume 31 July 2008 ISSN 2070-3740.
[13] Rai GD, Solar Energy Utilization Third Edition, Khanna Publishers Delhi-1100061987.
[14] Infield DG, Islam AKMS, Photovoltaic Technology for Bangladesh ISBN 98431-10854, pp. 87-88.
[15] Malodanado JA. Diseno y construccion de un sistema de control automatico para el posicionamiento de un pirheliometro. Memoria, Universidad Tecnica Federico Sunta Maria, Valparaiso, Chile, 1989.
[16] Maish AB, A self-aligning photovoltaic array tracking controller. In Proceedings of the 20th IEEE Photovoltaic Specialists Conference, 1988.

Appendix A. Comparison of algorithm

A.1. Software algorithm of single and two axis tracker

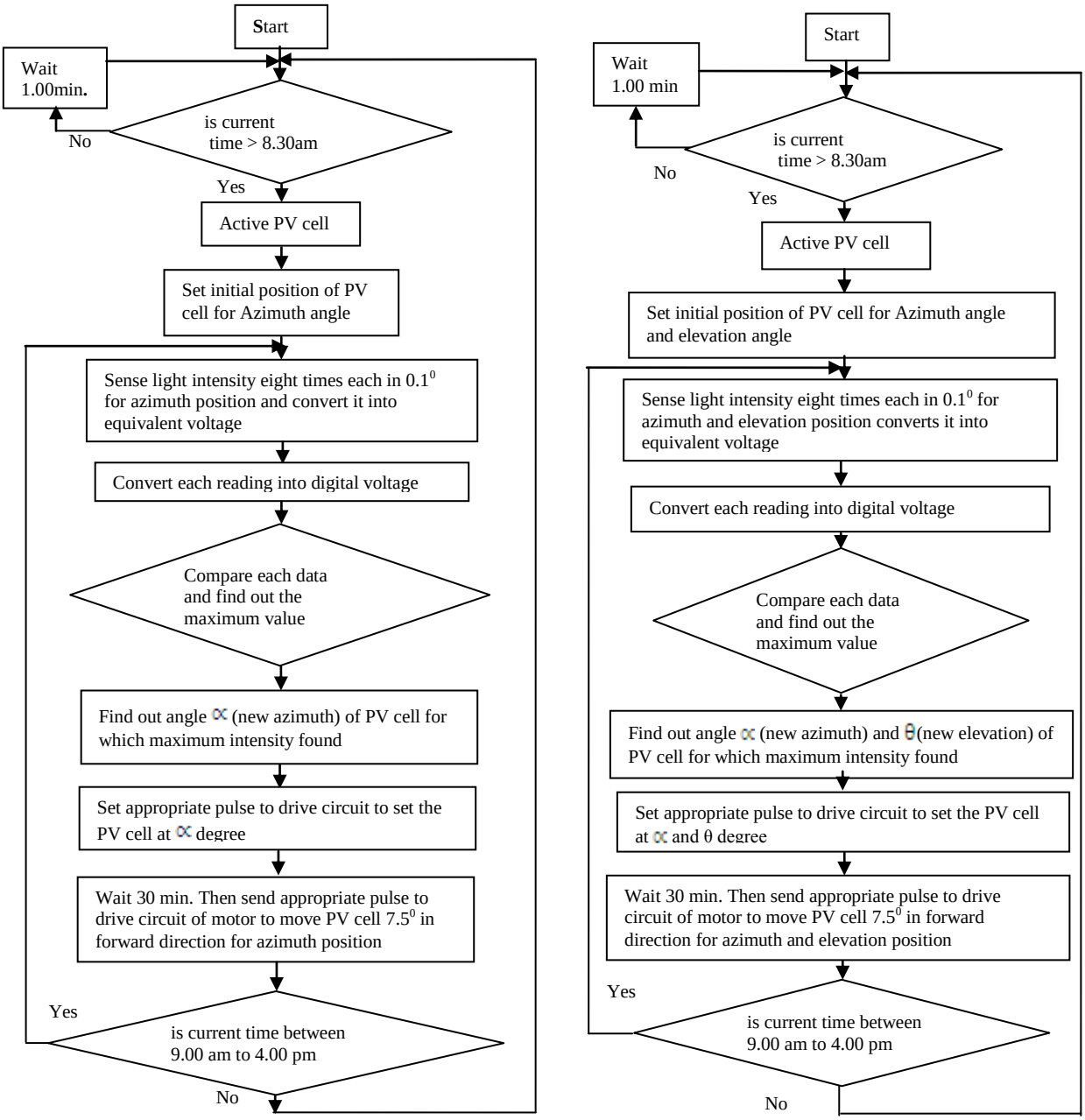

5th BSME International Conference on Thermal Engineering

Design and Fabrication of a Cost Effective Cyclone Separator

N. Nahar[a], M. A. Wazed[a], M. S. Rabbi[a], M. K. Islam[a,*]

[a]*Department of Mechanical Engineering, Chittagong University of Engineering and Technology (CUET), Chittagong 4349, Bangladesh*

Abstract

At present days air pollution is a great threat to human health. Major sources of air pollution are particulate matter, NOx, CO of various industries & mills. As the number of industries & mills increases, the concern of particulate pollution in the air also increases. The main objective of this project is to design and fabrication of a cyclone separator and to observe its functionality. Cyclone separator is a device that utilizes centrifugal forces caused by the spinning motion of gas to separate materials of differing density, size and shape. There are mainly two types of cyclone separators as axial and tangential. This project will deal with tangential type separator.

A cyclone separator of tangential type is fabricated. High speed rotating air or gas flow is established within the cyclone using a blower. Air or gas flows tangentially from top (wide end) of the cyclone and then spun rapidly. Flow pattern is helical in shape. Larger (denser) particles in the rotating stream have too much inertia to follow the tight curve of the stream. Again a centrifugal force is created by the circular airflow. This inertia & centrifugal force throw the dust particles towards the wall of the cyclone. Once the dust particle hits the wall it falls into a hopper below. 'Clean' exhaust is then blown through the vortex finder. It is observed that the separator is working well and clean air is obtained.

Keywords: Cyclone separator, Air pollution;

1. Introduction

The products of combustion of coal-fed (or any solid fuel) fires contain particles of solid matter floating in suspension [1]. This may be smoke or dust. Smoke indicates that the combustions are faulty and its proper remedy is in the design and management of the furnace. Dust particles such as fly ash may be mixed up with air. In many sensitive sectors such as establishment of petroleum industry, coal mining and handling operations, metal mining etc. dust free air is one of the primary requirements [2]. In power plant engineering the quantity and effect of the solid content in flue gas is one of the most considerable matters. There is always the possibility that adjacent residents may bring damage resulting from the fall of excessive ash or cinder on their premises. Nowadays there are legal restrictions on the dust content that may be emitted to the environment. Hence only a minimum amount of dust is allowed to emit into the environment. This controlled amount can be ensured only through separation technique. Hence dust separation from air and generally from flue gas is one of the most important considerations.

The removal of dust and cinders from air as well as from flue gas can usually be effected to the required degree by commercial dust collectors. There are some typical systems for the removal of particulates. These include (a) a sudden decrease in gas velocity, (b) an abrupt change in the direction of the gas flow, (c) the impingement of the gas stream on a series of baffles, and (d) the use of centrifugal force as in the 'cinder catchers' and are commonly used on stoker and small cyclone furnaces where crushed coal is burned rather than the very fine pulverized coal [3].

There are also more mechanical and electrical techniques of dust separation/collection. Electrical separators combine merits of cyclone precipitation and electrostatic precipitation. The basic idea is to use high voltage impulse electrostatic field in cyclone, when airflow with particles passes, the particles are separated from gas by centrifugal force and impulse electrostatic force. The mechanical collectors are subdivided into wet type and dry type.

Cyclone separators are commonly used for separating dispersed solid particles from gaseous Phase. Cyclone separator is used in dust separation technique due to its low capital and operating cost, simple construction & low maintenance, high dust load accepting capacity & its adjustability at high temperature. Therefore, they are widely used in Environmental Engineering to remove particulate pollutants, in Chemical Engineering and

* Corresponding author. Tel.: +880-1553-282819; fax: +880-31-714910.
E-mail address: awazed@gmail.com

Mechanical Engineering to collect valuable particle products, by Industrial Hygienists to sample particles in working environments, by Pharmaceutics to classify their powdered drugs. The main purposes of this article are to design a cyclone separator for high separation rate of dust from gas, to fabricate the designed cyclone separator and to measure its performance.

2. Design of Cyclone Separators

There are certain relationships among cyclone dimensions that should be observed for efficient cyclone performance, and which are generally related to the cyclone diameter. A cyclone separator uses inertial and gravitational forces to separate particulate matter from gas. The particle laden gas enters the cyclone separator with a high rotational velocity. The rotational flow then descends near the wall through the cyclone body and conical part until a reversal in the axial velocity making the gas flow in the upwards direction [4]. Where this occurs is called as the vortex end position. The upward rotating flow continues along the cyclone axis forming a double vortex structure. The inner vortex finally leads the flow to exit through a central duct, called the vortex finder. The vortex finder protrudes within the cyclone body [5]. It serves both in shielding the inner vortex from the high inlet velocity and stabilizing its swirling motion. The solids are separated due to the centrifugal force and descend helicoidally along the cyclone walls and leave the equipment through the exit duct.

In a typical cyclone separator, the gas-dust mixture enters the top cylindrical section of the cyclone through a tangential opening. It is essential that the particles must reach the wall of the cyclone before they can be recovered from the gas stream. The main areas of pressure loss in a cyclone are due to the contraction of the inlet and outlet ducts [6]. If the ratio of outlet area to inlet area is less than one, an increased pressure drop is experienced and the cyclone must be lengthened to avoid dust re-entrainment in the spiraling gas stream. In designing a cyclone separator relation of various parameters to cyclone efficiency should be considered.

Cyclone separators, the technology are commonly used for separating dispersed solid particles from gas phase. This section discusses about design and fabrication of a typical cyclone separator. A typical cyclone separator is shown in Fig. 1. The geometrical design of the cyclone separator is given in Table 1. For convenience, the dimensions of various cyclone parts are usually stated in dimensionless form as a ratio to the cyclone diameter, D is shown in Table 2.

3. Fabrication of the cyclone separator

Parts used in the construction are Elbow socket, Gate Valve, Plain Socket, T socket, one side threaded pipe (vortex finder), Top plate, Cyclone body, Cone section, Dust hopper, Vortex guide, Dust reservoir and Setup supporting Frame.

Elbow socket are used to connect two hollow pipes for continuation of fluid flow. 900 elbow socket is used here to connect the vortex finder with the exit pipe. The plain socket connects two pipes straightly. It ensures joint between two pipes. Tee socket are used to adjoin three pipes. In cycle separator, it makes joint of the inlet pipe, dust reservoir and gate valve. The gate valve is a valve that opens by lifting a round or rectangular gate/wedge out of the path of the fluid. Gate valves are primarily used to permit or prevent the flow of fluids. In the top portion of cyclone body a plate is used to cover the fluid flow and ensure that it pass through the exhaust pipe. The body, in which the air is forced to cyclone and makes it dust free, is the cyclone body. It is designed with specific dimensions to create such cyclone operation within the flow. GI (galvanized iron) pipe of specific dimension is used as cyclone body. A cone section (as shown in Fig. 1) made by metal sheet is placed at the bottom part of the cyclone body for removal of the dust from the cyclone body. Vortex Finder is a cylindrical pipe inserted inside the cylinder body which is fitted with top plate of the separator. Fresh air is (dust free air) exit to the environment through vortex finder after separation of dust. Its certain portion remain inside the cyclone body which some shorter in length than the body rest portion remain outside the body. A dust hopper which is a plastic box is used to collect the dust coming through the cone section. Vortex Guide is used to guide the air to create vortex in a specified direction. It is located just below the top plate and connected with inlet pipe. Its diameter is same as inlet diameter. It ensures a spiral path for the upcoming air containing dust. There must be some dust with air to make the experiment successful. So different kinds of dusts are placed in a conical dust reservoir and the dusts are made to mix with the air supplied by the blower. A frame made of mild steel is used to support the whole setup. It is strong enough to give support to the setup of the experiment. The dimension of different parts is given in Table 3. The complete set of the cyclone separator is shown in Fig. 2

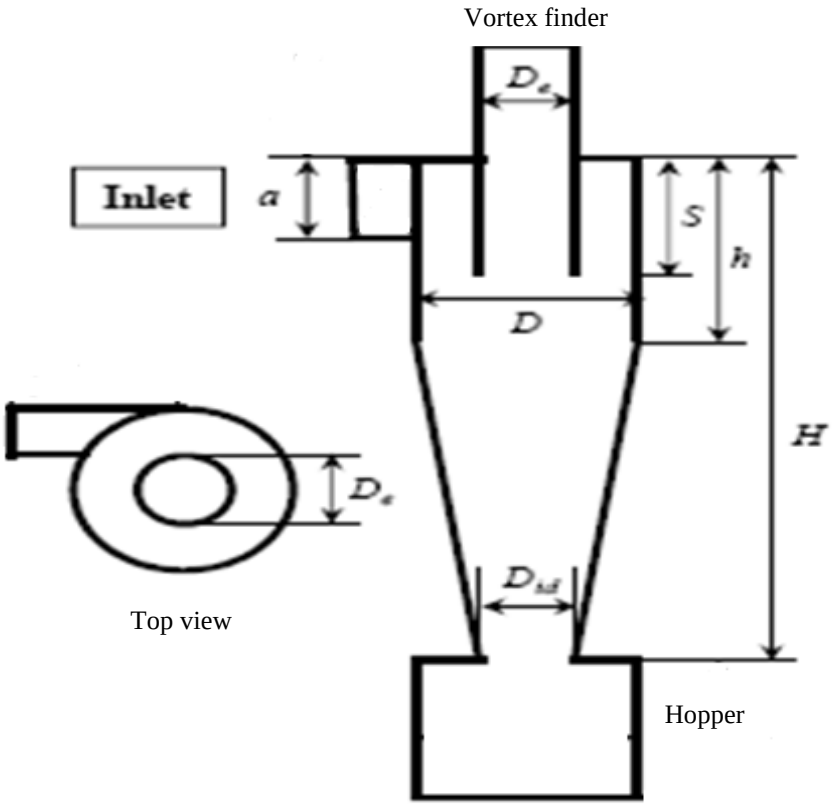

D = Cyclone diameter; a = Inlet diameter; De = Gas outlet diameter; s = Vortex finder length inside cyclone; h = cylinder length; H = Cyclone length; D_{id} = Duct collector (hopper) diameter

Fig. 1. A typical cyclone separator

Table 1. Geometrical design of cyclone separator

D	a/D	De/D	S/D	h/D	H/D	D_{id}/D
1	0.08	0.25	1.17	1.5	4	0.33

Fig. 2. Experimental setup

Table 2. Design dimensions

D cm	a cm	De cm	S cm	h cm	H cm	D_{id} cm
15.24	1.27	3.81	17.78	22.86	60.96	5.08

Table 3. Dimensions of different parts that are used in fabrication are given below

Serial	Name of the parts (material)	Dimensions
01	Elbow socket (GI)	2” dia
02	Plain socket (GI)	0.5”dia
03	Tee socket (GI)	0.75” dia
04	Gate valve	0.75” dia
05	Vortex finder: One side threaded GI pipe	1.5” dia 9” length, 7” inside the cyclone body
06	Top plate	6” dia × 0.25” thick
07	Cyclone body (GI pipe)	6”dia × 9” length
08	Cone section (GI sheet)	Upper section: 6” dia; Lower section :2.5”dia Length:15”
09	Dust hopper (plastic pot)	Approximately 8” length
10	Vortex guide (GI pipe)	0.5” dia
11	Setup supporting frame (mild steel)	0.75” thick angle bar and 0.375” flat bar

4. Performance analysis

The collection efficiency is used to measure the performance of the cyclone separator. The fraction of solids separated at the outlet is defined as the collection efficiency. The swirling motion within the cyclone separator causes large particles to travel swiftly to the cyclone walls and roll down to the outlet. On the other hand, the smaller particles are often drifted in upward spiral flow due to the slower speed and escape through the gas outlet. The collection efficiency is a primary measure of the performance of a cyclone separator and depends on the operating conditions and the geometrical characteristics. Table 4 shows the effects of various parameters on the efficiency.

Table 4. Impact of various parameters on cyclone efficiency

Parameter	When parameter increases, cyclone efficiency...
Cyclone body diameter compared to body length	Decreases
Ratio of cyclone body length to diameter	Increases
Smoothness of cyclone inner wall	Increases
Gas inlet duct area	Decreases
Gas exit pipe diameter	Decreases

It is observed that the smaller particles (< 10μm) tend to be dispersed and hauled by the gas flow and escape from the vortex finder at the top of the cyclone separator. But on increasing the particle mass loading, a sweeping effect of the coarser particle is observed. The swept particles then roll down and are collected at the bottom of the cyclone. This effect is also responsible for the formation of agglomerates. Agglomeration causes increased centrifugal force on the smaller particles improving their collection efficiency.

The inlet gas velocity also has an effect on the collection efficiency (Fig. 3). The collection efficiency increases with the inlet gas velocity. For smaller particle sizes (< 10 μm), the increase in the efficiency with respect to the gas velocity is more pronounced. As the particle size increases, the effect of the inlet velocity becomes insignificant.

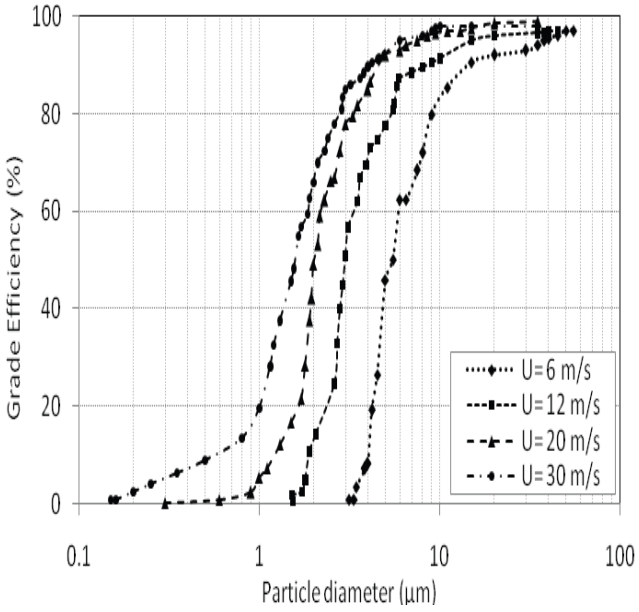

Fig. 3. Grade efficiency for different inlet velocity

5. Conclusions

From this research, it is concluded that-

- The cyclone separator is functioning well.
- As the GI pipes are used as main fabrication material the overall cost is economical.
- Fabrication technology is very simple, so it can be fabricated in a workshop.

References

[1] Frederick T. Morse, M.E., E.E. Power Plant Engineering. New Jersey: D. VAN NOSTRAND COMPANY, INC., June 1953.

[2] Md. Monir-Uz-Zaman and Sumon, Effect Of EGR and Cyclonic Separator on Emissions in DI Diesel Engine, Undergraduate Thesis, Rajshahi University of Engineering & Technology, 2009.

[3] Atakan Avci, Irfan Karagoz (2003), Effects of Flow and Geometrical Parameters on the Collection Efficiency in Cyclone Separators, Journal of Aerosol Science, 34, 937-955.

[4] Chuen-Jinn Tsai, Daren-Ren Chen, HungMin Chein, Sheng-Chieh Chen, Jian-Lun Roth, Yu-Du Hsu, Weiling Li, Pratim Biswas (2004), Theoretical and Experimental Study of an Axial Flow Cyclone for Fine Particle Removal in Vacuum Conditions, Journal of Aerosol Science, 35, 1105-1118.

[5] Utikar1, R., Darmawan1, N., Tade, M., Li, Q, Evans, G., Glenny, M. and Pareek, V. Hydrodynamic Simulation of Cyclone Separators

[6] Jiwu Lia, Weijian Cai, Bingyan Dong (2003), Study of solid–gas separation mechanism of cyclone with impulse excitation, Journal of Electrostatics, 57, 225–232.

5th BSME International Conference on Thermal Engineering

Finite Element Analysis on MHD Mixed Convection in a Lid-Driven Cavity with Semi-Circular Heater

A.K. Azad[a,] *, M.J.H. Munshi[b] M.M. Billah[c], M.M. Rahman[d]

[a]*Department of Business Administration, International Islamic University, Chittagong, Bangladesh*
[b]*Department of Mathematics, Hamdard University Bangladesh, Gazaria, Munshiganj, Bangladesh*
[c]Department of Arts and Sciences, *Ahsanullah University of Science and Technology (AUST), Dhaka-1208, Bangladesh Bangladesh*
[d]*Department of Mathematics, Bangladesh University of Engineering and Technology, Dhaka-1000, Bangladesh*

Abstract

A numerical analysis is conducted on MHD mixed convection in a lid-driven enclosure with a heated semi-circular heater on one wall under constant heat flux. The horizontal walls are assumed to be adiabatic. The left wall of cavity moves upward direction and buoyancy forces are also effective. Temperature of the moving wall, which has constant flow speed, is lower than that of the semi-circular heater. A uniform horizontal magnetic field is assumed to be applied to the fluid. The governing equations along with boundary conditions are expressed in a normalized primitive variables formulation. Finite element method is used in solution of the normalized governing equations. The dimensionless governing parameters affecting the velocity and temperature profiles are the Rayleigh number, Hartmann number. It is found that average Nusselt number can be decreased with increasing of Rayleigh number in the presence of magnetic field. The magnetic field is also a good control parameter for heat transfer and fluid flow.

***Keywords*:** lid-driven cavity, semi-circular heater, mixed convection and finite element method.

Nomenclature

B_0	magnetic induction (Tesla)	x, y	dimensional coordinates (m)
D	drag force	X, Y	dimensionless coordinates
g	gravitational acceleration (ms^{-2})	V_0	lid velocity (ms^{-1})
Ha	Hartmann number	$\bar{V}$	cavity volume (m^3)
k	fluid conductivity ($Wm^{-1}k^{-1}$)	*Greek symbols*	
L	length of the cavity (m)	α	thermal diffusivity (m^2s^{-1})
L_s	Length of the semi-circular (m)	β	thermal expansion coefficient
Nu	Nusselt number	σ	electrical conductivity (Sm^{-1})
p	dimensional pressure (Nm^{-2})	μ	dynamic viscosity (Kg $m^{-1}s^{-1}$)
P	non-dimensional pressure	ν	kinematic viscosity (m^2s^{-1})
Pr	Prandtl number	θ	non-dimensional temperature
Re	Reynolds number	ρ	density (kgm^{-3})
Ra	Rayleigh number	*Subscripts*	
T	temperature (K)	h	hot
u, v	dimensional velocity components (ms^{-1})	c	cold
U, V	dimensionless velocity components		

* Corresponding author. Tel.: +8801552556549; fax: +880-2-8613046.
E-mail address: azadmacu@gmail.com

1. Introduction

Natural convection heat transfer in enclosures is important from both theoretical and practical points of view. It is important to analyze cooling of electronic equipment, solar energy, heating and cooling of buildings, geothermal applications and heat exchangers. Magnetic force is one of several forces that may influence natural convection in an enclosure. The influence of magnetic forces on natural convection employing electrically conducting fluids causes significant changes on the temperature and flow distribution [1]. Kahveci and Oztuna [2] studied the problem of MHD natural convection in a laterally heated partitioned enclosure. Oztop et al. [3] studied the effects of non-isothermal boundary condition of MHD flow in a square enclosure. Chamkha [4] studied the MHD combined convection flow in a lid-driven cavity with internal heat generation or absorption for steady, two-dimensional, laminar flow. Rahman et al. [5] studied the effects of magnetic field with Joule effect in a lid-driven cavity with a circular body insertion. Sivasankaran et al. [6] made a numerical work by using finite volume technique on mixed convection in a square cavity of sinusoidal boundary temperatures at the sidewalls in the presence of magnetic field. Basak et al. [7] performed a penalty finite element analysis with bi-quadratic elements to investigate the effects of uniform and non-uniform heating of inclined walls on natural convection flows within an isosceles triangular enclosure.

The main aim of this work is to present the effects of magnetic field in a heated semi-circular object attached to a wall of square lid-driven cavities. The main contribution of this study to literature is to examine of effects of heated semi-circular cavity under magnetic force.

2. Physical Model

Fig. 1 shows the schematic of the system under consideration. It is a two-dimensional square cavity of length L. The left wall of the cavity is allowed to moves upward direction in its own plane at a constant velocity V_0 and to be kept at a constant temperature Tc. The right wall is the source for heat with a heated semi-circle at constant temperature T_h. Horizontal walls is assumed to be adiabatic and impermeable. The fluid is assumed to be electrically conducting, while walls of the cavity are considered to be electrically insulating. Still, gravity acts in vertical directions and magnetic field with uniform strength B_0 is effective in the horizontal direction normal to the moving wall. The magnetic Re is assumed to be small so that the induced magnetic field is neglected and the Hall effects of magneto-hydrodynamics are to be negligible. All fluid physical properties are assumed to be constant except the density variation in the body force term of the momentum equation according to the Boussinesq approximation.

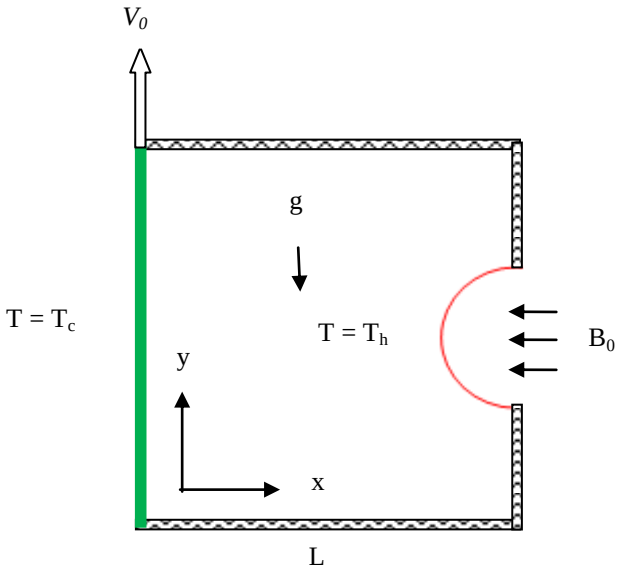

Fig. 1. Schematic diagram for the problem with boundary conditions

3. Mathematical Formulation

The governing equations for the problem under consideration are based on the balance laws of mass, momentum and thermal energy in two dimensions. Following the previous assumptions, these equations can be written in non-dimensional form as:

$$\frac{\partial U}{\partial X}+\frac{\partial V}{\partial Y}=0 \tag{1}$$

$$U\frac{\partial U}{\partial X}+V\frac{\partial U}{\partial Y}=-\frac{\partial P}{\partial X}+\frac{1}{Re}\left(\frac{\partial^2 U}{\partial X^2}+\frac{\partial^2 U}{\partial Y^2}\right) \tag{2}$$

$$U\frac{\partial V}{\partial X}+V\frac{\partial V}{\partial Y}=-\frac{\partial P}{\partial Y}+\frac{1}{Re}\left(\frac{\partial^2 V}{\partial X^2}+\frac{\partial^2 V}{\partial Y^2}\right)+\frac{Ra\,\theta}{Re^2 Pr}-\frac{Ha^2}{Re}V \tag{3}$$

$$U\frac{\partial \theta}{\partial X}+V\frac{\partial \theta}{\partial Y}=\frac{1}{Re\ Pr}\left(\frac{\partial^2 \theta}{\partial X^2}+\frac{\partial^2 \theta}{\partial Y^2}\right) \tag{4}$$

where the dimensionless variables are introduced as:

$$X=\frac{x}{L},Y=\frac{Y}{L},U=\frac{u}{V_0},V=\frac{v}{V_0},P=\frac{p}{\rho V_0^2}\ and\ \theta=\frac{T-T_c}{T_h-T_c}$$

The variables have their usual sense in fluid mechanics and heat transfer as listed in the nomenclature. As can be seen from the Eqs. (2) - (4), five parameters that preside over this problem are the Reynolds number (*Re*), Rayleigh number (*Ra*), Prandtl number (*Pr*), Hartmann number (*Ha*), which are defined respectively as

$$Re=\frac{V_0 L}{\nu},\ Pr=\frac{\nu}{\alpha},\ Ra=\frac{g\beta\left(T_h-T_c\right)L^3}{\nu\alpha},Ha=B_0 L\sqrt{\sigma/\mu}$$

The dimensionless boundary conditions corresponding to the considered problem are as follows:

on the top and bottom walls: $U=V=\frac{\partial\theta}{\partial N}=0$

on the left vertical wall: $U=\theta=0,V=1$

on the right vertical wall except semi-circular: $U=V=\frac{\partial\theta}{\partial N}=0$

on the semi-circular: $U=V=0,\theta=1$

where *N* is the non-dimensional distances either *X* or *Y* direction acting normal to the surface.

The average Nusselt evaluated along the heated surface of the cavity based on the dimensionless quantities may be expressed as

$Nu=-\frac{1}{L_s}\int_0^{L_s}\frac{\partial\theta}{\partial X}dY$ and the average temperature of the fluid is defined as $\theta=\int\theta\,d\bar{V}/\bar{V}$, where $\bar{V}$ is the cavity volume.

4. Solution Scheme

In this investigation, the Galerkin weighted residual method of finite-element formulation is used as a numerical procedure Basak et al. [8]. The finite-element method begins by the partition of the continuum area of interest into a number of simply shaped regions called elements. These elements may be different shapes and sizes. Within each element, the dependent variables are approximated using interpolation functions. In the present study, erratic grid size system is considered especially near the walls to capture the rapid changes in the dependent variables. The coupled governing equations (2)-(5) are transformed into sets of algebraic equations using the finite-element method to reduce the continuum domain into discrete triangular domains. The system of algebraic equations is solved by iteration technique. The solution process is iterated until the subsequent

convergence condition is satisfied: $\left|\Gamma^{m+1}-\Gamma^{m}\right|\leq 10^{-6}$ Where, m is number of iteration and Γ is the general dependent variable.

A trial calculation is made using various non-uniform grids of triangular elements: 2980, 4602, 6676, 8874 and 9402 in order to obtain grid independent solutions as shown in Fig. 2. These experiments reveal the magnitude of average Nusselt number Nu for 4602 elements illustrates a very slight difference with the results obtained for the other higher elements. Finally 4602 elements is selected for the balance between the calculation accuracy and the speed. The comparison of the calculated average Nusselt number using the present numerical code for Ra = 10^6, X_p = 0.5, w = 0.1 and k = 0.001 with the published work done by Kahveci [9]. The present study was modified according to Kahveci's case. Comparatively good agreement is found as shown in Table 1. We are, therefore, confident that the results reported in our paper are accurate.

Table 1. Comparison of Nusselt number between present study and Kahveci [9] for *Ra* = 10^6, X_p = 0.5, w = 0.1 and k = 0.001

Kahveci [9]		Present work	
Partition wall	Cold wall	Partition wall	Cold wall
1.63	1.94	1.65	1.93

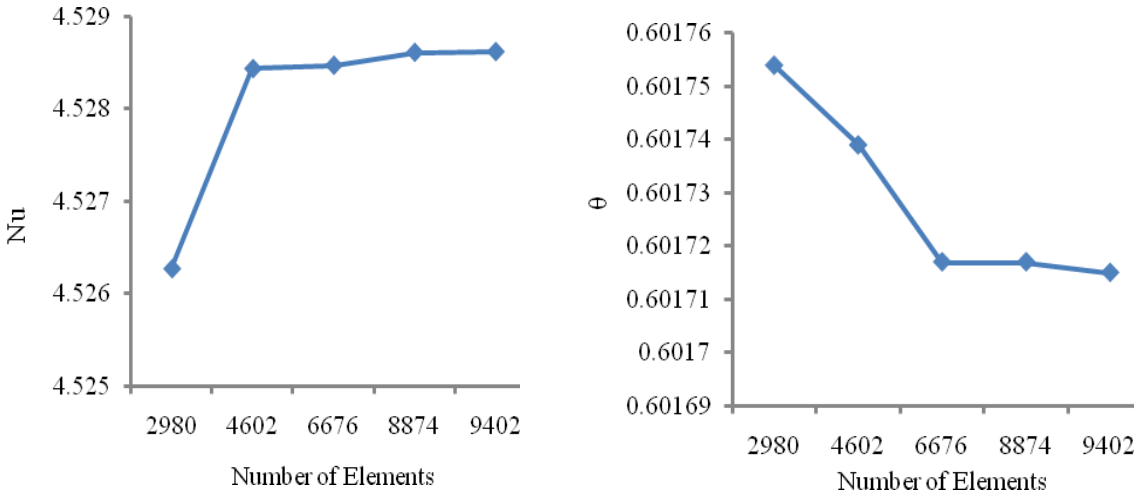

Fig. 2. Average Nusselt number (left) and bulk temperature (right) for different grid elements with Ra = 10^5. and Ha = 10

5. Results and Discussion

A computational analysis has been performed to investigate the effects of magnetic field on natural convection in semi-circular heated pipe inserted enclosures using finite element method. The effective parameters are Hartmann number, Rayleigh number and distance between heaters. Results will be present via streamline, isotherms, average Nusselt numbers and average fluid temperature.

Fig. 3 lists the effects of Hartmann number on streamlines (left column) and isotherms (right column) for and Ra = 10^5. As seen from the figure, double cells are formed inside the enclosure. The left cell (clockwise direction) is created by moving wall due to its shear effects on fluid and the main cell (counterclockwise direction) is formed with the presence of buoyancy forces. Due to presence of heated semi-circular shaped object, the flow impinges on the bottom side of the object and it shows streamlined behavior due to curved boundary. The figure is also showed that the Hartmann number is an effective parameter on streamlines. The elongated cell is broken and a small two cells were formed with increasing of Hartmann number. The location of the main cell is changed from left side to the top. The flow strength is also decreased with increasing of

Hartmann number. These results are supported by Chamkhas study [10]. Also, thin temperature boundary layer is formed for low Hartmann number as seen from isotherms and they are more parallel to the vertical wall for the highest value of Hartmann number. The thermal boundary layer becomes stronger at the bottom of the heated circle than the top due to stagnation point and maximum velocity of that area.

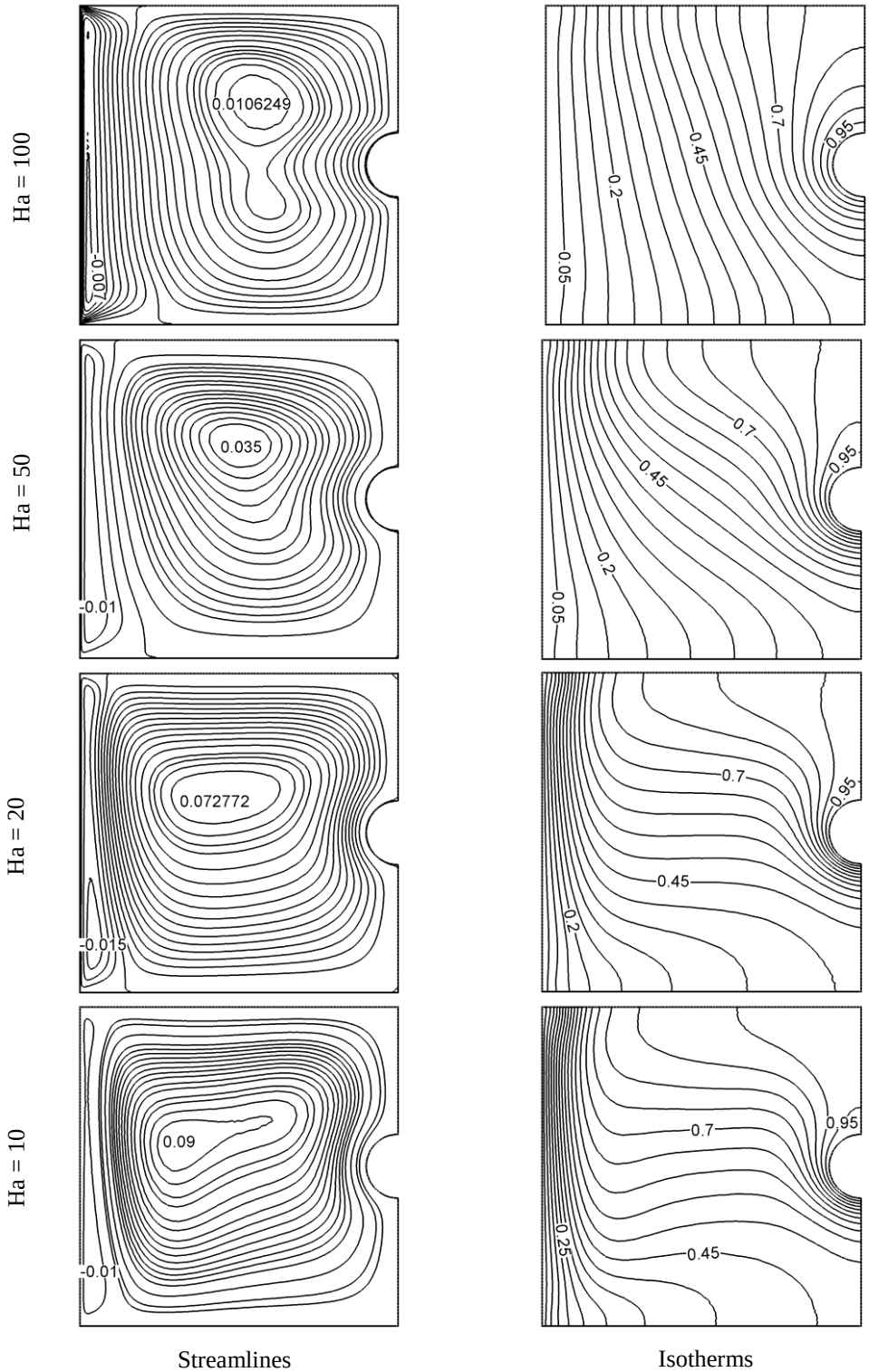

Fig. 3. Effect of Hartmann number on streamlines and isotherms, while Ra = 10^5.

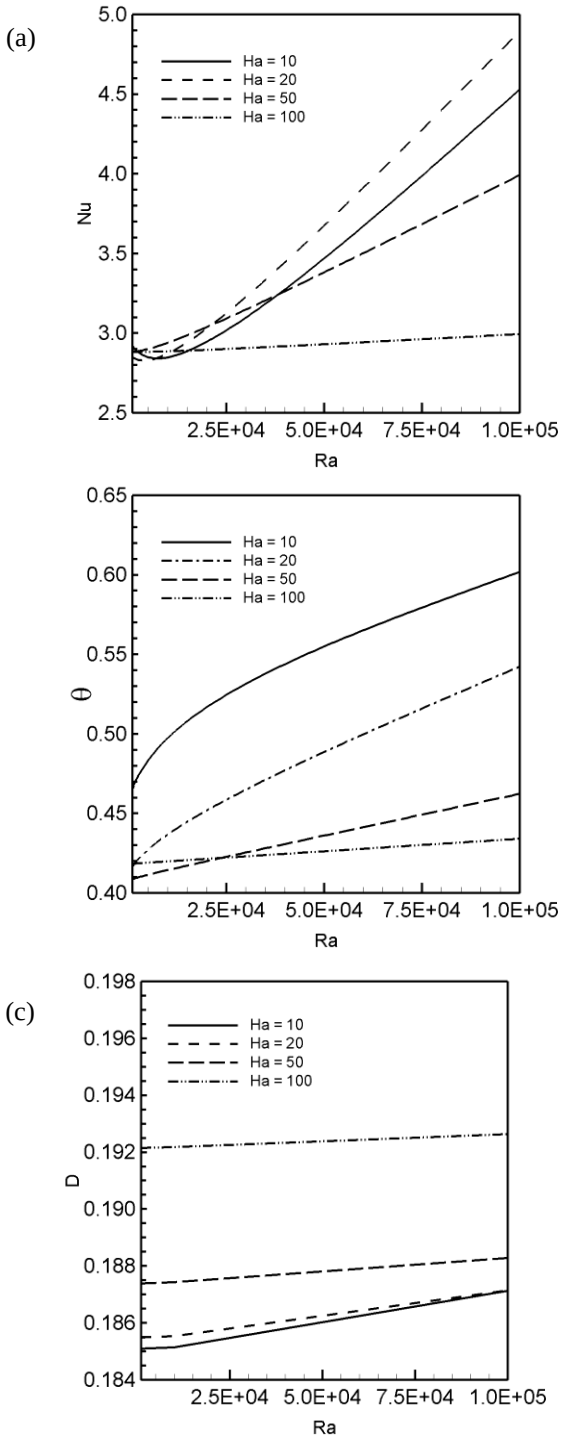

Fig. 4. a) Average Nusselt number, b) Average fluid temperature, c) Drag force, for different Rayleigh numbers and Ha numbers.

The average Nusselt number *Nu* is calculated along the hot surface, which is a measure of the overall heat transfer rate, is plotted in Fig. 4(a) as a function of Rayleigh number for the aforementioned values of Hartmann number. The average Nusselt number increases sharply for the lower values of *Ha* (= 10 and 20) and mildly for the highest values of Ha (= 50) with the increasing *Ra*. Moreover, the values of *Nu* are always highest for the value of *Ha* (= 20). As seen from the figure, Hartmann number becomes insignificant for low values of Rayleigh number due to domination of forced convection. Average Nusselt values are almost same for the considered values of *Ra* at Ha (= 100). It means that it is a specific case that the flow due to moving lid is not affected at this value of Hartmann number. In any case, the figure summarized that Hartmann number of the cavity with

moving lid can be a control parameter for heat transfer. The effect of Hartmann number on average fluid temperature in the enclosure is shown in Fig. 4(b). The average fluid temperature θ increases strictly for the lower values of Ha (= 10 and 20) and moderately for the higher values of Ha (=50 and 100). The drag force is plotted in Fig. 4(c) for different Rayleigh numbers. As seen from the figure, the drag force show linear increment with Rayleigh number for all values of Hartmann number and its value increase with increasing of Hartmann number due to increasing of shear stress.

6. Concluding Remarks

Mixed convection heat transfer and fluid flow in a two-dimensional lid-driven cavity with a heated semi-circular object on the wall is investigated numerically for a wide range of governing parameters. Effects of magnetic field are investigated on mixed convection. The governing equations were solved using finite element method. The obtained results showed that the flow field and temperature distribution are affected from the magnetic field. The flow strength and heat transfer are decreased with increasing of Hartmann number. The drag forces are also affected from the magnetic field. The heated semi-circular object can be cooled via cold lid-wall. It shows a familiar behavior with fluid for low values of Rayleigh number and does not affect the fluid near the lid.

Acknowledgements

The authors like to express their gratitude to the department of Business Administration, International Islamic University, Chittagong, Bangladesh.

References

[1] Ogut, E.B., 2010. Magnetohydrodynamic natural convection flow in an enclosure with a finite length heater using the differential quadrature (DQ) method, Numerical Heat Transfer, Part A 58, p. 900.

[2].Kahveci, K., Oztuna, S., 2009. MHD natural convection flow and heat transfer in a laterally heated partitioned enclosure, European J. Mechanics B/Fluids 28, p. 744.

[3] Oztop, H.F., Oztop, M., Varol, Y., 2009. Numerical simulation of magnetohydrodynamic buoyancy-induced flow in a non-isothermally heated square enclosure. Comm. in Nonlinear Sci. Numerical Simulation 14, p. 770.

[4] Chamkha A.J., 2003. Hydromagnetic combined convection flow in a vertical lid-driven cavity with internal heat generation or absorption, Num. Heat Transfer, Part A 41, p. 529.

[5] Rahman, M.M., Alim, M.A., Sarker, M.M.A., 2010. Numerical study on the conjugate effect of joule heating and magneto-hydrodynamics mixed convection in an obstructed lid-driven square cavity, Int. Comm. Heat Mass Transfer 37, p. 524.

[6] Sivasankaran, S., Malleswaran, A., Lee, J., Sundar, P., 2011. Hyro-magnetic combined convection in a lid-driven cavity with sinusoidal boundary conditions on both sidewalls, Int. J. Heat Mass Transfer 54, p. 512.

[7] Basak, T., Roy, S., Babu, S.K., Balakrishnan, A.R., 2008. Finite element analysis of natural convection flow in a isosceles triangular enclosure due to uniform and non-uniform heating at the side walls, Int. J. Heat Mass Transfer 51, p. 4496.

[8] Basak, T., Roy, S., Paul, T., Pop, I., 2006. Natural convection in a square cavity filled with a porous medium: effects of various thermal boundary conditions, Int. J. Heat Mass Transfer 49, p. 430.

[9] Kahveci, K., 2009. Natural convection in a partitioned vertical enclosure heated with a uniform heat flux, J. Heat Transfer 129, p. 717.

[10] Chamkha, A.J., 2003. Hydromagnetic combined convection flow in a vertical lid-driven cavity with internal heat generation or absorption, Num. Heat Transfer, Part A 41, p. 529.

5th BSME International Conference on Thermal Engineering

Fabrication of continuous flow down draught rice husk gasifier

Dr. Md. Arefin Kowser[a*], Nayeem Md. Lutful Huq[b], Dr. Hasan Mohammad Mostofa Afroz[b]

[a,b]Department of Mechanical Engineering, Dhaka University of Engineering and Technology, Gazipur-1700, Bangladesh

Abstract

Bangladesh is an agriculture based developing country. Most of the people of this country are farmers and they mostly grow paddy in several seasons. Huge amount of rice husks are produced from paddy which create a significant disposal. Although some rice husks are used as fuel for cooking, boiling paddy, electricity generation, and other purposes, but in most of these applications the maximum energy loss occurs due to inefficient burning process. To utilize maximum energy, rice husks should be burned properly. Down draught rice husk gasification is one of the systems where rice husks are burned properly for the utilization of maximum energy. In the present work, a down draught rice husk gasifier is fabricated, where; primary gasification air is introduced above the oxidation zone in the gasifier. The producer gas is removed at the bottom of the apparatus, so that fuel and gas move in the same direction. Using the rice husk gasifier a continuous flow gas is produced which ensures a continuous supply of usable form of energy. In this method once the processes is started it can be kept running as long as needed. The burnt solid waste is removed automatically after a certain period. As it gives efficient energy conversion it leaves a less environmental impact. Thus the system has made the burning process a user and environment friendly one.

Keywords: Rice husk gasifier, reactor, Energy efficient, Continuous flow, Environment friendly;

1. Introduction

Alternative energy sources, like biomass, have become the point of interest to the people around the world. This is because the supply of fossil fuel is becoming scarce, causing its price to be high enough for domestic as well as for industrial usage. In addition to this, emission of burnt gases, brought about by the production of these fossil fuels, create a lot of problems to the environment.

An agricultural residue that could be utilized in a large number of countries for the recovery of energy because of its reasonably high energy content (12–18MJ/kg) is rice husk. Large quantity of rice husk is generated annually as the major by-product of rice milling industry. The total annual rice production worldwide is about 500 million tones [1]. Assuming 20% rice husk recovery rate from rice grains [2] the annual rice husk production of about 100 million tonnes. Kandpal TC *et. al.*, 1996 carried out a work for testing the viability and estimated per unit electricity production cost to be 0.05-0.2 USD [3].

Near about 7 million tons of rice husk is produced in Bangladesh per year. Despite the increasing trend of the rice husk surplus, proper methods of its utilization are yet to be developed. Many countries have imposed new regulations to restrict field burning of rice husks, primarily for environmental reasons. Consequently, this has increased the interest in the utilization of rice husk as a renewable source of energy [4]. Moreover converting rice husk into gaseous or liquid fuels will be beneficial to the countries who have no conventional energy resources and whose economies are tied to agriculture and local industries.

Gasifying rice husk means, burning it with limited amount of air. Several studies in the past revealed that a bluish-flame gas can be generated from rice husk when gasified. Using the biomass as a source of energy was started in early 1980s [5]. At that time the EERC conducted a series of research projects involving the utilization of sunflower hulls, wood residue, and sewage sludge for power using both combustion and gasification technologies. In the year 1999 Ghaly AE *et. al.*, 1999 [6] used a dual distributor type fluidized bed gasifier for producing fuel gas. The San San Rice husk Gasifier Stove developed in Myanmar, 2005, offers smokeless combustion of rice husk in an efficient manner [7]. Alexis TB *et. al.*, in the year 2010 designed a continuous flow rice husk gasifier for thermal applications, such as, cooking, drying etc. [8].

Corresponding Author: Dr. Md. Arefin Kowser. Tel.:+880 1754262832, Fax: +88029204710
E-mail address: nadimduet@yahoo.com

Thus attempts have been made in several rice producing countries in Asia to develop rice husk gasification plants. However, this technology is still not well proven till today and the problems are still arising even in the commercial systems. Further research and development work needs to be undertaken to improve this technology.

Nomenclature	
CFRHG	Continuous Flow Rice Husk Gasification
CRH	Carbonized rice husk
DAQ	Data acquisition
EERC	Energy and Environmental Research Center
RHA	Rice husk ash

1.1. Objectives

The main objective of this work is to fabricate a feasible rice husk gasifier working in a controlled temperature below 1000 K to produce syngas. Laboratory and bench scale rice husk gasification experiments were conducted in the present study to develop an operationally simple and economically attractive process.

2. Background

Around 20% of the paddy weight is husk. In 2008, 132 million tons of rice husk were produced. But, it is often considered as a waste product in the rice mill and therefore is often either burnt in the open field or dumped on wasteland. Husk has a high calorific value and thus can be used as a source of renewable energy.

2.1. Characteristics of rice husk

- Rice husk is difficult to ignite and it does not burn easily with open flame unless air is blown through the husk. It is highly resistant to moisture penetration and fungal decomposition. Husk therefore makes a good insulation material.
- Rice husk has a high silica (SiO_2) contents which means that it decomposes slowly when brought back to the field.
- Handling of rice husk is difficult because it is bulky and dusty. It has an angle of repose of about 40°-45° which indicates that it's flow ability, e.g. in feed hoppers is very poor.
- It has low bulk density of only 70-110 kg/m³, 145 kg/m³ when vibrated or 180kg/m³ in form of pellets. It thus requires large volume for storage and transport capacity, which makes the transportation over long distances uneconomical.
- It has a high average calorific value of 3410 kcal/kg and therefore is a good, renewable energy source.

3. Fabrication

The gasifier was fabricated using the available materials in Bangladesh so that the system can be constructed at any corner of the country economically.

3.1. Reactions in gasifier

Table 1. Principal chemical reactions in a gasifier

Reaction type	Reaction
Combustion	$C + O_2 = CO_2$
Water gas	$C + H_2O = CO + H_2$
Water shift reaction	$CO + H_2O = CO_2 + H_2$
Boudouard reaction	$C + CO_2 = 2CO$
Methane reaction	$C + 2H_2 = CH_4$

3.2. Main components of CFRHG

- Feed hopper
- Reactor
- Blowers
- Burner
- Char chamber
- Scraping system
- Data acquisition system
- Support frame

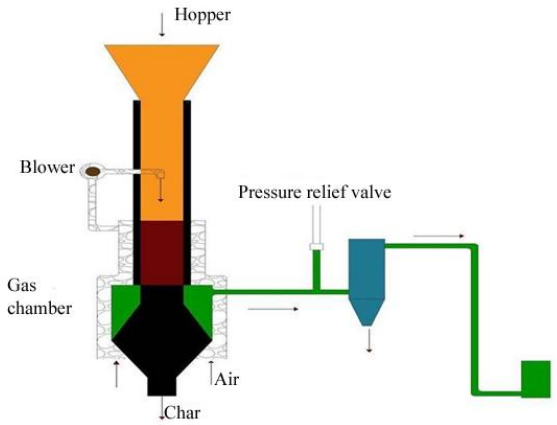

Fig. 1. Schematic diagram of CFRHG

3.3. Important data about CFRHG

Table 2. Major operational data

Parameter	Dimension
Reactor diameter (cm)	25
Startup time (min)	15-25
Rice husk consumption (kg/hr)	8
Gas temperature (^{o}C)	90-130
Air temperature (^{o}C)	20-25
Flame temperature (^{o}C)	400-800

The gasifier, as schematically shown, has the following components: a 25cm diameter by 110-cm high single reactor, where rice husk is gasified using limited amount of air for combustion; a feeding hopper situated directly above the reactor that feeds rice husks by gravity mode; a char chamber positioned directly beneath the reactor used to hold burnt rice husks and also served as an exit duct for combustible gases to the burner; a char separator attached to the char chamber for cleaning the gas leaving the reactor before the gas enters the burner; and an air injector positioned beneath the char chamber to gradually remove the char from the chamber pneumatically through a cyclone separator. An electric blower supplies the air needed for gasification and an electric motor drives the pneumatic conveyor.

3.4. Description about Individual parts

3.4.1. Fuel Feeding System

The feed hopper is a conical part that serves as the temporary storage for rice husk. It is located on the top of reactor. This device is provided with a door that can be opened for easy disposal of rice husk. The funnel shaped hopper, which serves as a reservoir for the fuel material, has a capacity of about 15 kg of rice husk.

3.4.2. Air supply system

The air is supplied to the reactor by two identical supply units. Each unit consists of a blower, a pressure valve, a main valve to control the air flow rate, a bypass valve to prevent overheating of the electric motor, and a steel pipe having an inner diameter of 50 mm. Each blower inlet has a filter with a micron rating of 25 and a maximum flow of 7.08 m^3/min. The filter cleans the incoming air from contaminants, such as, dust particles, water etc. The primary air supply (from blower 1) is used to supply air to the after burner, whereas the secondary air supply (from blower-2) is used to create a jet of air within the secondary column which carries the bed material (char).

3.4.3. Start-up system

The start-up burner is used to burn the rice husk initially .It works by a spark plug. The start-up unit does not work until both the air supply and the ignition systems are turned on. Rice husk should be combusted at temperatures not above 800°C, provided that there are no hot spots or localized high temperatures, which in practice (in directly fired furnaces/gasifiers) is not possible. This requires a large grate area and quick dissipation of heat. So burner should have an ability to resist 800°C. A net is used to support the weight of husk.

3.4.4. Reactor

Since the rice husks gasifier operates at relatively high temperature inside the reactor, the amount of CO_2, also known as the greenhouse gas, varies from 5 to 15% which is half of the amount derived when rice husks are burned by direct combustion. The heating value of gas ranges from 1200 to 1400 kcal/m^3, with measured black carbon content of 10 to 50 gm/m^3 and tar content of 56 to 100 mg/m^3.

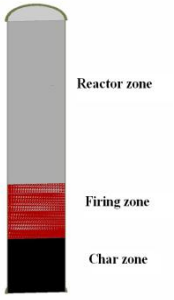

Fig. 2. Reactor

3.4.5. Char chamber

The char is deposited in char chamber. The temperature in this zone is about 50°C to 87°C. It is produced in the gasifier and is completely black, which is good for soil conditioning. Rice husk contain about 75% organic volatile matter and the balance 25% of the weight of this husk is converted into ash during the burning process which is known as char or rice husk ash (RHA). This RHA in turn contains around 85% - 90% amorphous silica.

3.4.6. Scraper

The scraper is one of the most important elements in this set up. Here it is used to remove the char from the combustion chamber and driven by a dc motor that rotates after every five minutes. It is made of a shaft and a net. The shaft is coupled with a motor by a chain sprocket arrangement. The net should have ability to resist high temperature and the weight of a mass of about 15 to 20 kg.

Fig. 3. Scraping system Arrangement

3.4.7. Blower

There are two electric blowers in the system. One is used to supply the required air into the combustion chamber so that the husk can burn easily and the other is to remove the char from the scraping zone.

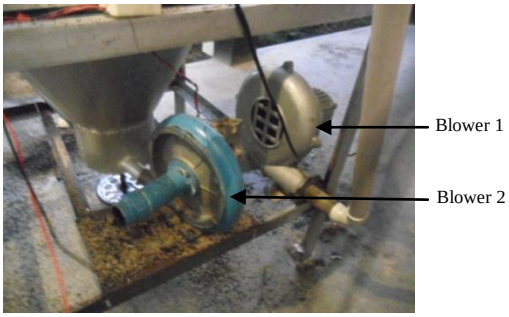

Fig. 4. Blower Arrangement

3.4.8. Data acquisition system

A data acquisition (DAQ) system is used for online recording and processing of the data, like temperature and pressure, collected from the gasifier. This system consists of temperature probes, pressure transducers, power supply, microcontroller, personal computer, and signal conditioning extinctions for instrumentation (SCXI). The National Instruments SCXI is a multi channel signal conditioning and control system for using with personal computers. It is comprised of a chassis that can house a variety of modules for any I/O needs. The SCXI system is programmed with Lab VIEW (Laboratory Virtual Instrument Engineering Workbench), a National Instruments applications software package. A library of functions included in Lab VIEW is used to develop a model for data acquisition, instrument control, data analysis, data presentation and data storage.

Fig. 5. The complete setup

4. RESULTS

4.1. Observations

The CFRHG system has been tested successfully in a continuous mode. Continuous operation is accomplished by simply loading rice husks onto the feed hopper while simultaneously discharging char from the char box. Rice husk fuel produced combustible gas within 15 to 25 minutes after ignition. Almost no smoke emitted from the gasifier during operation. One or two persons are sufficient to operate the CFRHG i.e., to facilitate loading of fuel and removing char from the site.

The temperature of the gas leaving the reactor varies from 150° to 270°C. Preheated air, with a temperature of 90° to 180°C, is mixed with the burning gas at the burner producing a yellowish-to-bluish flame in color having a temperature of 400° to 800°C.

4.2. The positive features of the technology

- The heat energy generated from the gasifier is in gaseous form and can be efficiently supplied for various heating tasks;
- The operation is convenient for it does not require much attendance and easy control on burning makes it more suitable for sensitive applications like seed drying and food cooking;
- The gasifier can easily be built even in a small shop;
- The gas emitted from the burner contains fewer amounts of black carbon, tars, CO_2, and other gases.

5. CONCLUSION

There are seasonal, geographical distribution and other variables in the availability of conventional energy sources in Bangladesh. Using of this technology in rice processing industries will help to avoid the need (and hence cost) of handling and transportation of energy. A substantial proportion of the energy demand in rice processing operations in Bangladesh can be met with the currently available technologies for exploitation of the energy potential of husk. Of course in future, with the availability of more realistic input data based on increased field experience, the method outlined in the present work can be used to arrive at more optimized conclusions.

The CFRHG technology clearly demonstrates that rice husks can be efficiently gasified in a continuous mode following the principle of a moving-bed inverted-downdraft technology. The use of scraper eliminates the problem of char clogging during operation.

The technology can provide more benefits to the users, particularly in terms of convenience of operation and cost. It does not require advanced knowledge and high-tech component and equipment in the fabrication; thus, it can easily be built using locally available resources and manpower. It also addresses the environmental aspect, since it is considered a clean technology based on black carbon and CO_2 emissions, which are basically low. The by-products can be further used as valuable commodity products for agriculture and construction sectors.

Moreover, the adoption of this technology in other countries simply indicates the significance of its contribution in the advancement of utilizing renewable energy.

5.1. Future recommendations

The present system is a preliminary one that gives the basic understanding of the method. But to have a commercially viable system it needs farther development and optimization. The factors that need to be determined for optimized output include;

- The rate of air flow for maximum energy output.
- The inlet air temperature.
- Optimum temperatures at different zones in the reactor.
- Optimum height of different zones in the reactor.
- Optimum fuel gas temperature.

References

[1] Food and Agriculture Organization. Yearbook Production 1995. Rome: FAO, 1996.
[2] Beagle E. Rice husk conversion to energy. In:Agricultural Services Bulletin, 31. Rome, Italy: FAO,1978.
[3] Kapur T, Kandpal TC and Garg HP. Electricity Generation from Rice Husk in Indian Rice Mills: Potential and Financial Viability. Biomass and Bioenergy 1996;10(5/6):393-403.
[4] Boateng AA, Walawender WP, Fan LT, Chee CS. Fluidized bed steam gasification of rice hull. Bioresource Technology 1992;40(2):235-9.
[5] The Energy and Environmental Research Center. A History of Biomass Experience and Expertise. EDGE 2007; 18(1).
[6] Mansaray KG, Ghaly AE, Al-Taweel AM, Hamdullahpur F, Ugursal VI. Air gasification of rice husk in a dual distributor type fluidized bed gasifier. Elsevier Science Ltd. Biomass and Bioenergy 1999;17:315-32.
[7] SAN SAN INDUSTRIAL Cooperative., Ltd., Myanmar. Accessed 20 Feb 2005. http://www.benergyssic.com/sansanrice.htm
[8] Alexis TB, Daniel AHB, Lucio L. Continuous-flow rice husk gasifier for thermal applications. 10th PCIERD Regional S&T Fora and Compitition February 26, 2010;

Effect of Bamboo Bandalling Structures on Velocity Distribution in the Open Channel Flow

Md. Lutfor Rahman[a*] , B.C.Basak[b] , Md. Showkat Osman[c]

[a*]*Chief Scientific Officer (CSO), River Research Institute, Faridpur and Ph.D.Research Fellow, Department of Civil Engineering, DUET, Gazipur, Bangladesh; e-mail:mdlutforrahman10@yahoo.com*
[b]*Professor & Chairman, Department of Civil Engineering, Stamford University Bangladesh, email: bcbasak@stamforduniversity.edu.bd*
[c]*Professor, Faculty of Civil Engineering, DUET, Gazipur, Bangladesh; e-mail: pd_cobit@yahoo.com*

Abstract

There is a laboratory experimental study for the effect of Bamboo Bandalling Structures in river flow & morphology. A series of bamboo bandalling structures are constructed in laboratory flume. Due to the effect of the bamboo bandalling structures, river bank sedimentation & navigational channel is developed. The velocity distribution at the upstream & downstream of the constructed bandals plays a vital role for the navigational channel development and river bank sedimentation. The velocities in between the bamboo bandalling structures are very less than that of the velocity away from the bandals. It is important to note here in this paper so that the point velocity is less behind bandals and that of higher velocity in the upper portion of the bandals.

Keywords: laboratory; bamboo bandalling structures; river bank sedimentation; navigational channel

1. Introduction

River bank erosion and channel shifting are recurrent problems in Bangladesh that usually occur during the monsoon (more specifically, during rising stage and recession stage) when huge sediment load is generated by means of bank erosion and bed changes. Conventionally, spurs, groins, revetments or combination of them are used in order to manage sediment load thus generated and mitigate river erosion and related problems. Spurs, groins or revetment-like structures are too expensive to adapt along the longer reaches of the large-scale alluvial rivers in Bangladesh. Therefore, it is important to develop alternative low cost approaches that can be adaptive within local socio-economic and environmental condition.In Bangladesh, over the years, channel width is increasing and depth is decreasing because of unfavorable geographic location and discharge control by the countries in the upstream reaches that lead to unexpected erosion-siltation processes along the major rivers. It is very difficult and even impossible to maintain in-stream flow requirement that is very important for the maintenance of river ecology and aquatic habitat necessary for the healthy life cycle of plants and animals. Rivers are loosing their navigability and waterways are severely obstructed during the dry season. On the other hand, conveyance capacity of rivers is reducing and is insufficient for safe and expeditious passage of floodwater and sediment discharge during the monsoon. As a result, country had experienced severe flood disasters during the past such as in 1988 and 1998. However, the situation seems to get more severe gradually as compared with the past events.

Floodplains and riverbanks are developed from recent deposits consisting mostly silt and fine sand that are highly susceptible to erosion. As a result, the river channels often shifts within wide range of river belt. To prevent the river erosion groins, spurs, revetments, porcupines, sand bags, boulders etc are applied. Some of these methods (groins, revetments) are very expensive considering the large river dimensions and corresponding limited financial strength of Bangladesh. On the other hand, porcupines, sand bags, boulders are being used from experience of local people against river bank erosion and none of these methods have been proved to be effective for the protection of river erosion in long-term basis. Bandals are one of the local structures developed in the Indian sub-continent that obstruct flow near the water surface and allow it to pass near the riverbed.

* Corresponding author. Tel.: +88-01715-039646; fax: +88-0631-63065.

E-mail address: mdlutforrahman10@yahoo.com

These are made of naturally available materials such as bamboo, wood etc. and regarded as inexpensive method over conventional structures and mostly applied for the improvement of navigational channels during the low flow season. But application of Bandalling for riverbank protection is not yet practiced in Bangladesh. It is mention here that the river channel stabilization is studied by Rahman et al (2003) and also there is a study for the river bank stabilization with the application of Bamboo Bandalling Structures by Rahman,Md.Lutfor (2011).

In recent past some field tests along the Jamuna was executed for the bank protection using Bandalling (FAP 21/22, 2001). At the laboratory scale, the preliminary idea on the possibility of use of Bandalling for sediment management (erosion and siltation) was discussed (Rahman et al., 2003, 2004).

2. Objectives of the Study

The main objective of the laboatory experimental study are being carried out to investigate the effect of bandalling on river flow and morphology.

- to measure the flow field around bandals.
- to analyze the velocity around the bandal
- to get idea about the sedimentation and navigational phenomenon in the open channel

3. Methodology

To achieve the objectives of the study, an experimental set are taken in re-circulated straight flume that is 22 m long, 2.2 m wide and 2 m deep. The flume setup was in live-bed condition. The effect of a series of bandals structures are examined in terms of the arrangement of spacing & with certain angle of the flow direction in the channel. The laboratory experimental set-up with the circulated water supply system is shown below in Figure 1.

Fig.1: Experimental set-up for the open channel with the water supply system

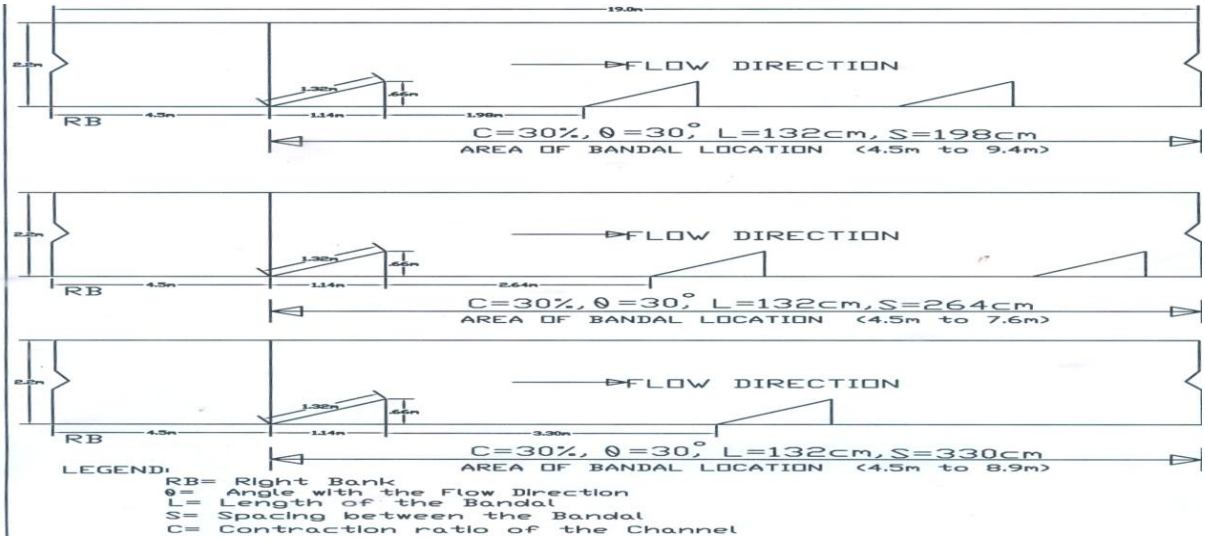

Fig. 2 Bandals location in different orientation for the openning below the chatai are 40%, 50% and 60%

4. Data Collection & Analysis

Data are collected at the different cross-section with an interval @25 cm as well as along the open channel flow. The velocities in two dimensions at the different depth level such as 0.1d, 0.3d, 0.5d, 0.7d and 0.9d are plotted and presented as in Fig. 3 to Fig. 6.The point velocity data was collected at upstream and downstream of the constructed bandals in different distance from the start point of the constructed bandals. The bed topography data was also collected through sounding method. This bathymetry data were analyzed and plotted is shown as in Fig.7.

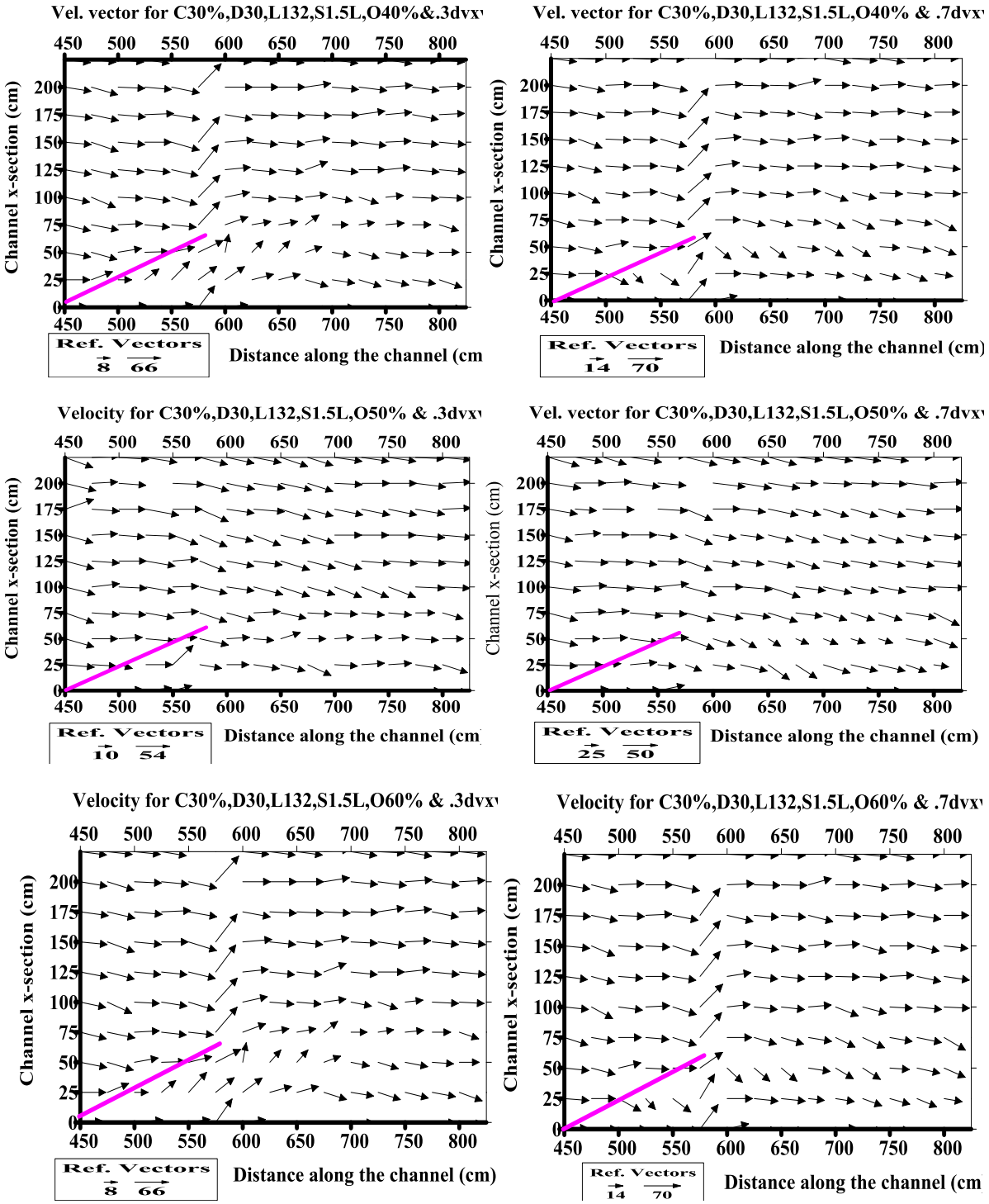

Fig.3: Velocity vector for the 40%, 50% & 60% oppenning below bamboo chatai at different depth level

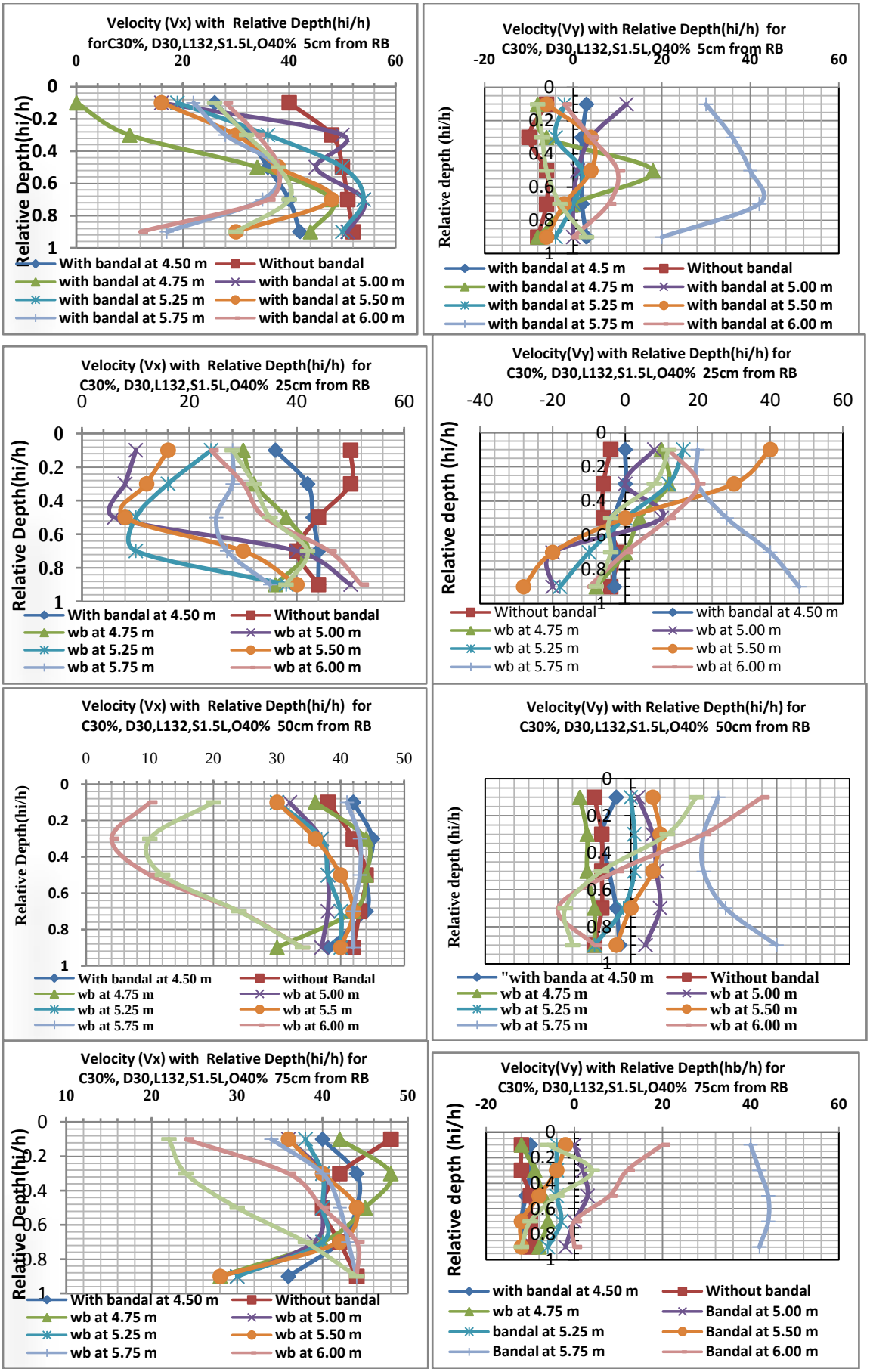

Fig.4: Velocity vector diagram for the 40% opening below bamboo chatai in different distance from the right bank

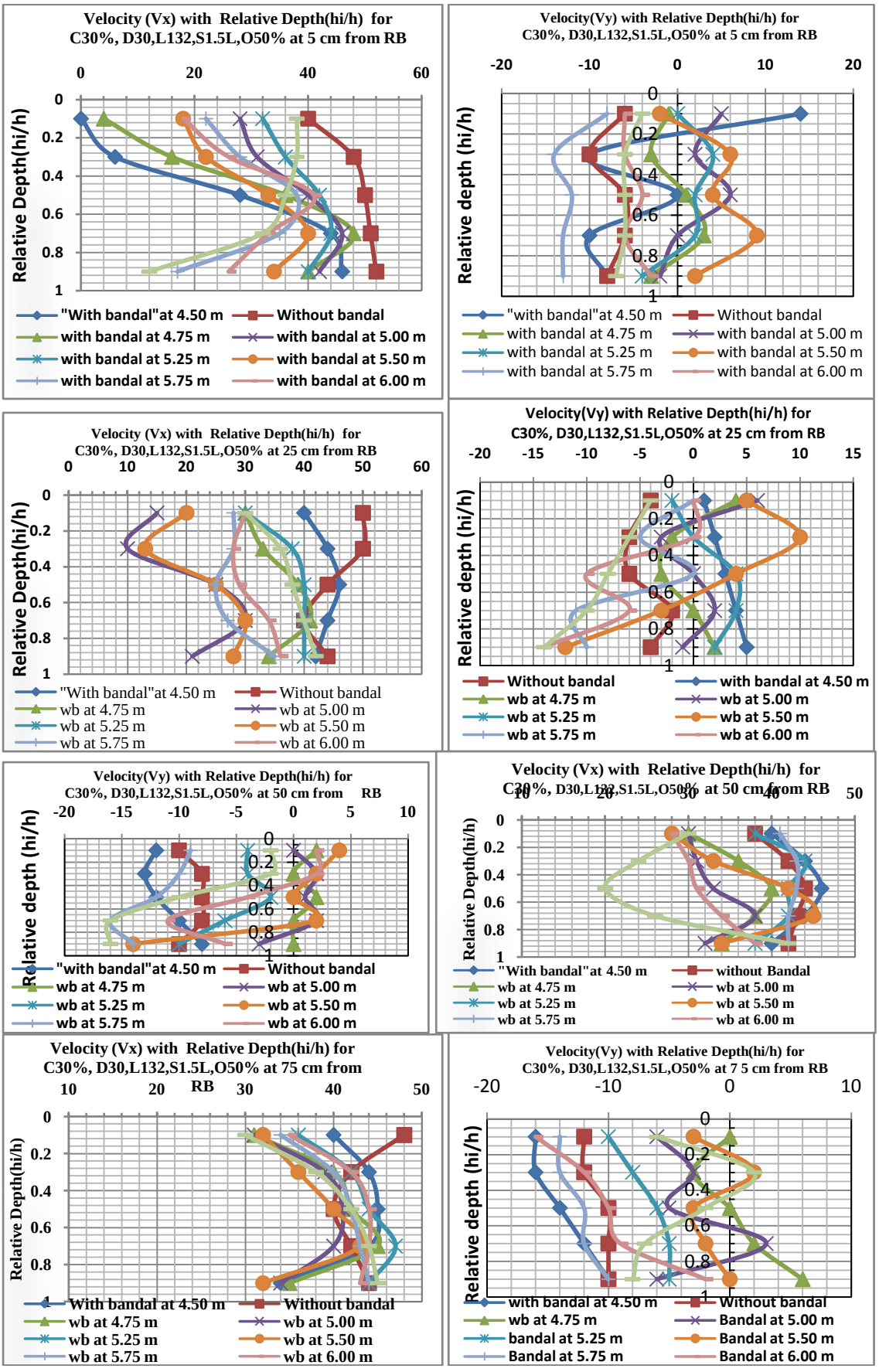

Fig.5: Velocity vector diagram for the 50% opening below bamboo chatai in different distance from the right bank

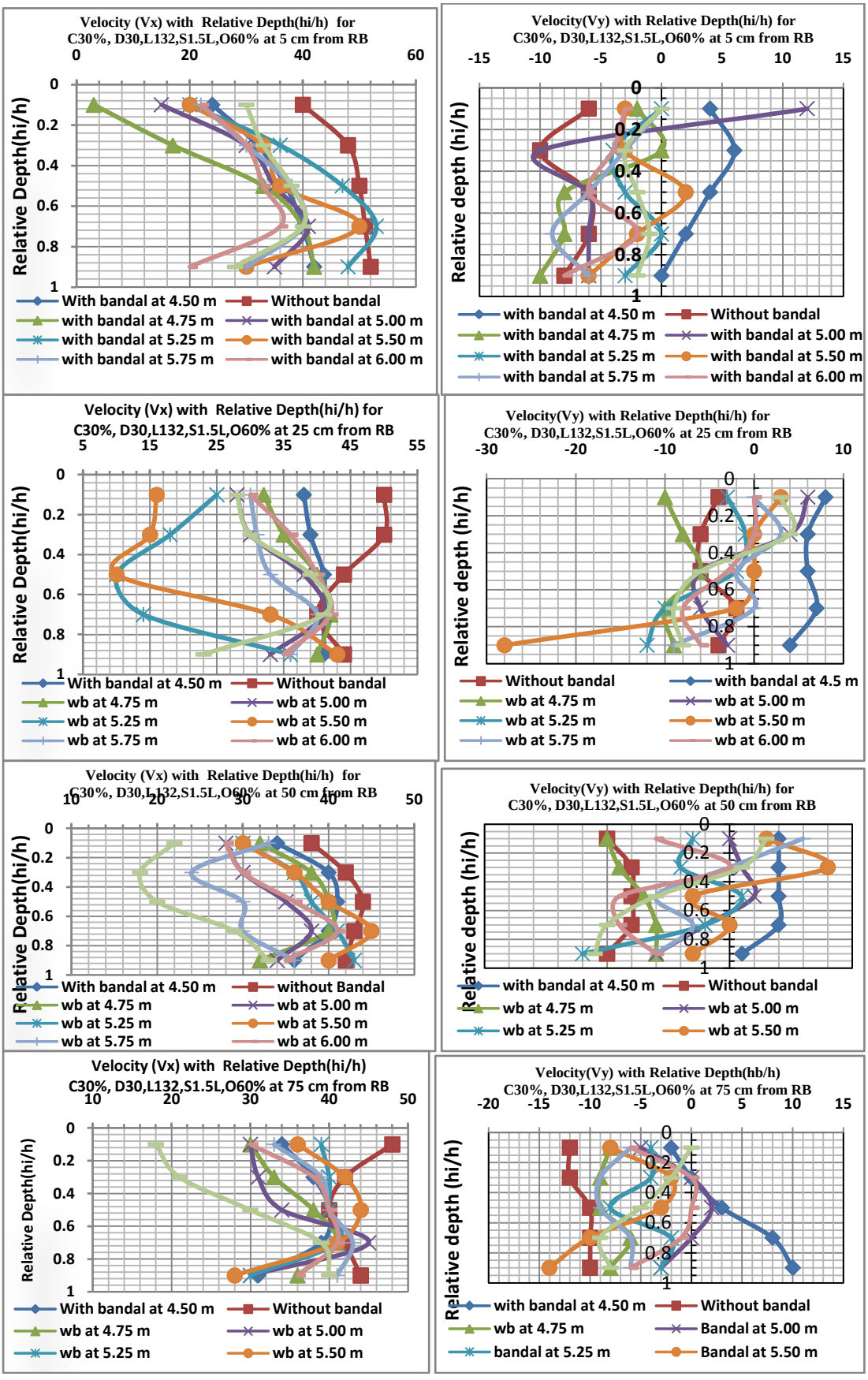

Fig.6: Velocity vector diagram for the 60% opening below bamboo chatai in different distance from the right bank

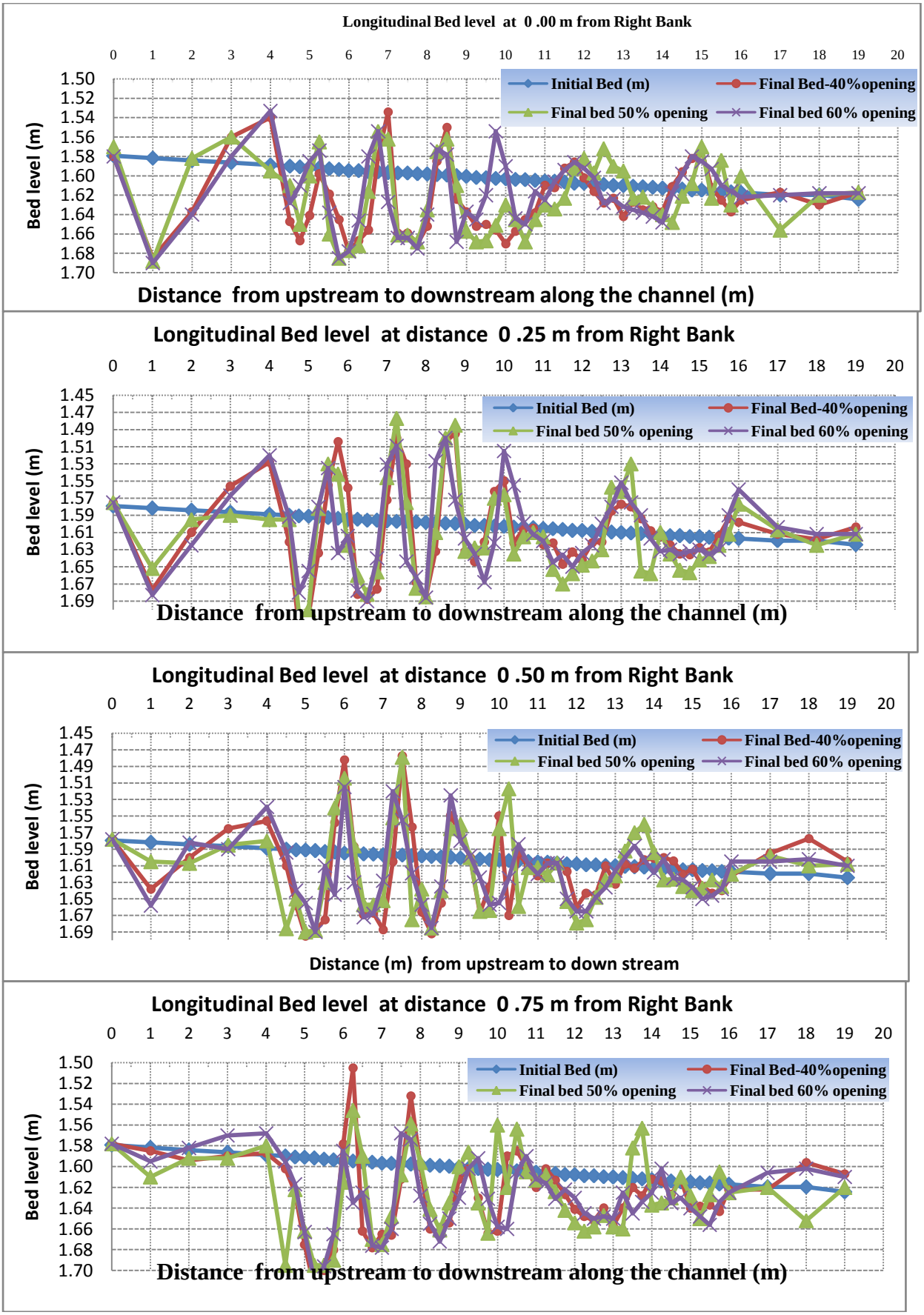

Fig.7: Comparison of initial and final bed due to the effect of velocity for the 40%,50% & 60% opening below bamboo chatai

5.Result and discussions

From Fig. 3 to Fig.6, it is seen that there is less velocity at the top & bottom of the constructed bamboo bandalling structures at a depth of o.1d and 0.9d whereas the velocity is higher at the 0.3d and 0.5d level of the bandals. It is also evident that less velocity for the less opening below the bamboo chatai and that of higher velocity due to higher opening below the bamboo chatai. From the figure 7, it is clear that due to the less velocity, the sediment is deposited behind the bandals and the deep navigational channel is developed away from the bank. The velocity in the Vy is always unstable and the velocity in the flow direction Vx is always more or less value near the bank so that there is sedimentation near the bank. So the effect of bamboo bandalling is vital for the river bank erosion protection in the open channel river flow.

6. Conclusions

In conclusion, we can say that bandals are capable for protecting river banks by flow diversion towards the main channel leading to deep navigational channel formation. Flow velocities are reduced near the bank lines that ensure bank protection by the deposition of sediment. If the bandal structure functions optimistically, the river can get sufficient time for its adjustment and new main channel and bankline development. The output of the present research for the stabilization of river course can solve the river erosion & navigation problems of Bangladesh that is more or less inherent due to its complex geographical location at the lower riparian of the catchments.

Acknowledgements

The author is highly to the authority of River Research Institute, Faridpur for giving financial support to conduct such innovative research work.

References

[1] FAP 21, Guidelines and design manual for standardized bank protection structures, Bank protection pilot project, Flood Action Plan, Govt. of Bangladesh, 2001.
[2] FAP 21/22 (2001), Bank protection & river training pilot project, Flood Action Plan, Govt. of Bangladesh,2001
[3] Rahman, M.M., Nakagawa,H. Khaleduzzaman and AT.M. and Ishigaki, T. (2003), "Flow and scour-deposition around bandals." Proceeding of the Fifth International Summer Symposium, JSCE, 177-180.
[4] Rahman, Md.Munsur, Hajime Nakagawa, Taisuke Ishigaki and ATM Khaleduzzaman (2003), " Channel Stabilization Using Bandalling ." Annuals of Disas. Prev. res. Inst., Kyoto Univ., No. 46
[5] Rahman, M.M., Nakagawa,H. Khaleduzzaman, AT.M., Ishigaki, T. and Yasunori M. (2004), " On the Formation of stable River course." Annuals of Disas. Prev. res. Inst., Kyoto Univ., No. 47
[6] Rahman,Md.Lutfor et al (2011), "River Bank Stabilization with the application of Bamboo Bandalling Structure: A case study." 4th Annual paper meet and 1st Civil Engineering Congress, December 22-24, 2011, Dhaka, Bangladesh ISBN: 987-984-33-4363-5, Noor,Amin, Bhuiyan, Chowdhury and Kakoli (eds), www.iebconferences.info

5th BSME International Conference on Thermal Engineering

Production of Biodiesel from Waste Vegetable Oil

Md. Mamunur Roshid[a], Dr. Jamal Uddin Ahamed[b], Md. Shakar Ullah Chowdhury[c]

[a,c]Lecturer, [b]Assistant Professor, Deparment of Mechanical Engineering, Chittagong Univrsity of Engineering & Technology, Chittagong-4349, Bangladesh

Abstract

Biodiesel, a promising substitute as an alternative fuel has gained significant attention due to the finite nature of fossil energy resources and does not produce sulphur oxides and minimize the soot particles in comparison with the existing one from petroleum diesel. The utilization of liquid fuel such as biodiesel produced from vegetable oil by trans-esterification process represents one of the most promising options for the use of conventional fossil fuels.
In the first step of this experimental research, waste soybean vegetable oil used as test material and converted into soybean oil ethyl ester which is known as biodiesel and they are prepared in the presence of homogeneous acid catalyst and optimized their operating parameters like reaction temperature, quantity of alcohol and the catalyst requirement, stirring rate and time of esterification. In the second step, the physical properties such as density, flash point, kinematic viscosity, cloud point and pour point were found out for the above biodiesel. The same characteristics study was also carried out for the diesel fuel for obtaining the base line data for analysis. The values obtained from the biodiesel produced from waste vegetable oil are closely matched with the values of conventional diesel and it can be used in the existing diesel engine without any hardware modification. In the third step the storage characteristics of biodiesel are also studied.

Keywords: Biodiesel, Trans-esterification, Soybean oil ethyl ester

1. Introduction:

Biodiesel is an alternative fuel similar to conventional or 'fossil' diesel. Biodiesel can be produced from straight vegetable oil, animal oil/fats, tallow and waste cooking oil. The process used to convert these oils to Biodiesel is called transesterification. This process is described in more detail below. The largest possible source of suitable oil comes from oil crops such as rapeseed, palm or soybean. Most biodiesel is produced from waste vegetable oil sourced from restaurants, chip shops, industrial food producers such as Birdseye etc. Though oil straight from the agricultural industry represents the greatest potential source it is not being produced commercially simply because the raw oil is too expensive. After the cost of converting it to biodiesel has been added on it is simply too expensive to compete with fossil diesel. Waste vegetable oil can often be sourced for free or sourced already treated for a small price. (The waste oil must be treated before conversion to biodiesel to remove impurities). The result is Biodiesel produced from waste vegetable oil can compete with fossil diesel.

2. Scope and Limitation of the Study:

2.1 Advantages of biodiesel:

a) Biodiesel reduces emissions of carbon monoxide (CO) by approximately 50% and carbon dioxide by 78.45% on a net life cycle basis because the carbon in biodiesel emissions is recycled from carbon that was already in the atmosphere, rather than being new carbon from petroleum that was sequestered in the earth's crust.
b) Biodiesel contains fewer aromatic hydrocarbons: 56% reduction for Benzofluorathene and 71% reduction for Benzopyrenes. Biodiesel also eliminates sulfur emissions (SO_2) since not containing sulfur.
c) Biodiesel reduces by as much as 65% the emissions of particulates, which consist of small particles of solid combustion products. According to testing sponsored by the department of energy, this can reduce cancer risks up to 94%.
d) Biodiesel does produce more NO_x emissions than petrodiesel, but these emissions can be reduced through the use of catalytic converter. The increase in NO_x emissions may also bidets the higher cetane rating of biodiesel. Properly designed and tuned engines may eliminate this increase.
e) Biodiesel has a higher cetane rating than petrodiesel, and therefore ignites more rapidly when injected into the engine. It also has the highest BTU content of any alternative fuel (Ethanol, LPG) in its pure form (B100).

f) Biodiesel is biodegradable and non-toxic tests sponsored by the United States department of agriculture confirm biodiesel is less toxic than table salt and biodegrades as fast as sugar.
g) Biodiesel is the only alternative fuel to have successfully completed the health effects testing requirements of the clean air act (1990).
h) Biofuel extraction is an easy process, which can be done by small scale operations in local villages and it is used in third world countries like Zimbabwe, Zambia, Nicaragua and India. In these countries biofuel is widely utilized to operate cooking stoves, diesel water pumps and electric generators.

2.2 Disadvantages of Biodiesel:

a) Biodiesel is currently about one and half times more expensive than petroleum diesel fuel. Part of this cost is because the most common source of oil is the soybean which only is only 20% oil. However, the costs of biodiesel can be reduced by making biodiesel from recycled cooking oils rather than from new soybeans or by making it from plant matter with higher oil content.
b) It takes energy to produce biodiesel fuel from soy crops including the energy of sowing, fertilizing and harvesting.
c) Biodiesel fuel can damage rubber hoses in some engines, particularly in cars built before 1994. You should check with the manufacturer before using biodiesel to see if you need to replace any hoses or rubber seals.
d) Biodiesel cleans the dirt from the engine. This dirt then collects in the fuel filter, which can clog it. Clogging occurs most often when biodiesel is first used after a period of operation with petroleum diesel, so filters should be changed after the first several hours of biodiesel use.
e) Biodiesel is not distributed as widely as traditional, petroleum diesel but distribution infrastructure is improving.

3. Methodology of the study:

The major steps required to synthesize biodiesel from waste vegetable oil are as follows:

3.1 *Purification:*

If waste vegetable oil is used, it is filtered to remove dirt, charred food and other non-oil material often found. Water is removed because its presence causes the triglycerides to hydrolyze to give salts of the fatty acids instead of undergoing transesterification to give biodiesel. At home, this is often accomplished by heating the filtered oil to approximately 120ºC. At this point, dissolved or suspended water will boil off. When the water boils, it spatters (chemists refer to it as “bumping”). To prevent injury, this operation should be done in a sufficiently large container (at most two thirds full) which is closed but not sealed.
In the laboratory, the crude oil may be stirred with a drying agent such as magnesium sulphate to remove the water in the form of water of crystallization. The drying agent can be separated by decanting or by filtration. However, the viscosity of the oil may not allow the drying agent to mix thoroughly.

3.2 *Neutralization of free fatty acids:*

A Sample of the cleaned oil titrated against a standard solution of base in order to determine the concentration of free fatty acids (RCOOH) present in the waste vegetable oil sample. The quantity (in moles) of base required to neutralize the acid is then calculated.

3.3 *Transesterification:*

While adding the base, a slight excess is factored into provide the catalyst for the transesterification. The calculated quantity of base (usually sodium hydroxide) is added slowly to the alcohol and it is stirred until dissolves. Sufficient alcohol is added to make up three full equivalents of the triglyceride and an excess is added to drive the reaction to completion.
The solution of sodium hydroxide in the alcohol is then added to a warm solution of the waste oil and the mixture is heated (typically 50ºC) for several hours (4 or 8 typically) to allow the transesterification to proceed. A condenser may be used to prevent the evaporative losses of the alcohol. Care must be taken not to create a closed system which can explode. An example of the transesterification reaction equation, shown in skeletal formulas:

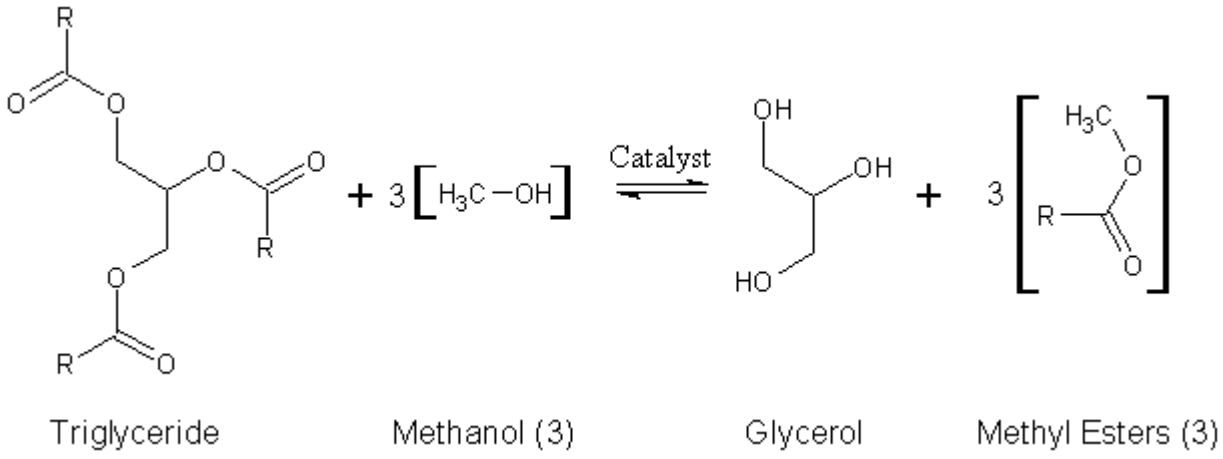

Since natural oils are typically used in this process, the alkyl groups of the triglyceride are not necessarily the same. Therefore, distinguishing these different alkyl groups, we have a more accurate depiction of the reaction: R_1, R_2, R_3: Alkyl group.

During the esterification process, the triglyceride is reacted with alcohol in the presence of a catalyst, usually a strong alkali (NaOH, KOH, or Alkoxides). The main reason for doing a titration to produce biodiesel, is to find out how much alkaline is needed to completely neutralize any free fatty acids present, thus ensuring a complete transesterification. Empirically 6.25 g / L NaOH produces a very usable fuel. One uses about 6 g NaOH when the WVO is light in color and about 7 g NaOH when it is dark in color.

The alcohol reacts with the fatty acids to form the mono-alkyl ester (or biodiesel) and crude glycerol. The reaction between the bio-lipid (fat or oil) and the alcohol is a reversible reaction so the alcohol must be added in excess to drive the reaction towards the right and ensure complete conversion.

3.4 *Workup:*

Once the reaction is complete, the glycerol should sink. When ethanol is used, it is reported that an emulsion often forms. This emulsion can be broken by standing, centrifugation or the addition of a low boiling (easily removed) non-polar solvent, decanting and distilling.
The top layer, a mixture of biodiesel and alcohol, is decanted. The excess alcohol can be distilled off or it can be extracted with water. If the latter, the biodiesel should be dried by distillation or with a drying agent.

3.5 *Quality Testing:*

Diesel engines require fuel of a certain quality. You just can't pour poor-quality biodiesel into the tank and expect the engine to go on and on without problems. You have three very dangerous enemies: free glycerin, poorly converted oils/fats and lye catalyst. Free glycerin and mono-, di- and triglycerides (poor ester conversion) will form gum-like deposits around injector tips and valve heads, lye can damage the injector pump. The key to good fuel is to just do it right and finish it. Use pure chemicals (sulfuric acid, lye and methanol) and measure them accurately. A proper wash will get rid of any glycerin and remaining lye.

3.5.1 *Wash Test:*

This is the most useful all-round test, and it's very simple: Put 150 ml of unwashed biodiesel (settled for 12 hours or more, with the glycerin layer removed) in a half-liter glass jar or PET bottle. Add 150 ml of water (at room temperature), screw the lid on tight and shake it up and down violently for 10 seconds. Then let it settle. The biodiesel should separate from the water in half an hour or less, with amber (and cloudy) biodiesel on top and milky water below, and no more than a paper-thin white interface layer between the oil and water. This is quality fuel, a completed product with minimal contaminants. Wash it and use it with confidence. But if it turns into something that looks like mayonnaise and won't separate, or if it only separates very slowly, with a thick, creamy white layer sandwiched between the water and the biodiesel, it's not quality fuel and your process needs improvement.

- Either you've used too much catalyst and made excess soap. Or,
- An incomplete reaction with poor conversion has left you with half-processed monoglycerides and diglycerides, fuel contaminants that also act as emulsifiers. Emulsifiers are used to make stable mixtures of oil and water, such as, indeed, mayonnaise. Or,
- Both -- too much catalyst as well as poor conversion.

3.5.2 *Reprocessing Test:*

The barnyard tests for your fuel are to take a liter of finished fuel, process it again as if it were new vegetable oil. If any more glycerin drops out, then you know it wasn't as good as it could have been. Also, look at your wash water. The second wash should be almost completely clear. The third wash should be nearly crystal clear. After settling 24 hours after a third wash, the fuel should be transparent when held up to light in a glass jar. If slightly hazy, simply heating the fuel to 9 deg Fahrenheit (32°C) should clarify it. If it clarifies with minimal application of heat, throw it into your tank and go see your mum for the weekend. If all the above 'tests' turn out well, you probably have a fuel that would analytically beat fuel produced using continuous process (i.e. commercial) methods.

3.5.3 Methanol Test:

Take exactly 25 ml of biodiesel and dissolve it in exactly 225 ml of methanol in a measuring glass. The biodiesel should be fully soluble in the methanol, forming a clear bright phase. If not, there is pollution in the biodiesel. Each ml of undissolved material corresponds to 4% by volume. Is there any undissolved material at the bottom of the measuring glass? If there is, your reaction is not complete and this is causing you trouble with the water test. This method does not cover every aspect of quality, but it gives a hint. It is valid only for biodiesel made from vegetable and animal oils. It is not valid for biodiesel made from oils with a very wide fatty acid pattern, such as fish oils.

3.5.4 *Viscosity Test:*

Viscosity levels are a comparative indicator of biodiesel quality. Unfortunately, and despite to the country, that's all they are, a comparative indicator: this batch is better than that batch. Even at the laboratory or industrial level, viscosity testing alone cannot tell you if the process has gone far enough before reaching equilibrium and that there are not unacceptably high levels of harmful unreacted and partly reacted materials in your fuel.Unconverted monoglycerides (MGs) and diglycerides (DGs) are fuel contaminants that can cause injector coking and engine damage. MGs and DGs are very similar in viscosity to biodiesel and stay in solution with it after an incomplete reaction, they cannot be washed out. The allowed maximums are low: less than 1% for DGs and less than half that for MGs. Viscosity tests might get you within 5% accuracy, not nearly close enough for a useful quality check. Viscosity is that property of a fluid by virtue of it offers resistance to shear. Kinematic and Dynamic viscosities are very important properties of oil.
In this test, I used Saybolt Universal Viscometer to determine the viscosity of the biodiesel using following formula:
$\upsilon = 0.224\ t - 185/t$ When $115 > t > 34$
υ = Kinematic viscosity in Centistroke.
t = Saybolt Universal viscosity in seconds

3.5.5 *More quality checks:*

AleksKac has provided some useful quality checks:
There is a rule of thumb: the brighter yellow in color, the better the crack. As a standard you should take virgin sunflower oil yellow color in see-through sunlight. (It's a sort of colorometry). Then take a glass jar of your fuel and place it in front of a white wall in the evening. When seen in the reflected light of a tungsten bulb it should not change to orange (a very simple case of absorption spectrometry).

- Nicely cracked biodiesel: very pale yellow (less than virgin sunflower oil) and no change in color with artificial lighting;
- Acceptable biodiesel: yellow like virgin sunflower oil or straw, but will get orangey undertone in reflected tungsten light;
- Deeper color biodiesel has a lot of glycerin in it in the form of various glycerides. Not good for standard engines. Remedy: If the diesel is too dark and you are sure that you used the correct quantities(s) of catalyst(s), add a pinch more alcohol -- you could be losing it due to evaporation.

4. Flow Chart of the Production Process:

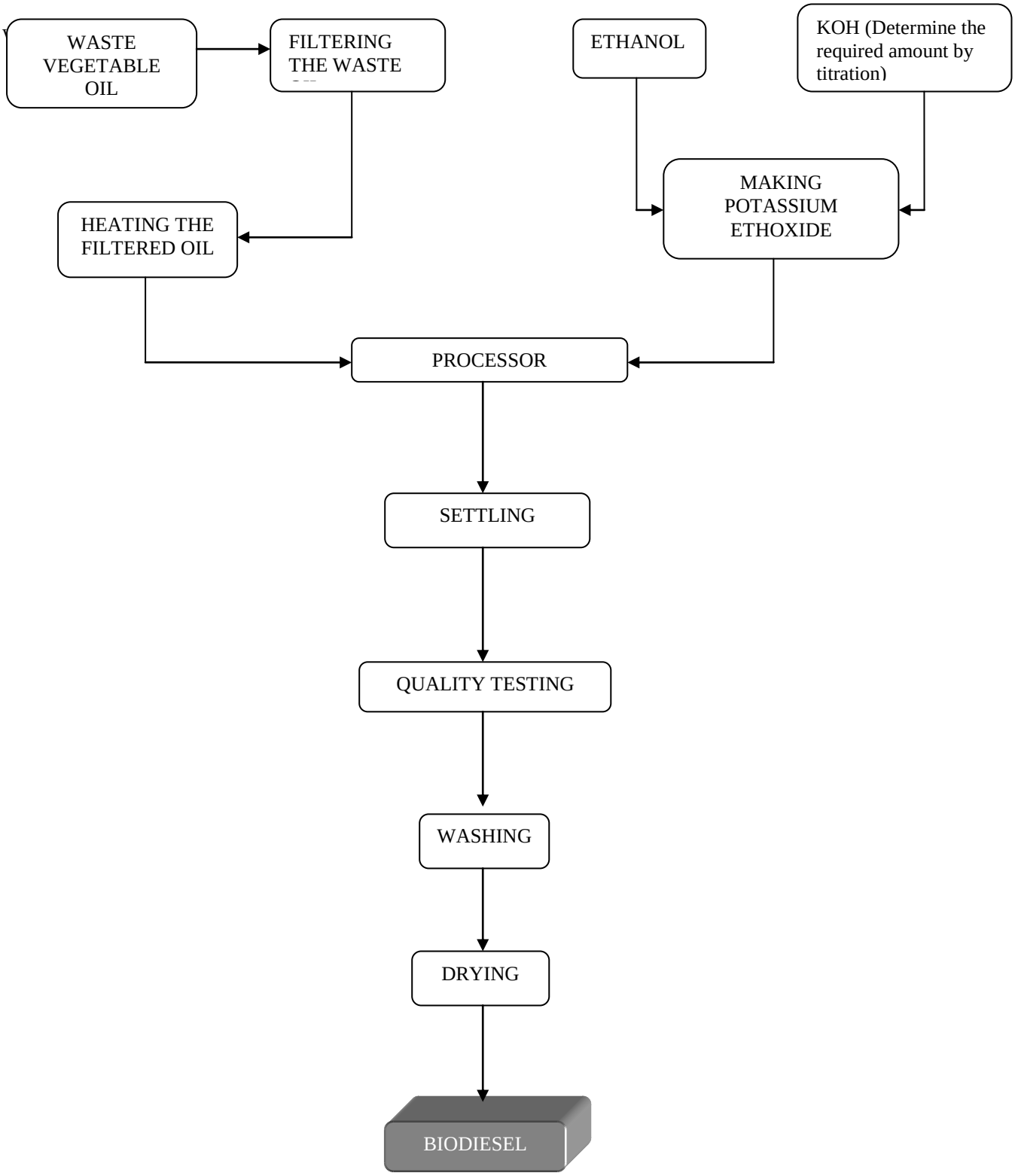

5. Comparison between diesel and biodiesel:

Comparison between Properties of Diesel, Canola oil & Commercial US Biodiesel			
	Diesel	**Canola Oil**	**Biodiesel**
Density kgL^{-1} @ 15.5ºC	0.84	0.92	0.88
Calorific value MJL^{-1}	38.3	36.9	33 – 40
Viscosity mm^2s^{-1} @ 20ºC	4 – 5	70	4 – 6
Viscosity mm^2s^{-1} @ 40ºC	4 – 5	37	4 – 6
Viscosity mm^2s^{-1} @ 70ºC	-	10	-
Cetane Number	45	40 - 50	45 – 65

6. Results:

Name of the Test	**Reading**	**Standard Value**	**Comments on Quality**
Wash Test	Exists a thin layer between oil and water	Exists a very thin layer between oil and water	**MEDIUM**
Ethanol Test	Form a moderate bright phase	Form a strong bright phase	**MEDIUM**
Viscosity Test	5.8 Centistokes @ 40ºC 5.0 Centistokes @ 60ºC 4.0 Centistokes @100ºC	4-6 Centistokes @40ºC	**MEDIUM**

Conclusions:

Production of biodiesel from waste vegetable oil is no so as easy as from fresh oil but it can be done if one try to do it carefully and perfectly. Titration of the waste oil should be done carefully to determine the amount of lye required for neutralize the free fatty acid. The quality of the chemicals should be high for producing top quality biodiesel. Biodiesel is an environment friendly fuel than petrol, diesel and other fossil fuel. It will be helpful for decreasing the global warming. If we use unused and less fertile land for cultivating vegetable oil or jatrova in a large scale, then it does not make any hamper in the food production for the mankind. Above all, Biodiesel is a safe, clean and environment friendly fuel which can be used in the automobile without major change in the configuration of the engine.

References:

[1] Biodiesel Production – Dr. G Matt
[2] An overview of Biodiesel and Petroleum diesel lifecycles, May 1998, Sheehan, et al. NREL (60pp pdf file)
[3] National Biodiesel Board. "Biodiesel" www.biodiesel.com
[4]Iowa State University Mechanical Engineering Department."BEACON:Biodiesel Education."www.me.iastate.edu/biodiesel/pages/biodiesel11.html
[5] www.iowadnr.com/energy/renewable/biodiesel.html
[6] www.biodiesel.org/pdf_files/fuelfactsheets/Lubricity.pdf
[7] www.biodiesel.org/pdf_files/fuelfactsheets/performance.pdf
[8] www.mdac.state.ms.us/n_library/programs/alt_energy/alt_biodiesel_performance
[9] www.sizes.com/units/cetane_number.html
[10] www.pacfuel.com/FAQs.html
[11] www.aces.uiuc.edu/~asap/research/fs-organic-soybeans.html
[12] www.eere.energy.gov/afdc/progs/ddown.cgi?afdc/FAQ/13/0/0
[13] Egov.oregon.gov/ENERGY/RENEW/Biomass/cost.shtml
[14] www.greencarcongress.com/2005/11/us_biodiesel_pr.html
[15] En.wikipedia.org/wiki/biodiesel
[16] www.nrel.gov/docs/logosti/fy98/24089
[17] www.nrel.gov/docs/logosti/fy98/24090
[18] www.nrel.gov/docs/logosti/fy98/24091
[19] www.uidaho.edu/bioenergy/biodieseled/publication/04
[20] www.journeytoforever.org/making your own biodiesel

Finite Difference Solution of MHD Mixed Convection Flow with Heat Generation and Chemical Reaction

Tanvir Ahmed and Md. Mahmud Alam*

Mathematics Discipline, Khulna University, Khulna-9208, Bangladesh

Abstract

Unsteady MHD mixed convection flow from a vertical plate in porous media in the presence of internal heat generation with chemical reaction, Hall current and thermal radiation has been studied. To obtain the non-similar momentum, energy and concentration equations, usual non-dimensional variables have been used. A finite difference technique with stability and convergence analysis is used to solve the obtained non-similar, coupled, non linear partial differential non-dimensional equations. The obtained solutions are shown graphically. Finally, a qualitative comparison with previous work is shown in tabular form.

Keywords: Hall current; MHD; Soret, Dufour; Chemical reaction; Finite Difference

1. Introduction

The effect of chemical reaction and thermal radiation on MHD boundary layer flow has become important in several industrial, scientific and engineering fields. The growing need for chemical reactions in chemical and hydrometallurgical industries requires the study of heat and mass transfer with chemical reaction. There are many transport processes that are governed by the combined action of buoyancy forces due to both thermal and mass diffusion in the presence of the chemical reaction. These processes are observed in nuclear reactor safety and combustion systems, solar collectors. From the point of applications, Das et al. [1] investigated the effect of the first-order homogeneous chemical reaction of an unsteady flow past a vertical plate with the constant heat and mass transfer. For industrial applications such as glass production, furnace design, space technology applications, cosmical flight aerodynamics rockets, and spacecraft re-entry aerothermodynamics which are operated under the higher temperature with radiation effects are significant. In view of this, Sattar and Kalim [2] studied the unsteady free convection interaction with thermal radiation in a boundary layer flow past a vertical porous plate. Aydin and Kaya [3] investigated the effect of radiation on MHD mixed convection flow about a permeable vertical plate. The Soret and Dufour effects have been found to influence the flow field in mixed convection boundary layer over a vertical surface embedded in a porous medium. Stanford et al. [4] has studied the effect of thermal radiation, Hall currents, Soret and Dufour on MHD flow by mixed convection over a vertical surface in porous media. Recently, Aurangzaib and Shafie [5] investigated the effects of Soret and Dufour on unsteady MHD flow by mixed convection over a vertical surface in porous media with internal heat generation, chemical reaction and Hall current.

Hence our aim of this research is to extend the work of Aurangzaib and Shafie [5] to solve the problem by implicit finite difference scheme. The proposed model has been transformed into non-similar coupled partial differential equation by usual transformations. Finally, the comparison of the present results with the results of Aurangzaib and Shafie [5] has been shown. The obtained results are shown graphically as well as tabular form.

2. Mathematical Formulation

Consider MHD mixed convective heat and mass transfer flow of a viscous incompressible fluid over an isothermal semi-infinite vertical flat plate through a porous medium. The flow is also subjected to a constant suction velocity. The positive x coordinate is measured along the plate in the direction of fluid motion and the positive y coordinate is measured normal to

* Corresponding author. Tel.: +88-041-725741; Cell: +8801912982811; fax: +88-041-731244.
E-mail address: alam_mahmud2000@yahoo.com

the plate. The leading edge of the plate is taken as coincident with $z-$axis. A uniform magnetic field B_0 is applied normal to the flow region. The imposed magnetic field vector B_0 can be taken as $\mathbf{B}=(0,B_0,0)$. The magnetic Reynolds number of the flow is taken to be small enough field and the magnetic field is negligible in comparison with applied magnetic field and the magnetic lines are fixed relative to the fluid. Initially, it is considered that the plate as well as the fluid is at the same temperature $T(=T_\infty)$ and concentration level $C(=C_\infty)$. Also it is assumed that the fluid and the plate is at rest after that the plate is to be moving with a constant velocity U_∞ in its own plane. Instantaneously at time $t>0$, the temperature of the plate and spices concentration are raised to $T_w(>T_\infty)$ and $C_w(>C_\infty)$ respectively, which is there after maintained constant, where T_w, C_w are temperature and spices concentration at the wall and T_∞, C_∞ are the temperature and concentration of the species outside the plate respectively. The physical configuration of the problem is furnished in Fig. 1.

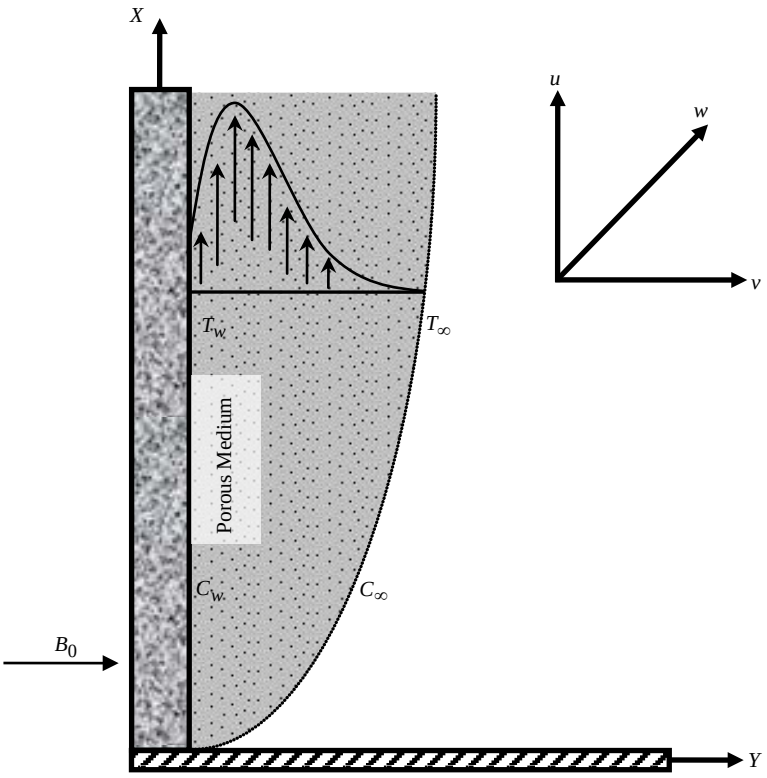

Fig. 1. Physical configuration and coordinate system.

Under the electromagnetic Boussinesq approximations, the MHD unsteady flow and heat and mass transfer with heat generation and chemical reaction are governed by the following equations are given by:

Momentum equation in $x-$axis:

$$\frac{\partial u}{\partial t}-v_0\frac{\partial u}{\partial y}=\upsilon\frac{\partial^2 u}{\partial y^2}+gB_T(T-T_\infty)+gB_C(C-C_\infty)-\frac{\sigma B_0^2}{\rho(1+m^2)}(u+mw)-\frac{\mu}{\rho k_1}u \qquad (1)$$

Momentum equation in $x-$axis:

$$\frac{\partial w}{\partial t}-v_0\frac{\partial w}{\partial y}=\upsilon\frac{\partial^2 w}{\partial y^2}+\frac{\sigma B_0^2}{\rho(1+m^2)}(mu-w)-\frac{\mu}{\rho k_1}w \qquad (2)$$

Energy equation:

$$\frac{\partial T}{\partial t}-v_0\frac{\partial T}{\partial y}=\frac{\kappa}{\rho c_p}\frac{\partial^2 T}{\partial y^2}+\frac{Dk_t}{c_s c_p}\frac{\partial^2 C}{\partial y^2}+\frac{\sigma B_0^2}{\rho C_p\left(1+m^2\right)}\left(u^2+w^2\right)-\frac{1}{\rho C_p}\frac{\partial q_r}{\partial y}+\frac{Q}{\rho c_p}\left(T-T_\infty\right)^p \tag{3}$$

Concentration equation:

$$\frac{\partial C}{\partial t}-v_0\frac{\partial C}{\partial y}=D\frac{\partial^2 C}{\partial y^2}+\frac{Dk_t}{T_m}\frac{\partial^2 T}{\partial y^2}-k_0\left(C-C_\infty\right)^q \tag{4}$$

with the corresponding boundary conditions are

$$u=U_\infty,\ w=0,\ T=T_w,\ C=C_w \quad \text{at } y=0 \tag{5}$$

$$u=0,\ w=0,\ T\to T_\infty,\ C\to C_\infty \quad \text{as } y\to\infty \tag{6}$$

where u, v and w are the x, y and z components of velocity vector, $m=\omega_e t_e$ is the Hall parameter, where ω_e is the electron frequency, υ is the kinematic coefficient viscosity, μ is the fluid viscosity, ρ is the density of the fluid, κ is the thermal conductivity, c_p is the specific heat at the constant pressure , k_0 is the rate of chemical reaction and D is the coefficient of mass diffusivity, k_t is the thermal diffusion ratio, c_s is the concentration susceptibility, respectively. Here p and q are considered as positive constant. The radiative heat flux q_r is described by the Rosseland approximation such that $q_r=-\frac{4\sigma^*}{3k^*}\frac{\partial T^4}{\partial y}$, where σ^* and k^* are the Stefan-Boltzman constant and the mean absorption coefficient, respectively. We assume that the temperature difference within the flow are sufficiently small so that the T^4 can be expressed as a linear function after using Taylor series to expand T^4 about the free stream temperature T_∞ and neglecting higher-order terms. This result in the following approximation: $T^4\approx 4T_\infty^3 T-3T_\infty^4$.

To obtain the governing equations and the boundary condition in dimension less form, the following non-dimensional quantities are introduced as;

$$Y=\frac{yU_\infty}{\upsilon},\ U=\frac{u}{U_\infty},\ W=\frac{w}{U_\infty},\ \tau=\frac{tU_\infty^2}{\upsilon},\ \overline{T}=\frac{T-T_\infty}{T_w-T_\infty} \text{ and } \overline{C}=\frac{C-C_\infty}{C_w-C_\infty}$$

Substituting the above relations in equations (1)-(4) and corresponding boundary conditions (5) and (6) are;

$$\frac{\partial U}{\partial \tau}-S\frac{\partial U}{\partial Y}=\frac{\partial^2 U}{\partial Y^2}+G_r\overline{T}+G_m\overline{C}-\frac{M}{\left(1+m^2\right)}\left(U+mW\right)-KU \tag{7}$$

$$\frac{\partial W}{\partial \tau}-S\frac{\partial W}{\partial Y}=\frac{\partial^2 W}{\partial Y^2}+\frac{M}{\left(1+m^2\right)}\left(mU-W\right)-KW \tag{8}$$

$$\frac{\partial \overline{T}}{\partial \tau}-S\frac{\partial \overline{T}}{\partial Y}=\left(\frac{1+R}{P_r}\right)\frac{\partial^2 \overline{T}}{\partial Y^2}+D_u\frac{\partial^2 \overline{C}}{\partial Y^2}+\frac{ME_c}{\left(1+m^2\right)}\left(U^2+W^2\right)+\beta\overline{T}^{\,p} \tag{9}$$

$$\frac{\partial \overline{C}}{\partial \tau}-S\frac{\partial \overline{C}}{\partial Y}=\frac{1}{S_c}\frac{\partial^2 \overline{C}}{\partial Y^2}+S_r\frac{\partial^2 \overline{T}}{\partial Y^2}-\gamma\overline{C}^{\,q} \tag{10}$$

boundary conditions are;

$$U=1,\ W=0,\ \overline{T}=1,\ \overline{C}=1 \text{ at } Y=0 \tag{11}$$

$$U=0,\ W=0,\ \overline{T}=0,\ \overline{C}=0 \text{ as } Y\to\infty, \tag{12}$$

where τ represents the dimensionless time, Y is the dimensionless Cartesian coordinate, U and W are the dimensionless velocity component in X and Z direction, $\overline{T}$ is the dimensionless temperature, $\overline{C}$ is the dimensionless concentration, $S=\frac{v_0}{U_\infty}$ (Suction Parameter), $G_r=\frac{gB_T\left(T_w-T_\infty\right)\upsilon}{U_\infty^3}$ (Grashoff Number), $G_m=\frac{gB_C\left(C_w-C_\infty\right)\upsilon}{U_\infty^3}$ (Modified Grashoff Number), $K=\frac{\mu\upsilon}{\rho k_1 U_\infty^2}$ (Permeability of the porous medium), $M=\frac{\sigma B_0^2\upsilon}{\rho U_\infty^2}$ (Magnetic Parameter), $R=\frac{16\sigma^* T_\infty^3}{3k^*\kappa}$ (Radiation Parameter), $P_r=\frac{\rho c_p\upsilon}{\kappa}$ (Prandlt Number), $D_u=\frac{Dk_t}{\upsilon c_s c_p}\frac{\left(C_w-C_\infty\right)}{\left(T_w-T_\infty\right)}$ (Dufour Number), $E_c=\frac{U_\infty^2}{c_p\left(T_w-T_\infty\right)}$ (Eckert

Number), $\beta = \dfrac{Q_0 \upsilon (T_w - T_\infty)^{p-1}}{\rho c_p U_\infty^2}$ (Heat Generation or Absorption Parameter), $S_c = \dfrac{\upsilon}{D}$ (Schimidt Number), $S_r = \dfrac{Dk_T}{\upsilon T_m} \dfrac{(T_w - T_\infty)}{(C_w - C_\infty)}$ (Soret Number) and $\gamma = \dfrac{k_0 \upsilon (C_w - C_\infty)^{q-1}}{U_\infty^2}$ (Chemical Reaction Parameter).

3. Shear Stress, Nusselt and Sherwood Number

From the velocity field, the effects of various parameters on the shear stress have been calculated. Shear stress in x-direction, $\tau_x = \mu_0 \left(\dfrac{\partial U}{\partial Y} \right)_{Y=0}$ which is proportional to $\left(\dfrac{\partial U}{\partial Y} \right)_{Y=0}$. Shear stress in z-direction, $\tau_z = \mu_0 \left(\dfrac{\partial W}{\partial Y} \right)_{Y=0}$ which is proportional to $\left(\dfrac{\partial W}{\partial Y} \right)_{Y=0}$. From the temperature field, the effects of various parameters on Nusselt number have been investigated. Nusselt number, $Nu = -\mu_0 \left(\dfrac{\partial \overline{T}}{\partial Y} \right)_{Y=0}$ which is proportional to $-\left(\dfrac{\partial \overline{T}}{\partial Y} \right)_{Y=0}$. And from the concentration field, the effects of various parameters on Sherwood number have been analyzed and the Sherwood number, $Sh = -\mu_0 \left(\dfrac{\partial \overline{C}}{\partial Y} \right)_{Y=0}$ is proportional to $-\left(\dfrac{\partial \overline{C}}{\partial Y} \right)_{Y=0}$.

4. Numerical Solutions

In order to solve the non-dimensional system by the implicit finite difference technique, it is required a set of finite difference equations. In this case, the region within the boundary layer is divided by some perpendicular lines of Y-axis,

Fig. 2. Finite difference system grid.

where Y-axis is normal to the medium as shown in Fig. 2. It is assumed that the maximum length of boundary layer is $Y_{\max} = (25)$ as corresponds to $Y \to \infty$ i.e. Y varies from 0 to 25 and the number of grid spacing in Y directions is $\overline{p}(= 400)$, hence the constant mesh size along Y axis becomes $\Delta Y = 0.0625 (0 \le Y \le 25)$ with a smaller time-step $\Delta t = 0.001$.

Let $U', W', \overline{T}'$ and $\overline{C}'$ denote the values of $U, W, \overline{T}$ and $\overline{C}$ of a time-step respectively. Using the implicit finite difference approximation, the following appropriate set of finite difference equations are obtained as;

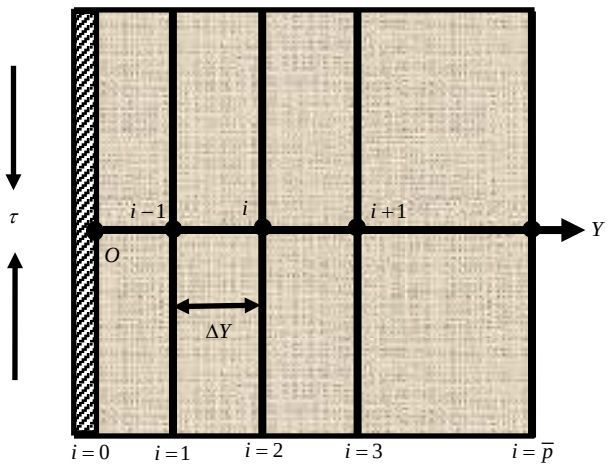

$$\frac{U_i^{n+1}-U_i^n}{\Delta\tau}-S\frac{U_{i+1}^n-U_i^n}{\Delta Y}=\frac{U_{i+1}^n-2U_i^n+U_{i-1}^n}{(\Delta Y)^2}+G_r\overline{T}_i^n+G_m\overline{C}_i^n-\frac{M}{\left(1+m^2\right)}\left(mW_i^n+U_i^n\right)-KU_i^n \quad (13)$$

$$\frac{W_i^{n+1}-W_i^n}{\Delta\tau}-S\frac{W_{i+1}^n-W_i^n}{\Delta Y}=\frac{W_{i+1}^n-2W_i^n+W_{i-1}^n}{(\Delta Y)^2}+\frac{M}{\left(1+m^2\right)}\left(mU_i^n-W_i^n\right)-KW_i^n \quad (14)$$

$$\frac{\overline{T}_i^{n+1}-\overline{T}_i^n}{\Delta\tau}-S\frac{\overline{T}_{i+1}^n-\overline{T}_i^n}{\Delta Y}=\left(\frac{1+R}{P_r}\right)\frac{\overline{T}_{i+1}^n-2\overline{T}_i^n+\overline{T}_{i-1}^n}{(\Delta Y)^2}+D_u\frac{\overline{C}_{i+1}^n-2\overline{C}_i^n+\overline{C}_{i-1}^n}{(\Delta Y)^2}$$
$$+\frac{ME_c}{\left(1+m^2\right)}\left\{\left(U_i^n\right)^2+\left(W_i^n\right)^2\right\}+\beta\left(\overline{T}_i^n\right)^p \quad (15)$$

$$\frac{\overline{C}_i^{n+1}-\overline{C}_i^n}{\Delta\tau}-S\frac{\overline{C}_{i+1}^n-\overline{C}_i^n}{\Delta Y}=\frac{1}{S_c}\frac{\overline{C}_{i+1}^n-2\overline{C}_i^n+\overline{C}_{i-1}^n}{(\Delta Y)^2}+S_r\frac{\overline{T}_{i+1}^n-2\overline{T}_i^n+\overline{T}_{i-1}^n}{(\Delta Y)^2}-\gamma\left(\overline{C}_i^n\right)^q \quad (16)$$

with the finite difference boundary conditions,

$U_0^n=1, W_0^n=0, \overline{T}_0^n=1, \overline{C}_0^n=1$ (17)

$U_L^n=0, W_L^n=0, \overline{T}_L^n=0, \overline{C}_L^n=0$ where $L\to\infty$ (18)

Here the subscript i designates the grid points with Y coordinate and the superscript n represents a value of time, $\tau=n\Delta\tau$ where $n=0,1,2,\ldots\ldots$. The primary velocity (U), secondary velocity (W), temperature $(\overline{T})$ and concentration $(\overline{C})$ distributions at all interior nodal points may be computed by successive applications of the above finite difference equations. The numerical values of the local shear stresses, local Nusselt number and local Sherwood are evaluated by **Five-point** approximate formula and the average shear stresses, average Nusselt number and average Sherwood number are calculated by the **Simpson's** $\frac{1}{3}$ integration rule. The stability conditions of the method are;

$$-\beta\Delta\tau+2\left\{S\frac{\Delta\tau}{\Delta Y}+\left(\frac{1+R}{Pr}\right)\frac{2\Delta\tau}{(\Delta Y)^2}\right\}\le 2,\ \gamma\Delta\tau+2\left\{S\frac{\Delta\tau}{\Delta Y}+\frac{2\Delta\tau}{Sc(\Delta Y)^2}\right\}\le 2, \text{ and } \left(K+\frac{M}{1+m^2}\right)\Delta\tau+2\left\{S\frac{\Delta\tau}{\Delta Y}+\frac{2\Delta\tau}{(\Delta Y)^2}\right\}\le 2 \text{ and}$$

convergence criteria of the problem are $m<<1$, $D_u<<1$ or $S_r<<1$, $K\le 911$, $\beta\ge -1760$, and $\gamma\le 846$ when $S=2.00$, $R=0.20$, $P_r=7.00$, $S_c=0.94$.

5. Results and Discussion

To observe the physical situation of the problem, the steady-state solutions have been illustrated in Figs. 3-7 when $p=2$ and $q=2$. The primary velocity, secondary velocity and temperature distributions are displayed for various values of Dufour number D_u respectively illustrated in Figs. 3(a), 3(b) and 4(a). These results show that the primary velocity, secondary velocity and temperature distributions increase with the increase of D_u. The effect of Soret number S_r on the primary velocity, secondary velocity and concentration distributions are respectively illustrated in Figs. 4(b), 5(a) and 5(b). These results show that the primary velocity, secondary velocity and concentration distributions increase with the increase of S_r. The concentration distribution is shown in Fig. 6(a) for various values of chemical reaction parameter γ with two values of Schimdt number $S_c=0.60$ (water vapor) and $S_c=0.94$ (carbon dioxide) respectively. It is noted that the concentration decreases with the increase of γ, where $\gamma<0$ and $\gamma>0$ are treated as genarative and destructive chemical reaction respectively. The concentration also decreases with the increase of S_c leads to thining of the concentration boundary layers. Fig. 6(b) displays the temperature distribution for several values of heat generation or absorption parameter β and Prandlt number P_r. It is noted that the temperature increases with increase of β, where $\beta<0$ and $\beta>0$ are treated as heat absorption and genaration respectively. The temperautre increases with the increase Prandlt number P_r. This is consistent with the well known fact that the thermal boundary layer thickness increasing with the increase P_r. The Nusselt number for different values of heat genaration or absorption parameter β and Prandlt number P_r are displayed graphically in Fig. 7(a). The Nusselt number decreases with the rise of β and increases with the rise of P_r. The Sherwood number for different values of chemical reaction parameter γ and Schimdt number S_c are displayed graphically in Fig. 7(b). The Sherwood number increases with the increase of γ and S_c.

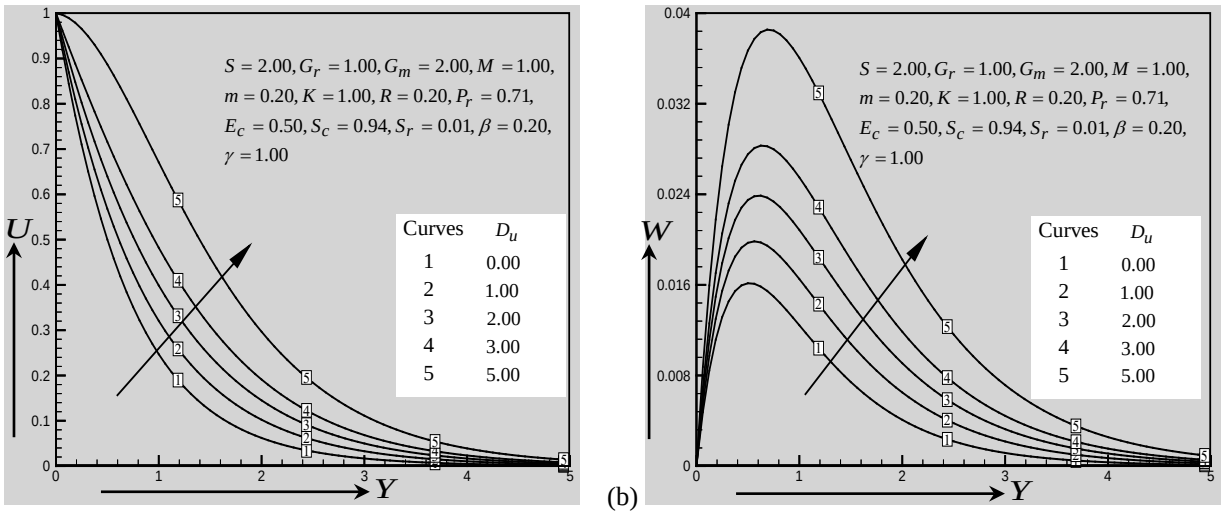

Fig. 3. Illustration of (a) Primary velocity profiles and (b) Secondary velocity profiles for various values of D_u when $p = 2$ and $q = 2$.

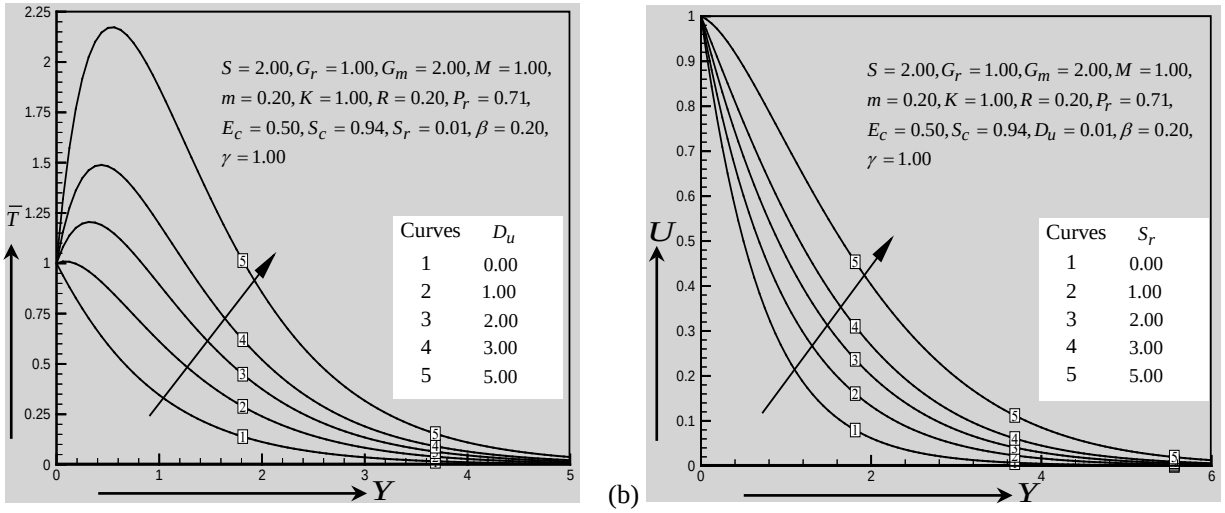

Fig. 4. Illustration of (a) Temperature profiles for varios values of D_u and (b) Primary velocity profiles for various values of S_r when $p = 2$ and $q = 2$.

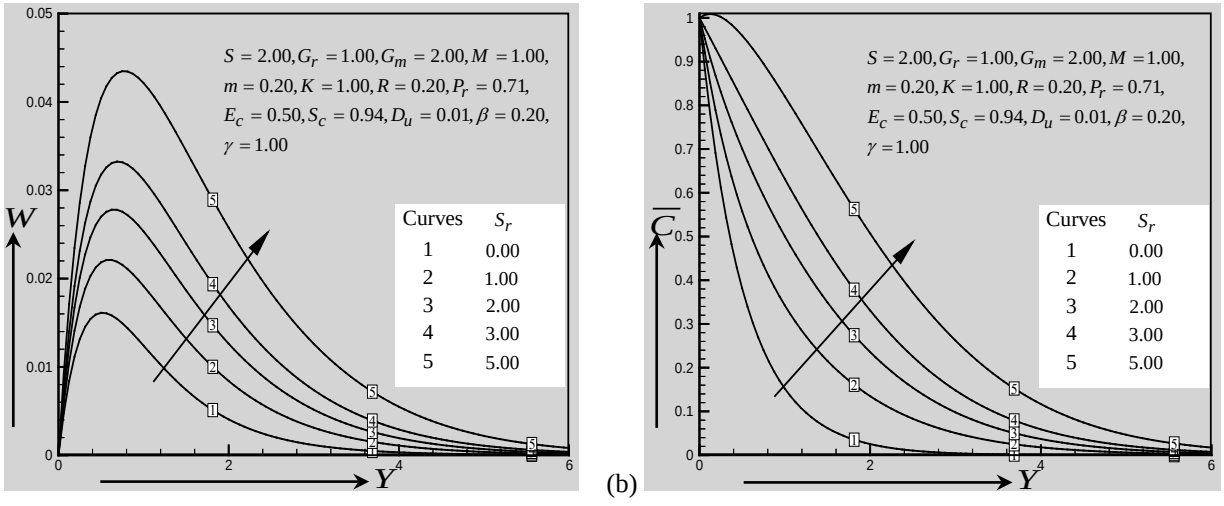

Fig. 5. Illustration of (a) Secondary velocity profiles and (b) Concentration profiles for various values of S_r when $p = 2$ and $q = 2$.

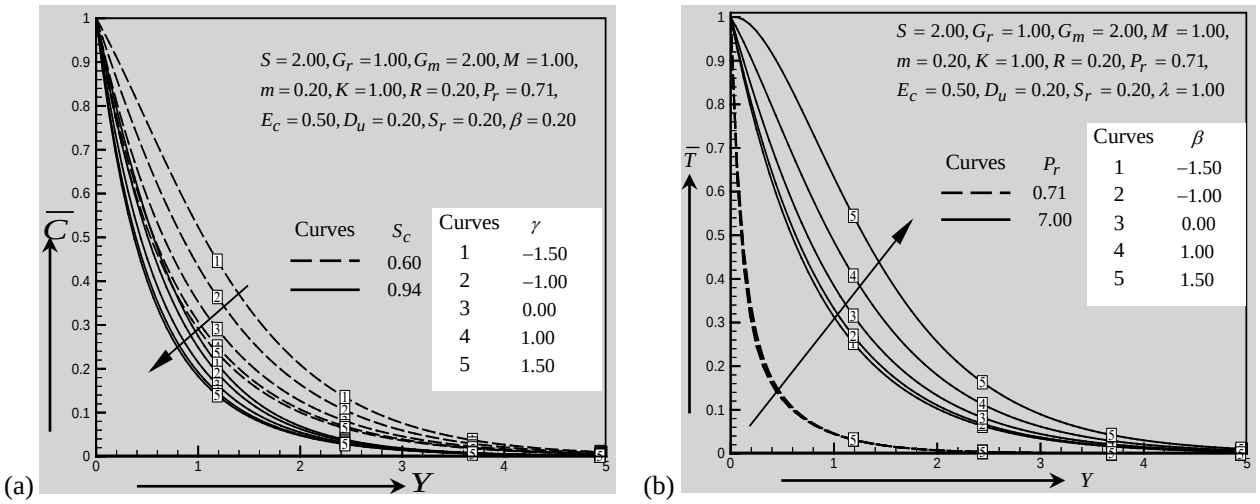

Fig. 6. Illustration of (a) Concentration profiles for various values of γ and (b) Temperature profiles for various values of β when $p = 2$ and $q = 2$.

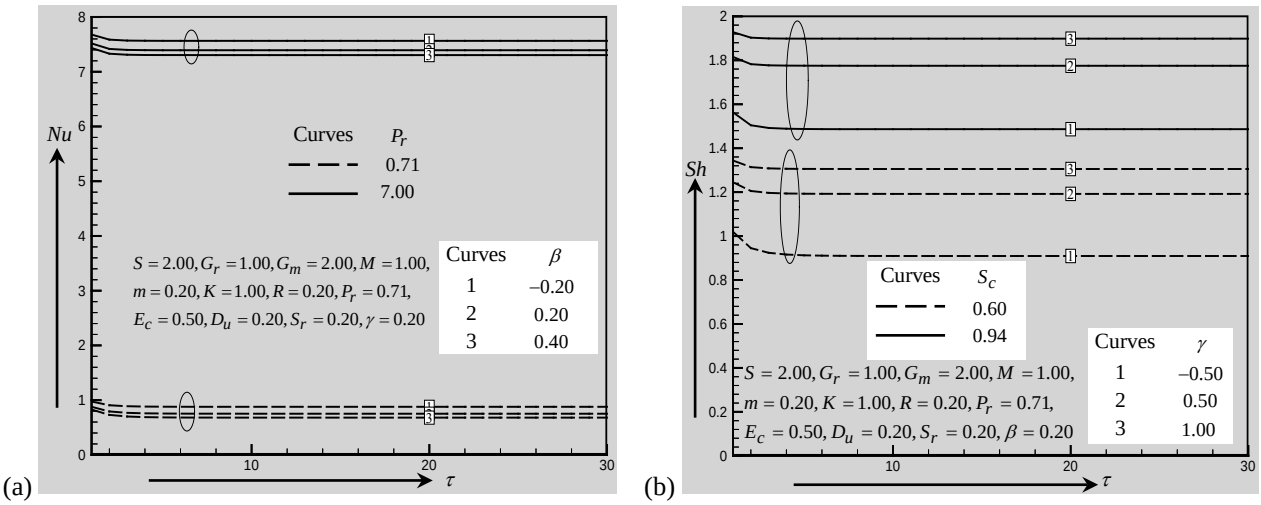

Fig. 7. Illustration of (a) Nusselt number for various values of β and P_r and (b) Sherwood number for various values of γ and S_c when $p = 2$ and $q = 2$.

Finally, a qualitative comparison of the present steady-state results with the published results (Aurangzaib and Shafie **[5]**) is presented in table 1. The accuracy of the present results is qualitatively as well as quantitatively good in case of all the flow parameters.

Table 1. Qualitative comparison of the present results with the previous results

Increased Parameter	Previous results given by Aurangzaib and Shafie **[5]**						Present results					
	$f'(\eta)$	$h(\eta)$	$\theta(\eta)$	$\phi(\eta)$	Rate of H. T.	Rate of C.	U	V	T	C	Nu	Sh
Du	Inc.	Inc.	Inc.				Inc.	Inc.	Inc.			
Sr	Inc.	Inc.		Inc.			Inc.	Inc.		Inc.		
γ				Dec.		Inc.				Dec		Inc.
Sc				Dec.		Inc.				Dec.		Inc.
β			Inc.		Dec.				Inc.		Dec.	
Pr			Dec.		Inc.				Inc.		Inc.	

R	Inc.	Inc.

6. Conclusions

In this study, In this study, the finite difference solution of unsteady MHD mixed convection heat and mass transfer over a permeable vertical plate in the presence of heat generation, chemical reaction, thermal radiation and Hall current for $p \leq 2$ and $q \leq 2$ is investigeted. In present investigation, the primary velocity, secondary velocity and temperature distributions increase with the increase of Dufour number. The primary velocity, secondary velocity and concentration distributions increase with the increase of Soret number. The concentration decreases with the increase of chemical reaction parameter and Schimidt number. It is also seen that temperature increases for the increase of heat genaration or absorption parameter and Prandlt number. The Nusselt number decreases with the increase of heat genaration or absorption parameter and increases with the and Prandlt number. The Sherwood number increases with the increase of chemical reaction parameter and Schimdt number.

References

[1] Das, U. N., Dekha, R., Soungalgekar, V. M., 1994. Effects on m ass transfer on flow past an impulsively started infinite vertical plate with constant heat flux and chemical reaction, Forschungim Ingenieurwesen 60, pp. 284-287.

[2] Satter, M. A., Kalim, H., 1996. Unsteady free-convection interaction with thermal radiation in a boundary layer flow past a vertical porous plate, J. Math. Phys. Sci. 30(1). Pp. 25- 37.

[3] Aydin, O., Kaya, A., 2008. Radiation effect on MHD mixed convection flow about a permeable vertical plate, Heat Mass Transfer 45, pp.239-246.

[4] Stanford Shateyi, Sandile Sydney Mosta and Precious Sibanda, 2010. The effects of thermal radiation, Hall currents, Soret and Dufour on MHD flow by mixed convection over a vertical surface in porous media, Mathematical Problems in Engineering, Article ID 627475.

[5] Aurangzaib, Sharidan Shafie, 2011. Effects of Soret and Dufour on unsteady MHD flow by mixed convection over a vertical surface in porous media with internal heat generation, chemical reaction and Hall current, Canadian Journal on Science and Engineering Mathematics 2(4), pp-153-162.

5th BSME International Conference on Thermal Engineering

Power Generation By Multiple Pedaling And Comparison With Solar Panel

Md. Arif Hossain[a,*], Asif Tanveer [a]

Department of Mechanical Engineering
Bangladesh University of Engineering and Technology,
Dhaka-1000, Bangladesh

Abstract

'Power generation by using multiple pedaling' is fabricated using local technology and available materials. It uses human energy to produce electricity. It's potentiality in the field of micro level electricity generation is quite significant. Here an alternator is connected to a belt-pulley and chain-sprocket arrangement in a rigid structure. The input rotation is given on the pedal and final rotational speed is obtained in the alternator rotor that consecutively produces current. A new and improved technique is developed through this project that is a single shaft can be coupled by multiple pedal which not only reduce individual's afford but also helps to generate more power by engaging more people on this work. 'Power Generator by multiple pedaling' can be an attractive renewable energy source for the production of electricity. In the developing country like ours, it can be used in the villages as useful source of power for a small family where the family members themselves can charge the battery by pedaling daily for a short period of time. It can be used for partial power supply in gymnasium, apartment, school and other public places. This will not only provide electricity according to their need but also provide a useful way of physical exercise and a handsome amount of payment to them which can be good source of income for the poor people. Due to the low manufacturing cost and very low maintenance effort, wide scale application "Power generation by multiple pedaling" can be a suitable source of renewable energy instead of solar panel. we are successful to reduce the production cost up to 30% compare to the production of solar panel.

***Keywords*:** alternator, current, human afford, multiple pedaling, solar panel

1. Introduction

Living in 21st century, only a few recognizes the great ingenuity that is required to bring electricity in to our lives. Our proposal seeks to raise hands on awareness of electricity production, while demonstrating alternatives to the current standard in an exciting and engaging way. It is important to visualize new ways to bring power to the people as population continues to grow and power shortages continue to occur. Much of the power that is provided to people today is done in very un-sustainable ways; new ideas are needed to transition in to a post cheap-petroleum era. Electricity is one of the most important driving forces of human civilization. The main sources for producing electricity are non-renewable sources and day by day they are exhausting due to rapid growth of electricity consumption. So need for alternate renewable sources for electricity generation has become of a matter great interest.

Energy cannot be created and destroyed. It can be changed from one from to another. There are many form of energy like Thermal energy, Sound energy, Kinetic energy, Potential energy, Electric energy and so one. Among them Electric energy is the most useful terminal form of energy. Using human energy can be an attractive source of small-scale electricity production. Paddle Power Generator uses this human energy to produce electricity. It is based on the alternator principle where an alternator is rotated to produce electricity and stored in a battery.

* Corresponding author. Tel.: +88-01717-337199.
E-mail address: arif_buet_06@yahoo.com

2. Structure of Multiple pedaling unit

2.1 Major components

- Rickshaw/Bicycle framework
- Chain-drive system
- Belt-pulley system for transmission
- Alternator with DC output and regulator
- Battery

2.2 Working Principal

The entire system can be divided into three steps of energy conversion. First, the human muscle energy is converted into mechanical energy through pedaling. This mechanical energy is represented in the form of rotation of chain-sprocket system. Second, the mechanical energy is transferred through the chain drive and converted to electrical energy in the alternator. Finally, the electrical energy is stored in the battery as chemical energy.

2.2.1 Conversion of energy

The mechanical energy is produced by the cycling action. The rotation of the larger sprocket (with the pedals) drives the smaller sprocket on the rear shaft. Motion and power are transferred with the help of a chain. The chain pulley system has a teeth ratio of 48:22. The shaft rotates and rotates a large pulley, which drives the smaller pulley of the alternator with the help of a belt drive. The belt pulley has a diameter ratio of 18:2. This ratio is chosen so to attain the charging speed of the alternator, which is around 1000 to 1200rpm. This reduces pedaling effort.
Conversion from mechanical energy to electrical energy is done with the help of an automotive alternator. An alternator is simply an electromechanical device used to convert mechanical energy to electrical energy in the form of alternating current. Since battery charging needs DC voltage, a rectifier is used to convert the AC current to DC current. This is done by the battery. As the alternator generates the charging voltage, terminals of the battery connected to the alternator draws in charging current and the battery charges itself, and stores the energy in chemical form. The typical chemical reaction that occurs in an automotive lead-acid battery (similar to one used in experiment) is shown below:

$$PbO_2 + Pb + 2H_2SO_4 \underset{\text{Charge}}{\overset{\text{Discharge}}{\rightleftarrows}} 2PbSO_4 + 2H_20$$

2.3 Main Structure

The main structure consists of two bicycle frameworks for two users to pedal simultaneously. The frameworks are placed parallel to each other and connected by a rod. The rod improves stability and vibration of the whole structure. The framework is been welded to horizontal angle bars for support. Chain drive transfers power to the shaft. Free-wheeling sprockets on the shaft allow two users to pedal simultaneously or individually. The shaft also has a large pulley that is connected to the alternator via a belt drive system. The alternator can be moved horizontally along the parallel setup to loosen or tighten the belt, or to remove it if the belt wears out. It also allows greater flexibility in selecting the length of the belt.

(a) (b)

Fig. 1. (a) proposed design; (b) actual design

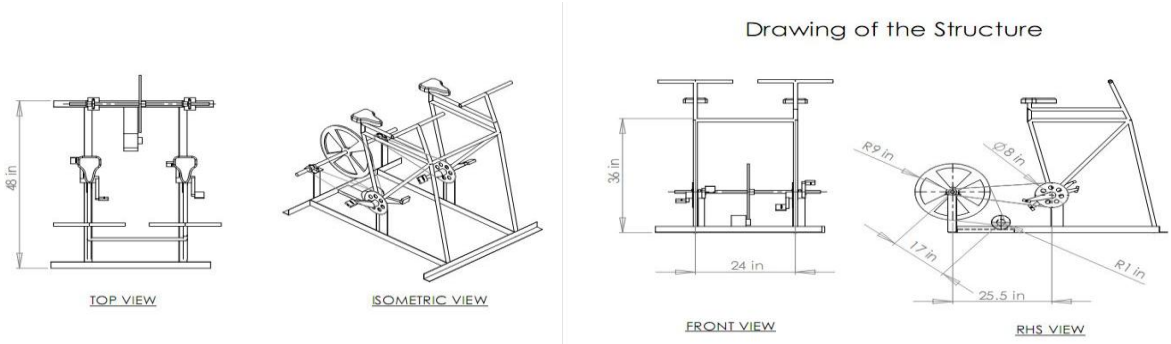

Fig. 2. detail drawing of the structure

2.4 Technical parameters

Table 1. Technical specification

No	Feature	Dimension / specification
1.	Overall Dimension	48 inch X 24 inch X 48 inch
2.	Diameter of Large pulley	18 inch
3.	Diameter of small pulley	2 inch
4.	Teeth no of Large sprocket	48
5.	Teeth no of small sprocket	22
6.	Centre Distance between pulley	17 inch
7	Height of hand rest	48 inch
8.	Speed multiplying factor	19.63
9.	Alternator Driving belt	Belt No: A 68
10.	Storage Battery	Brand : Non brand , 35 AHr-12V Battery
11.	Alternator	60 Amp-12V, Automotive type.

2.5 Power transmission

The design of the system is such that there are two stages of power transmission needed to reach the minimum effective charging speed of the alternator. The first transmission occurs by a chain-sprocket system and the second by a belt-pulley system which in turn is connected to a single rotating shaft. When the user pedals, the large sprocket is rotated at a speed equal to the rotation of the pedal. This large Sprocket has 48 teeth. The large sprocket is connected by a chain to the small sprocket of 22 teeth.

Let the large sprocket rotate at a speed N_1 and the small sprocket rotate at a speed N_2. So the relation of the rotation of the two sprockets is [1]

$$\frac{N_2}{N_1} = \frac{48}{22} \quad (1)$$

Now the small sprocket has the same shaft with the large pulley of the belt pulley system. So the large pulley rotates at the same speed as the small sprocket. So if the speed of the large pulley is N_3 then

$$N_2 = N_3 \quad (2)$$

Here diameter of the large pulley is 18 in and small pulley is 2 in; let the speed of the small pulley is N_4. So

$$\frac{N_4}{N_3} = \frac{18}{2} \quad (3)$$

Now as the small pulley is coupled with the alternator so the speed of the small pulley will ultimately be the speed of the alternator. Form equation 1, 2 and 3 speed of the alternator

$$\frac{N_4}{N_1} = \frac{48}{22} \times \frac{18}{2} = 19.63$$

So, the ultimate speed multiplying factor = 19.63
If pedal rpm is 60, then alternator rpm becomes 60x19.63 = 1177.
Rpm are calculated and verified using a contact-type tachometer.

2.6 Belt pulley selection

Known data,
Diameter of Larger pulley, d_1 = 18 in = 45.72 cm
Diameter of small pulley, d_2 = 2 in = 5.08 cm
Centre distant between two pulley, c = 17 in = 43.18 cm

Then, length of the belt, $L = \frac{\pi}{2}\left(d_1 + d_2\right) + 2c + \frac{(d_1 - d_2)^2}{4c}$

= 176 cm (~70in)

3. Results

Charging an automotive battery is the primary goal of this Alternating power generator. This setup is used to charge a battery up to a certain level in relation to the electrical power consumed from the battery. To determine the exact state of the battery for desire charging level, the following parameters need to be known.

- Rotational speed of the alternator rotor.
- Generated voltage and current from the alternator.
- Open circuit voltage (OCV) of the battery.
- Specific gravity of the battery electrolyte

The performance test results regarding various parameters, data table and graphs are shown below.

Table 2.1 Observation for a single person pedaling

Obs NO:	Time(min)	Voltage(Volt)	Avg Voltage (Volt)	Current (amp)	Power (Watt)
1	1	12.38-12.45	12.41	3.5	43.57
2	1	12.36-12.62	12.49	2	25.24
3	1	12.58-12.70	12.64	2.2	27.94
4	1	12.57-12.75	12.66	2	25.5
5	1	12.64-12.80	12.72	2.1	26.88
6	1	12.72-12.78	12.75	2.2	28.05
7	1	12.75-12.79	12.77	2	25.54
8	1	12.74-12.78	12.76	2.1	26.8
9	1	12.78-12.92	12.85	2.3	29.55
10	1	12.75-12.86	12.80	2.2	28.17

Table 2.2 Observation for double person pedaling

Obs NO:	Time(min)	Voltage(Volt)	Avg Voltage (Volt)	Current (amp)	Power (Watt)
1	1	12.32-12.52	12.42	4.75	58.9
2	1	12.38-12.64	12.51	3.63	45.4
3	1	12.56-12.68	12.62	3.28	41.1
4	1	12.58-12.72	12.65	3.14	39.7
5	1	12.62-12.78	12.70	3.00	38.1
6	1	12.66-12.76	12.71	3.12	39.6
7	1	12.69-12.78	12.73	3.08	39.2
8	1	12.72-12.80	12.76	3.10	39.5
9	1	12.75-12.84	12.79	3.00	38.3
10	1	12.78-12.85	12.81	3.13	40.1

Initially there is a large amount of current flow which is known as surge current. As time passes current become stable and power varies with the current flow. Terminal Voltage varies with current and if the battery is fully charged then it with show approximately 12.80 volt. For a single person rotor speed varies from 700-1000 rpm. And in the observation current varies from 3.5-2 amp.

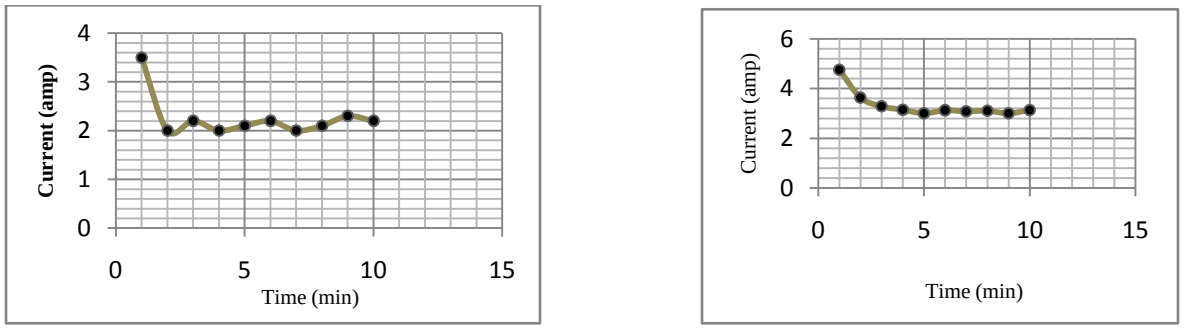

(a) *(b)*

Fig. 3.(a) Charging current Vs Time (single person); (b) Charging current Vs Time (Two person)

Charging current varies with rotor speed. As the alternator's rated rpm is 3000rpm [2] but in this project maximum rotor speed recorded was 1350 rpm. Charging current are recorded for the rotor speed varies from 700 rpm to 1350 rpm and the corresponding current varies from. The recorded data are given below.

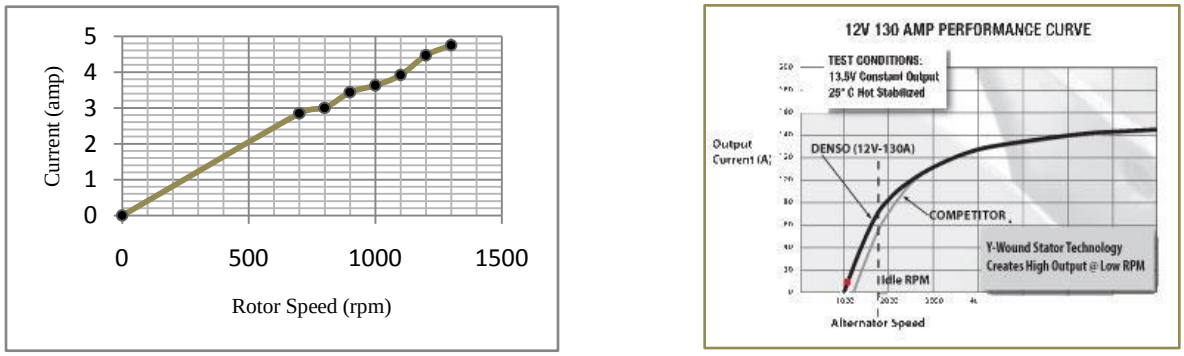

(a) *(b)*

Fig.4. (a)Charging current Vs Rotor Speed; (b) performance curve of a typical alternator

Power obtained by a single person and two persons are given below.

Table 3. Power output for single person and two person

Output Power (Watt) Single Person	Output Power (Watt) Two person
43.57	58.9
25.24	45.4
27.94	41.1
25.50	39.7
26.88	38.1
28.05	39.6
25.54	39.2
26.80	39.5
29.55	38.3

4. Comparison with solar panel

Table 4. Cost analysis

Components		Price (BDT)
Structure		
	Frame	1160
	Axle	500
	Pulleys, sprockets and chains	1080
	Angle Bar (17.5 kg)	1200
	Accessories	970
Alternator		4000
Battery		5000
Total		13330

Table 5. cost comparison

Power Source	Cost (BDT)	Power (Watts)
Solar Energy	10000	8
Human Power	15000	30

5. Discussion and conclusion

Human power generation can be an attractive renewable source as far as small-scale production of electricity is concerned. Although, initially it may not be popular to city-dwellers where electricity is available at a much cheaper rate and consumption is huge, the prospect of using human power generation in rural areas is brighter, where electricity is scarce and often completely unavailable. This system can, under such circumstances, help produce enough electricity for lighting individual homes at a village. Also, the concept of multiple pedaling can reduce the physical effort needed and charging time, which are vital in rural areas where agrarian life often demands human energy for other uses, such as farming. Other fields of application of this pedal-powered generator may include supplying necessary amount of electricity during long term load-shedding, charging small electronic equipments and so on. Another interesting use can be powering and charging portable research equipments in isolated and inhospitable places, such as in the arctic region or the jungle. In that case, the design needs to be adapted for portability, since the current design is quite bulky. The preliminary studies on the paddle power generator are encouraging as the system has a low cost when compared to a solar photovoltaic home system of similar energy output. Also materials needed to make the setup are available and fabrication is quite simple; maintenance required is therefore low.

References

[1] Khurmi, R.S. and Gupta, J.K.,*Theory of Machines,* S' Chand & Co, New Delhi, India.
[2] Crouse, W.H. and Angline, D.L., *Automotive Mechanics*, Tata Mcgraw-Hill,New Delhi, India.
[3] Theraje, B.L. and Theraje, A.L., E*lectrical Machines*, S' Chand & Co, New Delhi, India.
[4] Hannah, J. and Stephens, R.C., *Mechanics of Machines*, Viva Books Private Ltd, Mumbai, India.
[5] World Energy Council Report 2007, *Deciding the future: Energy Policy Scenario 2050*

5th BSME International Conference on Thermal Engineering

Reverse Osmosis-based-Recovery of used Caustic Solution

[a]Md. Imran Hosain, [b]Ahsanul Kabir Didar, [b]Iqbal Hossain

"[a,b]Department of Chemical Engineering, Bangladesh University of Engineering & Technology, Dhaka-1000, Bangladesh"

Abstract

In mercerizing waste-waters there remains sufficient amount of caustic soda. To recover this generally multistage evaporators are used but this process is energy & capital intensive. As an alternate method membrane technologies can be used for this recovery. Although membrane technologies are economic and environmentally favourable, the use of these technologies is very much limited in Bangladesh. Hence, a comprehensive study is conducted to develop a caustic recovery process in the context of Bangladesh on the basis of membrane technologies. In the developed algorithm, sedimentation, and activated carbon are used for pre-treatment, and the well-known reverse osmosis (RO) process is applied for actual recovery. The effect of temperature on recovery is also studied considering the real operating conditions. Caustic recovery is found to be economic when caustic use exceeds 11,300 tons per year of 100% cotton goods or 22,700 tons per year of 50/50 cotton polyester fabrics. Therefore, the reverse osmosis-based-recovery of used caustic solution from mercerizing waste-water is very promising for Bangladesh.

Keywords: Mercerizing waste-waters, recovery, Membrane technology, filtration, Coagulation, flocculation, sedimentation, Reverse Osmosis

Nomenclature

VFR	Volumetric Flow Rate
RO	Reverse Osmosis
COD	Chemical Oxygen Demand
BOD	Biological Oxygen Demand
TMP	Temperature

1. Introduction

The intensive use of water and a large quantity of chemicals is characterized by the textile industry. Consequently, the effluents of textile industries are characterized by high COD and presence of non biodegradable components e.g. pigments, dyes, some newly introduced polymers or chemicals. A wide range of chemicals are used such as softeners, stain release agents, and wetting agents. Many of these chemicals become part of the final product whereas the rest are removed from the fabric and are purged in the effluent stream which is very much harmful for environment [1], [2]. For that the local authorities have begun to enforce the textile industry to clean up the discharged wastewater. Experts in regulatory body are looking for toxicity due to high salt content, Biological Oxygen Demand (BOD) and, non-destructible COD, heavy metals, and color of the effluent [3]. Bangladesh is considered as a developing economy which has recorded in GDP growth sector, 75% of exports revenues come from garment industry. So this sector is very significant for Bangladesh. In Bangladesh, textile industry often faces shortage of water resources not only because of water scarcity but also discharge limits. These facts have shifted considerations toward water saving and recovery alternatives for the textile industry.

* *Md. Imran Hossain, Tel.: +880 172 655 90 26*
E-mail address: *imran.chebuet@yahoo.com*

The applicability of membrane technology which is a new but becoming a prevalent technology in this area has been investigated. With this intend RO processes have been studied. Furthermore some pre-treatment options prior to these membrane processes to increase the capacity of membrane were implemented. Effluents from textile industry are of complex composition and require more than a single treatment technology to achieve and maintain compliance with currently enforced environmental legislations. Traditional treatment interventions comprise of but not limited on the followings: physical treatments, biological treatments & chemical treatment (e.g. neutralization, oxidation, reduction, coagulation & flocculation etc) [3], [4]. These used methods are insufficient and uneconomic not only for obtaining the required water quality but also for water and chemical recovery.

The prime purpose of this study is to evaluate caustic recovery from mercerizing waste-water and to provide a caustic stream at reusable concentrations by membrane processes. After membrane separation, further processing (evaporation) is to be applied using waste heat from stack gases for the production of a caustic stream at the desired concentration.

2. Caustic Recovery

There are two types of caustic recovery methods from mercerizing wastewater in practice. These are evaporation technique & membrane based recovery. Although use of evaporation technique has good examples, it becomes unsuitable for some manufacturers due to operational difficulties arising from wide range of chemicals applied. These problems have induced the development of membrane based caustic recovery methods (RO) from mercerizing wastewaters.

2.1. Principle of Reverse Osmosis

RO is a process by which low molecular solutes such as inorganic or small organic solutes are separated from solvents. Much denser and hydrologically resistant membranes are used. Normally, a semi permeable membrane separates a dilute solution from a concentrated solution, solvent crosses from the dilute to the concentrated side of the membrane in an attempt to equalize concentrations. The magnitude of the pressure required to completely impede the flow of solvent is defined as the "osmotic pressure". The flow of solvent can be prevented by applying an opposing hydrostatic pressure to the concentrated solution. If the applied hydrostatic pressure exceeds the osmotic pressure, flow of solvent will be reversed, that is, solvent will flow from the concentrated to the dilute solution. This phenomenon is referred to as Reverse Osmosis [5], [6]. The figure illustrates the concepts of osmosis, osmotic pressure and reverse osmosis schematically.

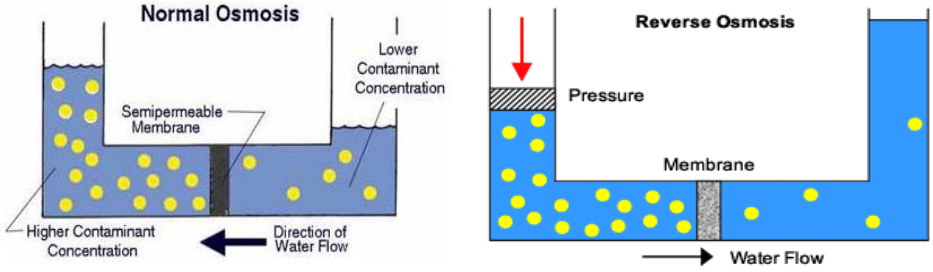

Fig.1. Normal osmosis and Reverse osmosis.

2.2. Experimental

As in Reverse Osmosis (RO) unit only solvent is allowed to pass through the membrane and larger particles are restricted to pass. Along with caustic, mercerizing waste-water also contains solids (polymers). These solids must be cleaned before feeding this solution to RO unit to enhance the capacity and longevity of the membrane used in RO unit. So it is very more convenient to use a pre-treatment unit before the RO unit to separate most of the solids from the solution before feeding to RO unit. For that sediment filter1, activated carbon filter, sediment filter2 are used as pre-treatment unit (fig.2). In sediment filter most of the solids are separated and activate

carbon filter is used to absorb colored solids. In RO unit the feed solution is splits into two streams, one is permeate stream which is very lower concentration of caustic solution and retantate stream which is higher concentration of caustic solution. Fig. 3(a) shows a spiral wound membrane through which the mechanism of splitting feed stream and fig. 3(b) shows recovery of caustic from mercerizing waste-water using RO unit along with pre-treatment unit.

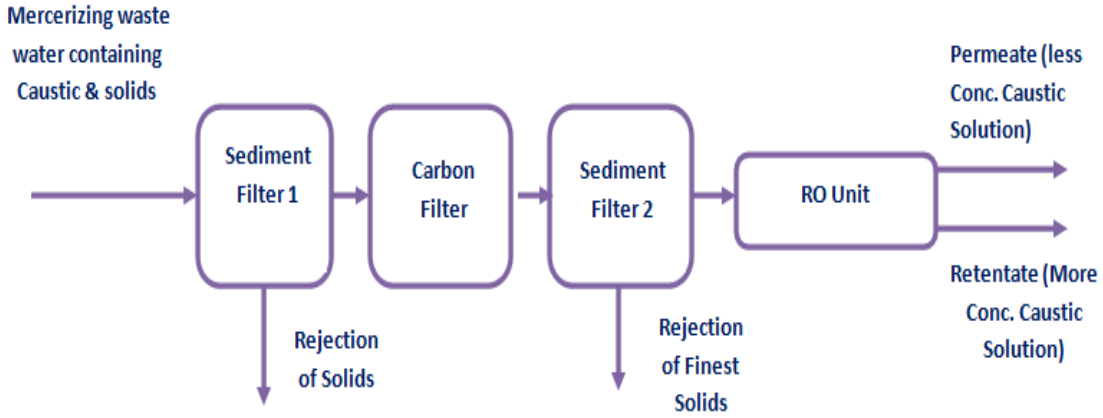

Fig.2. RO unit along with pre-treatment unit for caustic recovery from mercerizing waste-water

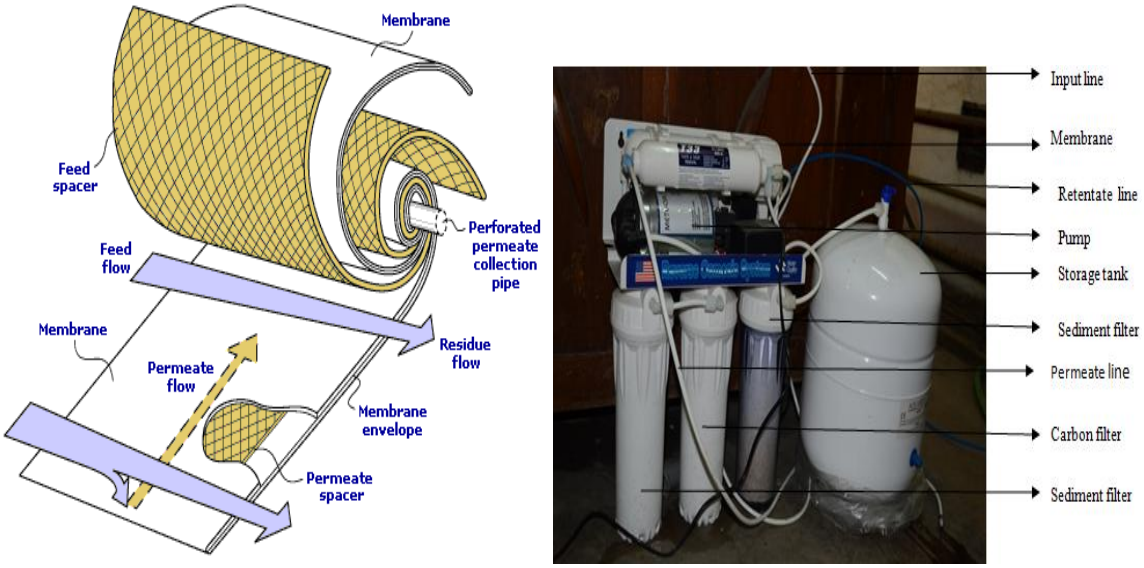

Fig. 3. (a) A spiral wound membrane; (b) experimental caustic recovery RO system.

3. Results and Discussion

In the experimental setup Polyamide membrane (a thin-film composite membrane) is used in the RO unit which has a P^H range (3~13) limitation and a limitation of maximum operating temperature (45^oC). Using this membrane we got a better caustic recovery from feed mercerizing waste-water stream (Table 1. shows the percentage of recovery in retantat stream). As higher and higher the concentrated caustic containing mercerizing waste-water is fed to the RO unit the percentage of recovery becomes lower. This may due to the rapid blocking of pores of membrane by containing solids in the feed stream so that the permeability of membrane gradually

decreases which lowers the flow rate of permeate and the ultimately results in lower concentrated retantate caustic stream. Another reason may be due to the use of high P^H range as operating condition which might lead to degrade membrane's permeability. The percentage of recovered caustic in Retantate with respect to the conc. (wt %) of caustic in mercerizing waste-water fed to RO unit is shown in fig.4. Again temperature (TMP) is one of the important operational parameter that determines the membrane performance. Flow rates of permeate and retantate decline with temperature which is shown in fig. 5.

Table 1. Caustic recovery in RO unit

TMP	Maxi. Working Pressure	Mother Solution Fed to RO unit		Volumetric Flow Rate (VFR)		Permeate from RO Unit		Retantate from RO Unit		Percentage of Recovered Caustic in Retantate
(^{o}C)	(Psi)			(CC/min)						
		Wt%	P^H	Permeate	Retantate	Wt%	P^H	Wt%	P^H	
30.0	100	2.4	12.78	2.7	5.35	0.4	12.00	4.4	13.0	83
32.0	100	4.0	13.00	2.63	5.25	0.42	12.04	6.2	13.2	55
32.8	100	5.0	13.01	2.55	5.20	0.50	12.09	7.3	13.3	46
34.0	100	8.0	13.30	2.35	5.10	0.70	12.24	11.1	13.5	39

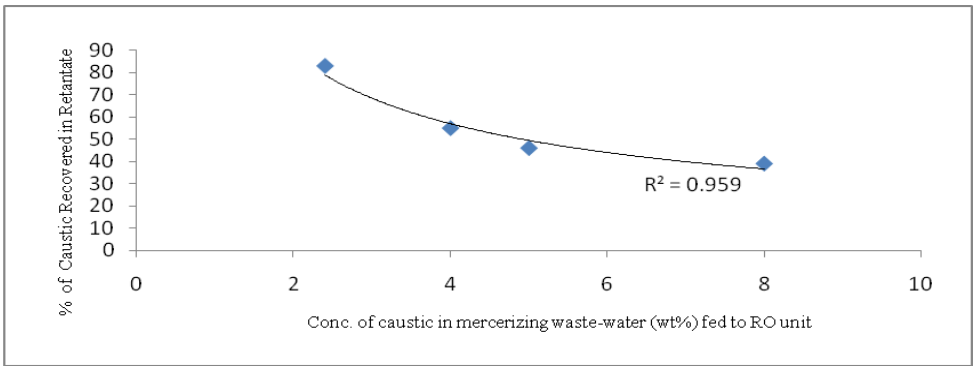

Fig. 4. Percentage of recovered caustic in Retantate stream with respect to the conc. (wt %) of caustic in mercerizing waste-water fed to RO unit

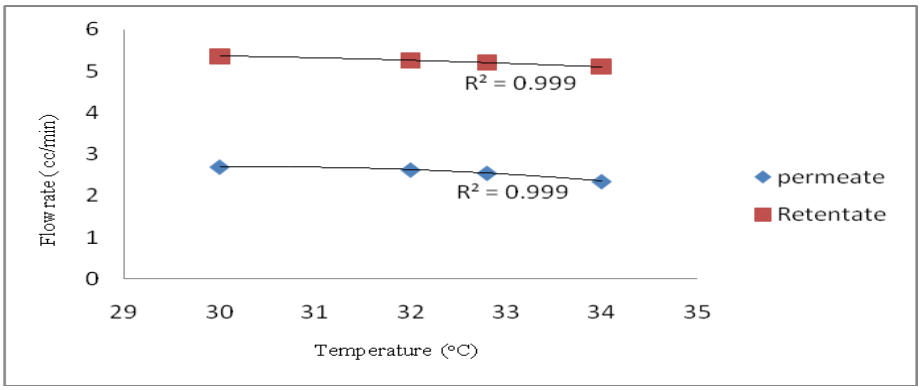

Fig. 5. Permeate & Retantate flow rate varies with temperature

5. Conclusion

RO based caustic recovery process is considered as a cost effective process in textile industry by not only recovering caustic from mercerizing waste-water but also reducing consumption of water, wastewater treatment costs, waste disposal costs and minimizing required heat in evaporation system. Again RO based caustic recovery has gained significance due to environmental regulation and conservation of water resource issue. The experiment indicates the suitability and large scope of RO membrane in Bangladesh.

Acknowledgement

The supports from the Department of Chemical Engineering, Bangladesh University of Engineering and Technology are gratefully acknowledged.

References

[1] Caustic recovery from highly alkaline denim mercerizing wastewaters using membrane technology, M.Sc. Thesis: Middle East Technical University

[2] Aslam, M. M., Baig, M. A., Hassan, I., Qazi, I. A., Malik, M., & Saeed, H.(2004). Textile wastewater characterization and reduction of its COD & BOD by oxidation, Environmental Agricultural and Food Chemistry, 3, 804-811

[3] Wagner, Jorgen (2001) "Membrane Filtration Handbook", 2nd ed., Osmonic. Woerner, Douglas L. "Membrane Technology in Textile Operation" incomplete

[4] Jul 4, 2010 ... BOD/COD ratio and characterized by the limits of toxic, biochemical oxygen demand (BOD) and chemical oxygen demand (COD). Aslam, M.M., M.A. Baig, I. Hassan, I.A. Qazi, M. Malik and H. Saeed, Textile wastewater ... J. Environ. Agric. Food. Chem., 3 (6): 804-811, (2004). 9. Blonskaja, V., I.

[5] http://en.wikipedia.org/wiki/Reverse_osmosis

[6] Srikanth, G. (n.d.). Retrieved 06 08, 2008, from Membrane Separation Processes Technology and Business Opportunities: http://www.biologica.eng.uminho.pt/PSB/docs/TextoFicha3.pdf

5th BSME International Conference on Thermal Engineering

Experimental study on variation and distribution of droplet size of a cylindrical falling jet

Md. Nazmus Sakib[a]*, Raihan Tayeb[b], Mohammad Ali[b]

[a,b] *Department of Mechanical Engineering, Bangladesh University of Engineering and Technology, Dhaka-1000, Bangladesh*

Abstract

This study focuses on the size of the droplets formed during the breakup of a cylindrical falling jet. The size of the droplets at a fixed distance from the jet outlet is measured from photographs. Variations in average droplet diameter with jet velocity are investigated for low Weber number. A correlation between average droplet diameter and Weber number has been drawn. The distribution of droplet size for a certain jet velocity is also studied. Droplet diameters for a certain jet velocity at a fixed position from jet outlet are measured and a frequency distribution curve is plotted. The trend of the frequency distribution curve is in conformity with the Nukiyama-Tanasawa distribution that is widely used as an experimental correlation. Frequency distribution of droplet diameters is also observed with the variation in Weber number.

Keywords: Jet breakup; droplet diameter; droplet size distribution; Nukiyama-Tanasawa distribution.

1. Introduction

The qualitative study of the disintegration process of a liquid jet emanating into another fluid has a history of more than a century. It is in fact fascinating to know that the knowledge of hydrodynamic instability and jet breakup has found its application not only in the field of engineering but also helps us to understand the large scale structure of the universe and the support of the galaxy clusters. The instability of space and time has been found to be analogous to the jet breakup process. Like a liquid column a black hole is stretched along some arbitrary dimension into a "black string" and then perturbed along this dimension. Cardoso, 2006 hypothesized that the black string will breakup into smaller black holes as in the Rayleigh-Plateau instability.

Study of jet instability and jet breakup has led to many engineering application. The most common application is in inkjet printing, where printers use this phenomenon to improve performance. Here small stream of droplets of precise diameter arises in a predictable manner. In case of coating of fibre optic cable to prevent the droplet formation the process from wetting to curing must be accomplished within a time scale significantly smaller than the critical time for Rayleigh-Plateau droplet formation. In digital micro fluidics problems a process known as flow focusing employs Rayleigh-Plateau instability for efficient mixing of droplets having sizes on the order of a picoliter. In biological context, Duclaux, 2004 hypothesized that Rayleigh-Plateau instability may occur inside human lungs creating droplets or lenses that may impair respiratory performance.

Laplace, 1805 and Young, 1805 first noted the crucial role of mean curvature made up of contributions from both the axial and radial curvature in jet breakup process. By early 19th century some experimental progress came first, particularly in the works of Savart F, 1833. Savart first noted that the breakup of jet is spontaneous and independent of any external force and the direction to which the jet is projected. Joseph Plateau, 1873 first characterized the jet instability through experimental observations building on the works of Savart. He noted that the instability arises when the liquid column length exceeds the column diameter by a factor of about 3.13. Rayleigh L, 1879, later corroborated Plateau's work by giving an analytical explanation of this observation. After Rayleigh many experiments have been performed on liquid jet by many scientists notably the jet experiments of Rutland and Jameson, 1970 as well as those of Goedde and Yuen, 1970 with water jet and those of Kowalewski, 1996 with high viscosity jets. All these experiments revealed the high nonlinearity of jet breakup process.

In recent years jet breakup has been studied extensively using high speed digital cinematography. Researchers tried to find the relationship between jet breakup, Reynolds number, Weber number, wave length of perturbation and temperature. In our experimental study we focused on the droplets formed during jet breakup. The variation of droplet size with jet velocity is studied and also the size distribution of droplets is plotted.

2. Experimental Setup

A schematic of the experimental setup is shown in Fig 1. The setup consists of a reservoir of water with arrangement to maintain constant water level, a nozzle to produce a vertical jet directed toward the collection bucket and a transparent plastic scale attached aside the jet to measure the breakup length and droplet size. The constant water level is maintained using a siphon, that transfers water to the reservoir from another reservoir and the excess water is released with an overflow pipe set at a certain height of the reservoir. The diameter of the jet is 4 mm. The droplet diameters are measured from photographs by image processing. Photographs are taken with a digital camera (Sony, 14.1 MEGA PIXEL, 26 mm wide angle lens). A digital balance is used to measure the weight of the water collected in the collection reservoir. There were arrangements to keep the whole setup dark except the jet to get good and clear photographs. The disintegration of liquid jet is very much sensitive to the vibration of the floor. To eliminate the vibration water is transferred from the reservoir to the nozzle through a soft hose and the transfer hose and the nozzle is suspended through a soft spring. The base of the experimental frame was covered with rubber pad to damp out the vibration that transferred from the floor to the nozzle.

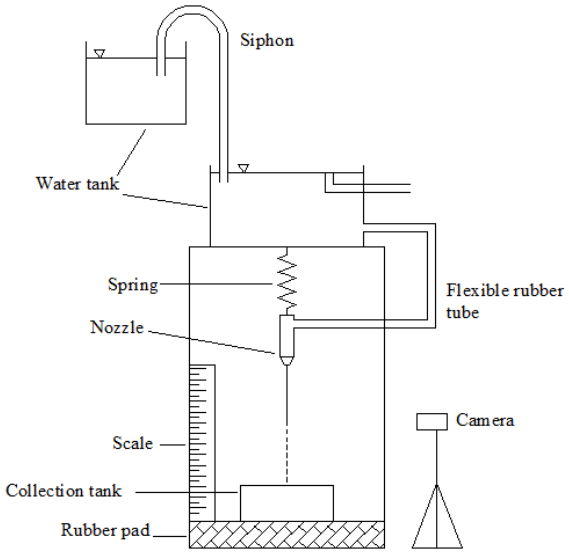

Fig. 1. Schematic of the experimental arrangement

2.1 Photography and visualization

To measure the droplet diameter and analyze the effect of different parameter on jet disintegration, photographs of the jet are taken. But to obtain measureable photographs proper illumination of the jet is a must. The surrounding of the jet is kept dark and only the jet is illuminated with a diffused light. A board covered with brown paper is placed behind the jet and light is cast on the board, which reflected the diffused light on the jet. The reflection of camera flash on the jet is avoided by focusing the scale aside the jet. The velocity of the jet was obtained by dividing the flow rate with the cross-sectional area of nozzle outlet. Flow rate of the jet was measured by bucket method. The discharge from the nozzle is collected in the collection reservoir, whose weight is known. The weight of the water collected with the help of a digital balance (TANITA, KD 160-3). The sensitivity of the scale is up to 1 gram. Fig 2 shows the jet disintegration at different jet velocities and from this figure it can be seen that the droplet diameter increases with jet velocity. Though the jet breakup process and swelling, necking and droplet formation cannot be

observed with the naked eye, with the help of a stroboscope we can have a visual observation of jet breakup process.

(a)

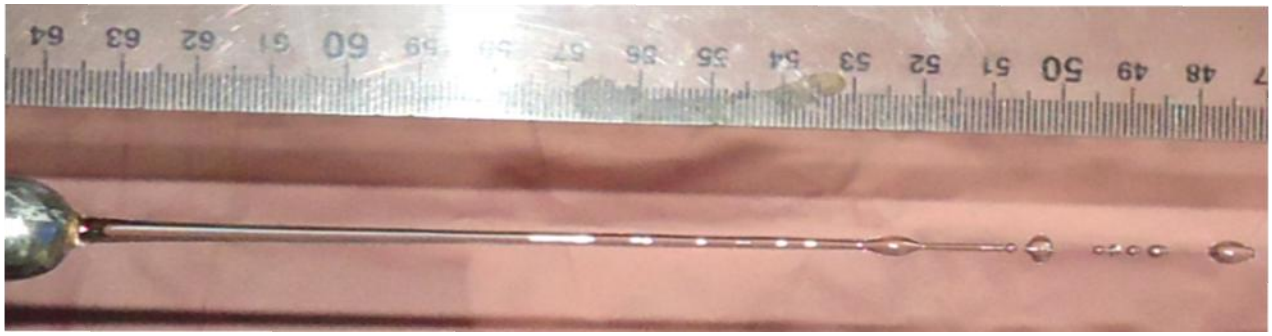

(b)

(c)

Fig. 2. (a) Jet velocity, V = 0.1971 m/s, (b) Jet velocity, V = 0.248 m/s, (c) Jet velocity, V = 0.281 m/s

2.2 Measurement of droplet diameter

In this study size of the droplets are measured at a distance of 20 cm from the jet outlet. This distance is found to be sufficient to ensure the breakup of jet at all the velocities we considered. Droplet diameters are measured from the photographs. The number of pixels along droplet diameter is measured. This is then compared with the number of pixels between two points of known distance to measure the breakup length. To measure droplet diameter we used image processing software. From the image, number of pixels equivalent to a unit length is found out. Then this relation is used to find the droplet diameter from the image. The droplet diameters cannot be measured from visual observation of photographs. Because the perspective of different pictures is different so we cannot compare the lengths. Breakup length measurement process is shown in Fig 3, a similar method is used to measure droplet diameter.

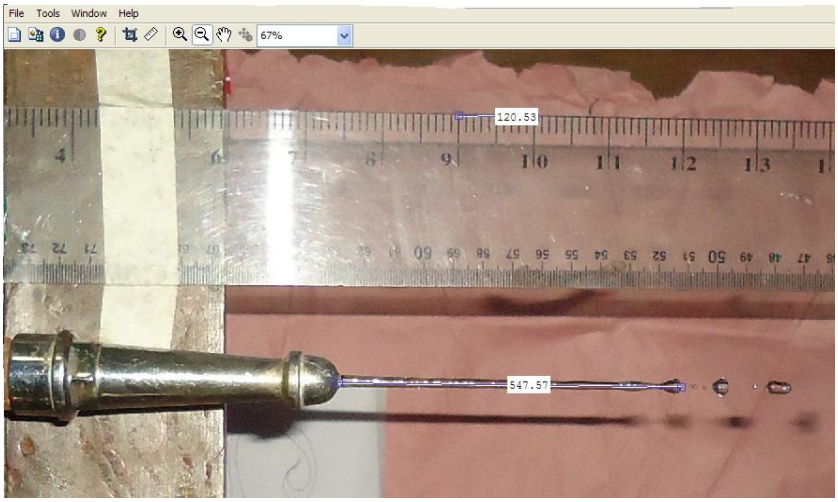

Fig. 3. Measurement of breakup length

3. Results and discussion

The variation of droplet size with flow velocity is shown in Fig 4. It is observed that at lower Weber number with increased jet velocity the sizes of the droplets increases. This may be explained by the Weber number which is the ratio of inertia force and surface tension force. At lower Weber number with increasing jet velocity the total amount of liquid passing through a certain cross section increases. The propagation of disturbance needs some time to cause the breakup of the jet. So the ultimate result is the formation of droplets with relatively large diameter. But at higher Weber number the surface tension force is relatively weaker which leads to smaller droplet size.

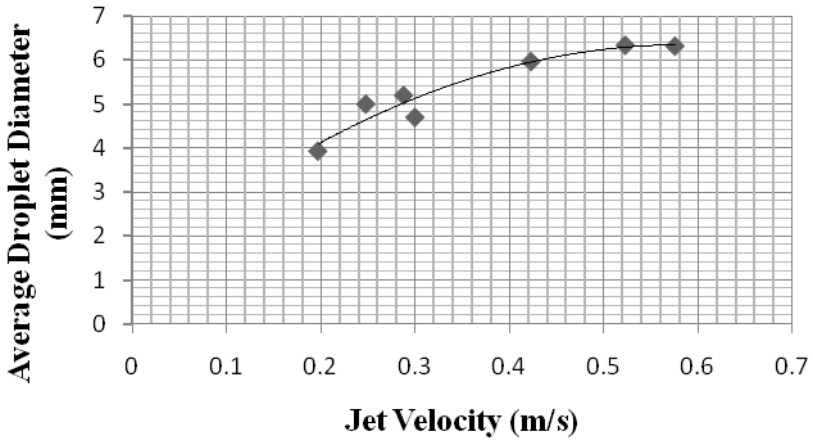

Fig. 4. Effect of jet velocity on average droplet size

The effect of Weber number on droplet size is studied by plotting droplet diameters against Weber number on a log-log graph which is shown in Fig 5. A correlation between droplet diameter and jet velocity within laminar flow regime is drawn as

Droplet diameter, $\mathbf{d = 3.584\ We^{0.208}}$

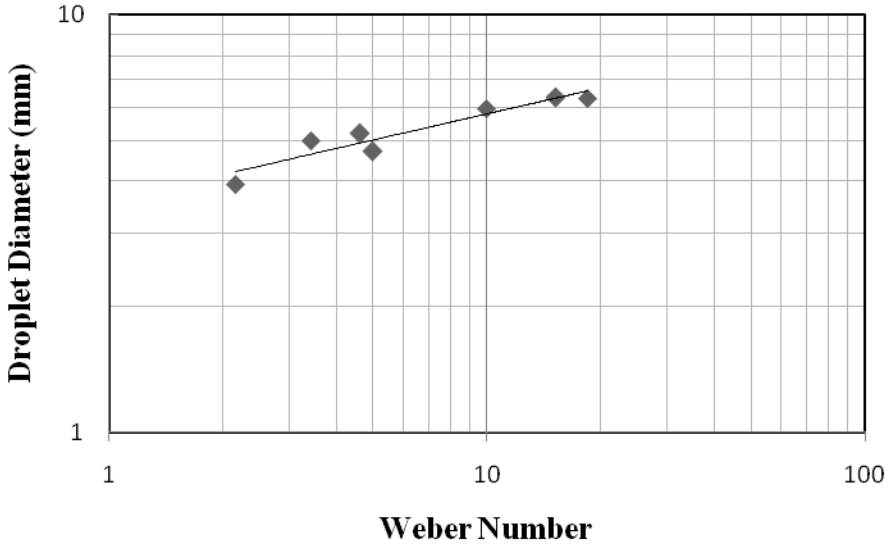

Fig. 5. Effect of Weber number on droplet size

To find the distribution of droplet size, the diameters of droplets at a certain distance from jet outlet can be plotted against frequency. The droplet sizes do not follow a normal distribution rather it fits well with log-normal and the frequency distribution of Nukiyama-Tanasawa, 1939. The droplet size distribution is showed in figure 8. There is a peak of the distribution curve and most of the droplets have a diameter around the peak. From this curve it can also be seen that the peak of the distribution curve rises with Weber number.

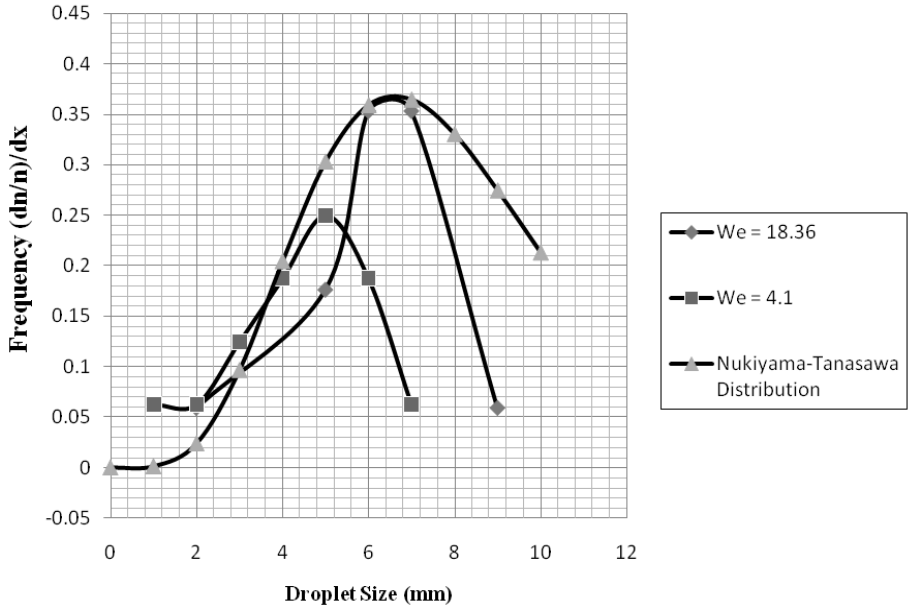

Fig. 6. Distribution of droplet size

4. Conclusion

The variation and distribution of droplet size with jet velocity is studied experimentally. The droplet size increases with jet velocity at low Weber number from which a correlation between average droplet diameter and Weber number has been drawn. The size distribution of droplets at a certain distance from jet outlet is studied by plotting a frequency distribution curve. The frequency distribution curve is found to agree well with the Nukiyama–Tanasawa distribution. The size distribution with increasing Weber number shows that the peak frequency rises with Weber number. Moreover it can be found that with increase of Weber number the diameters of droplet increases which indicates the higher accumulation of liquid particles in droplet.

References

[1] Cardoso, Vitor, Ó. Dias. Black Holes and Strings in the Water Tap. Phys. Rev. Lett. 96, 181601; 2006.

[2] Duclaux, Virginie; Quéré, David; Clanet, Christophe. Does Plateau-Rayleigh instability occur in our lungs? American Physical Society, 57th Meeting of the Division of Fluid Dynamics; 2004.

[3] de Laplace P S. Mechanique Celeste Supplement au X Libre. Paris: Courier; 1805.

[4] Young T. An essay on the cohesion of fluids. Trans. R. Soc. Lond. 95 65–87; 1805.

[5] Savart F. Memoire sur la constitution des veines liquides lancees par des orifices circulaires en mince paroi. Ann. Chim. 53 337–98; 1833.

[6] Plateau J. Statique Experimentale et Theorique des Liquids Soumie aux Seules Forces Moleculaire. vols. 1, 2. Paris: Cauthier Villars. 450 pp. 495 pp; 1873.

[7] Rayleigh L. On the instability of jets. Proc. London Math. Soc. 10:4–13; 1879.

[8] Rutland, D. F., and G. J. Jameson. Theoretical prediction of the sizes of drops formed in the breakup of capillary jets. Chem. Eng. Sci. 25; 1970.

[9] Goedde EF, Yuen MC. Experiments on liquid jet instability. J. Fluid Mech. 40:495–512; 1970.

[10] Kowalewski, T. A. On the separation of droplets from a liquid jet. Fluid Dyn. Res. 17, 121; 1996.

[11] S. Nukiyama, Y. Tanasawa. An experiment on the atomization of liquid (3rd Report, On the distribution of the size of droplets). Trans. Jpn. Soc. Mech. Engineers, 5, 131–135; 1939.

5th BSME International Conference on Thermal Engineering

Experimental Study on Aerodynamic Characteristics of Basic Airfoils at Low Reynolds Number

Md. Amzad Hossain*, Mohammad Mashud and Sharmin Sultana

Department of Mechanical Engineering, Khulna University of Engineering & Technology, KUET, Khulna-9203, Bangladesh

Abstract

The airfoil is one of the common and elemental devices to control flow and its reacting force. In the Reynolds number region lower than approximately 1.0×10^5, which corresponds to the Reynolds number region of a Micro Air Vehicle, thinner and sharper leading edge airfoil performs better than thicker and blunter one. This research focuses on the difference in flow fields which are clarified by means of surface pressure distributions measurements. But the aerodynamic characteristics of airfoils have been researched in higher Reynolds-number ranges more than 10^6, in a historic context closely related with the developments of airplanes and fluid machineries in the last century. However, our knowledge is not enough at low and middle Reynolds-number ranges. So, in this project, I have investigated such basic airfoils as a NACA0015, a flat plate and the flat plates with modified fore-face and after-face geometries at Reynolds number ranges from $2.9\times10^4< Re <7.2\times10^4$, using two dimensional computations together with wind-tunnel. As a result, I have revealed the effect of the Reynolds number Re upon the pressure coefficient C_p. Besides, I have shown the effects of attack angle α upon various aerodynamic characteristics such as the coefficient of pressure C_p at $Re=2.9\times10^4$ to 7.2×10^4, discussing those effects on the basis of both near-flow-field information and surface-pressure profiles. Such results suggest the importance of sharp leading edges, which implies the possibility of an inverse NACA0015. Furthermore, concerning the flat-plate airfoil, I have investigated the influence of fore-face and after-face geometries upon such effect

Key words: Loe Reynolds Number; Airfoil; Aerodynamics; Cp; Experiment; Wind Tunnel

1. Introduction

Airplanes are transportation devices which are designed to move people and cargo from one place to another. Airplanes come in many different shapes and sizes depending on the mission of aircraft. However, most of the aerodynamic characteristics of airfoils have been investigated at higher values of Reynolds number Re than about 1.0×10^6, where Re is defined using a chord length c as a characteristic length scale. On the other hand, we have been requiring more precise knowledge about the aerodynamic characteristics of airfoils especially at $Re < 10^6$. Concerning the aerodynamic characteristics at low values of Re, there have been several studies. Among them, Sunada et al. (1997) have conducted a series of water tank experiments on various airfoils including a NACA0006, a NACA0012 and a flat plate at $Re= 4.0\times10^3$. Motohashi (2001) and Nakane et al. (2003) have carried out wind tunnel experiments on a flat plate at $Re= 4.8\times10^3 – 1.5\times10^5$, and on a NACA0012 at $Re=5.0\times10^3$-7.0×10^5, respectively. Few years ago, Sun & Boyd (2004) have computed the flow past a flat plate at Re= 1.4-1.4×10 and at a Mach number Ma=0.2. However in such a lower range of Re, our knowledge has not been enough yet, due to non-negligible and complicated Re effects related with the laminar to turbulent transition whose strong non-linearity brings us some technical difficulties in the accuracies of analyses, computations and experiments.

In the present study, in a Re ranges from $2.9\times10^4< Re<7.2\times10^4$, we investigates two kinds of basic two dimensional airfoils, namely a NACA0015 and a flat plate, using two dimensional computations with wind tunnel experiments. Specifically speaking, at first, we try to reveal the effect of attack angle α upon various aerodynamics characteristics such as the pressure coefficient Cp.

* Corresponding author. Tel.: +88-01721269426
E-mail address: amzad.kuet.me@gmail.com

And then, in order to discuss the αeffects, we show such near flow field information as pressure distributions around the airfoils at α=4 and 16 deg, together with surface-pressure profiles of the airfoils. Furthermore, concerning the flat plate, we investigate the influences of fore-face and after-face geometries upon the α effect introduce the paper, and put a nomenclature if necessary, in a box with the same font size as the rest of the paper.

Nomenclature

U_∞	Free stream velocity
Re	Reynolds number
t/c	cross-section ratio
C	Cord length [m]
S	Surface area [m^2]
T	Flat-plate thickness[m]
α	Angle of attack
C_p	Coefficient of pressure
μ_∞	free stream viscosity
ρ_∞	free stream density

1.1. Aplication Overview

On 11 January 1999, the Pentagon and Lockheed Martin began airborne flight test on an aircraft with a wingspan of 15cm and a weight of 85 grams. This type of aircraft is considered a Micro Air Vehicle (MAV). MAVs of this size or even smaller, will enable soldiers to significantly enhance their fighting capability. Such a vehicle can be fitted with miniature cameras and other surveillance equipment to allow a soldier to have instant information about their battlefield environment. MAVs can also be used to sniff for chemical and biological agents, detect mines, jam radars and communications and assistance with micro weapons. Besides military uses, they can be employed to monitor airborne pollutants and traffic, fly into burning buildings to search for victims, or survey the activities of criminal suspects. The MAV's in the near future are expected to have a total wingspan of 10-15cm with a total weight of about 10-50grams. A typical mission will require it to be airborne for about 20-60 minutes while carrying a payload of 2-5 grams and a fly distance of about 10km at approximately 13m/s. However, these specifications have presented problems. At a wingspan of about 15cm, the laws of aerodynamics make flight very much more difficult than just scaling down a larger aircraft. At that size, the performance of most conventional airfoils deteriorates as these airfoils were tailored for Reynolds number, Re of 105 and above. They give insufficient lift at the relatively low speed which the MAV flies at. Thus some investigation into performance of airfoils at below Re=105 is necessary. In shortly, we have been requiring more precise knowledge about the aerodynamic characteristics of airfoils especially at Re < 106, because of the recently increasing importance in such applications as unmanned aerial vehicles known as UAVs, micro air vehicles known as MAVs, insect/bird flight dynamics, small –scale machines like micro fluid machineries and fluid machineries and micro combustion engines and so on.

2. Method

2.1. Model Construction of

Figure 1 shows the present models. They are two kinds of fundamental airfoils such as a NACA 0015 and a flat plate. The flat plate has a cross section ratio t/c= 0.05, where t and c denote the thickness and the chord length, respectively. They are two dimensional ones with basic and symmetric cross sections: the NACA 0015 is a typical streamlined airfoil for high Re and the flat plate is the simplest thin airfoil with sharp leading and trailing edges. I investigate the NACA0015 and the flat plate also experimentally. Furthermore, in order to investigate the influences of fore-face & after-face geometries, the flat plate is transformed into six kinds of modified flat plates, which are hereinafter referred to as MFP1-MFP6. Strictly speaking, the MFP1-MFP3 is the flat plates with their fore faces partially expanded in the upstream & the MFP4-MFP6 are those with their after-faces partially expanded in the downstream. These modified models are designed, being intended to reveal representative effects of sharp edges. All the modified models are shown in Fig.1, as well.

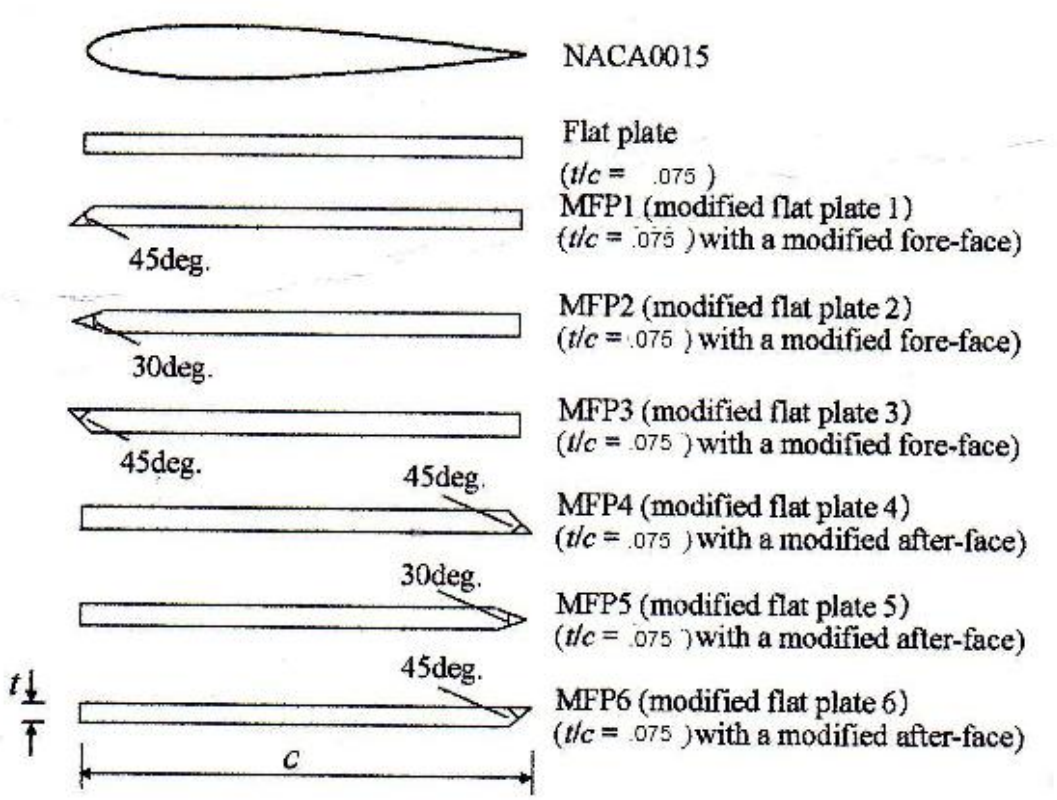

Fig. 1. Models (Two Dimentional Airfoils)

According to this design, I have prepared my Airfoil models which are made of wood. The pictures of the models are given here:

Fig. 2. Airfoil NACA 0015, Flat Plate Model

Fig. 3. Modified Flat plates with modified fore- face (MFP1, MFP2, MFP3)

Fig. 4. Modified Flat plates with modified after-face (MFP4, MFP5, MFP6)

2.2. Experimental Setup

The experiments were conducted using 36×36×100 cm wind tunnel. Figure 5 shows a schematic of the experimental setup. A small sized model is appropriate to examine the aerodynamic characteristics for the experiments. The model was placed in the middle of the test section supported by a frame. The frame is constructed by four 5mm diameter threaded iron rod, bolts, a flat plate and two bars with angle measuring system. The four threaded rods placed the plate tightly inside the wind tunnel. This plate holds the two bars & these bars hold the model tightly inside the wind tunnel. One bar has an extended part which is used to measure the angle of attack. The surface of the model is drilled through 2mm diameter holes & small sizes pressure tubes are placed inside the drilled holes. One end of the vinyl tubes are attached to each pressure tube & the other end are connected to a digital manometer for measurement of the surface pressure of the model at different points.

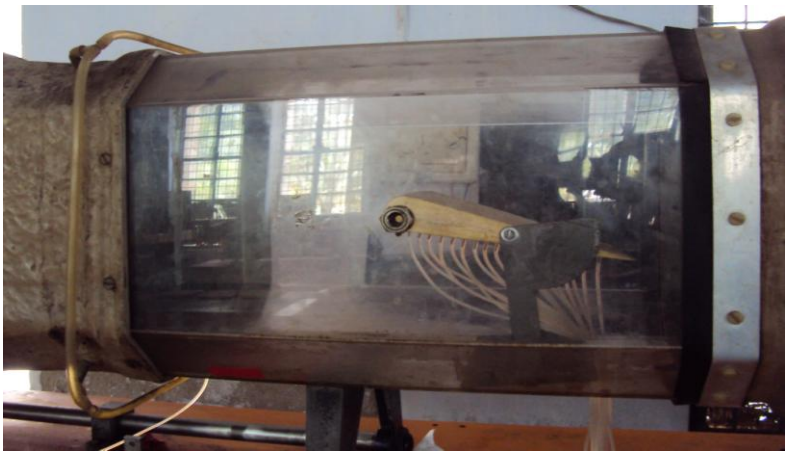

Fig. 5. Experimental setup(The NACA0015 airfoil mounted in the wind tunnel)

3. Results And Discussions

Aerodynamic force (AF) was the resultant of all static pressure acting on an airfoil in airflow, multiplied by the plan form area that was affected by the pressure. The line of action of the AF passed through the chord line at a point called the Centre of Pressure (CP). When Angle of Attack (AOA) changed, the magnitude & direction of the aerodynamic force also changed & the location of Centre of Pressure (CP) also moved. These changes made the analysis of the forces on airfoils very complicated. The centre of pressure on the top of airfoil & that on the bottom were located at the same point on the chord line (for symmetric airfoil).The surface pressure distribution was measured for various attack angles. The experiment was done in three different speeds. In this experiment the aerodynamic characteristics of an airfoil shape & flat plate including modified flat plate were determined by plotting C_p Vs X/C.

Pressure distribution around the surface of the model is calculated by following equation
Co-efficient of pressure, $C_p = P - P_\infty / q_\infty$

$$C_p = P - P_\infty / .5\ \rho_\infty\ u_\infty^2$$

Where,

P_∞= free stream pressure
u_∞= free stream velocity
q_∞= dynamic pressure

Using this equation the co-efficient of pressure for various attack angles for the model have been calculated and plotted C_p vs. X/C graphs.

In these graphs,

C_p1 = Upper surface Co-efficient of Pressure at 2 m/s
C_p2 = Upper surface Co-efficient of Pressure at 4 m/s
C_p3 = Upper surface Co-efficient of pressure at 5 m/s
C_pL = Lower surface Co-efficient of Pressure

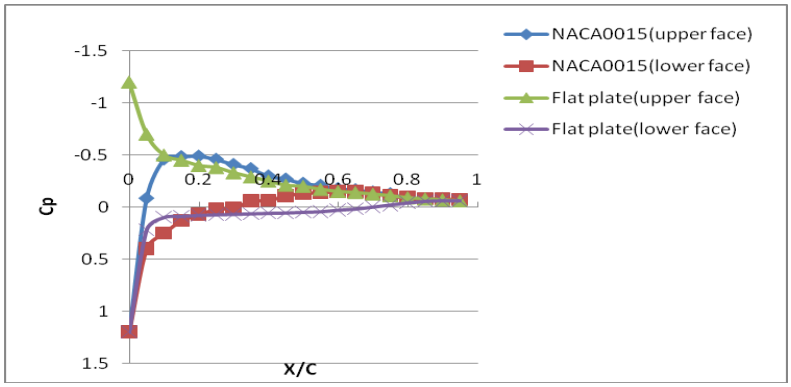

Fig. 6. Coefficient of pressure vs. distance for 4° angle of attack at Re=72640 (NACA0015 & Flat plate)

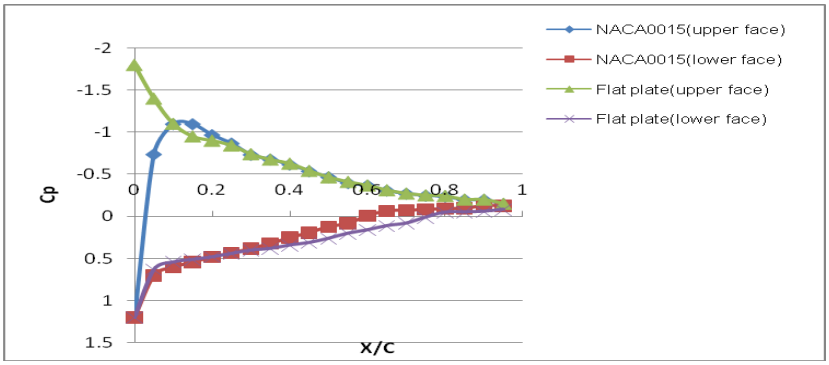

Fig. 7. Coefficient of pressure vs. distance for 16° angle of attack at Re=72640 (NACA0015 & Flat plate)

From the figure 6 & figure 7 show the surface pressure profiles on both the airfoils at Re= 72640. The abscissa x denotes the distance from the leading edge in the leeward direction which are normalized by c. Figure 6 are at α= 4 deg. & figure 7 are at 16 deg. First we consider the NACA0015. When we see figure 6, we can confirm the features representing the similarities between α= 4 & 16 deg. such as (i) the widely distributed low-pressure area over the upstream portion of the upper surface and (ii) the concentrated high pressure area just below the fore-face. We also know that the features representing the slight discrepancies between α=4 & 16 deg. such as (iii) the pressure reduction in the widely distributed low pressure area over the upstream portion of the upper surface with the increasing α and (iv) The leeward expansion of the concentrated high-pressure area just below the fore-face with almost the same peak value of Cp with increasing α. However, we cannot find any features representing the clear discrepancy (v) between α= 4 & 16 deg. related with the flow separation on the middle upper surface.

Finally, we compare the NACA0015 & the flat plate. We can easily find one clear difference between both the airfoils; namely, a sharp and very low pressure drop near the upper fore-face is seen not for the NACA0015, but for the flat plate. Besides, we can see another difference between both the airfoils, namely, slightly higher pressure of the flat plate than the NACA0015, which is widely distributed over the middle portion especially of the lower surface.

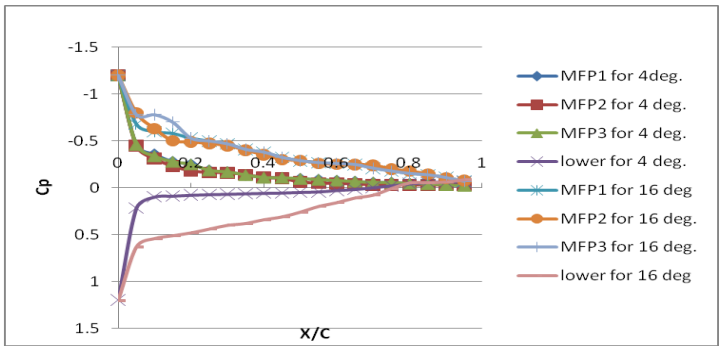

Fig. 8. Coefficient of pressure vs. distance for 4° & 16° angle of attack at Re=72640 (MFP1, MFP2, MFP3)

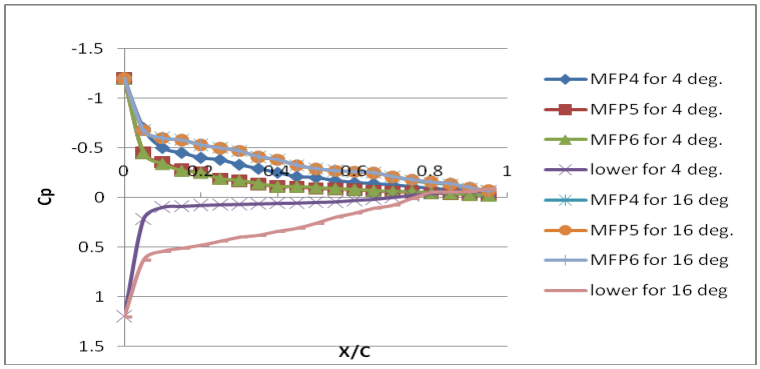

Fig. 9. Coefficient of pressure vs. distance for 4° & 16° angle of attack at Re=72640 (MFP4, MFP5, MFP6)

From figure 8 and figure 8, the variation of coefficient of pressure with the distance from leading edge can be observed for various angles of attack. Here The angle of attack, $\alpha = 4^{o}$ & 16^{o}. From figure 8 & figure 9 show variation of pressure over the upper surface of the airfoil with 4^{o} and 16^{o} angle of attack. The pressure is high on the lower surface close the leading edge of the airfoil. The pressure is high on the lower surface and positive at maximum points for the value of x/c from 0 to .81. 5 m/s free stream velocity was used to calculate the pressure at different values of x/c from 0 to 1. The pressure decreases with the increase of free stream velocity. Pressure was started to increase after the point x/c=0.15.

As the flow expands around the top surface of the airfoil P decreases rapidly. At the point where P decreases rapidly C_p goes negative. In those region where $P < P_{\infty}$, the value of C_p is negative. By convection plots of C_p for airfoils were shown with negative values above the abscissa. Similarly, I have observed the value of Cp for all the models at Re=29056 & Re= 56112. The Characteristics are pretty similar with the above Reynolds Number. The only difference is that pressure decreases with the increase of free stream velocity. The minimum value of C_p was found at the free stream velocity of 2m/s that means at Re=29056.

4. Conclusion

We have investigated such basic airfoils as a NACA0015, a flat plate and the flat plates with modified fore-face and after-face geometries in a low Reynolds number, using two dimensional computations with wind tunnel. Obtained results are as follows:
At low Re, the aerodynamic characteristics of the flat plate are qualitatively similar with those of the NACA0015 and are quantitatively superior to those of the NACA0015. The sharp and very low pressure drop near the upper fore-face, which can be seen not for the NACA0015 but for the flat plate, contributes to such superior aerodynamic characteristics, due to the existence of sharp leading edges. Both a non convex lower surface and the appropriate after-face geometry can also improve aerodynamic characteristics. The latter of both is actually effective only at large α. For the airfoil with any sharp leading edges, the effects of the fore-face geometry upon aerodynamic characteristics can be negligible at such a low Re as 7.2×10^{4}, while the after-face geometry can be effective actually at $\alpha >= 10$ deg. Among the after-face modified flat plates, the MFP4 shows superior aerodynamic characteristics.

5. References

[1] John D. Anderson, J.R, "Introduction to flight", Third Edition, McGraw-Hill International Editions, Aerospace Science Series.
[2] E. L. Houghton and P. W. Carpenter, "Aerodynamics for Engineering Students", Fourth Edition, Edward Arnold Publisher.
[3] Dr. P. N. Modi and & Dr. S. M Seth, "Hydraulics and Fluid Mechanics Including Machine" (In SI Unit), new edition 2005-2006, Standard Book House.
[4] William H. Rae, Jr. & Alan Pope, "Low Speed Wind Tunnel Testing", Second Edition, A Wiley-Inter science Publication.
[5]Charles E. Dole, "Flight Theory and Aerodynamics", A Wiley Interscience Publication.
[6] Sun, Q. and Boyd, I. D., "Flat-Plate Aerodynamics at Very Low Reynolds Number," Journal of Fluid Mechanics, Vol. 502 (2004), pp. 199-206.
[7] Donald T. Ward, "Introduction to Flight Test Engineering ", Elsevier Science Publishers. Richard Eppler, "Airfoil Design and Data".
[8] Francis J. Hale, "Introduction to Aircraft Performance, Selection and Design", John Wiley & Sons Publishers.
[9] Sunada, S Sakagusi, A. and Kawachi, K., "Airfoil Section Characteristics at a low Reynolds Number", Transaction ASME, Journal of Fluids Engineering, Vol. 199(1997), pp.129-135.
[10] Motohashi, T., "Characteristics of Rectangular Wings at Low Reynolds Number", Proc. 39th aircraft Symposium JSASS, 3D6 (2001), pp.1-4(in Japanese).Herrmann Schlichting & Klaus Gersten,"Boundary-Layer Theory", Eighth edition, Spring Publication.

Flow Separation Control of Thick Airfoil by a Trapped Vortex

Mohammad Mashud*, Meer Md. Alam-Al-Raze and Mausumi Ferdous

Department of Mechanical Engineering, Khulna University of Engineering & Technology, KUET, Khulna-9203, Bangladesh

Abstract

To ensure a high lift-to-drag ratio, wing of modern airplanes are thin and streamlined. However the tendency to design commercial aircraft of ever-larger dimensions, or innovative configuration as Blended-Wing-Body airplanes requests innovative solution in the field of wing structures. In order to carry a larger load having thick wing would be beneficial. The drawback of this type of airfoils is a low efficiency due to high value of the drag coefficient. These airfoils are affected by early flow separation phenomenon even for small incidence angle. Nowadays many research activities are aimed to investigate system dedicated to flow control. As a scientific discipline and as a technological curiosity, flow control is perhaps more hotly pursued by scientists and engineers than any other area in fluid mechanics This paper represents the experimental campaign performed at KUET A-2 wind tunnel aimed to investigate the potential benefit obtainable using a trapping vortex cell system on a high thickness airfoil with and without steady suction and/or injection mass flow. The behavior of a 2D model, equipped with a span wise oriented circular cavity, has been investigated. Pressure distribution on the model surface and inside the cavity and the complete flow field around the model and inside the cavity have been measured. An extensive test campaign has been carried out in an open circuit wind tunnel, with test section size of 360x360x700 mm^3 and maximum speed of 20 m/s. Due to the limited dimensions of the Wind Tunnel, the model has been mounted on the bottom wall of the wind tunnel in order to avoid blockage problems. The model represents a two dimensional high thickness airfoil with a chord length of 350mm. The model angle of attack ranges between 0° to 16° with a step of 1°.The installation of the model on the wind tunnel bottom wall presented heavy flow instability under the front part of the model. The flow instability has been solved applying a flow suction in front the model trough a porous wall installed on the bottom wind tunnel wall. The cavity has been realized with transparent material in order to allow optical access. The model has been designed in order to permit flow suction and/or blowing inside the cavity. The influence of different parameters has been investigated. Tests have been performed varying the wind tunnel speed (form 1 m/s, to 15 m/s), varying the suction mass flow (from 0 m^3/h to 10 m^3/h) varying the blowing mass flow (from 0 m^3/h to 20 m^3/h) applying suction and blowing at the same time, and varying the model angle of attack (AoA).

Keywords: Airfoil, Flow Seperation, Trapped Vortex.

* Mohammad Mashud. Tel.:+880 1713 255226.
E-mail address: mdmashud@yahoo.com

5th BSME International Conference on Thermal Engineering

Construction of Unmanned Aerial Vehicle (UAV) using Coanda Effect

Mohammad Mashud*, Md. Tanvir Ibny Gias and Abir Mahmud

Department of Mechanical Engineering, Khulna University of Engineering & Technology, KUET, Khulna-9203, Bangladesh

Abstract

A small UAV will often have the capability to carry a significant payload. This gives the opportunity for it to carry: High definition video & stills, Thermal imaging and infra-red cameras, Explosive equipment, Small delivery packages, Listening devices and Mine detectors. With so many restrictions for the pilot of a UAV to consider, in an ideal world UAVs would operate without the requirement for human control. Autonomy is a very challenging solution from the developers' perspective but it will ultimately lead to the most efficient systems. In recent years the demand for Unmanned Aerial Vehicles (UAV's) has increased rapidly across many different industries and they are used for various applications. The objective of this research work is to construct an Unmanned Aerial Vehicle using Coanda effect which have the ability to enter dangerous or inaccessible environments and allow vital information to be collected without human risk. Lift on a conventional airfoil is generated by circulation around the wing. As air is accelerated downwards, it causes the pressure below the wing to increase, and the pressure above to decrease, resulting in lift. In order to carry out a task, a UAV has to face many different challenges. This has led to the development of novel platforms that move away from traditional aircraft design in order to make them more capable. A good example of this type of craft is one which uses the Coanda Effect to assist propulsion. This effect was discovered in 1930 by Henri-Marie Coanda who found that if a thin film of air is directed over a curved body, then the air follows the curve. When used to propel a UAV, the Coanda Effect also entrains air from above and lowers the air pressure in this region, which in turn generates more lift. In this project a UAV will develop which is based on the Coanda Effect "By creating an air velocity in the centre of the craft with the aid of a fan and then directing the air flow out of the outlet it will follow over the curved surface. The amount of lift generated is dependent upon the velocity, mass and density of the air". This phenomenon can be harnessed to produce lift in two ways. Firstly, it can be used to change the direction of airflow to point downwards, resulting in vertical thrust. Secondly, it can be used to entrain air from above which causes a region of low pressure above the body, which results in lift. The propose UAV will be hollow hemisphere shaped and hemisphere surface mounted with airfoil shaped flaps. The majority of the lift will generate from the downwards pointing airflow at the perimeter of the craft, and a remarkable part of lift will generate from the mail body through the Coanda Effect. From the proposed UAV, a significant amount of lift (the Coanda Effect can improve lift by up to 300%) can be achieved, which would be sufficient for the UAV to take off.

Keywords: UAV, Coanda Effect, Lift coeffecient.

1. Introduction

A flying saucer (also referred to as a flying disc) is a type of flying craft with a disc or saucer-shaped body. Sometimes flying saucers are believed to be of alien origin, in which case they are referred to as unidentified flying objects or (UFO's). These are usually described as silver or metallic, sometimes reported as covered with running lights or surrounded with a glowing light, hovering or moving rapidly, either alone or in tight formations with other similar craft, and exhibiting high maneuverability. Some flying saucers are man-made though, such as the American Chance Vought V-173 / XF5U "Flying Flapjack", the British GFS flying saucer or the British "S.A.U.C.E.R" ("Saucer Aircraft Utilizing Coanda Effect Reactions") flying saucer. Actually the flying saucers acquire considerable lift for the flying by the means of coanda effect reactions and initially fly to the vertical direction. By using the Coanda rule to make raising, it has rattling soft downwash and is aerodynamically steady.

* Corresponding author. Tel.: +88-01713255226
E-mail address: mdmashud@yahoo.com

The air jets change a intelligent way do seize to walls when pursy shut to them. After the air jetis is sued into the quiescent surrounding it entrains the air between the jet and the protect. Low pressure location is cast deed the jet to disconcert towards the surround. This phenomenon legendary by the personage of the Coanda-effect had saved diverse applications ever since it was disclosed. Galore saucer shaped steep take-off and landing (VTOL) bomb designs use Coanda-effect to create the straight jut to arise.

2. Method

2.1. What is coanda effect

The Coanda Effect has been discovered in 1930 by the Romanian aerodynamicist Henri-Marie Coanda (1885-1972). He has observed that a stream of air (or an other fluid) emerging from a nozzle tends to follow a nearby curved surface, if the curvature of the surface or angle the surface makes with the stream is not too sharp. If a stream of water is flowing along a solid surface which is curved slightly from the stream, the water will tend to follow the surface. The Coanda Effect works with any of our usual fluids, such as air at usual temperature, pressures and speeds.

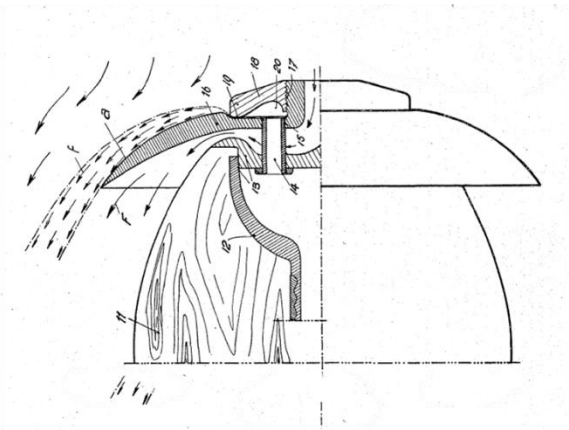

Fig. 1.Schematic diagram of coanda effect

- ***Types of coanda effect***

  In practice there are two types of coanda effect can be seen, such as-
  - Repulsion type
  - Electro-Hydrodynamics devices(EHD)

- ***Repulsion type***

When the main electric engine is started, the Coanda effect begins to create a differential aerodynamic pressure between the outer and the inner surface of the primary hull. At a higher speed, the vortex chamber becomes a kind of high electrostatic generator due to the air particles in high speed motion acting as an electrical charges transporter. The paper is focused on repulsion type coanda effect only. Where the lift is gained by the pressure difference between inside and outside of the hull. As the motor starts to rotates then there creates air flow over the hull.

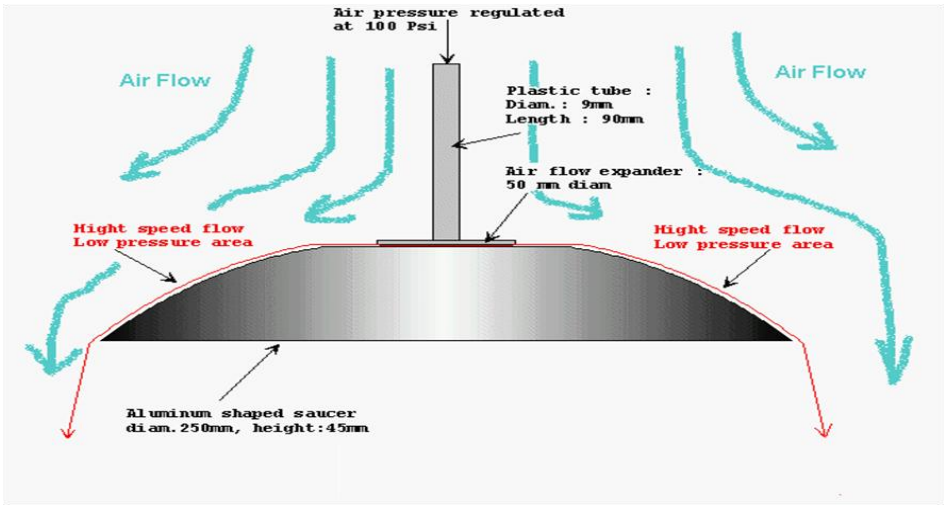

Fig. 2. Repulsion type coanda effect

2.2. Design and instrument

- **Computer design of the true UAV(Unmanned Air Vehicles) model**

Here is the full plan of the GFS-UAV model N-01A.We are going to construct this structure as well as will try to give a considerable lift(with the help of a BLDC and a propeller mounted to the top of the structure) to this structure so that it could fly.

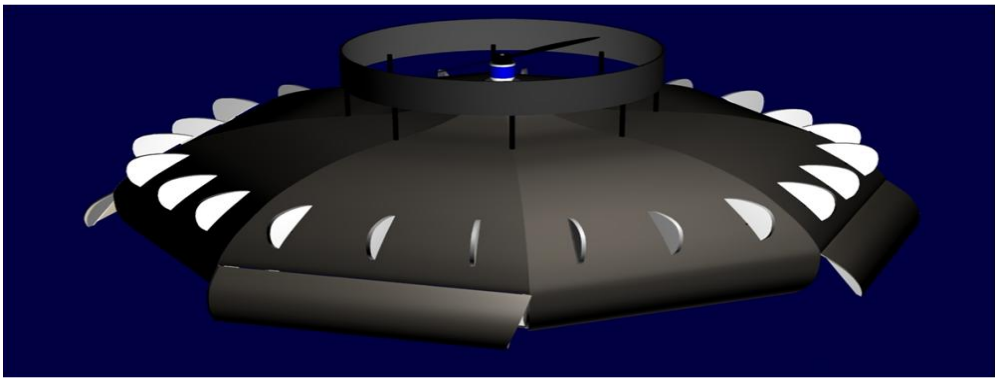

Fig. 3. Computer design of the true UAV model

- ***Necessary Instrument***

Here is the lists of all the necessary equipments those are needed for constructing the full structure as well as give lift to the structure.

Table 1. Necessary instruments

Function	Part name	Weight(gm)
Brushless motor	MP JET AC 28 7/30D	56
Speed controller	JETI Advance 30 plug	28
Lipo battery	Power House 3S1P 950 mA 25C	97
Propeller	APC 10*7 E	10
Depron Foam(To make GSF Hull)	GSF Hull	100

So, the full structure with all the necessary instruments is weighted about 292 (gm). This will be lifted to a considerable height with the rotation of the propeller. The propeller effect will be enough to lift the structure vertically. Here is brief description of all the parts that is needed to construct the model.

- ***Brushless motor***

The AXi 2808/24 brushless out runner with rotating drum and high power neodymium magnets is suitable for 400-500 sized models, and up to 1,300g/45.9oz in weight. The 2808/24 is probably about the most powerful and efficient out runner available for outdoor 3D models up to 800g/28oz. If you are an accomplished R/C pilot looking to upgrade your outdoor 3D plane, look no further. The hardened steel 4mm diameter shaft and is supported by two ball bearings, ensuring very good mechanical stability. Due to it's high torque characteristics this motor is capable of turning large propellers with a high level of efficiency and without the need for a gearbox.

Fig 4. BLDC(Brushless DC motor with three terminal and two phase)

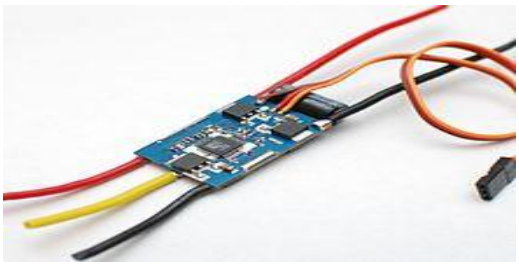

Fig 5. Jeti Eco range of brushless speed controller

- ***Speed controller***

The Jeti Eco range of brushless speed controllers are a quality range of speed controllers for brushless motors, with a continuous current rating ranging from 8-40 amps for 2 or 3 cell lithium polymer batteries or 6-12 NiCd/NiMH cells. The Eco range offers simple access to the most common programming requirements of a speed controller, with all settings being selected simply using the supplied jumper plug. Each unit features a linear BEC, a power cut-off system to protect battery voltage and temperature overload protection, which cuts power to the motor if the temperature of the controller exceeds 100 °C. These controllers automatically detect the number of poles and set timing appropriately, with no intervention required.

- ***Lipo battery***

Desire Power 1,500mAh 3s/11.1V lithium polymer battery with standard JST-XH type balance connector. The main wires do not arrive with a plug fitted, so you can fit your own preferred connector here. This 1500mAh pack is the ideal size for many different models from park-flyers to aerobatic and 3D fixed-wing models.

Fig 6. Lipo Battery(- Desire Power 1,500mAh 3s/11.1V)

Fig 7. APC 10x7 E Thin Electric RC Airplane Composite Propeller

- ***Propeller***

APC Landing Products RC thin electric composite model airplane propeller A10070E / LP 10070E is designed for use with electric rc airplanes. Includes locating rings in various sizes and instructions on adaptation procedures.

- ***Depron Foam(To make the Hull) :***

Depron is an extruded polystyrene foam product, manufactured into sheets of a standard size. It is extremely lightweight and moisture resistant. Developed as a high performance Wall and Floor Insulation, now Depron has a wide variety of uses such as food packaging, but more recently in Modeling due to it's light weight and righty.

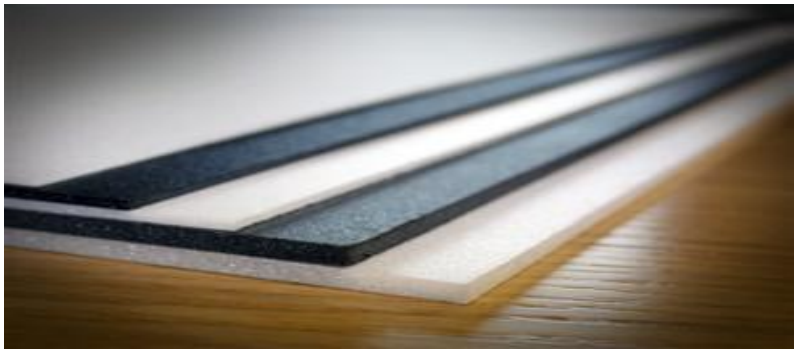

Fig 8. Depron Foam

2.3. Design construction

- **Dimension of different parts of GFS hull and Cutting the parts according to the proper dimension**

The first step is to determine the dimension of different parts of the GFS hull which is the main aerodynamic structure and which will fly and will carry all the equipments.

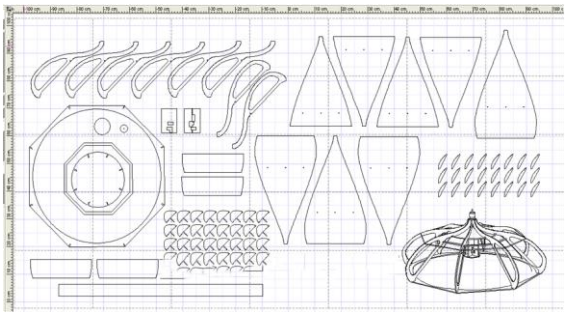

Fig 9. Dimensions of different parts of the UAV

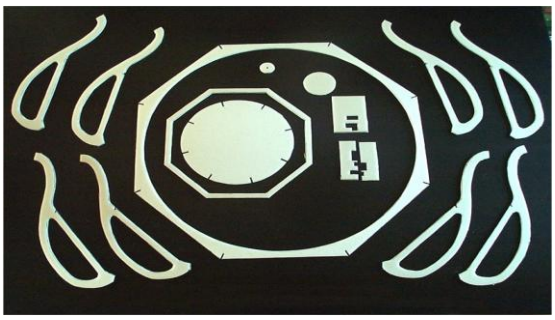

Fig 10. Different parts of the UAV (Cut according to the dimension)

- **Making the main frame of the hull**

Above all the GFS-UAV parts has been cut in the Styrofoam with a brand new cutter and with a low angle of cut. Here the post important factor is precession cutting.

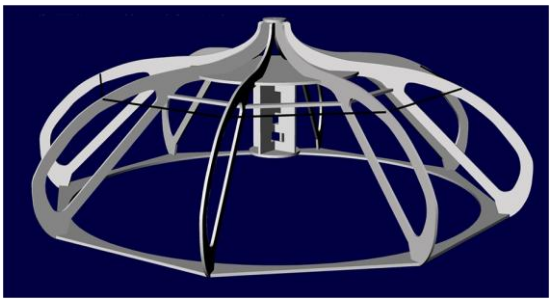

Fig 11. Semi structure of the (UAV) model

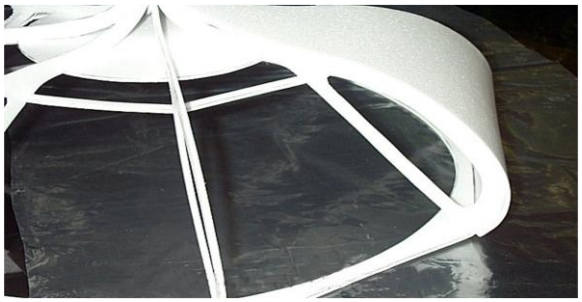

Fig 12. Attachment of the curved petal parts to the main frame

The curved petals, the key of the Coanda effect, are carefully assembled and glued on the main structure. Cracks on the curved surface were carefully avoided .For bending the different parts of the structure we used some cylindrical shaped smooth materials so that the bending edges are smooth enough and can be easily attached to the main frame.

- **Final structure of the UAV**

For more aerodynamic stability a rounded shed is added at the top of the hull. So that the air can be directed as a synchronize manner rather than spread out randomly over the hull. And the final structure is such

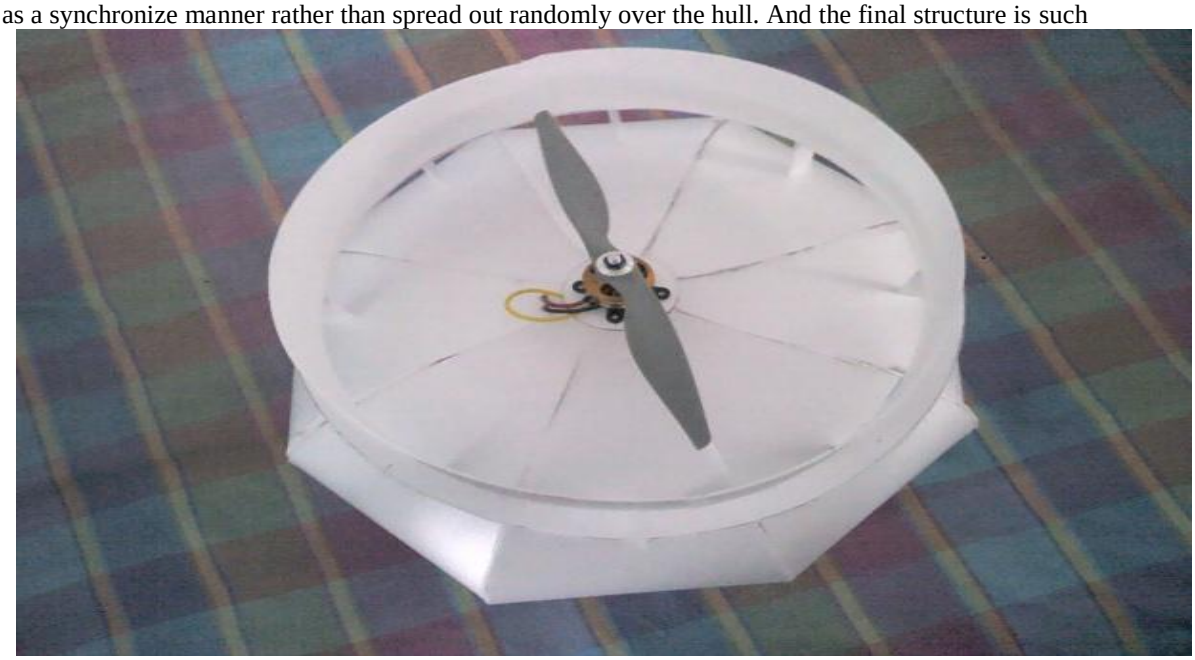

Fig 13. Final structure of the UAV(Coanda effect flying saucer)

2.4. Electrical equipment setup

The AXi 2808/24 with a 30A speed controller, 11.1V Li-Poly battery and a 10"x7" propeller is a great setup in 3D models up to 800g/28.2oz such as the Telink SU29 and Yak 55 3D EPP models and also performs efficiently in sailplanes up to 1,300g/45.9oz with 9"x5" folding propellers. The AXi 2808-24 is also suitable for flying wings like the MS Composit Maxi Swift with 9×5 folding propellers on 3s Li-Po packs. We have used the best setup here. That is The AXi 2808/24 with a 30A speed controller, 11.1V Li-Poly battery and a 10"x7" propeller.

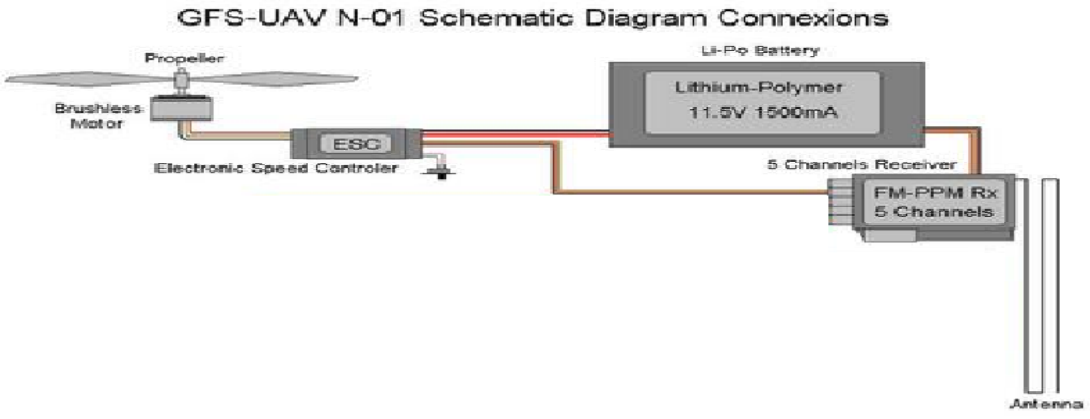

Fig 14. Schematic diagram of the circuit connection

- ***Connection of motor with the battery***

Brushless DC motors (BLDC motors, BL motors) also known as electronically commutated motors (ECMs, EC motors) are synchronous motors which are powered by a DC electric source via an integrated inverter. The motor part of a brushless DC motor is often permanent magnet synchronous motor, but can also be a switched reluctance motor, or induction motor. BLDC motors may be described as stepper motors, however, the term *stepper motor* tends to be used for motors that are designed specifically to be operated in a mode where they are frequently stopped with the rotor in a defined angular position. Two key performance parameters of brushless DC motors are the Motor constants Kv and Km. BLDC motors develop maximum torque when stationary and have linearly decreasing torque with increasing speed. Limitations of brushed DC motors overcome by BLDC motors include lower efficiency and susceptibility of the commutator assembly to mechanical wear and consequent need for servicing, at the cost of potentially less rugged and more complex and expensive control electronics.

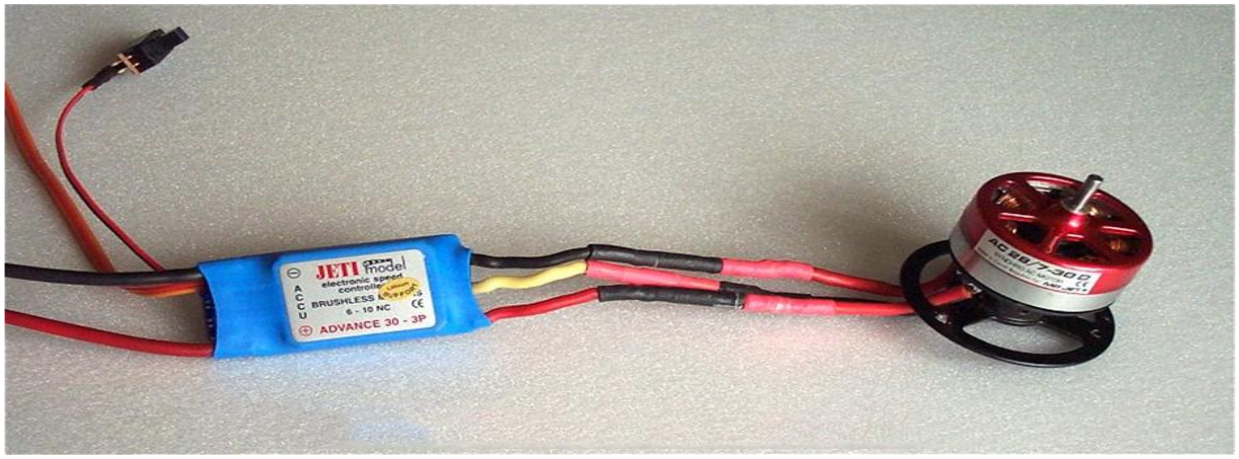

Fig 15. The brushless motor is connected to a speed controler JETI Advance 30-3P

A typical BLDC motor has permanent magnets which rotate and a fixed armature, eliminating the problems of connecting current to the moving armature. An electronic controller replaces the brush/commutator assembly of the brushed DC motor, which continually switches the phase to the windings to keep the motor turning. The controller performs similar timed power distribution by using a solid-state circuit rather than the brush/commutator system.

Controller implementation

Because the controller must direct the rotor rotation, the controller requires some means of determining the rotor's orientation/position (relative to the stator coils.) Some designs use Hall effect sensors or a rotary encoder to directly measure the rotor's position. Others measure the back EMF in the undriven coils to infer the rotor position, eliminating the need for separate Hall effect sensors, and therefore are often called *sensor less* controllers. A typical controller contains 3 bi-directional outputs (i.e frequency controlled three phase output) , which are controlled by a logic circuit. Simple controllers employ comparators to determine when the output phase should be advanced, while more advanced controllers employ a microcontroller to manage acceleration, control speed and fine-tune efficiency. Controllers that sense rotor position based on back-EMF have extra challenges in initiating motion because no back-EMF is produced when the rotor is stationary. This is usually accomplished by beginning rotation from an arbitrary phase, and then skipping to the correct phase if it is found to be wrong. This can cause the motor to run briefly backwards, adding even more complexity to the startup sequence. Other sensor less controllers are capable of measuring winding saturation caused by the position of the magnets to infer the rotor position.

3. Discussion

An effective and modern structure was designed with proper dimension so that it could gain a considerable lift and can have a vertical fly. All the parts were cut precisely with a long cut angle as well as with the proper dimension so that the structure looks fine and have a good lift. A round shed was attached at the top of the GSF

Hull so that the propelled air can be scattered in a synchronized manner rather than scatter away randomly. That is why if the air which will be propelled by a propeller(With a maximum speed of 15000 RPM) scatter randomly over the GSF Hull then the structure would not be gained a considerable lift that was needed indeed to give the structure a vertical flight. And the structure was made compact as much as possible so that air can not be flow through the blank space. Because that would produce a considerable drug which would reduced the lift effect as a result indeed. And as the motor was a brushless DC motor(BLDC) with three terminal it was necessary to design a speed controller so that the rotation can be maintained as a synchronized manner. The sequence of the motor rotation was controlled by the back E.M.F method as it was a sensor less Brush less DC motor in manner. The propeller was connected with the motor which rotates with a maximum speed of 15000 RPM. The was controlled with a range of 1190 RPM per volt(approximately). And a remote control device to control the system was designed to control the system from the distance. And finally the UAV that was designed was able to fly vertically to a considerable lift and a good height.

4. Conclusion

Now a days the UAV(Unmanned Air Vehicles) is an important filed in the field of aeronautics engineering. For an increase in efficiency, the electrical driven propeller itself can be mounted in a central duct. In this particular arrangement, also the air volumes entrained by the Coanda effect became several times multiplied. UAVs are designed and manufactured depending on their mission and they may perform. This technology can be used in surveillance that represents a monitoring process of the humans', objects' or processes' behavior, to be compared to the expected or required norms (for example, detecting some nuclear, biological or chemical activities or phenomena) . Intelligence considered to be a military branch of knowledge, which concentrates upon the gathering, analysis, protection and the dissemination of the information about the enemy, field and weather in the military operations area or within the area of interest.

Acknowledgements

All praises belong to Almighty Allah, the most kind hearted and bounteous to all his creatures and their actions and also help me to acquire knowledge.

The author wish to express gratitude and profound respect to supervisor Dr. Mohammad Masud, Professor and Head, Department of Mechanical Engineering, Khulna University of Engineering & Technology (KUET) for his supervision, advice and guidance from the very early stage of this thesis which were essential to carry out this work.

References

[1] History of Unmanned Aerial Vehicles - www.vectorsite.net

[2] The Role and Importance of UAV Within the Actual Theaters of Operations NICULAE MARIN, ELENA MARIN, AFASES 2010 BRASOV

[3] Civil Aviation Authority - CAP 658, Model Aircraft: A Guide to Safe Flying, United Kingdom, June 2003;

[4] Policy for Unmanned Aerial Vehicle (UAV) certification, EASA- AMENDAMENT (NPA) No 16/2005;

[5] Pahonie R., Cîrciu I., Boşcoianu M.- „ AN ANALYSIS OF DIFFERENT ROTARY WING MICRO AIR VEHICLES SOLUTIONS"- Metalurgia Internaţional No.7 Special

[6] Geoffrey Hatton, Simon McIntosh, GFS Projects Ltd., *Craft having flow-producing rotor and gyroscopic stability*, UK Patent Office no. GB 2,424,405 /23.03.2005

[7] http://en.wikipedia.org/wiki/Flying_saucer

[8] http://jlnlabs.online.fr/gfsuav/index.html

[9] http://diydrones.com/profiles/blogs/coanda-effect-saucer-ces-uav

5th BSME International Conference on Thermal Engineering

Design of a Grid Tied Solar Photovoltaic (PV) System with the Reduction of the Energy Storage Devices

Maruf Mohammad Ali[a*], Md. Mehedi Farhad[b], Sadia Safwat[c], Nahid Ashraf[d], Iftekhar Alam Abbasi[e], Md. Maruf Hossain[f]

[abcde]*Student, Ahsanullah University of Science and Technology, Dhaka-1208, Bangladesh*
[f] *Assistance Professor, Ahsanullah University of Science and Technology, Dhaka-1208, Bangladesh*

Abstract

Energy is inevitable for human life and a secure and accessible supply of energy is crucial for the sustainability of modern societies. With the increasing concern about the global demand for Renewable Energy (RE) energy, it is very much important to reduce the cost of the whole solar photovoltaic (PV) system. Still now most of the solar photovoltaic (PV) system is highly expensive. In this paper we have shown that grid tied solar system can be developed by omitting the energy storage device like large capacity battery bank. It will not only reduce the internal losses for charging and discharging of battery bank but also at the same time a large amount of cost of the battery will be reduced. So, the system maintenance cost will be reduced also. We have proposed a new approach to design a photovoltaic (PV) solar power system which can be operated by feeding the solar power to the national grid along with the residential load. Again if there is an extra power demand for residential load along with the solar power then this system can also provide an opportunity to consume the power from the national grid. The total system is controlled with the help of some sensors and a microcontroller. As a whole a significant reduction in the system costs and efficient system performance can be realized.

Keywords: Photovoltaic (PV); solar power; grid connected PV system; energy conversion.

1. Introduction

Bangladesh is one of the world's poorest and most densely populated country. Energy crisis is the biggest obstacle for economical development of any country as well as in Bangladesh. Due to the rising cost and depleting storage of fossil fuels along with the increasing concern for global climate change, utilization of RE in national scale has become essential for this country. At present, Bangladesh relies heavily on fossil fuels especially Natural Gas (NG) resources for its power generation and its present proven NG reserve would be ceased by 2015 [3]. The only way to save the fossil fuels like Natural Gas, Furnace Oil, Coal etc are in small scale use of them. According to the National Energy Policy the projected demand in 2005 was 5720MW with deficiency of around 700MW and will increase gradually to 11,794MW by 2020 for low economic growth of 6% and for a higher growth rate of around 8% it should be 17,580 MW. That is why Bangladesh government recognizes the indispensability of Renewable Energy policy on 18 December 2008 where target has been set to generate 5% of the total electricity from Renewable Energy sources by 2015 and 10% by 2020.

This target is incredible but not impossible: mainly due to the geographical location of Bangladesh. To achieve this target we need to install more solar PV system with the most effective manner. According to the data up to September 2011, more than 1 million off-grid solar PV systems have been installed in the rural area throughout this country having capacity 50MW. But still the growth rate of PV system and its contribution to the national energy is not sufficient due to the technical inconvenience and installation cost of the PV system. This paper presents an improved and cost efficient way to synchronize the PV array output with the utility grid using a special control scheme. So that, an individual solar PV system owner can acts as an electricity provider to the national power grid.

2. Conventional Off-Grid and Grid-Tied system

Most of the PV systems installed in rural area in Bangladesh are off grid system and most of these systems make use of the large capacitive battery as energy storage device. They store the energy in day time and use it at night time. One the other hand there is a very little use of on grid or grid tied system.

*Maruf Mohammad Ali. Tel.:+88-016-86355803
E-mail address: marufeeeaust@yahoo.com

2.1. Performance of a conventional Off-Grid PV system with storage

The Off-Grid PV system is consists of a PV array with a charge controller, battery and Dc load. This can be operated to drive a AC load by using an Inverter.

As Bangladesh is a compact, flat country with little geographic variation, the solar radiation data collected at one point may be treated as reasonably representative of the whole country. Fig. 1(a) and 1(b) shows the graph of Ampere-hour vs. days and Battery voltage vs. days respectively. Here for this system we have used a solar panel of Pmax 87W, Vpmax 17.4V, Ipmax 5.02A, Voc 21.7V and Isc 5.34 A rated at temperature 25^{o}C. The data for this graph was collected on April 2012.

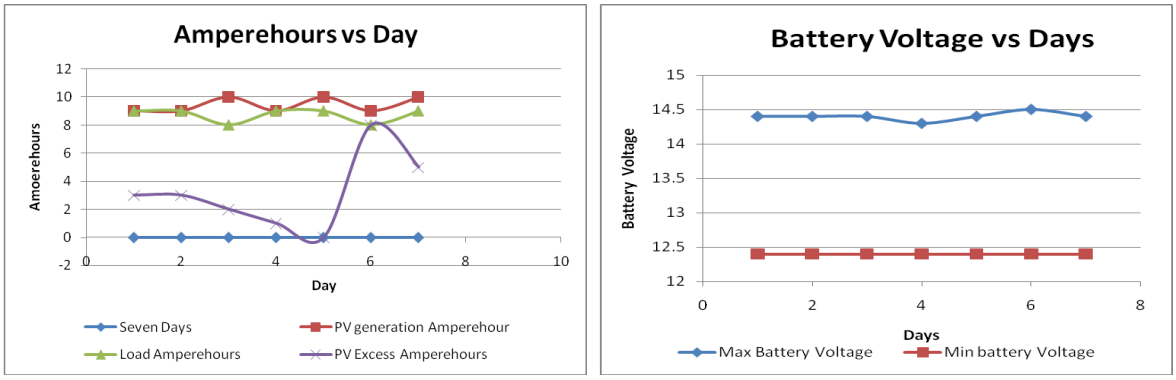

Fig. 1. (a) Ampere-hour vs. days of a typical system; (b) Battery voltage vs. days of a typical system

2.2. Conventional Grid-Tied PV system

Still grid tied PV system is not a popular PV installation system in Bangladesh. Some of the grid tied system has been designed earlier which was not so efficient at al. But to reach the goal of having 10% energy from renewable sources, we need to grab every opportunity of scaling up. Configuration of a typical grid-tied PV system is given below in Fig. 2.

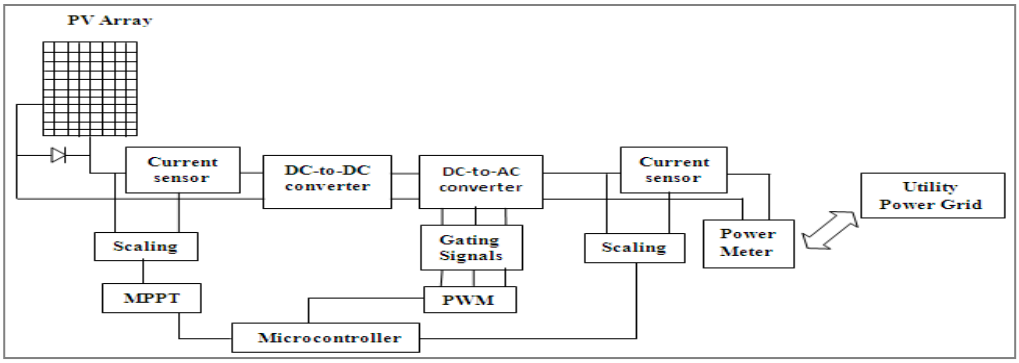

Fig. 2. Block diagram of a conventional grid-tied PV system

3. Proposed design of a Grid-Tied PV system

Energy is vital for the progress of a nation and it has to be conserved in a most efficient manner. Here we proposed an innovative design of a grid-tied PV system without storage device. This system is capable to feed solar energy to the utility power grid when grid power is available and backup the on-site load as well when the grid power is unavailable.

3.1. System layout

As shown in Fig. 3 the planed grid-tied PV system is consists of an internal processing junction box with its three end points. These are solar power, Utility power grid and Residential load. Here this system always tries to

feed the solar power to the utility power grid. At the same time the residential load will consume the load demand power from the utility power grid. But if the grid power is unavailable then the residential load demand will supply by the solar power.

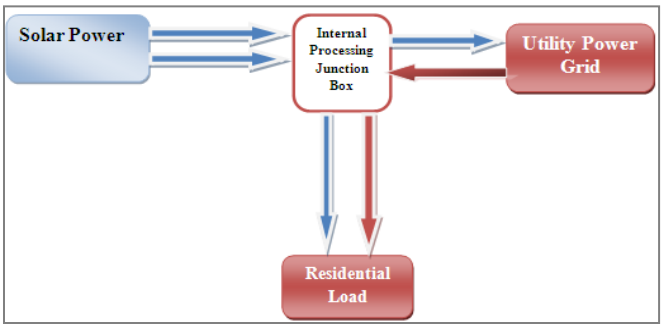

Fig. 3. Layout diagram of the planned grid-tied PV system

3.2. Schematic diagram and the relay position

As the illustration in Fig. 4 the power flow from the PV array and the utility power grid is controlled by three relay. The positions of the relays are also shown in Fig. 4. During normal operation relay 3 always at Normally Closed (NC) position. At day time when sunlight and grid power is available relay 1 and relay 2 both will be at NC position. So that the solar power will feed to the grid through relay 1 and at the same time residential load will consume the load demand power from utility power grid through relay 2. But if grid power is unavailable relay 2 will be off and relay 1 will be at Normally Opened (NO) position. So that, the solar power can directly flows to the residential load. Again if there is any overloading situation due to the residential load the relay 3 will be operate at NO position to disconnect the connection and ensure the safety of the system. At the same time it will generate a signal to the consumer for reducing the load. This is how the system will operate with a most efficient manner.

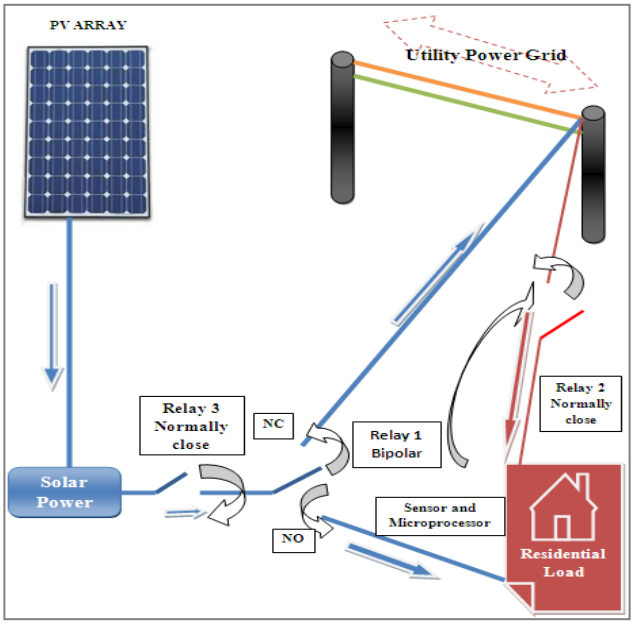

Fig. 4. Schematic diagram of the planed grid-tied PV system.

4. Proposed Grid-Tied PV system block diagram

Fig. 5 demonstrates the block diagram of the control scheme. The system block diagram consists of solar PV array, MPPT charge controller, DC to DC converter, High efficient Grid Tie inverter, AC three phase synchronizer, Microcontroller, DC power measuring device, CT, PT, ADC (Analogue to Digital converter), Relays and Metering device. We can describe all those elements in three parts:

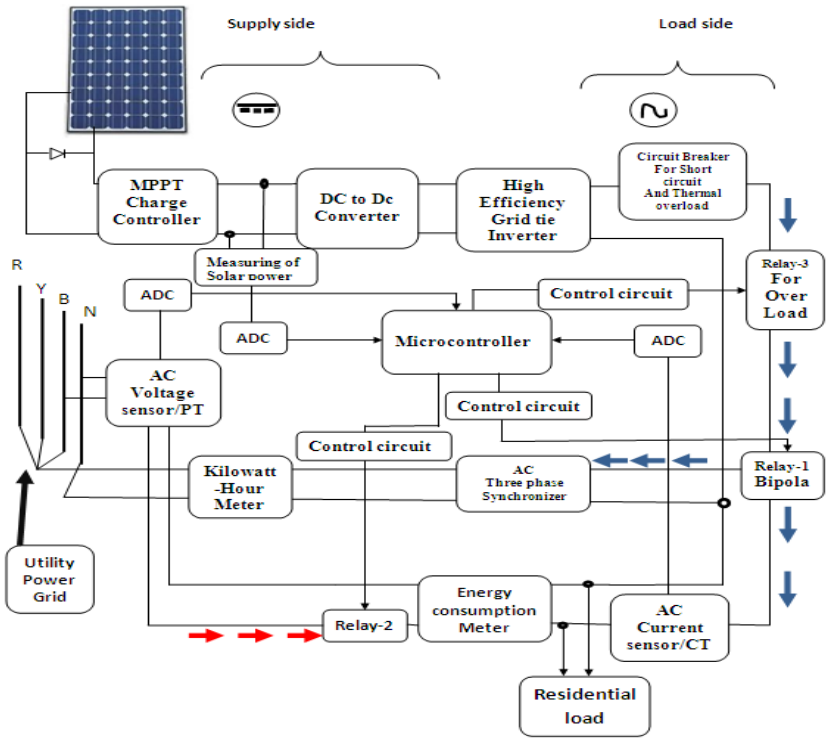

Fig. 5. Proposed Grid-Tied PV system block diagram.

4.1. *Voltage Control of Solar PV Array*:

The power output of a PV array depends on the voltage level where it operates under a given condition of irradiance and cell-surface temperature. For efficient operation, a PV array should operate near at the peak point of the V-I curve [2]. Various Maximum Power Tracking (MPPT) techniques have been proposed in [4] and [5]. The MPPT block of the block diagram in Fig.5 always tries to stable the PV output voltage and also ensure the maximum power output of the PV system.

4.2. Grid Tie Inverter

An inverter is a device that converts direct current to alternating current. The PV inverters are classified into two categories, Stand Alone Type and Synchronous Grid Tie Type. Synchronous Grid Tie Type inverter is a special type of inverter which is always collect the data of voltage and frequency from utility power grid by a AC synchronizer and synchronize the inverter output with the utility power grid. So that, it is possible to install a medium to large-size PV array and remain hooked up to the utility power grid [1].

4.3. Control Section and net metering system

The power measuring block measures the solar power with respect to time. The AC current sensor senses the residential load current which can be converted in power by multiply with the system voltage. The output of the measured solar power and the load demand goes to the microcontroller through two ADC (Analogue to Digital converter). The availability of the grid power can be detected by a PT. The output of the PT goes to the microcontroller through another ADC. With the help of these data microcontroller will take decision to send signal to the relay control circuit. Then the relays will operate according to the decision of the microcontroller. The relay control circuit consists of a 1K Resistance and a NPN Transistor (BD135). Fig.6 (a) shows the relay control circuit. Here pic16F88, 28 pin microcontroller with 16MHZ clock pulse generator and IC7805 voltage regulator can be used to obtain best performance of the system.

In our system a solar system owners can also enjoy the opportunity of net metering by selling energy to the grid when the consumed energy is less than the Delivered energy. Here we use two meter for metering consumed and delivered power. The energy consumption/billing meter will record how much energy is consumed by the costumer from the utility power grid. When the kilowatt-hour meter will record the amount of energy is delivered from the solar system to utility power grid. Fig.6 (b) shows the net metering system.

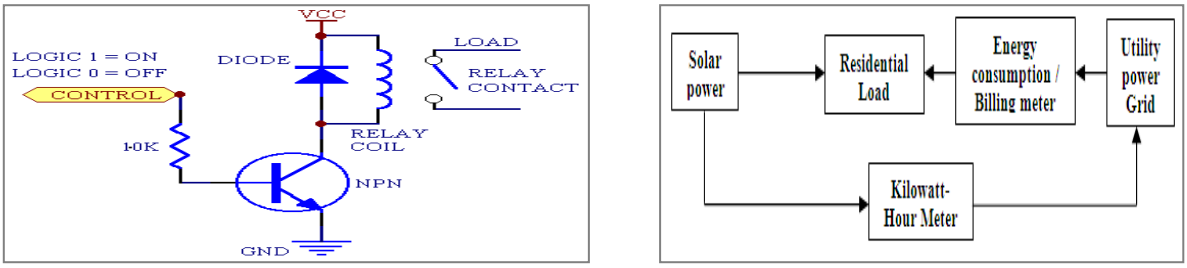

Fig. 6. (a)Relay control circuit ;(b) Net metering system

5. Flow Chart of the Control Scheme with Description

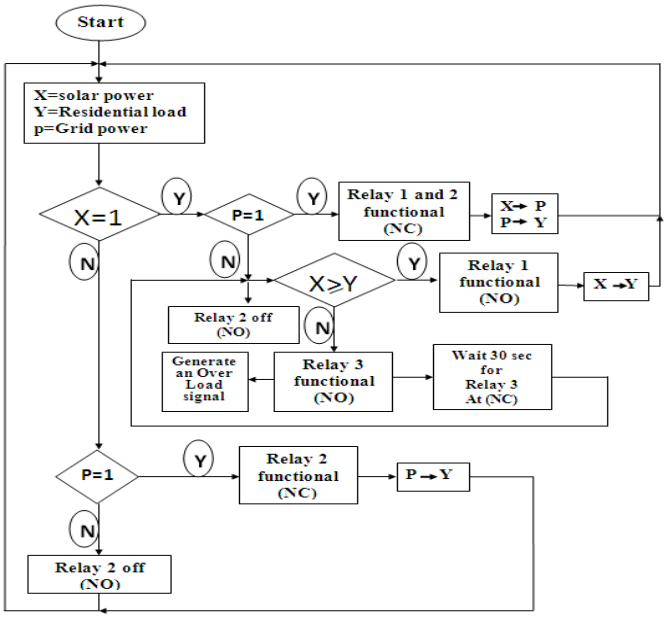

Fig. 7. Shows the flow chart of the control scheme

According to the flow chart as shown in Fig. 7 we develop a program in MicroC and also in assembly code to check the system performance. Here, after initialization of the system parameter the microcontroller always check the availability of grid power and solar power and take decision to control the relay 1 and relay 2. The microcontroller also compares the solar power with the residential load to control the relay1 and relay 3. According to the technical requirement in IEEE 1547, to prevent islanding situation the microcontroller always monitor the voltage and frequency of the grid and disconnect the inverter from the grid for any worse situation by controlling relay 1.

6. Comparative cost analysis of the Off-Grid solar PV system

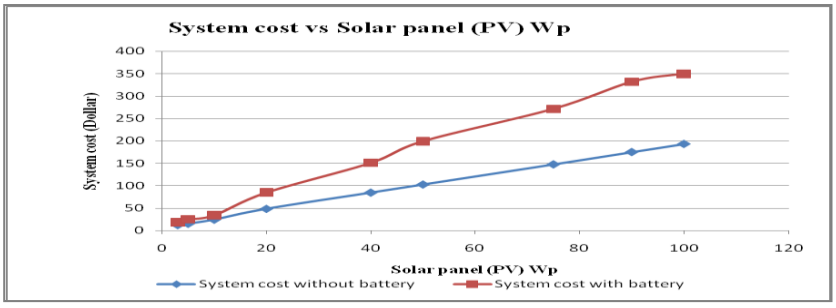

Fig. 8. System cost vs. solar panel (PV) Wp

Fig.8 shows the graph of installation cost vs. PV array Wp of a PV system with and without storage device. Here for a typical system we assume the relative cost components as: PV array $ 1.207 per Wp, Battery $1.207 per AH, Inverter $ 0.6030 per Watt, Charge controller $1.207 per Amp. This graph shows that the system cost will be cheap for a same Wp PV array installation without storage device (Battery).

7. Advantages of the Designed System

- Grid tied system is more power efficient than a conventional solar system. It ensures full utilization of solar energy whereas battery discharge rate is 60% to 65% in conventional off-grid solar system in Bangladesh.
- Properly configured, this grid-tied system represents the consumer as an energy provider to the utility power grid.
- Net metering allows system owners to get credit for any electricity the system sends to the grid.

8. Limitation of the designed system

In this paper we have come within the reach of a new PV system design. So that, we can produces more power from the renewable energy sources. But in our design we have some limitations. This grid-tied system without storage can't supply power if utility power grid is disconnected during night or rainy day when sunlight is not sufficient. Again power output from certain renewable energy sources, like wind and solar, can be intermittent. Fluctuation in output can negatively affect power grid frequency, voltage, component performance, causing instability in the power generation system and interrupted service to the customers.

9. Conclusion

This system has been designed with a concept of micro photovoltaic power station. Still the solar PV system installation cost is not within an acceptable limit. To fulfil the requirement of the predicted 10% of total energy which will produce from renewable energy by 2020, we need to install more PV system. And to do so, proper step should be taken to reduce the solar PV panel cost. So that, the general electricity consumer can concentrates their attention in grid-tied PV system. We hope there will be occur a lot of activity regarding grid-tied PV system in Bangladesh and then our work may help to decide an optimized way.

So, in this paper we have shown an advanced grid-tied PV system which is suitable for produce more energy from renewable energy sources. Thus every photovoltaic system which is installed in any where can be treated as a micro PV power station. No matter what ever the generation capacity of the plant.

Acknowledgements

This study was made possible with the help of the installed PV system at Ahsanullah University of Science and Technology. Special thanks to Assistant Professor Md. Maruf Hossain, Assistant Professor Md. Jakaria Rahimi and Embedded System Engineer Fahad Mirza for their useful discussion.

References

[1] M. Gohul, T. Jayach, A. Mohamed Syed Ali, T.G. Raju, N. Santhosh Kumar, M.R. Saravanan, "Anew design of grid tie inverter for a grid interactive solar photovoltaic power generation-An alternative option for energy conservation & security" IJECT Vol. ,2, Issue 3, Sept.2011.

[2] Md. Rejwanur Rasid Mojumder, Arif Md.Waliullah Bhuiyan, Hamza Kadir, Md. Nizamul Haque Shakil, Ahmed-Ur-Rahman, "Design & analisis of an optimized Grid-Tied PV system: Perspective Bangladesh" IACSIT international journal of engineering and technology, Vol.3, No. 4, August 2011.

[3] "Bangladesh Energy Crisis: Soul Searching", Energy Bangladesh, June, 2009.

[4] T. Noguchi et al, "Short-current pulse-based maximum-power-point tracking method for multiple photovoltaic-and-converter module system," IEEE Trans. Ind. Electron., vol. 49, no. 1, pp. 217–223, Feb. 2002.

[5] K. H. Hussein, "Maximum photovoltaic power tracking: An algorithm for rapidly changing atmospheric conditions," Proc. Inst. Electr. Eng.—Generation, Transmission, Distribution, vol. 142, no. 1, pp. 59–64, Jan. 1995.

5th BSME International Conference on Thermal Engineering

Future aspect of nuclear power in Bangladesh

*N. Paul[a], P. K. Halder[b] and M. E. Hoque[a]

[a]*Rajshahi University of Engineering and Technology, Rajshahi-6204, Bangladesh*
[b]*Jessore Science & Technology University, Jessore-7408, Bangladesh*

Abstract

Economic development and civilization of any country depends on reliable energy supply. However, Bangladesh is experiencing a severe electric power capacity crisis that is only likely to worsen over the next 15 years. Further, over 80% of Bangladesh's population still lives with no electricity. Recently the total electricity supply is 3000 MW/day within the demand of 5000MW/day. To meet this increasing demand of electricity, it is necessary to find out the alternative approaches to electrify the country. Nuclear power is one of the alternatives, considered as the pollution and carbon dioxide free that can create electric power with economic and ecological advantages. This paper outlines the prospects for nuclear power in Bangladesh and estimates the potential for commercial applications now and in future. The paper concludes that Bangladesh holds the potential to cost-effectively meet a significant fraction of its future electricity demand through the use of nuclear power generation technology.

Keywords: Nuclear power; nuclear fusion; nuclear fission and Renewable energy.

1. Introduction

Non-renewable energy like fossil fuels, oils and natural gases are often scarce due to rapid depletion of these resources. So, the energy crisis is the main problem to mankind facing today. Although the actual reserve of this most important fossil fuel of Bangladesh has not yet been ascertained, a recent survey shows that there is as much as 33 TCF (trillion cubic feet) of proven probable natural gas reserves in the country [1]. At present the country has 2,041 million tons of coal reserve [2]. Total storage capacity of petroleum products (Diesel, kerosene, petrol and octane) in the country is 687,500 tons which is only 8% of the total demand [3]. In rural, remote, coastal and isolated area development has long been considered as one of the major policy objectives of the government of Bangladesh because over 85% of the population live in those areas. Energy is the key ingredient for the socioeconomic development of a country. In Bangladesh poverty and lack of access to energy are closely linked. Energy in Bangladesh is indispensable for almost all economic activities, ranging from farm irrigation to the manufacture of goods by small and micro enterprises. Energy is also indispensable for attaining the Millennium Development Goals (MDGs) for Bangladesh. Although endowed with natural gas resources and some good quality coal deposits, Bangladesh continues to reel from widespread power shortages due to a lack of investment in power generation and the inadequate distribution of infrastructure. While there has been some improvement in generation capacity in the recent past, the demand far outstrips the supply [4]. The civilization is dependent on electric power. People in rural areas suffer more than those in urban areas from low access to electricity. Even those who have electricity experience frequent outages and poor quality power. Only 49% of Bangladeshis having access to electricity, the per capita energy use is only 180 Kilowatt-hours (kWh) however, with the passage of time and access to electricity and demand will increase dramatically in near future. It is required to improve electricity generation in order to meet overall goals of the national development viz. millennium development goals (MDGs). It is estimated that about 6,000 MW additional capacity needs to be added over the period up to 2015. It would increase the per capita availability of electricity to 200 kWh. It is understood that an average 1,000 MW electricity generation is needed in every year to access electricity for all by 2020 [5]. Indigenous natural gas supply now is the principal fuel and accounts for about 86% of electricity generation. If natural gas is used for power generation at the present rate, this would result in the complete depletion of existing reserves within 10-12 years. At present to meet total demand of energy, Bangladesh imports annually about 1.3 million metric Tons of crude oil and 2.7 million metric Tons (approx.) of refined petroleum products per annum is imported [4-6]. In order to meet the increasing energy demand for development of agriculture and industry and for the generation of better employment opportunities, it is necessary to harness all the available alternative sources of energy immediately. Thus, the interest in renewable energy has been revived over the last few years, especially after global awareness regarding the ill effects of fossil fuel burning. Nuclear power plants can offer an alternative source of limitless energy. Generally, construction of the first nuclear plant takes longer time, 8-15 years, from inception in developing countries [5]. The first nuclear chain reaction produced electricity experimentally in a reactor in Chicago in 1945 and the first commercial nuclear power plant was built in 1954, nine years later. Since then, nuclear power reactors have grown fast and about 390 of them were built until 1986. At present, 22 countries in the world consume more than 15% of nuclear

electricity. Nuclear power stations are usually situated in a load dispatch Centre and act as a base load station (above 85% plant factor) and should thus provide reliable electricity in a grid system. The percentage of electricity produced by nuclear power plants all over the world has remained stable and nuclear power is now producing 16% of the world's electricity. It may be noted that it takes in a long time to complete a nuclear power station (5 years). Starting with a modest nuclear power station of 600 MW (to supply power from, say 2011-2012), the target could be to produce 15% of electricity from nuclear power by 2030 [5-17]. In Bangladesh context, nuclear power technology is identified as a viable option in the overall energy mix.

2. Bangladesh Power Sector

Total generation capacity of electricity in the country was 6,727 MW (up to June 15, 2011) including 3,534 MW in Public sector and 3193 MW in Private sector including Rural Electrification Board (REB) as shown in Table I [18, 19]. In the public sector, a good number of generating units have become very old and has been operating at a much-reduced capacity. As a result, their reliability and productivity are also poor. For the last few years, actual demand could not be supplied due to shortage of available generation capacity. Besides, due to a shortage of gas supply some power plants are unable to reach their usual generation capability.

Table 1. Present power generation scenario

Sl. No.	Items	FY 2010-2011 (Up to 15 June'11)
1	Generation Capacity , MW	6,727
2	Maximum Generation , MW (13 June'11)	4,890
3	Net Generation, MWh (FY 2009-2010)	29,247
4	Transmission Line, km	8,500
5	Grid Substation Capacity, MVA (a)400 kV& 230 kV (b)132 kV	 6,850 9,899
6	Distribution Line, km	2,70,000
7	Number of Consumers (Million)	12
8	Number of Village Electrified	53,281
9	Per Capita Generation, kWh	236
10	Access to Electricity	49%

The installed capacity by owner basis for FY 2010-11 (up to 15 June'11) is shown in Fig 1.

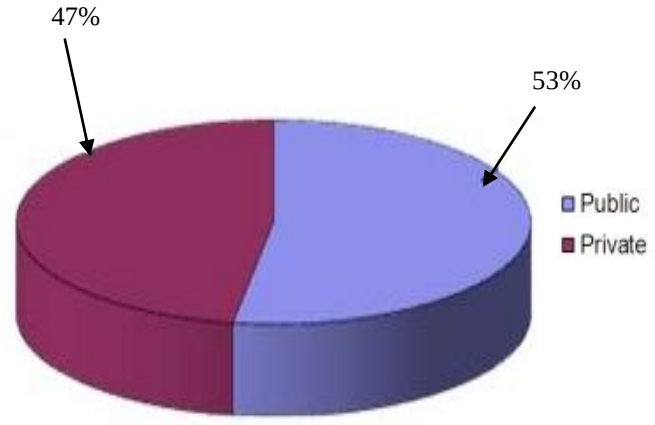

Fig 1: Total generation capacity

3. Present Electricity Situation in Bangladesh

The supply of electricity and access to it has great impact on the national economy. Only about one third of the country's population has access to electricity. The present peak load generation, which is stated to be about 4500 MW (draft background document of National Energy Policy, March 2006) is fluctuating due to faulty performance of individual power plants, many of which are too old and should be replaced. The power sector reform road map aims to accommodate 8% growth in electricity generation with a 25% reserve margin, encourage private sector power development and improve the sector performance. The demand of electricity is also increasing at about 8% per year. The average generation of electricity is about 3000 MW compared to average demand of 4400 MW. Temporary operational failures of power stations add to the shortage and make the situation more difficult. The crises of electricity become most critical at dry season during the irrigation season. The demand of Electricity is not constant. It varies over time and location based on the people's activity. Demand also varies over the year for irrigation and summer. Irrigation activity does not start simultaneously in all part of the country. Similarly commercial demand varies over the period of the day. If such factors are not included in the allocation of electricity it cannot be rationalized. Since the resource is limited, a rational approach has to be established to priorities between demands to address the most critical needs that would have more contribution to the national growth. The present estimate of base peak generation in 2025 is about 20,000 MW to produce over 100,000 GWh of electrical energy [18, 19].

4. Renewable Energy Resources in Bangladesh

Renewable Energy is the energy which is renewable. Their reserves are not diminished and the resources are not exhausted in course of time as they are used.

4.1 Natural Gas

In Bangladesh, natural gas is the most important source of energy that accounts for 75% of the commercial energy of the country. So far in Bangladesh 23 gas fields have been discovered with the rate of success ratio is 3.1:1 of which two of the gas fields are located in offshore area. Gas is produced from 17 gas fields (79 gas wells).Oil was tested in two of the gas fields (Sylhet and Kailashtila) [20, 21].

4.2 Biogas

Biogas may be the most promising renewable energy resource. Presently there are about 50,000 households and village-level biogas plants in place throughout the country. Table 2 shows the Biogas potential in Bangladesh [20, 21].

Table 2. Bio gas Potential in Bangladesh

Raw materials	Organic Fertilizer (million tons)	Yearly gas production (million cubic meter)
1. Cow/Buffalo dung	60.20	2971.10
2. Poultry droppings	2.05	191.60
3. Human excreta	32.85	1226.40
4. Garbage	1.72	115.00
5. Water hyacinth	10.00	740.00
6. Pressed mud	0.07	384.00

4.3 Solar Energy

Bangladesh is situated between 20.30 - 26.38 degrees north latitude and 88.04 -92.44 degrees east which is an ideal location for solar energy utilization. Daily average solar radiation varies between 4 to 6.5 kWh per square meter. Maximum amount of radiation is available on the month of March-April and minimum on December-January. Potential of solar energy is good in Bangladesh. But due to its higher cost of equipment it

has to go a long way to become commercially viable. However, in remote areas of Bangladesh it is gradually becoming popular and government has undertaken lot of scheme to subsidize on it. Presently there are about 2, 64,000 solar panels installed throughout the country [20, 21].

4.4 Bio-Diesel

Bio-diesel may also be one of the promising sources of energy. Though Bangladesh is a densely populated country with 150 million people just in 147,570 Sq. Km areas, except the hilly areas, most of the areas are covered with fertile land that producing high yielding crop. Diesel from Jatropha plant may be a source of renewable energy in our country. Jatropha trees can be planted in both the sides of rail way tracks & high ways, marshy land & costal belt of the country. These Jatropha plant can also be used for coastal protection [20, 21].

4.5 Hydro Power

At present only 230 MW of hydro power is utilized in Karnafuli Hydro Station, which the only hydro-electric power plant operated by Bangladesh Power Development Board (BPDB). BPDB is considering extension of Karnafuli Hydro Station to add another 100 MW capacity which will add energy marginally, however, will be effective to operate it as a peaking power plant. The additional energy will be generated during the rainy season when most of the year water is spilled. Apart from Kaptai, two other prospective sites for hydro power generation at Sangu and Matamuhuri River are identified by BPDB. However, no pre-feasibility study has been made so far [20-22].

5. Nonrenewable Energy Resource in Bangladesh

Non-renewable Energy is the energy which is not renewable. Their reserves diminish and the resources are exhausted in course of time as they are used. And so the sources are considered limited and not usable for an unlimited period of time.

5.1 Coal

Coal played a key role as a primary source of organic chemical feed stocks in the world till 1950s, and maintained its large share as a primary energy source throughout the 20th century. Although its percentage contribution decreased from 55 in 1900 to 22 in 1997, coal plays a vital role as an energy resource. The present coal reserve of Bangladesh is 2,041 million tons as shown in Table 3 [2].

Table 3. Estimated Coal Reserve

Field	Reserve (million ton)	Depth (m)	Area (sq. km)
Jamalganj	1053.00	640-1036	10.36
Barapukuria	303.00	119-506	5.50
Khalaspir	685.00	257- 482	12.26
Total	2041.00	---	---

5.2 Petroleum Products

Various types of Petroleum products such as Diesel, kerosene, petrol and octane are most commonly used in different sectors. Total storage capacity of petroleum products in the country is 687,500 tons. Table IV shows the petroleum products consumption [3].

Table 4. Petroleum products consumptions 1997 (in tons)

Products	Power sector	Industry sector	Agriculture sector	Domestic sector	Transport sector	Grand Total
Octane	---	92	---	195	58,793	59,080
Petrol	4	292	---	115	212,283	212,694
Kerosene	53,251	239	---	532.227	129	585,846

Diesel	179,344	36,274	451,179	17,546	857,661	1,542,004
LDO	498	1,002	---	---	784	2,284
Jute Batching Oil	---	22,087	---	---	---	22,087
Furnace Oil	110,834	94,973	---	9,490	6,611	221,908
Lubs/Gr.	1,184	8,532	8,508	204	25,932	44,360
LPG	---	---	---	13,539	---	13,539
Bitumen	---	---	---	---	71,042	71,042
JP-1	---	5,524	---	---	---	5,524
SBP/MTT	---	5,524	---	---	---	5,524
Grand Total	345,115	169,015	459,687	573,316	1,361,082	2,908,215
%	11.87	5.81	15.81	19.71	46.80	100.00

6. Energy Situation and Energy Mix in Bangladesh

Per capita energy consumption of Bangladesh is one of the lowest in the world. Major portion of energy is consumed for subsistence (e.g. cooking, lighting, heating etc.) & Small portion for economic growth (e.g. agriculture, industry, transport, commerce etc.). In developed countries higher proportion of energy is consumed for economic growth and smaller proportion for subsistence. Increase in per capita commercial energy consumption is necessary to increase per capita gross national income (GNI). Primary energy supply of Bangladesh in 2005 depends on indigenous & imported energy sources. Fig. 2 shows the consumption of energy from various sources [5].

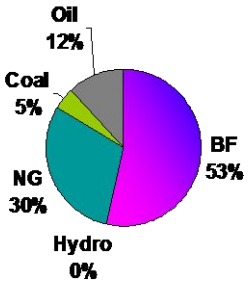

Fig.2: Various sources of energy

Total=31.78MTOE [Per Capita=226kgOE],
Renewable Energy (Biomass & Hydro) = 53.7%,
Nonrenewable Energy (NG, Oil, Coal) = 46.3%,
Indigenous Energy (Biomass, Hydro, NG) =83.5%,
Imported Energy (Coal, Oil) =16.5%,
Approximate Cost of Imported Energy=$1.8 billion.

7. Nuclear Power in Bangladesh

The government started feasibility studies for possible nuclear power in Bangladesh in 1961. The International Atomic Energy Agency supported such a possibility in 1962 and an US firm recommended the setting up of a 50 MW station in 1963. A site along the Padma River, measuring 262 acres of land in Rooppur and another 12 acres of land, a few miles away for residential colony were acquired. But the project was abandoned because the expected US aid was not available. Since then many other projects proposals, including

one from the Soviet Union (offered by Prime Minister Mr. Kosygin himself) in 1968 and a private sector offer from Belgium in 1969 were not considered for various reasons by the government. Soon after Chernobyl accident started building up against nuclear power. A Nuclear Safety and Radiation Control Act was passed by the Parliament in 1993 [23-28].

8. Present Situation of Nuclear Power in Bangladesh

In view of the failure of the past nuclear projects, mainly for lack of funds, IAEA had recommended that Bangladesh should try for implementation of nuclear power projects by private sector, which could organize both technology and funding for an IPP project. The recovery of the cost will be made through a power purchase agreement (PPA) with an agency of the Government. Further, an expert group meeting in Vienna was convened in which a draft National Nuclear Power Action Plan for Bangladesh was reviewed. IAEA agreed to provide assistance for training of manpower, evaluation of an updated site report as well as the preparation of a Request for Proposal (RFP) document. A revised Site Safety Report (especially considering low surface water in Rooppur, as at present) and a comprehensive "Bid Evaluation Document" comprising of technical and financial offers for the implementation of the project on a BOO or BOOT basis have been prepared by BAEC. IAEA has wanted a stamp of priority by the government before the RFP could be sent to pre-qualified manufacturers. This is awaited for some years now [23-28].

9. Nuclear as a form of Energy

Nuclear energy is the energy that directly releases after controlled Atomic reactions. Nuclear power is obtained from release of nuclear energy, a type of nuclear technology involving the controlled use of nuclear reactions. A nuclear reactor is a device in which controlled fission & fusion reactions are carried out at a steady rate in order to produce thermal energy. This thermal energy can then be used to supply heat, for industrial or home heating, or to produce electricity. While small reactors have been developed for specific purposes (e.g., ship or submarine propulsion), most nuclear reactor applications are associated with the production of electricity. Typically, heat produced from fission & fusion reactions is used to power steam turbines which are coupled to alternators to generate electrical power. Nuclear power can come from the fission of uranium, plutonium or thorium or the fusion of hydrogen into helium.

9.1 Nuclear Fission Technology

Nuclear fission is the splitting of a massive nucleus into photons in the form of gamma rays, free neutrons, and other subatomic particles. A typical nuclear fission reaction involves ^{235}U and a neutron. The nucleus of ^{235}U has 92 protons and 143 neutrons. When bombarded by extra neutrons on ^{235}U, it loses atomic balance and becomes unstable to split into smaller pieces of fission products and releases more neutrons. This post splitting mass difference causes to release huge energy in the form of heat. The extra neutrons produced responsible for further chain reaction within the leftover mass of uranium [29, 30].

$$^{235}_{92}U + n = {}^{236}_{92}U \qquad (1)$$

$$^{236}_{92}U = {}^{144}_{56}Ba + {}^{89}_{36}Kr + 3n + 177\ MeV \qquad (2)$$

For a fission reaction, two conditions need to be satisfied such as,

A. Critical mass of the substance (the minimum amount of mass is required for fission to be self-sustaining).
B. A relatively slow neutron is required to initiate the process.

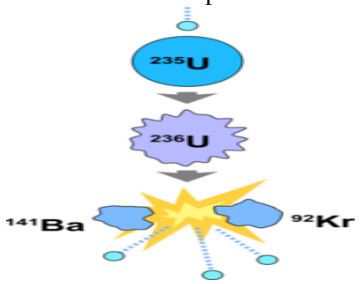

Fig.3: Nuclear fission reaction

9.2 Nuclear Fusion Technology

Nuclear fusion is the reaction in which two or more nuclei combine together to form a new element with higher atomic number (more protons in the nucleus). The energy released in fusion is related to $E = mc^2$ (Einstein's famous energy-mass equation). On earth, the most likely fusion reaction is Deuterium–Tritium reaction. Deuterium and Tritium are both isotopes of hydrogen. Fusion of deuterium with tritium creates helium-4, frees a neutron, and releases 17.59 MeV of energy [29, 30].

$$^{2}{}_{1}Deuterium + {}^{3}{}_{1}Tritium = {}^{4}{}_{2}He + {}^{1}{}_{0}n + 17.6\ MeV \qquad (3)$$

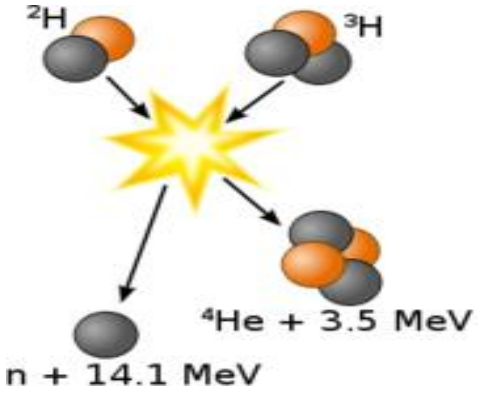

Fig.4. Nuclear fusion reaction

9.3 Effects of fusion and fissions

If accidentally, a fission reaction goes out of control as a result of not controlling the emission of neutrons, a nuclear meltdown can happen which can then release highly radioactive particles in the atmosphere. In contrast, in case of nuclear fusion if the reaction goes out of control, the reaction would stop automatically as it will cool down because, fusion reactors cannot sustain a chain reaction, therefore, they can never melt down like fission reactors. In addition, in case of nuclear fusion reaction, the amount of radioactive materials produced as waste is very small or, if the right atoms are chosen, no radioactive waste. With regards to these factors it can be said that a fusion reaction is a more environmentally friendly method of producing nuclear power. The energy released by fusion is three to four times greater than the energy released by fission. This is because the amount of mass transformed into energy is that much greater in a fusion reaction than in a fission reaction. Fission reaction takes little energy to split two atoms but extremely high energy is required to bring two or more protons close in fusion reaction [23-28]. Thus, fission reactors were developed first, and fusion reactors have not been developed yet.

10. Importance of Nuclear Energy

There are several advantages to the use of nuclear power when the situation makes it possible. First, it is an energy source which delivers low - cost electricity. It is possible to generate a high amount of electrical energy in one single plant using small amount of fuel. Furthermore, this cost is stable over several decades. Another greatest advantage of nuclear power is that it avoids the wide variety of environmental problems arising from burning fossil fuels - coal, oil, and gas. Nuclear fuels do not emit CO_2 during operation, so it does not contribute to the greenhouse effect. Thus 'global warming' process can be minimized - changing the earth's climate, acid rain, which is destroying forests and killing fish; air pollution etc. It checks degrading our quality of life; i.e., the destructive effects of massive mining for coal; and oil spills which do great harm to ecological systems can be prevented. Even if one takes into consideration the entire fuel cycle, including CO_2 emitted at each stage of the nuclear process, for example, extraction and processing of the ore, enrichment of the uranium, and construction of the reactor and reactor housing, the total emissions are below that emitted when fossil fuels are used to supply the same amount of energy. The total emissions can vary, of course. Obviously, if uranium enrichment is done using electricity produced by fossil fuels, there is a larger contribution to CO_2 emission than if it is done with electricity provided by nuclear power. As nuclear energy is a concentrated form of energy, the weight or volume

of nuclear waste produced by nuclear energy sources is also relatively small. Nuclear energy is a rather young energy source, having been used a little less than half a century [23-28].

11. Conclusions

Bangladesh has gone a long way in getting ready for nuclear power. Manpower has been trained, radiation safety bill has been passed, land for the first nuclear power station has been acquired and many feasibility studies have been made. Energy policy has clearly stated the necessity for energy security and keeps all options for power production open. International Atomic Energy Agency (IAEA) has always supported Bangladesh in her search for nuclear power and will provide more help in implementing a nuclear power program. Bangladesh also has many hilly and unused lands. Therefore, these available unused lands can be used for nuclear power plants. The initial cost, though high, will still produce electricity at a comparable generation cost. If the political will is there, the opponents of nuclear power will honor the will, as long as commitment to the peaceful uses of atomic energy remains and sufficient precautions have been made for safety and safeguards. After all, 75% of electricity in France is generated from nuclear power stations and there is no dearth of nuclear fuel in the world, with prospect of endless new fuel from fast breeder reactors. Land is available and many other preparatory studies have already been made by Bangladesh Atomic Energy Commission (BAEC). The developer has to arrange fuel for the entire period of operation of the power reactor and take back the burnt fuel so the Bangladesh does not have the problem of the main waste disposal. Safety and safeguards issues can be dealt with by BAEC and IAEA. Therefore, it has been recommended that, if Bangladesh is to get out of the chronic power shortage problem and look for energy security, entry into a long term nuclear power program should not be delayed anymore and a decision has to be made by Bangladesh itself as soon as possible

Acknowledgement

The authors are thankful for the supports received from the department of Mechanical Engineering, Rajshahi University of Engineering & Technology, Bangladesh.

References

[1] Titas Gas Transmission and Distribution Company, 2011. htpp: //www.bloomberg.com/apps
[2] Barapukuria Coal Mining Company Limited (BCMCL), Bangladesh, 2011. http://www.bcmcl.org.bd
[3] Bangladesh Petroleum Corporation (BPC), 2011.htpp://www.mof.gov.bd
[4] ADB (2003) Promotion of Renewable Energy, Energy Efficiency, Greenhouse Gas Abatement (PREGA) Operating Procedures, Country Study Report of Bangladesh, Asian Development Bank, p 73.
[5] Challenges and Opportunities to Introduce the First Nuclear Power Plant in Bangladesh, Reactor Operation and Maintenance Unit, Bangladesh Atomic Energy Commission Dhaka, Bangladesh.
[6] Building renewable electricity supply in Bangladesh Fulton, L.M. Energy Conversion. Engineering Conference, 1997, IECEC-97. Proceedings of the 32nd Intersociety, Volume 3, Issue 27 Jul-1 Aug 1997 Page(s):2187 - 2192 vol. 3.
[7] Japan Nuclear Cycle Development Institute, Monju Reactor Website. www.jnc.go.jp/zmonju/mjweb/index.htm (October 30, 2000).
[8] *Nuclear Power in an Age of Uncertainty*. Congress of the United States, Office of Technology Assessment, OTA-E-216, February 1984.
[9] *Nuclear Proliferation and Safeguards Summary*. Congress of the United States, Office of Technology Assessment, OTA-E-148, March 1982.
[10] Hulme, H. R., *Nuclear Fusion*. London: Wykeham Publications Ltd., 1969.
[11] Semat, Henry, *Introduction to Atomic and Nuclear Physics*. New York: Holt, Rinehart & Winston, 1959.
[12] Glasstone, Samuel, *Principles of Nuclear Reactor Engineering*. New York: D. Van Nostrand, 1960.
[13] Glasstone, S., and Sesonske, A., *Nuclear Reactor Engineering.* New York: Van Nostrand Reinhold, 1981.
[14] Winterton, R. H. S., *Thermal Design of Nuclear Reactors.* New York: Pergamon Press, 1981.
[15] Nero, Anthony V. Jr., *A Guidebook to Nuclear Reactors.* Berkeley, Calif.: University of California Press, 1979.
[16] Nealey, Stanley M., *Nuclear Power Development.Prospects for the 1990s*.Columbus, Ohio: Battelle Press, 1990.
[17] International status and prospects of nuclear power, 2010 edition. International atomic energy agency, Vienna.
[18] http://www.powerdivision.gov.bd/index.php?page_id=262.
[19] Energy: The Changing Climate: Royal Commission on Environmental Pollution 2000.

[20] Assessment of Renewable Energy Resources of Bangladesh, Mazharul Islam, EBook1,version 1, May 2002, pp. 1-51.
[21] http://www.emrd.gov.bd/43221.html.
[22] Salequzzaman M., Newman P., Ellery M. and Corry B. (2000), Prospects of Electricity in Coastal Regionof Bangladesh: Tidal Power as a Case Study, Journal of Bangladesh Studies, vol.2, no. 1, June 2000.
[23] World List of Nuclear Power Plants. *Nuclear News*, February 1991.
[24] Nuclear Regulatory Commission, .Nuclear Reactors.www.nrc.gov/NRC/reactors.html (November 2, 2000).
[25] Nuclear Regulatory Commission, .U.S. Commercial Nuclear Power Reactors.www.nrc.gov/AEOD/pib/states.html (November 2, 2000).
[26] Environment News Service, .World Total: 434 Nuclear Power Plants.ens.lycos.com/ens/may99/1999L-05-06-06.html (November 4, 2000).
[27] Postnote January 2003 Number 192 Nuclear Fusion, Parliamentary Office of Science & Technology.
[28] Bromberg, Joan Lisa, *Fusion*. Cambridge, Mass.: MIT Press, 1982.
[29] J. Wesson. *The Science of JET*. JET Joint Undertaking, 2000. URL http://www.iop.org/Jet/fulltext/JETR99013.pdf.
[30] K. S. Krane. *Introductory Nuclear Physics*. John Wiley & Sons, Inc., 1988.

5th BSME International Conference on Thermal Engineering

Modification of an SI Engine into a Compressed Air Engine to Work with Compressed Air or Gas

Debashish Saha, SKM Ashikul Islam, Aashique Alam Rezwan* and Maglub Al Nur

Department of Mechanical Engineering, Bangladesh University of Engineering & Technology, Dhaka-1000, Bangladesh

Abstract

The environmental pollution in the metropolitan cities is increasing rapidly mostly because of the increased number of fossil fuel powered vehicles. Many alternative options are now being studied throughout the world. One of the alternative solutions can be a compressed air powered vehicle. The present study focuses on converting an SI engine into a compressed air engine. A two stroke single cylinder SI engine is converted to operate using compressed air because of its design simplicity. The cylinder head of the engine is modified by replacing the existing cam with a set of newly designed flank cam and an inlet-exhaust air passage. As the cylinder head of the engine is modified, the engine is tested for different timing of the valve opening and duration of opening. Three sets of valve timing are used to test the converted compressed air engine. The air pressure used in the present study is 7 bar which is obtained using a compressor. The design and experimental test result presented here can be used for further research and modification of the technique.

Keywords: Compressed Air Engine; Valve Timing, SI Engine;

1. Introduction

A compressed-air engine is a pneumatic actuator that creates useful work by expanding compressed air and converting the potential energy into motion. A pneumatic actuator is a device that converts energy into motion. The motion can be rotary or linear, depending on the type of actuator. Compressed Air Engine (CAE) are fueled by compressed air, which is stored in a tank at a high pressure of about 30 MPa. The difference between the compressed air engine and IC engine is that instead of mixing fuel with air and burning it to drive pistons with hot expanding gases, CAE's use the expansion of previously compressed air to drive their pistons.

The greatest advantages of compressed air vehicle are no burning process and no waste gas discharge to the surrounding environment. It can be said as a green environmental protection vehicle with near zero pollution (1) in the metropolitan cities. With the policy of energy conservation and environment protection, studies on air powered car become more and more warming-up. Recently, its researches in domestic and aboard have achieved notable achievements. Zhejiang University and Hefei University of Technology of China have accumulated abundant experience in theory analyses and experimental test. The MDI Company in France has realized the design, manufacture, and application of air powered car (2) (3). The engines of compressed air cars are piston type, vane type, rotary type and so on, and the piston engine is widely taken now (4) (5). At present, the piston engine power system has some disadvantages such as complex structure, easy wearing, high noise and low efficiency. Therefore, to develop and optimize engine power system is the key technique for compressed air car.

2. Project Overview

In the present study, emphasis was given to conversion of a two stroke single cylinder SI engine into a compressed air engine with minimum possible modification of the existing design. The design is based on a rather simple working principle.

The compressed air is the source of energy that is stored in a high pressure cylinder. Basically this cylinder is re-filled by the compressor. But in the present case, the compressed air is supplied directly from a compressor at a pressure of 7 bar. When the piston is at TDC (Top dead centre) then the inlet cam allows the inlet follower rod to open the inlet port and let the compressed air enter into the air chamber. In this situation the exhaust port is closed by the respective follower controlled by the exhaust cam. The high pressure air introduced to the

* Corresponding author. Tel.: +8801552364999
E-mail address: aashiquear@gmail.com

chamber passes through the inlet passage and creates a downward thrust on the piston and the piston starts moving downwards. After pushing the piston downwards the air is then reflected towards the other passage of the chamber and meanwhile the exhaust cam opens the exhaust port to leave the air by the use of a follower rod. The inlet cam has to close the inlet port with the help of the inlet follower before the piston reaches the BDC (Bottom dead center).

An extra supply of power is needed to give the piston an upward motion after it reaches BDC. Therefore the reciprocating motion of the piston is influenced by the application of a flywheel mounted on the extended crank shaft. The power storage capability of the flywheel is used to supply the extra energy to the piston movement. The transmission of power from the crank shaft to the cam shaft is done directly by a chain sprocket mechanism. The mechanism of cam shaft rotation is done by mounting the shaft on two ball bearing holders. The two follower rods are mounted on separate springs placed above the air chamber. The restoration of force carried out by spring allows the follower to lift back to its initial position when the cam position is at zero displacement. The use of a one way valve is to ensure a unidirectional flow of the high pressure air from the compressor to the air chamber.

3. Structural Design

In the present study, a CDI H1100S motorcycle engine has been used for modification into compressed air engine. There are several structural change required to be done to run the engine with compressed air.

3.1. Extended Cylindrical Chamber

The cylinder head on top of the engine cylinder has been replaced with a new cylindrical chamber made of mild steel with pressure coating. The hole provided for the spark plug has been bored further to match the outer diameter of the new cylindrical chamber. The cylinders have two through holes (diameter = 15 mm) for the intake and exhaust valves to operate. At 60 mm from the top of the cylinder, two 10 mm holes were drilled for the purpose of intake and exhaust ports.

Fig. 1. Cylindrical Chamber

3.2. Inlet-Exhaust Passages

To avoid complexity in the design, providing inlet passage with bypass air chamber as before, whereas keeping the exhaust passage open the whole time, which aroused ambiguity in operation when tested the previous design, two separate passages has been bored in the newly designed air chamber. A solid partition has been provided in between the through passages for the safe operation of valves.

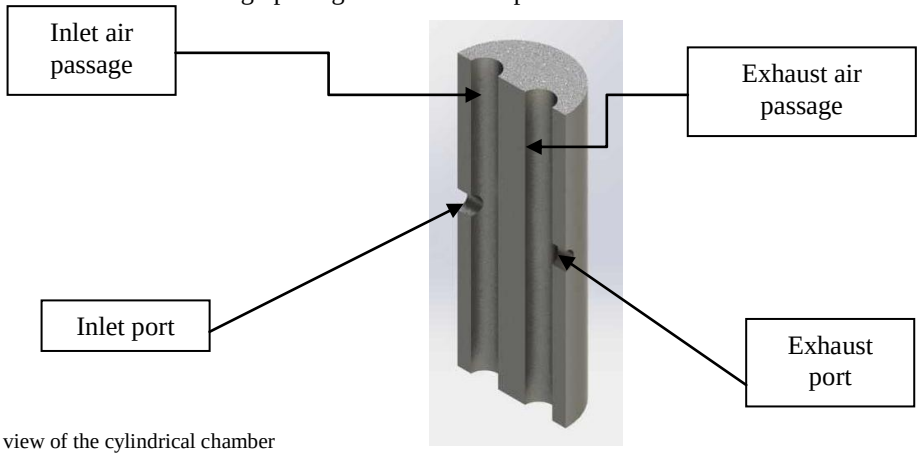

Fig. 2. Cut-way view of the cylindrical chamber

3.3. Inlet-Exhaust Valves

These are basically two mild steel shafts of varying cross section combining the action of both: a flat faced cam follower and a valve. The varying cross section of the flat face valve sits on a spring leaving the rest of the valve hanging inside the air passage.

Fig. 3. Inlet Exhaust Valve

3.4. Cam Shaft

It is a 10 mm diameter solid shaft. The shaft is supported on two ball bearings staged in their housing and linked with the output shaft of the engine via chain and sprocket.

The cams are tightly attached to the shaft with the help of Allen key screw.

3.5. Flywheel

A 150mm diameter and 12mm thick mild steel disc has been cut in lathe machine and attached to the previously modified output shaft. These dimensions were obtained from the engine specification (Engine torque = 60 N-m) and some assumption made according to engine space constraints. The weight of the flywheel is 6kg.

4. Cam Design

For replacing the original cylinder head, a new set of two flank cams has been designed for operating the inlet and exhaust valves of the modified engine. Both the exhaust and inlet cams are symmetric about the center line of the cam shaft. The cams are made of mild steels. These cams are cut out from 90mm diameter 40 mm thick cylindrical discs on milling machine and lathe machine on the basis of the full scale drawing provided to get the specific cam profile obtained from calculation and theoretical assumptions. These cams provide determined motion to the follower based on the assumed cam profile which is done in actual practice.

The inlet cam profile is designed to give the valve a maximum ascent/descent of 18 mm while it is 15mm for the exhaust cam. The inlet cam has an ascent angle of 40° and a descent angle of 320°, while the exhaust cam has an ascent angle of 150° and descent angle of 210°.

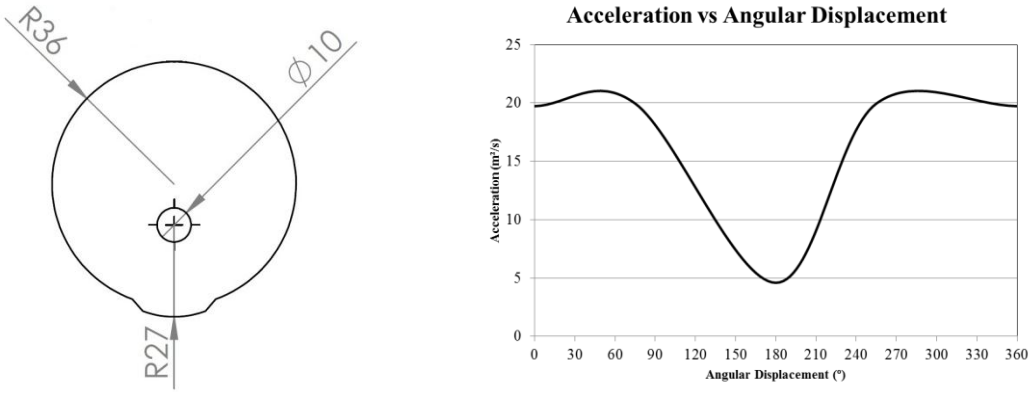

Fig. 4. Inlet Cam

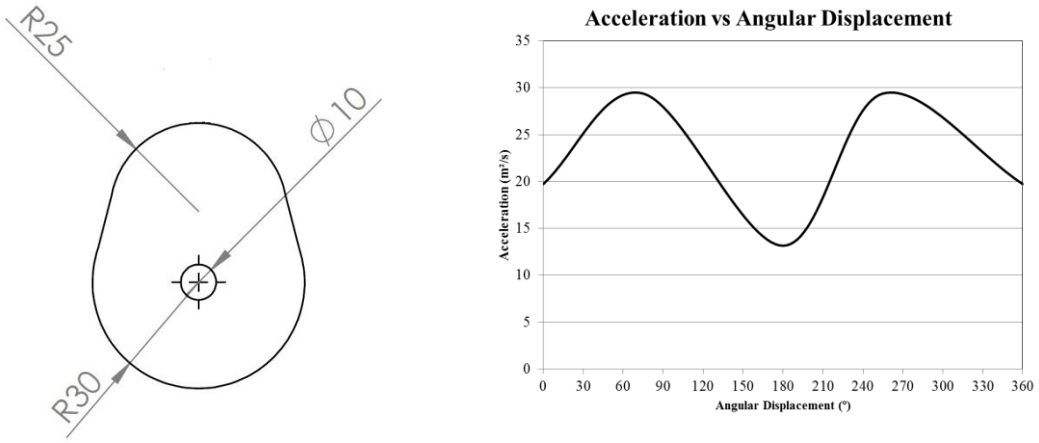

Fig. 5. Exhaust Cam

4.1. Valve Timing

The converted compressed air engine has been tested for a set of three valve timings. In the first case, the inlet and exhaust cam are set in symmetric in angle in both side of TDC and BDC respectively. The inlet cam gives a lift of 18mm to the follower. When the piston is at TDC the inlet valve is at fully opened condition and as the compressed air starts entering into the chamber, the valve has to close the inlet port of 10mm diameter before the piston reaches BDC. To ensure the complete closure of the 10mm inlet port, the inlet follower is given a movement of 18mm. When the crank is at 20 degrees after TDC, the closure of the inlet port is started by the valve and it is completely closed when the crank is at 45 degrees after TDC. During this period the inlet port remains fully closed and no air is allowed to pass through the inlet port. The inlet port starts to open and allow the air to pass into the cylinder just 45 degrees before the TDC and reaches its maximum opening condition 20 degrees before TDC.

The exhaust port is at fully closed condition when the piston is at TDC and the exhaust valve starts to open the exhaust port just 75 degrees after TDC. For the next 210 degree rotation of the crank, the exhaust port is kept at fully opened condition and the air is allowed to leave the chamber. The exhaust follower is given a displacement of 15mm to completely close the outlet port of 10mm diameter. Exhaust valve starts to close the outlet port just 75 degrees before TDC and it is moved to completely closed condition just when the piston is at TDC.

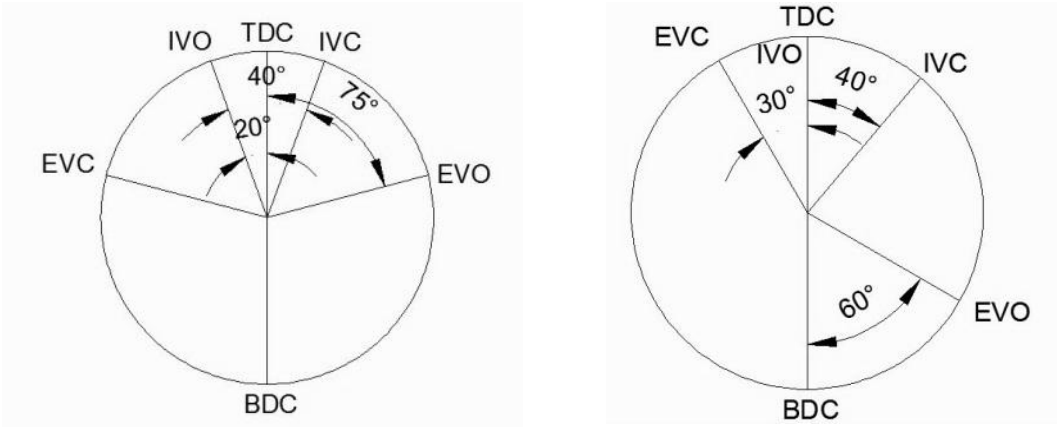

Fig. 6. (a) Valve Timing Diagram 1; (b) Valve Timing Diagram 2

With the modification a second valve timing was tested with inlet valve starts to open at 25º before TDC and fully open at TDC. The total opening time remains the same at 40º of cam rotation. The exhaust valve starts to open at 60º before BDC and closed after 30º of cam rotation before the piston reaches the TDC.

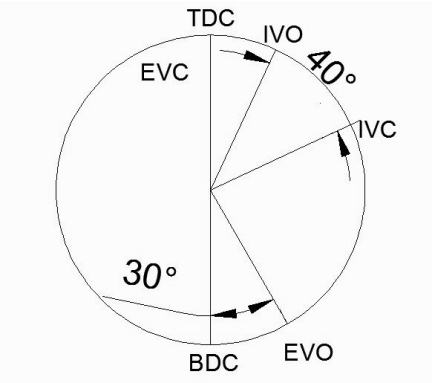

Fig. 7. Valve Timing Diagram 3

With the modification a third valve timing was tested with inlet valve starts to open at TDC and fully open at 25º after TDC. The total opening time remains the same 40º of cam rotation. The exhaust valve starts to open at 30º before BDC and closed when the piston reaches the TDC.

5. Testing Results

The engine has been tested with compressed air of 7 bar pressure. In the first design of the valve timing diagram, the engine starts running with the opening of the compressed gas line. But after a full cycle the engine gradually slows down and eventually stops. This may have occur due to the fact that in the return stroke, the inlet valve opens before TDC. This acts against the piston in the return stroke and eventually slows down the engine.

In the second valve timing design, the engine starts running after the compressed air has started to flow into the engine cylinder. But after several full cycles the engine again slows down and stopped. In this case, the inlet valve is started to open before TDC. As the compressed air started to flow into the engine cylinder, before the piston reaches TDC in the return stroke, the compressed air again pushes the piston back in the return stroke. Thus the engine again slows down and stopped.

In the third valve timing design, the engine starts running with compressed air flow into the cylinder. This time, the engine runs for half an hour before the pressure of the compressed air dropped below a certain limit. The rpm of the engine has been measured and is found to be 420 rpm.

6. Conclusion

In the present modification project, a two stroke single cylinder SI engine has been reassembled with new cylinder head and cam. The engine has been tested with three different valve timing diagram. For first two simplified valve timing, the engine didn't run for long time. Thus the design of the valve timing can't be used for the modified engine. The valve timing diagram has been further modified and with the third valve timing diagram. This time the engine runs until the gas pressure dropped. The maximum rpm of the engine is 420.

In future, further modification can be done so that the engine itself can run the compressor. The engine can also be attached with other engines in support to the main engine. The high pressure gas exhausted from the primary engine can be used as input air for the compressed air engine. The pressure of the air can also be increased up to the limit of the engine structure. This kind of engine can be used for different purposes.

References

[1] **Tokhi, M, O, Al-Miskiry, M and Brisland, M.** Real Time Control of Motors using a Pneumatic H-bridge. *Control Eng Pract.* 2001, pp. 449-457.
[2] **Huang, K, D, Quang, K, V, Tseng, K, T.** Study of Recycling Exhaust Gas Energy of Hybrid Pneumatic Power System with CFD. *Energy Converstion Management.* 2009, pp. 1271-1278.
[3] **Thipse, S, S.** Compressed Air Car. *Tech Monitor.* 2008, pp. 33-37.
[4] **Liu, X, Y, Wang, Y.** Overview of Developement of Compressed Air Engine. *Machine.* 2008, Vol. 35, pp. 1-5.
[5] **Shen, Y, T, Hwang, Y, R.** Design and Implementation of Air Powered Motorcycles. *Applied Energy.* 2009, Vol. 86, pp. 1105-1110.

5th BSME International Conference on Thermal Engineering

Harvesting energy from speed breaker

M.B Hossain[a]*, M. E. Hoque[b] , M. M. Billah[b] and A. A. Rahman[b]

[a]*Dinajpur polytechnic Institute, Dinajpur – 5200, Bangladesh*
[b]*Rajshahi University of Engineering and Technology, Rajshahi – 6204,Bangladesh*

Abstract

In today's world with the increasing population, the world's energy needs are growing steadily and the crisis for power is also increasing. The scope of this paper concentrates on an approach to produce power from an unconventional source by the implementation of the integration of gear assembly, generator/DC motor and rechargeable battery installed at speed breakers. In this work, prospect and feasibility of power generation by using speed breakers has been investigated. A mechanism is used to generate power by converting the potential energy generated by a vehicle going up a speed breaker into kinetic energy. This arrangement is made one rotation as soon as a vehicle moves over the speed breaker and has been increased using gear assembly. After producing the electricity, a storing unit has been used to hoard the generated electricity during the vehicle movement and will be used when necessary. A prototype has been made using rack and pinion gear, spur gear, springs and generator from which a considerable amount of energy is obtained. Nonetheless the cost of the prototype is inexpensive which proves the feasibility of this project and the idea can be applied on heavy traffic roads. Several challenges are associated with the implementation of such project before considering speed breaker as a major source of energy in the world. This paper attempts to identify major technical, financial, environmental, political as well as social challenges associated with speed breaker energy utilization from feasibility study to generate electricity for regular consumption.

Keywords: Energy harvesting; micro-power generation; energy from speed breaker; electro-mechanical system

1. Introduction

The demand of electricity is increasing day by day. As energy costs continue to rise worldwide, the researchers desire to seek out new technologies to meet the rising demand for sustainable energy. Future security of supply, particular of oil and gas is uncertain and indigenous production is declining rapidly. The energies produced from burning fossil fuels are responsible for carbon emission and global warming. Therefore, finding an inexpensive and reliable source of energy is a challenge in many developed and even in developing countries like Bangladesh. Although energy surrounds us in all aspects of life, the ability to harness it and use it for constructive ends as economically as possible is the challenge before mankind. Alternative energy refers to energy sources which are not based on the burning of fossil fuels or the splitting of atoms. The renewed interest in this field of study comes from the undesirable effects of pollution both from burning fossil fuels and from nuclear waste byproducts. Fortunately there are many means of harnessing energy which have less damaging impacts on our environment.

Power plays a great role wherever man lives and works-in industry, agriculture transportation and so on. The living standard and prosperity of a nation vary with increase in use of power. As technology is advancing the consumption of power is steadily rising. The energy consumption mix was estimated as: indigenous biomass 60%, indigenous natural gas 27.45%, and imported oil 11.89%, imported coal 0.44% and hydro 0.23% [9]. Bangladesh has one of the lowest per capita energy consumption in the region and about 51% of its 155 million populations have no access to power. The government of Bangladesh has undertaken a master plan under the Vision-2021 to reach electricity facilities to every village of the country. Approximately 48,754 villages out of 87,372 villages have been brought under electricity facilities till April 2011 [7]. Even then, the national power generation capacity is only 4500-4750 MW against a peak demand of 6500 MW. The current rate of increase in consumption is 10% annually [10]. Moreover, per capita power generation is only 236 kWh. The cumulative efforts of exploration for oil and gas resources in Bangladesh has resulted in the discovery of 23 gas fields of

* Corresponding author. Tel.: +880 1816272309
E-mail address: belayet9328@gmail.com

various sizes producing 2000 mncft of natural gas . Currently, from our 5 discovered mines only Barapukuria Coal Mine is producing at this stage. In 2008 it produced about 0.8 million tones. The estimated reserves of coal are close to 3300 million tons, while the proven reserve is about 884 million tones [11]. The scope of hydropower generation is very limited in Bangladesh because of its plain lands, except in some hilly region in the northeast and southeast parts of the country. At present only 230MW of hydropower is utilized in Karnafuli hydro station through 5 units of Kaplan turbine [12]. However, the chronic energy crisis is now an alarming issue. Consequently, any type of attempts to produce electricity is of the essence. In this work, an idea endeavors to show how energy can be trapped from a commonly used system, the road- speed breakers. The number of vehicles passing over the speed breaker in roads is increasing day by day. There is possibility of tapping the energy and generating power by making the speed breaker as a power generation unit. moreover, the useful purpose for these types of generators is as a remote source of small power generation (MW to W range) where access to a fixed grid supply is not available and other options of remote power are less viable (such as solar, batteries, diesel generator, etc). Next time on the roads, don't scoff at the speed-breakers. They could actually light up small villages off the highway. An amateur innovator in Guwahati has developed a simple contraption that can generate power when a vehicle passes over a speed breaker. The innovation has caught the eye of the Indian Institute of Technology (IIT), Guwahati, which will fund a pilot project to generate electricity from speed-breakers. IIT Guwahati has evaluated the machine and recommended it to the Assam ministry of power for large scale funding. A K Das, a professor at IIT's design department says it is a 'very viable proposition' to harness thousands of mega watts of electricity untapped across the country every day [13]. A survey has been conducted about electricity consumption from Tamil Nadu electricity board website. It says that: The amount of electricity consumed in one night by all the street lights around Chennai city is equal to consumption of electricity in a remote village for one month and 14 day. This survey inspired us a lot and made us to think about saving this wasted power which made us introduce this new technique [14].

2. Road and transportation scenario of Bangladesh

In Bangladesh, under the communication ministry the total length of road 21288 km in which 3538 km national Highways (No. of roads 71), 4278 km regional Highways (No. of roads 121), 13472 km Zilla roads (No. of roads 635) are available. Table 1 represents Road and Highway Department (RHD) road network [8] .

Table 1. RHD road network

Road Type	No. of road	Total Road (Km)
National Highways	71	3538
Regional Highways	121	4278
District Roads	635	13472
Total	827	21288

Table 2. Number of year wise registered motor vehicle in Bangladesh

Type of vehicle	Up to 2003	2004	2005	2006	2007	2008	2009	2010	January to June 2011	Grand total
Motor Car	116196	5410	6431	8447	11941	16927	21461	20690	8283	215786
Jeep/St. Wagon/Micro	49364	2514	3963	5540	5650	6537	9027	8040	3623	94258
Taxi	10932	540	515	275	15	9	12	0	9	12307
Bus	30617	857	783	1020	1368	1342	1184	1233	704	39108
Minibus	33364	622	361	241	382	307	320	311	180	36088
Truck	51375	2583	2791	3065	2521	2609	6561	10056	5621	87182
Auto-rickshaw/ Auto-tempo	98479	8974	4877	6898	10530	19071	14902	19018	8404	191153
Motor-Cycle	321347	24941	43226	51106	85131	93541	85142	88499	55439	848372
Others	25726	2761	2931	3713	3734	4076	6634	13331	8840	71746
TOTAL	737400	49202	65878	80305	121272	144419	145243	161178	91103	1596000

Table 3. vehicle characteristics : weight and dimension

Category	Make	Axles no.	Tare kg	GVW kg	Length mm	Width mm	Height mm
Medium Truck	Tata SE 1612/42	2	4015	15660	6970	2434	3625
Small Truck	Isuzu NKR55L	2	2750	5200	6025	1880	2220
Large Bus	Hino AK3HMKA	2	4145	12500	10005	2430	1995
Mini Bus	Tata LP909/36	2	3300	9000	5970	2159	1900
Micro Bus	Toyota Liteace	2	1180	2150	4453	1695	1870
Utility (Jeep)	Mitsubishi Pajero	2	1930	2800	4645	1695	1865
Car	Toyota Corolla Sedan 1300 GL	2	998	1510	4270	1685	1380
Auto Rickshaw	Bajaj Baby Taxi	2	200	580	1900	745	1020
Motor Cycle	Honda CG 125	2	96	N	1900	745	1020
Bicycle	nc	2	nc	50	nc	nc	nc
Rickshaw/Van	na	2	nc	304	nc	nc	nc
Animal Cart	na	1	nc	1800	nc	nc	nc

From Bangladesh Road Transport Authority (BRTA), the total registered vehicle in Bangladesh up to June 2011 is 159600 among them 643003 registered vehicle in Dhaka. Total registered Motor Car in Bangladesh is 215786 among them 174122 is in Dhaka. Except Motor Cycle other registered vehicle is about 75% only in Dhaka city and 25% registered vehicle out of the country. BRTA is not responsible for non-motorized traffic registrations, which are left to the local authorities to regulate. Non-registration is common and the actual number of NMTs is unknown. However, this report has dealt with the operating costs of both motorized vehicles as well as NMTs. Table 2 shows BRTA figures for vehicles registered in Bangladesh from up to 2003 to June 2011 [3]. The Bangladesh vehicle fleet is characterized by a large number of different vehicle types spanning up to three decades in age. Road and Highway Department (RHD) have derived a classification of motorized vehicles and non-motorized vehicles for traffic counting which categorizes vehicles into two broad groups: one for eleven standard motorized vehicles and the other for four standard non-motorized vehicles. Table 3 set out the physical characteristics of the representative vehicle.

2.1. Speed breaker

Speed breaker is a speed-reducing feature of road design to slow traffic or reduce through traffic. A speed breaker is a bump in a roadway with heights typically ranging between 3 and 4 inches (7.6 and 10 cm). The length of speed breaker are typically less than or near to 1 foot (30 cm); whereas speed breaker are longer and are typically 10 to 14 feet (3.0 to 4.3 m) in length. Speed bumps can be made of recycled plastic, asphalt or rubber. The advantages to the recycled plastic version are that they consistently will keep the original bright color, warning drivers of their approach without fading or having paint chip off. Speed bumps of various sizes can be placed on a road, from using two four foot or six foot devices on it with a space on either side for avoiding the bump on one side of the car, or connected across the entire road surface. The use of speed breaker is widespread around the world, and they are most commonly found where vehicle speeds are statutorily mandated to be low, usually 25 mph. Although speed breakers are very effective in keeping vehicle speed down, their use is sometimes controversial as they can cause noise and possibly vehicle damage if taken at too great a speed.

2.2. History

On June 7, 1906, The New York Times reported on an early implementation of what might be considered speed bumps in the U.S. town of Chatham, New Jersey, which planned to raise its crosswalks five inches above the road level: "This scheme of stopping automobile speeding has been discussed by different municipalities, but Chatham is the first place to put it in practice". The average automobile's top speed at the time was around 30 mph. According to a publication by the Institute of Transportation Engineers, the first speed bump in Europe was built in 1970 in the city of Delft in the Netherlands.

2.3. Provision of speed breaker

Speed breakers can be set up for producing electricity on the following critical locations:

- All manned and unmanned railway crossings.
- Junction of rural road with higher order roads (MDRs, SH & NH).
- Near Schools / Health Centers.
- Entry points of habitation
- Entry of bridge to receive toll

3. Experimental setup

Figure 1 shows the schematic diagram of power generation from speed breaker and Fig. 2 shows the developed energy harvester from speed breaker. The model is prepared comprising flexible speed breaker, flexible sheet, compression spring, wooden block, rack and pinion gear, spur gear, generator and battery to store power. When the vehicle moves over the speed breaker, it comes down resulting the compression of spring and the rack moves downwards. A small pinion coupled with a big gear is meshed with the rack.

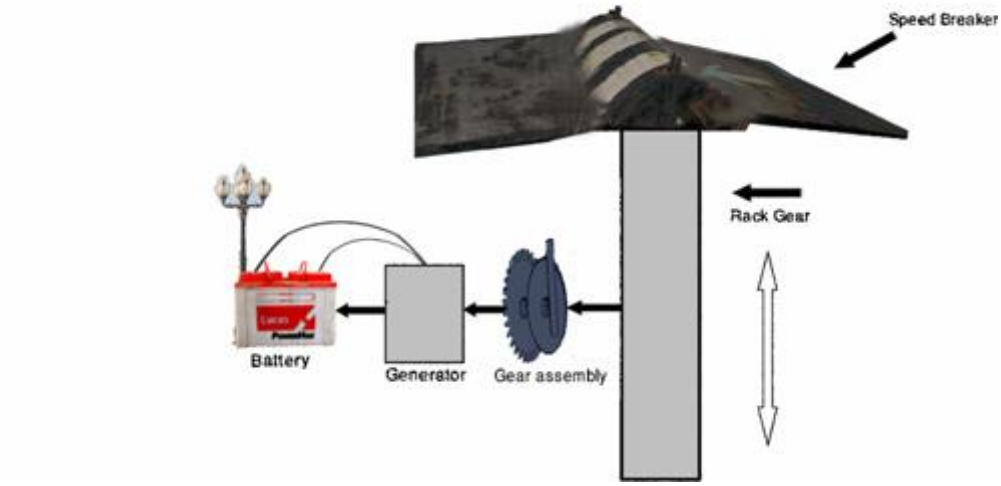

Fig. 1. Schematic diagram of power generation from speed breaker

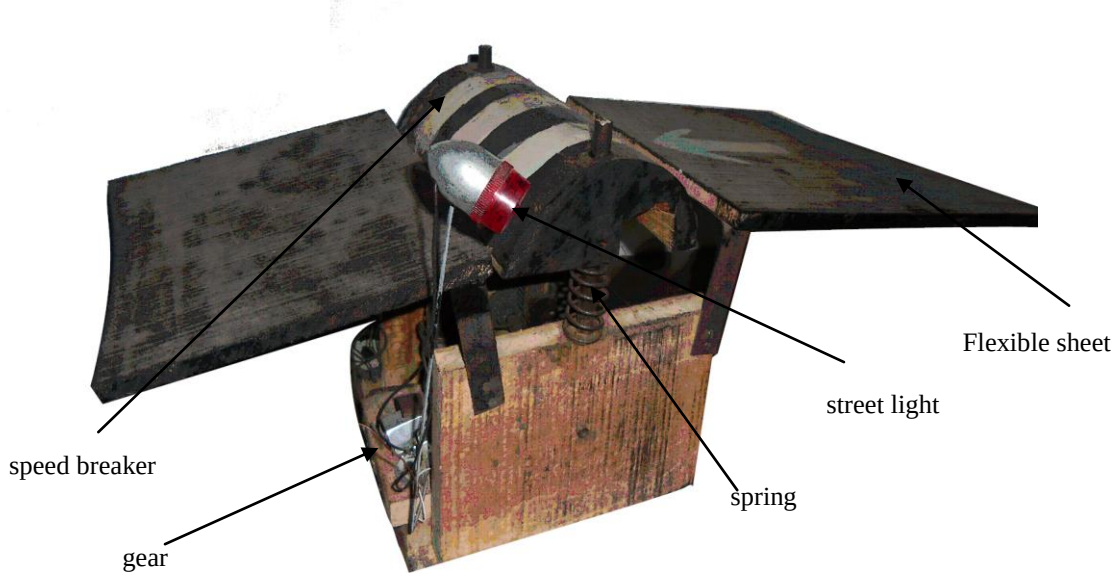

Fig. 2. The developed energy harvester from speed breaker

The downward motion of the rack causes the rotation of the pinion which is transmitted to the big gear. A small pinion is attached to the dynamo/ DC motor shaft which is mashed with the big gear. The rotation of the big gear is now transferred to the dynamo shaft and the kinetic energy is converted into electricity. Due to the using of different gear ratio, the linear movement of the rack is increased step by step and finally the speed of the dynamo shaft becomes about 30 times to the rack speed. This electricity is stored in a battery. Then the output of the battery is used to lighten the street lamps on the road. As during daytime electricity is not required for lightening the street lamps so a control switch is incorporated in order to automatic control of electricity output. The control switch is connected by wire to the output of the battery. The control switch has ON/OFF mechanism, which allows the current to flow when considered necessary.

5. Selection of dynamo

Gear box contain compound gear and a pinion which coupled with dynamo. Compound gear consists of a smaller gear and a larger gear. Smaller gear has 14 teeth and larger gear has 140 teeth. Larger gear is meshed with pinion. Pinion has 15 teeth.

As larger gear is meshed with pinion, its speed ratio is

$$N_A / N_B = T_B / T_A \quad (1)$$

Where, NA = speed of larger gear

T_A = number of teeth on larger gear

N_B = speed of pinion

T_B = number of teeth on pinion

If N_A = 1 rpm, then from equation. (1)

$N_B = 9$

Thus the speed ratio between compound gear and pinion 1:9

For maximum mass, m = 200kg

rpm of dynamo = 150

The speed ratio between compound gear and pinion 1:9

Then, rpm of gear mesh with rack = 16.67

Height of deflection, r = 0.04cm

Torque (T) = Force (F) × Radius (r)

= m × g × r

= 200 × 9.8 × 0.04

=78.4 Nm

Input power = torque × angular velocity

= 78.4 × (2 × 3.14 × 16.67/60)

= 136.79W

Considering various loss such as friction loss

Let, efficiency = 50%

Output power = 68.39W

For this, a dynamo can be chosen of maximum power output 68.4 W

4. Result and discussion

Several investigations have been accomplished to find out the performances of the prototype systems. From the collected data, the power output of the systems is acquired. Fig. 3. shows the output power of the prototype with maximum power 16.50W for the object (vehicle) weight of 200 kg.The graph also represents increasing weight produce higher power. From the above mentioned performance of the prototype implies vivid prospect of the project. Implementation of the concept in highways, where enormous vehicles run in everyday will generate massive power throughout the day. This project will more effective near Toll plaza where the bus speed is very low. Bangabandhu setu is the ideal place where thousands of vehicles run in a day.

Fig. 4. shows the variation of current when a motor cycle passing over the speed breaker. There is three consecutives passing of motor cycle with same load.

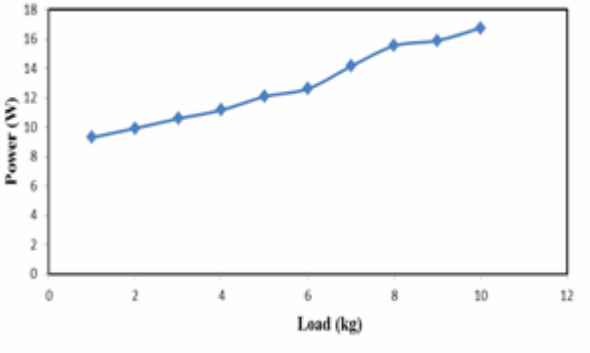

Fig. 3. Load versus power characteristics

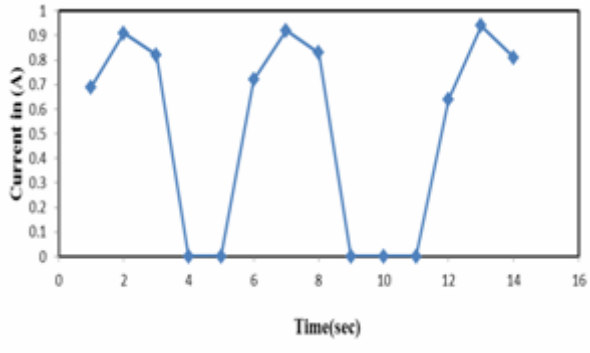

Fig. 4. Time versus current characteristics

5. Conclusion

In this world where there is shortage of electrical power supply, this project will be helpful to solve the power crisis to some extent. This project has some advantages such as; it is economical and easy to install, free from all types of pollutions as well as maintenance cost is low . A speed breaker power generator prototype has been designed, built and experimentally tested. The generator relies on the use of different gear combination to harness power from the speed breaker. This concept is quite promising due to its good efficiency as well as energy recovery criteria. Further investigation is being carried out to introduce the technology for practical approach.

References

[1] Van Mithal GK. Electronic devices & Circuit. ISBN: 8121924971
[2] Mehta VK, Mehta R. Principle of power system. ISBN- 13: 9788121924962
[3] www.brta.gov.bd (02.05.2012)
[4] National renewable energy laboratory (NREL), www.nrel.gov (22.11.2011)
[5] http://www.neweysonline.co.uk/...The-Energy-consumption...light/static.raction (20.02. 2011)
[6] www.journals.elsevier/renewable-energy (20.12.2011)
[7] Rural electrification board (REB), www.bangladeshgov.org (12.06.2007)
[8] Road and highway department, www.rhd.gov.bd (25.04.2012)
[9] Islam MR, Islam MR, Beg MRA. A renewable energy resources and techniques practice in Bangladesh. Renewable and sustainable energy reviews, 2008; 12, 299-343
[10] Hossain AK, Badr O. Prospect of renewable energy utilization for electricity generation in Bangladesh. Renewable and sustainable energy reviews 11, 2007; 1617-1649
[11] Petrobangla, 2010; Bangladesh
[12] Rahman M. executive board report at the 15th Council of ICC, B, 2010.
[13] http://wiki.answers.com/ (20.06.2011)
[14] www.tneb.gov.in (20.06.2011)
[15] Costa MAD, Schuch L, Michels L, Rech C, Pinheiro JR, Costa GH. Autonomous street lighting system based on solar energy and LEDs. IEEE, 2010; pp.1143-1148.
[16] Nunnoo S, Attachie JC, Charles JC, Abraham K. Using solar power as an alternative source of electrical energy for street lighting in China. IEEE, 2010; PP.467-471
[17] IEEE PES Committee report. Electric power engineering curricula content in the 21st century. IEEE transactions on power system. 1994; vol. 9, no. 3 pp.1145-1151
[18] Gunte quipment for engineering education. www.usdidactic.com/html/p3562.htm
[19] Materials by design: Piezoelectric materials. [online].available: http:// www.mse.cornell.edu/ course/ engrill/ piezo.htm; 1996.
[20] Ottman GK, Hofmann HF, Bhatt AC, Lesieutre GA. Adaptive piezoelectric energy harvesting circuit for wireless remote power supply. IEEE Trans. Power electron. 2002; vol. 17, no.5, pp.669–676.
[21] Roundy S, Otis B, Chee YH, Rabaey JM, Wright P. A1.9 GHz RF transmit beacon using environmentally scavenged energy. presented at the Int. Symp. Low power electronics and design; 2003.
[22] Ottman GK, Hofmann HF, Lesieutre GA. Optimized piezoelectric energy harvesting circuit using step-down converter in discontinuous conduction mode. IEEE trans. Power electron. 2003; vol. 18, pp. 696-703.
[23] IEA. World energy outlook. Paris: international energy agency (IEA); 2006.

Available online at www.sciencedirect.com

SciVerse ScienceDirect

Procedia Engineering 00 (2012) 000–000

Procedia Engineering

www.elsevier.com/locate/procedia

5th BSME International Conference on Thermal Engineering

Heat Transfer Enhancement in an Air Process Heater using Semi-Circular Hollow Baffles

Aashique Alam Rezwan*, Sarzina Hossain, S M Ashrafur Rahman and MA Islam

Department of Mechanical Engineering, Bangladesh University of Engineering & Technology, Dhaka, Bangladesh

Abstract

Air process heater is one of the crucial equipment for many industries. Process heater is used in Baking, Drying, Laminating, Metal Working, Packaging, Plastic Welding, Preheating, Sealing, Soldering, Shrink Fitting, Synthetic Fabric Sewing and in other industries. But heating of air to a very high heat flux is sometimes impossible without the degradation of air quality, because many industries use combustion of gases for the purpose of heating the air to a very high heat flux. Electric heater can be alternative heating equipment, but it requires costly and long heating apparatus for the desired air temperature. In the present study, heat transfer enhancement in an air process heater was investigated both numerically and experimentally. A circular duct with 5 semi-circular hollow baffles and 4 cartridge electric heaters was designed for the process heating. Air was supplied from a wind tunnel at 3.17×10^4 Reynolds number. Total supplied electric power was 3 kW. The results showed the temperature ratio (Ambient Temperature/Air Temperature) to be decreased up to 0.72 where in many electric air heaters the temperature ratio is about 0.9. The designed air process heater supplies air at velocity 19 m/s and temperature up to 147ºC. The experimental results were also matched with the numerical simulation values of the designed heater. The results were also compared with some of the existing air process heater for investigating the enhancement of heat transfer.

Keywords: Air Process Heater; Heat Transfer Enhancement; Baffle; Cartridge Heater;

1. Introduction

Air process heater is important equipment in many industrial applications. Process heater is used in Baking, Drying, Laminating, Metal Working, Packaging, Plastic Welding, Preheating, Sealing, Soldering, Shrink Fitting, and Synthetic Fabric Sewing and in other industries. But heating of air to a very high heat flux is sometimes impossible without the degradation of air quality, because many industries use combustion of gases for the purpose of heating the air to a very high heat flux.

In the present study, a simulation approach has been conducted to increase the efficiency of the air process heater within size limit. The principle goal of the project is to design a heater that can be used to heat the air from a blower with certain velocity. The length of the heater is also a factor to be considered. The target length of the heater was given to be within 2 feet. Different types of combinations have been considered for the design, including using nicrome wire heater. But the calculated value showed that most of them can't be used due to inefficiency of heating to the air within the target range. Thus for better understanding and design, many complex geometry like series heater, heating by suddenly slowing down the air etc., has been simulated and compared. After several considerations finally the design with semi-circular hollow baffle showed a comprehensive improvement of the heating process within the target range.

* Corresponding author. Tel.: +8801552364999
E-mail address: aashiquear@gmail.com

Previously, similar type of heating system has been developed by MAT Ali and Hasan [1-2], but the capacity of the heating system is low compared to the present design [3]. Many other researchers has been experimented about the proper condition of an air process heater. Siviryuk et al. [4] has developed and diagnosis method for the air process heater, Vikhman et al. [5] has presented a technical and economic rationale for selecting an air process heater. The design process and the comparison of simulated value and the experimental value of the fabricated heater are described. The heater has been fabricated using the local available material and equipment, and the total fabrication has been done under the authors' supervision. The local availability of material and cost are also taken into consideration for the final design.

2. Design of Heater

Figure 1 shows the different parts of the heater section. The overall length of the heater section is 0.9 m. It consists of 4 cartridge heaters of total power consumption of 3 kW. Five half circular baffles are placed in series in the heating section to enhance the heating capacity of the air. Air from the wind tunnel is passed through the entrance section, heating section and settling chamber and then finally through the nozzle to produce the desired jet of air.

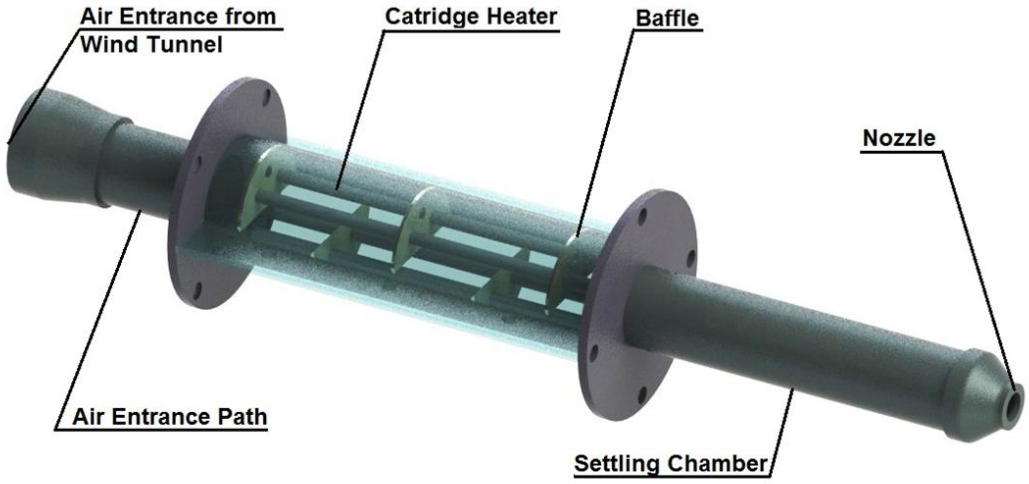

Fig. 1 Different Parts of the Heater Section

Swirling effect of the air due to the baffles ensures the uniform heating of air from the heater surface. The heated air then passes through the long settling chamber to the nozzle having a diameter of 25.4 mm. This is to note that the settling chamber is insulated with asbestos cloth and heat tape to prevent the heat loss to the surrounding from the hot air.

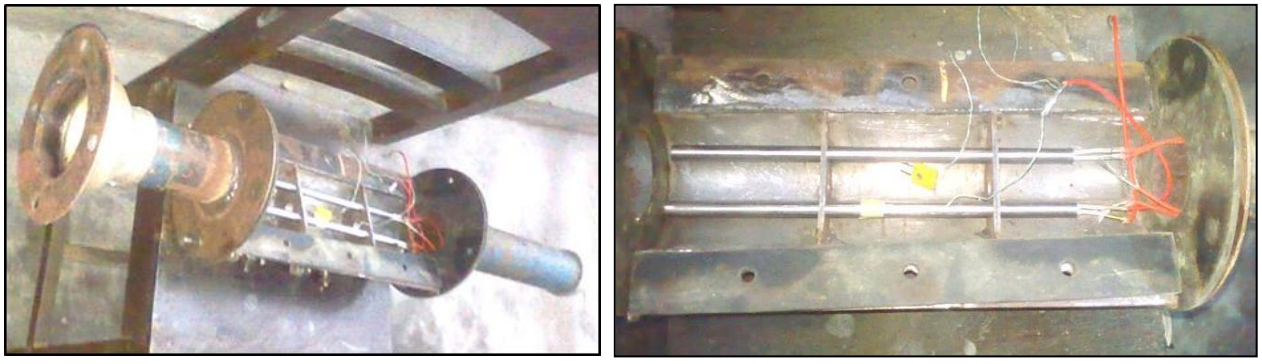

Fig. 2 Fabricated Heater Section [3]

3. Simulation of the Air Process Heater

For designing the heater computer simulation has been used. In the present works, ANSYS CFX has been used to simulate the air flow and heating process in the heater section. Figure 3(a) shows the contour plot of air temperature through the heater section. It can be seen that the swirling effect of the baffle greatly enhance the heating process.

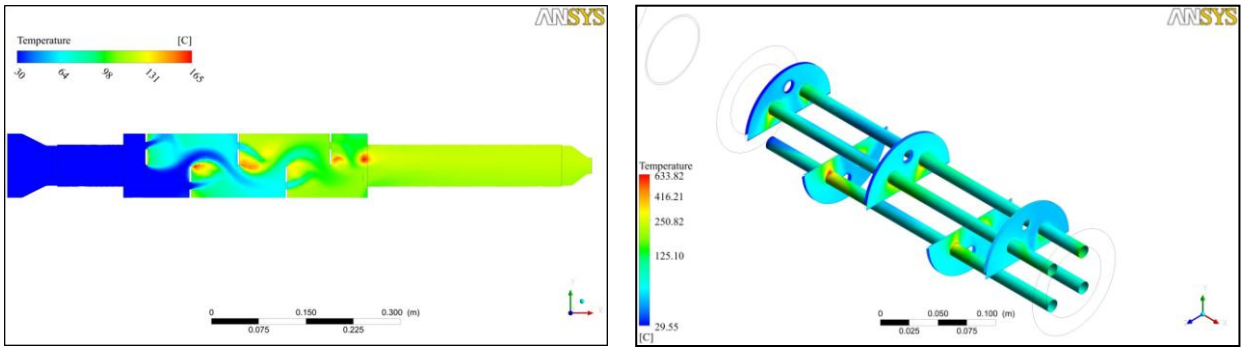

Fig. 3 (a) Temperature of Air through Heater Section (b) Heater Surface Temperature

In the fig. 3(b) the surface temperature of individual cartridge heater has been showed. This measurement is required for the safe heating of air. Due to the lack of heat transfer capability of air, the confined air in the section does not heat up properly. If the air near the surface of the heater can't transfer heat to the surrounding air in the section, the surface of the cartridge heater will be increase due to the lack of heat transfer. If the temperature increases in excess of the safe temperature for the heater, the heater could be break. Fig. 4 shows the mid line air temperature along the heater section.

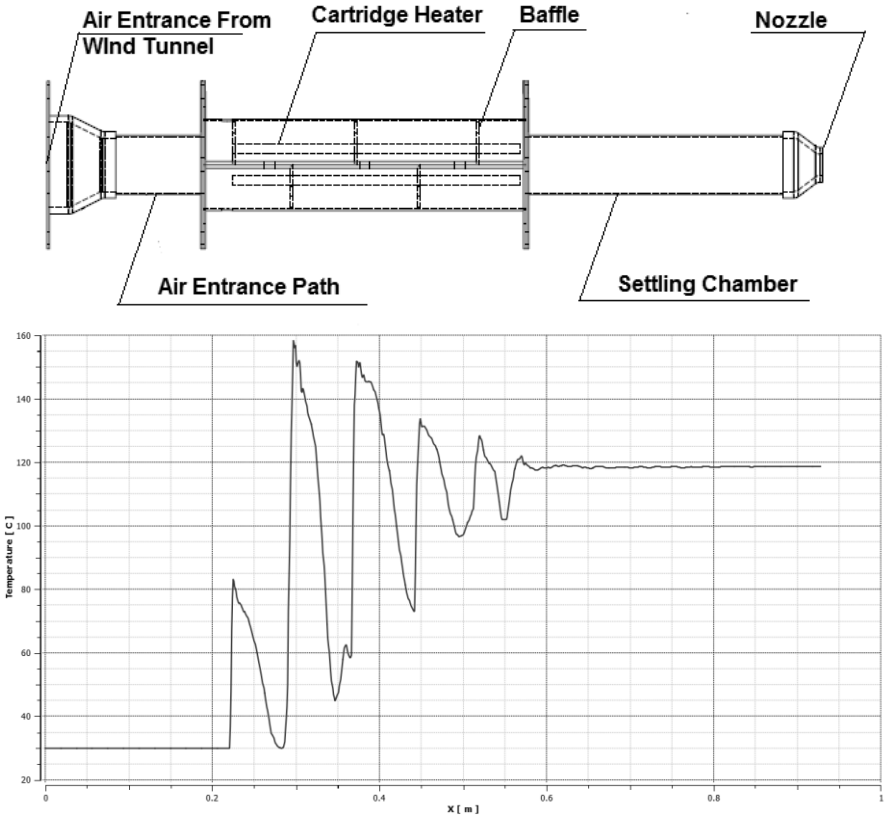

Fig. 4 Temperature of Air (mid line) along the Heater Section

4. Experimental Setup

The experimental study has been carried out by using a circular air jet facility as shown in Fig. 5. Detail explanation of different segment of the facility has been given in the previous studies [1-2]. The overall length of the flow facility is 9.0 m.

It has axial flow fan unit, two settling chambers, two diffusers, a silencer and a flow nozzle. The fan unit consists of three Woods Aerofoil fans of the same series. The fan unit receives air through the butterfly valve and discharges it into the silencer of the flow duct. Flow from the silencer passes on to the settling chamber through a diffuser. At the discharge, side of this chamber there is a flow straighter and wire screen of 12 meshes to straighten the flow and to breakdown large eddies present in the air stream. Air from this chamber then flows to the second settling chamber through a nozzle and second diffuser. The flow straighter and wire screens are used here to ensure a uniform axial flow free of large eddies which may be present in the upstream side of the flow. The flow from the second settling chamber then enters the 100 mm long and 80 mm diameter circular nozzle. At the farthest end the diameter of the flow facility is reduced from 475 mm to 88.9 mm where the heating section is placed [1-2].

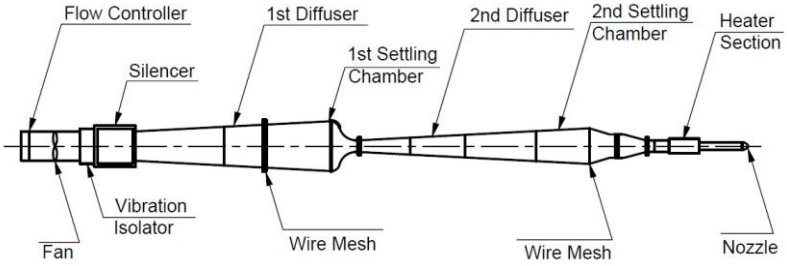

Fig. 5 Wind Tunnel for the Circular Jet Facility [1]

The air flow through the nozzle is controlled by regulating the speed of the fan units. The temperature of the jet is regulated by controlling the supply voltage of the heater. The whole setup is mounted on rigid frames of M.S. pipes and plates and these frames are securely fixed with the ground so that any possible unwanted vibration of the system is reduced to a minimum. To avoid the effect of ground shear, the setup is installed at an elevation of 1.4 m from the ground.

5. Results and Discussions

To ensure that the designed heater has been performing up to the requirement the heater section has been tested to its limit and compare with the computer simulation. Figures 6(a) depict the air jet temperature and fig. 6(b) temperature ratio of the jet of air for the increasing electrical energy input. With the increasing input energy the temperature of the jet of air increases exponentially. The surface temperature of the heater section (Fig. 6c) has been determined for the safety of the cartridge heater as described in the previous section. Then the experimental result has been compared with the computer simulation result. Fig. 7 shows the comparison between experimental result and the computer simulation result.

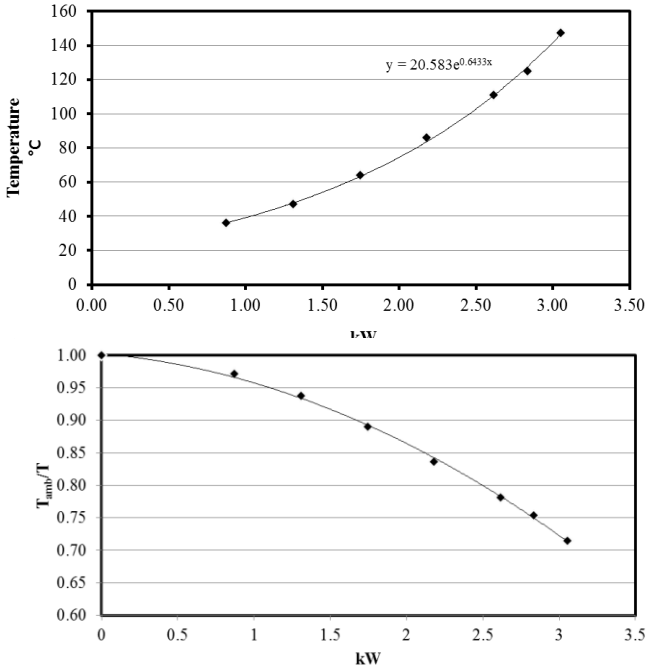

Fig. 6 (a) Temperature of Air Jet with Electrical Energy Input and (b) Temperature Ratio with Electrical Energy Input

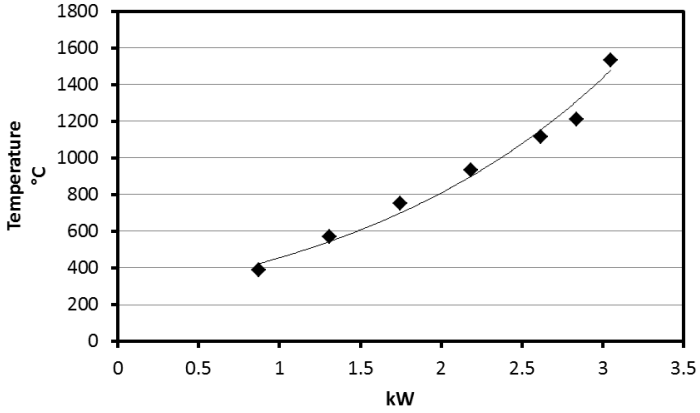

Fig. 6 (c) Temperature of Heater Surface with Electrical Energy Input

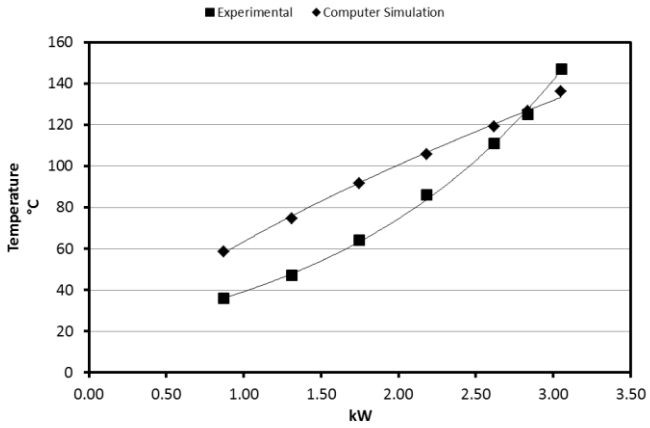

Fig. 7 Comparison between Simulation Result and Experimental Result

From the figure 7 it can be seen that at low power input, the temperature of air for the computer simulation is quite greater than the experimental result. As the power input increases, the difference between the two values also decreases and become equal at the rated condition for safe limit of the heater. After that, the experimental value of the temperature is increases more than the computer simulation result. This may due to the heat loss at low power, as there is cooler air in the surrounding. At high power input, as the time of heating increases, the temperature of the baffles and the pipe also increases. This restricts the air to loose heat to the surrounding environment.

Table 1. Summary of Previous & Designed Air Jet Heater Section [2]

Comparison Criteria	**Previous Heater [2]**	**Designed & Constructed Heater**	
		Simulation Value	**Experimental Value**
Heater Type	Electric Resistance Wire and Mica Sheet	Cartridge Heater 1200W (each)	
Number of Section	4	3	3
Number of Heaters	6	4	4
Maximum Design Capacity	3 kW	3 kW	3 kW
Maximum Capacity	-	4.8 kW	4.8 kW
$\frac{T_{amb}}{T}$ (minimum)	0.925	0.74	0.72
Maximum Jet Temperature	54°C	136°C	147°C
Re_d	3.72×10^4	3.17×10^4	3.17×10^4
Intermittent Mixing Capability	Present	Present	Present
Temperature Control	Varying the Supply Voltage	Given Input	Variable Voltage Supply

6. Conclusion

An air process heater has been designed and fabricated which can heat the air up to 147ºC. The designed Reynolds' number is 3.17×10^4.The surface temperature of the heater has also been determined for the safety limit of the heater. Total supplied electric power was 3 kW. The results showed the temperature ratio (Ambient Temperature/Air Temperature) to be decreased up to 0.72 where in many electric air heaters the temperature ratio is about 0.9. The designed air process heater supplies air at velocity 19 m/s and temperature up to 147ºC. The experimental results were also matched with the numerical simulation values of the designed heater. The results were also compared with some of the existing air process heater for investigating the enhancement of heat transfer. This type of heater can be adopted in any industrial process without adulterating the air.

References

1. Ali, M. A. T., Bhattacharjee, S., 2009, "Experimental Study of Thermally Stratified Co-Axial Jets with Trip Ring Excitation", *Proc. Int. Conf. on Mechanical Engineering (ICME2009), Dhaka, Bangladesh.*
2. Hasan, M. N., 2008, "Experimental Study of Flow Characteristics in the Near Field of a Thermally Stratified Co-axial Free Jet", M.Sc. Thesis, Bangladesh University of Engineering & Technology, Dhaka, Bangladesh.
3. Islam, MA, Rezwan, A.A., Hossain, S. and Islam, AKMN, 2011, "Study of Transient Heat Transfer of Solid with Protective Fabric Under Hot Air Jet Impingement", *Proc. Int. Conf. on Mechanical Engineering (ICME2011), Dhaka, Bangladesh.*
4. Siviryuk, V.L., Gramotnik, I.,V., and Bezrukov, A.,N., 2011, "Diagnostics of T\the Air-Heater Casings in Blast Furnaces.", Steel in Translation, Volume 41, Issue 1, pp36-40.
5. Vikhman, A.,G. and Kharichko, M.,A., 2006, "Selecting an Air Heater. Technical and Economic Rationale.", Chemistry and Technology of Fuels and Oils, Volume 42, Issue 4, pp 262-270.

5th BSME International Conference on Thermal Engineering

Numerical Investigation of Aerodynamics of a Sweptback Wing

Shakerur Ridwan[a]*,Md.Mamun[b]

[a]*Graduate Student, Department of Mechanical Engineering, Bangladesh University of Engineering and Technology, Dhaka-1000*
[a]*Associate Professor, Department of Mechanical Engineering, Bangladesh University of Engineering and Technology, Dhaka-1000*

Abstract

In modern aircraft design, sweptback wing is very popular due to its advantage for increasing the speed of the aircraft. The range of the speed of a subsonic aircraft depends on the local Mach number on the upper surface of the aircraft. The critical Mach number depends on that local Mach number. To prevent the aircraft from the shockwave at a higher speed critical Mach number is needed to be increased and so the wing is swept. But the wing has also the effect on induced drag. This study aims to investigate the effect of sweeping an aircraft wing at different angles. It also gives the vision of the local flow field of the wing and economical aspect of using a swept back wing. The study uses CFD analysis by validating the data with an authentic experimental result. This analysis helps the designer selecting the expedient wing shape for the design of the aircraft.

Keywords: Sweptback wing; CFD analysis; Aerodynamics

1. INTRODUCTION

With the progress of civilization human started to dream to fly like a bird. Gradually human started to think about flying, analyzed the different position of flying animal and eventually took the step to fly. Now human is moving with high velocity even far faster than many flying creature. They have developed many theories, analyses, experiments to be sure in many purposes. And finally human has started to fly with a very good control over the machines and devices. NACA has made different model of swept back wing and found experimental results. A trial to find better economical swept back wing was the purpose of the paper and for this purpose, a simulation of modified model shows higher lift to drag ratio.

Nomenclature

C_L	Lift coefficient
C_D	Drag coefficient
$C_{D,i}$	Induced drag coefficient
α	Angle of attack
α_i	Induced angle of attack
Ω	Sweep angle
AR	Aspect ratio

* Shakerur Ridwan. Tel.: +8801675698826
E-mail address: shaker043@yahoo.com

2. Simulated Model

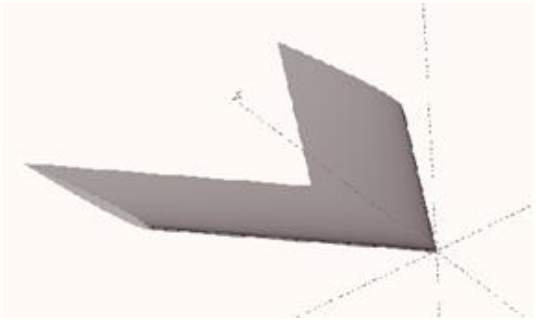

Figure 1. NACA-0012 sweptback 60 degree

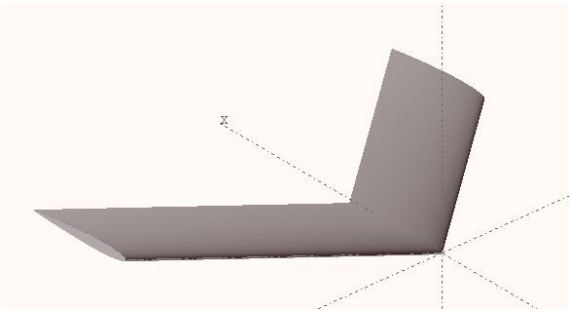

Figure 2. NACA-0012 sweptback 41 degree(modified)

Figure 1 represents an aircraft wing model swept at an angle 60 degree ($\Omega=60^0$) of NACA-0012 airfoil[1],[2],[4] section. This model is an experimental model prepared by NACA[5] and the data of lift and drag coefficient has also been supplied by NACA[3]. This wing, with an aspect ratio of 1.49, has the wingspan of 29.6 inch, root and tip chord length of 19.8 inch and hence the taper ratio of 1, the surface area of 586.06.

This wing is modified by changing the sweep angle, reducing the sweep angle to 41 degree($\Omega=41^0$), and hence increasing the aspect ratio as a trial for reducing the induced drag because the higher the aspect ratio the lower will be induced drag. The modified shape becomes alike the figure 2. The modified model has the same surface area. Hence the aspect ratio has been changed from 1.49 to 3.41. The wing becomes wider and hence the wingspan increases. The wingspan is 1134.84mm. The chord length of tip and root is 333.19mm.

3.1 Results and Analyses

The comparison of lift coefficient between experimental and the simulated value for a swept back wing can be depicted as follows:

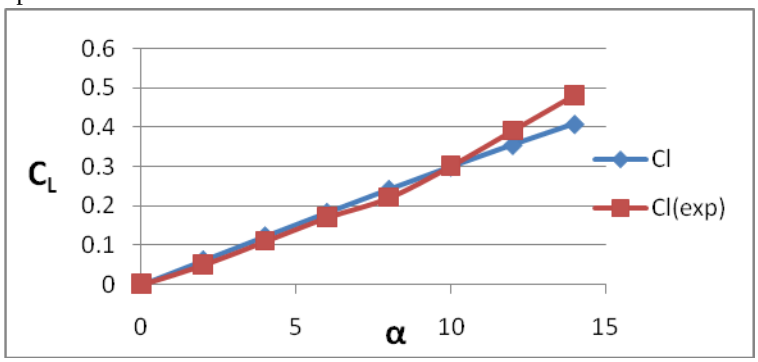

Figure 3. Comparison of lift coefficient between experimental and simulated result for NACA-0012 swept back wing

The vortex lattice method in combination with drag polars from 2d sections was used for the simulation of the wing. In graph it can be seen that upto 14 degree the value of lift coefficient almost coincides with the experimental value. The percentage of error varies from 7% to 15% except for the angle of 2 degree. At this angle the difference of value is very small. But in case of percentage of error it is about 23%. Here, it can be seen that the value of lift coefficient is 0 at 0 degree angle of attack although the wing has been swept.

The value of drag coefficient can also be found from the software using vortex lattice method. The comparison of drag coefficient between experimental and the simulated value can be depicted as follows:

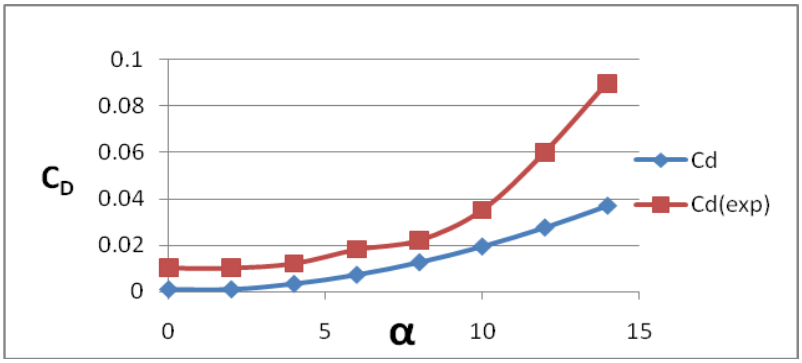

Figure 4. Comparison of drag coefficient between experimental and simulated result for NACA-0012 swept back wing

The two curve is of similar type. But there is a percentage of error between the experimental and simulated value.

The pressure coefficient at the angle 12 degree:

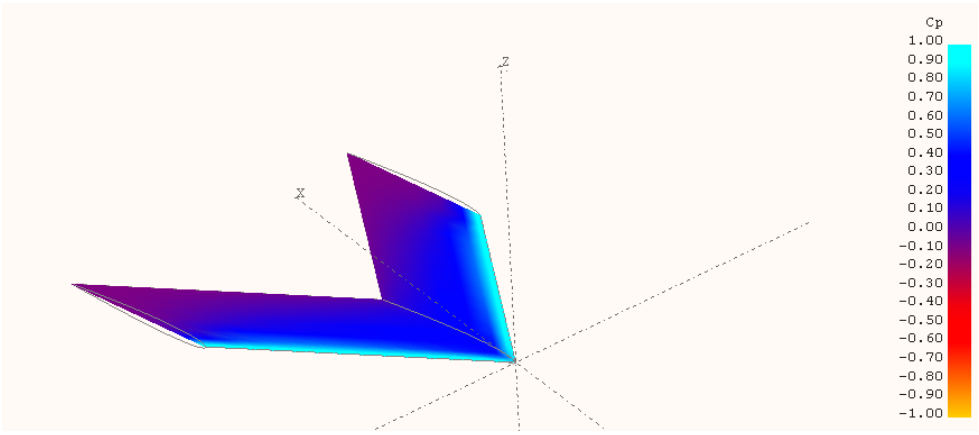

Figure 5. Pressure coefficient distribution

The downstream flow of the swept back wing clearly represent the presence of **vortices**[1],[2] at the two tip end of wing. These vortices plays vital role in the change of lift and drag co-efficient. The wing that has been simulated has a very low aspect ratio of 1.5. So the downwash is very effective and contribute a significant change of the lift and drag.

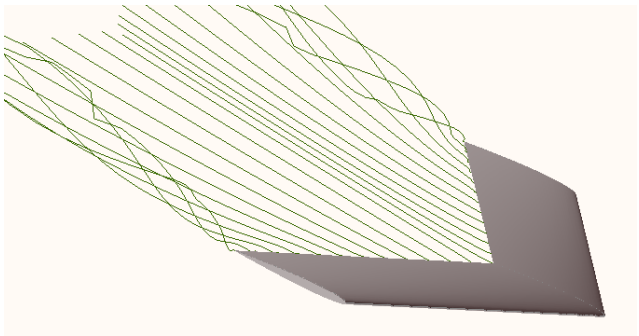

Figure 6. The flow pattern at the downstream

After changing sweep angle to 41 degree this wing model is again simulated and the value is compared with model of sweptback wing of 60 degree.

The graph that represents the comparison of the lift coefficient of the experimental value and the value of the modified model is as follows:

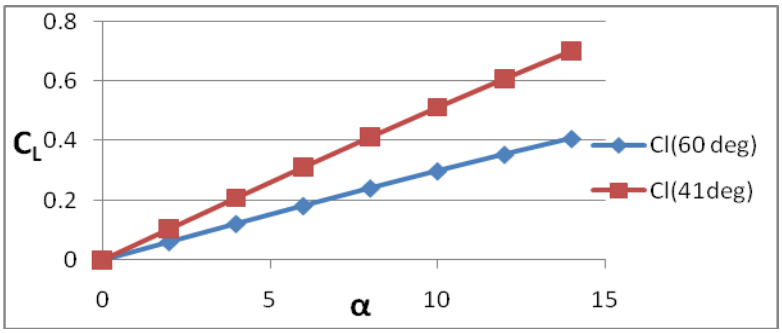

Figure 7. Comparison of lift coefficient between 60^0 and 41^0 swept back wing

Here, it can be seen that the lift coefficient value is higher for 41 degree angle of attack than the 60 degree angle of attack. From theory, **induced drag**, $C_{D,i}$ [1],[2], is inversely proportional to the **aspect ratio**,AR[1],[2]. The higher the aspect ratio the lower will be the induced drag and downwash. Then the lift coefficient will be of higher value. Because the higher the **downwash**[1] the loss of lift will be higher and the lower will be the lift coefficient value. Hence the simulated result perfectly supports the theoritical derrivation.

The comaparative value of drag coefficient for the same two models is as follows:

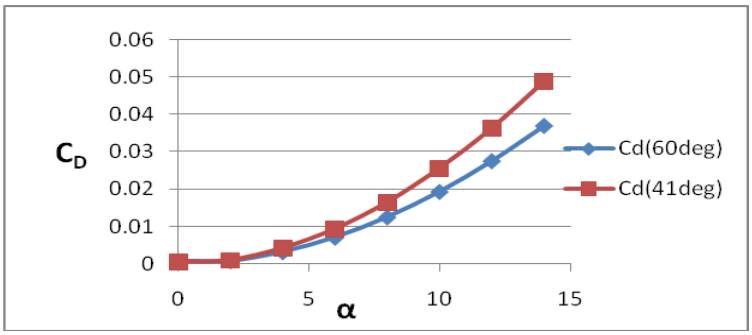

Figure 8. Comparison of drag coefficient between 60^0 and 41^0 swept back wing

This graph represents a significant important factor for the aerodynamic analysis of aircraft wing. Here, it is obvious that the drag coefficient for the 60 degree swept back wing is lower than the 41 degree swept back wing. Now, the induced drag coefficient is inversely proportional to the aspect ratio. As the 41 degree swept back wing has higher aspect ratio so induced drag will be lower for that model. But the simulated value shows that for the same angle of attack the total drag coefficient value is higher for the 41 degree swept back wing. This is because the total drag coefficient includes the skin friction drag, pressure drag and induced drag. When the same airfoil is swept at higher degree the wing becomes thinner. So skin friction drag and pressure drag will be less. These affect the total drag and finally it becomes higher.

3.2 COMPARISON OF C_L/C_D

The lift to drag ratio is important for economic aerodynamic design of the aircraft. Because at the time flying the only power that is needed for aircraft to overcome the drag force. So it is better if higher lift can be obtained from the same drag.

If the two curve is compared in the same graph then it looks like this:

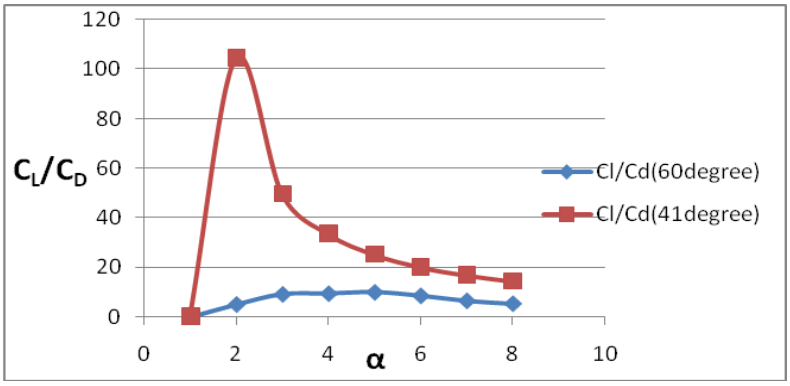

Figure 9. Comparison of C_L/C_D between 60^0 and 41^0 swept back wing

From two graph of C_L/C_D it can be seen that in the two graph C_L/C_D gradually increases with angle of attack and then decreases. These graph is quite similar that should be obtained for normal airfoil. In the graph at an angle of attack of 2 degree for 41 degree swept back wing the value becomes very higher. It shows a little bit different shape.

But from the graph of comparison of C_L/C_D it is obvious that the C_L/C_D value is higher for 41 degree swept back wing. So it can be said that for making the design more economical it is better if the swept angle is less. But when the speed of the aircraft need to be higher it is better to keep the swept angle higher. Because in that case the drag will be less and more speed can be obtained avoiding shockwave[7],[8]. So for high speed aircraft the swept angle is kept higher and delta wing is also a good choice.

4. Conclusion

For designing an aircraft wing it is obvious that for attaining higher speed the wing need to be swept and the higher the sweep angle the higher will be the speed of range. But from simulated value of 60 degree and 41 degree swept back wing, C_L/C_D for 41 degree swept back wing is higher than the 60 degree swept back wing. So considering fuel economy less swept wing, 41 degree in simulation, can be endorsed for real aircraft design.

Reference

[1] Anderson jr. John D "Fundamentals of Aerodynamics" 4th edition, McGraw-Hill, New York
[2] Anderson jr. John D "Introduction to Flight" 5th edition, McGraw-Hill, New York
[3] Purser Paul E. and Spearman M. Leory, "WIND TUNNEL TESTS AT LOW SPEED OF SWEPT AND YAWED WINGS HAVING VARIOUS PLANFORM," NACA.
[4] Abott Ira Herbert and Doenhoff Alber E. Von "Theory of wing section", McGraw-Hill, New York
[5] https://www.naca.com/nacaWeb/index_main.aspx
[6] Anderson jr. John D "Computational Fluid Dynamics", McGraw-Hill, New York
[7] Roskam Jan "Airplane Flight Dynamics and Automatic Flight Control", DAR Corporation, Lawrence
[8] Roskam Jan and Lan Chuan-Tau Edward "Airplane Aerodynamics and Performance", DAR Corporation, Lawrence

5th BSME International Conference on Thermal Engineering

Effects of Heat Generation on Salt Water Flow through in an Ocean by Inclined Angle

Ifsana Karim[a] , Md. Mahmud Alam[b,*], Md. Shakhaoath Khan[c]

[a,b,c] *Mathematics Discipline; Science, Engineering and Technology School, Khulna University, Khulna-9208, Bangladesh*

Abstract

The numerical studies are performed to examine the MHD heat and mass transfer (salt water) flow in an ocean by inclined angle with heat generation effects. The governing equations are transformed into nonlinear ordinary differential equations which depend on the magnetic parameter, Grashof number, prandtl number, modified prandtl number, heat source parameter and soret number with the different angles respectively. The obtained non linear coupled ordinary differential equations are solved numerically using Nactsheim-Swigert shooting iteration technique together with Runge-Kutta six order iteration schemes. The velocity, temperature and salinity distributions are discussed and presented graphically. Finally the skin-friction coefficient surface heat and salinity transfer rate are investigated.

Keywords: Salinity; Magnetic field; inclined angle; heat generation

1. Introduction

Ocean plays an important role in both under-standing current climatic conditions and predicting future climate change. In situ oceanographic instruments provide only sparse measurements over the world ocean. Although remote-sensed data from satellites cover the globe, they only provide information on the ocean surface. In order to improve the sustainable development of ocean resources, the well understanding and acknowledgement of oceanographic and meteorological phenomena should be emphasized and carried out. Temperature, pressure, and salinity are three most important properties of sea water, and they determine the physical properties associated with sea wave motion and the presences of small suspended particles in sea water are also important variables that affect the properties of sea water. The ocean is now well known to play a dominant role in the climate system, because it can initiate and amplify climate change on many different time scales. The best known example is inter-annual variability of Philander [1] and the potential modification of the major patterns for oceanic heat transport as a result of increasing greenhouse gases**.** Yet the ocean has been very much under measured for most of the history of ocean Science Even though systematic observations began in the 1880s with pioneering observations by Nansen et al.[3] the seagoing and theoretical efforts were mainly oriented toward describing large scale circulation which was often regarded as steady for lack of more detailed information. To gain some appreciation for the model's ability to simulate coastal ocean circulation Blumberg and Mellor [4] has investigated the potential impact, mathematical modelling, and physical behaviour for their model.

Ezer [8] studied the importance of ocean circulation model. He has created and maintain The Princeton ocean model web site. Institutionally the model was developed and applied to Oceanographic problems, the Geophysical Fluid Dynamics, Laboratory of NOAA and dynalysis of princeton.

Wang et al. [2] have studied parallel computation of the regional ocean modelling system. They investigates the regional ocean modelling system (ROMS) is a regional ocean general circulation modeling system solving the free surface, hydrostatic, primitive equations over varying topography. Very recent Sourav and Chakraborty [5] have analyzed numerical simulation of seasonal variations in circulations of the Bay of Bengal. The seasonal variations in circulation at different layers of the Bay of Bengal (BOB) basin have been studied here using multilayered regional ocean modelling system (ROMS). Alam et al. [6] showed the similarity solution for MHD flow through vertical porous plate with suction. They applied a uniform magnetic field normal to the plate and investigate the effect of various parameters on the velocity and the temperature fields across the boundary layer.

* Corresponding author. Tel.: +88-041-2831544; fax: +88-041-731244.
E-mail address: alam_mahmud2000@yahoo.com

Nomenclature

x, y	Cartesian coordinates	C_p	Specific heat at constant pressure
G_r	Grashof number	υ	Kinematic viscosity
u, v	Velocity components	$\bar{\alpha}$	Heat source parameter
P_s	Modified Prandtl number	τ	Dimensionless time
P_r	Prandtl number	$f'(\eta)$	Dimensionless velocity components
S_r	Soret number	$\theta(\eta)$	Dimensionless temperature
g	Acceleration due to earth gravity	$\phi(\eta)$	Dimensionless Salinity
F_s	Molecular diffusion	η	Similarity variable
M	Magnetic Parameter	β	Thermal expansion coefficient
$U_\circ$	Uniform velocity	β^*	Thermal expansion coefficient due to salinity

The objective of this study is to present an effect of heat generation on salt water flow through in an ocean by inclined angle. The governing equations are transformed into nonlinear ordinary differential equations which depend on the magnetic parameter (M), Grashof number (G_r), the prandtl number (P_r), modified prandtl number (P_s), the heat source parameter $(\bar{\alpha})$ and the soret number (S_r). The obtained non linear coupled ordinary differential equations are solved numerically using Nactsheim-Swigert [7] shooting iteration technique together with Runge-Kutta six order iteration schemes. The velocity, temperature and Salinity distributions are discussed and presented graphically, and also the skin-friction coefficient, the surface heat and salinity transfer rate are investigated.

2. Mathematical Model of Flow

Introducing the Cartesian co-ordinate system the *X*-axis is chosen along the plate in the direction of flow and the *Y*-axis is inclined to it. Here α is the angle of inclination between *X* and *Y* and α is considered for different angle. Initially it is assumed that the plate as well as the fluid is at the same temperature $T(T_\infty)$ and the Salinity level $S(S_\infty)$ everywhere in the fluid is same. Also it is assumed that the fluid and the plate is at rest after the plate is to be moving with a constant velocity. The temperature of the plate and spices salinity raised to $T_w(>T_\infty)$ and $S_w(>S_\infty)$ respectively, which are these after maintained constant where T_w, S_w are temperature and spices salinity at the wall and T_∞, S_∞ are the temperature and salinity of the spices far away from the plate respectively. The Physical configuration and coordinate system have been shown in the Fig.1. Under the boundary layer approximation the governing equation for the effects of heat generation on salt water flow through in an ocean by inclined angle;

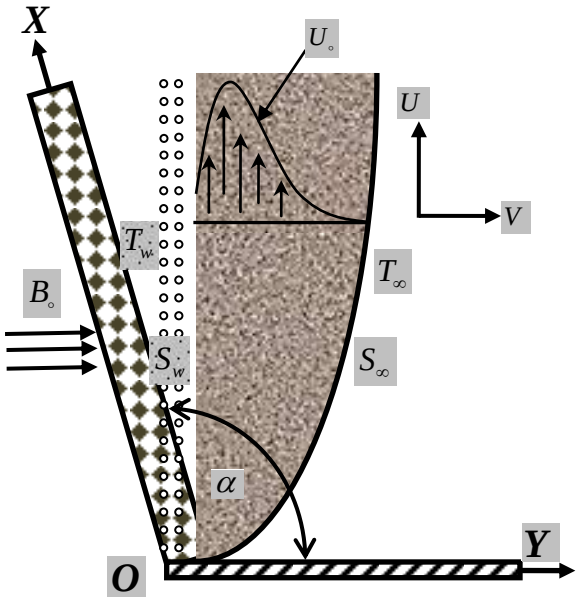

Fig 1. Physical configuration and coordinate system.

The continuity equation

$$\frac{\partial u}{\partial x}+\frac{\partial v}{\partial y}=0 \tag{1}$$

The momentum equation

$$u\frac{\partial u}{\partial x}+v\frac{\partial u}{\partial y}=\upsilon\frac{\partial^2 u}{\partial y^2}+g\beta(T-T_\infty)sin\alpha-\frac{\sigma B_\circ^2 u}{\rho} \tag{2}$$

The Salinity equation

$$u\frac{\partial s}{\partial x}+v\frac{\partial s}{\partial y}=K_s\frac{\partial^2 s}{\partial y^2}+F_s\frac{\partial^2 T}{\partial y^2} \tag{3}$$

The temperature equation

$$u\frac{\partial T}{\partial x}+v\frac{\partial T}{\partial y}=K_T\frac{\partial^2 T}{\partial y^2}+\frac{Q_T}{\rho C_p} \tag{4}$$

Corresponding boundary conditions are;

$$u=0,\ v=0,\ T=T_w=T_\infty+\sin\alpha,\ S=S_w=S_\infty+\sin\alpha \qquad \text{at}\ \ y=0$$

$$u=0,\ V=0,\ T=T_\infty, S=S_\infty \qquad \text{as}\ \ y\to\infty \tag{5}$$

where υ is the kinematic viscosity, $K_S=\dfrac{K}{\rho C_S}$ is the thermal conductivity due to salinity, $K_T=\dfrac{K}{\rho C_p}$ is the thermal conductivity due to temperature, F_s is the molecular diffusion, C_p is the specific heat at constant pressure, $U_\circ$ is the uniform velocity, σ is the conductivity of the material, g is the acceleration due to earth gravity, β is the volumetric thermal expansion coefficient, β^* is the volumetric thermal expansion coefficient due to salinity, $Q_T=(T-T_\infty)Q^*$ is the heat generation, $B_\circ$ is the magnetic induction and ρ is the density.

3. Mathematical formulation

In order to obtain the solution of equations (1) to (4) with the boundary conditions (5), the following dimensionless variables have been introduced;

$$\eta=y\sqrt{\frac{U_\circ}{2\upsilon x}},\ \psi=\sqrt{2\upsilon U_\circ x}\,f(\eta),\ \theta=\theta(\eta)=\frac{T-T_\infty}{T_w-T_\infty},$$

$$\phi=\phi(\eta)=\frac{S-S_\infty}{S_w-S_\infty}\ \text{ and }\ u=\frac{\partial\psi}{\partial y},\ v=-\frac{\partial\psi}{\partial x}. \tag{6}$$

The non dimensional, non linear compiled ordinary differential equations from the equations (2), (3) and (4) become

$$f'''+ff''+G_r\theta\cdot\sin\alpha-Mf=0 \tag{7}$$

$$\theta''+P_r f\theta'+P_r\bar{\alpha}\cdot\theta=0 \tag{8}$$

$$\phi''+P_S f\phi'+P_S\cdot S_r\theta''=0 \tag{9}$$

the boundary conditions are;

$$f=0,\ f'=0,\ \theta=1,\ \phi=1 \text{ at } \eta=0$$

$$f'=0,\ \theta=0,\ \phi=0 \qquad \text{as}\ \ \eta\to\infty \tag{10}$$

where the notation primes denote differentiation with respect to η and $G_r=\dfrac{g\beta(T_w-T_\infty)2x}{U_0^2}$ is the Grashof number, $M=\dfrac{\sigma\beta_\circ^2 2x}{U_\circ}$ is the magnetic parameter, $P_r=\dfrac{\upsilon\rho C_p}{K}$ is the prandtl number, $P_s=\dfrac{\upsilon\rho C_S}{K}$, is the modified prandtl number, $\bar{\alpha}=\dfrac{2xQ^*}{U_0\rho C_p}$ is the heat source parameter and $S_r=\dfrac{F_s}{\upsilon}\left(\dfrac{T_w-T_\infty}{S_w-S_\infty}\right)$ is the soret number.

4. Skin-Friction Coefficients, Nusselt and Sherwood Number

The physical quantities of the skin-friction coefficient, the Nusselt number (rate of heat transfer) and Sherwood number (rate of salinity) are calculated respectively by the following equations,

$$C_f\,(R_e)^{-\frac{1}{2}}=-f''(0),\ N_u\,(R_e)^{-\frac{1}{2}}=-\theta'(0)\ \text{ and }S_h\,(R_e)^{-\frac{1}{2}}=-\phi'(0)$$

where R_e is the Local Reynolds number.

5. Numerical Solutions

The non dimensional, nonlinear, coupled ordinary differential equations (7) to (9) with boundary condition (10) are solved numerically using initially value solver the shooting method. For the purpose of this method, the Nactsheim-Swigert shooting iteration technique together with Runge-Kutta six order iteration scheme is taken and determines the temperature and salinity as a function of the coordinate η. Extension of the iteration shell to above equation system of differential equations (10) is straightforward, there are three asymptotic boundary condition and hence three unknown surface conditions $f''(0)$, $\theta'(0)$ and $\varphi'(0)$.

6. Results and Discussion

In order to investigate the physical representation of the problem, the numerical values of velocity (f'), temperature (θ) and salinity (ϕ) with the boundary layer have been computed for different parameters as magnetic parameter (M), Grashof number (G_r), prandtl number (P_r), modified prandtl number (P_s), heat source parameter $(\bar{\alpha})$ and soret number (S_r) with different angle and 120° respectively.

Figs. 2 and 3 represent the dimensionless velocity distribution $f'(\eta)$ for different values of Grashof number G_r where $M = 1.0, P_r = 0.125, P_s = 10, S_r = 1.0, \bar{\alpha} = 0.80$ with the corresponding angle 90° and inclined angle 120°. It has been found that, the momentum boundary layer thickness decreases as G_r increase.

Figs. 4 and 5 represents the salinity distribution $\phi(\eta)$ and temperature distribution $\theta(\eta)$ respectively for different values of angle α where, $M = 1.0, G_r = 4.0, P_r = 0.50, P_s = 1.0, S_r = 1.0, \bar{\alpha} = 0.5$. It has been seen that the salinity and temperature boundary layer thickness decrease respectively as α increases.

Fig.6. shows the dimensionless skin-friction coefficient $(-f'')$ plotted against heat source parameter $(\bar{\alpha})$ for the different values of Magnetic parameter M where $G_r = 1.0, P_r = 0.125, P_s = 10, S_r = 1.0$ and $\alpha = 90^\circ$. It is noted that there is decrease in skin-friction coefficient as magnetic parameter M increases.

Fig.7. shows the dimensionless salinity rate $(-\phi')$ plotted against heat source parameter $(\bar{\alpha})$ for the different values of modified prandtl number P_s where $M = 1.0, G_r = 4.0, P_r = 0.71, S_r = 1.0$ and $\alpha = 90^\circ$. It is noted that there is decrease in salinity rate as modified prandtl number P_s increases.

Fig.8. shows the dimensionless heat transfer rate $(-\theta')$ plotted against Heat source parameter $(\bar{\alpha})$ for the different values of prandtl number P_r where $M = 1.0, G_r = 4.0, P_s = 1.0, S_r = 1.0$ and $\alpha = 90^\circ$. It is noted that heat transfer rate decrease as prandtl number P_r increase.

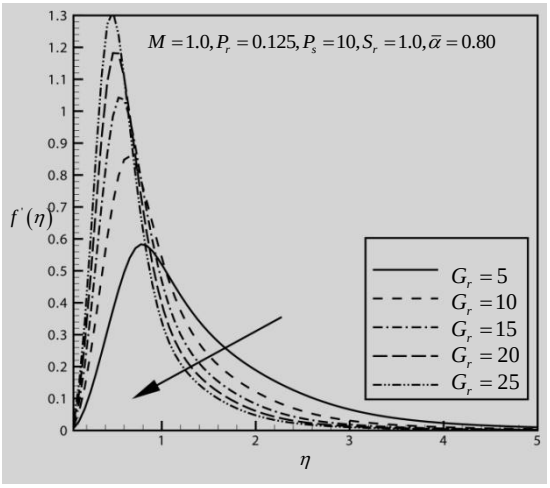

Fig.2. Effect of G_r on Velocity profile with the angle 90° .

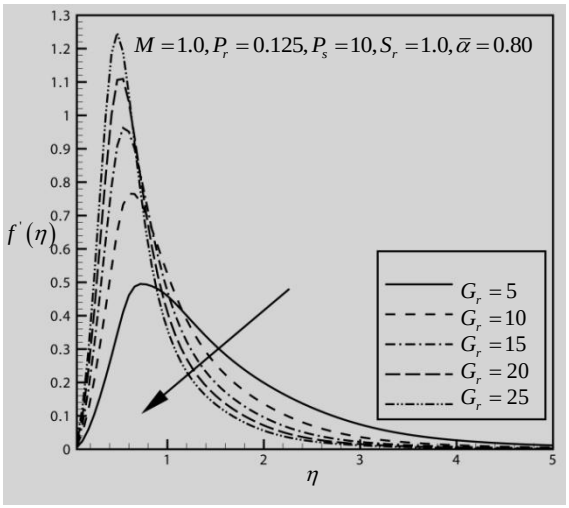

Fig. 3. Effect of G_r on Velocity profile with the angle 120° .

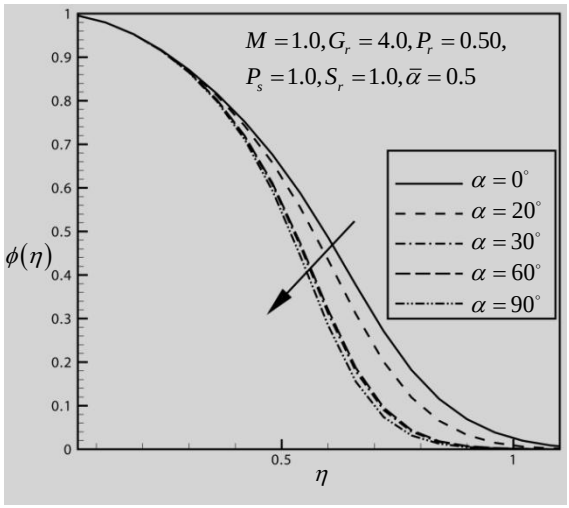

Fig.4. Effect of angle α on Salinity profile.

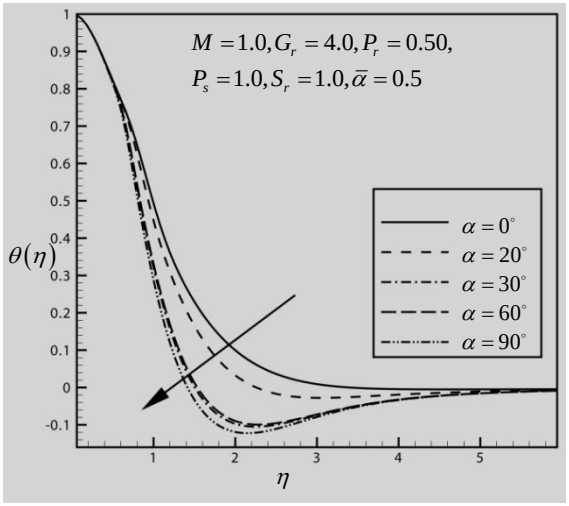

Fig.5. Effect of angle α on Temperature profile.

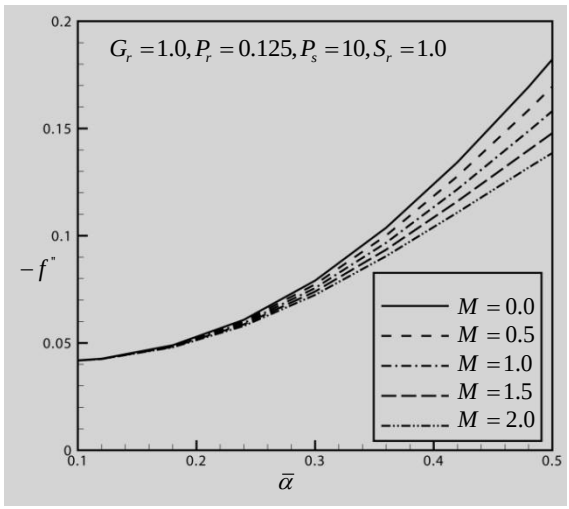

Fig.6. Effect of M on Skin-friction Coefficient.

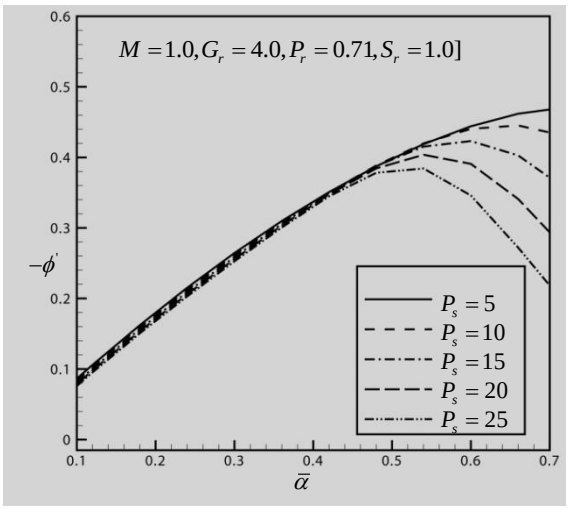

Fig. 7. Effect of P_s on the Rate of Salinity.

7. Conclusions

This paper investigated the effects of heat generation on salt water flow through in an ocean by inclined angle. The important findings of the investigation from graphical representation are listed below:

1. The momentum boundary layer thickness rises as the Grashof number increase. Also the skin-friction coefficient decreases as magnetic parameter increase.
2. The temperature and salinity boundary layer thickness decrease as α increase.
3. The salinity rate decreases as the Modified Prandtl number increase.
4. The surface heat transfer rate decrease as the Prandtl number increase.

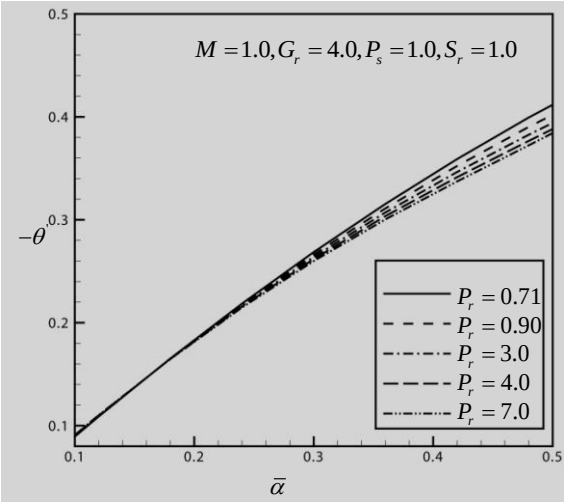

Fig.8. Effect of P_r on the Rate of heat transfer.

Acknowledgements

The authors wish to express their very sincerely thanks to the reviewers and the 5th BSME ICTE committee for their valuable comments and suggestions.

References

[1] Philander, SGH. El Niño, La Nina, and the Southern Oscillation. Academic Press, San Diego 1990: 293.
[2] Ping Wang et al. Parallel computation of the regional ocean modeling system, The International Journal of High Performance Computing Applications 2005; 19: 375–385.
[3] Nansen, F. Oceanography of the North Polar Basin. Science Research1902; 3:427 .
[4] Blumberg, AF. and GL. Mellor. A whole basin model of the Gulf of Mexico. Proceeding sixth annual Ocean Thermal Energy Conversion Conference. Department of energy. Washington, D.C 1979a: 13.15-1 to 13.15-10.
[5] Sourav Sil and Arun Chakraborty. Numerical simulation of seasonal variations in circulations of the Bay of Bengal, Journal of Oceanography and Marine Science 2011; 2(5) :127-135.
[6] Alam, M. et al. Similarity Solution for MHD Flow through a Vertical Porous Plate with Suction, J. of Comp. and App. Mech. 2005; 6:15–25.
[7] Nachtsheim, P.R. and Swigert P. Satisfaction of the asymptotic boundary conditions in numerical solution of the system of non-linear equations of boundary layer type. NASA 1965 TND-3004.
[8] Ezer, T. and Mellor, G.L. A generalized coordinate's ocean model and a comparison of the bottom boundary layer dynamics in terrain-following and z-level grids. Ocean Modelling 2004; 6:379-403.

5th BSME International Conference on Thermal Engineering

Production and exhaust gas analysis of bio diesel from bio fuel

Yamin Rekhu[a] , Shabab Mottakin Chowdhury[b,*]

[a]Military institute of science and technology (MIST), Mirpur, Dhaka-1216, Bangladesh.
[b]Military institute of science and technology (MIST), Mirpur, Dhaka-1216, Bangladesh.

Abstract

Biodiesel, made from partially renewable sources of oil such as soybean, coconut or palm oil, has been heralded as an environmentally-friendly alternative to petroleum derived diesel. It can be used in diesel engines without any engine modification and past studies have shown biodiesel to be less polluting than petroleum-derived diesel. However, new research has shown that the quality of the biodiesel used as fuel has a significant impact on emissions. Petroleum diesel engines are heavily polluting. They emit nitrogen oxides and particulate matter that are harmful to human health. There are serious concerns especially over children exposed to exhaust pollutants. Previous studies of engines fuelled by biodiesel, on the other hand, have suggested that biodiesel produces less carbon monoxide, hydrocarbons and particulate matter. This work considers the use of vegetable oil for the production of alternative renewable and environmental friendly biodiesel fuel from coconut and soybean oil. We have prepared biodiesel through transesterification reaction using1000gm coconut/soybean oil, 20.0% methanol (wt% soybean oil), 0.8% potassium hydroxide as catalyst at 65°Creaction temperature and 30 minutes reaction time. The experiment was carried out three times and average results evaluated. We designed an engine test bench and tested the exhaust gas property by using exhaust gas analyzer. We have found that with the increase of load it was seen that CO, CO_2, SO_2 and O_2 emission in exhaust gas reduced when we used biodiesel in comparison with diesel .but NO emission increased in emission when we use biodiesel instead of diesel. With the increase of fuel flow rate CO, CO_2 and SO_2 emission increased in both type of fuel but reduced for O_2 also for both fuel. The important output of the test is sulfur reduction and carbon monoxide which are very harmful for health and environment. The carbon footprint of biodiesel was found promising and better than diesel.

1. Keywords: Bio diesel;transesterification;exhaust gas;carbon footprint.

1. Introduction

The use of vegetable oils as an alternative fuel for diesel engines dates back to around a century. Due to rapid decline of crude oil reserve and increase in price, the use of vegetable oils is again prompted in many countries. Depending upon the soil condition and climate, different nations are looking for different vegetables oils for example, soybean oil in U.S.A, rapeseed and sunflower oil in Europe, Palm oil in Malaysia and Indonesia, Coconut oil in Philippines are being considered to substitute of diesel fuel (1). The potential of bio diesel production from soybean have been found to be a promising fuel for diesel engine in number of studies. Soybean is a widely growing seed in Bangladesh. It is generally used for cooking. Through transesterification, these vegetable oils are converted to the alkyl esters of the fatty acids present in the vegetable oil (2).These esters are commonly referred to as biodiesel.

In view of the current instability in oil prices, biodiesel stands as an attractive source of alternative energy. By adopting and increasing the use of biodiesel, European countries have reduced from her over-dependence on crude oil reserves (3). Besides, conventional fossil fuel has been reported as being finite. While it is worthy to note that biodiesel will not completely displace petroleum diesel, biodiesel has its place as an alternative fuel and can be a source of lubricate as an additive to diesel fuel. The emissions produced from biodiesel are cleaner compared to petroleum-based diesel fuel. Particulate emissions, soot, and carbon monoxide are lower since biodiesel is an oxygenated fuel. However, emissions of oxides of nitrogen (NO_X) are higher when biodiesel is used (4). The cause of the rise in NO_X is unknown and is being studied.

One particular problem of biodiesel is its cold flow properties. Neat biodiesel such as methyl soy ate has a pour point (i.e. the lowest temperature at which the fuel is pourable) of -3°C (5). In colder climates, crystallization can occur, which leads to the plugging of fuel filters and lines. Typically, taking U.S as a case study, biodiesel is blended with diesel fuel. A B20 blend would be 20% biodiesel in diesel fuel (6).Such a blend would have better cold flow properties compared to neat biodiesel. This work is therefore aimed at producing biodiesel from ethyl esters of soybean oil and comparing some properties of the produced biodiesel with ASTM standards.

* Yamin Rekhu. Tel.: +8801717531449; fax: +8029011311.
E-mail address: rekhu.mist@gmail.com

2. Biodiesel

Biodiesel is produced from vegetable oils. The main component of vegetables oils are triglycerides. Triglycerides are esters of glycerol with long chain acids, commonly called fatty acids. Biodiesel is defined as mono alkyl esters of long chain fatty acid derived from renewable feed stock such as vegetable oil or animal fats, for use in compression ignition (CI) engines (7). This name is given to esters when they are for use as fuel.

2.1. Blends.

Blends of biodiesel and conventional hydrocarbon-based diesel are products most commonly distributed for use in the retail diesel fuel marketplace. Much of the world uses a system known as the "B" factor to state the amount of biodiesel in any fuel mix:

- 100% biodiesel is referred to as B100, while
- 20% biodiesel, 80% petro diesel is labelled B20
- 5% biodiesel, 95% petro diesel is labelled B5
- 2% biodiesel, 98% petro diesel is labelled B2

2.2. Transesterification Process

Soybean oil like any other vegetable oils and animal fats are triglycerides, inherently containing glycerine. The biodiesel process (transesterification) turns the oils into esters, separating out the glycerine from the main product (biodiesel). The glycerine sinks to the bottom and the biodiesel floats on top and can be decanted off. The process is called transesterification, which substitute's alcohol for the glycerine in a chemical reaction, using a catalyst.

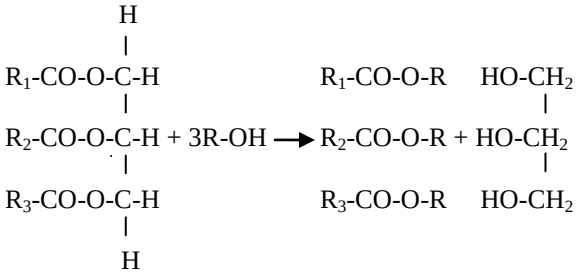

Oil of fats Alcohol Biodiesel Glycerine

2.3. Materials Used in Biodiesel Production

In the Laboratory scale production of soybean oil biodiesel, the following materials were used; 1 litre of soybean oil, 200 ml of methanol (99+% pure), Sodium hydroxide (NaOH), blender, scales accurate to 0.1 grams. The major feedstock source used in this work is soybean oil, locally produced in Bangladesh. It was purchased at the local market in kawran bazar Dhaka. By the stoichiometric equation of the process, 1 mol of soybean oil is required to react with 3 moles of methanol to produce 3 moles of the biodiesel and 1 mole of glycerol (8). 100g soybean oil was used for the transesterification process. Reaction temperature for the process must be below the boiling point of alcohol (methanol, 78°C) used (9); therefore, a reaction temperature of 65°C was selected. Different researchers have reported different reaction times for transesterification process as well as the entire biodiesel production process. The reported reaction time ranges from less than 15 minutes to more than 60 minutes (10). Reaction time of 30 minutes was therefore selected.

Most researchers have used 0.1 to 1.2 % (by weight of oil) of catalyst for biodiesel production (11). 0.8% NaOH (by weight of soybean oil) concentration was therefore selected while 20% methanol was used. NaOH used was manufactured by a German company.

2.4. Synthesis of Biodiesel from Soybean Oil

For the transesterification of soybean oil, the following steps were being followed in this work First 200 ml methanol was mixed with 150 ml (1 N) NaOH. As this is an exothermic reaction, so the mixture would get hot. This solution is known as sodium meth oxide, which is a powerful corrosive base and harmful for human skin. So, safety precautions should be taken to avoid skin contamination during meth oxide producing.

Next, sodium meth oxide was added with 1 litre of soybean oil, which was preheated about 65°C. Then the mixture was shaken for 5 minutes in a glass container. After that the mixture was left for 24 hours (the longer is

better). For the separation of glycerol and ester this mixture then gradually settles down in two distinctive layers. The uppermost transparent layer is 100% biodiesel and the lower concentrated layer is glycerol. The heavier layer is then removed either by gravity separation or with a centrifuge. In some cases if the soybean oil contains impurities, then a thin white layer is formed in between the two layers. This thin layer composes soap and other impurities. Then the biodiesel has been washed with distilled water in order to remove waste and a dry wash has been done by air-stone.

Biodiesel produced in the above process contains moisture (vaporization temperature 100°C), methanol (vaporization temperature 60°C) and usually some soap. If the soap level is low enough (300-500 ppm), the methanol can be removed by vaporization and the methanol will usually be dry enough to directly recycle back to the reaction. Methanol tend to act as a co-solvent for soap in biodiesel, so at higher soap levels the soap will precipitate as a viscous sludge when the methanol is removed. Anyway, heating the biodiesel at temperature above 100 °C would cause the removal of both the moisture and methanol as well.

2.5. Washing Method

Washing was done in two steps. In the first step, the collected biodiesel after transesterfication reaction was taken into a beaker. Hot water (40°C) was poured into the biodiesel slowly. Then the mixtures were shaken slowly and the solution was kept 4 hours in stable position. Then a layer of soap has formed in the bottom of beaker. Then the biodiesel was collected by a pipe followed by siphoning method. The process had been repeated 4 times and gradually soap formation was reduced.

In other step, an air stone was used for producing bubbles in the solution for dry wash. Dry wash confirmed the formation of glycerol and soap rest in the mixture. A heater was used which had been kept always 35°C for removing the water from biodiesel. After the process finally the biodiesel was collect and its properties were tested in the laboratory.

3. PROPERTIES OF BIODIESEL AND THEIR BLENDS ANALYSIS

Biodiesel produced from soybean oil has comparable fuel properties with the conventional fossil diesel. A comparative study of fuel properties with the conventional fossil diesel, neat biodiesel and their blends have been carried out in this work to find out suitable blending of biodiesel. In the study B40, B60, B80 and B100 blend have been prepared to compare the fuel properties of different blends.

3.1. Heating Value

Heating value indicates the energy density of the fuel. In our study, ASTM 2382 method has been applied to measure the heating value of biodiesel and their blends. Table 1 shows the heating value of diesel, neat biodiesel and their blends in MJ/kg.

Table.1: Comparison of heating value of different fuels

Fuel	Heating Value (MJ/kg)
Fossil diesel	45.71
B100	42.78
B80	42.92
B60	43.12
B40	43.24

From table 1 it is observed that, diesel fuel has heating value about 45 MJ/kg. Heating value of the fuel decreases as we choose higher blending of biodiesel. This is because, biodiesel has lower energy density than diesel fuel, so higher amount of biodiesel is required for producing same amount of energy as compared to diesel fuel.

3.2. Viscosity

Viscosity of the fuel exerts a strong influence on shape of the fuel spray; high viscosity for example, causes low atomization (large droplet size) and high penetration of spray jet. Note that cold engines, with higher viscous oil, discharge will act almost a solid stream of fuel into the combustion chamber and starting may be difficult while a smoky exhaust will invariably appear. On the other hand, very low viscous fuel would cause to pass through leakage of the piston and piston wall especially after wear has occurred, which subsequently prevents accurate metering of the fuel. Fig. 1 indicates that, B40, B60 and B80 have almost the same viscosity at

room temperature and it is about 1.5-2% higher than fossil fuel. But a slight preheating would cause to achieve comparable viscosity as that of diesel fuel. So using B40, B60, B40 and B80 blend would not cause much change on the fuel spray pattern, and thus these fuels can be used in the diesel engine without modification of the fuel supply system.

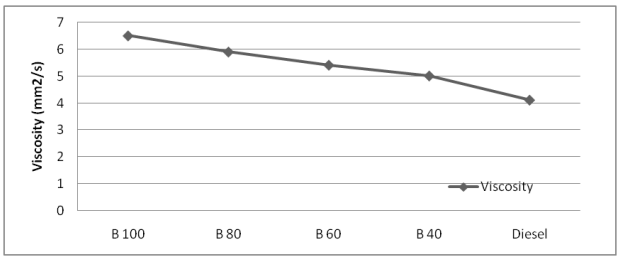

Fig.1. Viscosity for diesel and biodiesel blends

On the other hand B100 is a much viscous fuel, and its viscosity is much higher than diesel fuel. The high viscous fuel would exhibit almost a solid stream of spray pattern in the combustion chamber and so cold starting of the engine would be difficult. So, using B100 fuel in the existing diesel engine would require modification of that fuel system so that fuel supply system exerts high sprat pressure to achieve the desired spray pattern inside the engine cylinder.

3.3. Flash Point

Flash point is an important property of CI engine fuel. Fig. 2 shows flash point for diesel, biodiesel and their blends.

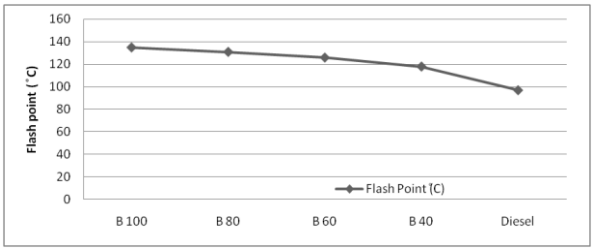

Fig.2. Flash point for diesel and biodiesel blends

4. Exhaust gas in diesel engine

Diesel exhaust (known as clag when emitted by locomotives, or diesel engine emissions in scientific papers) is the exhaust gas of an engine. In diesel engines, conditions in the engine differ from the spark-ignition engine, since power is directly controlled by the fuel supply, rather than by controlling the air supply. Thus when the engine runs at low power, there is enough oxygen present to burn the fuel, and diesel engines only make significant amounts of carbon monoxide when running under a load.

Diesel exhaust is well known for its characteristic smell; but in Britain this smell in recent years has become much less (while diesel fuel getting more expensive) because the sulphur is now removed from the fuel in the oil refinery, plus the effect of converters. Diesel exhaust has been found to contain many toxic air contaminants. Among these pollutants, fine particle pollution is perhaps the most important as a cause of diesel's deleterious health effects.

4.1. Particulates in exhaust gas

Diesel particulate matter (DPM), sometimes also called diesel exhaust particles (DEP), is the particulate component of diesel exhaust, which includes diesel soot and aerosols such as ash particulates,

metallic abrasion particles, sulphates, and silicates. When released into the atmosphere, DPM can take the form of individual particles or chain aggregates, with most in the invisible sub-micrometer range of 100nanometers, also known as ultrafine particles (UFP) or PM0.1. Soot is a general term that refers to impure carbon particles resulting from the incomplete combustion of a hydrocarbon. It is more properly restricted to the product of the gas-phase combustion process but is commonly extended to include the residual pyrolyzed fuel particles such as ecospheres, charred wood, petroleum coke, and so on.

4.2. Exhaust gas analyzer

Exhaust gas analysis is a machine which can detect the percentage of exhaust gas contaminants like CO, CO2, SO2, H_2S Etc and also measure the exhaust gas draught ,AF ratio, exhaust gas temperature and some other property depending on machine standards .they measure the data using chemical, electrochemical ,chemical and optical sensors . We use the model IMR 400.

Fig.3. Exhaust gas analyzer IMR 4001

4.3. Experimental data of different engines using different fuels

Using the exhaust gas analyzer we measured data of a diesel engine using diesel fuel and using Biodiesel. Data's are entitled below in the table

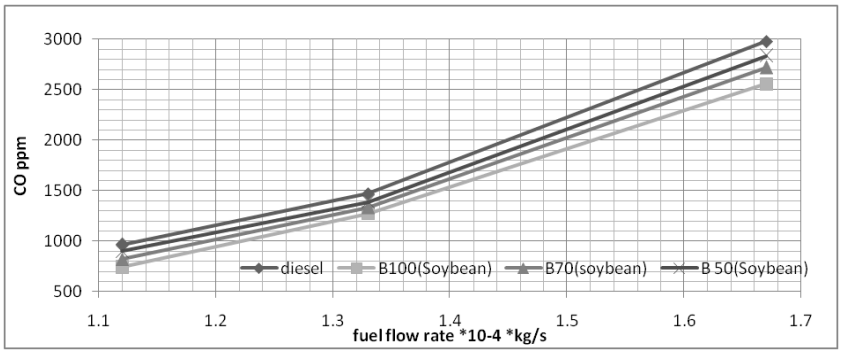

Fig.4.1.CO emission graph in diesel engine

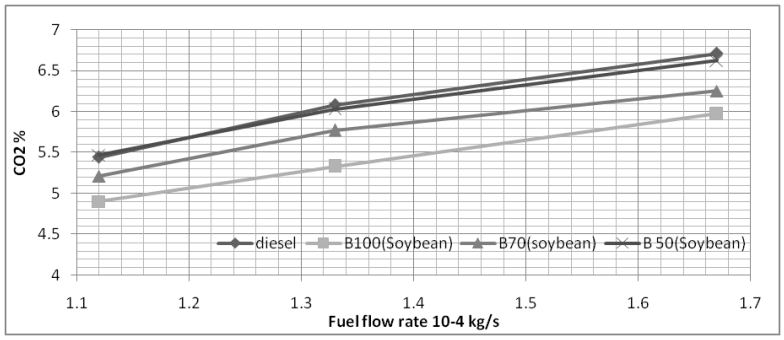

Fig.4.2. CO_2 emission graph in diesel engine

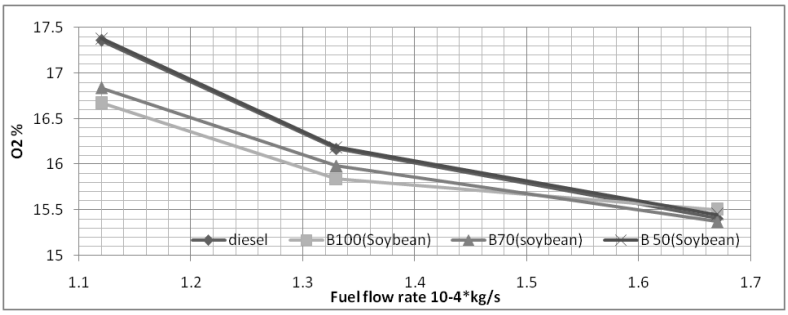

Fig.4.3. O_2 emission graph in diesel engine

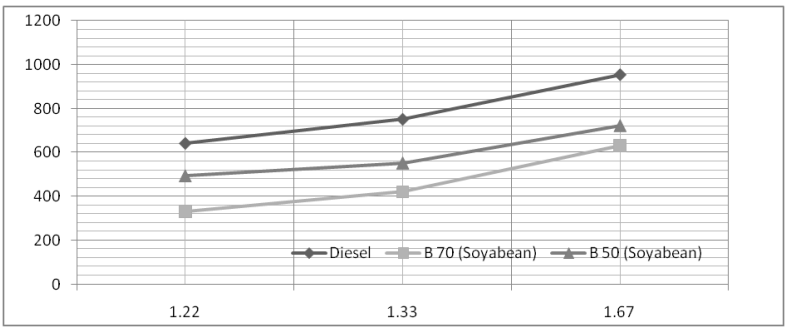

Fig.4.4. SO_2 emission graph in diesel engine

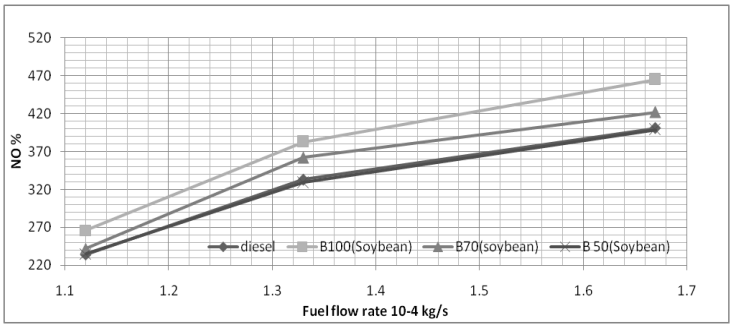

Fig.4.5. NO emission graph in diesel engine

4.4. Results analysis

With the increase of load it was seen that CO, CO_2, SO_2 and O_2 emission in exhaust gas reduced when we used biodiesel in comparison with diesel .but NO emission increased in emission when we use biodiesel instead of diesel. With the increase of fuel flow rate CO, CO_2 and SO_2 emission increased in both type of fuel but reduced for O_2 also for both fuel. Some irregular data also found in the experiment.

The important output of the test is sulphur reduction and carbon monoxide which are very harmful for health and environment. The carbon footprint of biodiesel was found promising and better than diesel.

5. Conclusion

Now a day, the developing countries are suffering greatly from energy crisis, Bio Diesel can be used as a good alternative source. Although production cost of biodiesel is high but it is environmentally friendly and a good source of renewable energy. Detailed Studies need to be done about the prospect of biodiesel in Bangladesh. Biodiesel production from soybean oil is comparatively higher than soybean and rapeseed. But energy output and fuel consumption rate is better than the following two. Beside this soybean oil has a much better lubrication property than other bio-fuels.

6. References

1. *"Triglyceride based diesel fuels".* A. Srivasata, R.Prasad. Vols. Renewable and sustainable Energy reviews,vol. 4, No. 2, pp.111-133,2000.
2. Ramadhas A.S., Jayraj S. and Muraleedharan C,,. 2005. Vols. Biodiesel production from high FFA rubber seed fuel ,84 p.335-340.
3. *Biodiesel Production from Nigerian Palm Kernel Oil: Effect of KOH Concentration on Yield.* Alamu O.J, Waheed M.A., Jekayinfa S.O. 2007. Energy for Sustainable Development. Vol. XI(3), pp. p. 77-82.
4. *Comparison of relevant exhaust gas emissions from biodiesel and fossil diesel fuel.* Munack A., Schroder O., Krahl J., Bunger J. Agricultural Engineering International: the CIGR Journal of Scientific Research and Development., p. Manuscript EE 01 001 Vol.
5. Peterson C.L., Cruz R.O., Perkings L., Korus R., Auld D.L. No. 90-610. *Transesterification of vegetable oil for use as diesel fuel: A progress report.* 1990. ASAE Paper.
6. *A study of some fuel properties of local ethanol blended with diesel fuel.* Ajav E.A., Akingbehin A.O. Agricultural Engineering International: the CIGR Journal of Scientific Research and Development., pp. Manuscript EE01 003 Vol. IV, 2002.
7. Y.Yosiomoto, M.Onodera and H. Tamaki. *Production and emission Charecteristics of diesel engine fuelled by Vegetable oils.* s.l. : The Society of Automotive Engineers, 2001. Vols. 2001-01-1807.
8. Kavitha, P.L. *Studies on transesterified mahua oil as an alternative fuel for diesel engines.* India : M.Sc. thesis: Anna University, Chennal-600 025., 2003.
9. J., Van Gerpen. *Biodiesel processing and production.* s.l. : Fuel Processing Technolngy, 2004,. pp. 1-11. Vols. XX,.
10. *Optimisation of experimental conditions for biodiesel production from alkali-catalysed transesterification of Jatropha curcus oil.* Chitra P., Venkatachalam P., Sampathrajan A. 2005. Energy for Sustainable Development. Vol. IX(3), pp. 13-18.
11. *Catalytic production of biodiesel from soybean oil, used frying oil and tallow. .* Alcantara R., Amores J., Canoira L., Fidalgo E., Franco M.J., Navarro A. 2000. Biomass and Bio energy. pp. 515-527.

5th BSME International Conference on Thermal Engineering

Production and comparison of performance of biodiesel produced from different bio-fuel

Yamin Rekhu[a] , Shabab Mottakin Chowdhury[b,*]

[a]Military institute of science and technology (MIST), Mirpur, Dhaka-1216, Bangladesh.
[b]Military institute of science and technology (MIST), Mirpur, Dhaka-1216, Bangladesh.

Abstract

Due to energy crisis and environmental pollution world has taken renewable energy as a remising source of energy. Now a day when developing countries are suffering from energy crisis; Bio Diesel can be used as an alternative source. . Although production cost of biodiesel is high but it is environment friendly and a good source of renewable energy. Many researchers have successfully worked on generating energy from different alternative sources including solar and biological sources such as the conversion of trapped energy from sunlight to electricity and conversion of some renewable agricultural products to fuel. This work considers the use of vegetable oil for the production of alternative renewable and environmental friendly biodiesel fuel as an alternative to conventional diesel fuel. It would certainly help to develop new ideas and machines even. Moreover the fuel properties of is diesel i.e. flash point, fire point, carbon residue, viscosity etc are also rich. We tested bio-fuel property and produced biodiesel from coconut and soybean through transesterification reaction .We designed a diesel engine test bench with preheating system and tested the performance of biodiesel. We compared the property of bio-fuel with biodiesel and also the performance in a diesel engine. We compared the biodiesel performance produced from coconut and soybean in our designed test bench.

Keywords: environmental pollution;alternative source;flash point;fire point;carbon residue

1. Introduction

The use of vegetable oils as an alternative fuel for diesel engines dates back to around a century. Due to rapid decline of crude oil reserve and increase in price, the use of vegetable oils is again prompted in many countries. Depending upon the soil condition and climate, different nations are looking for different vegetables oils for example, soybean oil in U.S.A, rapeseed and sunflower oil in Europe, Palm oil in Malaysia and Indonesia, Coconut oil in Philippines are being considered to substitute of diesel fuel (1). The potential of bio diesel production from soybean have been found to be a promising fuel for diesel engine in number of studies. Soybean is a widely growing seed in Bangladesh. It is generally used for cooking. Through transesterification, these vegetable oils are converted to the alkyl esters of the fatty acids present in the vegetable oil (2).These esters are commonly referred to as biodiesel.

In view of the current instability in oil prices, biodiesel stands as an attractive source of alternative energy. By adopting and increasing the use of biodiesel, European countries have reduced from her over-dependence on crude oil reserves (3). Besides, conventional fossil fuel has been reported as being finite. While it is worthy to note that biodiesel will not completely displace petroleum diesel, biodiesel has its place as an alternative fuel and can be a source of lubricate as an additive to diesel fuel. The emissions produced from biodiesel are cleaner compared to petroleum-based diesel fuel. Particulate emissions, soot, and carbon monoxide are lower since biodiesel is an oxygenated fuel. However, emissions of oxides of nitrogen (NO_X) are higher when biodiesel is used (4). The cause of the rise in NO_X is unknown and is being studied.

One particular problem of biodiesel is its cold flow properties. Neat biodiesel such as methyl soy ate has a pour point (i.e. the lowest temperature at which the fuel is pourable) of -3°C (5). In colder climates, crystallization can occur, which leads to the plugging of fuel filters and lines. Typically, taking U.S as a case study, biodiesel is blended with diesel fuel. A B20 blend would be 20% biodiesel in diesel fuel (6).Such a blend would have better cold flow properties compared to neat biodiesel. This work is therefore aimed at producing biodiesel from ethyl esters of soybean or coconut oil and comparing some properties of the produced biodiesel with ASTM standards.

* Yamin Rekhu. Tel.: +8801717531449; fax: +8029011311.
E-mail address: rekhu.mist@gmail.com

2. Biodiesel

Biodiesel is produced from vegetable oils. The main component of vegetables oils are triglycerides. Triglycerides are esters of glycerol with long chain acids, commonly called fatty acids. Biodiesel is defined as mono alkyl esters of long chain fatty acid derived from renewable feed stock such as vegetable oil or animal fats, for use in compression ignition (CI) engines (7). This name is given to esters when they are for use as fuel.

2.1. Blends.

Blends of biodiesel and conventional hydrocarbon-based diesel are products most commonly distributed for use in the retail diesel fuel marketplace. Much of the world uses a system known as the "B" factor to state the amount of biodiesel in any fuel mix:

- 100% biodiesel is referred to as B100, while
- 20% biodiesel, 80% petro diesel is labelled B20
- 5% biodiesel, 95% petro diesel is labelled B5
- 2% biodiesel, 98% petro diesel is labelled B2

2.2. Transesterification Process

Coconut and soybean oil like any other vegetable oils and animal fats are triglycerides, inherently containing glycerine. The biodiesel process (transesterification) turns the oils into esters, separating out the glycerine from the main product (biodiesel). The glycerine sinks to the bottom and the biodiesel floats on top and can be decanted off. The process is called transesterification, which substitute's alcohol for the glycerine in a chemical reaction, using a catalyst.

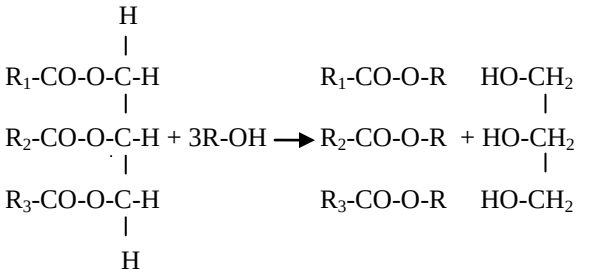

Oil of fats Alcohol Biodiesel Glycerine

2.3. Materials Used in Biodiesel Production

In the Laboratory scale production of soybean and coconut oil biodiesel, the following materials were used; 1 litre of soybean or, coconut oil, 200 ml of methanol (99+% pure), sodium hydroxide (NaOH), blender, scales accurate to 0.1 grams. The major feedstock source used in this work is soybean and coconut oil, locally produced in Bangladesh. It was purchased at the local market in kawran bazar Dhaka. By the stoichiometric equation of the process, 1 mol of soybean or coconut oil is required to react with 3 moles of methanol to produce 3 moles of the biodiesel and 1 mole of glycerol (8). 100g soybean or coconut oil was used for the transesterification process. Reaction temperature for the process must be below the boiling point of alcohol (methanol, 78°C) used (9); therefore, a reaction temperature of 65°C was selected. Different researchers have reported different reaction times for transesterification process as well as the entire biodiesel production process. The reported reaction time ranges from less than 15 minutes to more than 60 minutes (10). Reaction time of 30 minutes was therefore selected.

Most researchers have used 0.1 to 1.2 % (by weight of oil) of catalyst for biodiesel production (11). 0.8% NaOH (by weight of soybean or coconut oil) concentration was therefore selected while 20% methanol was used. NaOH used was manufactured by a German company.

2.4. Synthesis of Biodiesel from Soybean or coconut Oil

For the transesterification of soybean or coconut oil, the following steps were being followed in this work First 200 ml methanol was mixed with 150 ml (1 N) NaOH. As this is an exothermic reaction, so the mixture

would get hot. This solution is known as sodium meth oxide, which is a powerful corrosive base and harmful for human skin. So, safety precautions should be taken to avoid skin contamination during meth oxide producing.

Next, sodium meth oxide was added with 1 litre of soybean or coconut oil, which was preheated about 65°C. Then the mixture was shaken for 5 minutes in a glass container. After that the mixture was left for 24 hours (the longer is better). For the separation of glycerol and ester this mixture then gradually settles down in two distinctive layers. The uppermost transparent layer is 100% biodiesel and the lower concentrated layer is glycerol. The heavier layer is then removed either by gravity separation or with a centrifuge. In some cases if the soybean or coconut oil contains impurities, then a thin white layer is formed in between the two layers. This thin layer composes soap and other impurities. Then the biodiesel has been washed with distilled water in order to remove waste and a dry wash has been done by air-stone.

Biodiesel produced in the above process contains moisture (vaporization temperature 100°C), methanol (vaporization temperature 60°C) and usually some soap. If the soap level is low enough (300-500 ppm), the methanol can be removed by vaporization and the methanol will usually be dry enough to directly recycle back to the reaction. Methanol tend to act as a co-solvent for soap in biodiesel, so at higher soap levels the soap will precipitate as a viscous sludge when the methanol is removed. Anyway, heating the biodiesel at temperature above 100 °C would cause the removal of both the moisture and methanol as well.

2.5. Washing Method

Washing was done in two steps. In the first step, the collected biodiesel after transesterfication reaction was taken into a beaker. Hot water (40°C) was poured into the biodiesel slowly. Then the mixtures were shaken slowly and the solution was kept 4 hours in stable position. Then a layer of soap has formed in the bottom of beaker. Then the biodiesel was collected by a pipe followed by siphoning method. the process had been repeated 4 times and gradually soap formation was reduced.

In other step, an air stone was used for producing bubbles in the solution for dry wash. Dry wash confirmed the formation of glycerol and soap rest in the mixture. A heater was used which had been kept always 35°C for removing the water from biodiesel. After the process finally the biodiesel was collect and its properties were tested in the laboratory.

3. PROPERTIES OF BIODIESEL AND THEIR BLENDS ANALYSIS

Biodiesel produced from soybean and coconut oil has comparable fuel properties with the conventional fossil diesel. A comparative study of fuel properties with the conventional fossil diesel, neat biodiesel and their blends have been carried out in this work to find out suitable blending of biodiesel. In the study B40, B60, B80 and B100 blend have been prepared to compare the fuel properties of different blends.

3.1. Heating Value

Heating value indicates the energy density of the fuel. In our study, ASTM 2382 method has been applied to measure the heating value of biodiesel and their blends. Table 2 shows the heating value of diesel, neat biodiesel and their blends in MJ/kg.

Table.1: Comparison of heating value of different bio diesel from soybean

Fuel	Heating Value (MJ/kg)
Fossil diesel	45.71
B100	42.78
B80	42.92
B60	43.12
B40	43.24

Table.2: Comparison of heating value of different bio diesel from coconut

Fuel	Heating Value (MJ/kg)
Fossil diesel	45.71
B100	42.78
B80	42.92
B60	43.12
B40	43.24

From table 1 and 2 it is observed that, diesel fuel has heating value about 45 MJ/kg. Heating value of the fuel decreases as we choose higher blending of biodiesel. This is because, biodiesel has lower energy density than diesel fuel, so higher amount of biodiesel is required for producing same amount of energy as compared to diesel fuel.

From table 1 and 2 it is observed that, diesel fuel has heating value about 45 MJ/kg. Heating value of the fuel decreases as we choose higher blending of biodiesel. This is because, biodiesel has lower energy density than diesel fuel, so higher amount of biodiesel is required for producing same amount of energy as compared to diesel fuel.

3.2. Viscosity

Viscosity of the fuel exerts a strong influence on shape of the fuel spray; high viscosity for example, causes low atomization (large droplet size) and high penetration of spray jet. Note that cold engines, with higher viscous oil, discharge will act almost a solid stream of fuel into the combustion chamber and starting may be difficult while a smoky exhaust will invariably appear. On the other hand, very low viscous fuel would cause to pass through leakage of the piston and piston wall especially after wear has occurred, which subsequently prevents accurate metering of the fuel. Fig. 1 indicates that, B40, B60 and B80 have almost the same viscosity at room temperature and it is about 1.5-2% higher than fossil fuel. But a slight preheating would cause to achieve comparable viscosity as that of diesel fuel. So using B40, B60, B40 and B80 blend would not cause much change on the fuel spray pattern, and thus these fuels can be used in the diesel engine without modification of the fuel supply system.

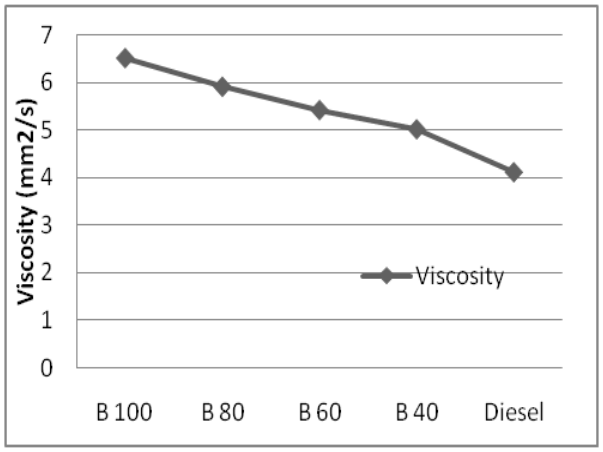

Fig.1. (a) Viscosity for diesel and biodiesel blends (soybean)

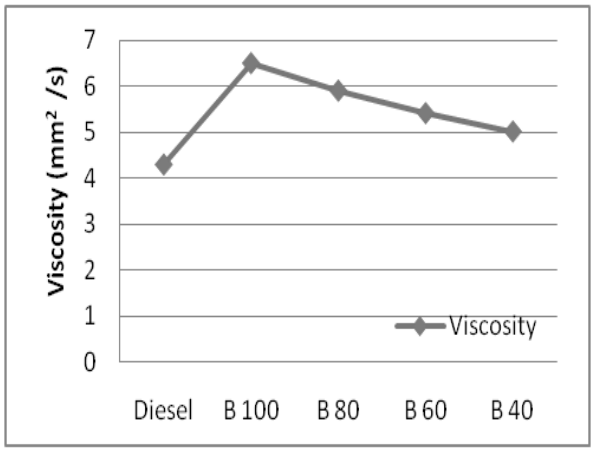

(b) Viscosity for diesel and biodiesel blends (coconut)

On the other hand B100 is a much viscous fuel, and its viscosity is much higher than diesel fuel. The high viscous fuel would exhibit almost a solid stream of spray pattern in the combustion chamber and so cold starting of the engine would be difficult. So, using B100 fuel in the existing diesel engine would require modification of that fuel system so that fuel supply system exerts high sprat pressure to achieve the desired spray pattern inside the engine cylinder.

3.3. Flash Point

Flash point is an important property of CI engine fuel. Fig. 2 shows flash point for diesel, biodiesel and their blends.

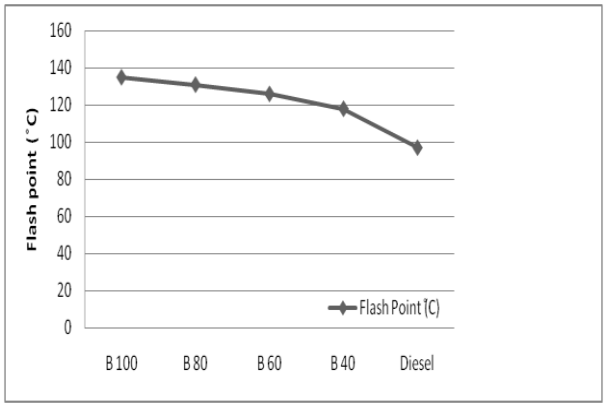

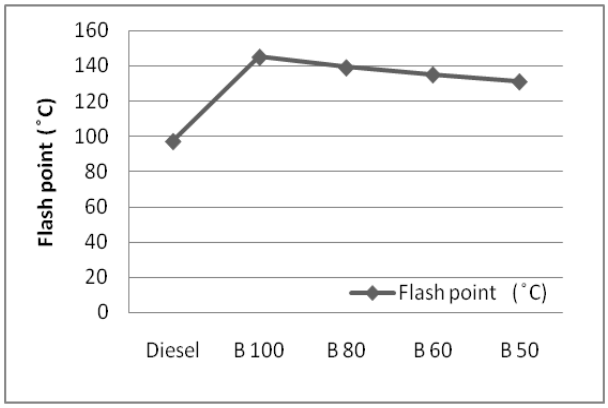

4. Engine Performance Testing and Analysis

4.1. Engine Parameter

The final product of biodiesel from coconut oil was used as an alternative fuel to operate a diesel engine and the performance data were recorded. The specification of the engine is given in table.

Table.3: Engine Specification

1. Model	ZS1110
2. Method of starting	Hand starting
3. Type	Horizontal, 4- stroke, 1 cylinder
4. Cylinder dia	70mm
5. Piston stroke	75mm
6. Nominal speed	2600 rpm
7. Nominal power	3HP
8. Cooling system	Air cooled
9. Rotation	Anti clockwise
10. Fuel filter	Present
11. Lube oil filter	Present

4.2. Experimental Setup

The experimental setup consisted of engine test bed with fuel supply system and different measuring and metering devices with the engine. A preheating system was made in diesel engine test bed with the help of heater and thermo couple for measuring the temperature. A control unit was used to set temperature and automatic control of heater .Separate tank had been used for direct use of coconut oil with mixing with diesel. Single tank has been used for testing biodiesel performance and a typical heater was used to preheat the oil both bio diesel and the direct using of oil. Brake horse power (BHP), Brake specific fuel consumption (bsfc), brake thermal efficiency of the engine was measured for Diesel, B100, B80, B60 and B40 blends. For measuring BHP, brake type dynamometer had been used. Test was run by varying fuel flow rate which was measured in kg/s. Fuel flow rate had been varied to change the output results which is shown in Fig.

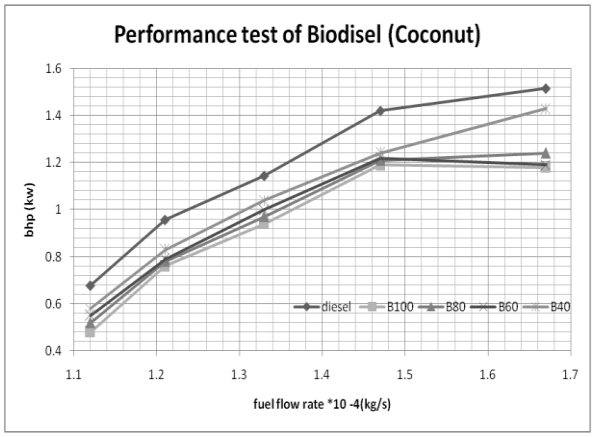

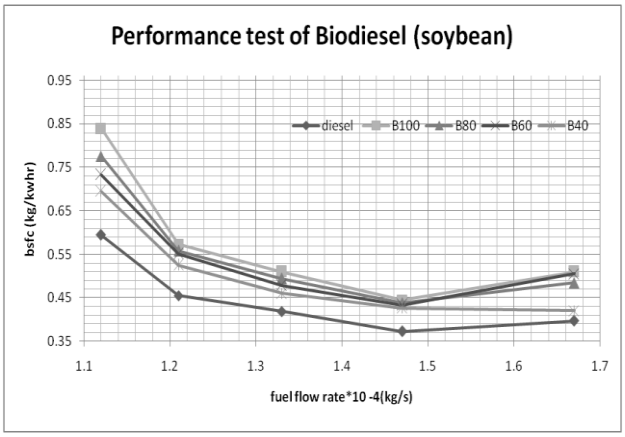

Fig.2 . (a) BHP vs. fuel flow rate for biodiesel (coconut) at preheat temperature 60°C (b)BHP vs. fuel flow rate for biodiesel (soybean) at preheat temperature 60°c

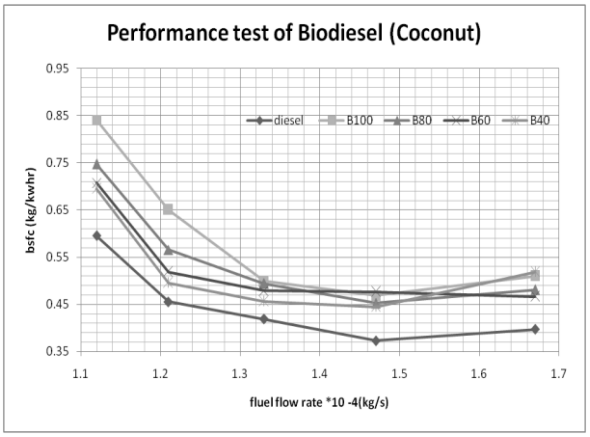

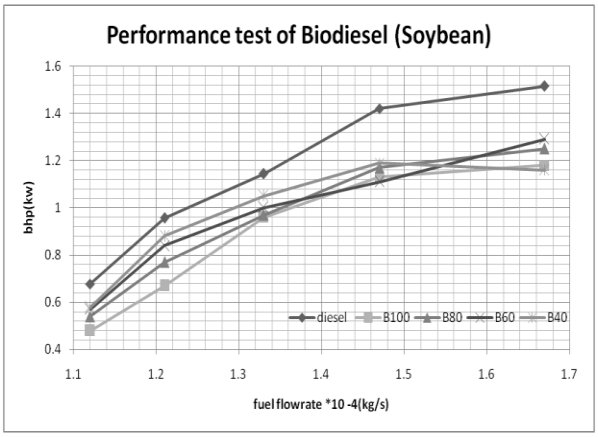

Fig.2. (a) bsfc vs. fuel flow rate for biodiesel (coconut) at preheat temperature 60°C (b)bsfc vs. fuel flow rate for biodiesel (soybean) at preheat temperature 60°c

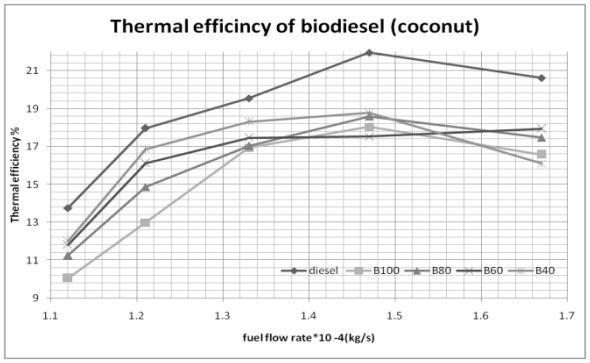

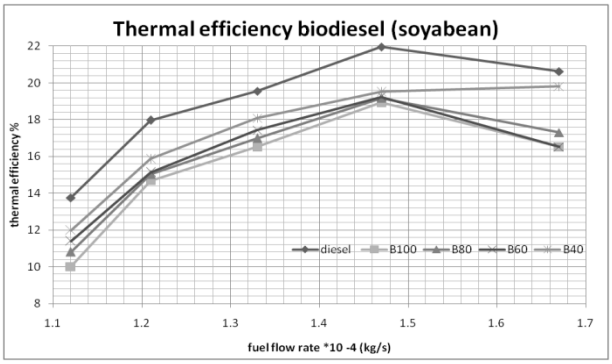

Fig.2. (a)Thermal efficiency vs. fuel flow rate for biodiesel (coconut) at preheat temperature 60°C (b) Thermal efficiency vs. fuel flow rate for biodiesel (soybean) at preheat temperature 60°c

5. Conclusion

Now a day, the developing countries are suffering greatly from energy crisis, Biodiesel can be used as a good alternative source. Although production cost of biodiesel is high but it is environmentally friendly and a good source of renewable energy. Detailed studies need to be done about the prospect of biodiesel in Bangladesh. Biodiesel production from coconut oil is comparatively higher than soybean and rapeseed. But energy output and fuel consumption rate is better than the following two. Beside this coconut oil has a much better lubrication property than other bio-fuels.

6. References

1. *"Triglyceride based diesel fuels"*. A. Srivasata, R.Prasad. Vols. Renewable and sustainable Energy reviews,vol. 4, No. 2, pp.111-133,2000.

2. Ramadhas A.S., Jayraj S. and Muraleedharan C,,. 2005. Vols. Biodiesel production from high FFA rubber seed fuel ,84 p.335-340.

3. *Biodiesel Production from Nigerian Palm Kernel Oil: Effect of KOH Concentration on Yield.* Alamu O.J, Waheed M.A., Jekayinfa S.O. 2007. Energy for Sustainable Development. Vol. XI(3), pp. p. 77-82.

4. *Comparison of relevant exhaust gas emissions from biodiesel and fossil diesel fuel.* Munack A., Schroder O., Krahl J., Bunger J. Agricultural Engineering International: the CIGR Journal of Scientific Research and Development., p. Manuscript EE 01 001 Vol.

5. Peterson C.L., Cruz R.O., Perkings L., Korus R., Auld D.L. No. 90-610. *Transesterification of vegetable oil for use as diesel fuel: A progress report.* 1990. ASAE Paper.

6. *A study of some fuel properties of local ethanol blended with diesel fuel.* Ajav E.A., Akingbehin A.O. Agricultural Engineering International: the CIGR Journal of Scientific Research and Development., pp. Manuscript EE01 003 Vol. IV, 2002.

7. Y.Yosiomoto, M.Onodera and H. Tamaki. *Production and emission Charecteristics of diesel engine fuelled by Vegetable oils.* s.l. : The Society of Automotive Engineers, 2001. Vols. 2001-01-1807.

8. Kavitha, P.L. *Studies on transesterified mahua oil as an alternative fuel for diesel engines.* India : M.Sc. thesis: Anna University, Chennal-600 025., 2003.

9. J., Van Gerpen. *Biodiesel processing and production.* s.l. : Fuel Processing Technolngy, 2004,. pp. 1-11. Vols. XX,.

10. *Optimisation of experimental conditions for biodiesel production from alkali-catalysed transesterification of Jatropha curcus oil.* Chitra P., Venkatachalam P., Sampathrajan A. 2005. Energy for Sustainable Development. Vol. IX(3), pp. 13-18.

11. *Catalytic production of biodiesel from soybean oil, used frying oil and tallow. .* Alcantara R., Amores J., Canoira L., Fidalgo E., Franco M.J., Navarro A. 2000. Biomass and Bio energy. pp. 515-527.

Briquette: An Efficient Alternative Fuel in Bangladesh

Mahbubul Alam[a], Hafizul Islam[b], Md. Mahmudul Hasan[b,*], Tanvir Ahmed Siddique[b]

[a]*Professor, Dept. of ME, BUET, Dhaka-1000.*
[b]*Student, Dept. of ME, MIST, Dhaka-1216*

Abstract

Energy crisis is now a major problem throughout the world. So, everyone is searching for an efficient renewable energy. Biomass briquette is a good example of renewable energy. Biomass Briquette, a dense form of bio-fuel has gained a large popularity in poor developing countries as an alternate cooking fuel. In developed countries, it is used in power generation or space heating. In Bangladesh, it has gained much popularity in many regions. But, a little work has been done on it. This paper will provide information about briquette in Bangladesh, its production, physical and fuel properties, field survey on local acceptance, challenges and future potential. Though it will not highlight the complete scenario, but at the end of the paper, one can have an overview of present condition, lacking in this sector etc. This will help to make biomass briquette more popular as an alternative fuel in Bangladesh.

Keywords: Energy crisis, Renewable energy, Briquette, Physical and fuel properties, Alternative fuel

1. Introduction

From the beginning of human race, human beings have been consuming energy. A world without energy cannot be imagined. Since developing countries are at initial stages of industrialization, their energy consumption has been growing at greater rates compared with developed countries. Again the developed countries also try to consume as much energy as they can. The whole world is now in a race to meet their demand with limited energy sources. So the world is now in extreme energy crisis. This will become a more severe condition in future. That's why; renewable energy is now a popular energy sources throughout the world. Biomass briquette is one of the most used renewable energy at present. It is used for different purposes in different regions. Developing countries like Bangladesh mostly use it as a cooking fuel. Biomass briquette is produced from various kinds of raw materials. The most common raw materials are rice husk, saw dust and forest residues. Biomass briquette has an improved characteristic. There are still a lot of limitations in briquette production technology. These limitations may decrease the efficiency of biomass briquette. That's why, continuous works are being done to identify the problems and solve them. So, this technology is regarded one of the most updated technology in the world. Latest technologies are applied to this sector especially in developed countries which is being done in developing countries too.

2. Biomass Densification Technology

Biomass densification technology is nothing but a technology used for the production of densified biofuel which is a well-known alternate fuel throughout the world. Biomass densification technology is used in compacting a low bulk density material into a product of high density. Biomass densification technology refers to the technology used in the process whereby biomass in the form of small particles like straw, sawdust or chips, is concentrated by machines into small pellets or briquettes. **[1]** Biomass briquette is the product of biomass densification technology. Briquette is a type of solid fuel in a compacted form. Raw materials are compressed with the application of pressure thus increase the density. That's why; it is known as biomass densified fuel. Biomass densification technology has become a focusing technology throughout the worldwide in recent years as a technique of beneficiation of residues for utilization as energy source. To meet the demand of alternate fuel against the recent energy crisis, this technology is being adopted by many countries at present.

*Correspnding author, Tel.:+8801670852119
Email address:morshed.0825@yahoo.com

Research is being promoted on this technology to improve its performance. So this technology is also regarded as one of the latest technologies at present. Now it is equally popular in developed and developing countries. The following Fig. 1 provides the energy sources scenario of the whole world.

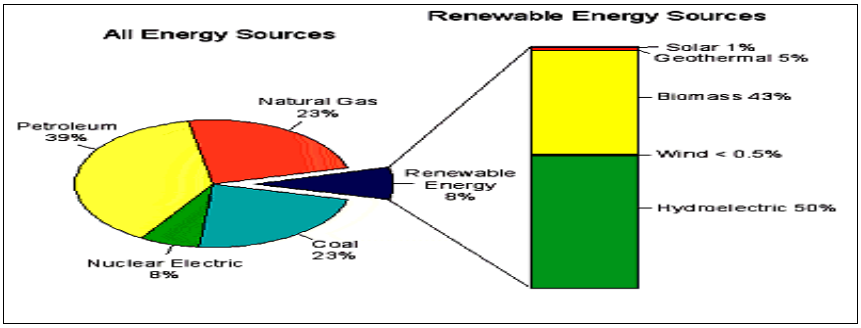

Fig. 1: Total energy sources scenario of the world **[1]**

3. Biomass Briquette System in Bangladesh

Biomass briquette system is not very old to Bangladesh. As heard and found from investigation, briquette system was first introduced in the eastern part of the country, in Sylhet in 1990's. It was first introduced there by a rice mill owner who imported a briquette production unit from Taiwan to tackle problems related to disposal of rice husk, which had become a major hurdle for the boatmen and fishermen there. Eventually briquette system spread to neighbouring districts and slowly throughout the country. The biomass briquette production technology has been developed in our country by entrepreneurs without any support from government and donor agencies. The briquetting machines used are of heated-die screw press type similar to Thailand, Malaysia and South Korea. Bangladesh Institute of Technology (BIT), Khulna [Now, Khulna University of Engineering Technology (KUET)] conducted a survey on densification activities in Bangladesh in the year 1999, and reported about 906 number of machine are running throughout the country and all machines are the heated die screw extruder type. The region wise distribution of the biomass densification technology in Bangladesh is shown in Fig. 2. The highest number of machines was found in Sylhet district (248 no. of machine) where the first machine was launched. Briquette unit's availability is mostly subjected to raw materials availability. According to another survey conducted in year 2004, the number of briquette units was found to be more than 1000. Thus following the growing trend it may be estimated that present number is around 1200 **[2][3][4].**

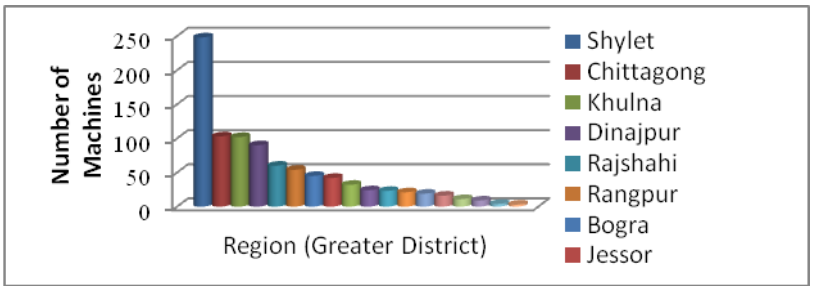

Fig. 2: Distribution of rice husk briquette machines by region in Bangladesh **[4]**

Among the mentioned raw materials, rice husk is the most used raw material in Bangladesh. Around 26% of biomass energy in Bangladesh comes from rice husk. The most of the units use rice husk as their raw material. This is due to the huge production of paddy in our country annually. Bangladesh is one of most rice production countries in Asia. The following Fig. 3 shows the percentage of rice production annually in Bangladesh **[4].**

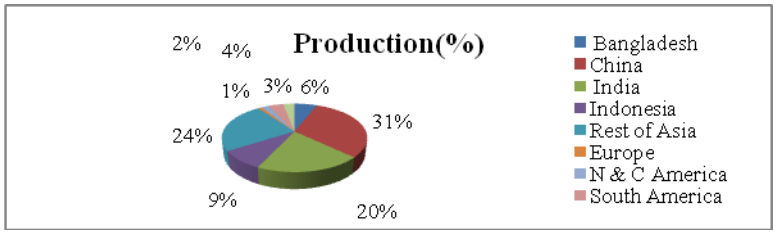

Figure 3: Percentage of rice production in Bangladesh **[4]**

Production of rice husk energy is steady over decades and day by day it is increasing. This high production rate of rice husk energy than others inspires the producers to take it as a raw material for briquette production without any hesitation. That's why, almost in briquette available districts, rice husk briquette is seen.

4. Properties

Briquette is a long cylindrical shaft with an inner bore for high burning efficiency. It is hard and brittle and has a black coating on outer side caused by heating during extrusion. Normally two types of properties are determined to evaluate the efficiency of a biomass briquette. The properties tested of a briquette are given in the following Fig. 4:

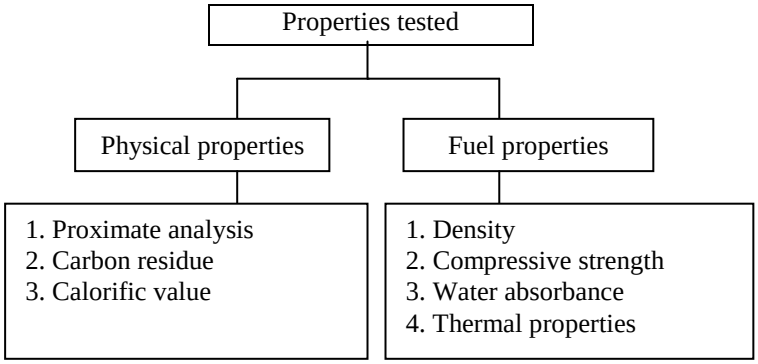

Fig. 4: Physical and fuel properties

4.1 Physical Properties

To determine the mechanical properties mentioned in Fig. 4, the following samples (Table 1) were taken:

Table 1: Sample distribution

Sample no.	1	2	3
District	Sylhet	Khulna	Sirajgong

Generally the external diameters of the above sample vary from 58-60 mm and the internal diameters are 20-22 mm. The height is normally 1m.

4.1.1 Density

The following table (Table 2) provides a feature of the increase of bulk density by using densification technology.

Table 2: Density of different samples tested at lab

Sample 1	Sample 2	Sample 3	Average	Rice husk (Raw)	Rice husk (Grinded)
1084.4 Kg/m^3	1109.34 Kg/m^3	1140.14 Kg/m^3	1111.3 Kg/m^3	147.64 Kg/m^3	279.07 Kg/m^3

4.1.2 Compressive Strength

Average compressive strength of the samples was found to be 10.7 MPa or N/mm^2. A briquette with higher compressive strength is safer for storage and transportation.

4.1.3 Thermal Properties

For understanding thermal properties of briquette a heated rod was inserted into the bore of briquette and then temperature reading was taken continuously after certain time intervals from the source, temperature at surface of briquette. Table 3 is given below to have a look of the thermal conduction through briquette. Then Fig. 5 is provided to show the temperature increasing with time.

Table 3: Data chart for rise in temperature with time.

Time (min)	0.00	5.00	10.00	15.00	20.00	25.00
Source temperature (^{0}C)	88	92	98	102	105	105
Briquette surface temperature (^{0}C)	35	37	39	40	41	42

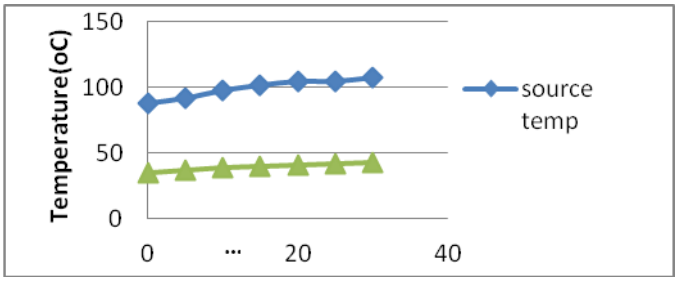

Fig. 5: Time vs. temperature curve

4.1.4 Water Absorbance

For water absorbance test, the samples were submerged under water at room temperature for certain duration of time and weight of the samples was taken at certain time intervals. This property would enable us the storage method of briquette. Table 4 and Fig. 6 are given below according to test result.

Table 4: Weight of different samples under water at various time periods

Time (minutes)	Sample 1 (Weight in grams)	Sample 2 (Weight in grams)	Sample 3 (Weight in grams)
00.00	216.94	136.8	231.3
01.00	239.70	151.70	287.2
02.00	250.55	170.69	310.85
03.00	255.30	182.75	318.17
04.00	264.11	192.2	327
05.00	269.1	200.18	330.96
10.00	277.36	206.5	335.6
15.00	288.86	211	345
20.00	292.12	204	345.95
25.00	294.00	209	352
30.00	298.77	212.9	345.89

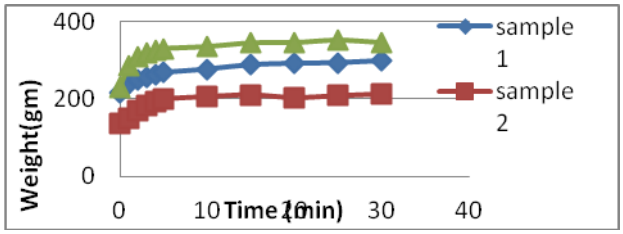

Figure 6: Weight vs. Time curve for water absorbance test

4.2 Fuel Properties

Briquette is a moderate quality fuel for cooking and other purpose. It can be ignited easily and burns with a long and steady flame, low smoke and almost no odor. It also has a high burning efficiency. As before for testing fuel properties two samples were taken from Sylhet (sample 1) and Khulna (sample 2). For comparison rice husk was from Gazipur was also tested. All experiments were done in atmospheric pressure and room temperature and humidity. The sample grade size was 60 (250 microns).

4.2.1 Proximate Analysis

A proximate analysis, as defined by ASTM, is the determination by prescribed methods of moisture, volatile matter, fixed carbon (by difference) and ash. The sample of 60 grades was heated 107^0C, 750^0C and 950^0C accordingly to determine the moisture, ash, volatile and fixed carbon contents. The composition of biomass briquette is given in following figure (Fig. 7).

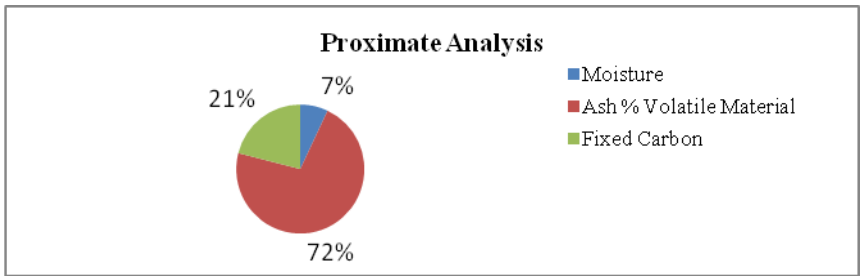

Fig. 7: Average composition in %

4.2.2 Carbon Residue

The carbon residue of a fuel is the tendency to form carbon deposits under high temperature conditions in an inert atmosphere, and may be expressed commonly as Micro Carbon Residue (MCR). The carbon residue provides information on the carbonaceous deposits which will result from combustion of the fuel.

Table 5: Data chart for Carbon Residue

Sample 1 (%)	Sample 2 (%)	Average value (%)	Rice husk (%) (Gazipur)
42.39	41.42	42.6	40

4.2.3 Calorific Value or Heating Value

Calorific value determines the heat energy produced during combustion. The calorific value of briquette was tested in a bomb calorimeter. The calorific value found during testing is given in following Table 6.

Table 6: Data chart for Calorific Value

Sample 1	Sample 2	Average value	Rice husk (Gazipur)
4300 cal/gm or 18 Kj/gm	4580 cal/gm or 19.7 KJ/gm	4250 – 4600 cal/gm	4270 cal/gm 17.87 KJ/gm

5. Field Survey

The survey was conducted in four different locations of the country namely Kawran bazaar, Shavar, Joypurhat and Bagerhat. Several users of biomass fuel were interviewed in the selected locations and their opinions have been listed understanding the reasons behind the rapid development of biomass briquette and its possible further development. In Table 7, the user comments on briquette found by survey are given and the graphical representation of briquette price and cost is given in Fig. 8.

Table 7: Highlights of user review on use of Briquette

User no & Location	User type	Period of use (years)	List of Advantages				
			Easy to use	Easy storage	Low cost	No smoke & odor	Good fuel properties
User 1, Kawran Bazaar	Commercial	2	Y	N	N	N	Y
User 2, Shavar	Commercial	7	Y	Y	Y	N	Y
User 3, Bagerhut	Commercial	10	Y	Y	Y	N	N
User 4, Joypurhut	Commercial	2.5	Y	N	Y	N	N
User 5, Joypurhut	Residential	2.5	Y	N	N	Y	Y

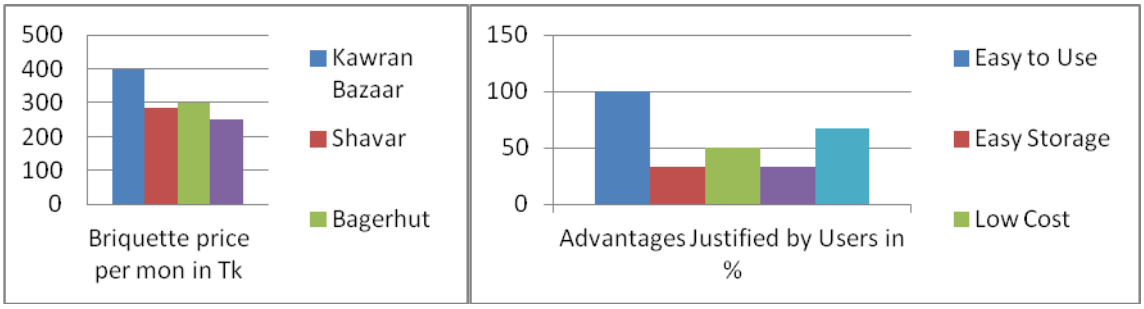

Fig. 8: (a) Briquette price at different regions of the country; (b) Advantages supported by users in %

6. Conclusion

Biomass briquetting technology has immense potential in an agricultural country like Bangladesh. The technology allows effective use of the residues which otherwise would have been used inefficiently or wasted. There is scope for development in this sector by researching for more effective ways to use bio fuel and make it more environment and user friendly. For this, the assistance of the government is must. It can be replaced the other traditional fuels.

Acknowledgements

For this study on briquette, we are grateful to the Head of Me department of BUET and MIST to permit us to use the labs such as fuel testing lab, solid mechanics lab. We are also grateful to those lab technicians helped us in testing.

References

[1] H. Islam, M. Hasan, T. A. Siddique, "A Study of Biomass Briquette in Bangladesh" B.Sc. thesis, MIST, Bangladesh, 2011.
[2] M. M. Alam, H. Islam, M. Hasan, T. A. Siddique, "**A Study of Biomass Briquette in Bangladesh**", in proc. of the 9th International Conference on Mechanical Engineering (ICME 2011), BUET, Dhaka, Bangladesh, 18-20 December, 2011, PI-RE-02.
[3] M. M. Alam, H. Islam, M. Hasan, T. A. Siddique, "**A Study of Biomass Densified Fuel (Briquette) in Bangladesh**", in the proc. of the 1st International Conference on Mechanical Engineering & Renewable Energy (ICMERE 2011), CUET, Chittagong, 22-24 December, 2011, PI-214.
[4] Md. Ahiduzzaman, Production and use of densified biofuel in Mymensingh district (Bangladesh) under

technical and socio-economical respect, M.sc. thesis, University of Flensburg, Germany, 2006.

5th BSME International Conference on Thermal Engineering

Numerical Study of Double-diffusive Natural Convection in a Triangular cavity

M. Borhan Uddin[a]*, M.J.H. Munshi[b], M.M. Rahman[c], M.K. Chowdhury[c]

[a]*Department of Basic Science, World University of Bangladesh, Dhanmondi, Dhaka-1205, Bangladesh*
[b]*Department of Mathematics, Hamdard University Bangladesh, Gozaria, Munshiganj, Bangladesh*
[c]Department of Mathematics, Bangladesh University of Engineering and Technology, Dhaka-1000, Bangladesh

Abstract

This paper concerned with the numerical study of thermal and mass diffusive natural convection flow inside a triangular shape solar collector using finite element method for the governing equations expressing the velocity pressure formulation along with the energy and concentration balance equations. In the solution procedure, the isothermal and iso-concentration boundary conditions are assumed at the absorber and covers of collector. Local and mean heat and mass transfer rates for the thermal Rayleigh number and Lewis number are presented. Streamlines, isotherms and iso-concentration are also presented for the aforesaid parameters. The result found in this study fully agreed with the previous published work. But this result will be profitable for the design of the collector.

Keywords: Solar collector; natural convection; finite element method; absorber.

1. Introduction

Finite element method techniques are widely used in problems of consisting of complex geometry and partial differential equations. In this method of analysis, the considered domain is discretized into simple geometric shapes called finite elements. The materials property and the governing relationships are considered over these elements and expressed in terms of unknown values at element corner. An assembly process duly considering the loading and constraints, results in a set of equations. Solution of these equations gives us the approximate behavior of the continuum. Thompson [1] discusses solution of partial differential equations involved in areas such as Fluid Mechanics, Elasticity and Electromagnetic Field by using FEM. Details about fluid mechanics and heat transfer problems and their solution can be found in [2]. A more complex transient heat conduction equation is discussed in Winget and Hughes [3].

Natural convection flow and heat transfer in different geometrical enclosures such as triangular, square, rectangular and trapezoidal enclosures etc. which are the main piece of solar energy system, have been the topic of many research engineering studies. These studies consist of various technological applications such as solar collectors, building heating and ventilation, cooling electronically devices [4-6]. Double-diffusive natural convection occurs within the solar collector, owing to the collective thermal and mass diffusion buoyancy effects as well as the temperature difference between cover and absorber. Nowadays, the study of solar collectors is one of the most significant works to progress their performance with a competitive price [7]. Numerical solution has the advantage over an experimental investigation in that the important parameters, such as geometrical dimensions, glass thickness and covenant location may be simply changed. Therefore, its persuading on the overall heat and mass transfer can be studied at a low price. Numerical investigation is also helpful in testing the performance of solar collectors for different components.

Several experiments and theoretical investigations have been undertaken in this region. Boukar and Harmim [8] experimentally investigated design parameters of an indirect vertical solar still. Omri et al. [9] examined the thermal exchange by natural convection and effect of buoyancy force on flow structure. The authors provided useful information on the flow structure sensitivity to the governing parameters, the Rayleigh number and the tilt angle on the thermal exchange. Omri [10] numerically studied the flow characteristics inside an asymmetrical triangular still for the configuration optimization. Gao et al. [11] performed a study on natural convection inside

* Corresponding author. Tel.: +8801721109412; fax: +880-2-8613046.
E-mail address: mbuborhan@gmail.com

the wavy and inclined solar collectors, but they did not consider flow behavior and thermal fields. A numerical experiment is performed for inclined solar collectors by Varol and Oztop [12].

Different types of solar still available in the literature are conventional solar stills, single-slope solar still with passive condenser, double condensing chamber solar still [13], vertical solar still [14], the inverted absorbers solar still [15] and multiple effect solar still [16]. The heat transfer inside the isosceles triangular enclosure is studied by Varol et al. [17–19] for different thermal boundary conditions, including entropy generation. Double-diffusive natural convection inside an isosceles triangular solar collector was discussed by Rahman et al. [7]. In their study, the considered fluid inside the cavity was air with Pr = 0.71 and taking Lewis number was fixed at Le = 2.0. In this paper, natural convection heat and mass transfer in a triangular shaped enclosure for different Lewis and Rayleigh number are thoroughly studied.

Nomenclature

B_r	buoyancy ratio	T_h	hot wall temperature (source)
C	concentration of species	T_L	cold wall temperature (sink)
C_h	high species concentration (source)	u, v	dimensional velocity components
C_L	high species concentration (sink)	U, V	dimensionless velocity components
$C^{'}$	dimensionless species concentration	x, y	dimensional coordinates
D	species diffusivity	X, Y	dimensionless coordinates
g	gravitational acceleration	*Greek symbols*	
H	enclosure height	α	thermal diffusivity (m^2s^{-1})
Le	Lewis number	B_T	thermal expansion coefficient
Nu	Nusselt number	β_c	compositional expansion coefficient
p	dimensional pressure (Nm^{-2})	μ	dynamic viscosity (Kg $m^{-1}s^{-1}$)
P	non-dimensional pressure	ν	kinematic viscosity (m^2s^{-1})
Pr	Prandtl number	θ	non-dimensional temperature
Ra	Rayleigh number	ρ	density
Sh	average Sherwood number	Ψ	Stream function
T	temperature (K)	Γ	general dependent variable

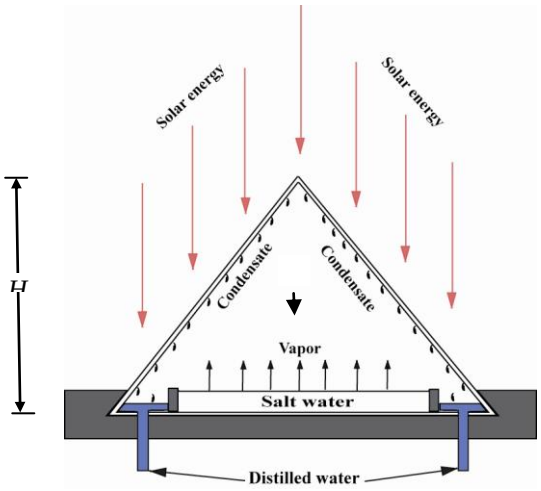

Fig. 1. Schematic diagram for the problem

2. Problem Statement

2.1. Physical description

The physical phenomenon of the considered domain is shown below. A triangular shaped solar collector is considered here. The enclosed space consists mostly of an absorber plate and two inclined glass covers that form a cavity. The absorber plate is represented by a horizontal bottom wall kept to a constant temperature T_h while the inclined walls are considered transparent and maintained at a constant temperature T_L with $T_h > T_L$.

2.2. Mathematical formulation

The governing equations for the problem under consideration are based on the balance laws of mass, momentum and thermal energy in two dimensions. Following the previous assumptions, these equations can be written in non-dimensional form as:

$$\frac{\partial U}{\partial X}+\frac{\partial V}{\partial Y}=0 \tag{1}$$

$$U\frac{\partial U}{\partial X}+V\frac{\partial U}{\partial Y}=-\frac{\partial P}{\partial X}+\mathrm{Pr}\left(\frac{\partial^2 U}{\partial X^2}+\frac{\partial^2 U}{\partial Y^2}\right) \tag{2}$$

$$U\frac{\partial V}{\partial X}+V\frac{\partial V}{\partial Y}=-\frac{\partial P}{\partial Y}+\mathrm{Pr}\left(\frac{\partial^2 V}{\partial X^2}+\frac{\partial^2 V}{\partial Y^2}\right)+Ra_T\,\mathrm{Pr}(\theta+BrC) \tag{3}$$

$$U\frac{\partial \theta}{\partial X}+V\frac{\partial \theta}{\partial Y}=\frac{\partial^2 \theta}{\partial X^2}+\frac{\partial^2 \theta}{\partial Y^2} \tag{4}$$

$$U\frac{\partial C}{\partial X}+V\frac{\partial C}{\partial Y}=\frac{1}{Le}\left(\frac{\partial^2 C}{\partial X^2}+\frac{\partial^2 C}{\partial Y^2}\right) \tag{5}$$

where the dimensionless variables are introduced as:

$$X=\frac{x}{H},Y=\frac{y}{H},\mathrm{U}=\frac{\mathrm{uH}}{\nu},\mathrm{V}=\frac{\mathrm{vH}}{\nu},\mathrm{P}=\frac{(\mathrm{p}+\rho\mathrm{gy})\mathrm{H}^2}{\rho\nu^2},\theta=\frac{T-T_L}{T_h-T_L},C=\frac{c-c_L}{c_h-c_L} \tag{6}$$

The variables have their usual sense in fluid mechanics and heat transfer as listed in the nomenclature. It can be seen from the Eqs. (2) - (5), five parameters that preside over this problem are the Prandtl number (Pr), the thermal Rayleigh number (Ra_T), Lewis number (Le) and buoyancy ratio (Br), which are defined respectively as

$$\mathrm{Pr}=\frac{\nu}{\alpha},Ra_T=\frac{g\beta_T(T_h-T_L)H^3}{\alpha\nu},Le=\frac{\alpha}{D},Br=\frac{\beta_c(c_h-c_L)}{\beta_T(T_h-T_L)} \tag{7}$$

The dimensionless boundary conditions corresponding to the considered problem are as follows

on the bottom wall: $U=V=0,\theta=C=1$

on the inclined walls: $U=V=0,\theta=C=0$

The local heat and mass transfer rates on the surface of heat and contaminant sources are defined respectively as

$$Nu=-(\frac{\partial\theta}{\partial Y})_{Y=0} \quad \text{and} \quad Sh_x=-(\frac{\partial c}{\partial Y})_{Y=0}$$

The average heat and mass transfer rates on the surface of heat and contaminant sources can be evaluated by the average Nusselt and Sherwood numbers, which are defined respectively as

$$Nu=-\int_0^1\frac{\partial\theta}{\partial Y}dX \tag{8}$$

and

$$Sh=-\int_0^1\frac{\partial c}{\partial Y}dX \tag{9}$$

The stream function is calculated from

$$U=\frac{\partial\psi}{\partial Y},V=-\frac{\partial\psi}{\partial X} \tag{10}$$

3. Numerical Solution

3.1. Solution procedure

The Gelarkin weighted residual technique of finite element method is used in this task. In the finite element method, the region of interest can be discretized using different types of element shapes and sizes, called elements. The dependent variables are then approximate over these elements. In this study, the triangular

element is considered. Using FEM, the governing Eqs (2-5) are transferred into a set of algebraic equations. The system of algebraic equations is solved using iterative method. The iterative process is continuing until the following convergence condition is satisfied: $|\Gamma^{i+1} - \Gamma^{i}| \leq 10^{-6}$ where i is the number of iteration and Γ is the general dependent variable.

3.2. Grid refinement checks and code validation

In FEM solution procedure, the accuracy of the numerical result can be enhanced by using either higher order elements or increasing the number of elements. The number of elements is increased to get the desired accuracy as well as to get the grid independent solution of this study. A trial calculation is made using various non-uniform grids of triangular elements: 1486, 3396, 4590 and 5112 in order to obtain the desired grid independent solutions. The calculation of average Nusselt number and Sherwood numbers are carried out using $RaT = 10^6$, Pr = 0.71 and Br = 10.0 for these five non-uniform grid. Finally, the grid size of about 3396 elements was chosen through this study for the balance between the calculation accuracy and the speed. The study is compared with an earlier work performed by Kent et al. [20] and found a good agreement which ensure the code validation of this analysis. The comparison result is shown in fig-2.

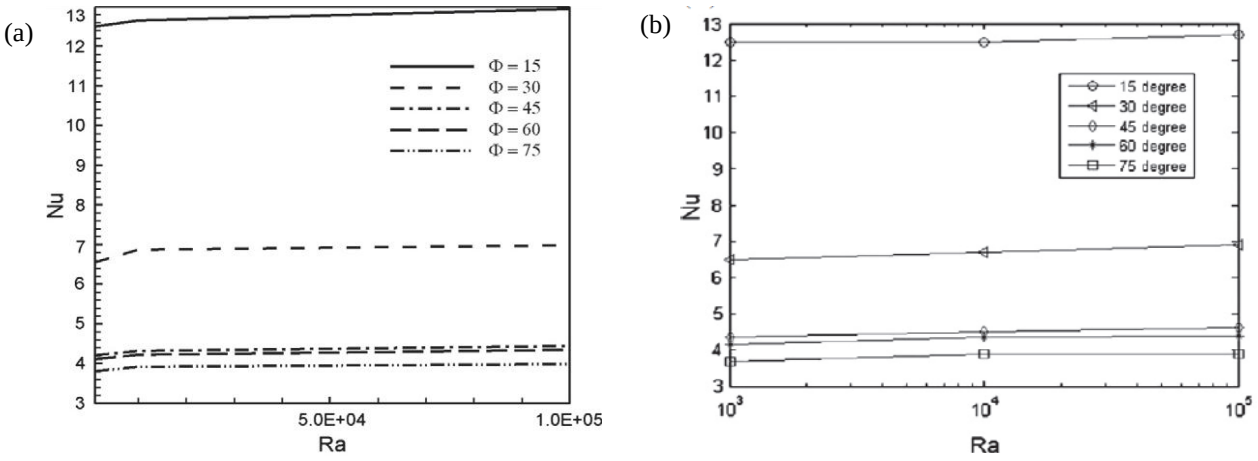

Fig-2. Comparison of the (a) present model with (b) the results of Kent [20] for natural convection inside a isosceles triangular enclosure for five different base angles.

4. Results and discussion

A computational analysis has been performed to investigate the effects of Lewis number on natural convection inside an isosceles triangular solar collector using Gelarkin weighted residual finite element technique. Air was used inside the cavity as a working fluid with Pr = 0.71.The effective parameters are buoyancy ratio, Rayleigh number, Lewis number etc. The buoyancy ratio and Rayleigh number were considered fixed at Br=10 and $Ra = 10^6$ throughout this analysis.

Fig-3 demonstrates the effect of Lewis number on streamline, isotherm and iso-concentration. As seen from the figures, symmetric flow distribution is observed inside the cavity according to the middle axis of the triangle. In the case of stream lines for low Lewis number, the number of circular cell trends to increase. But due to the increase of Lewis number from 1.0 to 10.0, there are only two circular cells inside enclosure and the strength of flow increases. The left cell rotates counterclockwise while the right cell rotates clockwise. In the case of temperature distribution, convective distortion of the isotherms occurs throughout the cavity due to the strong influence of the convective current in the cavity. It is evident that flow of the temperature increases with increase of Lewis number. A similar distribution of iso-concentration exhibits with increase of Lewis number.

Fig-4 illustrates the average heat transfer rate with the increase of Lewis and Rayleigh number. Average heat transfer increases from 0.1 to 1.0 and shows decreasing trends from 1.0 to 10 with increase of Lewis and Rayleigh number. But in the case of average mass transfer, it exhibits speedily increases with increase of Lewis and Rayleigh number which shows in fig-5.

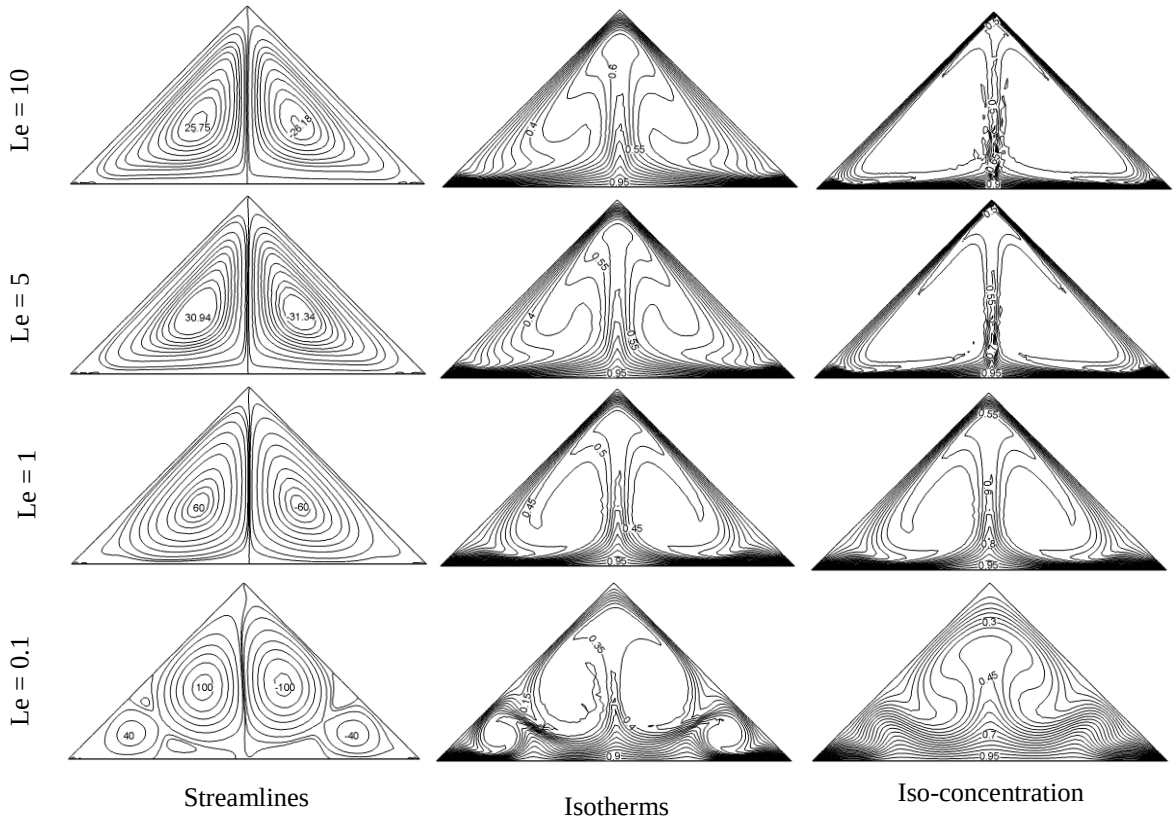

Fig. 3. Effect of Lewis number on streamlines, isotherms and iso-concentration, while Ra = 10^5

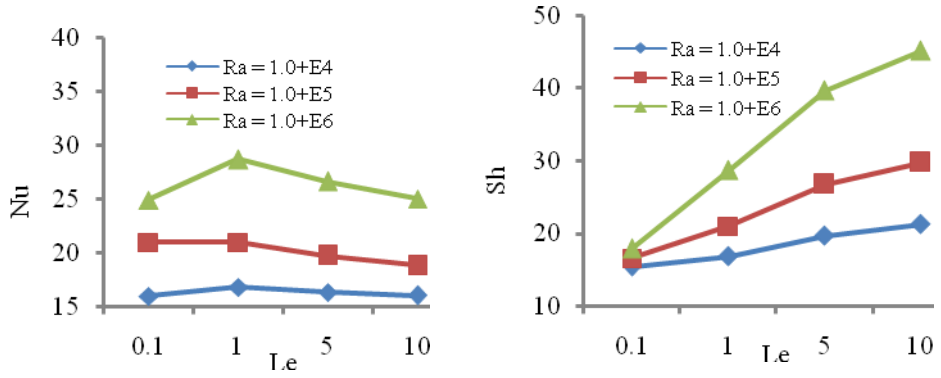

Fig-4 Effect of Lewis number on average Nusselt number (Nu) and average Sherwood number (Sh)

5. Conclusions

This numerical study concerned with the fluid flow, heat transfer and mass transfer inside triangular shaped solar collectors. The results are obtained for different values of Lewis and Rayleigh numbers. It is observed that mass transfer increases with increase of Lewis and Rayleigh numbers and formed symmetric flow field, temperature distribution and mass distribution according to the middle axis of the triangular cavity. But the heat transfer at first increases and then decreases with the increases of Lewis and Rayleigh numbers and formed symmetric flow field, temperature distribution and mass distribution according to the middle axis of the triangular cavity

Acknowledgements

The authors like to express their gratitude to the department of mathematics, Bangladesh University of Engineering and Technology (BUET).

References

[1] Thompson, Erik G., Introduction to the Finite Element Method: Theory Programming and Applications, John Wiley & Sons Inc, 2004
[2] Bejan A, Convection Heat transfer, John Wiley and Sons Inc, 1984
[3] Winget J. M, Hughes T.J.R., Solution algorithms for nonlinear transient heat conduction analysis employing element by-element iterative strategies, Computer Methods in Applied Mechanics and Engineering, 1985; 52:711–815.
[4] B. Gebhart, Y. Jaluria, R.L. Mahajan, B. Sammakia, Buoyancy induced Flows and Transport, Hemisphere, Washington, DC, 1988.
[5] G. De Vahl Davis, I.P. Jones, Natural convection of air in a square cavity: a comparison exercise, Int. J. Numer. Methods Fluids 3 (1983) 227–248.
[6] S. Ostrach, Natural convection in enclosures, J. Heat Transfer 110 (1988) 1175–1190.
[7] M. M. Rahman et al, Double-diffusive natural convection in a triangular solar collector, International Communications in Heat and Mass Transfer 39 (2012) 264–269
[8] M. Boukar, A. Harmim, Design parameters and preliminary experimental investigation of an indirect vertical solar still, Desalination 203 (2007) 444–454.
[9] A. Omri, J. Orfi, S.B. Nasrallah, Natural convection effects in solar stills, Desalination 183 (2005) 173–178.
[10] A. Omri, Numerical investigation on optimization of a solar distiller dimensions, Desalination 206 (2007) 373–379.
[11] W. Gao, W. Lin, E. Lu, Numerical study on natural convection inside the channel between the flat-plate cover and sin-wave absorber of a cross-corrugated solar air heater, Energy Conversion Management 41 (2000) 145–151.
[12] Y. Varol, H.F. Oztop, Buoyancy induced heat transfer and fluid flow inside a tilled wavy solar collector, Building and Environment 42 (2007) 2062–2071.
[13] G.N. Tiwari, A. Kupfermann, S. Agrawal, A new design of double condensing chamber solar still, Desalination 114 (1997) 153–164.
[14] J.P. Coffey, Vertical solar distillation, Solar Energy 17 (1975) 375–378.
[15] S. Suneja, G.N. Tiwari, Optimization of number of effects for higher yields from an inverted absorber solar still using the Runge–Kutta method, Desalination 120 (1999) 197–209.
[16] H. Tanaka, T. Nosoko, T. Nagata, Parametric investigation of a basin type multiple effect coupled solar still, Desalination 130 (2000) 295–304.
[17] Y. Varol, A. Koca, H.F. Oztop, Natural convection in a triangle enclosure with flush mounted heater on the wall, International Communications in Heat and Mass Transfer 33 (2006) 951–958.
[18] Y. Varol, H.F. Oztop, I. Pop, Entropy generation due to natural convection in non-uniformly heated porous isosceles triangular enclosures at different positions, International Journal of Heat and Mass Transfer 52 (2009) 1193–1205.
[19] Y. Varol, H.F. Oztop, I. Pop, Influence of inclination angle on buoyancy-driven convection in triangular enclosure filled with a fluid-saturated porous medium, Heat Mass Transfer, 44, Springer, 2008, pp. 617–624.
[20] E.F. Kent, Numerical analysis of laminar natural convection in isosceles triangular enclosures for cold base and hot inclined walls, Mechanics Research Communications 36 (2009) 497–508.

5th BSME International Conference on Thermal Engineering

Detection of fire through smoke and temperature analysis with an automatic extinguishing system

Yamin Rekhu[a],Md.Arifuzzaman[b *]

[a]*Military instiitute of science and technology,Mirpur,Dhaka-1216,Bangladesh.*
[b]*Univrsity of information technology and sccience,Gulsan,Dhaka-1212,Bangladesh.*

Abstract

Accident due to fire is a common phenomenon now a day. The domestic environment accounts for majority of fire related deaths. It can take place anywhere and anytime whether in the slums or in the high-raised buildings. It causes heavy loss of life and property. Taking some precaution and necessary steps can minimize this loss. Considering the problem we designed an automatic fire detection and preventive system to detect smoke and heat. Thereby get prevention. It is designed to detect the presence of fire in a room through smoke and heat detection. When a significant amount of smoke and heat will generate. It will raise the alarm and take preventive action if required. In this system heat was detected by RTD and smoke was detected by optical sensor. The density of fire can be detected by optical sensor through regulating resistance of the optical sensor. By setting designed resistance, a siren was controlled to generate an alarm. So the smoke from kitchen or cigarette not hampers the system as density of smoke was controlled. In the other hand temperature was detected By an RTD. Through a temperature controller the output signal of temperature was detected by an RTD .Through a temperature controller the output signal of temperature was controlled. At a set temperature it switches the solenoid valve for water spraying. We designed the system for ordinary fire (fire category-A). So when set temperature reached to the detected temperature then a pump sprayed water to extinguish the fire .The important outcome of the system was detection of both smoke and temperature. By accumulating both signal fire type (A, B, C & D) can be detected and actual automatic preventive system can be taken .The whole system fully fireproof and own electrical power system. Calibration was done by varying different criteria and some systems parameters was calculated like systems active area calculation, temperature range calculation and smoke density (in terms of voltage fluctuation). The system was very cheap in price, can be used both in industry and home.

Keywords: smoke, RTD, optical sensor, fire category, active area.

1. Introduction

This fire alarm system can detect both smoke and heat. As in case of fire in a certain place both the heat and smoke can be generated, our fire alarm system can sense automatically any of this fire property and will raise the alarm. In the market we have seen a lot of fire alarm system. But they are very expensive. Another thing is that most of the fire alarm system cannot be turned off by the user while doing any kind of fire related works in the room or certain place. Considering this in our mind we have designed it such a way that it can be turned off or on whenever a user wants. Moreover, the available fire alarm system cannot fight the fire i.e. they can only detect the presence of fire and there is no system to extinguish the fire (1). But our fire alarm system can also extinguish the fire by spraying water into the room. We have made a cheaper fire alarm system. We made it simple, easy to use and efficient fire alarm system with smoke and temperature detection**.**

* Corresponding author. Tel.:+08801717531449; fax: 88-02-8899531
E-mail address: rekhu.mist@gmail.com

1.1 Basic components

In this project we have used two types of components: Mechanical components & Electrical components. Mechanical components mainly responsible for water spraying and electrical side detects smoke and raise alarm. Another function of the electrical system is to control temperature signal.

1.2 Mechanical Components

Mechanical section is divided in two parts smoke detection set up and water spraying unit. For making smoke detection setup we have used a funnel. It has larger cross-sectional area at lower part and smaller at upper part. For this there is a pressure difference at two positions. So smoke created at lower part can easily pass through the funnel as there is lower pressure at upper portion of funnel. We add a pipe with the funnel to take the smoke to the smoke detection box. When the system is activated the optical switch is switched on and gives light of constant intensity (2).

For this fixed light optical switch has a fixed value of resistance. When smoke go through the duct there is change of intensity of light. So optical switch shows higher resistance. For the change of resistance in a certain value system make alarm. Upper part of funnel is tapper. We added a small length of pipe making it curved by heating, so as external light source cannot effect at our system light source.

For making water spraying system we placed a solenoid valve with controller. This valve can control water supply. Controller is connected with main circuit output and with 220V ac supply. We placed a water reservoir at a certain height and from this we made a water line with pipe and connected to the solenoid valve. When controller gets voltage from main circuit it activates the solenoid valve and there is a water flow through pipe. At the end of pipe we used a small shower. By making some small holes we made it to increase the target area for watering.

Fig.1. solenoid valve, smoke duct and water spraying element.

1.3 Electrical Component

Electrical components together responsible for generating electrical signal from smoke to control fire alarm and temperature detection. We used RTD for temperature detection.RTD-Resistance thermometers, also called resistance temperature detectors or resistive thermal devices (RTD), are temperature sensors that exploit the predictable change in electrical resistance of some materials with changing temperature. As they are almost invariably made of platinum, they are often called platinum resistance thermometers (PRT)(3,4). They are slowly replacing the use of thermocouples in many Industrial applications below 600 degree Celsius due to higher accuracy and repeatability.

Resistance thermometers are constructed in a number of forms and offer greater stability, accuracy and repeatability in some cases than thermocouples. While thermocouples use the Seebeck effect to generate a voltage, resistance thermometers use electrical resistance and require a power source to operate. The resistance ideally varies linearly with temperature.

A photoelectric sensor, or photo eye, is a device used to detect the distance, absence, or presence of an object by using a light transmitter, often infrared, and a photoelectric receiver. They are used extensively in industrial

manufacturing. There are three different functional types: opposed (a.k.a. through beam), retro reflective, and proximity-sensing(5).

We used temperature controller to controlling the temperature signal.Temperature controller is used to accurate the control process of temperature without extensive operator involvement; a temperature control system relies upon a controller, which accepts a temperature sensor such as a thermocouple or RTD as input. It compares the actual temperature to the desired control temperature, or setpoint, and provides an output to a control element. The controller is one part of the entire control system, and the whole system should be analyzed in selecting the proper controller(6).

We used a relay and rectifier for smoke signal. A **relay** is an electrically operated switch. Many relays use an electromagnet to operate a switching mechanism, but other operating principles are also used. Relays find applications where it is necessary to control a circuit by a low-power signal, or where several circuits must be controlled by one signal (7).

Rectifier is an electrical device that converts alternating current (AC) to direct current (DC), a process known as rectification. Rectifiers have many uses including as components of power supplies and as detectors of radio signals. Rectifiers may be made of solid state diodes, vacuum tube diodes, mercury arc valves, and other components. As our optical switch is dc current operated, so we need rectification.

2. working principle

This project has two working unit which are independent of each other. Units are –Smoke detection unit with alarm system & Temperature detection with water spraying system.

2.1 Smoke detection unit with alarm

Optical switch used in the system was 24dc volt operating system. Source (220volt AC) turns into 24 dc by a rectifier. Firstly smoke comes through a funnel to optical switch box. There the optical switch gives a week signal when smoke goes into smoke box. As the signal is so week Relay makes the signal to higher voltage signal. Alarm switches when it get signal from the relay. Optical switch signal can be controlled through resistance controller. That ensures the control of smoke.

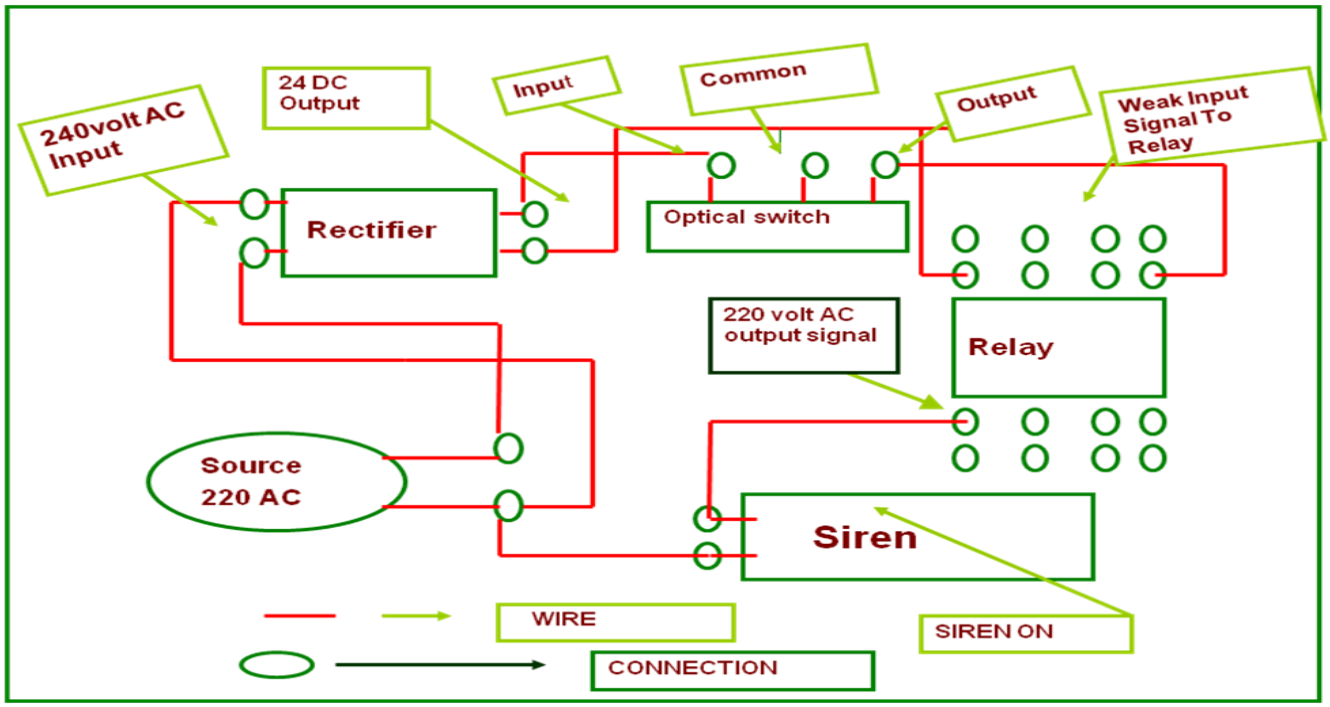

Fig .2 .Smoke detection circuit diagram

2.2 Temperature detection with water spraying system

Firstly the RTD sense the temperature. It is connected with a controller. Controller also connected with the solenoid valve. We set a temperature in controller. When the sensing temperature goes to setting temperature then a signal sends to the solenoid valve and finally the valve switch on.

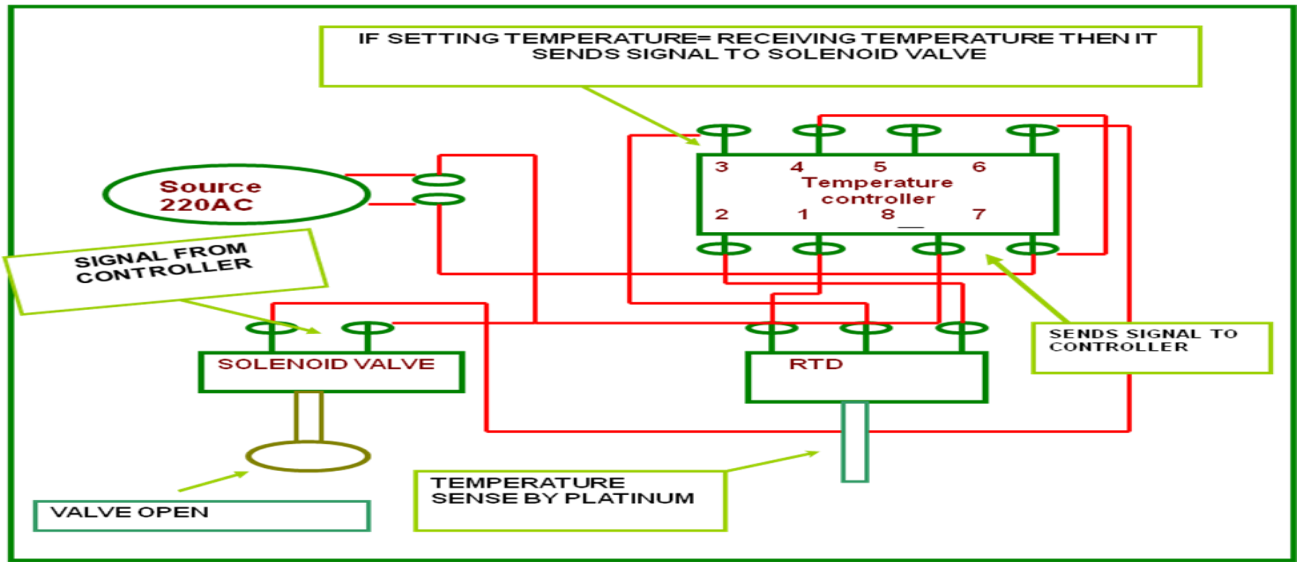

Fiq. 3. Circuit diagram of Temperature detection unit.

3. Calibration

Calibration was done to ensure the system's capacity and limitations. Two types of calibration were done. Optical switch area and Temperature controller accuracy were tested.

3.1 optical switch active areas

To calibrate the optical switch we set resistance setting in three position and create smoke of similar type at three position and take the relay or siren data to ensure its active area.

Table .1: calibration of optical switch

Distance (inch)	Stability setting	Signal to relay /siren
2	max	on
6	max	on
12	max	on
18	max	on
24	max	on
30	max	on
36	max	off
10	moderate	on
15	moderate	on
24	moderate	off
8	min	on
12	min	on
14	min	off

3.2 calibration of RTD accuracy

To test the accuracy of RTD and temperature controller we set a temperature for pump to spray water and took temperature reading when it actually give the signal to start the pump .

Table .2: calibration of RTD accuracy

Setting temperature (degree)	Circuit cut at (degree)	Solenoid valve condition
20	20	on
30	30	on
40	40	on
50	52	on
70	71	on
100	98	on
120	121	on

4. Analysis of the system

The designed system can detect smoke within its 12 inch from its set place of optical switch and special system was done by a funnel to reach the smoke easily into smoke box .so alarm switches quickly. RTD has high operating range and controller accuracy was high.

We have taken two independent systems to detect fire. Smoke sensing unit gives alarm for any kind of smoke. It may be due to fire or others like kitchen smoke. But the water spray will not on. Until it reaches the set temperature. If we use a single system for the project by using latch circuit then the system completely depends on temperature unit. Here then smoke will not a factor rather temperature turns the main and only on factor. In this case we get an alarm in every types of smoke like it may be from cigarette or kitchen that's helps us to be alert about the fire. So we think independent unit is better than latch circuit.

5. Conclusion

In Bangladesh we have seen that fire related accident is very common .Due to fire accident not only we losses life but also huge amount of property also. So strong preventive measurement should be taken to reduce fire related accident .This project was a small initiative after utilizing the fact. We explored through the market and search the fire detection system .we found weak systems with low capacity based. We designed the system with available devices, made it cheap and user-friendly. Automatic system was added to ensure the right action during fire.

6. References

1. W.K. Chow, N.K. Fong and C.C. Ho, "Analysis of unwanted fire alarm: case study", Journal of Architectural Engineering, pp. 62-65, June (1999).
2. M. Tuillard, "New methods for reducing the number of false alarms in fire detection systems", Fire Technology, Second Quarter, pp. 250-268 (1994).
3. Y. Okayama, "A primitive study of a fire detection method controlled by artificial neural net", Fire Safety Journal, Vol. 17, pp. 409-432 (1991).
4. C.Y. Yau, "A study on neural network for reducing false alarm in automatic fire detection system", 25th Anniversary Commemorative Magazine, pp. 95-104 (2000).
5. G. Pfisher, "Multisensor fire detection: a new trend rapidly becomes state of the art", Fire Technology, Vol. 33, pp. 115-139 (1997).
6. BRE information paper, IP13/92, Building Research Establishment, June (1992).
7. BS 5839-1:2002, Fire detection and fire alarm systems for buildings - Part 1: Code of practice for system design, installation, commissioning and maintenance

5th BSME International Conference on Thermal Engineering

Investigation of improved aerodynamic performance of isolated airfoils using CIRCLE method

M U Ahmed[a], E J Avital[a], T Korakianitis[a,b] *

[a]*School of Engineering, Queen Mary University of London, London E1 4NS, UK*
[b]*Parks College of Engineering, Aviation and Technology, Saint Louis University, Missouri 63103, USA*

Abstract

The PresCrIbed suRface Curvature distribution bLade dEsign (CIRCLE) method, proposed by T Korakianitis, is a direct method for designing (or redesigning) high efficiency turbomachinery and fan blades, and isolated airfoils. It was initially introduced to improve the design of high efficiency turbomachinery blades. It is now extended for use with 2D and 3D turbomachinery blades and isolated airfoils. The connection of the profile's leading edge (LE) to the trailing edge (TE), on both sides, is defined using continuity in the surface curvature and its derivatives. Improvements to the aerodynamic performance of the Eppler airfoil are presented in this paper. Improved geometries with continuous curvature have been produced using the CIRCLE method. The performances of Eppler and the redesigned A5 and A6 have been studied using CFD analysis. They are analyzed considering low subsonic flow condition (Reynolds number~10^5). These are compared to a previous airfoil A4. The redesigned blades' LE proved favorable as they succeeded in removing pressure 'spikes' on the suction side. Comparative analysis with the original results showed significant aerodynamic improvements. Airfoils A4, A5 and A6 have comparatively thicker TE section compared to Eppler. Despite the changes made to the geometry and continuous curvature distribution in A4, A5 and A6 (from Eppler), there appear a separated region on the suction side at about 60% of the chord downstream from the LE. The new blades exhibit higher aerodynamic efficiencies, in terms of overall lift-to-drag ratio up to 40% than the original. The investigations are performed at on and off design conditions.

Keywords: aerodynamics; blade; CIRCLE method; design;

Nomenclature

c_0, c_1…	thickness coefficients
C1,*C2*..	Bezier control points
C*=1/r*	curvature defined with its radius
k1,*k2*…	exponential thickness polynomials
M	Mach number
o	throat circle
p	pressure
P	points on airfoil
$C_{p/L/D}$	Co-efficient of pressure/lift/drag
Greek	
α	flow angle
β	blade surface angle
λ	stagger angle
ϕ	angle of throat diameter

Subscripts	
in	inlet station
o	stagnation point
ot	outlet station
p	pressure side
p2	pressure side TE circle to y1
pm	pressure side y1 to y2
pk	pressure side y2 to y3
p1	pressure side y3 to LE circle
s	suction side
s2	suction side TE circle to y1
sm	suction side y1 to y2
sk	suction side y2 to y3
s1	suction side y3 to LE circle

1. Introduction

Gas turbines have been among the most efficient energy conversion devices developed so far. Wind and hydro turbines have also secured a good place in the category. With increasing advancements in fluid dynamics and thermodynamics, the

* Corresponding author. Tel.: (314) 977-8283
E-mail address: korakianitis@alum.mit.edu (T. Korakianitis)

overall performances of these devices have enhanced [1]. One of the major components in these devices is the blade or airfoil [1]. They are placed in the fluid flow either to work on, or to extract work out of the flow. The blades operate under complex harsh conditions [2]. Blade design process, therefore, has a significant influence on the performance of the whole machine [3]. In general, 3D blade geometry is obtained by arranging 2D geometries along the center of gravity considering the associated limitations [3]. And the relevant 2D profiles are defined by streamlined curvature calculations based on the flow angles from hub to tip at the leading edge (LE) and trailing edge (TE) [3]. In order to make the design process simpler 3D blade cascades are considered to be 2D geometries placed in stream-wise direction [3, 4].

Performance of the blade profiles is expressed by blade surface and cascade passage property (such as Mach number, pressure, velocity, etc.) distribution along the chord [5]. Numerous techniques have been applied in blade designing, such as, direct method, inverse and semi-inverse method, optimization methods and etc. [5]. The objective of any method is to define the best profile which exhibits good aerodynamic and heat transfer performance with adequate structural integrity. This means disturbances upstream and downstream the profile should be minimized while complying with the constraints within the design conditions. For 3D profile generation, compromises are made to allow location of cooling and hollow passages. This paper presents a blade design approach using direct method. The process is defined by analyzing the aerodynamic performance of a specified blade profile. On the other hand, a typical inverse blade design method is defined as a method in which the preferred blade performance is defined and the geometry satisfying this performance is calculated [4].

Numerous works [3,4,6,7] have shown that it is difficult to obtain a desirable aerodynamic blade profile using inverse method. The inverse method has difficulties in both the LE and TE due to zero velocity at the stagnation points [3,4]. Inverse method can be applicable for generating compressor blades with very thin TE, but not to define a blade with thicker TE. Any blade which is designed with zero thickness TE becomes difficult to manufacture [4].

The work presented here, depicts a way of designing blades using PresCrIbed suRface Curvature distribution bLade dEsign (CIRCLE) method. It defines both turbomachinery and isolated profiles with continuous surface curvature and slope of curvature from the LE to TE for the suction and pressure sides. It can be used to design and redesign (improve) blades with higher efficiencies than their contemporaries, and can also be coupled with genetic algorithm based optimization method. CIRCLE method has evolved from a 2D turbomachinery blade design method to a 3D turbomachinery and isolated profile design method. Past studies [4,5] showed its applications in gas turbine blade redesign. Here the method's robustness in redesigning isolated wind turbine airfoils is presented. Following the global growing concern to switch to renewable energy source for the longevity of world's natural resources and environmental sustainability, wind turbine is one of the best choices for power plants. Results of redesigned wind turbine isolated airfoil, using CIRCLE method, is presented and discussed with few examples of other turbomachinery blades.

2. Background theory

The CIRCLE method defines each side of a 2D shape in three parts: *y1* near the LE; *y2* in the middle part of the surface; and *y3* near the TE. The stream-wise surface and slope of the curvature distribution is manipulated to optimize the aerodynamic performance. 2D shapes are designed near the hub, mean and tip regions and then the 3D shape is designed by maintaining continuity in the 2D parameters from hub to tip. This method does not use the traditional maximum thickness and maximum camber principles. It is guided by the surface pressure and Mach number distribution with their relation to continuous surface curvature distribution, and the outcome is the blade profile. Theoretical and experimental evidences presented in [5] show curvature and slope of curvature affects aerodynamic performance of blade profiles. Continuous slope of curvature requires continuous third derivative of the splines used in the method. It is illustrated in the following two equations for curvature ***C*** and slope of curvature ***C'***, where *y=f(x)* as:

$$C = \frac{1}{r} = \frac{y''}{\left[1+y'^2\right]^{\frac{3}{2}}} \tag{1}$$

$$C' = \frac{dC}{dx} = \frac{y'''\left[1+y'^2\right]-3y'y''^2}{\left[1+y'^2\right]^{\frac{5}{2}}} \tag{2}$$

Figure 1 depicts CIRCLE method's background and its modification for generating compressor and isolated profiles. The LE and TE shapes are circular geometries defined by their corresponding radii, and inlet and outlet flow angles α_1 and α_2 (Fig 1). Blade pitch plays an important parameter in turbomachinery profile while it is not used in isolated airfoils. Turbomachinery blades are set at their stagger angle λ (Fig 1a-c) while it is set to zero for isolated profiles. Turbomachinery blades are defined on the suction by the distribution of the flow area and the minimum area along the passage (Fig 1). The throat circle *o* and its angle ϕ determine the suction side blade control point P_{sm} and the corresponding blade angle β_{sm}. The corresponding input values for the pressure side control point P_{pm} and blade angle β_{pm} are arbitrary values. The P_{sm} and β_{sm}, for isolated airfoils, are independent of the passage area. The LE and TE circles are very difficult to connect with the other blade segments, as the circles have continuous curvature and rest of the surface have locally varying curvature. The TE radius and the λ locate the TE circle. The two sides disengage from the TE circle at P_{s2} and P_{p2}. This is controlled by β_{s2} and β_{p2}.

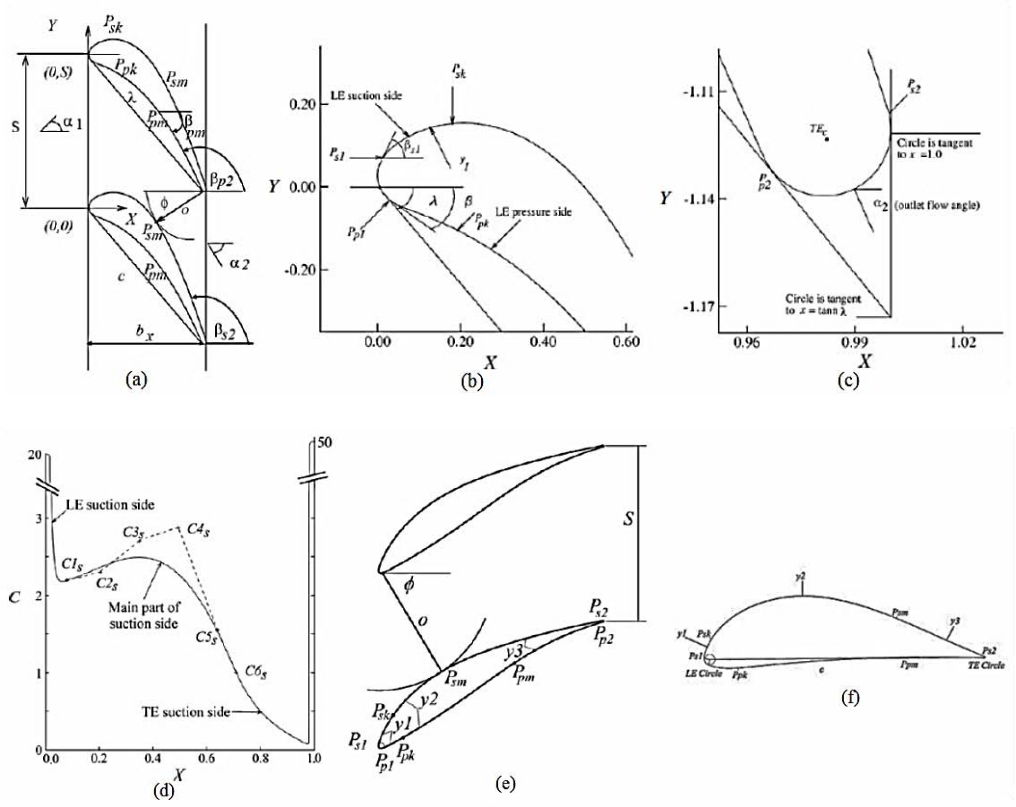

Fig. 1 CIRCLE method's blade geometry development process [3]

The TE segment *y3* from P_{s2} to P_{sm} is defined by an analytic polynomial *y=f(x)* of exponential form [5]:

$$y3 = f(x) = c_0 + c_1 x + c_2 x^2 + c_3 x^3 + c_4 k_1 [x - x(P_{s2})] + c_5 k_2 [x - x(P_{s2})] \quad (3)$$

where, k_1 and k_2 are exponential functions depending on P_{s2}. The six coefficients c_0 to c_5 are evaluated from the slope and other derivatives' continuity at P_{s2} and P_{sm}. The line segment *y2* between P_{sm} and P_{sk} is defined by mapping the curvature ***C*** vs *X* to the plane *Y* vs *X* using multiple point Bezier spline (e.g. Fig 1d). The curvature segment corresponding from P_{s2} to P_{sm} is evaluated from analytic polynomial *y1* using Eq. (3). It is plotted on the ***C*** vs. *X* plane, from the TE at X = 1.0 and to point $C6_s$ (Fig 1d). The slope of the curvature $\boldsymbol{C}_s(x)$ at point $C6_s$ is computed from Eq. (3) and becomes an input to further calculations. Using central difference Eq. (1) is written for curvature at airfoil point *I* as a function of *(x,y)*. Then the Bezier

spline is iteratively computed until the slope and the *y* coordinate at P_{sk}, and the shape of the curvature distribution matches reasonably. The LE circle similarly disengages at P_{s1} and P_{p1}, defined by β_{s1} and β_{p1}. Then a parabolic construction line *y* and a thickness distribution y_t are defined from the LE origin or circle center. They are defined to have continuous point and derivatives of the curvature at points P_{s1} and P_{sk}. For instance, construction line *y* may be defined as:

$$y = f(x) = Ax^2 + Bx + C \tag{4}$$

$$y_t = c_0 + c_1 x + c_2 x^2 + c_3 x^3 + c_4 k_{11}[x - x(P_{s1})] + c_5 k_{12}[x - x(P_{sk})] + c_6 k_{13}[x - x(P_{s1})] + c_7 k_{14}[x - x(P_{sk})] \tag{5}$$

where, k_{11}, k_{12}, k_{13} and k_{14} are exponential polynomials and are dependent on P_{s1} and P_{sk}. And similar to Eq. (3) the c_0 to c_7 are evaluated from the continuity in *y* and its derivatives at P_{s1} and P_{sk}. Thus the whole approach ensures that continuity of curvature and slope of curvature from the TE circle to the main part of the blade surface through the LE y_t and into the LE circle, for both surfaces of the blade. The control parameters C1, C2, C3 and C4 (Fig. 1) are specified smoothly to vary along the curvature's radius with the Bezier curves. Desired changes in 2D surface pressure or streamlines are compared with changes in 2D curvature distributions and the location of the 2D blade surfaces. After the first iteration (i.e. first geometric design and analysis) the user examines the resulting blade loading distributions, and decides where to alter local curvature and loading. After the second iteration the user gains an understanding of the magnitude of the required changes in curvature to cause the desired changes in Mach number or pressure distribution. The procedure is repeated until a desirable profile and aerodynamic performance are obtained.

3. 2D turbomachinery blade redesign

Performance of four redesigned cascades L25, L30, L35 and L40 was presented in [5]. For all cases, the cascades have been designed by changing the stagger angle while keeping the other variable constant. The computed results showed that increasing the λ, while keeping other parameters constant, results in thinner and more front loaded cascades. As λ increases, the *o* pushes both the blade surfaces farther down. This located the throat of the blade farther upstream on the suction side making the blade thinner. Consequently, this increased the curvature of the suction side and in turn increases the Mach number while loading the front accordingly [5]. It is predicted that there is one optimum λ for which the wake thickness is minimum.

The LE has significant effects on the aerodynamic performance of an airfoil. Defining airfoil's LE with any method is very difficult. The approach in CIRCLE method is discussed earlier. Hodson [8] detected spikes on the LE experimentally due to discontinuity in the curvature. They experimentally tested HD blade. The redesigned HD blade, in Fig. 2, shows that the leading edge seperation spikes have been removed. This improvement is depicted with CFD computations in Fig. 2. I1, I4 and I9 are the redesigned stages of the original HD blade. The modified blades are restricted to have the same LE circle diameter and chord length. Therefore they ended up being a bit thinner near the LE, due to the reduction in the wedge angle. The curvature distribution (Fig. 2b) shows smoother lines for the redesigned profile than the original HD profile, obtained from [9]. The Mach number plot shows successful removal of suction side discrepancies and pressure side diffusion in the LE region of the redesigned profiles compared to the experimental results obtained from [9]. Experimental and computational results for Kiock blade show the existence of significant disorders on both surfaces [10]. Fig. 3a shows the surface curvature distribution of Kiock and S1, which is evident enough to show the improvements in the surface curvature discontinuity. Fig.3b indicates a variation in the thickness to compensate for a smooth continuous curvature around the profile. This resulted in the removal of small disturbances in the blade's Mach number distribution (Fig. 3c). This has resulted in smoother boundary layer displacement thickness and reduced the local entropy generation [3].

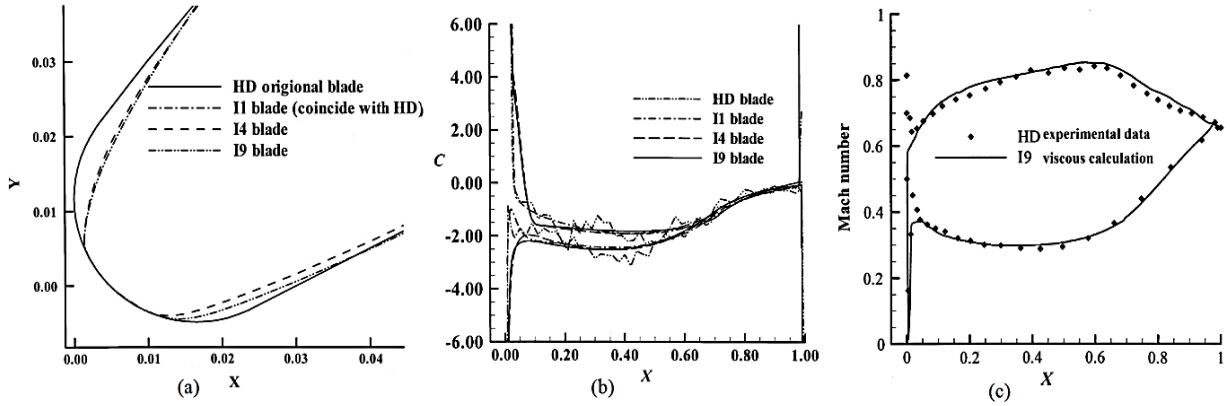

Fig. 2 Original and redesigned HD blade's (a) LE, (b) curvature distribution and (c) Mach number distribution [4]

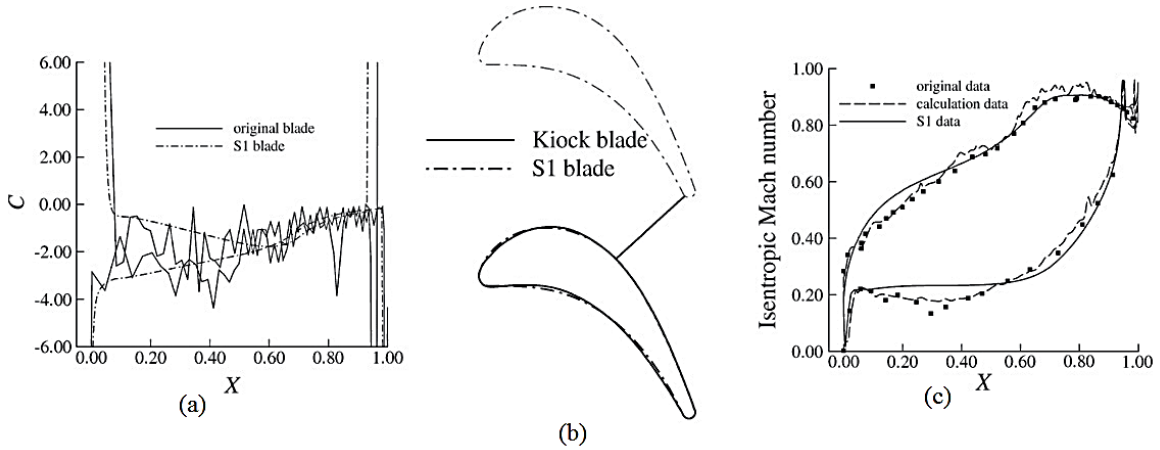

Fig. 3 Comparison of original Kiock blade with modified S1 blade (a) curvature distribution (b) geometry and (c) Mach number plot [3]

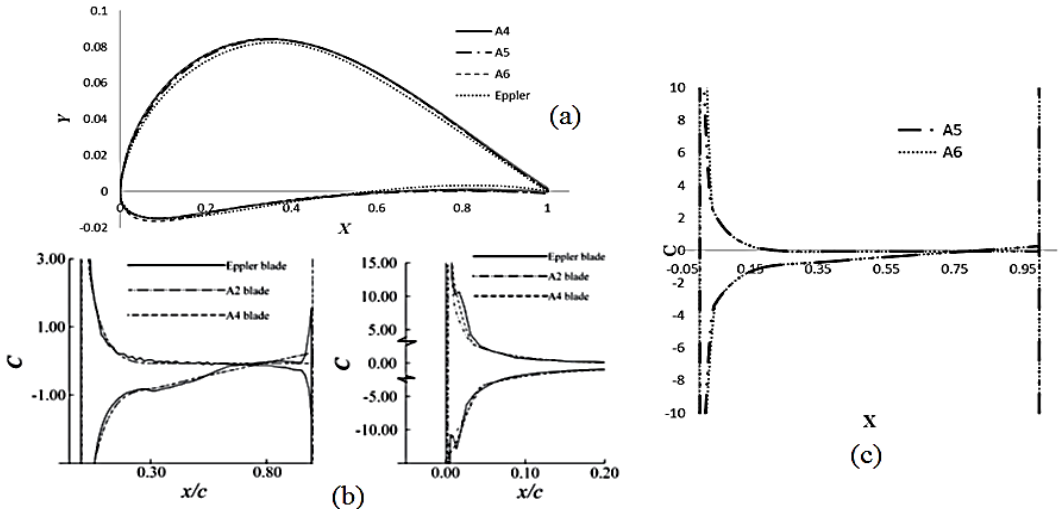

Fig. 4 (a) Geometries of Eppler, A4, A5 and A6; Curvature distribution of: (b) Eppler and A4, (c) A5 and A6

4. 2D isolated airfoil redesign

Isolated airfoils appear to be sparsely arranged, e.g. wind turbine airfoils, compared to clustered turbomachinery blades, i.e. turbine/compressor blades. Eppler 387 is a wind turbine airfoil candidate. From Fig. 4b, curvature discontinuity on its surface appears apparent. The CFD (depicted in Fig 4 and 5) and the experimental results [11] clearly show the LE

disturbances on Eppler. Isolated airfoil appears to have 'curved-out' pressure side; therefore a slight modification in the CIRCLE method to define the pressure side has been used to redesign Eppler. Fig. 4a shows the geometries of Eppler with its stages of redesign: A4, A5 and A6. The redesigned blades appear thicker in the LE and TE regions. This removed the LE curvature disturbances that exist in Eppler. A4 shows better continuity in curvature compared to Eppler (Fig. 4b). A5 shows further improvement than A4 and A6 more than A5 (Fig. 4c and 5). The computations are based on typical wind turbine flow conditions [3], unlike high speed unsteady turbulent flow in turbomachinery. It was computed in a flow with Reynolds number 10^5; turbulence intensity 0.5% at various incidences, i.e. on and off design points. The C_p contours are plotted using CFD RANS model – Transition SST in ANSYS 13.0, with a 2D structured C grid, giving a $y^+<1.5$. Figs 5a, b and c refer to computational and experimental C_p of Eppler and the redesigned blades. Figs 5b and c show the removal of the Eppler's LE noise from all the redesigned blades at $\alpha=4^\circ$ (comparison to experimental data [11]) and $\alpha=8^\circ$ (design point), respectively. Despite smooth curvature there exist boundary layer separation bubbles at 65-70% of the chord on the suction-side at $\alpha=4^\circ$, and 45-60% of the chord on the suction-side at $\alpha=8^\circ$; but reattaches turbulent soon after. This is due to the aerodynamic behavior of flow at such low Reynolds number. The laminar boundary layer becomes too weak to remain attached at that Reynolds number for those incidences. Nevertheless, suitable active or passive flow control method can be used to investigate further and optimize the aerodynamics at those instances. The polars results for the airfoils, which are obtained using XFoil [12], (Fig 5h, i & j) show the incremental aerodynamic improvement among the stages of Eppler's redesign. They exhibit a trend where A6 has overall better C_L, C_D and C_L/C_D performances, with a slight deviation near $\alpha=7^\circ$ where A4 dominated till $\alpha=8^\circ$.

Percentage improvements in C_D, C_L and C_L/C_D calculated as, for C_D: $(\Delta C_D/C_{D\text{-Eppler}})$ x 100; for C_L: $(\Delta C_L/C_{L\text{-Eppler}})$ x 100; and for C_L/C_D: $(\Delta(C_L/C_D)/(C_L/C_D)_{Eppler})$ x 100 at design point. The following table depicts the implicit values from the polar calculations.

Table 1 Showing the polar results for C_D, C_L and C_L/C_D and their percentage improvements

Items	Eppler	A4	A5	A6
C_D	0.031494	0.025046	0.02373	0.023304
C_L	1.156052	1.196228	1.177495	1.196925
C_L/C_D	36.70733	47.76206	49.62153	51.36147
% improvements from Eppler in C_D	--	20.47451	24.65324	26.00452
% improvements from Eppler in C_L	--	3.475276	1.854847	3.635568
% improvements from Eppler in C_L/C_D	--	30.11587	35.18153	39.92156

5. Conclusion

The paper presents the effect of CIRCLE method on airfoil design and redesign. It successfully comprehended the improvement of the Eppler 387 isolated airfoil. The references to the turbomachinery blade redesign show its overall proficiency in this field. From the polar results, it is found comparing with Eppler, the drag reduced 20.5% in A4, 24.7% in A5 and 26% in A6 at design point, and the lift improved 3.5% in A4, 1.9% in A5 and 3.6% in A6. These indicate an overall C_L/C_D performance improvement of 30.1% in A4, 35.2% in A5 and 40% in A6. It is deemed necessary for a paradigm shift to sustainable energy systems to meet global energy demand and emission targets. And it can be concluded from here, CIRCLE method can contribute in to the solution to current global energy crisis and emission problems.

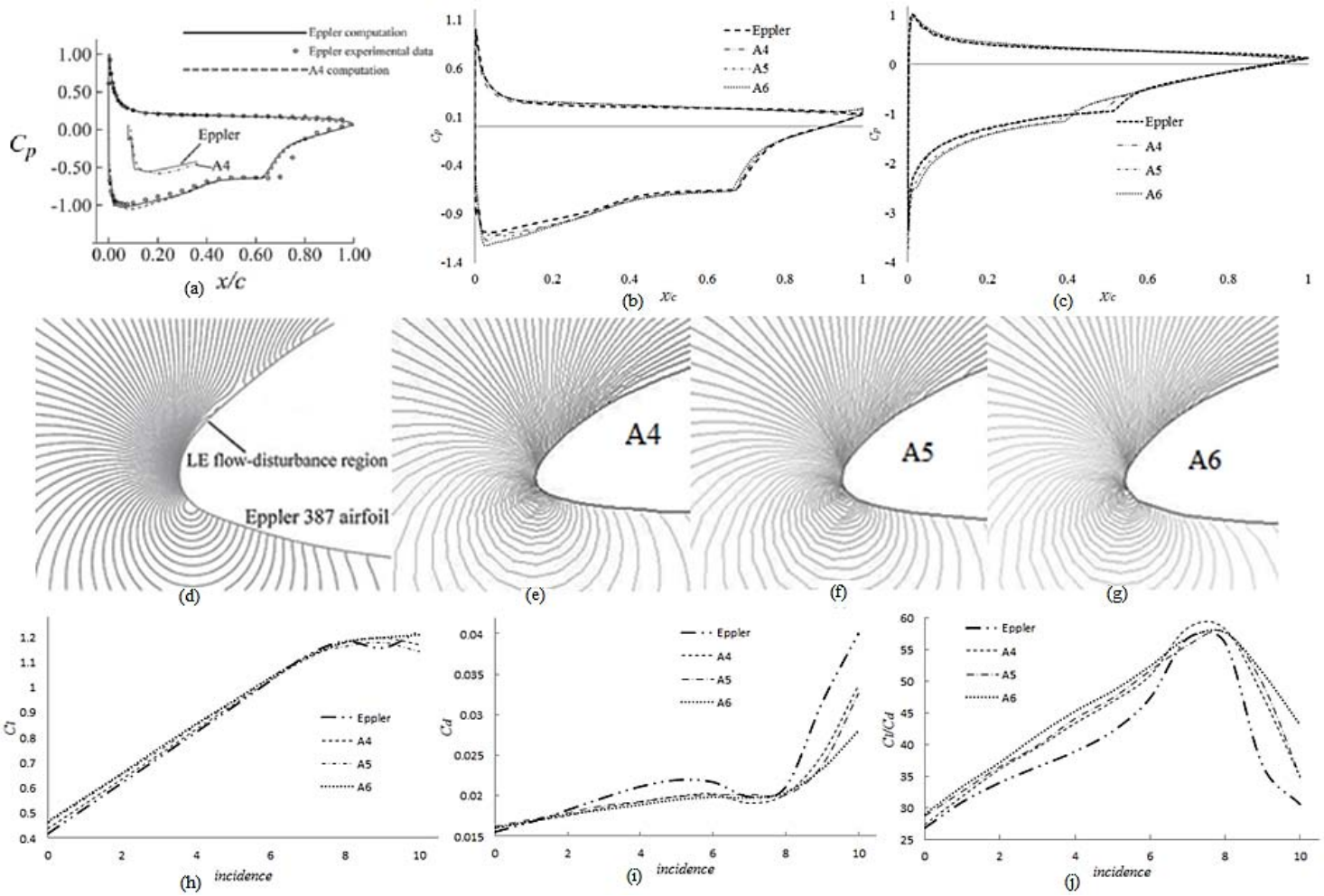

Fig. 5 Comparison of Eppler and the redesigned airfoils: (a) C_p distributions of Eppler computational with experimental and A4 computational results; C_p distributions of Eppler computational vs A4, A5 and A6 for: (b) $\alpha=4^{\circ}$, (c) $\alpha=8^{\circ}$ (design point); (d) LE C_p contour plot of Eppler; (e) LE C_p contour plot of A4; (f) LE C_p contour plot of A5; (g) LE C_p contour plot of A6; (h) C_L variation against α; (i) C_D variation against α; (j) C_L/C_D variation against α;

Reference

[1] Fast M, Assadi M, De S, 2009, Development and multi-utility of an ANN model for an industrial gas turbine, Applied Energy, 86(1): pp 9–17

[2] Massardo A, Satta A, 1990, Axial-flow compressor design optimization. Part 1. Pitchline analysis and multivariable objective function influence. Trans ASME, J Turbomach, 112(3): pp 399–404

[3] Korakianitis T, Hamakhan I, Rezaienia M, Wheeler A, Avital E, and Williams J, 2012, Design of High-Efficiency Turbomachinery Blades for Energy Conversion Devices With the Three-Dimensional Prescribed Surface Curvature Distribution Blade Design (CIRCLE) Method, Appl. Energy, 89: pp 215–227

[4] Hamakhan IA, Korakianitis T, 2010, Aerodynamic performance effects of leading edge geometry in gas turbine blades. Appl Energy, 87(5): pp 1591–601

[5] Korakianitis T, 1993, Prescribed-Curvature Distribution Airfoils for the Preliminary Geometric Design of Axial Turbomachinery Cascades, ASME J. Turbomachinery, 115(2): pp 325–333

[6] Dang T, Damle S, Qiu X, 2000, Euler-Based Inverse Method for Turbomachinery Blades, Part 2: Three-Dimensional Flows, AIAA J, 38(11): pp 2007–2013

[7] Phillipsen B, 2005, A Simple Inverse Cascade Design Method, 50th ASME Turbo-Expo, ASME Paper No. 2005-GT-68575

[8] Hodson H P, Dominy R G, 1987, Three-Dimensional Flow in a Low Pressure Turbine Cascade at its Design Condition, ASME J. Turbomachinery, 109(2): pp. 177–185

[9] Hodson H P, Dominy R G, 1987, The Off-Design Performance of a Low-Pressure Turbine Cascade, ASME J. Turbomachinery, 109(2): pp. 201–209

[10] Kiock R, Lehthaus F, Baines N C, Sieverding C H, 1986, The transonic flow through a turbine cascade as measured in four European wind tunnels. Trans ASME, J Eng Gas Turb and Power, 108(2): pp 277–284

[11] McGhee R J, Walker B S, 1988, Experimental results for the Eppler 387 airfoil at low Reynolds numbers in the Langley Low Pressure Turbine Tunnel, NASA-TM- 4062

[12] Drela M, Giles M B, 1987, Viscous-inviscid analysis of transonic and low Reynolds number airfoils, AIAA J, 25(10): pp 1347–55

Acknowledgements

The authors acknowledge the contributions of MSc and PhD students, and postdocs, who over two decades have contributed to coding various aspects of the CIRCLE blade design method in FORTRAN, C++ and MATLAB, and on various platforms and operating systems: George Pantazopoulos; Nick Vlachopoulos; Paschalis Papagiannidis; Dequan Zou; Richard Binzley; Sean Spicer; Brandon Wegge; Yan Tan; Mingyu Shi; Akbar Rahideh, M. Amin Rezaienia and Idres Hamakhan. The PhD research of Moin U Ahmed is partly sponsored by Cummins Turbo Technologies Ltd and partly by Queen Mary University of London.

5th BSME International Conference on Thermal Engineering

Escalation of Gasoline Combustion Efficiency Using Brown Gas

Noman Sadi[a*], Md. Istiak Shahriar[b], Rabiul Islam[b],
[a,b]*Department of Mechanical Engineering, Chittagong University of Engineering and Technology, Chittagong-4349, Bangladesh*

Abstract

This paper represents processes involved in Brown gas generation and finding the optimum values of all the factors to produce the gas consuming least power. Brown gas (HHO) or hydroxy gas has achieved the remarkable recognition as the alternative source of clean energy for IC engine. It is a mixture of monatomic and diatomic hydrogen and oxygen and a special form of water called Electrically Expanded Water (EEW). Brown Gas (HHO) is mainly produced by electrolyzing water through a unique and specified arrangement of electrolyzer. Brown gas is used as a supplementary fuel in SI and CI engine without any modification. The produced Brown gas from the onboard system effects on combustion characteristics and exhaust emissions of the engine by introducing the gas into intake manifold. On an average up to 35 % of energy can be extracted from burning hydro-carbon fuels whereas above 60 % of energy can be extracted in case of mixing air-fuel mixture with Brown gas including the energy required to electrolyze water. The gas acts as a catalyst for hydrocarbon fuel and increase the combustion efficiency, decreasing specific fuel consumption (SFC) and engine knocking. The gas also effects in reducing NO_X emissions and no CO emission. Brown gas has some unique properties like cool flame temperature at which it can sublimate Tungsten at only 130^0 C and the gas always implodes rather exploding while burning. As the gas is generated from the engine power so the main concern is to produce the gas efficiently. This study revealed the maximum production of Brown Gas with the optimum combination of voltage and current, frequency and different concentration of electrolytic (KOH) solution.

Keywords: Brown Gas; Electrolyser; Pulsed Current; Combustion Efficiency;

1. Introduction

Alternative sources of fuel consists extreme consequences as due to the total reserve of fuel is stepping down day by day and emission of deleterious components by fossil fuels. Fuel crisis, unrest in biggest oil producing countries impacts on the frequent price hike and makes the situation worst for the third world country. Fuel is the crucial factor which determines tranquillity of socio-economical aspects of the world. It is known that before 1970, energy was abundant and cheap and therefore it was not a major concern. However fossil fuels are limited and will be exhausted within 100-150 years. Another devastating term cogitating from few decades is the carbon emission by fossil fuel. Approximately 90% of our energy consumption comes from fossil fuels.

Nomenclature

V	volt
I	Ampere
V_d	Drift velocity
W	Energy consumed during the related process (Joule)
Pe	The free electron density of desired material
q	Charge of electron
PWM	Pulse Width Modulator
SFC	Specific Fuel Consumption

Diesel and spark plug engines are main sources of pollutions in urban areas. Carbon monoxide (CO), unburned hydrocarbon (HC), carbon dioxide (CO_2) and nitrogen oxides (NO_x) are produced during the incomplete combustion in IC engines. Emissions like SO_2, lead and smoke too are health hazards caused by motor vehicles. Especially, diesel engines are leading pollutant producers of SO_2 and smoke. These deleterious

* Tel: Noman Sadi. +88-01912188996
Email: noman.cuet@gmail.com

emissions are responsible for concerns such as global warming, greenhouse emissions, climate change, etc. Therefore using resource optimally is a major issue these days.

To reduce the fuel consumption significantly and to save our environment from deleterious emissions the design of IC engines are wavering continuously. At the same time to get the most effective solution the world is focusing on alternative sources of fuel. As of 2010, about 12% of global total energy consumption comes from alternative energy sources and it is endlessly increasing.

Hydrogen fuel was considered as the possible solution of these problems. Hydrogen has long been recognized as a fuel having some unique and highly desirable properties as a fuel in engines,but in practical it has several difficulties to use in cars. The storage of hydrogen is a major concern. Hydrogen must be stored at extremely low temperature and high pressure. A container capable of withstanding these specifications is larger than a standard gas tank. Hydrogen storage could be viewed as a problem by consumers. Another one is Hydrogen is extremely reactive. Hydrogen is combustible and flammable. The Hindenburg disaster, where hydrogen filled blimp exploded and many people died, has caused a fear of hydrogen. Another problem for hydrogen fuel is consumer demand and the cost to change all gasoline filling stations and vehicle production lines into hydrogen. Production of hydrogen takes a lot of energy. If we have to burn fossil fuels to make hydrogen then we gained nothing from it. Electrolysis of hydrogen cannot yield excess energy. The electrolysis of hydrogen follows the principle as given below.

Electrolysis: $H_2O + E_1 \rightarrow H_2 + O2$

Combustion: $H_2 + O2 \rightarrow H_2O + E_2$

Energy: E_1 always greater than E_2

Compared with other alternative sources of fuel Brown gas is considered as the most efficient, economic and environmentally friendly. Brown gas acts as a catalyst for combustion of fuel in IC engine which proliferate combustion efficiency fabulously, reduces specific fuel consumption and exclude emission of CO and NO_X by introducing the gas in combustion chamber with gasoline in any existing design of the engine. It has no difficulty as hydrogen gas because it is produced in a recycled a way during the running of the IC engine. Brown Gas is a mixture of monatomic hydrogen and oxygen created by electrolysis of water. It is a unique method for transmitting electrical energy directly into the atomic structure of materials. Within the compact structure of the system, water is electrolyzed by specially designed electrodes. Brown Gas has several distinctive properties, unlike its constituent gases. It has cool flame temperature and it implodes upon ignition. Brown gas can fuse brick, steel, sublimate tungsten, glaze quarts, neutralize nuclear waste, fuse two dissimilar substances and many more things. Brown Gas burns with a clean flame. It uses no atmospheric oxygen, and creates only pure water as its combustion product. One litre of water produces about 1866 litres of gas. When this gas is ignited, the volume is reduced to the original one litre of water (Michrowski, 1993).

Addition of HHO significantly enlarges the flammable region and extends the flammability limit to lower equivalence ratios. HHO has a low ignition energy and fast flame speed, the HHO-gasoline mixture can be more easily ignited and quickly combusted than the pure gasoline.According to the classic theory (the first theory), Brown Gas is a simple mixed gas of hydrogen and oxygen generated by electrolysis of water, which cannot explain the special characteristics of Brown's Gas. Accordingly, new theories about the entity of Brown's Gas have been recently introduced. Experimental results acquired to date show that a mixture of mono-atomic oxygen and hydrogen generated by a Brown Gas generator has remarkably larger reactivity than an equal amount of another mixture of oxygen and hydrogen (Yilmaz, 2010).

Yull Brown pioneered and advocated for HHO gas. He gave many public demonstrations in Australia, USA and received his own patents (US-4010777 and US-4081656). Production was transferred to the Peoples Republic of China at the inducement of its government, resulting in mass production of generators for national distribution. Yull Brown drove a number of cars on a variety of internal combustion engines, performing many measurements on them using his laboratory's fully instrumented dynamometer set-up. He has been officially monitored to drive 1,000 miles per gallon of water. The most well known legend of brown gas is Stanley Meyer. He invented the most efficient system of brown gas production system. Today's million dollar business of selling Brown gas kit in more than 12 countries is nothing but new version of Meyer's invention. In 1998 Stanley Meyer died mysteriously after his claim of inventing running engines by only Brown gas.

1.1, Reasons to be distinctive the Brown gas

Researchers explained the sources of exotic energy in Brown gas in a different way. Most accepted are

- Electrically expanded water
- Pulsed current
- Plasma charge gas cluster
- Trapping of Zero point energy

Brown gas is a special form of water called “Electrically Expanded Water (EEW)” or “Santilli Magnecules.This gas is a new phase of water that is not a result of heat, but electricity. The rapid heating of objects when exposed to a Brown Gas flame might be the result of this stored electricity being transferred to the object. In such a situation, the heat produced would be a simple by-product of electrical resistance.

Electricity + water = Brown Gas
Brown Gas + ignition = Electricity + Water.

Every material gets hot when used as a resistor for electricity. When this electric steam hits a piece of metal the extra electrons from the ‘electric steam’ travel with the speed of the gas plus original speed around the excited water molecule. This equation helps to determine the amount of energy and the speed of the electrons.

$$V_d = \frac{W}{P_e \times q}$$

In case of the Brown’s gas, it is like a moving wire at a speed of 7.4 m/s plus the original speed of the electrons (if the gas is stationary), so the material that is being hit by this high energy gas has those extra electrons transferred into the new material. Those electrons disperse causing high heat due to the electrical resistance of that material. These high energy electrons do not travel as fast as the gas. When they hit the surface of something, they lose big amount of their speed. Thus, they release their kinetic energy as heat, the more dense and resistive material gets hotter, the less dense or more conductive material results the less generated heat (however it still has a high heat because of the kinetic energy of the electrons). The Brown’s Gas flame is a unique method for transmitting electrical energy directly into the atomic structure of materials.

Another reason is pulsing the current causes electrodes to vibrate and emit a high pitch frequency. Pulse into the water creates a kind of feedback loop. In technical terms, this is called a "transverse wave effect". This effect just happens to loosen the molecular bond between the hydrogen and the oxygen atoms inside the water molecule. The stress produce by the effect allows breaking the bond between hydrogen and oxygen with only a small amount of current.

Most important explanation is the formation of especial form of water. A hypothesis is proposed that the dominant energy is not coming from hydrogen, but rather it is coming from charged water gas clusters, which activate and coherently trap zero-point energy. In Brown Gas there is a unique form of plasma in which electrons are weakly held rather than free floating. This is known as "Non-equilibrium plasma" or "cold plasma”. In this type of plasma the electrons have high energies but the molecules or atom that holds the extra electrons are relatively unenergetic. In a Brown’s Gas torch, these extra electrons are what produce the immense heat, while the molecule or atoms releasing these electrons remains relatively cool. By definition it an isomer is any molecule that has the same number and type of atoms, like H2O is always going to be water, but the structure or orientation of those atoms in the molecule may be different. Water original shape is bent with about 107 but the form of brown gas shows a new shape which is non-polar.

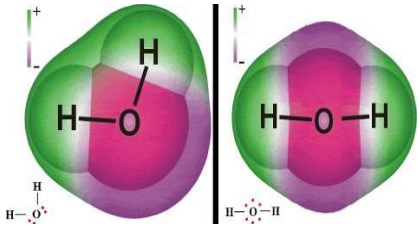

Figure:1. Comparison of chemical structure of H_2O and HHO

2. Materials and methods

For the electrolysis of water power is drown from the 12 volt DC battery of the installed car. The power rating of the battery should 120Ah or above for better longevity. For the experimentation a variable laboratory DC power source used. Tap water gradually forms non-conductive barriers on the electrolyzing plate. So it would be better to use distilled water. High corrosion resistance is considered as one of the major factors for electrode material because of corrosive working ambient. Therefore, 316L stainless steel due to its high corrosion resistance are normally used. The electrolyzing plate or reactor may be of different shapes like rectangular, cylindrical or wire type. Rectangular type reactor draws least amount of power (Yilmiz) while maximum production obtains by cylindrical shape electrolyzer.

Fig:2 Apparatus set up

The spacing between the electrodes is an important factor must be acute. For the best production spacing between the electrodes should be in the range of 0.6mm-2mm. The cells are in parallel connection. Now the 12 volt DC is passed to the cell through a Pulsed Width Modulatotion circuit. A 555 timer circuit or microcontroller circuit is commonly used to generate the desired frequency of square wave pulse type for switching operation through a MOSFET. The gas production greatly varies on magnitude and duty cycle of the frequency. At the resonance frequency of the electrode maximum gas generation obtains in exchange of low energy. Here we used oscilloscope to find the resonance frequency. Now the terminals of the cells are connected to the power source. Brown gas production is merely contingent to the current flow through the cell. The production shows a proportionality connection with current flow. As the brown gas is very unstable, the design next to gas production must aim to consume the gas within shortest possible time. The burning of produced gas along with correct air-fuel mixture increases the combustion efficiency.

3. Results and discussion

Three significant factors were obtained from the experiment for the optimum production of Brown gas at the expense of minimum energy. First one, the experiment showed that the voltage applied above 1.8 volt for each cell is merely wastage. The voltage above 1.8 volt had a very little effect on gas production. If the voltage maintains at 1.80 volt per cell then waste of energy drops dramatically. This improves overall efficiency. Anything over 1.80 volts is a waste, and will be expelled into the water as heat and increase the temperature of water. A conventional car battery has the voltage rating up to 14 volt. As the electrolyser have six cells, therefore total voltage required 10.8 volt. A laboratory DC power source having a rating of zero to thirty volt was used.

Table 1. voltage variation effects

Voltage	Temperature ˚C	HHO gas L/m
10.8	27	0.8
12	27.6	0.82
14	28.5	0.82
16	29.3	0.82
20	32.1	0.82
25	34.6	0.82

Generation of Brown gas is proportional to current flow. A good design of electrolyser and higher conductivity of water pushes up gas generation using least amperage. As the pure water has pure conductivity, addition of electrolyte increased the current flow and consequently the generation of HHO. Addition of KOH over 2% proliferate the current flow and also the brown gas generation dramatically.

Table 2.. Current flow rate with the change of percentage of electrolyte at 12 volt

Percentage of KOH	Current, I	HHO L/m
0	2.1	0.16
0.5	2.23	0.21
1.5	2.67	0.24
2.0	3.31	0.32
2.5	3.97	0.5
3.00	4.45	0.68
3.5	4.67	0.71

At resonance frequency of the electrode maximum HHO gas generated at lowest energy. A pulse width modulator made of PIC16F72 used as PWM. With this process we just switching the power (with varying on and off times with aid of a Metal Oxide Semiconductor Field Effect Transistor) to the electrolyser at the respective frequency. In this experiment square wave pulse of 52% Duty cycle for each reading were maintained. At 0.5 % of catalytic solution of KOH the given data we obtained,

Table 3.Response of current and gas generation on various frequency

Frequency	HHO L/m	current
1 KHz	0.6	2.3
20KHz	0.6	2.33
35 KHz	0.6	2.3
42 KHz	0.9	3.7
50KHz	0.6	2.8
65KHz	0.6	2.43
80KHz	0.6	2.39

Here we got the maximum current drown at a frequency of 42 KHz which is almost nearer to the resonance frequency of the type of metal we used.

3.1 confirmation of presence of brown gas

The brown gas at 42 KHz and 3.7 Amp had distinct burning characteristics and productivity from the same current but no PWM. The gas generated without any pulse showed similar characteristics of hydrogen gas. Without pulsing current the existed for few minutes in the chamber, i.e. it could be burned after few minutes of its production, but at resonance frequency the gas showed two types of burning characteristics. Within 1-2 seconds of production, the gas burned with explosive sounds and no observable flame and burning after the time limit produced a very little flame and no explosive sound. Also the burning temperature for the first condition was insignificant as it was same as ambient temperature.

4. Conclusion

Although the characteristics of high burning velocity, wide flammability range, oxygen content and absence of carbon make HHO gas an appropriate fuel which results in increasing combustion efficiency, decreasing SFC and deleterious emissions, but to make the system economical average power increment must bigger than the electrical power consumed. The result of this experiment discerns the generation of brown gas in the expense of lesser power consumption. In addition to control the gas generation in accordance with the varying speed of the engine Hydroxy Electronic Control Unit (HECU) is mostly used which makes the system efficient at low speed.

The experimental results we found

- Voltage over 1.8 causes to heat, decease the efficiency of the system
- 2% of electrolytic solution pushes up the gas production moderately.
- At resonance frequency the system shows highest efficiency.

Acknowledgement

The author is gratitude to Prof. Dr. Bodius Salam (Head, ME Dept. CUET) for his valuable discussion and funding the experiment, Mrs.Sumona Biswas (Asst. Prof. ME Dept. CUET) for her generous support for the experiment.

References

[1] P. Kelly, A practical guide to free energy devices. 1st ed. Jan.2006;163:51-9.
[2] Ali Can Yilmaz, Design and application of HHO system. Çukurova University,Turky, 2010
[3] Ruggero Maria Santilli, A new gaseous and combustible form of water. Institute for Basic Research USA,2010
4] Mohammed Awwad Al-Dabbas, The Simulation of Using Hydrogen Fuel in Gasoline Internal Combustion pacific journal, vol 10, 2009.
[5]Ammar A. Al-Rousan, Reduction of fuel consumption in gasoline engines by introducing HHO gas into intake manifold. Science Direct, 2010,
[6] Sa'ed A. Musmar, Effect of HHO gas on combustion emissions in gasoline engines. Mutah University,2011.
[7] M.B. King, Water Electrolyzers and the Zero-Point Energy. 2011.
[8] D.C. Cole, H.E. Puthoff, Extracting energy and heat from the vacuum Phys. Rev. E, 48 (1993), pp. 1562–1565
[9] Wiseman, Eagle Research: Brown's Gas. eagle-research.com, 2010.
[10] Michrowski, A. Yull Brown's Gas. Planet. Assoc. Clean Energy Newsl. 1993, 6 (4), 10-11.
[11] By Dr. Jay L. Wile , Advanced Chemistry in Creation.College Chemistry Book,
[12]APOSTOLESCU. N. and CHIRIAC. R, A Study of Combustion of Hydrogen-Enriched Gasoline in a Spark Ignition Engine. SAE Paper, 1996.
[13] PEAVEY, M, Fuel from Water: Energy Independence with Hydrogen.Eleventh Edition. New York, 2003.

5th BSME International Conference on Thermal Engineering

Feasibility Study About Micro Hydro and Solar Energy in Hill Tracts of Bangladesh

Khizir Mahmud[a*], Md. Abu Taher Tabir[b], Md. Ashraful Islam[b]

[a]*Department of Electrical Engineering, Northwestern Polytechnical University, X'ian-710072, China*
[b]*Department of Electrical & Electronic Engineering, Chittagong University of Engineering & Tech, Chittagong-4349, Bangladesh*

Abstract

The energy demand is expected to grow rapidly in most developing countries over the next decades. For Bangladesh, economic growth has been accelerating and it is expected that the population will grow from an estimated 162.20 million people in 2011 to 200 million by 2050, with almost half of the population living in urban areas. For meeting the expected energy demand as the population will rise and to sustain economic growth, alternative form of energy – renewable energy needs to be expanded. This paper tries to explore the possibility of finding the renewable energy mainly from micro hydro and solar in different places of Chittagong hill tract region by thoroughly describing present condition of energ**y** along with data collection, calculation and feasibility of power generation from July 2011 to Jan 2012.

Keywards: Bangladesh Hill Tracts; Micro hyro; Renewable energy; Solar intensity; Solar energy.

1. Introduction

The development of a country is mostly dependent on per capita energy use. Bangladesh is one of the poor countries in the South Asian region. A large number of its population is out of electricity. Only 48.5 percent of the total population has access to electricity [5]. Most of the power generation of Bangladesh is based on fossil fuel sometimes which is playing a negative impact on finance in the long run operation. So to supply the electricity to the rest people is a great challenge. In future fossil fuel will not be able to supply the electricity to the user as it will be finished & not environment friendly also. So to search and depend on environment friendly renewable energy is now a great desire of the country. Bangladesh has a great probability of renewable energy. It has much different form of renewable energy resources. Among them micro hydro and solar may play a major role specially to serve electricity in the remote area of Chittagong hill tract for ensuring economic growth of the country. Though a great potentiality of micro hydro and solar to serve power in remote areas but real feasibility of implementation of this type of power generations are still behind limelight. Development of micro-hydro power plant and solar power can reduce electricity scarcity problems so economically in remote areas of Chittagong Hill Tract without any major hassle.

2. Present power scenario of Bangladesh

In the South Asian region Bangladesh is one the most densely populated country (1099 people/km^2 in 2010) [7]. With high population Bangladesh is experiencing extreme energy challenges especially for the shortage of electricity. Shortage of electricity may be considered in two forms firstly, reviewing the scenario of per capita electricity consumption and percentage of population having access to electricity in Bangladesh compared to other countries and secondly, determining gap between demand and supply of electricity in respect of country's economic situation and GDP growth. By the dichotomy of power generation and demand Bangladesh faces a severe load shedding. Bangladesh relies greatly on fossil fuels for its energy which will be depleted in 2015[7].

* Corresponding author. Tel.: +8618392374190
E-mail address: khizirbd@gmail.com

Table 1. Rate of use of different types of energy in producing electricity.

Fuel	Percentage of use (2010)
Furnace oil	2.81
Diesel	1.75
Hydro	3.39
Coal	3.77
Gas	88.29

2.1 Production of power in Bangladesh

Bangladesh Power Development Board (BPDB), Ashuganj Power Station Company Limited (APSCL), Electricity Generation Company of Bangladesh (EGCB) is producing electricity in the public sector. On the other hand, through IPP (Independent Power Producer) and through Rental electricity is produced in the private sector which is purchased by the Government at a fixed rate[8]. At present nearly 54.40 percent of total electricity production is produced from public entities. BPDB alone produces 43.51 percent of total electricity production [5].

Table 2. Statistics of electricity production in Bangladesh (March, 2012).

Government Sector				Private Sector				
Organization	BPDB	APSCL	EGCB	IPPs	SIPP (BPDB)	SIPP (REB)	15 years rental	3/5 years rental
Production capability (MW)	3483	662	210	1272	99	226	168	1885
Total (MW)	4355					3650		

BPDB =Bangladesh Power Development Board, APSCL= Ashuganj Power Station Company Limited, EGCB = Electricity Generation Company of Bangladesh, SIPP = Small Independent Power Producer and REB =Rural Electrification Board.

2.2 Future plan of power production of Bangladesh

Bangladesh government has taken a long term plan to develop the power sector and mitigate the present power scarcity. According to the plan Electricity Generation in the country by 2013 will be 8500 MW and within 2015 this generation will rise to 11,500 MW and surplus power will be possible to give to national grid. Within the year of 2021 there is a plan to generate 20,000 MW power and to provide power to the whole area of the country [4].

Table 3. Year wise expected power generation statistics of Bangladesh Power Division.

Year	Government Sector	Private Sector	Total (Megawatt)
2010	360	432	792
2011	920	---	920
2012	505	1764	2269
2013	725	950	1675
2014	1170	---	1170
2015	---	2600	2600
Expected Extra Generation			9426

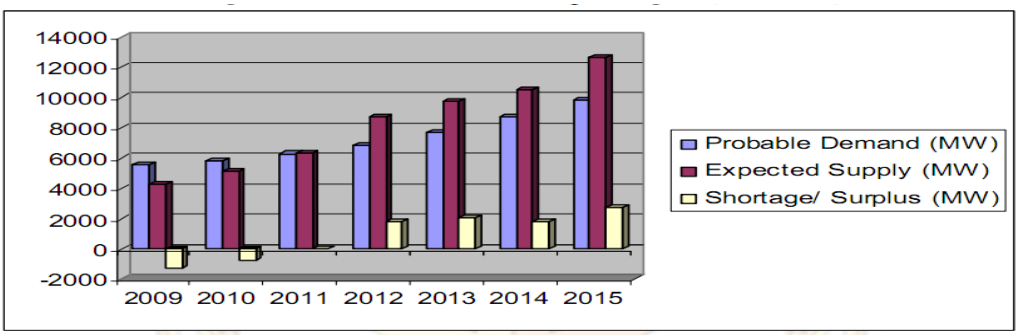

Fig. 2. Probable power shortage/ surplus of Bangladesh (2009-2015).

In last few years to meet up the scarcity of power so quickly government has taken some short term steps and thus establish quick rental power plant. So far, as many as 18 quick rental power plants have been approved and 14 of

them are operational now. To fuel these power plants, the additional cost for the current fiscal year, as projected by the World Bank is between Tk. 52 billion and Tk. 56 billion, which is about 0.6 per cent or 0.7 per cent of the Gross Domestic Product (GDP)[1]. Excess payment for quick rental power plants has already affected various government economic decisions and posing a serious threat to the economy. For this reason the topic to quest and establish renewable energy based power plant come to forward. So this paper has a little effort to meet the demand of searching that renewable energy sources and supply power to some remote areas.

3. Renewable energy scenario of Bangladesh

3.1 Solar energy

Bangladesh is located between 20.30 to 26.38^0 North latitude and 88.04 to 92.44^0 East which is an ideal location for solar energy utilization. Here, the daily average solar radiation varies between 4 to 6.5 kWh per square meter. Infrastructure Development Company Limited (IDCOL) has supported NGOs in installation of Solar Home Systems (SHSs) and a total of 801,358 SHSs having capacity of about 36.5 MW have been installed till January 2011[6]. About 10 kW central AC solar PV systems have been installed in one selected market in each of the three Rangamati district's sub-districts [3].

3.2 Wind energy

In Bangladesh, especially at coastal areas there are some Islands where wind energy can play a very important role to progress the economy of the country. BPDB installed a 160 feet tower at the Muhuri Dam site in the Feni district in May 2003. BPDB implemented a 1000 kW capacity wind battery hybrid power project (WBHPP) at the Kutubdia Island (Bay of Bengal) in the Cox's Bazar district. Under this project, total 50 nos. of 20kW capacity stand alone type wind turbines are being installed. The total capacity of all the wind turbines is 1 MW [9]. In another project, BPDB has implemented a 0.90 MW capacity of the Grid Connected Wind Energy (GCWE) at the Muhuri Dam areas in the Feni district in 2004 [3].

3.3 Biomass and biogas

Biomass covers all kinds of organic matter from fuel wood to marine vegetation. Biogas is a mixture of CH_4 (40 to 70 %), CO_2 (30 to 60 %) and other gases (1 to 5%) produced from animal dung, poultry droppings and other biomass wastes in specialized bio-digesters [2]. In Bangladesh biomass accounts 70% of the total final energy consumption. IDCOL financed a 250 kW Biomass based power plant at Kapasia upazila under Gazipur district [9]. From 1971 to October 2009 About 41000 biogas plants has been constructed by different NGOs, under National Domestic Biogas And Manure Program (NDBMP) of IDCOL. Under NDBMP of IDCOL, 5688 biogas plants have been constructed in Bangladesh in the year of 2010 [9].

3.4 Hydro Energy

Kinetic energy from flowing or falling water is exploited in hydropower plants to generate electricity. In Bangladesh about 1.4 trillion cubic meters (m^3) of water flows through the country in an average water year. Major rivers of the country have a high rate of water flow of about 5 to 6 months during monsoon season which is substantially reduced in winter season. At present only 230 MW of hydro power is utilized in Karnaphuli, Rangamati hydro station, which the only hydro-electric power plant operated by BPDB [9]. Microhydro and minihydro have limited potential in Bangladesh, with the exception of Chittagong and the Chittagong hill tracts. Hydropower assessments have identified some possible sites from 10 kW to 5 MW but no appreciable capacity has yet been installed. Hydropower plants are classified into two categories:

- Large hydropower plants (>10 MW), usually with reservoirs, that cannot only produce electrical energy Continuously, but also are able to adjust their output according to electricity demand.
- Small hydropower plants (<10 MW) that are less flexible with respect to load or demand fluctuation due to their dependence on the water resource.

4. Micro hydro potentialities in Bangladesh

The scope of hydropower generation is very limited in Bangladesh because of its plain terrains except in some hilly region in the North East and South East parts of the country. However there are lots of canals, tributaries of main river Karnafuli, Shangu, Matamuhuri as well as tiny waterfalls having good potentials for setting up mini/micro hydropower unit in Chittagong Hill Tracts (CHT) region. To explore potential sites of micro hydro; several studies have been conducted by Bangladesh Water Development Board (BWDB) and BPDB in 1981.

Table 4. Potential micro hydro sites in Bangladesh.

District	Name of The River/Chara/Stream	Potential Energy(KW)
Chittagong	Foy's Lake	4
Chittagong	Choto Kumira	15
Chittagong	Hinguli Chara	12
Chittagong	Sealock	81
Chittagong	Lungichara	10
Chittagong	Budia Chara	10
Sylhet	Nikhari Chara	26
Sylhet	Ranga Pani Gung	616
Jamalpur	Bi hugai-Kongsa at 2 miles U/S. of NalitabarI P.S	69 KW for 10 month, 48 KW for 2 month
Jamalpur	Marisi at Dukabad near Jhinaighati Thana Head Quarter	35 KW for 10 month, 20 KW for 2 month
Dinajpur	Dahuk at Burabari	24
Dinajpur	Chawai at U/S of Chawai L.L.P	32
Dinajpur	Talan at U/S of Talan L.LP	24
Dinajpur	Pathraj at Fulbari	32
Dinajpur	Tangon at D/S of Narun L.L.P	48
Dinajpur	Punarbhaba at Singraban	11
Rangpur	Buri Khora Chikli at Nizbari	32
Rangpur	Fulkumar at Raiganj Bazar	48

In 2004 Sustainable Rural Energy (SRE), Local Government Engineering Department has explored some potential micro-hydro sites in CHT region which is listed in table 5.

Table 5. Micro-Hydropower sites identified by SRE study in Hill Tract Region of Bangladesh in 2004.

Site	Potential Energy (KW)
Nunchari Tholipara, Khagrachari	3 KW
Chang-oo-Para, Bandarban	30 KW
Bangchari, Bandarban	25 KW
Liragaon, Bandarban	20 KW
Kamalchar, Rangamati	20 KW
Thang Khrue, Rangamati	30 KW
Monjaipara, Bandarban	7.5 KW

5. Micro hydro power calculation

The amount of power available from a micro hydropower system is directly related to the flow rate, head and the force of gravity which can be derived by the following equation:

$$P_{th} = Q \times H \times g$$

P_{th} = Theoretical power output in kW, Q = Usable flow rate in m^3/s, H = Gross head in m and g = Gravitational constant (9.8 m/s^2)

6. Micro hydro potentials survey in hill tract region of Bangladesh

Greater Chittagong Region has a great geographical diversity and thus has a potentiality to get the micro hydro power. In last few decades several attempts have been made to find out the potential of micro hydro power generation. To explore the possibility of hydropower from small hilly rivers/streams in the country, a working committee was constituted on February 1981 with officers from Bangladesh Water Development Board (BPDB). A study was also conducted by a group of Chinese experts and by LGED in 2002-2003 [9]. This research has a goal to find some places according to mathematical scrutiny where the establishment of micro hydro is possible. Some places like Choto Kumira in Chittagong, Mahamaya Chora in Mirsorai, Chittagong, Ruangchori Canal in Bandorban, Sailopropat Spring in Bandorban have a great potentiality to establish hydro power plant. The feasibility of the establishment of micro hydro power generation has been corroborated by the following calculation.

6.1 Choto Kumira Canal, Chittagong, Bangladesh

Head, H = 3 ft = .9144m

Table 6. Width survey of Choto Kumira Canal, Chittagong, Bangladesh.

No of observation	1	2	3	4	5
Width (ft)	7	11.3	12.5	11	10.8

Average Width, W = 10.52 ft = 3.21 m

Table 7. Depth survey of Choto Kumira Canal, Chittagong, Bangladesh

No of observation	1	2	3	4	5
Width (ft)	2.2	2.7	2.4	2.6	2.8

Average Depth, D= 2.54 ft = .774m and Area = W×D = 3.21×.77 = 2.48m^2

6.1.1 Measurement of flow

For passing the length of 13 ft or 3.96m following data were recorded.

Table 8. Flow survey of Choto Kumira Canal, Chittagong, Bangladesh.

No of observation	1	2	3	4	5
Time (t) (Sec)	4.35	4.30	4.58	4.86	4.82

Average time, t = 4.58 sec, Velocity, V = 3.96/4.58 = .86 ms^{-1}, Flow Rate, Q = V×A = .86×2.48 = 2.14 m^3/sec and Power, P = 9.81×Q×H = 9.81×2.14×.9144 = 19.19 kw.

6.2 Mahamaya Chora, Mirosorai, Chittagong, Bangladesh

Head , H = .9144 m, Width, W = 2 ft = .6096 m, Depth, D = 3 ft = .9144 m
Area = W×D = .6096×.9144 = .55741

6.2.1 Velocity measurement

For measuring the velocity we took the following data of time(t) to pass a distance of 16 ft.
Here, L = 16 ft = 4.88m

Table 9. Velocity survey of Mahamaya Chora, Chittagong, Bangladesh.

No of observation	1	2	3	4	5	6	7	8	9	10
Time (t)(Sec)	4.72	5.03	4.8	4.95	4.86	5.07	5.05	4.98	4.65	5.1

Average time, t = 4.92 sec, Velocity, V= L/t = 4.88/4.92 = .99 ms^{-1} and Flow Rate, Q = V×A= .99×.55741 = .5518359
Therefore, P = 9.81×Q×H = 9.81×.5518359×.9144 = 4.95 kw

6.3 Ruangchori Canal, Ruangchori, Bandorban, Bangladesh

Table 10. Width survey of Ruangchori Canal, Bandorban, Bangladesh.

No of observation	1	2	3	4	5
Width, W (ft)	69.5	65.3	89.1	77.7	82.5

Average width, w = 76.82 ft = 23.415 m, Average depth, d = 4.5 ft = 1.372 m and Cross sectional area, A = w x d = 32.12 m^2

6.3.1 Measurement of flow

For passing the length of L = 1.2192 m following time were recorded

Table 11. Time survey for flow in Ruangchori Canal, Bandorban, Bangladesh.

No of observation	1	2	3	4	5
Time, t (Sec)	50.45	51.08	50.3	50.45	51.25

Average Time, t = 50.706 sec, Velocity v = L/t = 1.2192/50.706 = .024 ms^{-1}, Flow, Q = V×A = .024×32.12 = .77088 m^3 /sec and Head, H = 5m.
Therefore Power, P = 9.81×Q×H = 9.81×.77088×5 = 37.81 kw

6.4 Sailopropat Spring, Sailopropat , Bandorban, Bangladesh

Head, H = 27.59 ft = 8.41m, Width , W = 2 ft = .61 m, Length , L = 4 ft = 1.2192 m
Area, A = W×L = .74 m^2

6.4.1 Measurement of flow

For passing the length of L= 1.2192 m following time were recorded.

Table 12. Time survey for flow measurement of Sailopropat Spring.

No of observation	1	2	3	4	5	6	7
Time, t (Sec)	1.75	1.73	1.65	1.81	1.79	1.64	1.78

Average time, t = 1.74 sec, Velocity, V = L/t = 1.2192/1.74 = .7ms^{-1}
Flow, Q = A* V = .74 *.7 ms^{-1} = .518m^3 /sec = 518 litre/sec
Power, P = 9.81 *Q*H = 42.74 KW

6.5 Raozan Power Plant Canal, Raozan, Chittagong

Cross sectional width of canal = 1.524m, Depth of canal =0.03175m

Table 13. Velocity measurement survey of Raozan Power Plant Canal.

No of observation	1	2	3	4	5	6
Length in meter	6.096	6.096	6.096	6.096	6.096	6.096
Required Time (Sec)	3.06	2.98	2.97	2.98	3.03	3.0

Average time = 3.0033 sec, Velocity=6.096/3.0033=2.097m/s
Area=W×D = 1.524×0.03175 = 0.04838m^2
Flow, Q =A×V = 0.04838×2.02976m =0.09821m^3/s
Power of the flow of water, P=1000 × 9.8 × Q × H = 1000 × 9.8 × 0.09821 × 1.0414 = 1.08 KW

7. Solar potentials survey in hill tract region of Bangladesh

Bangladesh is situated between 24^0 North latitude and 90^0 east longitude, which is an ideal location for solar energy utilization. Daily average solar radiation varies between 4 and 6.5 kWh/m2. Maximum amount of radiation is available on the month of March–April and minimum on December–January. Different R&D Organizations, Institutes and Universities are collecting solar radiation data. This paper has a little effort to collect solar radiation data of Hill Tracts region of Bangladesh to meet up the local demand from solar energy.

Table: Radiation intensity in Bandorban and Mirsorai, Bangladesh (2011)

Bandorban, Bangladesh Latitude: 21.59°, Longitude: 92.59°			Mirosorai, Bangladesh Latitude 22.864722°, Longitude 91.566389°		
Month	Clearness Index	Daily Radiation (Kwh/m^2/day)	Month	Clearness Index	Daily Radiation (Kwh/m^2/day)

January	.674	4.848	January	.626	4.404
February	.662	5.449	February	.606	4.912
March	.624	5.920	March	.599	5.637
April	.58	6.083	April	.553	5.786
May	.543	5.958	May	.519	5.706
June	.386	4.280	June	.381	4.242
July	.354	3.889	July	.346	3.817
August	.398	4.224	August	.380	4.030
September	.424	4.155	September	.413	4.022
October	.567	4.860	October	.564	4.776
November	.598	4.425	November	.599	4.346
December	.661	4.524	December	.643	4.293
Average	.524	4.882	Average	.504	4.66

Table: Solar intensity of Choto Kumira & Mirsorai, Bangladesh (September, 2011)

Choto Kumira, Time: 9.30 am to 10.30 am Latitude:22.505278^0, Longitude: 91.715^0		Mirosorai, Bangladesh Time: 12.00 am to 1.00 pm Latitude:22.86472^0, Longitude: 91.56639^0	
No. of obs	Solar Intensity	Solar Intensity (lux)	
		Cloudy Sky (9.30 am to 10.30 pm)	Sunny Sky (12.00 am to 1.00 pm)
1	28200	35800	90000
2	31500	36500	89500
3	30600	36700	89400
4	26500	36400	91500
5	63000	37000	89000
6	71300	37900	87400
7	38200	38000	98000
8	25000	44700	99700
9	80000	44800	96000
10	71000	45000	98700

8. Conclusion

There is a great potential of micro hydro in Chittagong hill tract region of Bangladesh. This paper shows some feasible places beside the government survey to establish micro hydro and generate power. There is a diversified geographical feature with hill, mountain, river, canal and spring exists in this region. This hill tract region has promising resources to play a great role in the economy of Bangladesh. But without abundant power and shortage of energy supply this promising resources can't be utilized. On the other hand it is so tuff to provide power from the national grid to the remote areas of Hill Tracts and it needs huge expenditure. So to provide the electricity in that region without extra expenditure it is very fruitful to establish the micro hydro power plant. This paper has an effort to bring the micro hydro power plant into limelight and also to show some new promising places with proper calculation where this kind of plant can be established. If it is possible to develop power plant using micro hydro then it will definitely change the overall scenario of electricity in these region which will certainly affect the life style and economic stability of the people in that region as well as Bangladesh.

Acknowledgement

We are grateful to the omniscience Allah that we have completed our thesis successfully. We started our thesis on 'Feasible Micro Hydro and Solar Potentiality Exploration in Hill Tracts of Bangladesh' in Chittagong hill tract region' with kindness of Allah. We are grateful to the teachers of Electrical & Electronic and Mechanical Engineering department of CUET for helping ourselves a lot and give outline in germane all the time.

References

[1] Anonymous, January 2012, Energy Bangla. "Prioritising strategy for power sector". http://www.energybangla.com/2012/01/02/216.html

[2] Anonymous, 2002. Ministry of Energy and Mineral Resources, Government of Bangladesh, "Draft Renewable Energy Policy of Bangladesh", Dhaka, Bangladesh, October, 2002.

[3] Anonymous, 2008. Renewable Energy Policy of Bangladesh, Power Division, Ministry of Power, Energy and Mineral Resources, Bangladesh, Nov. 2008.

[4] Anonymous, June 2010, Ministry of Finance, Government of Peoples Republic of Bangladesh, "Towards Revamping Energy and Power Sector: A Road Map"

[5] Key Statistics of power, Bangladesh Power Development Board (BPDB), http://www.bpdb.gov.bd/bpdb/

[6] Md M. Biswas, Kamol K. Das, Ifat A. Baqee, Mohammad A. H. Sadi, Hossain M. S. Farhad. July 2011. "Prospects of Renewable Energy and Energy Storage Systems in Bangladesh and Developing Economics" Global Journal of researches in General Engineering, Volume 11 Issue 5 Version 1.0

[7] Md. Mizanur Rahman and Piyas Chowdhury. 2012."Present Status and Future Development of Renewable Energy Technologies in Bangladesh" ,IJET: ISSN 1812-7711, Volume 9, Issue 1 2012.

[8] Power report, Power Division, Ministry of Power, Energy and Mineral Resources, Government of the Peoples Republic of the Bangladesh, http://www.powerdivision.gov.bd

[9] Projects, Local Government Engineering Department, Ministry of Local Government, Rural Development and Cooperatives, Bangladesh. http://www.lged.gov.bd

5th BSME International Conference on Thermal Engineering

Design & Fabrication of an Automated Solar Boat

Khizir Mahmud[a]*, Md. Imran Khan[b]

[a]*Department of Electrical Engineering, Northwestern Polytechnical University, X'ian- 710072, China*
[b]*Department of Mechanical Engineering, Chittagong University of Engineering & Technology, Chittagong-4349, Bangladesh*

Abstract

Environment awareness has developed worldwide so progressively over the last few decades. Engineers in all disciplines have a particular obligation of development which is environmentally friendly and lead towards sustainable future development. The future engineers are required to be trained in decision making and to act environmentally sensitive and responsible manner. It is essential for them to obtain the knowledge on new environmental friendly technologies e.g. renewable energy technology. Solar energy is a prodigious renewable energy source which has enormous energy existing as heat and light. By processing this energy we can convert it to electricity and which is already using in many domestic purposes without pollution and environmental hazard. Besides the domestic uses we can utilize it as the alternative of the oil in boat's fuel and minimize the water pollution. The purpose of this research is to design and fabricate a solar boat. The boat will be conducted by the energy processed from solar by minimizing environmental pollution.

Keywards: Boat material; photovoltaic system; renewable energy; solar boat; solar energy.

1. Introduction

With the increasing population of the world we should think about alternate sources of energy because the primary sources of fuel are limited in stock. So the scientists are looking for sustainable energy sources like Sun, wind, water and tidal flow. Of them solar energy is the prime source of renewable energy as it can get easily from nature. Bangladesh is situated between 20.30—26.38 degrees north latitude and 88.04— 92.44 degrees east which have at least 2500 hours of bright sunshine per year 10]. So Bangladesh is a promising country that can utilize solar energy in its different sectors like inland navigations. There are many water way in Bangladesh mainly in southern region like Hill track lake areas, Vhola, part of Barishal. So considering all of the features introducing solar boat will be a good transportation system for Bangladesh. This paper has an attempt to design and fabricate a solar powered boat that can satisfy the requirements of short transportation. The boat has a navigation capacity of 25km/Day with maximum total weight of the unit of 200kg. The boat's has two batteries provide power as well in short cloudy periods as if it be a reliable source of transportation.

2. Boat Sheet Specification

2.1 *Main dimensions*

Table I. – Different parts sizes of the solar boat.

* Corresponding author. Tel.: +8618392374190
E-mail address: khizirbd@gmail.com

Variable	Description	Dimension (m)
Loa	Length over all	4.50
Lhull	Length hull	4.00
Lwl	Length water line	3.50
Boa	Breadth overall	1.92
Bhull	Breadth hull	1.50
Bwl	Breadth waterline	1.30
D	Depth	0.45
T	Drought at design	0.23
H	Height	1.65

2.2 Hydrostatic/ Hydrodynamic

Table II. - Hydrostatics and hydrodynamics data of the boat

Lsw	Light ship weight	200 [kg]
Dw	Deadweight	160 [kg]
Vdesign	Volume at design draught	0.360 [m]
P	Density of freshwater	1000 [kg/m2]
Δdesign	Displacement at design draught	360 [kg]
Cb	Block coefficient	0.345
Fn	Froude number	0.358
Gm	Gm for heel φ=0o	0.12 [m]

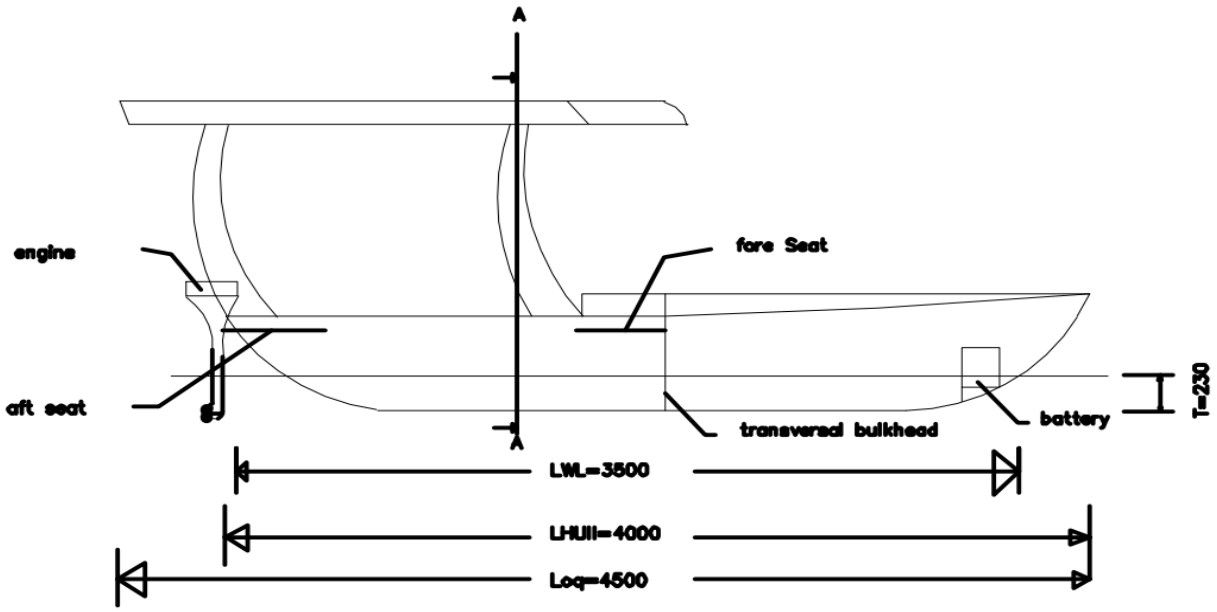

Fig 1: general view of solar boat dimension in centimetre

2.3 **Propulsion**

Table III. - Propulsion data of the solar boat

Notation	Size	Appearance
Vmax	Maximum speed	4 [kn]
Pmax	Max. Engine power output	2.7 [kw]
A	Area solar panels	7 [m2]
U/C	Voltage and capacity of the 2 batteries	24 [V] / 84 [Ah]

3. Boat material

In order to maintain the light weight for the light ship weight (LSW) it was necessary to use light composite materials. Though it made the boat quit expensive.

Table IV. - Boat material dates

Resin	Reinfor- Cement	Density [kg/m3]	Tensile Strength[Mpa]	Tensile Modulus [Gpa]	Comp. Strength
Epoxy	Aramid WR	1330	517	31	172
Polyester	E-Glass uni	1800	410-1180	1241	210- 480

Hull, bulkheads, pillars, deck, seats and roof are out of the very light Aramid WR. This has relative good material characteristics compared to the weight. The keel which has to contain the main forces and moments is out of the very strong E-Glass uni material [7].

3.1 Different Element Weight

For the determination of the weights was the hull shape approximated with geometrical surfaces like ellipses and parabolas and also with geometrical bodies like ellipsoids and paraboloides. For the preliminary design the precision of this method should be enough [7]. For the following design steps however more accurate calculation methods are necessary like e.g. SIMPSON [7].

Table V. - Weight of the different elements of the boat.

Element	Surface [m2]	Thickness [m]	Volume [m3]	Density [kg/m3]	Material	Mass [kg]
Hull aft	6.86	0.005	0,0343	1330	Aramid wr	5.62
Hull fore		0.005	0,0030	1330	Aramid wr	4.07
Flat keel	0.21	0.02	0,0042	1800	E-glass uni	7.54
Bulkhead trans.	0.49	0.005	0 ,0024	1330	Aramid Wr	3.28
Bulkhead long.	0.83	0.005	0,0041	1330	Aramid Wr	5.52
Deck	2.76	0.004	0,0082	1330	Aramid Wr	4.68
Roof	4.27	0.003	0,0128	1330	Aramid Wr	7.04
Pillar		0.003	0 ,0007	1330	Aramid Wr	1.01
Seat	0.53	0.005	0,0007	1330	Aramid wr	1.01

Table VI. - Total weight of the solar boat.

Element	Mi [kg]
Hull	49.69
Flat keel	7.54
Deck	14.68
Bulkhead transversal	3.28
Bulkhead longitudinal	5.52
Roof	17.04
Solar panel deck	16,56
Solar panel roof	25.62
2 fore pillars	2.01
2 aft pillars	2.01
Engine	22.00
2 batteries	30.00
Fore seat	1.01
Aft seat	1.01
	Σ= 198

The difference of 2kg between the denoted 200kg LSW in the data sheet and the 198kg LSW in this table is used as a reserve. This documentation contains a preliminary design. For this reason the weights were calculated with simple approximations. That means that there will probably be variations in the weight during the following design stages. The reserve of 2kg acts as a security factor to make sure that the total weight of the boat is less than the required 200kg.

4. Boat Propulsion

4.1 Significant boats

To approximate the needful power for the propulsion system 6 similar boats were compared to each other. The

effort to use the Admiralty coefficient was not effective:

$$Cadm = \frac{\Delta^{\frac{2}{3}} V^3}{pb}$$

Table VII. - Propulsion data of different types of boat.

Boat	L [m]	Δ [kg]	V [kn]	Pb [kw]	Cadm
Woolwich 20	5.9	1000	5.8	2.4	8130
Electric Boat	4	280	4.9	0.3	6784
Frauscher 560 Valencia	5.6	650	-	4.3	-
Frauscher 1500 W	5.4	350	-	1.5	-
Terhi (FI) Sea Fun C	4.06	185	-	2	-
Frauscher 600 Riviera	6	1400	5	4	3911

Mean values: = 5.16m; = 644kg; = 5.2kn; = 2.4kw

The Admiralty coefficient which is a crude but useful method of estimating power doesn't give any helpful values in this case. The main reason for that are probably the strong distinctions in the used values. As this method is confined to cases where the change in speed (V in kn) and displacement (Δ in kg) is relatively small. Besides the big distribution from the Admiralty coefficients the table shows that the Boat is with a length L of 4.50m, a displacement Δ of 360kg and an engine power Pb of 2.7 kw for a speed V of 4 knots well equipped.

5. Solar Energy

Table VIII. - Solar energy data.

Solar constant (terrestrial)	1 kw/m3
Effectiveness η of the solar panels	20 %
Surface of the solar panels	7.03m3
Area weight solar panel	6 kg/m3

The quantity of average solar energy in all season in Bangladesh is 1kw per 1m2 terrestrial surfaces. Mono crystalline solar cells are able to convert 20 % of the incoming solar energy into electrical energy:

$$1\frac{KW}{m^2} \times 0.20 \times 7.03 m^2 = 1.41\ KW$$

The solar panels on the Boat can provide 1.41kw, as illustrate in the above equation.

6. Batteries

The boat contains two batteries of the following type as show in the table IX.

Table IX. - Batteries specification

Manufacturer	Voltage/Capacity[V/Ah]	Dimensions(length x breath x hight) [mm]	Weight [kg]
DETA GEL	12/42	197 x 166 x 175	15
Total	24/84	-	30

The batteries are installed in the fore part of the boat. One stands on the portside and the other one on starboard. To ensure a good maintenance for each battery is a hatch in the deck installed. With the two batteries the Boat can store the solar energy. So she has propulsion even under non-perfect weather conditions [6].

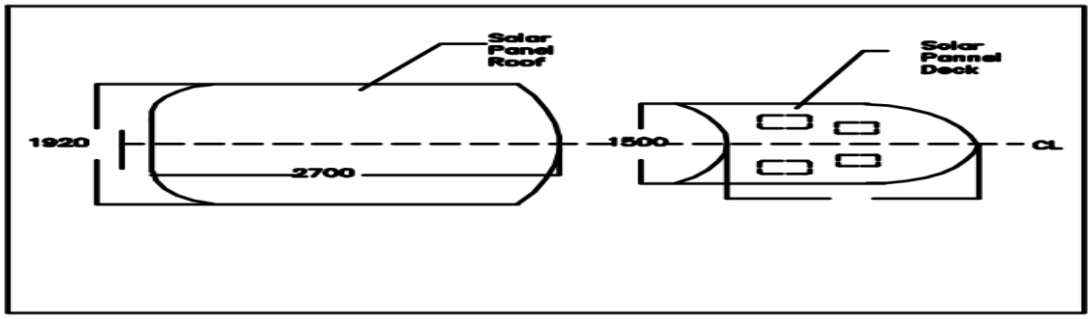

Fig 2: General view of the solar panel dimensions in centimeters.

7. Engine

Karvin 2700 engine has been chosen for the solar boat. The main advantage of this engine is that it can operate in direct current and has flexible options to speed control.

Table X. – Specification of KARVIN 2700 engine [9].

Amp hour rating min	80 Ah battery
Battery voltage	24V/36V/48V
Rpm max.	900 / 1200 / 1500
Power max. Kw/Hp	2.7 / 3.6
Torque	27.5 nm
Shaft length	long shaft l (510mm) / short shaft s (380mm)
Continuous regulation	Yes
Forward and reverse	Yes
Engine weight	22kg
Electronics	electronic control + electronic safety key

8. Boat Stability

For the determination of the centres of gravity of the sections valid the same as for the weight no numerical methods were used during the preliminary design. That results in the fact that all the given data are approximations and may change in the following design steps.

Table XI. - Stability dates

Element	Mi [kg]	Xcgi [m]	Mi x Xcgi [kg.m]	Zcgi [m]	Mi x Zcgi [kg.m]
Hull	49.69	1.77	88.05	0.15	7.50
Flat keel	7.54	2.07	15.59	0.08	0.57
Deck	14.68	2.93	32.23	0.45	6.61
Bulkhead trans.	3.28	2.80	6.57	0.32	1.05
Bulkhead long.	5.52	2.91	16.06	0.25	1.40
Roof	17.04	1.00	17.04	1.65	28.11
Solar panel deck	16.56	2.93	48.46	0.45	7.45
Solar panel roof	25.62	1.00	25.62	1.65	42.27
2 fore pillars	2.01	1.50	3.02	0.85	1.71
2 aft pillars	2.01	0.06	0.12	0.85	1.71
Engine	22.00	3.18	69.96	0.23	5.06
2 batteries	30.00	2.80	84.00	0.09	2.70
Fore seat	1.01	1.83	1.84	0.40	0.40
Aft seat	1.01	0.18	0.18	0.40	0.40
2 persons	160.00	1.00	160.00	1.20	192.00
Σ=	54.29	Σ=	582.09	Σ=	298.93
			Xcg=1.63		Zcg= 0.84

9. Calculation of GM (heel φ = 0o)

$$GM = KB + BM - KG$$

The distance between the base line K (Z = 0m) and the centre of buoyancy in z-direction (ZCB) equals to:

$$KB \sim \frac{2}{3}T - \frac{2}{3} \times 0.23\,m - 0.15m$$

The distance between the centre of buoyancy in z- direction (ZCB) and the metacentre (M) equals to:

$$BM = \frac{I_T}{V} \sim \frac{L \times B^3}{12 \times V} = \frac{3.5m \times (1.0m)^3}{12 \times 0.360m^3} = 0.81m$$

So the initial stability is:

$$GM = KB + BM - KG = (0.15 + 0.81 - 0.84)m = 0.12\ m$$

The initial stability was calculated considering 2 persons with a weight of 80 kg/person stand in the aft part of the boat. This was defined as the worst possible loading case. With a GM of 0.12m is the initial stability good.

10. Strength

Strength Considering the longitudinal strength the flat keel (50mm x 20mm) is the most important component of

the boat. It is designed for lakes and rivers. So it will not be subject to the strong torsion-and bending moments which can be created from heavy sea motions. But an inconvenient distribution of the Deadweight in the boat can also cause significant torsion and bending moments. The main structure that provides strength in the hull of the boat consists of:

- The flat keel (general longitudinal strength)
- The transversal bulkhead (receives torsion moments from the hull)
- The seats (prevent the twist of the hull through the reduction of the deck opening degree)
- The longitudinal bulkhead (prevents the warping of the transversal bulkhead and connects the keel with the deck).
- And the deck (prevents the twist of the hull and receives also the bending moments)

Besides a possible inconvenient distribution of the Deadweight the overland transport on a trailer is another critical condition regarding to the strength. In that case the whole weight of the Boat rests on a few points with a relatively small area. So there can be strong area forces on the hull. Those can be increased through additional impulse forces caused by bad road conditions during the overland transport. So during the transport the forces should be introduced in the hull basically through the flat keel and from the side through the transversal bulkhead. The area of the support points should be as big as possible. Due to optical-and strength-reasons the cross section of the pillars is relatively big and ellipses shaped.

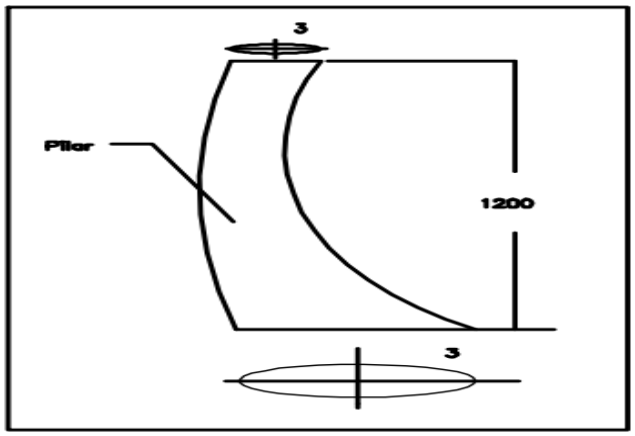

Fig 3: Cross sections of the pillar dimensions in centimeter.

11. Construction Mode

The hull can be produced in a negative form or in a positive form. In which several layers of the material can be put on top of each other. If the hull is ready and separated from the negative form the two bulkheads which can be produced as one single part can be glued in the hull. In the next step the deck (with the four holes for the hatches) must be glued on the hull. The pillars can be made around a positive form. When they are ready and separated from their form they can be installed on the hull. The connections between the pillars and the deck and the pillars and the roof are also glue connections. Like the hull the roof can be produced in a positive or negative form. When all composite parts are connected the solar panels can be bond on deck, roof and the four hatch covers. The montage of the four hatch covers is the next step. After that the electricity must be installed. That means the batteries and wires get assembled. (It may be favorable to install the batteries in the hull before the installation of the deck.) The last step is to install the engine.

12. Electrical Systems of Solar Boat

12.1 Photovoltaic System

According to Solar Splash rules, sunlight is the only power source for charging energy storage devices used for propulsion of boat. The sunlight is converted to electric energy by photovoltaic array (PV) made from semiconductor materials. The energy delivered by PV arrays is stored in lead acid batteries or directly used by propulsion devices. The output power (OUT P) of PV arrays may not have a one sun output greater than 480 watts and open circuit voltage (OC V) cannot be greater than 52V [8]. Following the characteristic tests, it was concluded that the maximum power point (MPP) of PV array is at the knee of I - V curve and it is unique point. Moreover, since solar cells are semiconductor devices, the power delivered by the PV array depends on the irradiance, temperature, and load voltage (battery voltage) [8]. As these parameters always change during

daytime, the current – voltage (I - V) characteristic of PV varies too. Due to this fact, if the PV is directly connected to load even at its MPP, it may not operate at its MPP. Therefore, the required power will not be obtained from PV array. This problem can be solved by using larger solar panels, but the solution is expensive. Instead of this, maximum power point tracker (MPPT) circuit is located between solar panel and load. MPPT is a microcontroller based, high switching frequency, DC – DC converter that forces PV array to operate at its MPP under both changeable atmospheric conditions and load voltage situation. As battery voltage (24V) is less than PV voltage (48V), a buck (step - down) converter was used. The analog signals such as voltage, current received by control circuit of MPPT were converted to digital signal by internal analog to digital converter (ADC) of microcontroller in order to be used for MPPT algorithm. Then, according to the result of MPPT algorithm, the duty cycle of buck converter was determined to operate PV array around MPP [1]. Complete electrical diagram of the solar cell is illustrated in the following figure.

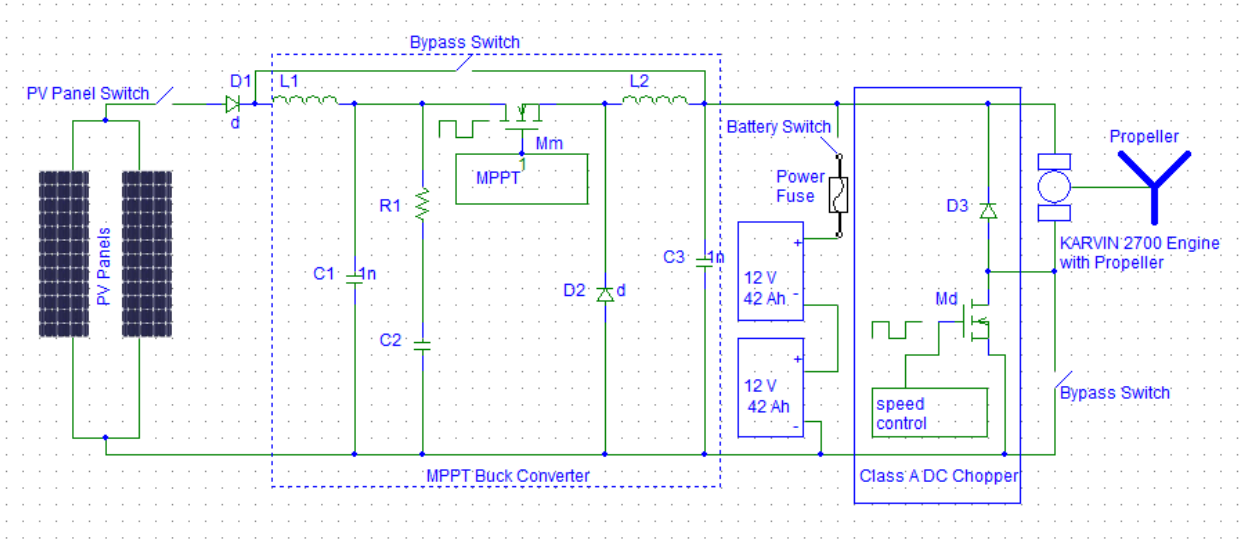

Fig 4: Electrical diagram of the solar boat

12.2 MPPT Design

The multipurpose control circuit was used as control circuit. A buck converter was designed for the solar boat because battery voltage was lower than the array voltage. Battery voltage was around 24V and PV array voltage was about maximum 48V. The most essential part of MPPT is its control algorithm [8]. MPPT algorithm was constructed so that it increases or decreases the duty cycle in order to determine MPP as the conditionals which change the maximum power point of PV array. Since the MPP of PV array is only one point on V - P curve, the algorithms used should operate efficiently as much as it is possible to operate the PV array at this point [2], [3]. By considering this fact, the various algorithms were tested to determine the most efficient methods. Before testing conventional MPPT methods, the PV array was operated at its MPP by manually adjusting duty cycle of buck converter to monitor MPP points during atmospheric condition changes.

12.3 Motor Controller

A first- quadrant (Class A) DC chopper illustrated in fig. 5 was designed and manufactured for controlling motor speed. In this part, a constant DC voltage has to be converted into a variable DC voltage to control the speed of motor. In this type of choppers, current and voltage values of load are both positive indicating a single-quadrant operation [4]. DC choppers have several advantages like soft start, smooth speed control and high efficiency [5]. For the control part of this chopper, the same multipurpose control circuit was used.

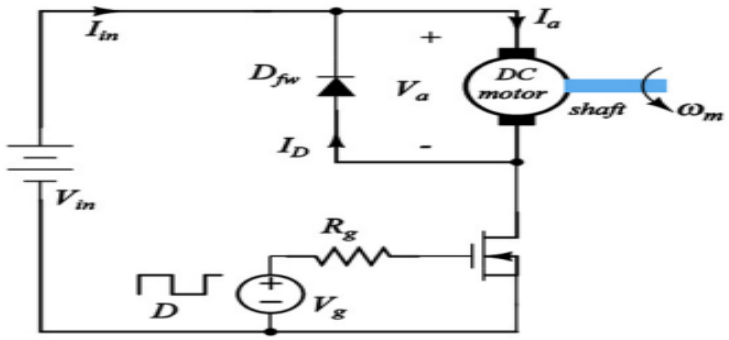

Figure 5: Class-A single quadrant DC chopper

Conclusion

Scientist always insists that this is the high time to minimize the dependency of fuel on conventional energy sources gradually and side by side to encourage the renewable energy sources. The use of renewable energy sources not only helps to reduce the environment pollution but also plays a great rule to reduce expenditure. For this reason the use of solar boat in inland navigation of developing country can help a lot to reduce cost. Alike the developing countries this boat can be a pertinent transportation system in Bangladesh. So this paper has an effort to introduce this kind of boat by proper design and fabrication.

Acknowledgement

We are grateful to the omnipotent Allah that we have completed our journal work successfully. We started our work on 'Solar boat' in the lab of Chittagong University of Engineering & Technology. We express our gratitude to the teacher of Electrical & Electronic and Mechanical Engineering department of CUET. Their sincere guidance and enthusiastic inspiration encouraged ourselves to complete the work.

References

[1] M. C. Ozden et al.; "Technical Report of the Istanbul Technical University Solar/Electric Boat", Advanced Energy Competitions, Inc. (Also on internet at www.solarsplash.com), 2007

[2] D.P. Hohm, M.E. Ropp: "Comparative Study of Maximum Power Point Tracking Algorithms Using an Experimental, Programmable, Maximum Power Point Tracking Test Bed". Photovoltaic Specialists Conference, 2000. Conference Record of the Twenty-Eighth IEEE 15-22 p.1699 – 1702, Sept. 2000.

[3] X. Weidong and W.G. Dunford: "A modified adaptive hill climbing MPPT method for photovoltaic power systems" Power Electronics Specialists Conference, 2004. PESC 04. 2004 IEEE 35th Annual Volume 3, p. 1957 - 1963 Vol.3, 2004.

[4] R.W. Erickson, "Supplementary notes on EMI and Layout Fundamentals for swiitched mode Circuits".

[5] S. Tweedie, "Experimental Investigation of Flow Control Techniques To Reduce Hydroacoustic Rotor-Stator Interaction Noise", 2006

[6] R. Leiner, "Research solar power boat - data management and online visualization", (2009).

[7] Juraci Carlos de Castro Nóbrega and Andrej Rössling, "Development of Solar Powered Boat for Maximum Energy Efficiency", International Conference on Renewable Energies and Power Quali (ICREPQ'12), 2012

[8] M. Cansin Ozden, "The Successful Design and Construction of Solar/Electric Boats Nusrat and Muavenet: An Overview", 2009

[9] Karvin electric outboard motor service instructions, http://www.karvin-polska.com

[10] Solar intensity, Banglapedia, http://www.banglapedia.org/httpdocs/HT/R_0175.HTM

[1]5th BSME International Conference on Thermal Engineering

Energy and Exergy analysis of a thermal power plant

Rabiul Islam[a*], Prasanjit Das[b], Noman Sadi[b]

[ab]*Department of Mechanical Engineering, Chittagong University of Engineering & Technology, Bangladesh*

Abstract

Exergy analysis is a method to evaluate the performance of devices, the degradation of energy during a process, entropy generation, the lost available energy to be used, and offers an alternative mean to improve the plant efficiency. In this paper the energy and exergy analysis of Chittagong Power Station, Chittagong, Bangladesh is presented. The main objectives of this paper are to analyze the components of the plant separately at different loads and different environmental temperatures, and to identify and qualify the largest losses of the plant. By this study, it is found that the largest energy losses of the plant is occurred in condenser, while the ratio of exergy destruction to the total exergy destruction is to be maximum at boiler followed by turbine and then the condenser. But the energy losses in boiler are far less than the condenser. Thus we concluded that the boiler is the main source of irreversibilities of this plant. Later the exergy destruction at different components is shown by bar chart.

Keywords: Exergy analysis, exergy efficiency, steam powerplant

1.Introduction

Bangladesh's energy market is one of the country's fast developing sectors. Annual demand for electricity is increased by 8% to 10% in this country where only 45% of the 155 million people are covered by the current power supply. In the May-October period last year, power outages occurred around 8 -12 hours per day, bringing life to a standstill and with factories being the worst affected.

On March this year (2012), there was a shortage of 1,304 MW, or nearly 25% of demand, with only around 3,769 MW of electricity generated against a total demand for 5,100 MW, according to the daily report of the Power Grid Company of Bangladesh. Shortages are higher during the summer, when demand can reach 6,000-6,300.

Nomenclature

h	specific enthalpy KJ/kg	Greek symbols	
I	Exergy destruction rate (W)	ψ	specific exergy (J/Kg)
$\dot{m}$	mass flow rate (ton/h)	η_{II}	exergy efficiency
P	pressure (P)	γ	exergy factor
$\dot{Q}$	heat transfer rate to the system (W)	Subscripts	
S	specific entropy (J/Kg.K)	i	inlet
T	temperature (K)	e	exit
W	work rate or power done by the system (W)	s	isentropic
$\dot{X}$	Total exergy rate	o	dead state condition

The Electricity production from natural gas sources (% of total) in Bangladesh was 89.38 in 2009, according to a World Bank report, published in 2010. So it is very important to analysis the power generation system for scientific interest and also essential for the efficient utilization of this energy resource. There are few methods to measure the performance of a power plant. The most commonly-used method of an energy-conversion process is the first law of thermodynamics. However there is increasing interest in the combined utilization of the first and second laws of thermodynamics, using such concepts as exergy and exergy destruction in order to evaluate the efficiency with

*Rabiul Islam. Tel: +880-1711319509
Email address: rabiulibs@gmail.com

which the available energy is consumed. The exergy method of analysis is based on the second law of thermodynamics and the concept of irreversible production of entropy. The fundamentals of exergy method laid down by Carnot in 1824 and Clausius in 1865 [1].

Scientists and engineers traditionally use the First law of thermodynamics to calculate the enthalpy balances to quantify the loss of energy, but it is unable to account the quality aspect of energy. This is where exergy analysis becomes relevant. The exergy concept has gained considerable interest in the thermodynamic analysis for thermal process and plant systems because it has been seen that the first law analysis has been insufficient from an energy performance stand point [1].

However exergy can specify where the process can be improved and therefore, it will signify what areas should be given consideration. The simple energy balance will not sometimes suffice to find out the defect of the system. In this circumstances the exergy analysis well thought-out to be significant to locate the systems imperfections.

The objective of this work is to analyze one generating unit of Chittagong Power Station from an energy and exergy perspective. Locations of energy loss and exergy destruction will be determined. The effects of load variation and the reference environment state on the exergy analysis will also be investigated.

2. Plant description

The power plant has a total installed capacity of 420MW. It is located in Raojan, Chittagong. It started to produce power in 1995. The power plant consists of two steam turbines unit (2×210) MW at 100% load. The power plant uses natural gas. The schematic diagram of the power plant is given in Fig. 1. Each unit has four LPH and three HPH. Steam is superheated to 804K and 12.44 MPa in the steam generator and feed to the high pressure turbine. At full the mass flow rate of the steam entering high pressure turbine is 713 ton/h, the pressure turbine exhaust steam at pressure 2.5MPa is sent to reheater where it is reheated to 784 K and enters the intermediate pressure turbine at a pressure of 2.34 MPa . The intermediate pressure turbine exhaust is fed to low pressure turbine at 0.11MPa and it exhausts to a water cooled condenser operates at .011 MPa. Then the cycle starts again.

Table 1. Operating conditions of power plant

Operating conditions	Value
Natural gas flow rate	52.1 (KNM^3/h)
Feed water inlet temperature to boiler	553 K
Main steam flow rate	712.9 (ton/h)
Steam temperature	804 K
Steam pressure	12.44 (MPa)
Power output	210MW
Number of pump	3

Table 2. Exergy destruction rate and exergy efficiency equations for power plant componenets

Components	Exergy destruction rate	Exregy efficiency
Boiler	$\dot{I}_{boiler}= \dot{X}_{fuel}+ \dot{X}_{in} - \dot{X}_{out}$	$\eta_{II,boiler}= \frac{\dot{X}_{out}-\dot{X}_{in}}{\dot{X}_{fuel}}$
Pumps	$\dot{I}_{pumps}= \dot{X}_{in} - \dot{X}_{out} + \dot{W}_{pump}$	$\eta_{II,pump}= 1- \frac{\dot{I}_{pump}}{\dot{W}_{pump}}$
Heaters	$\dot{I}_{heaters}= \dot{X}_{in} - \dot{X}_{out}$	$\eta_{II,heater}= 1- 1- \frac{\dot{I}_{heater}}{\dot{X}_{in}}$
Turbine	$\dot{I}_{turbine}= \dot{X}_{in} - \dot{X}_{out} - \dot{W}_{el}$	$\eta_{II,turbine}= \frac{\dot{I}_{turbine}}{\dot{X}_{in}-\dot{X}_{out}}$
Condenser	$\dot{I}_{condenser}= \dot{X}_{in} - \dot{X}_{out} + \dot{W}_{f}$	$\eta_{II,condenser}= \frac{\dot{X}_{out}}{\dot{X}_{in}+\dot{W}_{f}}$
Cycle	$\dot{I}_{cycle}= \sum_{\text{all components}} \dot{I}$	$\eta_{II,cycle}= \frac{\dot{W}_{net,out}}{\dot{X}_{fuel}}$

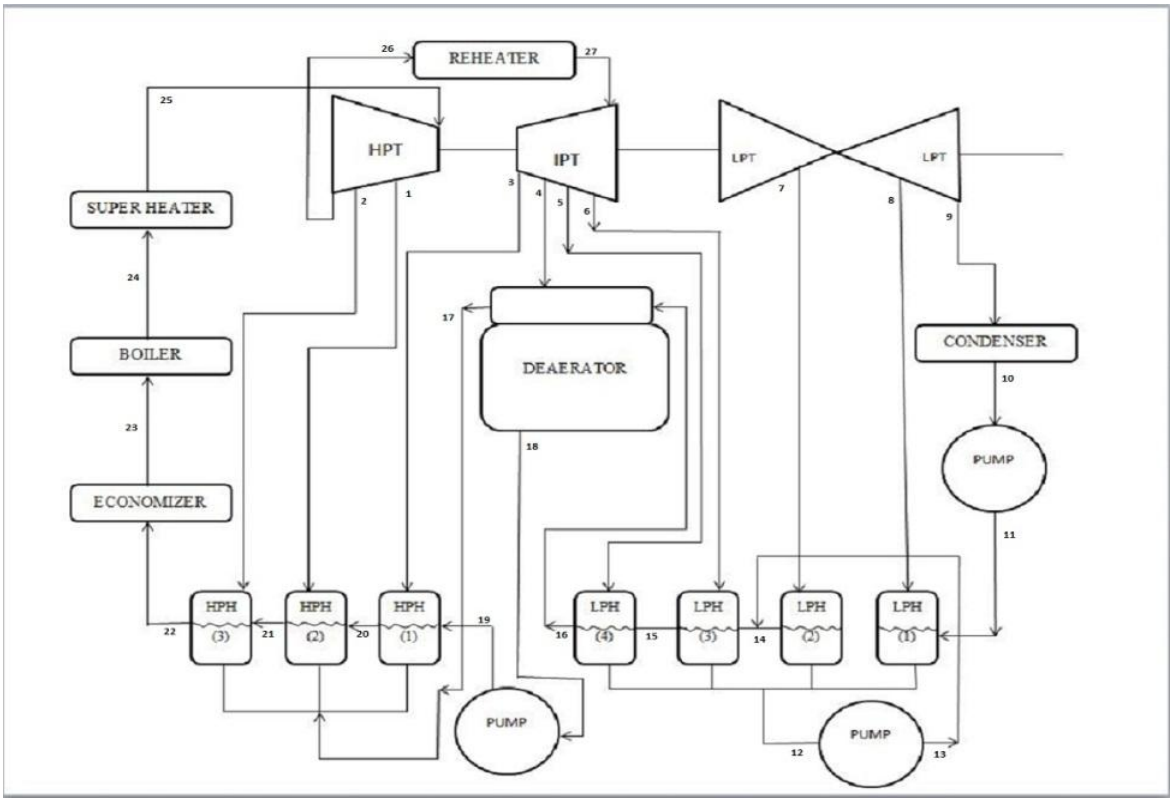

Fig.1. Schematic diagram of the power plant

3. Analysis

Exergy is a measure of the maximum capacity of a system to perform useful work as it proceeds to a specified final state in equilibrium with its surroundings. Exergy is generally not conserved as energy but destructed in the system. Exergy destruction is the measure of irreversibility that is the source of performance loss. Therefore, an exergy analysis assessing the magnitude of exergy destruction identifies the location, the magnitude and the source of thermodynamic inefficiencies in a thermal system [1].

Table 3. Exergy analysis of the power plant when T_O = 298.15K, P_O = 101.3KPa

Point	T (K)	P (MPa)	M (ton/h)	h (KJ/kg)	S (KJ/kgK)	Ψ (KJ/kg)	X (MW)
1	723	2.7	25.3	3308.4	6.76	1295.85	9.16
2	701	3.95	22.1	3208.3	6.43	1294.5	7.946
3	670	0.66	21.6	3259.6	7.38	1062.31	6.372
4	505	0.69	17.2	2838.2	6.64	861.82	4.117
5	463	0.38	9.4	2766.5	6.67	781.17	2.039
6	412	0.16	7.05	2728.7	6.96	656.71	1.286
7	357	0.025	14.5	2647.1	7.57	393.44	1.584
8	361	0.05	15.7	2674.6	7.36	483.55	2.108
9	331	0.011	583.1	2613.2	7.84	279.038	45.196
10	331	0.011	572.9	269.3	0.88	22.95	3.652
11	333.2	1.43	570.9	251.6	0.831	7.26	1.151
12	358	0.02	44.2	355.9	1.13	21.07	0.258
13	359	1.43	43.7	358.2	1.15	18.66	0.2265

14	375	1.40	602	424.4	1.32	34.176	5.714
15	394	1.93	599.4	507.5	1.54	51.683	8.605
16	413	1.25	597.8	587.1	1.74	73.99	11.280
17	520	1.5	56	1073.7	2.75	257.12	3.999
18	440	0.6	664	702.3	2.01	106.35	19.615
19	449	14.96	657.2	740	2.03	135.03	24.846
20	482	14.52	653.1	892.2	2.41	172.99	31.48
21	509	14.28	650.6	1010.8	2.70	184.21	33.466
22	537	13.92	648.2	1057.5	2.81	220.3	39.65
23	553	13.72	643.1	1236.8	3.06	327.79	58.556
24	574	13.39	717	2749.9	5.09	1080.7	215.326
25	804	12.44	713.1	3271.4	6.11	1453.03	287.821
26	602	2.5	663.3	3012.6	6.32	1131.63	208.502
27	784	2.34	658.2	3452.6	7.02	1362.92	249.187
28	388	0.11	600.4	2698.2	7.18	560.82	93.531

Table 4. Exergy balance of the power plant at different load, Heat added or loss

Components	Max Load	85.7% Load	77.67% Load
Condenser	381 MW	333.3 MW	313 MW
Net power	210 MW	180 MW	163 MW
Boiler	636.36 MW	557.27 MW	483.67 MW
Heaters	30 MW	69 MW	75 MW
Thermal efficiency	33%	32.3%	33.7%

Mass, energy and exergy balances for any control volume at steady state with negligible potential and kinetic energy changes can be expressed, respectively, by [1]

$$\sum \dot{m}_i = \sum \dot{m}_e$$
$$\dot{Q} - \dot{W} = \sum \dot{m}_e h_e - \sum \dot{m}_i h_i$$
$$\dot{X_{heat}} - \dot{W} = \sum \dot{m}_e \psi_e - \sum \dot{m}_i \psi_i + \dot{I}$$

where the net energy transfer by heat ($\dot{X_{heat}}$) at temperature T is given by

$$\dot{X_{heat}} = \sum (1 - T_O/T) Q$$

And specific exergy is given by

$\Psi = h - h_o - T_o(s - s_o)$

Then the total exergy rate associated with a fluid stream becomes

$$\dot{X} = \dot{m}\Psi = \dot{m}[h - ho - To(s - so)]$$

Choosing each component in Fig.1 as a control volume and for a steady state operation, the exergy destruction rate and exergy efficiency are defined as shown in Table 2. It includes the irreversibility of heat transfer to the steam in the boiler, exergy destruction associated with fuel combustion and exergy lost with exhaust gases from the furnace.

4. Results and Discussion

The power plant was analyzed using the above relations noting that the environment reference temperature and pressure are 298.15 K and 101.3 kPa, respectively. The thermodynamic properties of water at indicated nodes shown in Fig. 1 were calculated using steam table and summarized in Table 3.

The energy balance of the power plant at different loads is presented in Table 4. It shows that the thermal efficiency is about 33% at maximum load. Clearly, this efficiency was based on the specific heat input to the steam. The energy balance also reveals that about 59.8%of the energy added in the boiler is lost in the condenser and carried out into the environment. Nonetheless, efficiencies based on energy can often be non-intuitive or even misleading, in part because it does not provide a measure of ideality. In addition, losses of energy can be large quantity while it is thermodynamically insignificant due to its low quality. Exergy-based efficiencies and losses, however, provide measures of approach to ideality or deviation from ideality [7].

Table 5. Exergy destruction and exergy efficiency of the power plant components, when T_O = 298.15K, P_O = 101.3KPa

Components	Exergy destruction MW			Percent exergy destruction			Exergy efficiency at Max. load
	100%	85.77%	77.6%	100%	85.7%	77.67%	
Turbines	131	138	143.7	22.4	25.6	26.1	61.6%
Boiler	375	351	339	64.2	60.04	62.08	37.9%
Condenser	58.54	52.7	50.05	10.08	9.4	9.1	10.80%
Pumps	9.80	8.2	6.4	1.6	1.14	1.17	21.55%
Heaters	9.07	10.6	7.2	1.5	1.9	1.3	84.8%

Exergy destruction, percent of exergy destruction and percent exergy efficiency are summarized in Table 5 for all components present in the power plant. It was found that the exergy destruction rate of the boiler is dominant over all other irreversibilities in the cycle. It counts alone for (60%-62%) of losses in the plant, while the exergy destruction rate of the condenser is only (9.4%-10%). According to the first law analysis, energy losses associated with the condenser are significant because they represent about (60%) of the energy input to the plant. The real loss is primarily back in the boiler where entropy was produced. Contrary to the first law analysis, this demonstrates that significant improvements exist in the Boiler system rather than in the condenser and tremendous opportunities are available for improvement. However, part of this irreversibility cannot be avoided due to physical, technological, and economic constraints [4].

In order to quantify the exergy of a system, we must specify both the system and the surroundings. It is assumed that the intensive properties of the environment are not significantly changed by any process. The dead state is a state of a system in which it is at equilibrium with its surroundings. When a system is at the same temperature, pressure, elevation, velocity and chemical composition as its surroundings, there is no potential differences exist in such instances that would allow the extraction of useful work [7].

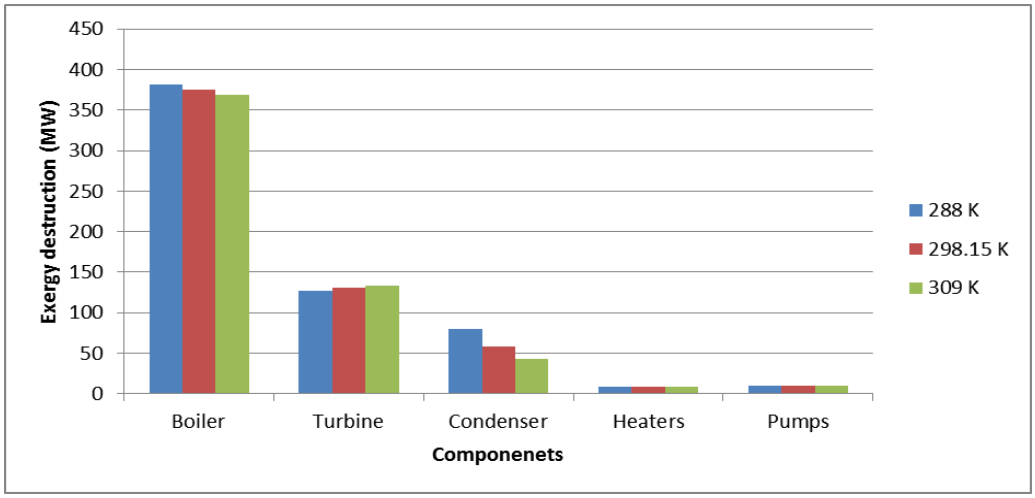

Fig. 2. Exergy destruction (MW) at differrent temperatures

The reference environment state is irrelevant for calculating a change in a thermodynamic property (first law analysis). However, it is expected that the dead state will have some effects on the results of exergy (second law) analysis. Although, some researchers assumed that small and reasonable changes in dead-state properties have little effect on the performance of a given system [3]. To find out how significant this effect will be on the results, the dead-state temperature was changed from 288 to 308 K while keeping the pressure at 101.3 kPa. Values of total exergy rates at different dead states for locations are shown in Fig. 2. Results of such analysis show that the major source of exergy destruction is the boiler no matter what the dead state is. However, the efficiency of the condenser at 308 K is much higher than the ambient temperature was 288 K. This can be explained by noting the diminution of temperature difference between the steam and the cooling air as the dead-state temperature is increased. This will decrease the exergy destruction and hence, will increase the exergy efficiency.

5. Conclusion

In this study, the energy and exergy analysis of Chittagong Power Station in Chittagong, Bangladesh is presented. The main objectives of this paper are to analyze the system components separately and to identify and quantify the locations having largest energy and exergy losses at different environmental temperature and loads.

The maximum energy loss was found in the condenser where 59.8%, 60% and 64.4% of the input energy was lost to the environment at full , 85.7%, and 77.6% load respectively. In addition, the calculated thermal efficiency of the cycle based on specific heat input to the steam was 33.7%, 32.3% and 33% at 77.6%, 85.6%, and full load respectively.

The exergy analysis of the plant showed that lost energy in the condenser is thermodynamically insignificant due to its low quality. In terms of exergy destruction, the major loss was found in the boiler where 375MW of the fuel exergy input to the cycle was destroyed at full load and it is 64.2% of the total exergy destruction. The percent exergy destruction in the condenser was 10.08%at full load, while all heaters and pumps destroyed less than 9.1% and 9.8% at full load respectively. Above 60% exergy destruction occurred in boiler. It indicates that tremendous opportunities are available for improvement. However, part of this irreversibility cannot be avoided due to physical, technological, and economic constraints

Acknowledgements

The authors are grateful to the management and stuffs of Chittagong Power Station for their generous helps.

References

[1] Isam H. Aljundi, Energy and exergy analysis of a steam power plant in Jordan. 2008.
[2] Rashadabd A. El Maihy, Exergy Analysis of a Steam Power Plant in Egypt. 2009.
[3] Chuang CC, Ishida M. Exergy analysis of an absorption heat pump by energy utilization diagrams. A future for Energy. Tokyo : Pergamon Press; 1990.
[4] Cengel, Y.A., Boles, M.A., Thermodynamics: An Engineering Approach", fifth ed. McGraw-Hill, New York. 2006.
[5] Szargut, J., Morris, D.R., Steward, F.R. Exergy Analysis of Thermal, Chemical, and Metallurgical Processes. Hemisphere Publishing Corp, New York. 1988.
[6] Kotas, T.J, The Exergy Method in Thermal Plant Analysis, Krieger, Malabar.1995.
[7] Bejan, A, Advanced Engineering Thermodynamics, third ed. Wiley, New York. 2006.
[8] Birnie, C, Obert, E. F. Evaluation and location of losses in a 60 MW power station, Proc. Midwest Power Conf, pp. 187-193, 1949.
[9] Keller, The evaluation of steam power plant losses by means of the entropy balance diagram, Trans. ASME, vol. 72, p. 949, 1959.
[10] Habib M. A.; Said ,' S. A. M. and Al zaharana, Optimization of Reheat Pressure
In Thermal Power Plants: Energy Vol. 20, No. 6, pp. 555-565, 1995.

Energy and Exergy Analysis in Agricultural Sector of Bangladesh

Rabiul Islam[a*], Noman Sadi[b] , Md Musleh Uddin[b]

[a,b]*Department of Mechanical Engineering, Chittagong University of Engineering and Technology, Chittagong-4349, Bangladesh*

Abstract

Bangladesh is an agricultural based country. Demand of food and other necessities of living based on agriculture are increasing day by day. Nowadays, many modern machineries of thermal efficiency is about 21% are used in agricultural sector of Bangladesh. So the thermodynamic losses take place in those machineries. To reduce these losses, it is important to identify and quantify them. An Exergy analysis is a method to identify the losses, evaluate the performance of devices, and it offers an alternative means to improve the efficiency. In this paper energy and exergy analysis of the agricultural sector in Bangladesh has been presented. Energy and exergy efficiencies, overall energy and exergy efficiencies of the fuel and electricity used to run the machineries have been estimated and graphically shown. Later, energy and exergy efficiencies of some countries are mentioned and compared with Bangladesh

Keywords: Exergy analysis, exergy efficiency, steam powerplant

1. Introduction

Agriculture supplies us with food and other necessities of living. Many kinds of machineries such as tractors, power tiller, shallow tube well, deep tube well, electric motors, etc, are used for agricultural activities. Before 70s, it is known that energy was abundant and cheap and therefore it was not a major concern. But it was not true. Fossil fuels are limited and may will be exhausted within 100-150 years. Emission released by burning fossil fuels is responsible for, greenhouse-gas emissions, global warming, climate change, etc. Therefore, using resources carefully and optimally is a major issue these days. For this reason in recent decades, practical concepts such as useful energy, computation of wasteful energy, have attracted the attention of many researchers. Scientists have been working on the thermodynamic quality aspect of energy for different sectors and countries. The main aim of their researches is to identify and assess thermodynamic losses taking place during the operation of different machineries in different sectors.

Nomenclature

h	specific enthalpy KJ/kg	Greek symbols	
I	exergy destruction J	ψ	specific exergy (J/Kg)
m	mass of the fuel (kg/s)	η_{II}	exergy efficiency
P_o	atmospheric pressure (P)	γ	exergy factor
E^W	exergy flow (J/s)	ε	specific exergy (J/kg)
E^Q	exergy flow for heat enrgy (J/s)	Subscripts	
S	entropy (J/KgK)	in	inlet
T_o	temperature (K)	ex	exit
W	shaft work (W)	ff	fuel
Y	energy consumed in the year,x	o	overall system

Energy analysis fails to indicate both the energy transformation and the location of energy degradation. In recent years, emerged a growing interest in the principle of special ability to measure different types of energy to work and popularly known as exergy [1].

Exergy analysis can lead to reduce the energy use and, thus, to decrease the environmental pollution. The main purpose of exergy analysis is to detect and assess quantitatively the thermodynamic imperfections' causes of thermal and chemical processes. The exergy method of thermodynamic analysis is based upon both the first and the second

laws of thermodynamics together, while the energy analysis is based only upon the first law. It is a feature of the exergy concept to allow quantitative assessment of energy degradation [2].

It also can distinguish between high-quality and low-quality energy sources and their uses in various sectors and thus gives an opportunity to match high-quality energy sources with high-temperature applications to acquire higher efficiencies. It is a suitable technique for furthering the goal of more efficient energy-resource uses, as it can identify the locations, types and true magnitudes of exergy destructions (losses) and wastes [2]. Many studies have already been carried out on energy and exergy utilizations, but it is found that there are limited studies on energy and exergy utilization in the agricultural sector. It is expected that this analysis will be useful for Bangladesh and some other countries. Policy makers in Bangladesh will be able to compare energy use and exergy efficiencies with other countries..

2. An overview of the agriculture sector in Bangladesh

The economic activities of Bangladesh are heavily dependent on agriculture in respect of employment, where about 48% of the human labor is involved. It contributes to about 18.29% of the gross domestic product (GDP) in 2010.(ministry of agriculture, 2010). So agriculture is fundamental prerequisite for the development of Bangladesh and improvement of it's people's life. Bangladesh is a developing country. It's economy is growing rapidly and the agriculture sector is important for both continuous economic growth and improving living standards. With the increasing demand of agricultural products along with unstoppable expansion of it's population the use of energy is growing year by year.

3. Theoretical and mathematical formulation for exergy analysis

These have been briefly presented in the following sections

3.1. The useful concept of exergy

Exergy can be defined as a measure of maximum capacity of an energy system to perform useful work as it proceeds to a specified final state in equilibrium within the surroundings. In simple words, we can describe exergy as the ability to produce work. The available work that can be extracted from an energy source depends on the state of the surrounding. The greater the temperature differences between an energy source and its surroundings, the greater the capacity to extract work from the system. Energy and exergy are different parameters (SimpsonandKay,1989) even though they were equivalent in their values [1].

In any real process irreversible), exergy is consumed or destroyed or lost since exergy cannot be conserved. The exergy balance equations can be shown as follows [2].

Exergy input -Exergy out-Exergy consumption =Exergy accumulation (1)

$$\sum_{in} \varepsilon_{in} m_{in} - \sum_{ex} \varepsilon_{ex} m_{ex} + \sum_{r} E^{0} - E^{W} - I - 0 \quad (2)$$

The amount of exergy destroyed within the system due to irreversibility during the process can be expressed by Eq. (2). $I=T_0 S_{gen}$ (3)

here the exergy consumption, I can be classified into two categories:

$I>0$ for an irreversible process, $I=0$ for a reversible process. Since $m_{in}=m_{ex}=0$, for a closed system, Eq.(2) can be simplified to $\sum_{r} E^{0} - E^{W} - I - 0$ (4)

3.2. Energy and exergy efficiencies for principle types of processes

The expressions of energy *(η)* and exergy *(ψ)* efficiencies for the principle types of processes can be presented by Eqs. (5) and (6), respectively [2]

Energy efficiency, $\eta = \frac{Energy\ in\ produdcts}{Total\ energy\ input}$ (5) and Exergy efficiency, $\psi = \frac{Exergy\ in\ produdcts}{Total\ energy\ input}$ (6)

Exergy efficiencies can often be written as a function of the corresponding energy efficiencies by assuming the energy grade function to be 'unity', which is commonly valid for the fuels encountered in the present [2]

3.3. Exergy efficiency calculations

The outputs of agriculture devices need to be in the form of kinetic energy (shaft work) and energy uses. The exergy associated with shaft work (W) can be expressed by

$E^W = W$ (7)

Thus, for electric shaft work production, the energy and exergy efficiencies of the devices used in agricultural activities can be expressed by

$\eta_{me} = \frac{W}{W_e}$ (8) and $\Psi_{me} = \frac{E^W}{E^{W,E}} = \frac{W}{W_e} = \eta_{m,e}$ (9)

Diesel and electric motor are used in agricultural activities in Bangladesh. First weighted mean energy efficiencies can be found for diesel and electricity by multiplying a weighing factor (f) with energy efficiency (η) for the fuel or electricity. A weighing factor is the ratio of energy input to the total sectoral input energy. This can be expressed by [2].

Weighing factor, $f = \frac{Energy\ inpput\ of\ any\ fuel}{Total\ energy\ input}$ (10)

Weighted energy efficiency of diesel, $\eta_{diesel} = \eta_0 \times f_{diesel}$ (11)

Weighted energy efficiency of electricity, $\eta_{electricity} = \eta_0 \times f_{electricity}$ (12)

Finally overall mean energy efficiency can be expressed by

$\eta_0 = \eta_{diesel} + \eta_{electricity}$ (13)

For fossil fueled shaft work production in agriculture devices, the exergy efficiency can be shown similar to the energy efficiency as follows:

$\eta_{m,e} = \frac{W}{m_{ff} H_{ff}}$ (14)

$\Psi_{m,e} = \frac{W}{m_{ff} \gamma_{ff} H_{ff}}$ (15)

$\Psi_{m,e} = \frac{W}{m_{ff} \gamma_{ff} H_{ff}} = \frac{\eta_{m,e}}{\gamma_{ff}}$ (16)

To assess the technical performance of agriculture devices, their exergy efficiency is considered as the quotient of the work output over the exergy input, corresponding to above equations. As devices are not operated at rated load (about 28) generally , so part load efficiencies of their devices are estimated to be 21% for road or agriculture devices such as tractor, deep tube well, shallow tube well ,low lift pump taken from [2]. Using weighing factor from Eqs. (10), weighted exergy efficiency of the diesel and electricity can expressed as follows,

$\psi_{diesel} = \frac{\eta_{m,e}}{\gamma_{diesel}} \times f_{diesel} = \frac{\eta_{diesel}}{\gamma_{diesel}}$ (17)

$$\psi_{electricity} = \frac{W}{W_e} = \eta_{electric\ motor,} \quad (18)$$

Thereof overall exergy efficiency can be expressed by

$$\psi_0 = \psi_{diesel} + \psi_{electricity} \quad (19)$$

4. Data sources and methodology

4.1. Data sources

Amount of fuel and electricity consumption by different machineries used in the agricultural activities are collected from Bangladesh Bureau of Statistics and presented in table 1

4.2 Steps and procedures taken for energy and exergy analysis

Energy and exergy efficiencies were determined using Eqs. (5) and Eqs. (6) Considering grade function as unity. The overall energy efficiency can be easily found by dividing total energy produced by total input energy [2]. The device exergy efficiencies are evaluated using data for the years (1990-2010) Energy and exergy efficiencies were then used to calculate the overall energy and exergy efficiencies of this sector.

Table 1. Energy uses data for the agriculture sector in Bangladesh for the year 1990-2010 (BBS)

	Energy consumption (GJ)			
Year	Diesel	% used	Electrical	% used
1990	14.39×10^6	87.5	2.13×10^6	12.5
1995	19.56×10^6	88.9	3.32×10^6	11.1
2000	26.60×10^6	90.23	3.29×10^6	9.77
2005	33.51×10^6	90.2	3.63×10^6	9.8
2010	38.72×10^6	92.26	3.25×10^6	7.74

5. Data analysis, results, and calculations

5.1 Overall energy and exergy efficiency:

With the help of data from table 1 and using equations (17) and (18) energy and exergy efficiencies of diesel oil and electricity are calculated. Then overall energy and exergy efficiency are calculated using Eqs. (13) and (19) and presented in table 2 and Fig. 1, Fig. 2, and Fig. 3.

Table 2. Energy, exergy and overall energy, exergy efficiencies for the period 1990-2010

Year	η_{deisel}	ψ_{diesel}	$\eta_{electrical}$	$\psi_{electrical}$	Overall energy efficiency	Overall exergy efficiency %
1990	18.37	17.17	10.60	10.60	28.99	27.79
1995	18.66	17.44	9.43	9.43	28.09	26.87
2000	18.95	17.70	8.30	8.30	27.25	26
2005	18.94	17.70	8.33	8.33	27.25	26
2010	19.37	18.10	6.58	6.58	25.95	24.68

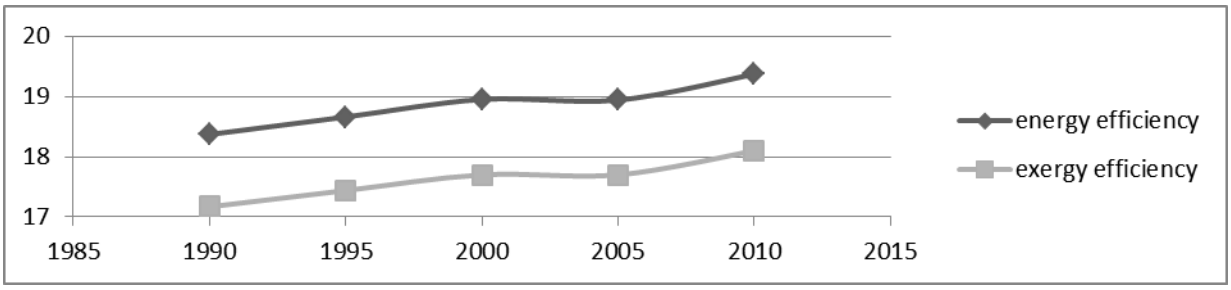

Fig. 1. Energy and exergy efficiency of diesel oil for Agriculture sector in Bangladesh for the period 1990-2010

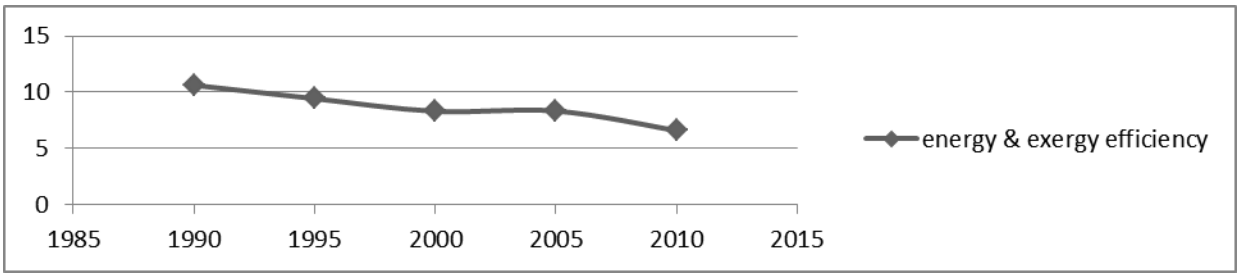

Fig. 2. Energy and exergy efficiency of electricity for Agriculture sector in Bangladesh for the period 1990-2010

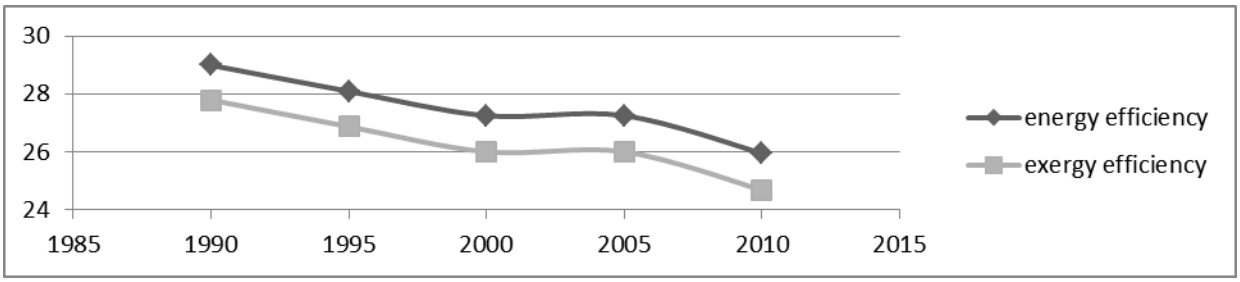

Fig. 3. Overall energy and exergy efficiency for Agriculture sector in Bangladesh for the period 1990-2010

5.2. Discussions

5.2.1. Energy and exergy analysis

In this section, we combined the overall energy and exergy efficiencies of Agriculture sector in Bangladesh. It is the ratio of energy or exergy products to the total energy or exergy inputs.

Overall energy efficiency= $\frac{\text{Total Energy Products}}{\text{Total Energy Inputs}} = \frac{40}{148} = 27.33\%$

And Overall exergy efficiency= $\frac{\text{Total Exergy Products}}{\text{Total Exergy Inputs}} = \frac{38.03}{143} = 26.54\%$

5.2.2. Comparison with other countries

In this section, energy and exergy efficiencies of agriculture sector in Bangladesh are compared with those of some selected countries. Overall energy and exergy efficiency of the agricultural sector in Bangladesh is compared with Turkey, Malaysia, Saudi Arabi), and Norway. Comparative results are presented in Fig.4. It has been observed that exergy efficiency of agriculture sector in Bangladesh is higher than Malaysia, Saud Arabia and Turkey but less exergy efficient than Norway.

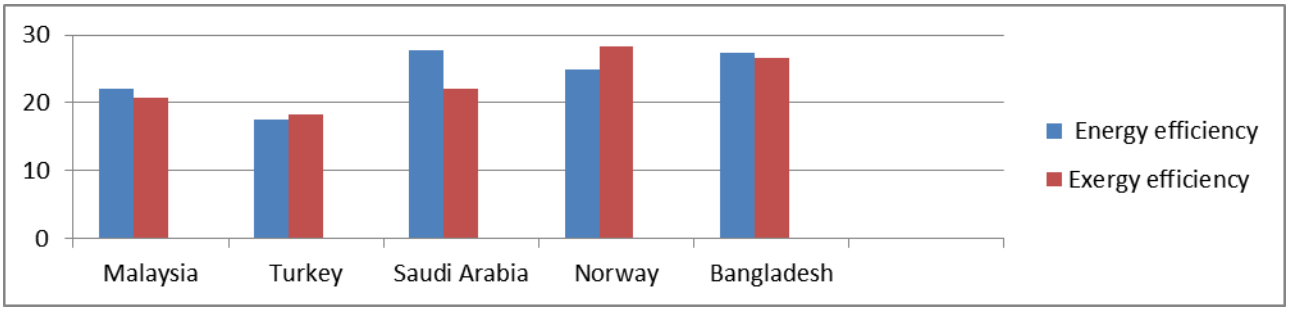

Fig.4. Comparison of energy and exergy efficiencies of the agriculture sector of Bangladesh with other selected countries

6. Conclusion

This study has achieved some important findings about energy and exergy analysis of the agricultural sector in Malaysia. Based on the obtained results, the following conclusions can be drawn:

- The energy and exergy efficiencies for the agricultural sector in Malaysia and the devices used in this sector are accurately determined. The average overall energy and exergy efficiencies of the sector have been found to be 27.33% and 26.54%, respectively, from 1990 to 2010.
- The highest exergy efficiency is about 27.79% for the year 2010.
- The exergy efficiency of the sector is lower than its corresponding energy efficiency. Therefore, a part of these losses can be reduced by applying appropriate technology, management and policy.

Acknowledgment

The authors would like to acknowledge JU Ahmed, their respected teacher, for his advices . The research has been carried out under the project CUET/ME/11

References

[1] J.U. Ahamed, R.Saidur, H.H.Masjuki, An application of energy and exergy analysis in agricultural sector of Malaysia, 2011.
[2] Dincer, I., Hussain, M.M., Al-Zaharnah, I., Energy and exergy utilization in agricultural sector of Saudi Arabia. Energy Policy 33,1 461–1467, 2005.
[3]Ediger, VS, Huvaz, O¨, Examining the sectoral energy use in Turkish economy (1980–2000) with the help of decomposition analysis. Energy Conversion and Management 47(6), 2006.
[4] Ahamed, J.U., Saidur, R., Masjuki, H.H., A review on exergy analysis of vapor compression refrigeration system. Renewable and Sustainable Energy Reviews 15 (3), 1593–1600, 2011.
[5] Bejan, A., Entropy Generation Through Heat and Fluid Flow. Willey, New York, 1982.
[6] Bejan, A., Advanced Engineering Thermodynamics. Wiley, New York, 1988.
[7] Dincer, I., On energetic, exergetic and environmental aspects of drying systems. International Journal of Energy Research 25 (8), 727–739, 2002.
[8] Dincer, I., On energetic, exergetic and environmental aspects of drying systems. International Journal of Energy Research 26 (8), 717–727, 2002.
[9]. Dincer, I., Hussain, M.M., Al-Zaharnah, I., Energy and exergy utilization in transportation sector of Saudi Arabia. Applied Thermal Engineering 24, 525–538, 2004a.

5th BSME International Conference on Thermal Engineering

Micro- Hydro Power: A Feasible Resolution for Power Scarcity in Bangladesh

Adib Ahmed Habib[a*]

[a]*Department of Electrical&Electronics Engineering, Islamic University of Technology (IUT,OIC), Gazipur-1704, Bangladesh*

Abstract

Energy crisis is one of the major hindrances to the development of Bangladesh. As bulk amount of our power generation rely on fossil fuel and there is incessant depletion of this source make energy crisis more acrimonious. Bangladesh is the eighth most populated country in the world, having power generation capability only 5000 MW and consumption of 146 kwh per capita. Hydropower is one of the prolific renewable energy sources, is one of the promising sources of energy used by human civilization. This is the most widely used form of renewable energy. Our only hydro power plant is situated in 50 km from the port city Chittagong named as Karnafuli Hydro Power Station Spillways, Chittagong Hill Tracts. It is not only generating power but also plays an important role in flood management installation for the areas downstream. Kaptai on Karnafuli river generating 218 MW of power. The potentiality of generation is 755 MW and the installed generation capacity is 4,120 MW. The other potential rivers are Matamuhuri and Sangu. Though this country has confined potentiality to generate power by water but there are few existing potential domains where we can utilize the hydro power as an alternative solution for energy crisis. There are also few barriers to promote hydro power such as topographical intricacies, lack of resource, high up frontal cost of dam construction. This paper depicts on the optimistic impacts of hydropower, the proceedings of hydro power plant in Bangladesh and also the initiatives which are needed to hold back the barriers.

Keywords: Energy crisis; Micro-Hydro Power; Power Scarcity; Karnafuly Hydro Power Station; Topographical intricacies.

1. Introduction

Hydropower or water power is power derived from the energy of falling water, which may be harnessed for useful purposes. Since ancient times, hydropower has been used for irrigation and the operation of various mechanical devices, such as watermills, sawmills textile mills, dock cranes, and domestic lifts. It is one of the ancient sources of power used by human civilization. It has been used hundreds of years ago to turn waterwheels for different purposes such as grind-ing grains, sawing logs and manufacturing cloths. Due to the huge contribution of 19% of the world's electricity power from both large and small power plants, hydro power is the most widely used renewable energy. Department of Energy (DOE) defines large hydropower as power plants having generation capacity of more than 30MW. Small hydropower plants are termed as having generation capacity of 100KW to 30MW. Micro hydropower plants are defined as having a generation capacity ranges from5KWto 100KW [1]. Hydropower is the one renewable energy resource with which mankind has long been familiar, and for which most efficient energy transformation technology is available. Most strikingly, the conversion efficiency from natural resource to electricity is 85% to 90% for hydropower compared to 20% to 30% for fossil fuels, nuclear and geothermal sources. People worldwide are now keen to go for hydropower because its environmental impact, except for land submergence under reservoirs, is minimal. The continued growth in the demand for electricity throughout the developed world has raised concern about the ability of the environment to sustain this development without harm to itself.

2. Functionality of Hydro Power

The principle of a hydro electric turbine is to convert the energy of flowing water into mechanical energy. A hydroelectric generator converts this mechanical energy into electricity.

* Corresponding author. Adib Ahmed Habib Tel.:+880-1675344748; .
E-mail address: adibiut@yahoo.com

The operation of a generator is based on the principles discovered by Faraday. He found that when a magnet is moved past a conductor, it causes electricity to flow. In a large generator, electromagnets are made by circulating direct current through loops of wire wound around stacks of magnetic steel laminations. These are called field poles, and are mounted on the perimeter of the rotor. The rotor is attached to the turbine shaft, and rotates at a fixed speed.. There is a dam on the large river that has a large drop in elevation. The energy flux of the water stream is dependent on the density, cross sectional area and velocity cubed. There are many concepts for harnessing this energy, but turbine is being the most com-mon and proven one. The equation governing the turbine out-put power is-

$P=1/2\ \rho KAV3$ (1)

The potential power can be calculated as follows:

Theoretical power (P) = Flow rate (Q) x Head (H) x Gravity (g) = 9.81 m/s^2)

When Q is in cubic metres per second, H in metres and g = 9.81 m/s^2) then,

$P = 9.81 \times Q \times H$ (kW) (2)

However, energy is always lost when it is converted from one form to another. Small water turbines rarely have efficiencies better than 80%. Power will also be lost in the pipe carrying the water to the turbine, due to frictional losses. By careful design, this loss can be reduced to only a small percentage. A rough guide used for small systems of a few kW rating is to take the overall efficiency as approximately 50%. Thus, the theoretical power must be multiplied by 0.50 for a more realistic figure.

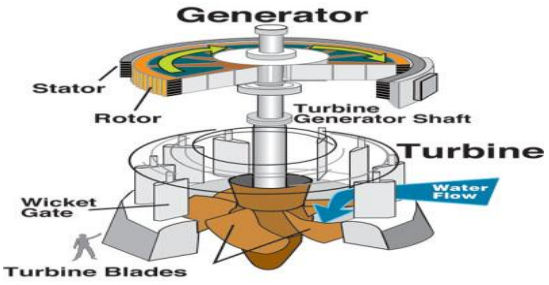

Fig. 1: Generation of power using Hydro electric Dam

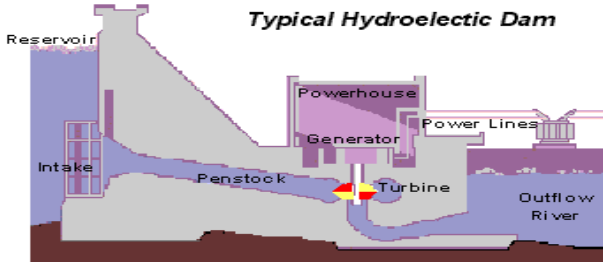

Fig. 2: Operation of Hydro electric Dam

3. Recent Energy Status &Collaboration of Hydro Power in Bangladesh

Currently, Bangladesh has a population about 160 million and it will be raise to 180 million by 2020. At present per capita energy consumption in Bangladesh is 170 kg-0e3, which is very low compared to South Asian nations [2]. At present the power demand in Bangladesh is about 6000MW, whereas the generation ranges only 4000-4600 MW. The generation capacity is 5936MW. As a result of power shortage causes excessive load shading throughout the whole year. Bangladesh relies greatly on fossil fuels for its energy, but the present reserve would be depleted by the year of 2015.

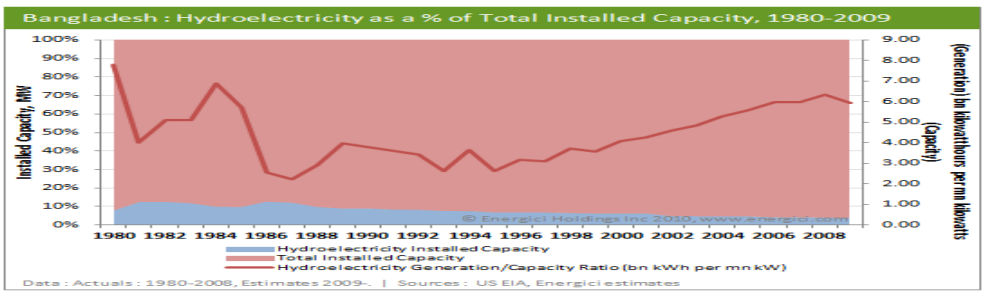

Fig.3: Bangladesh: Hydroelectricity as a % of Total Installed Capacity 1980-2009

Hydroelectricity had an installed capacity base of 230 MW in 2008, a change of 0 MW over the previous year. Its share of total installed capacity decreased from 4.88% in 2004 to 4.22% in 2008 and its share of renewable installed capacity remained unchanged at 100% in 2008.Hydroelectricity generated 1.46 billion kilowatt hours of electricity in 2008, equating to 4.43% of the total electricity generated. This is equivalent to 6.34 billion kilowatt hours of electricity per million kilowatts of capacity, which was the highest ratio amongst renewable

energy source. The Electricity production from hydroelectric sources (kWh) in Bangladesh was 1552000000.00 in 2009, according to a World Bank report, published in 2010. The Electricity production from hydroelectric sources (kWh) in Bangladesh was reported at 1474000000.00 in 2008, according to the World Bank. Sources of electricity refer to the inputs used to generate electricity. Hydropower refers to electricity produced by hydroelectric power plants.

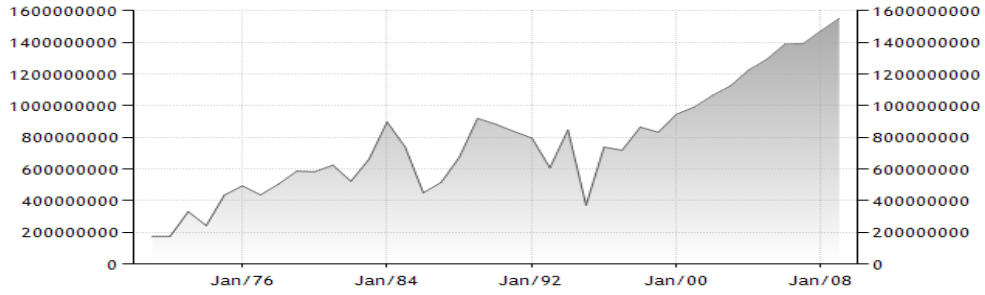

Fig.4: ELECTRICITY PRODUCTION FROM HYDROELECTRIC SOURCES (KWH) IN BANGLADESH

Table. 1: Present Energy Scenario in Bangladesh, 2011[3]

Sector	Status
Electricity Growth	10% in FY 2010 (Av. 7% since 1990)
Total Consumer	12 Million
Transmission Line	8500 km
Distribution line	2,70,000
Per Capita Generation	236 KWH
Access to Electricity	48.5%
Present Generation Capacity	5936 MW
Present Demand	6000 MW
Present Available Generation	4000-4600 MW
Recent Maximum Generation	4699 MW (August 2010)
Minimum Load Shedding in FY 2010	1500 MW (During hot Summer)

4. Projects & Installations of Micro Hydro Power in Bangladesh

In Bangladesh about 1.4 trillion cubic meters of water flows through the country in an average water year. Major rivers of the country have a high rate of water flow of about 5 to 6 months during monsoon season, which is substantially reduced in winter season. More than 90% of Bangladesh's rivers originate outside the country, due to which proper planning of water resource is difficult without neighbouring countries cooperation. Downstream water sharing with India is a highly contentious issue for Bangladesh. The annual average rainfall is about 2,300 mm, which varies from1, 200 mm in the north-west to 5,800 mm in the northeast. Most of the rainfall (about 80%) occurs during the months of May/June to September/October. At present only 230 MW of hydro power is utilized in Karnaphuli, Rangamati hydro station, which the only hydro-electric power plant operated by Bangladesh power development board (BPDB). Micro hydro and minihydro have limited potential in Bangladesh, with the exception of Chittagong and the Chittagong hill tracts. Hydropower assessments have identified some possible sites from 10 kW to 5 MW but no appreciable capacity has yet been installed. Sangu Project would be a new project with estimated annual energy of about 300 GWh/yr. For an installed capacity of 140 MW, the annual plant factor is 23 % and it is assumed that the plant would operate in a peaking mode (Rofiqul Islam, M., *et al* 2008; Micro Hydro Energy Potential in Bangladesh, 2007). Matamuhari hydroelectric Project would be a potential project of capacity 75 MW and approximate average annual energy 200 GWh/yr. (Rofiqul Islam, M., *et al* 2008; Micro Hydro Energy Potential in Bangladesh, 2007) [4]. Bangladesh has 0.08% of the total regional capacity for Hydroelectricity and ranks at #101 in the world for Hydroelectricity installed capacity. The Matamuhuri development would be a new project of capacity 75 MW and an approximate average annual energy 200 GWh per year. However, to obtain the required head for generating power a weir or barrage need to be constructed across the river channel. Based on mean monthly discharges and an assumed 5m head the hydro potential of the 10 major and medium perennial rivers of the Northeast Region is estimated at about 161 mw of continuous power with an annual energy production of about 1410 GWh. These are perennial rivers with

sufficient flow for power generation throughout the year [5].

Table 2 Hydro power potential

Site	Estimated Average Discharge (l/s)	Available Head, Ho (m)	Output Power, P (kW)
Sailopropat, Banderban [3]	100	6	3
Madhabkundu, Moulovibazar [3]	150	10	7.5
Faizlake [5]	42.5	12	2.5
Chota Karina chara[5]	311	6	9.3
Ringuli chara[5]	340	4.6	7.8
Sealock[5]	1132	9	51
Longi chara[5]	425	3	6.4
Budia chara[5]	170	7.6	6.5
Nikhari chara[5]	480	6.8	16.3
Madhab chara[5]	996	9.9	49

It shows some of these data. The head varies from 2m to10m whereas the flow rate varies from 40 to 1000 l/s. Again there is a seasonal variation both in flow rates and available head. The output power is calculated as P = 5 Q Ho (kW), where Q is the flow rate in m3/s and Ho is the available head in meter and assuming a 50% system efficiency.

Fig.5: Snaps of Kaptai Dam, Rangamati (Salient Hydro-electric Source of Bangladesh)

5.1 Prospects of Hydro Power in Bangladesh

Most of the identified places so far are in the hilly areas where mainly the tribal people have their habitat. Currently most of them are out of electrification facility. Exploration of further potential sites and proper utilization of the existing sites will create opportunity to bring them under electrification. Besides improving their standard of life it will enable them to start small-scale industries in those remote areas. Hence, there will be opportunities for jobs and self-employment. It would also encourage them to start home-based industry through the availability of three-phase power. Production of electricity in remote areas will save huge transmission and associated infrastructural cost. Also, these hilly areas being an attractive tourist spot undoubtedly tourism will

flourish due to the availability of power. Tourism has also been a good source of revenue for Bangladesh .Shrimp cultivation is one of the main sources of foreign revenue of the country [6]. But due to shortage of electricity, it has been very difficult to apply the modern techniques of cultivation. Potential river sites with run-off MHP facility will enable the local farmer to apply semi-intensive and intensive method of cultivation .There are more than 87,319 villages in Bangladesh, and most of them are unconnected to the national grid. It is only 10% of our rural householders are hooked on the grid. The electrification by grid extension or secondary power station can only reach a small minority of the population in rural areas. In view of the dispersion of localities and the low demand, the cost of production, transmission and especially distribution of electricity would be prohibitively expensive. Decentralized and standalone systems could effectively become a viable option in these areas.

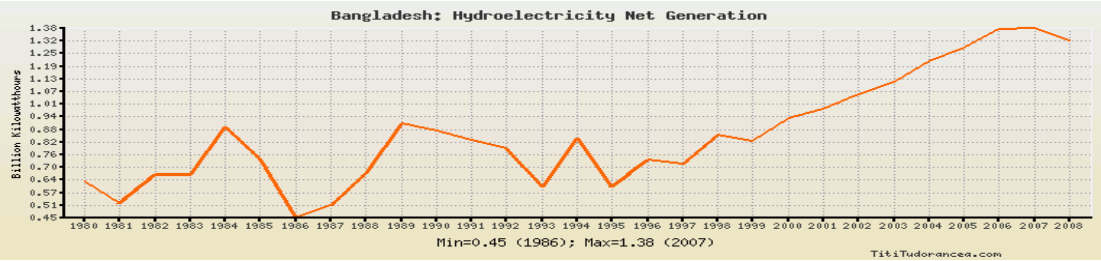

Fig.6: Hydroelectricity Net Generation in Bangladesh (1980-2008)

Installed capacity from hydro power source was 3.4% whereas from natural gas it was 76.14%. It disseminates the production of power from hydro power plants are still not satisfactory level.

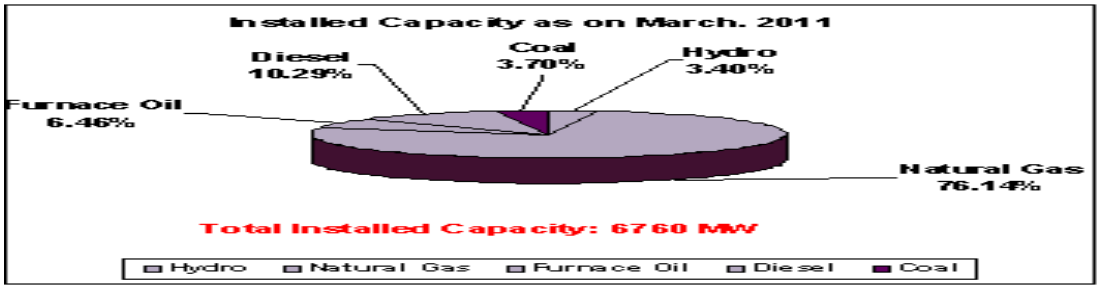

Fig. 7: Installed Capacity of Power in Bangladesh from different sources on March 2011

5.2 Hurdles of Hydro Power in Bangladesh

The plausibility of utilization of hydro power in Bangladesh is little as the country consists of low and flat land. Although there are few optimistic and extensive projects are in progress in hilly areas. The few salient hurdle are:

1) **Disrupts aquatic ecosystems**: The dams developed across the rivers can disturb aquatic life and lead to their large scale destruction. There is a chance that fish and other water animals may enter the penstock and ultimately the power generation turbines where they will be killed. Dams can also disturb the mating seasons and mating areas of the water animals.In some cases water animals have to swim against the water stream during breeding seasons. If a dam is built in the path of migrating fish they could be stuck there and killed, never reaching their destination. This could devistate a population of fish.

2) **Disruption in the surrounding areas**: Plant and animal life around rivers thrive due to continuous fresh flowing water in the river. Due to construction of the dams lots of areas have to be cleared that disrupt the plant and animal life. In many cases even a number of trees have to be cut that destroys not only the plant life but also the animals dependent on them. Even changing the course of flow of water in the river due to the construction of the dam disrupts the plants and animals life.

3) **Policy Hurdles**: As we have possessed the potential of capitalizing hydro power, but there are some policy barriers hindrance the path. Our research and development sectors for hydro power are not satisfactory. There

are also monitoring failure, lack of policy framework restrict the proceedings.

4) **Institutional and Technical Barriers** : Lack of acknowledgement about the importance of hydro power to the ordinary mass and shortage of technical adroit manpower and manufacturing equipments are the major cause of less production of hydro power. Lack of promptness of utilization of budget prediction of manufacturing power from water also opposes the growth.

5) **Requires large areas**: In order to build a dam, power generation unit and transformers, and connect them to the national grid, a huge amount of land is needed. This requires forests to be cleared disrupting many local, natural ecosystems.

6) **Large scale human displacement**: Because these dams take up such a large area, it is often necessary for humans to relocate. It is not easy to convince people to uproot their lives and businesses. Often they are not compensated fairly for their land and the inconvenience. This creates large scale opposition and revolts against construction of the dams.

Concluding Remarks

Energy is pre-requisite for human sustenance and development. Scarcity of energy is one of the major hindrances to the development of a nation.. Since micro-hydropower plant requires terrain and availability of high stream flow rate, so, it has a good potential in the north-eastern hilly regions of Bangladesh. Due to the abundance of rivers and canals, Bangladesh has a good run-off river micro-hydro potential but it is yet to be explored. To generate more power both the government and private sectors need to take measures and the impediments which restrict the progress are required to extract. In the case of fossil fuel depletion hydro power will be the promising solution for energy catastrophe in Bangladesh.

References

[1] Jahidul Islam Razan, Riasat Siam Islam, Rezaul Hasan, Samiul Hasan, and Fokhrul Islam, A Comprehensive Study of Micro-Hydropower Plant and Its Potential in Bangladesh, International Scholarly Research Network, Volume 2012, Article ID 635396.

[2]Engr. A.N.H. Akher Hossain PENG, FIEB, "Energy Mnagement for Sustainable Development" Engineers' Convention 2012, The Forum of Engineers and Architects of Bangladesh.(P-107-112)

[3] Khalid Md. Bahauddin, Tariq Md. Salahuddin, Prospect and Trend of Renewable Energy and Its Technology towards Climate Change Mitigation and Sustainable Development in Bangladesh, INTERNATIONAL JOURNAL OF ADVANCED RENEWABLE ENERGY RESEARCH, *Vol. 1, Issue. 3, pp. 14- 25, 2012.*

[4]M.A. Wazed and Shamsuddin Ahmed, A Feasible Study of Micro-Hydroelectric Power Generation at Sapchari Waterfall, Khangrachari, Bangladesh, Journal of Applied Sciences 9 (2) :372-376,2009.

[5] A.K.M. Sadrul Islam, M. Q. Islam, M. Z. Hossain, M. I. Khan and S. A. Uddin, "Appropriate Low Head Micro Hydro Systems for Bangladesh, "Second International Conference on Electrical and Computer Engineering, ICECE 2002, 26-28 December 2002, Dhaka, Bangladesh.

[6] A. Ahmed, "Prospects, Importance, Problems and Impacts of Shrimp Cultivation in Bangladesh: A Literature Review," May 2010, http://ssrn.com/abstract=1612845.

STUDY OF RESPONSE OF SPAR-TYPE FLOATING WIND TURBINE IN WAVES WITH EFFECT OF GYRO MOMENT

N. Mostafa[1], M. M. A. Sarker[2] and M. M. Karim[3]
[1]Department of Natural Science, Stamford University Bangladesh
[2]Department of Mathematics, Bangladesh University of Engineering and Technology
[3]Department of Naval Architecture and Marine Engineering, Bangladesh University of Engineering and Technology
E-mail: nmostafa79@gmail.com

Abstract

Nowadays, the annual energy consumption of the world is increasing more and more. These situations are mainly supported by consumption of fossil fuel. As global warming and exhaustion of fossil fuels become serious issues, the development of alternative energy sources has been become imperative. Therefore, a number of research groups have paid much attention to the study of floating offshore wind turbines (FOWTs). Similar to other offshore structures, the FOWTs are subjected to irregular waves and wind loads that cause a dynamic response in the structures. The motion of the FOWT might be changed by a change in gyroscopic effect which depends on the angular velocity and moment of inertia of the rotating blades. Therefore, to investigate the effect of the gyro moment on the motion of the FOWT, experiment was carried out in a water tank using a 1/360 scale model of a prototype FOWT. The interaction between the change of rotational speed as well as moment of inertia of the blade and the motion of the FOWT was studied. In this paper, the experimental results are compared with the results of numerical simulation and also discuss the findings. Numerical calculations have been carried out using potential theory based on the 3D panel method.

Keyword: SPAR, Response amplitude operator, Moment of inertia, Gyro moment;

1. Introduction

Nowadays, the energy problem is one of the fundamental issues facing the world. The development of renewable energy resources will help to reduce the effects of global warming. As global warming and exhaustion of fossil fuels become a serious issue, the development of alternative energy sources such as hydro energy, solar energy and wind energy has become indispensable. It is widely known that the vast marine space is one of the main sources of renewable energy. The offshore expansion of wind turbines is becoming increasingly common, especially in Europe. In future, it is expected that floating offshore wind turbines (FOWTs) will become a possible option. Therefore, many groups researching renewable energy are looking into the development of cost-effective FOWTs. Currently, there are a number of offshore wind turbines with floating foundation concepts in various stages of development. They are divided into four main categories: Spars-buoy type (SPAR-type), Tension leg platform type, Semi-submersible type and Barge-type. In general, the SPAR-type has a better heave performance than the Semi-submersible type due to its deep draft and reduced vertical wave exciting forces, as shown by Roddier et al. [1]. Therefore, the authors have selected the SPAR-type FOWT as the basis of their research because of its simpler shape and expected cost-effectiveness.

Up to the present time, several types of FOWT have been proposed such as, by Musial et al. [2] and Butterfield et al. [3]. In particular, Statoil Hydro [4] has installed a full scale SPAR-type FOWT, the Hywind project, offshore in Norway. Nielsen et al. [5] and Skaare et al. [6] examined the dynamic response of this SPAR-type FOWT under the action of winds and waves by experiment and numerical simulation. Several

concepts of FOWT have been proposed and are under research in Japan by Fukumoto et al. [7], Suzuki et al. [8] and Utsunomiya et al. [9].

Many problems have to be overcome before the FOWT can be considered suitable for practical use. Generally, the motions induced by waves and currents are a serious problem. The tower of a ground type wind turbine is fixed; the change in the rotor surface on revolution of the blades is extremely small. In contrast, in the case of the floating type wind turbine, the whole floating structure is affected by sea waves. Therefore, the rotor surface of the wind turbine always vibrates during revolution. It is well known that a rigid body having a rotating wheel has a moment of gyro effect from the change in the direction of the wheel. In the FOWT, this effect is clearly present.

The aim of the present study is to investigate numerically and experimentally the relationship between the motion of the FOWT and the change in gyroscopic effect induced by the change in inertia of the blade of the FOWT.

2. Formulation

Let (*x*, *y*, *z*) be the right-handed Cartesian coordinate system with the *xy* plane on the mean free surface and *z* the axis directed vertically upwards through the center of the FOWT as shown in Fig. 1. The motion of the FOWT in waves can be represented by equation of motion with six degrees of freedom. The six degrees of freedom are composed of three translational motions and three angular motions. The translational displacements in the *x*, *y*, *z* directions are ξ_1, ξ_2, ξ_3, respectively, where ξ_1 is the surge, ξ_2 is the sway, and ξ_3 is the heave motion. Furthermore, the angular displacements of the motions about the *x*, *y*, *z* axes are ξ_4, ξ_5, ξ_6, respectively, where ξ_4 is the roll, ξ_5 is the pitch and ξ_6 is the yaw angle.

The dynamic equation of motion in the frequency domain of a FOWT in waves can be written as follows:

$$\{(\mathbf{M}+\mathbf{m})\ddot{\xi}+\mathbf{N}\dot{\xi}+\mathbf{C}\xi\}=\mathbf{F} \tag{1}$$

where **M** is the 6×6 mass matrix, **m** is the 6×6 added mass matrix, and **N** is the 6×6 damping matrix of the

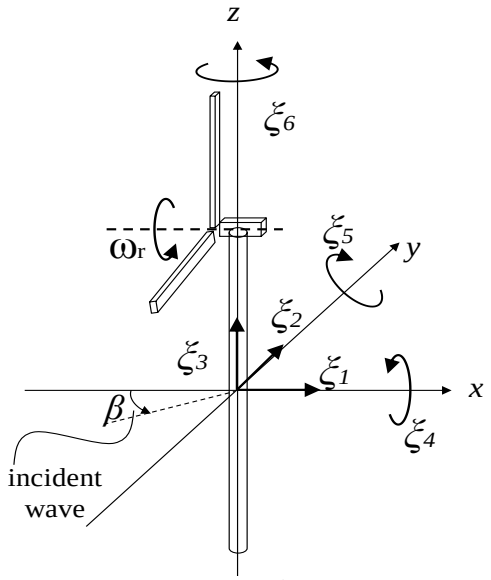

Fig. 1 Coordinate system of the FOWT

FOWT. The added mass and the damping are related to the hydrodynamic radiation force. The former one is proportional to the acceleration of the motion and the latter is proportional to the velocity of the motion. **C** is the 6×6 restoring force matrix, ξ is the motion response vector with 6 degrees of freedom. **F** is the vector of wave exciting forces with 6 degrees of freedom.

When the rotor of the FOWT is turned, there is an induced gyroscopic force which has an influence on the motion of the FOWT. Therefore, the equation of gyro moment is added to the dynamic equation of motion of the FOWT. The additional coordinate system proposed by Murai et al. [10] to expresses the rotational motion of blades. The center of the blades which rotate with angular velocity ω_r (=const) is at Or. The detail derivation of gyro effect has been derived by Mostafa et al. [11].

After derivation of gyro moment, the dynamic equation of motion of FOWT is obtained as follows;

$$\boldsymbol{\xi}=\{-\omega^2(\mathbf{M}+\mathbf{m})-i\omega(\mathbf{N}-\mathbf{M}_{gyro})+\mathbf{C}\}^{-1}\mathbf{F} \tag{2}$$

where $\mathbf{M}_{gyro}$ is written as follows:

$$\mathbf{M}_{gyro} = \begin{bmatrix} 0 & 0 & 0 & 0 & 0 & 0 \\ 0 & 0 & 0 & 0 & 0 & 0 \\ 0 & 0 & 0 & 0 & 0 & 0 \\ 0 & 0 & 0 & 0 & 0 & 0 \\ 0 & 0 & 0 & 0 & 0 & (I_{r3} - I_{r1})\omega_r \\ 0 & 0 & 0 & 0 & (I_{r1} - I_{r2})\omega_r & 0 \end{bmatrix} \tag{3}$$

3. Model Experiment

3.1 Experimental Set-up

In order to clarify the effects of change of gyro effect, simple experiment was carried out in a water tank at Yokohama National University, Japan. The dimensions of the water tank were 16m long, 1m wide and 2m deep. A plunger type wave maker was located at one end of the tank and a wave absorption beach at the other end. Regular waves were generated by the wave maker in water 1.5m deep. The assumed FOWT model was proposed by Suzuki et al. [8]. The experimental model of the SPAR-type FOWT is shown as a photo and sketch in Fig. 2. The parameters of the FOWT model are listed in Table 1.

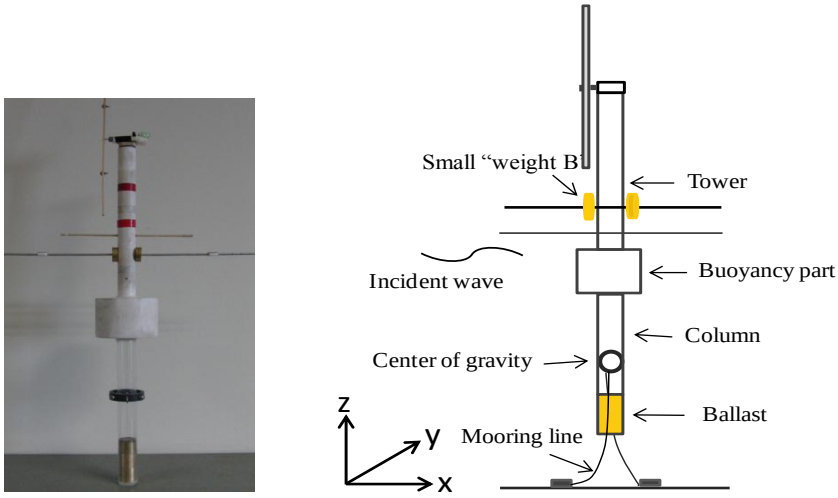

Fig. 2 Photograph (left) and sketch (right) of the experimental model

Table 1: Model parameters

Specimen	Experimental model	Actual model
Tower height	226.0 (mm)	80.0 (m)
Diameter of buoyancy part	70.0 (mm)	20.0 (m)
Height of buoyancy part	54.0 (mm)	20.0 (m)
Water plane area	315.0~318.0 (mm^2)	201.1(m^2)
Draft	277.0 (mm)	95.0 (m)
Total mass	245.6 (g)	10047.0 (ton)
Height of center of gravity from bottom	153.0 (mm)	35.0 (m)
Metacentric height (GM)[4]	42.3~45.0 (mm)	24.0 (m)
Spring constant for mooring	7.7 (N/m)	-

[4]Here, "GM" is the distance from the center of gravity and the metacenter of a FOWT

A flat blade with two small "weights A" was used as the rotor in the experimental model, as shown in Fig. 3. No attempts were made to create the wind force. A motor was placed at the top of the tower to create the gyroscopic effect. This well-known mechanical force arises when a rotor rotating around a certain axis undergoes a rotation around a different axis. The tower part and the buoyancy part were made of balsa and the column which was under water was made of polycarbonate pipe. Then ballast was used inside the column of the end part.

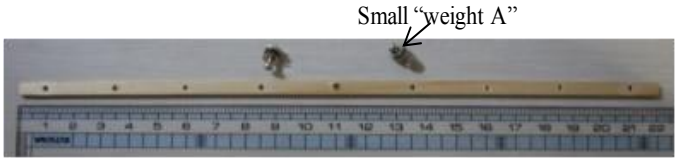

Fig. 3 Rotating flat blade with weights

Table 2: Effect of change of position of "weight A" on the flat blade

Distance from the center of blade to the "weight A", d (mm)	Angular velocity ω_r (rad/s)	Moment of inertia I_{r1} (kg·m^2)	Moment of inertia I_{r2} (kg·m^2)	Moment of inertia I_{r3} (kg·m^2)	$(I_{r1}-I_{r2})$	$(I_{r3}-I_{r1})\omega_r$
25.0	42.0	4.43×10^{-7}	2.38×10^{-7}	2.38×10^{-7}	8.64×10^{-6}	-8.64×10^{-6}
50.0	38.5	5.39×10^{-7}	3.33×10^{-7}	3.33×10^{-7}	7.92×10^{-6}	-7.92×10^{-6}
75.0	35.0	6.98×10^{-7}	4.93×10^{-7}	4.93×10^{-7}	7.19×10^{-6}	-7.19×10^{-6}
100.0	32.0	9.21×10^{-7}	7.16×10^{-7}	7.16×10^{-7}	6.58×10^{-6}	-6.58×10^{-6}

First, the variation of angular velocity of the rotating flat blade was measured when the small "weights A" were positioned at different locations on the flat blade. The holes in the flat blade were located every 25.0mm from the center of rotation. To calculate the angular velocity of the rotation, a CCD Laser Displacement Sensor was used. The change of gyroscopic effect depends on the change of angular velocity and moment of inertia of the rotating flat blade. In order to calculate the change of angular velocity as well as the change of moment of inertia of the flat blade, the attached "weights A" were varied from 25.0mm to 100.0mm from the center of the flat blade and results are listed in Table 2. From Table 2, it is concluded that, the angular velocity of the blade decreases with increasing the distance from the center of the flat blade. But the moment of inertia increases with increasing the distance from the center of the flat blade. The measured change of gyroscopic effect is higher at d=25.0 [mm] and decreases with increasing the distance. For each condition, a water tank experiment was carried out.

3.2 Experimental Method

A schematic diagram of the water tank with the experimental model is depicted in Fig. 4. In order to prevent the experimental model from drifting, it was moored by two spring mooring lines. The mooring lines were connected to the center of gravity of the model in the *y* direction. The mooring stiffness was measured by experiment and the measured stiffness is 7.7 N/m. The effect of mooring stiffness cannot be ignored. So, the value of mooring stiffness is added directly to the restoring force coefficient in numerical computation. The experiments were carried out with wave periods of 0.5, 0.6, 0.7, 0.8, 0.9, 1.0, 1.1, and 1.2s for 0° wave heading (head waves). In each wave period, a video of the surge, heave, pitch and yaw motion of the model was recorded with two digital cameras for 4 second of real time and analyzed an image of the animation using the color tracking method.

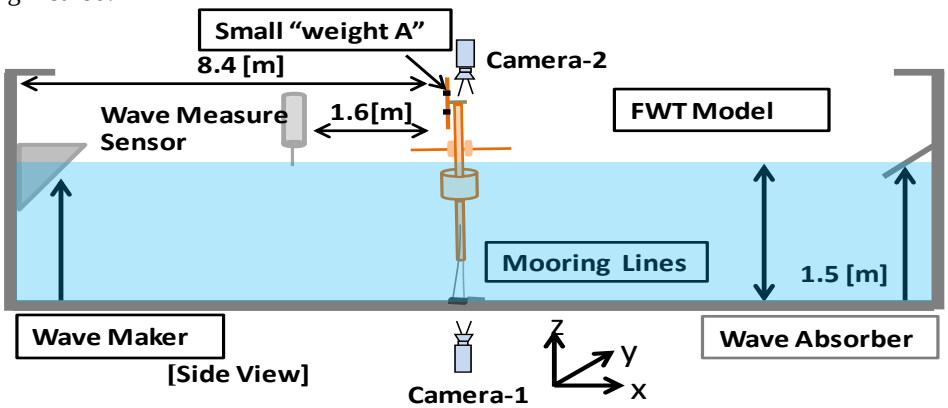

Fig. 4 Experimental set-up in water tank

A set method was followed for video analysis. The animation was separated which had been recorded with digital cameras (300 frames per second) into still images. The position of each tape was read from the still image and read the time trajectory of the tape. This time trajectory of the tape shows the time series response of the motion of the model.

4. Results and Discussion

Utilizing the time series response of each motion, graphs of the frequency response of the surge, heave, pitch, and yaw motion are obtained and compared those results to the results of numerical computation. The response amplitude operator (RAO) of the motion responses of surge, and heave is defined by the ratio of motion amplitude and incident wave amplitude (ξ_a). On the other hand, the RAO of pitch and yaw is defined by the ratio of motion amplitude and wave amplitude times wave number (k). The RAO is a function of normalized frequency, $2r\omega^2/g$ where r is the radius of the buoyancy part of the experimental model, ω is the wave frequency and g is the gravity acceleration. In the figures, symbols show the experimental results and solid lines represent numerical calculations.

Figure 5 illustrates the results of change of gyroscopic effect with the change of location of small "weights A" on the flat blade. The location of small "weights A" from the center of the blade was taken as d= 25.0, 50.0, 75.0, and 100.0mm. The change of gyroscopic effect does not affect the surge, heave, and pitch motion, but its effects appear on yaw motion. A resonant period of heave motion is seen near the normalized frequency, $2r\omega^2/g$=0.28. At frequencies above 0.28, the RAOs of surge, heave, pitch and yaw show a comparable response with the change of gyroscopic effect. But discrepancies are observed in the experimental result for normalized frequencies lower than 0.28. It can be considered that the main reason for such discrepancies is that the small scale model is not effective at lower frequencies. Hence, the responses between the normalized frequencies 0.28 to 1.13 are discussed. Peak response is observed in surge and heave motion in numerical computation. This response maybe due to neglecting the damping effect in the numerical calculation. From Eq. 3, it is seen that the yaw motion of the FOWT is affected by the gyro moment, which is clearly seen in numerical computations and experimental results above normalized frequencies of 0.28 (see Fig. 5). Figure 6 shows the results of RAO of yaw motion at the normalized frequencies 0.44 and 0.57 with the change of gyro moment of the rotating flat blade. This linear relationship demonstrates that the yaw response increases with increasing gyro effect (Table 2). As the change of gyro moment implies a lower response, the higher moment of inertia of the rotating blade plays an essential role in yaw response. Therefore, the change of gyro moment, which is presented theoretically in section 2, has an effect on the numerical and experimental results for yaw motion of the FOWT (see Fig. 6).

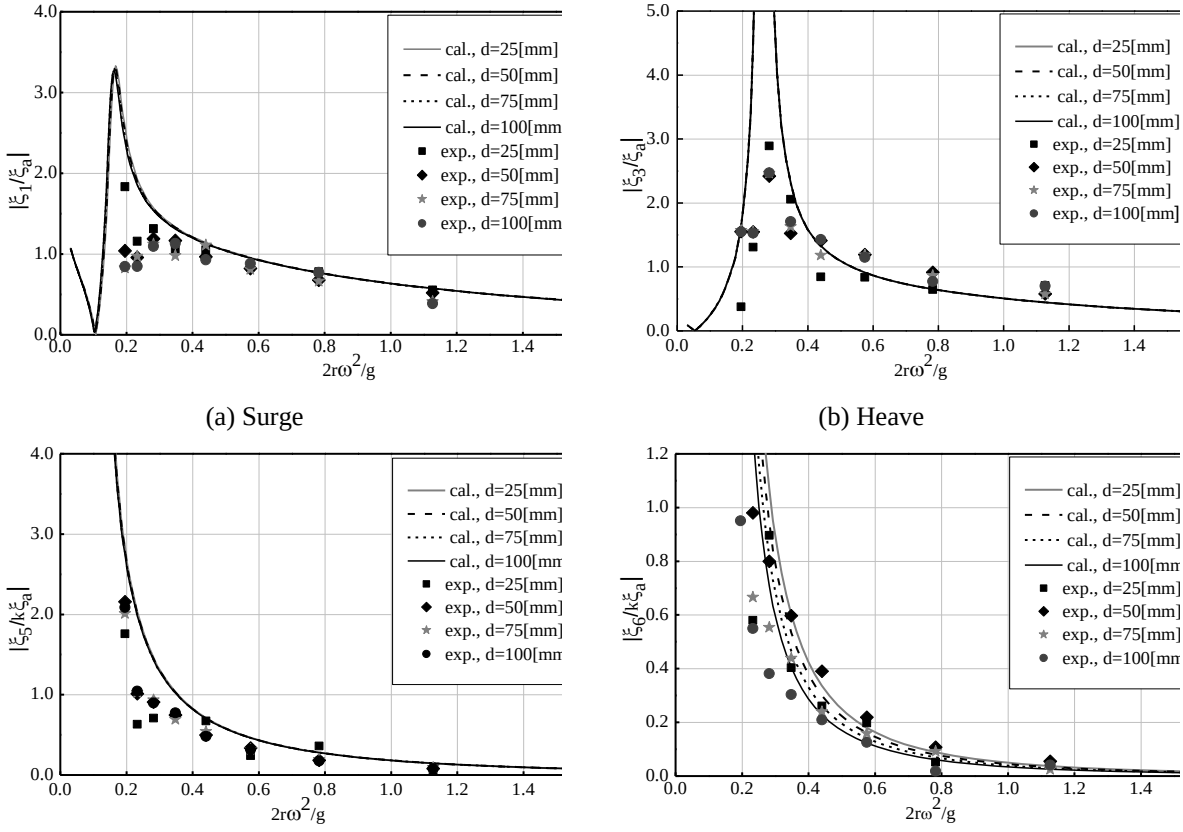

(a) Surge (b) Heave

(c) Pitch (d) Yaw

Fig. 5 RAO of (a) Surge; (b) Heave (c) Pitch; (d) Yaw motion at upright condition

Fig. 6 RAO of yaw with the variation of the moment of inertia of the blades for normalized frequencies, $2r\omega^2/g$=0.44 and 0.57

5. Conclusions

The floating wind turbine is a new technology in the offshore industry in the field of renewable energy. The gyroscopic effect of rotating rotor blade is a significant physical effect on FOWT. It is observed from this study that the gyroscopic effect caused by the rotation of flat blade has an effect on yaw motion of the FOWT. The response of yaw motion increases with the increasing gyroscopic force. As shown by numerical model, the change of yaw motion depends on the change of angular velocity as well as moment of inertia. Hence, the computed response of yaw motion of FOWT using potential theory exhibits a good agreement with experimental results above the normalized frequency 0.28. These results indicate that the effect of gyro moment on the FOWT could significantly influence the performance of the wind turbine in actual sea. Hence, from this experimental and numerical study, it can be claimed that the gyro moment results are very useful for the design of wind turbine and its tower structure to extract the energy from open sea.

References

[1] Roddier, D., Cermelli, C., Weinstein, A. Wind float: a floating foundation for offshore wind turbines, Journal of Renewable and Sustainable Energy, vol. 2(3), pp. 033104-1~34, 2010.

[2] Musial, W., Butterfield, S., Boone, A. Feasibility of floating platform system for wind turbines, The 23rd ASME WindEnergy Symposium, Reno, Nevada, January 5-8, 2004.

[3] Butterfield, S., Musial, W., Jonkman, J., Sclavounos, P. Engineering challenges for floating offshore wind turbines, Copenhagen Offshore Wind Conference, Copenhagen, Denmark, October 26-28, 2005.

[4] StatoilHydro, Hywind-Putting wind power to the test, 2009 (available at http:/www.statoil.com/en/TechnologyInovation/NewEnergy/RenewablePowerProduction/Offshore/Hywind/Pages/HywindPuttingWindPowerToTheTest.aspx).

[5] Nielsen, FG., Hanson, TD., Skaare, B. Integrated dynamic analysis of floating offshore wind turbines, Proceeding of 25th International Conference on Offshore Mechanics and Arctic Engineering, Hamburg, Germany, OMAE2006-92291.

[6] Skaare, B., Hanson, TD., Nielsen, FG., Yttervik, R., Hansen, AM., Thomsen, K., Larsen, TJ. Integrated dynamic analysis of floating offshore wind turbine, European Wind Energy Conference and Exhibition, Milan, May 7-10, 2007.

[7] Fukumoto, Y., Moriya, Y., Tsuchiya, K., Hara, M., Suzuki, H. A study of floating offshore wind turbine systems. Part III Investigation of reinforced concrete spar-buoy for offshore wind turbine, Proceedings of 28th Wind Energy Utilization Symposium, Tokyo, pp. 204-207, 2006.

[8] Suzuki, H., Ashida, T. Optimization of floating structure of a spar-type floating wind turbine, Proceedings of JASNAOE 2005S, pp.107-108.

[9] Utsunomiya, T., Nishida, E. On sea experiment of a hybrid SPAR for floating offshore wind turbine 1/10 scale model, Proceedings of the ASME 29th International Conference on Ocean, Offshore and Arctic Engineering, Shanghai, China, OMAE2010-20730.

[10] Murai, M., Nishimura, R. A study on an experiment of behavior of a SPAR type offshore wind turbine considering rotation of wind turbine blades, Oceans 2010, Sydney, May 24-27, 2010.

[11] Mostafa, N., Murai, M., Nishimura, R., Fujita, O., Nihei, Y. Study of motion of SPAR-type floating wind turbines in waves with effect of gyro moment at inclination, Journal of Navel Architecture and Marine Engineering, vol. 9, no.1, pp. 67-79, 2012.

5th BSME International Conference on Thermal Engineering

Comparison of Turbulence Models for Ahmed Car Body Simulation

Abul Kalam Azad[a], Mohammad Arif Hossain[a], AKM Sadrul Islam[b,*]

[a]*Department of Mathematics,Khulna University of Engineering & Technology, Khulna-9203, Bangladesh*
[b]*Department of Mechanical and Chemical Engineering, Islamic University of Technology, Dhaka,Bangladesh*

Abstract

In this study comparison among the different turbulence models, viz. k-ε, k-ω, SST and BSL, is done on the basis of the observed velocity profiles over Ahmed car body. Ahmed car body has become reference geometry. To check the performances of the turbulence models we have chosen 25^o rear window slant angle. For the simulation all the geometric quantities used are normalized with the body height (H=0.288m). The body is pleased in a channel of length about 8.8069 times of the body length and the blockage is about 4.27%. The ground clearance is 0.174H. In the simulations three different velocities viz. 40m/s, 20m/s and 15m/s are used. The velocity profiles with different turbulence models for the velocity 40m/s is compared with the benchmark. Little variations are observed among the different turbulence models.

Keywords: Ahmed car body; Turbulence models; CFD

1. Introduction

Turbulence are of great importance in computational fluid dynamics .The understanding of the physics of turbulence is critical and many different models have evolved to explain them. Sometimes the turbulence models are validated through vehicle aerodynamics. Computers have been used to solve fluid flow problems for many years. Numerous programs have been written to solve either specific problems, or specific classes of problems. From the mid-1970's, the complex mathematics required to generalize the algorithms began to be understood, and general purpose CFD solvers were developed. Recent advances in computing power, together with powerful graphics and interactive 3D manipulation of models have made the process of creating a CFD model and analyzing results much less labor intensive, reducing time and, hence, cost. Advanced solvers contain algorithms which enable robust solutions of the flow field in a reasonable time.

A real-life automobile is a very complex shape to model or to study experimentally (Lienhart et al., 2000). Because of the complexity of cars aerodynamics and in order to simplify studies Ahmed car body has become reference geometry (Montinat et al., 2008). The vehicle shape employed by Ahmed and Ramm, 1984 is known as Ahmed body. Several researchers have worked on the experiments and numerical modeling of the flow over the Ahmed body. Lienhart et al., 2000 conducted the experiments for two rear slant angles (25^o, 35^o) at LSTM. The velocity and turbulence kinetic energies have been measured by LDA at several key locations. Craft et al. 2001 compared the performance of linear and non-linear k-ε model with two different wall functions. Basara 1999 conducted the numerical modeling of this case by means of large eddy simulation (LES), Durand et al., 2002 compared the performance of the SST model and some other turbulence models.

In this study comparison is done among the velocity profiles at different locations over the Ahmed body for k-ε, k-ω, Shear Stress Transport (SST) and Baseline k-ω (BSL) turbulence models. Velocities 40, 20 and 15m/s are taken in these simulations and the respective velocity profiles are compared for the different turbulence models. The experimental data of the Linhart et al., 2000 is also compared with the chosen turbulence models velocity profiles for 40m/s velocity. A little discrepancy is observed.

2. Description

The geometry of body is shown in Fig.1(a,b). All the geometric quantities are normalized with the body height H=0.288m. The values of the geometric quantities are l_r/H=2.928, G/H=0.697 and W/H=1.35, where l_r.is the length from the beginning of the slant to the front, G is the length of the slant region and W is the width of the

* Corresponding author. Tel.: +880-1819147326
E-mail address: sadrul@iut-dhaka.edu

body. The front part is rounded with a radius of R/H=0.347in the plane, y=0 and z=0. The body is placed in the channel with a cross section of B × F=6.493H × 4.861H (width × height). The front face of the body is located at a distance of 7.3H from the channel inlet and the downstream length between the rear face of the body and the channel outlet is 21H. The body is lifted from the floor, producing aground clearance of C/H =0.174 on the four pillar. The slant angle is taken as 25^o. As a result the channel length is about 8.8069 times of the body length and the blockage is about 4.27%.

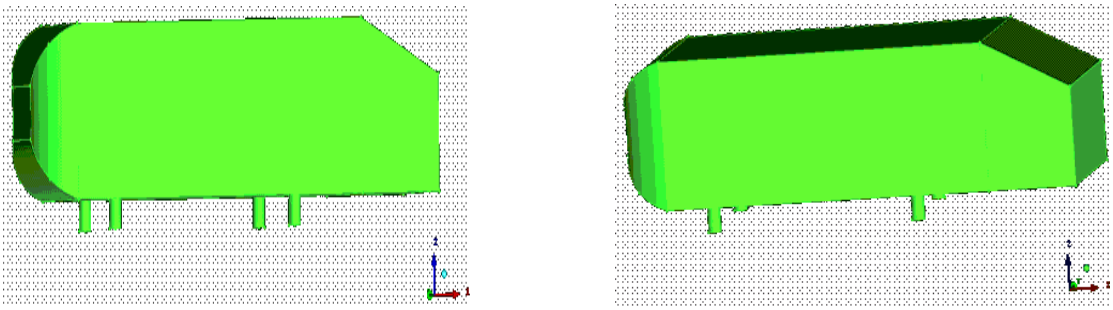

Fig. 1 (a,b)- Geometric presentation of the body from different angle.

In the simulations Ansys 11© with high resolution advection scheme along with Physical timescale (physical time = length of the tunnel/velocity of the fluid) is used. The following conditions are used as simulation parameters.

Simulation type :	Stationary	Boundary conditions and numerical schemes:	
Domain type	Fluid domain	Inlet:	
Fluid	Air at 25^o	Flow region	Subsonic
Buoyancy	Buoyant	Turbulence	Low(intensity=1%)
Gravity-	X= 0	Temperature	298K
	Y= 0	Outlet:	
	Z= -9.807m/s^2	Flow region	Subsonic
Buoyancy reference temperature	298K	Reference pressure	1 Pa
Domain motion	Stationary	Wall:	
Heat transfer option	Isothermal	Wall influence on flow	No slip
Wall function	Scalable	Wall roughness	Rough wall
Buoyancy turbulence	Production and dissipation	Roughness height	0.0001m
		Fixed temperature	298K

3. Results and Discussions

In the simulations 320924 nodes and 1344266 elements are used to create the mesh. The numbers are not accidental, rather they have been decided through simulations. The extension of the near wake separation bubble guided to determine the numbers. The origin of the Cartesian coordinate system considered is placed at the middle of the rear end of the body, for y- and x-axis respectively, and z axis is along the vertical. As a result the body is at the negative side of x. Velocity profiles at different locations are taken but for the sake of brevity only six key locations are presented here with velocity 40m/s. The locations are in front of the body, about the middle part of the body, close to the start of the slant, over the slant, close to the rear end and towards the outlet from the rare end. Velocity profiles of the simulations with k-ε, k-ω, SST and BSL turbulence models, for the inlet velocity 40m/s, are compared with the experimental data of Linhart et al., 2000. The velocity profiles at different locations along with the experimental data are presented in Fig 2(a-f).

In the front position (Fig 2a) the velocity profiles due to all the turbulence models matches well with the experimental value up to a certain height 0.45m. Above that height the velocity suggested by the models are more than the experimental, of them k-ε models velocity deviates more with the increase of height. Over the mid point of the body (Fig 2b) all the suggested patterns of the velocity profiles by the different turbulence model matches well with the experimental one but differ in terms of velocities expect nearer the body. Nearer the body the shape of the experimental velocity profile mismatches with the model. Of the four, suggested velocity by k-ε model is closer to the experimental (little more) near the body. Its suggested velocity remains more than the experimental all through the height. Except close to the body velocity profiles of BSL remain close to the experimental. At the position near the start of the slant (Fig 2c) velocity suggested by k-ω model is close to the experimental (near the body). Velocity produced by the k-ε model is next at near the body, but deviates more

with the increases in height. Over the slant, near the body k-ε model's velocity is in the best match with the experimental, BSL model suggested profile is next (Fig 2d). None of the model is showing the sharp turning as is found in the experiment. At the position after the rear end the shape prescribed by the experimental data is not found through models (Fig 2e). The models suggested shape is smooth but the experimental one is not that much. At the sharp turning performance of the k-ε is close to experimental. With the increase in height k-ε model's velocity differ more from the experiment. Away from the rear end the sharp turning is found in all the model's velocity profile (Fig 2f) but the velocities and heights of turning are different for the models. The velocity and height at the turning produced by the BSL model is close to the experimental, though the velocity-height relationship differ from the experimental before the free stream.

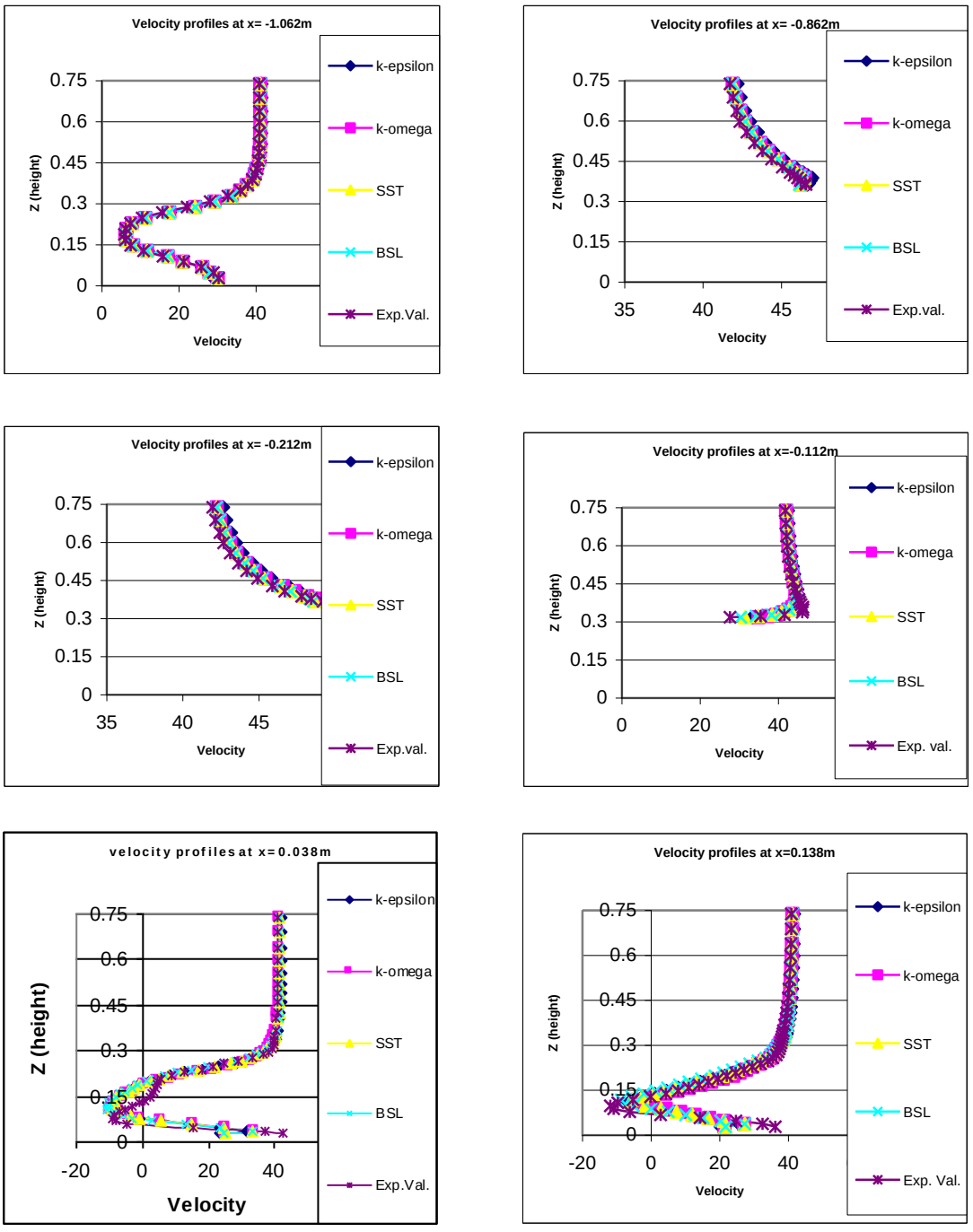

Fig. 2 (a-f) Velocity profiles at different locations with inlet velocity 40 m/s for different turbulence models

Velocity profiles with velocity 20m/s is presented in Fig 3(a, b). As we have no experimental value with this velocity so only two position's (over the slant and after the rear end) velocity profiles are presented here. For the same reason same are produced with the velocity 15m/s in fig 4(a, b). Over the slant the patterns in both the

cases are same and resemble with the profile at the same position for the velocity 40m/s. Thus the drag induced velocity reduction over the slant is independent of the velocity but how far the velocity will be reduced is depending on the free stream velocity and other factors. The shape and height of turning of the velocity profiles after the rear end are showing the same feature as shown by the velocity profiles over the slant.

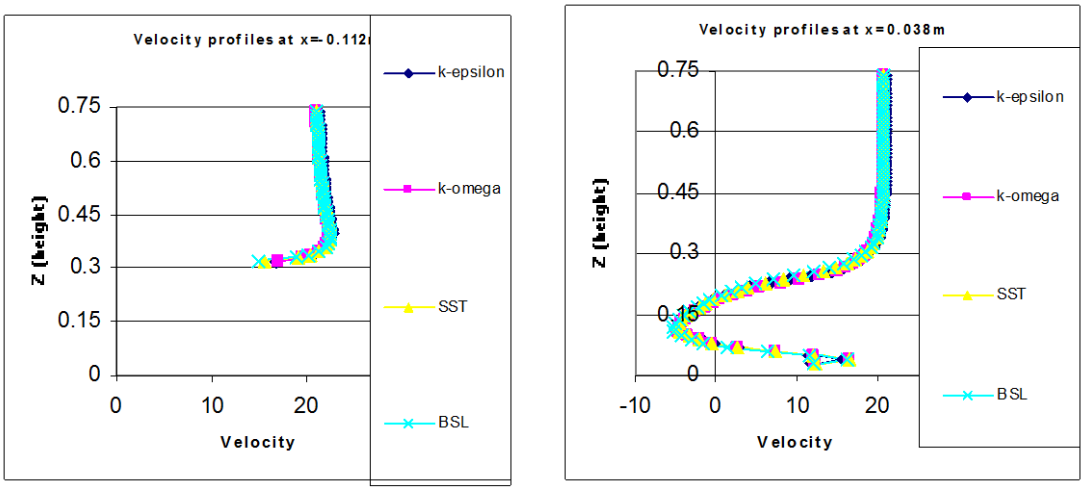

Fig 3(a,b) Velocity profiles at different locations with inlet velocity 20 m/s for different turbulence models

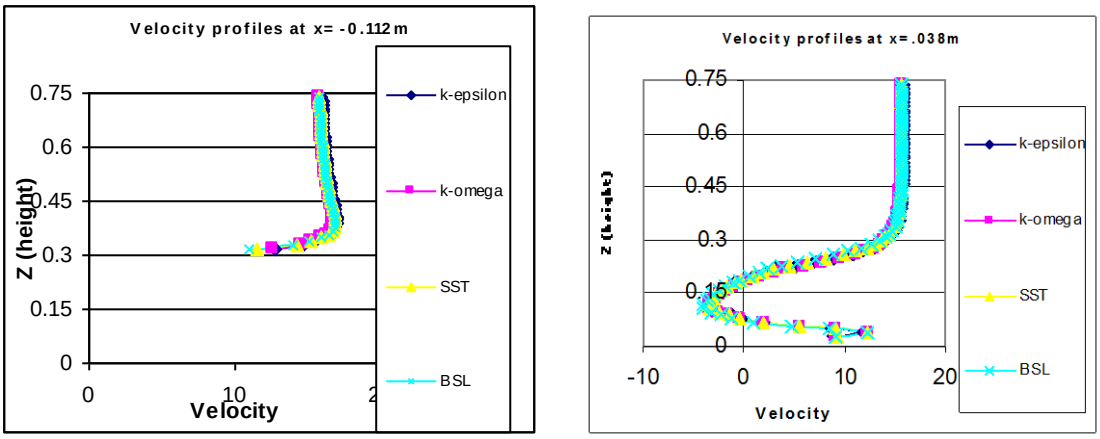

Fig 4(a,b) Velocity profiles at different locations with inlet velocity 15 m/s for different turbulence models

4. Conclusion

1) All the four turbulence models are capable to capture most of the features of the velocity profile of the experimental data.
2) Near the body the performance of the k-ε model is best among the models considered but the deviation from the experimental is also largest at the height considered.
3) Among the four models (k-ε, k-ω, SST and BSL), BSL is best.
4) The pattern/shape of the velocity profiles for different velocities do not differ significantly at the same location.

References

[1] Lienhart H, Stoots C, Becker S. Flow and turbulence structure on the wake of a simplified car model (Ahmed model), DGLR Fach. Symp. der AG ATAB,Stuttgart University, 2000.
[2] Martinat G, Bourguet R, Hoarau Y, Dehaeze F, Jorez B and Braza M. Numerical Simulation of the Flow in the Wake of Ahmed Body Using Detached Eddy Simulation and URANS Modelimg. Peng S-H and Haase W (Eds.): Adv. in Hybrid RANS-LES Modeling, 2008;NNFM 97:125-31
[3] Ahmed,S.R.,Ramm G.:Some Salient Features of the Time –Averaged Ground Vehicle Wake. SAE Technical Paper 840300,1984.

[4] Craft TJ, Gant SE, Iacovides H and Launder BE. Computational stady of flow around the Ahmed car body, 9 th ERCOFTAC workshop on refined turbulence modeling, Darmstadt University of Technology, Germany, 2001.
[5] Basara B. Numerical simulation of turbulent wakes around a vehicle, FEDSM 99-7324, 1999.
[6] Durand L, Kuntz M and Menter F. Validation of CFX-5 for the Ahmed car body, 10 th joint ERCOFTAC (SIG-15)- IAHR-QNET/CFD Workshop on Refined Turbulence Modelling, October 10-11, 2002.

5th BSME International Conference on Thermal Engineering

Analysis of Surface Temperature Distribution on MHD Natural Convection Flow Along a Vertical Flat Plate with Heat Conduction

A.K.M. Safiqul Islam[a], M. A. Alim[b]* , Md. Rezaul Karim[c] and M. M. A. Sarker[b]

[a]*Department of Mathematics, Gowripur Govt. College, Mymensingh, Bangladesh*
[b]*Department of Mathematics, Bangladesh University of Engineering and Technology, Dhaka-1000, Bangladesh.*
[c]*Department of Mathematics, Jagannath University Dhaka-1000, Bangladesh*
[b]*Department of Mathematics, Bangladesh University of Engineering and Technology, Dhaka-1000, Bangladesh,*
Emails: safiqis@yahoo.com, maalim@math.buet.ac.bd, rrezaul@yahoo.com, masarker@math.buet.ac.bd

Abstract

Natural convection surface temperature distribution flow of an electrically conducting fluid along a vertical flat plate with heat generation and Magnetohydrodynamic (MHD) combined effects are studied in this paper. The governing equations with associated boundary conditions reduce to local non-similarity boundary layer equations for this phenomenon are converted to dimensionless forms using a suitable transformation. The transformed non-linear equations are then solved using the implicit finite difference method. Numerical results of the velocity and temperature profiles, surface temperature and local rate of heat transfer distribution for different values of the magnetic parameter, Prandtl number and heat generation parameter are presented graphically. Detailed discussion is given for the effects of the aforementioned parameters. Significant effects are found in velocity and temperature profiles for Prandtl number and surface temperature and local rate of heat transfer distribution for heat generation parameter.

Keywords: surface temperature, heat transfer, magnetohydrodynamics.

Nomenclature

b	Plate thickness
C_p	Specific heat at constant pressure
f	Dimensionless stream function
g	Acceleration due to gravity
Gr	Grashof number
h	Dimensionless temperature
H_0	Applied Magnetic field strength
l	Length of the plate
M	Magnetic parameter
P	Conjugate conduction parameter
Pr	Prandtl number
Q	Heat generation parameter

* Corresponding author. Tel.: +88-01552345618; fax: +8802-8613046.
E-mail address: maalim@math.buet.ac.bd

T	Temperature of the interface
T_b	Temperature at outside surface of the plate
T_f	Temperature of the fluid
T_∞	Temperature of the ambient fluid
$\bar{u}$	Velocity component in x- direction
$\bar{v}$	Velocity component in y- direction
u	Dimensionless velocity component in x- direction
v	Dimensionless velocity component in y- direction
$\bar{x}$	Cartesian co-ordinates
$\bar{y}$	Cartesian co-ordinates
x	Dimensionless Cartesian co-ordinates
y	Dimensionless Cartesian co-ordinates
Greek symbols	
β	Co-efficient of thermal expansion
∇	Vector differential operator
η	Similarity variable
κ_∞	Thermal conductivity of the ambient fluid
κ_s	Thermal conductivity of the solid
κ_f	Thermal conductivity of the fluid
μ, ν	Viscosity and Kinematic viscosity of the fluid
μ_e	Magnetic permeability of the fluid
ρ	Density of the fluid inside the boundary layer
σ	Electrical conductivity of the fluid
τ_w	Shearing stress
Ψ	Stream function

1. Introduction

Magnetohydrodynamics involves magnetic fields (Magneto) and fluids (hydro) that conduct electricity and interact (dynamics). MHD technology is based on a fundamental law of electromagnetism. When a magnetic field and an electric current intersect in a liquid, their repulsive intersection propels the liquid in a direction perpendicular to both the field and the current.

Magnetohydrodynamics is that branch of science, which deals with the motion of highly conducting ionized (electric conductor) fluid in presence of magnetic field. The motion of the conducting fluid across the magnetic field generates electric currents which change the magnetic field and the action of the magnetic field on these currents give rise to mechanical forces, which modify the fluid. It is possible to attain equilibrium in a conducting fluid if the current is parallel to the magnetic field. Then the magnetic forces vanish and the equilibrium of the gas is the same as in the absence of magnetic fields. In the case when the conductor is either a liquid or a gas, electromagnetic forces will be generated which may be of the same order of magnitude as the hydrodynamical and inertial forces. Thus the equation of motion as well as the other forces will have to take these electromagnetic forces into account.
Electrically conducting fluid flow in presence of magnetic field and the effect of heat generation on free convection flow with heat conduction problems are important from the technical point of view and such types of problems have received much attention by many researchers.

Convection is the transfer of heat energy in a gas or liquid by movement of currents. Considerable convection is responsible for making macaroni rise and fall in a pot of heated water. The warmer portions of the water are less dense and therefore, they rise. Mean while, the cooler portions of the waterfall because they are denser. Conduction is most effective in solids but it can happen in fluids.

It is readily recognized that a wealth of information is now available on convective heat and mass transfer for viscous (Newtonian) fluids. The study of heat generation or absorption in moving fluids is important in problems dealing with chemical reactions and those concerned with dissociating fluids. Heat generation effects may alter the temperature distribution; consequently, the particle deposition rate in nuclear reactor, electronic chips and semiconductor wafers. In fact, the literature is replete with examples dealing with the heat transfer in laminar flow of viscous fluids.

A medium through which heat is conducted may involve the conversation of electrical, nuclear or chemical energy into heat (or thermal) energy. In heat conduction analysis, such conversion processes are characterized as heat generation. The safe and effective removal of this heat away from the sites of heat generation (the electronic circuits) is the subject of electronics cooling which is one of the modern application areas of heat transfer. Likewise, a large amount of heat is generated in the fuel elements of nuclear reactors as a result of nuclear fission that serves as the heat source for the nuclear power plants. The heat generated in the Sun as a result of the fusion of hydrogen into helium makes the Sun a large nuclear reactor that supplies heat to the earth. Heat generation is the ability to emit greater-than-normal heat from the body.

Model studies of the free and mixed convection flows have earned reputations because of their applications in geophysical, geothermal and nuclear engineering problems. Also the problems of various types of shapes over or on a free convection boundary layer flow have been studied by many researchers. Amongst them Takhar and Soundalgekar [1] analyzed dissipation effects on MHD free convection flow past a semi-infinite vertical plate. Pozzi and Lupo [2] investigated the coupling of conduction with laminar convection along a flat plate. Hossain [4] investigated the viscous and joule heating effects on MHD free convection flow with variable plate temperature. Mamun [5] studied the effects of conduction and convection on magnetohydrodynamic flow with and without viscous dissipation from a vertical flat plate. Alim et al. [7] analyzed joule heating effect on the coupling of conduction with MHD free convection flow from a vertical flat plate. Rahman et al. [8] investigated the effects of temperature dependent thermal conductivity on MHD free convection flow along a vertical flat plate with heat conduction. Alam et al. [11] studied viscous dissipation effects on MHD natural convection flow over a sphere in the presence of heat generation. Miraj et al. [12] investigated effect of radiation on natural convection flow on a sphere in presence of heat generation. Ali et al. [13] studied combined effects of radiation and heat generation on MHD natural convection flow along a vertical flat plate in presence of heat conduction

The present study is to incorporate the idea of the effects of MHD natural convection boundary layer flow along a vertical flat plate with heat generation.

The governing boundary layer equations are transformed into a non-dimensional form and the resulting non-linear system of partial differential equations is reduced to local non-similar partial differential forms by adopting appropriate transformations. The transformed boundary layer equations are then solved numerically. Numerical results of the velocity and temperature profiles, the surface temperature and local rate of heat transfer distribution for the magnetic parameter, Prandtl number and heat generation parameters are presented graphically.

2. Mathematical Formulation of the Problem

At first we consider a steady two-dimensional laminar natural convection flow of an electrically conducting, viscous and incompressible fluid along a vertical flat plate of length l and thickness b (Figure-1). It is assumed that the temperature at the outer surface of the plate is maintained at a constant temperature T_b, where $T_b > T_\infty$, the ambient temperature of the fluid. A uniform magnetic field of strength H_0 is imposed along the $\bar{y}$-axis i.e. normal direction to the surface and $\bar{x}$-axis is taken along the flat plate. The coordinate system and the configuration are shown in Figure-1.

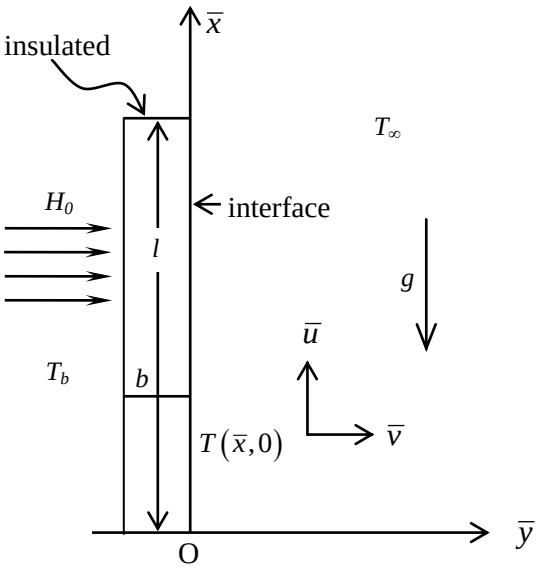

Figure-1: Physical model and coordinate system

The governing equations of such laminar flow with heat generation and also the magnetic parameter variation along a vertical flat plate under the Boussinesq approximations $\rho = \rho_\infty[1-\beta(T_b - T_\infty)]$, where ρ_∞ and T_∞ are the density and temperature respectively outside the boundary layer are given. For the present problem for continuity, momentum and energy equations take the following form

$$\frac{\partial \bar{u}}{\partial \bar{x}} + \frac{\partial \bar{v}}{\partial \bar{y}} = 0 \tag{1}$$

$$\bar{u}\frac{\partial \bar{u}}{\partial \bar{x}} + \bar{v}\frac{\partial \bar{v}}{\partial \bar{y}} = \nu\frac{\partial^2 \bar{u}}{\partial \bar{y}^2} + g\beta(T_f - T_\infty) - \frac{\sigma {H_0}^2 \bar{u}}{\rho} \tag{2}$$

$$\bar{u}\frac{\partial T_f}{\partial \bar{x}} + \bar{v}\frac{\partial T_f}{\partial \bar{y}} = \frac{1}{\rho C_p}\frac{\partial}{\partial \bar{y}}(\kappa_f \frac{\partial T_f}{\partial \bar{y}}) + \frac{Q_0}{\rho C_p}(T_f - T_\infty) \tag{3}$$

Here β is coefficient of volume expansion. The temperature dependent thermal conductivity, which is used by Rahman and Alim [6] as follows

$$\kappa_f = \kappa_\infty[1+\delta(T_f - T_\infty)] \tag{4}$$

Where κ_∞ is the thermal conductivity of the ambient fluid and δ is a constant, defined as

$$\delta = \frac{1}{\kappa_f}\left(\frac{\partial \kappa}{\partial T}\right)_f .$$

The appropriate boundary conditions to be satisfied by the above equations are

$$\left.\begin{aligned} &\bar{u} = 0,\ \bar{v} = 0 \\ &T_f = T(\bar{x}, 0),\ \frac{\partial T_f}{\partial \bar{y}} = \frac{\kappa_s}{b\kappa_f}(T_f - T_b) \end{aligned}\right\} \quad \text{on} \quad \bar{y} = 0,\ \bar{x} > 0$$
$$\bar{u} \to 0,\ T_f \to T_\infty \quad as \quad \bar{y} \to \infty,\ \bar{x} > 0 \tag{5}$$

The non-dimensional governing equations and boundary conditions can be obtained from equations (1) - (3) using the following dimensionless quantities

$$\begin{aligned} &x = \frac{\bar{x}}{l},\ \ y = \frac{\bar{y}}{l}Gr^{\frac{1}{4}},\ u = \frac{\bar{u}l}{\upsilon}Gr^{-\frac{1}{2}},\ v = \frac{\bar{v}l}{\upsilon}Gr^{-\frac{1}{4}}, \\ &\theta = \frac{T_f - T_\infty}{T_b - T_\infty},\ Gr = \frac{g\beta l^3(T_b - T_\infty)}{\upsilon^2} \end{aligned} \tag{6}$$

where l is the length of the plate, *Gr* is the Grashof number, θ is the dimensionless temperature.
Now from Equations (1)-(3), we get the following dimensionless equations

$$\frac{\partial u}{\partial x} + \frac{\partial v}{\partial y} = 0 \tag{7}$$

$$u\frac{\partial u}{\partial x}+v\frac{\partial u}{\partial y}+Mu=\frac{\partial^2 u}{\partial y^2}+\theta \tag{8}$$

$$u\frac{\partial \theta}{\partial x}+v\frac{\partial \theta}{\partial y}=\frac{1}{\Pr}(1+\gamma\theta)\frac{\partial^2 \theta}{\partial y^2}+\frac{\gamma}{\Pr}\left(\frac{\partial \theta}{\partial y}\right)^2+Q\theta \tag{9}$$

where $\Pr=\dfrac{\mu C_p}{\kappa_\infty}$ is the Prandtl number, $M=\dfrac{\sigma H_0^2 l^2}{\mu Gr^{1/2}}$ is the dimensionless magnetic parameter, and $Q=\dfrac{Q_0 l^2}{\mu C_p Gr^{1/2}}$ is the non-dimensional heat generation parameter .The corresponding boundary conditions (5) then take the following form

$$\begin{aligned} &u=0,\ v=0,\ \theta-1=(1+\gamma\ \ \theta)\ \ p\frac{\partial\theta}{\partial y}\ \ on\ \ \ y=0,\ x>0\\ &u\to 0,\ \theta\to 0\ \ as\ \ \ y\to\infty,\ x>0 \end{aligned} \tag{10}$$

here $p=\left(\dfrac{\kappa_\infty b}{\kappa_s l}\right)Gr^{\frac{1}{4}}$ is the conjugate conduction parameter. The described problem is governed by the coupling parameter p. In actual fact, magnitude of O(p) depends on b/l and $Gr^{1/4}$ being the order of unity. Since l is small, the term b/l becomes greater than one. For air, $\dfrac{\kappa_\infty}{\kappa_s}$ attains very small values if the plate is highly conductive and reaches the order of 0.1 for materials such as glass. Therefore in different cases p is different but not always a small number. In the present investigation we have considered p = 1 which is accepted for b/l of $O(\dfrac{\kappa_\infty}{\kappa_s})$.

To solve the equations (8) and (9) subject to the boundary conditions (10) the following transformations are

$$\begin{aligned} &\psi=x^{\frac{4}{5}}(1+x)^{-\frac{1}{20}}f(x,\eta)\\ &\eta=y\ \ x^{-\frac{1}{5}}(1+x)^{-\frac{1}{20}}\\ &\theta=x^{\frac{1}{5}}(1+x)^{-\frac{1}{5}}h\ \ \ (x,\eta) \end{aligned} \tag{11}$$

here η is the similarity variable and ψ is the non-dimensional stream function which satisfies the continuity equation and is related to the velocity components in the usual way as

$$u=\frac{\partial\psi}{\partial y}\ \ and\ \ v=-\frac{\partial\psi}{\partial x}.$$

Moreover, h (x,η) represents the non-dimensional temperature. The momentum and energy equations are transformed for the new co-ordinate system. At first, the velocity components are expressed in terms of the new variables for this transformation. Thus the following equations

$$f''' + \frac{16+15x}{20(1+x)} f\, f'' - \frac{6+5x}{10(1+x)} f'^2 - M\, x^{\frac{2}{5}}(1+x)^{\frac{1}{10}} f' + h = x\left(f' \frac{\partial f'}{\partial x} - f'' \frac{\partial f}{\partial x} \right) \tag{12}$$

$$\frac{1}{\Pr} h'' + \frac{\gamma}{\Pr}\left(\frac{x}{1+x}\right)^{\frac{1}{5}} hh'' + \frac{\gamma}{\Pr}\left(\frac{x}{1+x}\right)^{\frac{1}{5}} h'^2 + \frac{16+15x}{20(1+x)} fh' + Qx^{2/3}(1+x)^{1/10} h - \frac{1}{5(1+x)} fh = x\left(f' \frac{\partial h}{\partial x} - h' \frac{\partial f}{\partial x} \right) \tag{13}$$

where prime denotes partial differentiation with respect to η. The boundary conditions as mentioned in equation (10) then take the following form

$$f(x,0) = f'(x,0) = 0, \quad f'(x,\infty) \to 0$$

$$h'(x,0) = \frac{x^{\frac{1}{5}}(1+x)^{-\frac{1}{5}} h(x,0) - 1}{(1+x)^{-\frac{1}{4}} + \gamma x^{\frac{1}{5}}(1+x)^{-\frac{9}{20}} h(x,0)} \quad \text{and} \quad h(x,\infty) \to 0 \tag{14}$$

The set of equations (12) and (13) together with the boundary conditions (14) are solved by applying implicit finite difference method with Keller-box elimination technique [10] scheme.

For the numerical computation, it is important to calculate the values of the surface temperature. The numerical values of the surface temperature distribution are obtained from the relation. This can written in the non-dimensional form as

$$\theta(x,0) = x^{\frac{1}{5}}(1+x)^{-\frac{1}{5}} h(x,0) \tag{15}$$

In practical point of view, it is important to calculate the values of the local rate of heat transfer. This can written in the non-dimensional form as

$$Nu = (Gr^{-\frac{1}{4}} / \kappa_f (T_b - T_\infty)) q_w \tag{16}$$

where $q_w = -\kappa_f \left(\frac{\partial T_f}{\partial \bar{y}}\right)_{\bar{y}=0}$ is the heat flux.

Thus the rate of heat transfer is

$$Nu_x = -(1+x)^{-\frac{1}{4}} h'(x,0) \tag{17}$$

3. Numerical Method of Solution

In this paper investigates the effect of the surface temperature on electrically conducting fluid in natural convective heat transfer flow along a vertical flat plate with heat generation for strong magnetic field. Along with the boundary conditions (14), the solution of the parabolic non-linear differential equations (12) and (13) will be found by using in-house FORTRAN code based on the implicit finite difference method together with Keller-box elimination technique [9] which is well documented by Cebeci and Bradshaw [10] and used by Hossain et al. [14] and later by many other authors.

4. Results and Discussion

In this simulation the values of the Prandtl number *Pr* are considered to be 0.73, 1.00, 1.50, 2.00 and 2.50 that correspond to hydrogen, steam, sulfur dioxide, ammonia and methyl chloride respectively.

The velocity and the temperature profiles obtained from the solutions of equations (12) and (13) are depicted in Figures 2 to 4. Also the surface temperature and the local rate of heat transfer distribution profiles obtained from the solutions of equations (15) and (17) are depicted in Figures 5 to 7. Numerical computation are carried out for a range of magnetic parameter M = 0.02, 0.20, 0.40, 0.60, 0.80 and heat generation parameter Q = 0.02, 0.15, 0.25, 0.35, 0.50.

The interaction of the magnetic field and moving electric charge carried by the flowing fluid induces a force, which tends to oppose the fluid motion.

In fig. 2(a), it is shown that the magnetic field action along the horizontal direction retards the fluid velocity with Pr = 0.73 and Q = 0.02. Here position of peak velocity moves toward the interface with the increasing M. From fig. 2(b), it can be observed that the temperature within the boundary layer increases for increasing values of M from 0.02 to 0.80.

Fig. 3(a) and 3(b) illustrate the velocity and temperature profiles against η for different values of Prandtl number Pr with M = 0.02 and Q = 0.02. From fig. 3(a), it can be observed that the velocity decreases as well as its position moves toward the interface with the increasing Pr. From fig. 3(b), it is seen that the temperature shift downward with the increasing Pr.

In fig. 4(a) and 4(b) describe the velocity and temperature profiles against η for different values of heat generation parameter Q with M = 0.02 and Pr = 0.73. From fig. 4(a), it can be observed that the velocity increases as well as its position moves outward the interface with the increasing Q. From fig. 4(b), it is seen that the temperature profiles also the same as increasing within the boundary layer. It means that the velocity boundary layer and the thermal boundary layer thickness increase for large values of Q from 0.02 to 0.50.

The variation of the surface temperature distribution $\theta(x,0)$ and the local rate of heat transfer distribution Nu_x against x for different values of M with Pr = 0.73 and Q = 0.02 at different positions are illustrated in fig. 5(a) and 5(b), respectively. The velocity decreases as shown in fig. 2(a), due to the increasing M. It is observed from fig. 5(a) that the increased value of the magnetic parameter M leads to an increase the surface temperature factor on the plate. But from fig. 2(b) the temperature within the boundary layer increases for the increasing M. As a result, fig. 5(b) shows that the heat transfer rate from the plate to the fluid decreases due to the increased value of the magnetic parameter M. It can also be seen that the heat transfer increases along the downward direction of the plate for a particular M. The magnetic field acts against the flow and increases the surface temperature and reduces the heat transfer rate at the interface. It can be observed from figure that the surface temperature increases monotonically along the positive x direction due to the increasing of x for a particular M.

Fig. 6(a) and 6(b) deal with the effect of Prandtl number Pr on the surface temperature and the local rate of heat transfer with the increasing of axial distance x for the fixed value of controlling parameters M = 0.02 and Q = 0.02. It can be observed from fig. 6(a) that the surface temperature increases monotonically for a particular value of Pr due to the increasing of x. The values of Prandtl number are proportional to the viscosity of the fluid. So the increasing values of Pr the surface temperature decreases on the plate which is shown in fig. 6(a). From fig. 6(b), it can be seen that the rate of heat transfer increases due to the increasing values of Pr from 0.73 to 2.50.

Fig. 7(a) and 7(b) deal with the effect of heat generation parameter Q on the surface temperature and the local rate of heat transfer distribution against x with controlling parameter M = 0.02 and Pr = 0.73. It is seen that an increase value of heat generation parameter Q increase the fluid velocity within the boundary layer that shown in fig. 4(a). So, the corresponding surface temperature increase with the increasing values of Q. The opposite result is observed for the heat transfer distribution along with the increasing of heat generation parameter. Finally it can be noted that the surface temperature and the rate of heat transfer profiles increase and decrease for the increasing values of Q from 0.02 to 0.50.

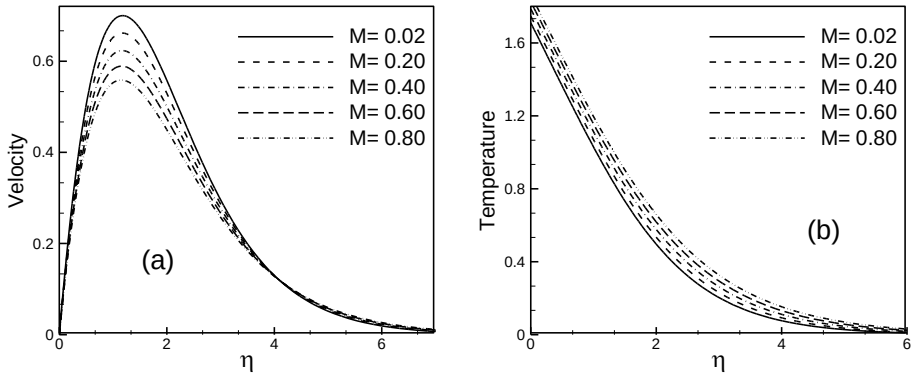

Fig. 2(a) Velocity and (b) temperature profiles against η for different values of M with Pr = 0.73 and Q = 0.02.

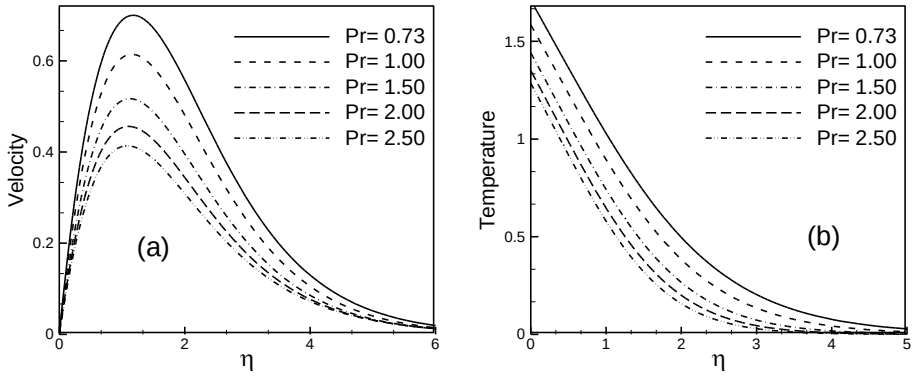

Fig. 3(a) Velocity and (b) temperature profiles against η for different values of Pr with M = 0.02 and Q = 0.02.

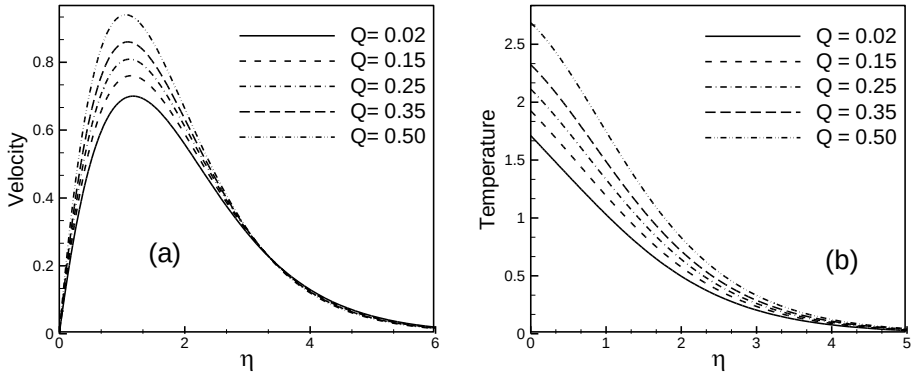

Fig. 4(a) Velocity and (b) temperature profiles against η for different values of Q with M = 0.02 and Pr = 0.73.

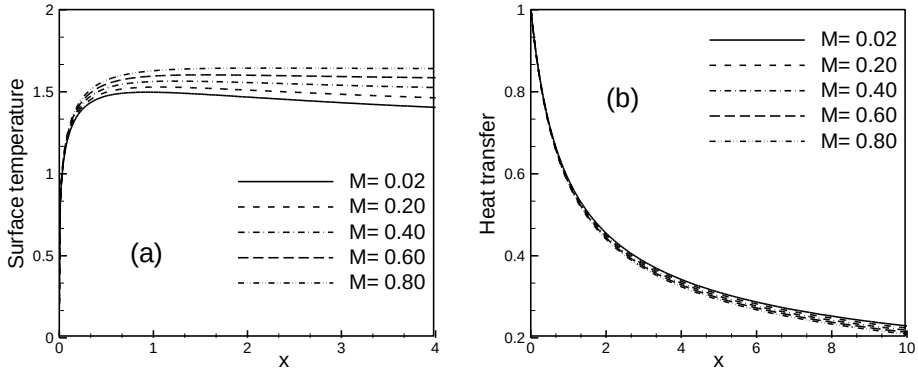

Fig. 5(a) Surface temperature distribution and (b) local rate of heat transfer against x for different values of M with Pr = 0.73 and Q = 0.02.

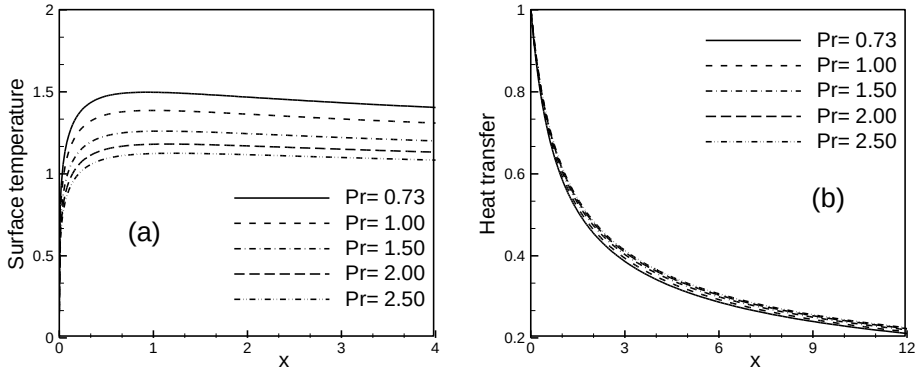

Fig. 6(a) Surface temperature distribution and (b) local rate of heat transfer against x for different values of Pr with M = 0.02 and Q = 0.02.

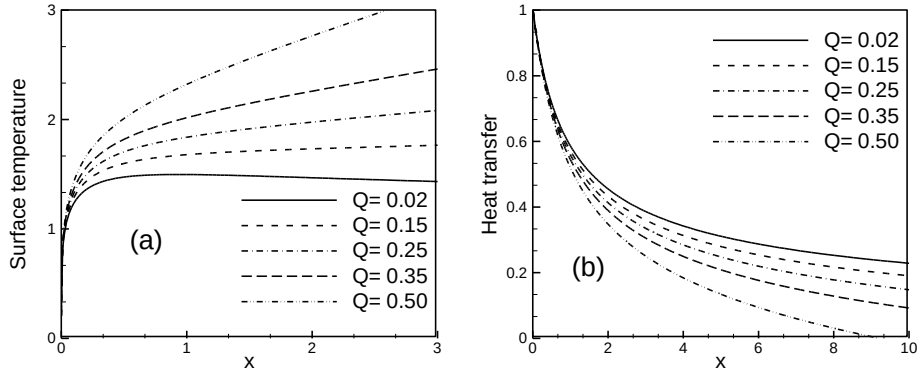

Fig. 7(a) Surface temperature distribution and (b) local rate of heat transfer against x for different values of Q with M = 0.02 and Pr = 0.73.

5. Comparison of the Results

The Table depicts the comparison of the present numerical results of the surface temperature distribution $\theta(x,0)$ with those obtained by Pozzi and Lopo [2] and Merkin and Pop [3] respectively. Here, the magnetic parameter M and heat generation parameter Q are ignored (i.e. M = 0.0 and Q = 0.0) and the Prandtl number Pr = 0.733 with $x^{1/5} = \xi$ is chosen. It is clearly seen that there is a strong agreement among the present results with the solutions Pozzi and Lopo [2] and Merkin and Pop [3].

Table 1: Comparison of the present numerical results of the surface temperature distribution $\theta(x,0)$ with Prandtl number Pr = 0.733, M = 0.0 and Q = 0.0 against x.

$x^{1/5} = \xi$	Pozzi and Lupo [2]	Merkin and Pop [3]	Present work
0.1	0.177	0.177	0.204
0.2	0.310	0.310	0.260
0.3	0.413	0.413	0.260
0.4	0.493	0.493	0.481
0.5	0.557	0.557	0.580
0.6	0.608	0.608	0.615
0.7	0.651	0.651	0.651
0.8	0.684	0.686	0.687
0.9	0.708	0.715	0.716
1.0	0.717	0.741	0.742
1.1	0.699	0.762	0.763
1.2	0.640	0.781	0.781

6. Conclusion

The MHD natural convective surface temperature and heat transfer flow along a vertical flat plate with heat generation has been investigated numerically and presented graphically. From this study the following conclusions may be drawn

- The velocity within the boundary layer increases for decreasing values of M, Pr and increases for increasing values of Q. Significant effect is found
- The temperature within the boundary layer increases for increasing values of M and Q and decreasing for values of Pr.
- The surface temperature increases for the increasing values of M, Q and decreases for the increasing values of Pr.
- An increase in the values of Pr leads to an increase in the rate of heat transfer. On the other hand, this decreases for increasing values of M and Q.

- Significant effects are found in velocity and temperature profiles for Prandtl number and surface temperature and local rate of heat transfer distribution for heat generation parameter.
- Significant effects are found in surface temperature distribution for magnetic parameter and Prandtl number. This is reverse for these two parameters.

References

[1] Takhar, H. S. and Soundalgekar, V. M., 1980, Dissipation effects on MHD free convection flow past a semi infinite vertical plate Applied Scientific Research, Vol. 36, No. 3, pp. 163-171.

[2] Pozzi, A. and Lupo, M., 1988, The coupling of conduction with laminar convection along a flat plate. Int. J. Heat Mass Transfer, Vol. 31, No. 9, pp.1807-1814.

[3] Merkin J. H and Pop I., 1996, Conjugate free convection on a vertical surface, Int. J. Heat Mass Transfer, Vol. 39, pp.1527- 1534.

[4] Hossain, M. A. 1992, The viscous and Joule heating effects on MHD free convection flow with variable plate temperature, Int. J. Heat transfer Vol. 35, No. 12, pp.3485-3487.

[5] Mamun, A. A., 2005, Effects of conduction and convection on magnetohydrodynamic flow with and without dissipation from a vertical flat plate. M. Phil thesis, Department of Mathematics, BUET.

[6] Rahman, M. M and Alim, M. A., 2009, Numerical study of magnetohydrodynamic (MHD) free convective heat transfer flow along a vertical flat plate with temperature dependent thermal conductivity, Journal of Naval Architecture and Marine Engineering, JNAME, Vol.6, No.1, pp.16-29.

[7] Alim, M. A., Alam, M.and Mamun, A. A., 2007, Joule heating effect on the coupling of conduction with MHD free convection flow from a vertical flat plate, Nonlinear Analysis: Modeling and Control, Vol.12, No. 3,pp.307-316.

[8] Rahman, M.M, Mamun A.A, Azim M.A and Alim, M. A., 2008, Effects of temperature dependent thermal conductivity on magnetohydrodynamic (MHD) free convection flow along a vertical flat plate with heat conduction, Nonlinear Analysis: Modeling and Control, Vol.13, No. 4,pp.513-524.

[9] Keller, H. B., 1978, Numerical methods in boundary layer theory, Annual Rev. Fluid Mech. Vol. 10, pp. 417-433.

[10] Cebeci, T and Bradshaw, P., 1984, Physical and Computational Aspects of Convective Heat Transfer, Springer, New York.

[11] Alam, Md. M., Alim, M.A. and Chowdhury, Md. M. K., 2007, Viscous dissipation effects on MHD natural convection flow over a sphere in the presence of heat generation, Nonlinear Analysis:Modeling and Control, Vol.12, No. 4,pp.447-459.

[12] Miraj, M., Alim, M. A. and Mamun, MAH., 2010, Effect of radiation on natural convection flow on a sphere in presence of heat generation, International Communications in Heat and Mass Transfer, Vol.37, pp. 660-665.

[13] Ali, Mohammad Mokaddes and Akther Rowsanara, 2009, Combined effects of radiation and heat generation on MHD natural convection flow along a vertical flat plate in presence of heat conduction, BRAC University Journal, Vol.VI ,No. 2,pp 11-20.

[14] Hossain, M. A. Alim, M. A. and Rees, D. A. S., (1999) The effect of radiation on free convection from a porous vertical plate, Int. J. Heat and Mass Transfer, Vol. 42, pp. 181-191.

5th BSME International Conference on Thermal Engineering

Analysis of dynamic characteristics of Multi-bladed S-shaped Rotor

"Z. Afroz[a*], M.Q. Islam[b], M. Ali[b]"

[a]*Assistant Engineer, BITAC, Tejgaon Industrial Area, Dhaka-1208, Bangladesh*
[b]*Professor, Department of Mechanical Engineering, BUET, Dhaka-1000, Bangladesh*

Abstract

In the present research work the dynamic conditions of Multi S-shaped bladed rotor at different Reynolds number has been analysed. The investigation on wind loading and aerodynamic effects on the four, five and six bladed S-shaped vertical axis vane type rotor has been conducted with the help of an open circuit subsonic wind tunnel. For different bladed rotor the flow velocities were varied from 5m/s to 9m/s covering the Reynolds numbers up to 1.35×10^5. It was observed that by increasing the number of blades of rotor to the optimum limit considering all significant factors and at the same time by increasing its Reynolds number, the power output can be increased to its maximum level. Finally, the nature of predicted dynamic characteristics has been analyzed by comparing with the existing research works.

Keywords: Multi-blade; S-shaped rotor; Vertical axis; Dynamic characteristics; Reynolds number.

1. Introduction

The utilization of wind energy is not a new technology but draws on the rediscovery of a long tradition of wind power technology. However, expected developments have not been achieved in wind driven machines to cope with the characteristics of wind turbines. Conventional machines are being used now a day even though they are not always suitable from the operational point of view. Arising from the increasing practical importance of wind turbine aerodynamics, there have been, over the past few decades, enormous increases in research works concerning laboratory simulations, full-scale measurements and more recently, numerical calculations and theoretical predictions of flows over a wide variety of vane type wind turbine. Bowden, G.J. and McAleese, S.A. [2] made some measurements on the Queensland optimum S-shaped rotor to examine the properties of isolated and coupled S-shaped rotor. Huda et al. [3] analyzed the performance of S-shaped rotor by placing a flat plate in front of the returning blade. Islam et al. [4] investigated Aerodynamic characteristics of a stationary Savonius rotor of two semi cylindrical blades. Islam et al. [5] investigated the aerodynamic forces acting on a stationary S-shaped rotor and made an attempt to predict the dynamic performance from these forces. Saha and Maity [6] experimented for augmenting the energy-harnessing effectiveness and finally, suggested that the use of the partially blocking wedge is highly desirable. Islam et al. [7] investigated the drag and torque coefficients of a stationary five bladed vane type rotor by measuring the pressure distribution on the blade surfaces at various rotor angles. Swamy and Fritzsche [8] investigated with the objective to improve the Darrieus type of motor.

This paper reports on the investigation on wind loading and aerodynamic effects on the four, five and six bladed S-shaped vertical axis vane type rotor conducted with the help of a subsonic wind tunnel together with the experimental set-up of the vane type rotor and a spring balance. This Vane type rotor of S-shaped cross section is predominantly drag based, but also uses a certain amount of aerodynamic lift. Drag based vertical axis wind turbines have relatively higher starting torque and less rotational speed than their lift based counterparts. Furthermore, their power output to weight ratio is also less. Because of the low speed, these are generally considered unsuitable for producing electricity, although it is possible by selecting proper gear trains. Drag based windmills are useful for other applications such as grinding grain, pumping water and a small output of electricity. A major advantage of drag based vertical axis wind turbines lies in their self–starting capacity, unlike the Darrieus lift–based vertical axis wind turbines.

* Corresponding author. Tel.: +88-02-8870725; fax: +88-02-8870728.
E-mail address: zakia_afroz@yahoo.com

2. Set-up of the experiment

The experiment was carried out in the open circuit subsonic wind tunnel [1] with an outlet test section of (490 mm x 490 mm) cross-section and the rotor was positioned at the exit section of the wind tunnel. The rotors were made of PVC material. Both the top and bottom ends of the rotor were fitted with end caps. The whole rotor was fixed on an iron frame by using a shaft that was inserted into it and two ball bearings. A pulley was attached at one end of shaft. A strip whose one side was tied to a spring balance and other side to a load carrying plate was prepared for passing over that pulley. A radium sticker was attached to that side of shaft. The spring balance was attached to the iron frame. The whole experimental set-up is shown in Figure 1.

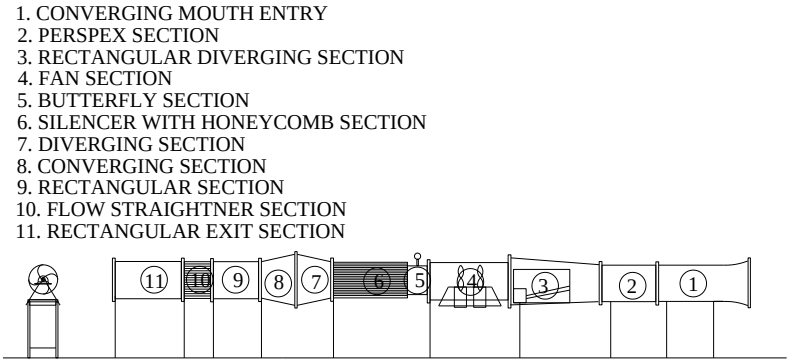

Figure 1. Schematic diagram of wind tunnel

The cross-sectional and three dimensional views of four, five and six bladed S-shaped vane type rotors are shown in Figure 2.

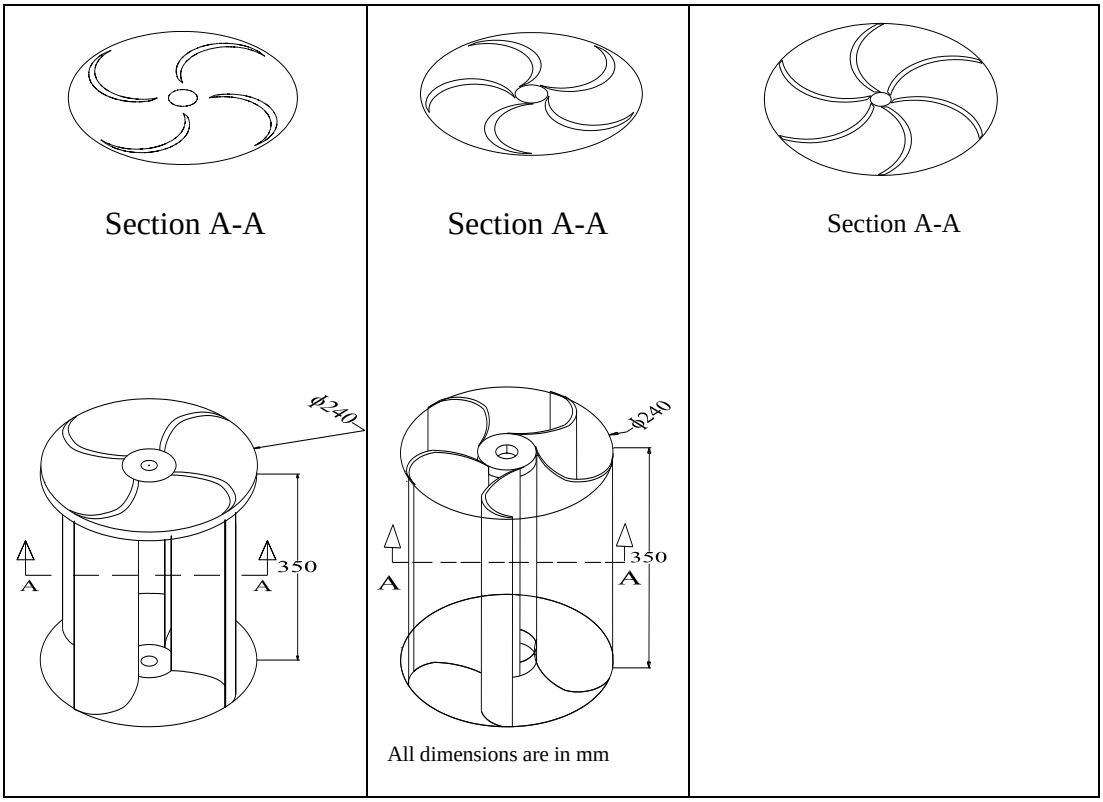

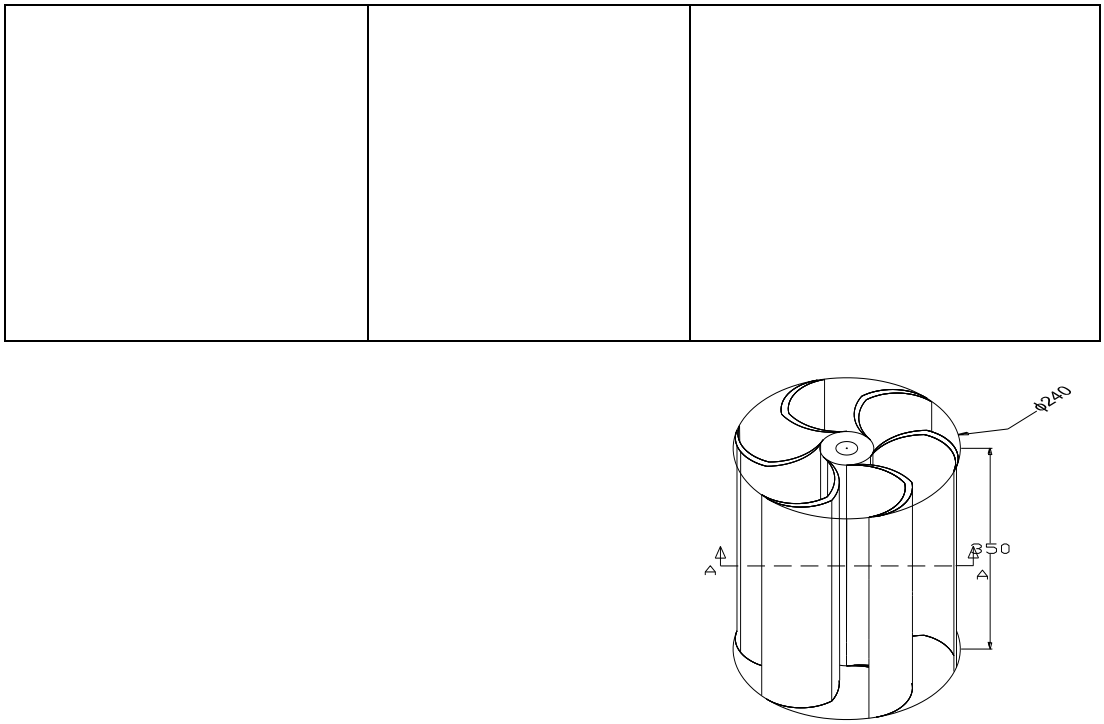

Figure 2. Cross-sectional and three dimensional views of four, five and six bladed rotor

3. Experimental procedure

In front of the wind tunnel without placing the rotor model the wind velocity was measured by an anemometer. The speed of the axial flow fan was then adjusted to obtain a particular free steam velocity of 5m/s at the exit section of wind tunnel. The four bladed vane type rotor with structural frame was placed in front of the wind tunnel. At rotating condition of rotor with shaft, the rpm reading was taken by digital non-contact tachometer at no load condition. At different loading condition the reading of rpm of the shaft using con-contact tachometer, the reading of weight from spring balance and the applied weight in the load carrying plate were noted down. After taking all the readings up to maximum loading condition, the free stream velocity was further adjusted to 6 m/s. And the same procedures were followed. Thus rapidly the free stream velocity was increased by 1 m/s and each time the same procedures were followed. The free stream velocity was raised rapidly up to 9 m/s. The same procedures were followed for five and six bladed vane type rotors. Experimental values of the power coefficients were calculated from the ratio of the total output power to the theoretical available power. Finally, experimental values of the Torque coefficients were calculated from the ratio of power coefficient to the tip speed ratio.

4. Results and discussions

The variation of results for four, five and six bladed S-shaped vane type rotor in terms of power co-efficient versus tip speed ratio for increasing Reynolds number are shown in Figure 3, 4 and 5 respectively.

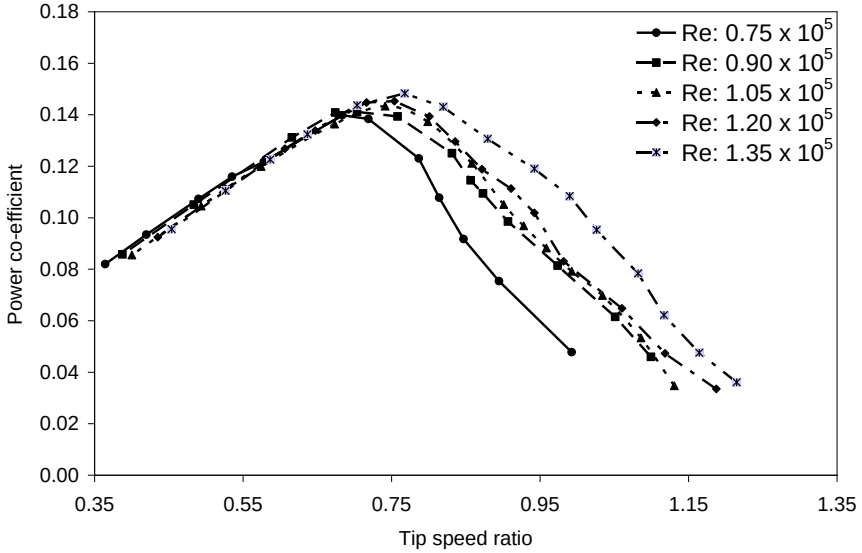

Figure 3: Comparisons of power coefficient vs. tip speed ratio for Four Bladed S-shaped Rotor at different Reynolds number

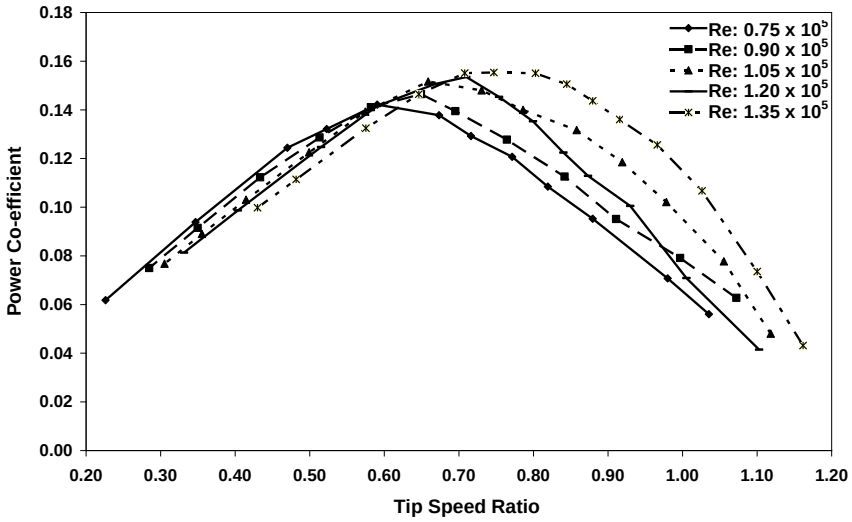

Figure 4: Comparisons of power coefficient vs. tip speed ratio for Five Bladed S-shaped Rotor at different Reynolds number

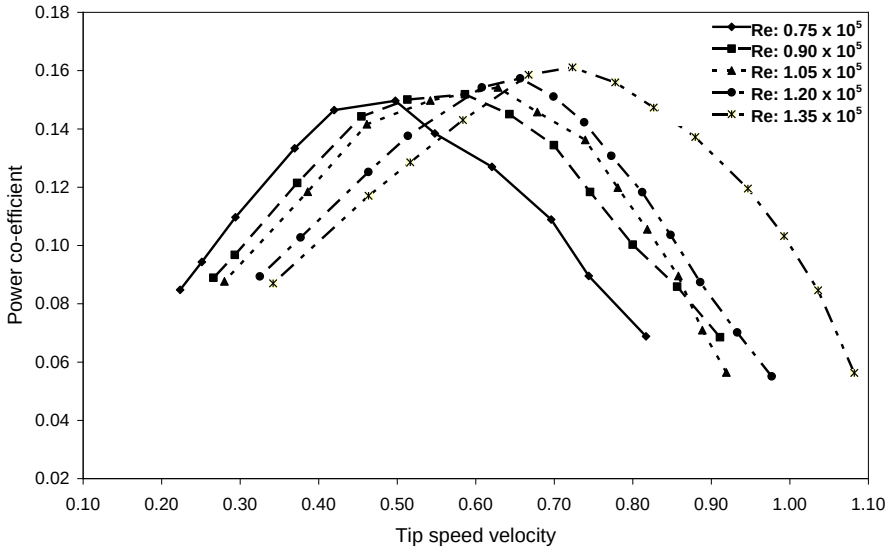

Figure 5: Comparisons of power coefficient vs. tip speed ratio for Six Bladed S-shaped Rotor at different Reynolds number

From these graphs (Figure 3-5) it is evident that with the increase of Reynolds number the maximum value of power coefficient also increases and it is shifted towards the higher values of tip speed ratios.

The results for four, five and six bladed S-shaped Vane Type Rotors in terms of torque co-efficient versus tip speed ratio for increasing Reynolds number are shown in Figures 6, 7 and 8 respectively.

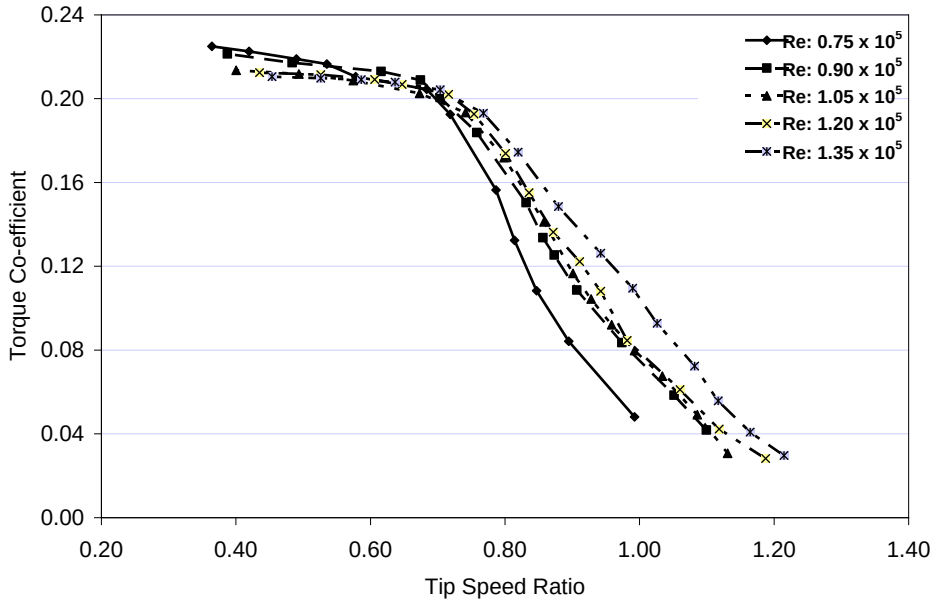

Figure 6: Comparisons of torque coefficient vs. tip speed ratio for Four Bladed S-shaped Rotor at different Reynolds number

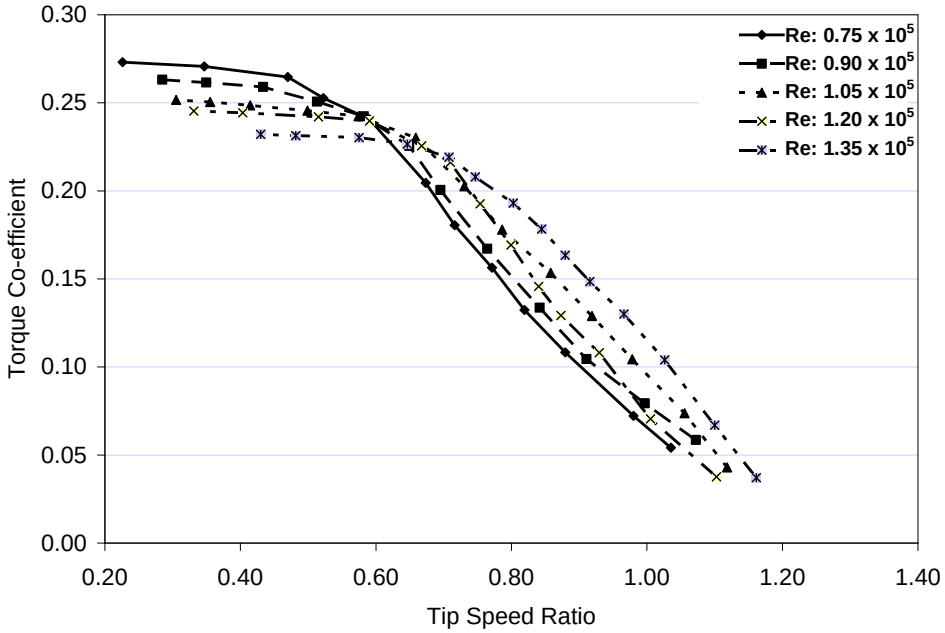

Figure 7: Comparisons of torque coefficient vs. tip speed ratio for Five Bladed S-shaped Rotor at different Reynolds number

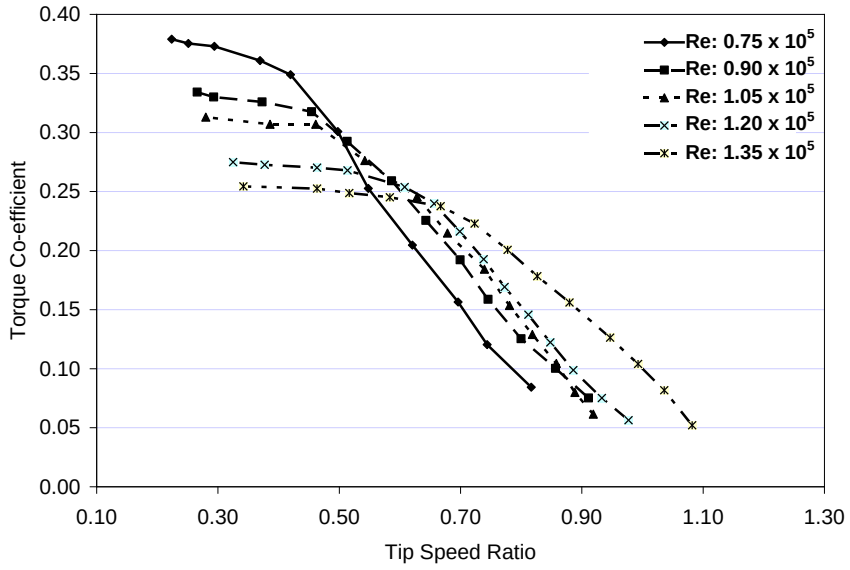

Figure 8: Comparisons of torque coefficient vs. tip speed ratio for Six Bladed S-shaped Rotor at different Reynolds number

From these graphs (Figure 6-8) it is evident that for higher Reynolds number the maximum value of torque coefficient is lower and it is shifted towards the higher values of tip speed ratio.

In Figures 9 and 10 the nature of predicted dynamic aerodynamic characteristics have been analyzed by comparing them with existing research works of Huda et al. [3].

In Figure 9 the nature of predicted power co-efficient versus tip speed ratio curves for free stream velocities of 6 and 7 m/s has been compared with the same curve of Huda et al. [3] (without attaching deflecting plate in the experimental setup) for free stream velocity of 6.5 m/s. From this figure it is seen that there is a close correlation between the values predicted by the present method and those predicted by Huda et al. [3]. In Figure 9 the nature of all curves are almost same although because of rotor swept area, blade number, its thickness and shape the curve predicted by Huda et al. is slightly oversize.

For the same reason the values of torque co-efficient with respect to tip speed ratio in the curve of Huda et al. of Figure 10 are slightly higher. However the nature of all curves is almost same.

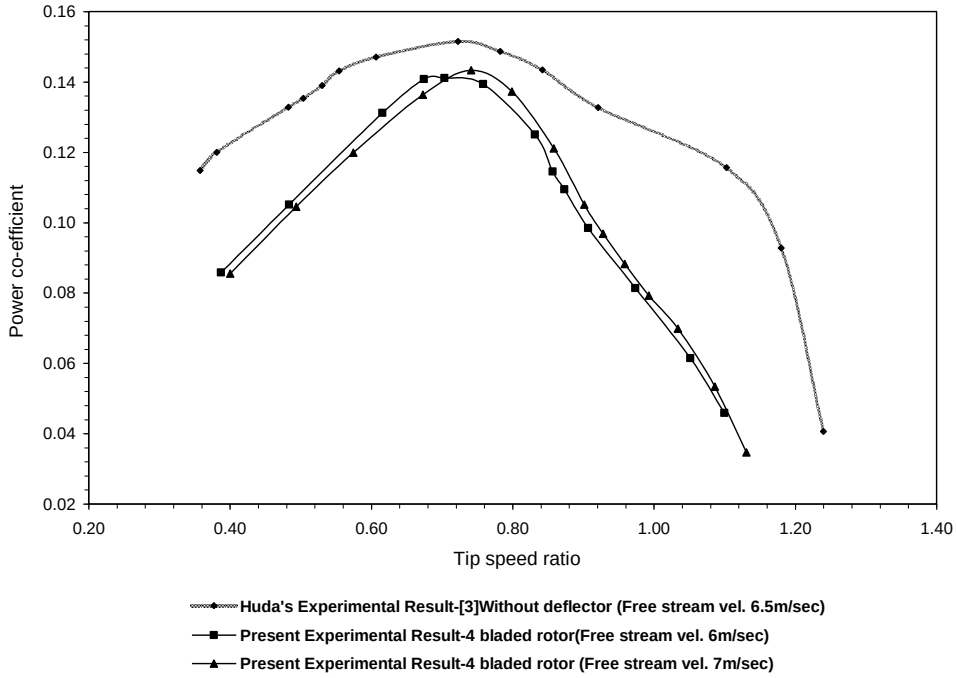

Figure 9: Comparisons of power coefficient versus tip speed ratio of present and existing experimental results [3]

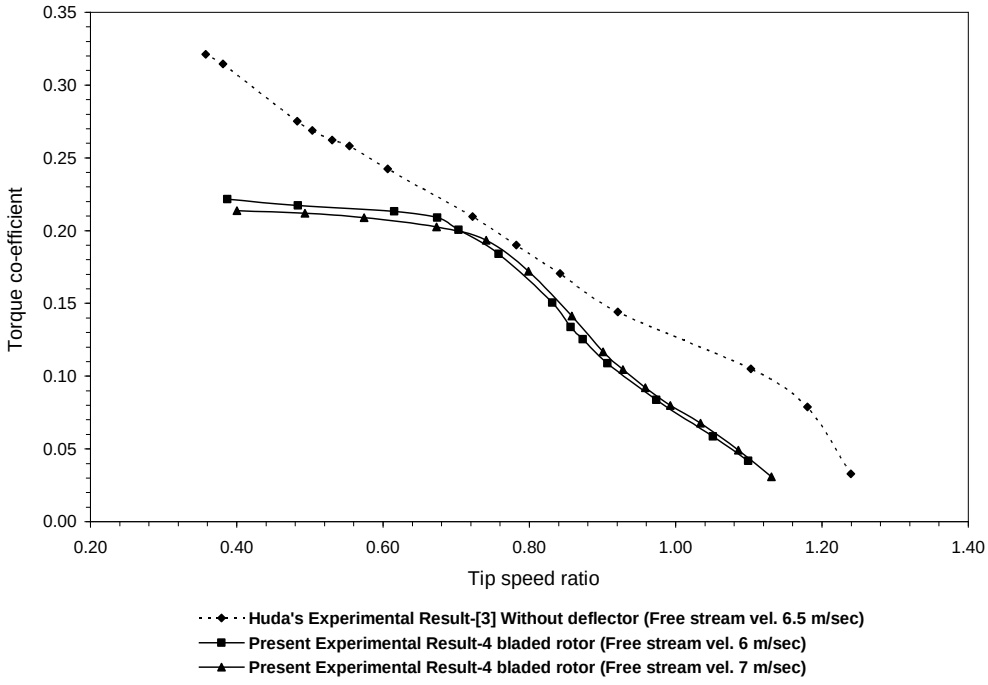

Figure 10: Comparisons of torque coefficient versus tip speed ratio of present and existing experimental results [3]

5. Conclusion

From the study, analysis and results of this research work, the following conclusions can be made:

1. For higher value of Reynolds number the value of maximum power coefficient is higher and it is shifted towards the higher value of tip speed ratio as the Reynolds number is increased.
2. For the same Reynolds number, the increase in number of blades makes the maximum value of power coefficient higher and it is shifted towards the lower value of tip speed ratio.
3. By increasing the number of blades of rotor to the optimum limit considering all significant factors and at the same time by increasing its Reynolds number, the power output can be increased to its maximum level.
4. At higher Reynolds number the value of maximum torque co-efficient is slightly lower.
5. At the same Reynolds number for rotor having higher number of blades the maximum value of torque coefficient is also higher and it is shifted towards the lower value of tip speed ratio. This point is very important for driving the irrigation pump especially positive displacement pump which needs higher starting torque.
6. The trend of all curves in each figure (showing comparison among the trend of predicted dynamic aerodynamic characteristics and similar research works) is almost same.

References

[1] Alexander, A.J. and B.P. Holownia. Wind Tunnel Tests on a Savonius Rotor. J. Industrial Aerodynamics, vol. 3, 1978.
[2] Bowden, G.J. and McAleese, S.A. The Properties of Isolated and Coupled Savonius Rotors. Journal of Wind Engineering, vol. 8, no. 4, pp. 271-288, 1984.
[3] Huda, M.D., Selim, M.A., Islam, A.K.M.S. and Islam, M.Q. The Perfomance of an S-Shaped Savonius Rotor with a Deflecting Plate. RERIC International Energy Journal: Vol. 14, No. 1, pp. 25-32, June 1992.
[4] Islam, A.K.M.S., Islam, M.Q., Mandal, A.C. and Razzaque, M.M. Aerodynamic Characteristics of a Stationary Savonius Rotor. RERIC Int. Energy Journal, Vol. 15, No. 2, pp. 125-135, 1993.
[5] Islam, A.K.M.S., Islam, M.Q., Razzaque, M.M. and Ashraf, R. Static Torque and Drag Characteristics of an S-Shaped Savonius Rotor and Prediction of Dynamic Characteristics. Wind Engineering, Vol. 19, No. 6, U.K., 1995.
[6] Saha, U.K. and Maity, D. Optimum Design Configuration of Savonius Rotor through Wind Tunnel Experiments. Journal of Wind Engineering and Industrial Aerodynamics, Volume 96, Issues 8-9, Pages 1359-1375, August-September 2008.
[7] Kamal, F.M. and Islam, M.Q. Aerodynamic Characteristics of a Stationary Five Bladed Vertical Axis Vane Type Wind Turbine. Journal of Mechanical Engineering, Vol. ME39, No. 2, IEB, December 2008.
[8] Swamy, N.V.C. and Fritzsche, A.A. Aerodynamic Studies on Vertical Axis Wind Turbine. International Symposium on Wind Energy Systems, Cambridge, England, September 7-9, 1976.

5th BSME ICTE

Investigation of Energy and Exergy Savings Using Hydrocarbon Mixture in the Air Conditioning System

Abstract

In this paper, the energy and exergy savings are investigated in a room air conditioner using R22 and its mixture with hydrocarbon (R290). A mixture of R22 and R290 with a mass ratio of 75:25 (M1) was used as the refrigerant. There are thermocouples, and pressure sensors used to measure the inlet and outlet temperatures and pressures in the compressor, evaporator, condenser and expansion devices. A digital data logger was used to interface the thermocouples and pressure transducers with the computer for data recording. The air conditioner unit was split type window air conditioner. Using mixture (M1), energy was saved by 5.22% in the domestic air conditioner with respect to R22. Exergy losses have been measured for all the components at varying evaporator temperatures. Exergy losses decreased with the increase of evaporator temperature, and it was found lower in low ambient temperatures. The refrigerating capacity or effect of the air conditioner was increased upto 2 to 6% while using the mixture, M1 instead of R22 at different evaporator temperatures. It is found that with the increase of 4°C set point indoor temperature, 24.40% energy was saved. It is concluded that the mixture (M1) can be the suitable candidate for the replacement of R22 based on energy, exergy and heat transfer performance.

Keywords: Exergy savings, Energy savings, set point temperature, hydrocarbon

1. INTRODUCTION

Refrigeration and air-conditioning systems are the main sectors of the vapor compression air conditioning system (Ahamed, 2012, Sattar et al, 2008)). In early date, the performance of the air conditioning system and refrigerator were measured based on only the energy performance of the system. Refrigerants were selected based on the high energetic performance (Ahamed et al., 2011). Early refrigerants were ammonia, carbon dioxide, etc. After twentieth century, CFCs took over the field. At present, Ammonia is used in the air conditioner for commercial uses but R22 is used in the air conditioner for domestic purposes. In some of the regions, R407C is being used as refrigerant.

Energy analysis deals with the first law of thermodynamics. It measures the coefficient of performance of the vapor compression system which is used in the refrigerator and air conditioner. Energy analysis tells the information of how efficiently the systems can work. High energy performance system means amount of heat absorption in the evaporator is higher compared to the electrical power consumption by the compressor. In the developed countries, performance of air conditioner is treated also as the term energy efficiency ratio (EER).

Exergy creates a link between the second law of thermodynamics and environmental impact (EI). Exergy measures the deviation of any state from the environment (Edgerton, 1992 ; Szargut, 1980; Dincer et al., 2008). The exergy efficiency is mostly influenced by the system and the states of the environment. The decrease in EI of any process shows the increase of exergy efficiency. Exergy analysis is used to improve the sustainability of the system. Cornelissen (1997) suggested that exergy losses can be minimized to obtain sustainable development using non-renewable energy forms. The author also found that EI is connected to the emissions and resource depletion which can be defined with exergy (Rosen et al., 2008).

Many literatures are based on energy analysis for air conditioning systems. But very few analyses are based on hydrocarbon mixture (R290) with R22 which will cause low GWP and ODP. Objectives of these experimental investigations are to find energy savings as well as exergy savings using the mixture with suitable proportions.

2. Potentials of Energy and Exergy Savings

To find a suitable refrigerant for energy and exergy savings it is essential to study the thermal properties of the refrigerants. From the literature, it is found that Refrigerants R22, R134a, R 290, R410a are already in used in the air conditioner. A mixture of R290 with R22 with proportion 25: 75 (M1) by mass was also considered for analysis.

2.1 Based on thermal properties

As R290 has high latent heat of vaporization, less amount of R290 will be capable to cool a room. Hence, the total exergy losses also will be reduced.

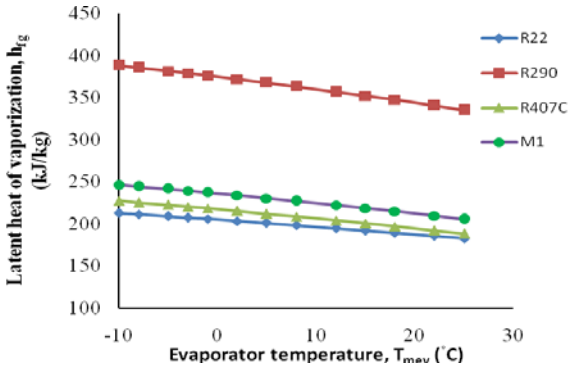

Fig. 1. Variation of heat of vaporization with evaporator temperatures for different refrigerants

From Fig. 1, it is clear that propane has higher heat of vaporization than that of R22 and the others. M1 also shows higher heat of vaporization than that of R22. R290 shows similar heat of vaporization to R22 but M1 and R290 show higher heat of vaporization than R22 at every evaporator temperatures.

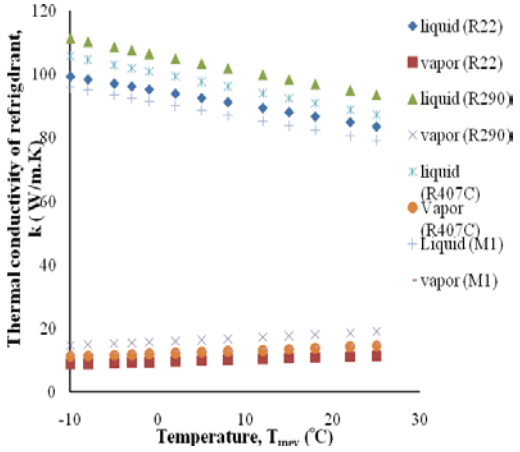

Fig. 2. Variation of thermal conductivity of the fluid with evaporator temperature

Thermal conductivity is important in heat transfer in both single and two phase flows. If thermal conductivity is higher, the heat transfer also will be higher. In the Fig.2, it is observed that thermal conductivity of propane is higher than that of the others. Thermal conductivity of the mixture (M1) in both cases (single and 2 phase flows) is higher than that of R22 at every evaporator temperatures. Higher thermal conductivity will influence the heat transfer. But the thermal conductivity in liquid state is decreasing with increasing the evaporator temperature. The thermal conductivity of the vapor does not increase/decrease with temperature changes (Pelletier & Palm, 1996).

2.2 Based on GWP and ODP

A comparative study based on GWP and ODP are necessary among the refrigerants used in the vapor compression systems.

Table 1: Global warming potential and ozone depletion potential of some refrigerants are used in the vapor compression refrigeration system

No.	Code	Chemical Formula	ODP	GWP
1	12	CCl_2F_2	0.82	8100
2	134a	CH_2FCF_3	0	1300
3	50	CH_4/methane	0	20
4	170	C_2H_6/ethane	0	20
5	290	C_3H_8/propane	0	20
6	22	$CHClF_2$	0.05	1810
7	407C	HFC32/HFC125/HFC134a	0	1530
8	M1	Mixture of R22 and R290 (3:1)	0	1075
9	22	$CHClF_2$	0.05	1810

3. Experimental Facility

In this work, a split- type- air conditioner, provided by the Institute of air conditioner research unit was adopted as the refrigerant unit and some parts of it were revised for operation convenience. The settings consist of four T-type thermocouples, three pressure transducers in the different positions and an ABB type flow meter. Refrigerant temperatures, tube wall temperatures were measured with T-type thermocouples. Flow meter was of magnetic type and can detect the flow rate through the evaporator. It measured the flow rate as mass flow rate or volume flow rate what unit is selected for measuring. In this experiment, mass flow rate was measured in gm/sec. Properties of the refrigerant were found using the REPROF7 software.

All the thermocouples and pressure transducers were connected with the PC through a data logger wind. Fig. 3 shows the schematic diagram of the experimental system, where the left part is indoor environment room while the right is outdoor environment room. First time, it is necessary to evacuate the compressor before charging refrigerant in to compressor. With the help of vacuum pump, the refrigerant inside the pipes and other ingredients are discharged. This supervac system pulls the contaminants creating a vacuum to 15-17 micron. Then placing the cylinder on the scale and connecting with the service port and control panel refrigerant is charged upto 4.26 bar pressure. The amounts of refrigerants are different for different refrigerants. During refrigerant charging the compressor is on. The desired room temperature is set. The data logger and flow meter is observed. After sometimes the condition of controlled room will be steady state and temperature reading will be steady. Then the temperatures and pressures reading are recorded and at the same time dry bulb and wet bulb temperatures are also recorded.

In the similar fashion, seven readings are taken for each refrigerant. Refrigerant charge is changed and a mixture of refrigerant R290 with R22 are charged with mass ratio of 25: 75. Different types of data are recorded. From these data energy analysis, exergy analysis and heat transfer parameters are calculated.

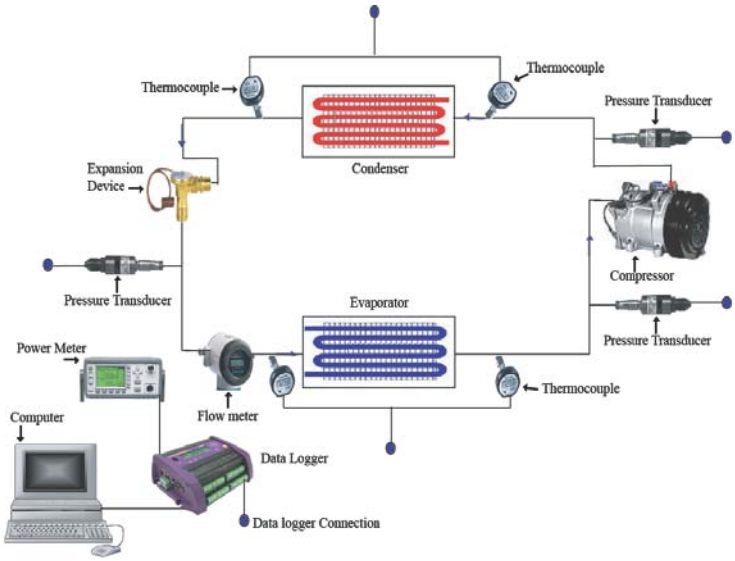

Fig. 3. Experimental Setup

4. Results and Discussion

4.1 Energy savings

Energy savings is the main objective of the most researches in the energy sectors. Usages of hydrocarbon mixture are capable to reduce energy expenses in the vapor compression air conditioning sector. Besides, some techniques are very much useful to reduce the energy usage also. Most of the techniques were utilized for analytical study. But in practice, some techniques are applied in some cases. Following methods are proposed to be used for the enhancement of the energy savings for this experimental study:

a) Changing thermostat temperature
b) Using hydrocarbon mixture as a refrigerant
c) Changing operating temperatures

d) Changing thermostat temperature

4.2 Changing thermostat temperature

Generally, the thermostat temperature of the indoor room is a set point at 20 °C. But in this experimental investigation, it was changed in order to save the energy usage. The air conditioner was running from 10.00 am upto 6.00 pm. Total running time daily was 8 hrs. Total consumption of energy at different set point temperatures is shown in Table 2. Using Equations 1-2 with the data found from the experimental work are tabulated and shown in Table 2.

$$EST\%_{20-T} = \frac{AET_{20} - AET_T}{AET_{20}} \times 100\% \tag{1}$$

$$AES = TEC_{ac} \times \%EST_{20-24} \tag{2}$$

From the literature (Saidur, 2008, 2009), it is found that total energy consumption in Malaysia was 127,752 MWh. Author found that energy consumption in the residential sector was 19% of the total energy uses. The air conditioner consumed 20% of the energy consumed by the residential sector in Malaysia. Hence, it is found that a total energy used by air conditioner in the residential sector is as follows:

$$TEC_{ac} = 127752 \times \frac{19}{100} \times \frac{20}{100} \Rightarrow 4854.576 \text{ MWh} \tag{3}$$

Total energy usage by domestic air conditioner = 4854.576 MWh
Annual bill savings can be calculated using following Equation (3)

$$Bill \quad Savings = AES \times Unit \text{ Price}$$

Table 2: Annual energy and bill savings in the air conditioning sectors in Malaysia

Set point (T)	Average daily Energy Usage, AEU	%Energy Savings (%EST)	Average Energy Savings per ° C (%)	Total annual Energy usage (in air conditioner) TEC_{ac}	Total Energy savings (TES)/year	Total bill savings yearly (Thousands)
°C	kWh			MWh/year	MWh/year	RM (k)
20	7.738	-			-	-
21	7.250	6.31	6.09	4754.576	30001.37	6540.30
22	6.810	11.99			57007.37	12427.61
23	6.280	18.84			89576.21	19527.61
24	5.850	24.40			116011.7	25290.54

4.3 Using hydrocarbon mixture as a refrigerant

Normally, R22 is used as a refrigerant in the air conditioner but in this experimental work, M1 is considered as an alternative refrigerant to R22. Using data from Table 2 and incorporating these data into the Equation (4), average energy savings are obtained as follows:

$$AES\% = \frac{AEU_{R22} - AEU_{M1}}{AEU_{R22}} \times 100\% \tag{4}$$

$$\Rightarrow \frac{7.65_{R22} - 7.25}{7.65} \times 100\% \Rightarrow 5.22\%$$

The above result indicates that using only 25% propane with R22, energy consumption will be reduced. Another thing is that this mixture caused to increase the coefficient of performance.

4.4 Changing the operating temperature

Operating temperatures have a great influence on the coefficient of performance. Hence, it has an effect on energy consumption also. In the case of vapor compression system, operating temperatures are condensing temperature and ambient temperature. But changes of operating temperatures are not easy. Evaporator temperature and condenser temperatures were changed due to the changes of refrigerants. It is observed in the experiment that in the morning, average power consumption was 1.58 kW and at noon, power consumption was 1.68kW for a particular range of evaporator temperatures. But during experimental work, in the morning, the ambient temperature was around 26°C and at noon it was 31.8°C. So, for 5.8 °C increase in ambient temperature (though other operating temperatures are not constant) caused 6.33% increase of power consumption. If it is possible to maintain ambient temperature for whole day at 26°C, the energy consumption will be reduced 6.33%. But this cannot be possible exactly. By limiting the use of substances having more global warming potential in the energy sectors, it is possible to maintain the atmospheric temperature at minimum level. Planting more trees in the country will also help to reduce emission, warming, etc. Thus, environment will become cool. Indirectly using high thermal capacity refrigerant, enhancement devices in the evaporator and condenser, pressure ratio as well as power consumption will be reduced.

4.5 Replacement of refrigerant R22 with M1

Total exergy losses of the refrigerant R22 and the M1 at different mean evaporator temperatures for two different ambient temperatures are calculated and presented in Table 3. By using Equation 5, annual exergy losses reductions are calculated. It is observed that exergy loss can be reduced using M1 instead of R22. Exergy savings are found higher at lower ambient temperatures. Table 4.5 shows the differences in exergy losses for both refrigerants used in the experimental work.

$$AIS_{refrigerant} = \frac{Ix_{R22} - Ix_{M1}}{Ix_{R22}} \times 100\% \tag{5}$$

Table 3: Average exergy savings at different mean evaporator temperatures and different ambient temperatures for both the refrigerants

At T_a= 27 °C				At T_a= 29 °C			
Mean evaporator temperature, T_{mev}°C	Exergy losses, Ix (kJ/kg) For R22	Exergy losses, Ix (kJ/kg) for M1	Exergy Savings %	Mean evaporator temperature, T_{mev}°C	Exergy losses, Ix (kJ/kg) For R22	Exergy losses, Ix (kJ/kg) for M1	Exergy Savings %
4	542	537	0.92	4.5	535.0	532	0.56
5	538	534	0.74	5	532.5	531	0.28
7	532	528	0.75	6	531.0	529	0.38
8	528.5	525.5	0.57	8	528.5	527	0.28

4.6 Increasing mean evaporator temperature

Total exergy losses are calculated for the refrigerants at different mean evaporator temperatures using the Equation 6. Ambient different are also varied. But for clear understanding and comparison, data for two distinct ambient temperatures are described and presented in Table 4.

$$AIS_{mevT2} = \frac{Ix_{mevT1} - Ix_{mevT2}}{Ix_{mevT1}} \times 100\% \quad (6)$$

Table 4: Exergy savings at different mean evaporator temperatures for different ambient temperatures

Mean evaporator Temperature, T_{mev} (°C)	Exergy loss at T_a= 27 °C	Exergy savings % at T_a=27 °C	Mean evaporator Temperature, T_{mev} (°C)	Exergy loss at T_a= 31°C	Exergy savings % at T_a=31°C
3.47	543.96	-	6.10	540.31	-
4.82	541.43	0.47	6.17	534.5	1.08
5.45	539.34	0.85	7.01	531.69	1.60
5.96	538.92	0.93	8.32	519.57	3.84
6.21	538.48	1.01	9.00	513.00	5.05
8.15	533.25	1.97	10.00	504.00	6.72
9.44	529.30	2.70			

Total exergy losses and exergy savings at T_a= 27°C and 31°C for different mean evaporator temperatures are calculated using Equation 3.34. It is clear that exergy savings increased with the increase of evaporator temperature for both ambient temperatures. It is also concluded that exergy savings are higher at T_a= 31°C than that of at T_a= 27°C. It is because at higher ambient temperature, the deviation of condenser temperature from the atmosphere is reduced. Hence, the exergy losses are reduced.

4.7 Exergy savings by decreasing condenser temperature

Table 5 shows a variation of exergy savings with different condenser temperatures.By reducing condensation temperature, exergy losses can be reduced for the refrigerants. Using data from experiment and putting it into Equation (7), exergy savings for the refrigerant R22 are calculated. These results are summarized and shown in Table 5 shows that exergy savings increased with the decrease of condensation temperature. In this experiment, the base condensation temperature for comparison was taken to be 45°C.The lowest condensation temperature was 38.8 °C.

$$AES_{cond} = \frac{Ix_{Tc=45} - Ix_{Tcond}}{Ix_{Tc=45}} \times 100\% \quad (7)$$

Table 5: Exergy savings with decreasing condenser temperature

Condenser temperature, T_c (°C)	Exergy losses, Ix (kJ/kg)	Temperature decrease, ΔT_c (°C)	Exergy savings (%)
45.0	548.17	-	-
44.0	543.10	1.0	0.93
43.3	542.60	1.75	1.02
42.5	541.75	2.5	1.17
41.5	540.31	3.5	1.43
40.8	539.80	4.2	1.536
39.8	538.75	5.2	1.72
38.8	537.10	6.2	2.019

5. Conclusion

Using the mixture M1 with respect to R22 as a refrigerant, it found energy consumption and exergy losses are found to be reduced. Summary of the findings are follows:

- The power consumption decreases by 4.5 to 5.5 % while using M1 instead of R22.
- With increasing the set point indoor temperature by 4°C, 24.40% of the energy consumption can be saved annually. Using M1 as a refrigerant instead of R22, up to 5.22% energy can be saved.
- More exergy savings can be possible by increasing mean evaporating temperature. At T_a= 27°C, by increasing evaporator temperature from 3.5 to 9.5°C, 2.7% exergy loss can be reduced whereas, at T_a= 31°C, by increasing evaporator temperature from 6.1 to 10°C, 6.72% exergy loss can be reduced.

References

[1] Edgerton, R. H. (1992). Available Energy and Environmental Economics. D. C. Heath, Toronto.

[2] Szargut, J. (1980). International progress in second law analysis. Energy 5, 709-718.

[3] Cornelissen, R. L. (1997). Thermodynamics and sustainable development. PhD Thesis, University of Twenty, The Netherlands.

[4] Rosen, M. A., Dincer, I., & Kanoglu, M. (2008).Role of exergy in increasing efficiency and sustainability and reducing environmental impact, Energy Policy 36,128-137.

[5] Pelletier, O., & Palm, B. (1996). Propane for heat pump applications using brazed plate heat exchangers, Report number 3. (8).

[6] Saidur, R. (2008). Energy, exergy and emission analysis in Malaysian residential sector. PhD Thesis, Mechanical Engineering Department, University of malaya, Kuala Lumpur, p. 189.

[7] Saidur, R. (2009). Energy consumption, energy savings, and emission analysis in Malaysian office buildings.*Energy Policy, 37*, 4104-4113.

[8] Ahamed J. U, (2012). Energy, exrgy and heat transfer performance investigation of air conditioning system, PhD Thesis, Department of Mechanical Eng. University Malaya, Malaysia, pp. 202.

[9] Sattar, M. A. (2008). Performance investigation of domestic refrigerator using hydrocarbons and mixture of hydrocarbons as refrigerant.A Thesis of Masters in Science and Engineering, Dept. of Mech. Engg. University of Malaya, Malaysia.

[10] Ahamed, J. U., Saidur, R., & Masjuki, H. H. (2011).A Review on Exergy analysis of vapor compression refrigeration system.*Renewable and Sustainable Energy Reviews, 15*(3), 1593-1600.

[11] Rosen, M. A., Dincer, I., & Kanoglu, M. (2008).Role of exergy in increasing efficiency and sustainability and reducing environmental impact, Energy Policy 36,128-137.